JOINT DOCTORAL PhD THESIS

Sorbonne University & Nanyang Technological University

Synthesis of hypercoordinated silicon species and asymmetric radical reaction via chiral ion-pairing

By

Alexandre Millanvois

A thesis submitted to the

Sorbonne University and Nanyang Technological University

in partial fulfilment of the requirement for the degree of Doctor of Philosophy

Under supervision of

Prof. Louis Fensterbank, Prof. Tan Choon Hong and Dr. Cyril Ollivier

Presented the 17 February 2023

M. THORIMBERT Serge	Professor, Sorbonne University	Internal Examiner
M. TLILI Anis	Researcher, Lyon University	External Examiner
M. CHIBA Shunsuke	Professor, Nanyang Technological University	Internal Examiner
M. YEUNG Ying yeung	Professor, The Chinese University of Hong Kong	External Examiner
M. OLLIVIER Cyril	Research Director, Sorbonne University	Supervisor
M. TAN Choon Hong	Professor, Nanyang Technological University	Supervisor
M. FENSTERBANK Louis	Professor, Sorbonne University	Supervisor

Statement of Originality

I hereby certify that the work embodied in this thesis is the result of original research done by me except where otherwise stated in this thesis. The thesis work has not been submitted for a degree or professional qualification to any other university or institution. I declare that this thesis is written by myself and is free of plagiarism and of sufficient grammatical clarity to be examined. I confirm that the investigations were conducted in accord with the ethics policies and integrity standards of Nanyang Technological University and Sorbonne University and that the research data are presented honestly and without prejudice.

. . . .

13/12/2022 Alexandre Millanvois

Supervisors Declaration Statement

I have reviewed the content and presentation style of this thesis and declare it of sufficient grammatical clarity to be examined. To the best of my knowledge, the thesis is free of plagiarism and the research and writing are those of the candidate's except as acknowledged in the Author Attribution Statement. I confirm that the investigations were conducted in accord with the ethics policies and integrity standards of Nanyang Technological University and that the research data are presented honestly and without prejudice.

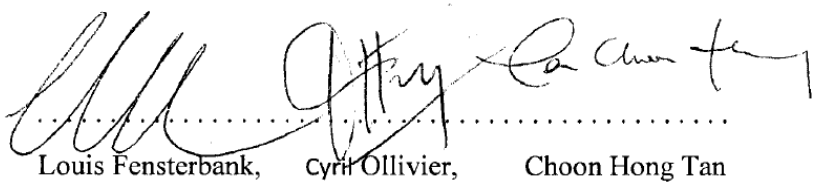

. . . . . .

16/01/22

Louis Fensterbank, Cyril Ollivier, Choon Hong Tan

Authorship Attribution Statement

This thesis contains material from 4 papers published in the following peer-reviewed journal(s) in which I am listed as an author.

Chapter 1.1 is published as A. Millanvois, C. Ollivier, L. Fensterbank, *European Journal of Inorganic Chemistry* **2022**, *2022*, e202101109. DOI: 10.1002/ejic.202101109

Chapter 1.3 is published as M. Abdellaoui, A. Millanvois, E. Levernier, C. Ollivier, L. Fensterbank, *Synlett* **2021**, *32*, 1513–1518. DOI: 10.1055/a-1374-9384

Chapter 2.2.2 is published as G. Lemière, A. Millanvois, C. Ollivier, L. Fensterbank, *The Chemical Record* **2021**, *21*, 1119–1129. DOI : 10.1002/tcr.202100049

Chapter 2.3 is published as A. Millanvois, C.-H. Tan, C. Ollivier, L. Fensterbank, *European Journal of Organic Chemistry* **2023**, *26*, e202300223.

. . . .

13/12/2022   Alexandre Millanvois

Abstract

The PhD was conducted between Sorbonne University (France) and Nanyang Technological University (Singapore) under the supervision of Prof. Louis Fensterbank, Dr. Cyril Ollivier and Prof. Choon-Hong Tan. It started at the end of 2019 until beginning of 2023.

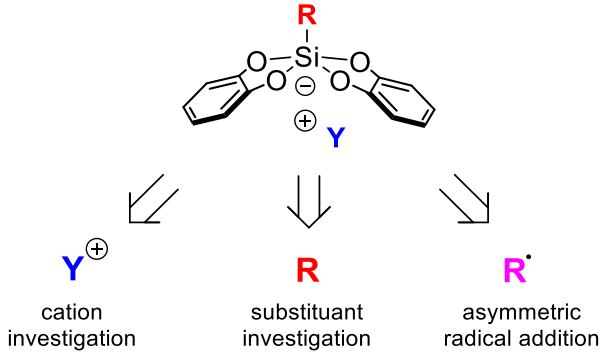

Since 2014, Prof. Fensterbank and Dr. Ollivier have studied the use of hypercoordinated silicon species (bis(catecholato)silicate) as radical precursors under photocatalyzed conditions. The classical cation used by our laboratory is mainly a chelated potassium with crown-ether, to prevent high molecular mass and resulting a poor atom economy when employed in organic synthesis, synthesis and study of several alkali derivative was done.

Their synthetic pathway has permitted to reach new alkali derivatives (Li, Na, K) with several substituent. Their physical properties were studied (NMR, cyclic voltammetry, X-Ray) and compared with the already known silicates. Their use as radical precursors in a dual nickel/photoredox methodology was then developed and published. (*Synlett,* 2021, *32*, 1513–1518)

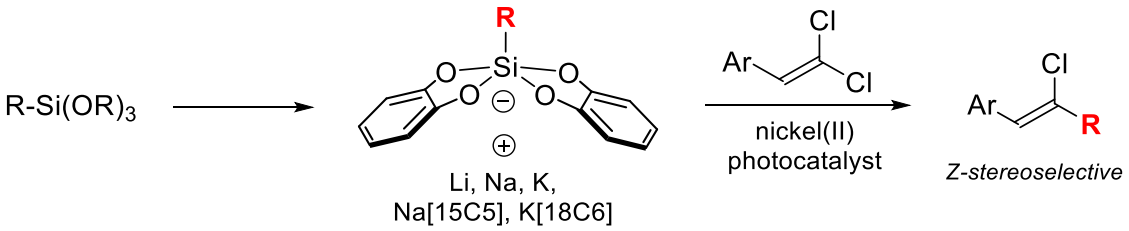

During our study oriented on the synthesis of these derivatives, we provided an overview on the synthesis of bis(catecholato)silicate and published a review on this topic. (*EJIC*, 2022 (17), e202101109). In addition, we published more specific reviews regarding the use of hypercoordinated species in our laboratory (*TCR,* 2021, *21* (5), 1119–1129) and organometallic/photoredox catalysis. (*Photochem Photobiol Sci* 2022, *21* (4), 585–606)

Owing to the limitations in commercially available trialkoxysilanes, we have investigated the synthesis of some silane derivatives, mainly substituted by cyclopropane or fluorinated alkyl chain, to access nontrivial radicals. The recent use of Martin's spirosilicates as radical precursor has allowed the synthesis of new potential precursors on this hypercoordinated derivative.

The development of these cyclopropane alkoxysilanes was achieved in gram scale, as well as the synthesis of the corresponding bis(catecholato)silicates. The methodology involved commercially available vinyl silane engaged in a formal [2+1] cycloaddition and our classical methodology to reach hypercoordinated species selectively.

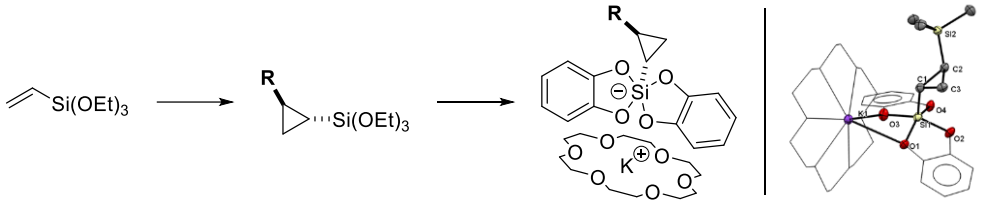

Indeed, the preparation of bis(catecholato) and Martin's silicate led to the formation of pentavalent silicons bearing the cyclopropyl both known to act as radical precursors under oxidative condition. Early results show a lack of reactivity concerning the generation of cyclopropyl radical from hypercoordinated silicon species. (*The manuscript on this work is currently in preparation)*

The synthesis of polyfluorinated alkyl hypercoordinated silicon species (R = $-CF_3$, $-(CF_2)_nCF_3$) is also ongoing to prepare of silane and bis(catecholato) derivative or Martin's silicate.

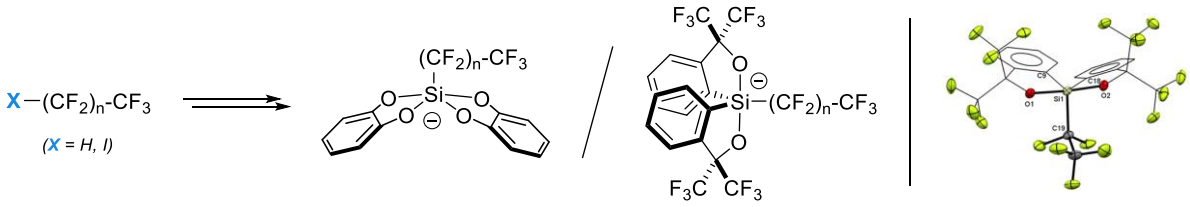

The desired bis(catecholato) trifluoromethyl silicate was not achieved but interesting results were obtained with the Martin's silicate. The observation of the desired $-CF_3$ species and later isolation of the $-C_2F_5$ one were achieved. The oxidation of the pentafluorosilicate was unsuccessful and the inability of the silicon species to act as radical precursor was rationalised. The nucleophilic behaviour on those silicon species was finally observed in solution at the cesium fluoride interface between and in solid-state under mechanochemical conditions. The mechanism of the reaction was studied and mechanistic insights were obtained by DFT calculations. (*EJOC, **2023**)*

In collaboration with Prof. Tan, we have questioned the ability of these anionic radical precursors with several small cations to be employed in a phase transfer reaction using chiral guanidinium derivative. This topic would later be extended to classical anionic radical precursors (R-BF_3K, carboxylate, anionic single electron donor..) with the idea of controlling radical species using the chiral ion-pair strategy.

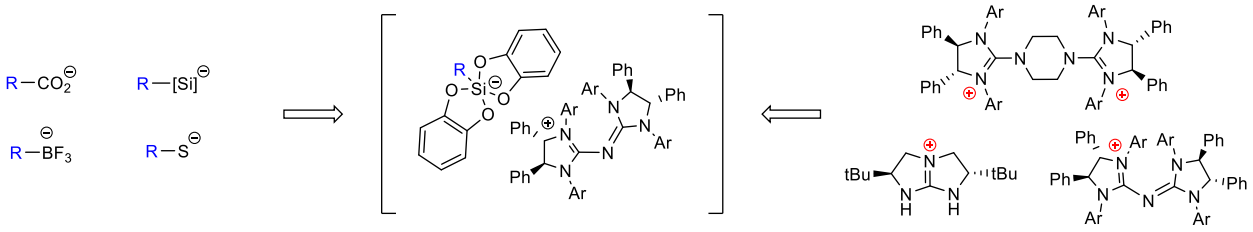

Radical precursor *Example of chiral ion-pair* *Phase transfer catalyst*

During our study, we have found that anionic salts, such as potassium 2-nitropropane salt or thiolate, act as single electron donor performing some radical reaction inside the chiral catalyst's pocket. This work was done in direct collaboration with Dr. Ban Xu in NTU. My work involved the design and investigation about the mechanistic part for this project.

Interestingly, we were able to perform this reaction in solution and solid state under mechanochemical conditions allowing us to reach high yield and high enantioselectivity. The mechanistic study (involving: UV, NMR, DFT calculation using ORCA on NSCC supercomputer, solution and solid EPR, ATR-FTIR) has showed similitude between both medium and has allowed us to propose a mechanism for this methodology. (*The manuscript on this work is currently in preparation)*

Finally, the solid-state oxidation of several radicals precursors (trifluoroborate, pentafluorosilicate and bis(catecholato) silicate) was investigated using organic and inorganic oxidants. To our delight, conditions were found allowing the generation and trapping of the desired radical species from all these precursors.

Acknowledgements

First, I would like to thank Prof. Thorimbert, Prof. Chiba, Dr. Tlili and Prof. Yeung for accepting to be part of the thesis committee and reviewing this PhD thesis work. This work has been done in collaboration between Sorbonne University (SU) and Nanyang Technological University (NTU).

I would like to express my deepest gratitude to Sorbonne University (previously UPMC) for giving me the possibility to study here even if I obtained my *Baccalauréat* in *second session*. I would also like to thank the university for all the opportunities it gave me during my bachelor and master, and finally for this incredible opportunity of performing a joint doctoral program. I obviously thank NTU for accepting the realization of such project.

This PhD journey began with both of my Master 2 professors in radical chemistry whom are now my SU supervisors, Prof. Fensterbank and Dr. Ollivier, that I want to thank for this opportunity. Firstly, I would like to thank you Cyril, you are an incredible professor and you have a tangible passion for this field. It was a pleasure to think about organic chemistry from a new perspective, it was the most intellectually challenging course from the Master 2. Then, thanks to Louis, firstly also for those courses oriented toward triplet state radical chemistry and the introduction to modern radical one. It was also nice to discover you and your chemistry through your explanations. I would also like to thank both of you regarding the end of the Master 2, when we firstly talked about internship to defend my Master then for talking about a PhD. Thank you for trying to build a first agreement with Japan, then a second with Singapore and finally for believing in me (and my curriculum) enough to give me the opportunity to defend a project and a funding for this program.

Concerning the PhD, and more about the best silicon lab of France, thank you for encouraging me to stretch my comfort zone out again and again. For example, with the synthesis of several interesting silicon-based targets and the related autonomy to develop this chemistry especially the fluorinated gaseous one. This made me learn so much, obviously experimentally and on the related knowledge and bibliography. It really developed my love for inert chemistry, group 14, fluorine, and glassware. Thank you also for letting me have interesting responsibilities in the lab, it's definitely valuable knowledge. So once again, thanks for letting me investigate new chemistry that needed some knowledge the lab didn't possessed at the time. Thank you for giving me the opportunity to do a lot of bibliography related work (EJIC❤) and to let me express a lot of creativity, drawing included. Thank you for being yourself since the M2 and also *accepting* me as I am since then. It is a pleasure to be true with others for the best and the worst as always. I wish you all the best for the future, I will come back some time if you don't cast me away me completely.

Then I need to thank my third supervisor, Prof. Tan. Thank you for your curiosity, it was a pleasure to talk about chemistry during my stay in the TCH lab, to learn about your work and your vision as a PI and of course talking about SG in its globality. Thank you for encouraging your team to discuss about chemistry since the beginning, I totally agree with your opinion on the future of chemistry, related to knowledge in DFT for all organic chemists. Thank you to "*force*" Choon Wee to put motivated people on good tracks, and therefore thank you for giving me the opportunity to start investigating this field. I am grateful for the opportunity and trust you gave me to work on the reaction developed by (Dr.) Ban Xu, it was a pleasure to push myself further at the end of my stay and to conduct this work. I also appreciate that you let me present again and again some of the main group chemistry for the lit. meeting. I hope to see you again in conferences or maybe when I will go back to SG for vacation, until that, I wish you also the best. Finally, thank you for all the liquor I discovered during the TCH's party, it was incredibly good.

Following the timeline of the PhD, I need to start talking about the MACO team, this place (actually 32-42, 5^{ieme}) is a marvellous place to learn a lot a thing from a lot of unique people with unique personalities about chemistry and social science. Based on what I know from the past and what I see when leaving, I believe this place will continue to be so much different from every classical IPCM's team. I will now talk about PI and past and present students.

Let's back up a little bit during Winter 2019. Firstly, thank to all the members, I need to thank Anthony (V.) et Alex. (S.) from the *Cobalt team* that were the firsts to talk to me without basing themselves on the shit people were spreading. Thank you both for our conversations about chemistry and for trying to unite the MACO team before your respective departure, you did your best. Then, thank you Etienne (L.) for introducing me fully to the lab and then into the *silicate team*. I do not regret how often I managed to prove you how far I can go to make you desperate. Thanks for the initial tips about crystallisation that put me on good track. It was a pleasure to spend some time with you, during your good and bad time here.

Then I need to thank Mehdi (A.) that started to talk to me because some Postdocs forced him to (you know the unity of the team blablabla). You quickly became my *co-worker*, and it was a pleasure to talk about chemistry with you during these years. I will be forever grateful for what I managed to learn by listen to you and explaining to you why you were talking shit. There were not some easy years, but not the worst ones neither let's be honest. I'm happy that you *stepped-up* on some points, and I wish you the best on continuing to do it everywhere (study your books carefully). It's now a pleasure to count you as one of my ~~friend~~ *ex-co-workers* ✓, I am waiting to see and hear about your following journey.

Still in the silicon community, I need to thank you Cedric (S.), for all the knowledge you passed to me on glassware, distillation, about chemistry and all the conversation we had. You are a very nice human being; a real part of this team and it was a pleasure to inherit your responsibilities in the lab.

Then also in the silicon area, Gilles (L), thank you for this year I have spent in the 511, it was a pleasure to exchange with you about chemistry, to learn more about science and to get to know you as a person. It was so nice to try to push ourselves to clean this lab by doing kind of a competition and to try several technics and improvements for the lab. Thank to Daisuke (S.) that was first a visiting student and that is now full member of the team, it was a pleasure to share the lab with you and Gilles.

The lab improvement spread a little bit in the 509's to Valerie-Anne (R.) & Fen (Z.), my neighbors at this time in 509. Thank you VA for sharing the few we got at this time by doing the addition of the stuff (509 + 511, so nearly nothing) especially the UV lamp for TLC at first. I need to thank my neighbour of the 510, Hengrui (Z.), for being such a nice person, It was a pleasure to exchange with you during my stay in this office. The 510 was also a great place, being the internship office also, so thx to all the M2 I had the chance to meet at this time (Pierre, Luis, Franck…)

Thanks to Etienne (D.), it has always been nice to discuss with you and have a drink. I still like after these years, just like for the other Etienne, *to go too far for you*. Thank you also for my forever memory about the XRD.

Following the team, thanks to Cassandre (B.). I firstly saw you in Master 2 and at the time, we didn't really talked but I heard a lot about your "*my email address doesn't work*" in every course we shared. I was quite happy to talk to you and to discover how nice you are. It's always a pleasure to exchange about chemistry and life in the 515 or 520. Thank you for being always available, it will be a forever memory to see your first so fcking violent -NO_2 reduction during my distillation of $TMSCHN_2$. Thank you also for asking at this time to work on some Saturdays, it's a pleasure for a workaholic (thanks to Alex S. also). As for MEA I am curious to heard about your next journey, hopefully we will have the opportunity to meet again.

Still in the 515 I need to thank Marion (B.) as said later, an incredible organic professor, when I was in bachelor, always here to exchange and guide people. I am happy to have had the opportunity to share some time with you years after being your student, thank you for everything.

To finish about the 514 office, thank you Marc (P.), our relationship was firstly a rollercoaster (still happen sometimes) but rapidly evolved to something great. It was also a pleasure to exchange about chemistry and learn about yours. I really appreciate everything I learned about inert chemistry and about my

gaseous chemistry mano apparatus. I also learned a lot from your relevant participation in seminar and when you fixed nearly everything in the lab. For all this and all the good you do in this team, thank you.

Another important person in the lab, Empress of 513, Virginie (M.) needs to be highlighted. Thank you for our positive interactions since the M2, and thank you also for talking about the opportunity with Sanofi that made me meet Patrick (Dr., B.). We often *agree that we disagree* even though we also think alike about quite a lot of the common sense things, but anyway it's often fun to discuss with you. Thank you for helping pushing the individualism a little bit further away when it is possible, this is obviously good for the team. Thanks to Clement (C.), for sharing so much about chemistry and your chemistry. Also, more specifically about glassware and inert technics. Having the opportunity to see you at your bench when you arrived in the team made me a better chemist. I deeply know that I obtained several of my targets due to meeting you. Thanks to Corinne (A.), an infinite source of culture and joy/unity in the team, it was nice to exchange and learn from you, wish you the best for your last project this year. And then obviously thanks to all the other members of the team at this time.

Special thanks for Thomas (D.) that I had the chance to introduce to the MACO team before SG. You are a very good (curious) chemist, a nice human being and moreover *consistent* as a person and this is an incredible quality. It was so nice during these few months and still up to now to present you my *old German fuming superacid* chemistry and my related apparatus. It is a pleasure to share with you Baptiste's (N.) responsibility for the distillation and to manage the glassware together. Special thanks to Florie (L.), and all the discussions we shared in her workshop. Finally, thank you for everything you taught me back when I started to apply this gaseous knowledge on your *spiraniques silylés*. It was quite funny to see how much I felt that I knew you at the beginning of my third year with only 2 months of being neighbors. I am happy to know you more now and I wish you the best for the end.

Then I need to thank members of the TCH labs. Firstly, my deepest one for Ban Xu, we firstly started to speak by mail before my arrival and then in person when I was in the lab. It was so nice to exchange about chemistry and life with you during this year, I will forever be grateful for suggesting me to work with you on your project with Prof. Tan and to perform the mechanistic investigation. This pushed me out my comfort zone and made me a better scientist. I wish you all the best in Henan with Jiang (Prof. Z.) and also the best to your family. I'm sure you will develop some very nice chemistry and hopefully we will have the opportunity to collaborate again.

I would like to thank a lot Ester (A.), for helping me setting up my chemistry in the lab, you taught me so much about SG and helped me to understand so much. Thank you so much for this and wish you the

best with the *animals* in the dormitory and for the end of PhD. A special one also to Chin Lee (L.) who helped me also at first when we both arrived for the beginning of our projects in SG. A big thank to ZiQi also, it was so nice to share the lab with you and try to help you with your XRD. Hopefully it will end well.

Finally, a big thank to Zhang Xin, it was soo cool to have you as direct neighbor in the lab that we shared 7/7 a week until late during months. Thank you for all our discussions about chemistry, for accepting to debate hours and hours about politics and for making me discover 二锅头 (èrguōtóu, a fabulous drink). Wish you the best for your career. A special one also to Kuo, thanks for sharing your culture, I still believe you will do great things in science, wish you the best. To finish with the lab's postdoc, thanks to Genevieve (L.). I am grateful that you asked me to read and discuss about your proposal as first conversation. It was a pleasure to discover your favourite bar with BX and your husband and to talk about everything. I really appreciated the frank conversations we had all the time; I wish you the best.

Another big thanks to the DFT team of the Lab, firstly thank to Choon Wee (K.), you gave me some precious orientation to start my DFT journey, it was nice to heard about your opinion during meetings and to debate with you also. I will remember our discussion during the hiking. A huge thanks to Kevin (W.), I will never have been able to start doing some real calculation without you, you are an incredible person, you bring so much good in the team. Thank you for all these (late) evening discussions we had about literally everything, my stay would have been different if I did not met you. I also wish you the best.

To conclude, all the best to all the news members of the teams during the end of my stay. Thanks a lot to the staff of the SPMS, special thanks to Ee Lings (G.) for your time and help, a huge one to Prof. Webster Thank you so much for all the knowledge you gave me concerning the EPR and fitting of signal, thank you for all the discussions we had during our time performing the analysis.

Finally, Thanks to Peenut (L), an incredible artist, thank you again and forever for your time and your art. I also would like to thank my both incredible landlords, Melissa and Thapelo, it was so nice to discuss with you about everything and discover SG from another point of view. Thanks to Po Kai, It was nice to meet you in France, nice to see you again in SG, wish you the best.

My last (PhD related) thanks goes to members of the IPCM and the MACO team I met during my last year. Firstly, thanks to Claire (T.), Aurelie (B.), Regina (M.) for their help concerning the NMR, and these nice discussions we had during these years. Thanks to Jeremy and Geoffrey concerning the XRD, you both taught me a lot regarding your field and I deeply appreciate how available you both were. Thanks to Gilles (C.) for the MS, thank to Omar (K.), it's always nice to see you and exchange a little bit.

Special thanks to the best office ever of the MACO and IPCM, obviously the 506 and its members. Thanks to my new (incoming, u will see Norby) brother Baptiste (N.), if the beginning was harsh, coffee included, it is now a pleasure to discuss with you about everything and to perform some stupid thing with the same energy. As a (future) member of my family, you can always count on me, good luck for the end of your PhD, do what you think is reasonable for your project *insert smiley clin d'oeil on sait*. Thanks to Baptiste's "kind of son", *le dénomé Valade*, you brought so much joy in the lab/office, wish you the best for the Quebec journey. Thanks again to Thomas (D.) for welcoming me in the office at the time, I am quite happy that we share the love of St. P. collection. Thank you again for welcoming me in the 509 lab where I met Maria (B.) a wonderful person. Thank you for being so nice, the peaceful member (or just the most reasonable one) of this office and lab. I wish you the best for the end of your PhD, as for all the first-year students I have no doubt that you will do a lot of interesting findings. A big thanks to *Maria bis* alias *Djuro* also known as *Alex IV* or *Alex* or Alexandre (D.). We first met 3 years ago in a bar, then again during my last year. You are also, like a lot of the MACO members, an incredible human being. We had so much fun in the lab, from the music to the whale vocalization.. Wish you the best in your Nordic journey.

Then thanks to the rest of the team. Firstly thanks to Omar (S.), thanks also to Jade (D.), if the beginning was a little bit harsh and even if apparently, we "hate each other" thank you, it was very nice to exchange with you and thanks for being supportive to all the lab. Hopefully one day we will finish at least one of the conversations we started but never ended. Thanks to Amal (L.), it's a real pleasure to always discuss with you frankly for the best and the worst, all the best for the end. Thanks to Norbert "Norby" (R.), one of the most important students for this lab's unity, it is always a pleasure to discuss and debate with you, I also wish you the best for the following Norby's adventures. Thank to Vincent D. and his countless MACO CDDs, best for the industry and thanks for exchanging on Grebs chemistry. Danke schön Maxim-A (W.), it was a pleasure to meet you, hopefully we will see us again (in Deutschland ?), anyway Chemie gibt dir Freiheit. All the best for the "old (but new student to me)" Xue Yan and Salem Lamine, and to the others new students, Lukmonjon, Fabio, Hang, Jorge and all the new M2..

Going back to my long stay in SU, one opportunity I had was obviously to discover organic chemistry under guidance of a lot of wonderful chemists. And a lot that gave me a chance to work and to become a better chemist and human being. Going back in L2, I firstly need to thank Prof. Frédéric Lemaitre. He is the most pedagogue Professor I have met in my life and the one that give me a goal in my life, organic chemistry. I will never be able to express all my gratitude for giving me so much knowledge, a factual overview of a classical organic lab and about public research. I also definitely need to thank Prof. Franck

Launay, for being so much available to his students, to me and for giving my first internship in a laboratory. Thank you for your instruction and for allowing me to organize my work freely during this time. Thank you also for being open to discussion and talking honestly about research from the scientific (but not only) point of view. Then, in L3, I had the chance to meet several incredible organic chemists such as Luc (D.), Serge (T.) then Marion (B.). Thank you respectively, for the TP (then courses in M1), CM (then courses in M1 also), and TD. Each of you taught me so much, it was a real pleasure to meet you. Then I need to thank more Luc who offered me my first organic chemistry internship and Serge that allowed it in the Chembio Team (Special thanks to the team, to Candice and Vincent also). Thank you, Luc, for letting me work and discover the total synthesis field, to take time every day to talk about chemistry with a coffee a black board and a lot of questions to stimulate my brain. Thank you for the autonomy you gave me (and thanks to Liang and Anto, in the lab at this time, for helping me on some occasions) it helped me ever since then. Thank you, Serge, also, for calling me randomly from the corridor and asking me to draw my chemistry to the black board, it obviously made me a better chemist. Anyway, thank you to both of you for everything you've done for me since I've met you, it is a pleasure to visit you from time to time and talk about science and life. I need to express my gratitude to Anne-Lise (D.) that believed in my project of performing total synthesis in Japan. Thank you for *fighting* to build the agreement with Okadai to reach Prof. Kadota, it was one of the best experiences of my life, it was heaven to perform total synthesis and being a lab rat. I learned so much during my stay, thanks to Prof. Kadota that taught me a lot also during this time. Thanks to Andy (-reas, M.) for being such a nice friend in Japan, it is always a pleasure to send you some too long emails from time to time. Thank you again Anne-Lise because this opportunity later allowed me to discover the industry and the fluorine chemistry under guidance of Dr. Bernardelli and Anne-Marie (P.). Thanks to both of you for your kindness and for the challenging subject.

Special thanks to all the wonderful people I met during my bachelor and master (M. Mintec, Meghane H., A.-E. Kasmi, Imane S., Camille M., Urielle R., Adrien S., Anais S., Gredy K., …)

I will finish with my deepest thanks for the most important persons in my life.

To Robin Z. (A.) & Felix (B.) F.; Julie K., Ingrid S. ; it aged well, thank you so much.

To the more recent but it does not matter; Nihel H.S. and *Madame* Carlota B.; I will not develop here why but thank you for everything, I owe you all so much.

Finally, I would like to thank my small family, thank you for being so supportive since the beginning.

Merci Papa, merci Maman, merci Boubou

À toute personne m'ayant enseigné,

"...
Je défends l'égaré, le faible, et cette foule
Qui, n'ayant jamais eu de point d'appui, s'écroule
Et tombe folle au fond des noirs événements ;
Etant les ignorants, ils sont les incléments ;
Hélas ! combien de temps faudra-t-il vous redire
A vous tous, que c'était à vous de les conduire,
Qu'il fallait leur donner leur part de la cité ;
Que votre aveuglement produit leur cécité ;
D'une tutelle avare on recueille les suites,
Et le mal qu'ils vous font, c'est vous qui le leur fites.
Vous ne les avez pas guidés, pris par la main,
Et renseignés sur l'ombre et sur le vrai chemin ;
Vous les avez laissés en proie au labyrinthe.
Ils sont votre épouvante et vous êtes leur crainte
..."

Victor Hugo (did not knew about PhD at this time)
L'année terrible (8e édition) (À ceux qu'on foule aux pieds)

Contents

List of abbreviations

ax	Axial
Ac	Acetate
ALIE	Average Local Ionization Energie
ATR-FTIR	Attenuated Total Reflectance - Fourier Transform InfraRed spectroscopy
BDE	Bond dissociation energy
BG	Bis(guanidinium)
bpy	Bispyridine
Cp	Cyclopentadienyl
DABCO	1,4-Diazabicyclo[2.2.2]octane
DFT	Density Functional Theory
dme	Dimethoxyethane (aka glyme)
dtbbpy	ditertbutylbispyridine
EDA	Electron Donor Acceptor
EFEI	External Force is Explicitly Included
EnT	Energy transfer
EPR	Electron paramagnetic resonance
ESP	Electrostatic potential
eq	equatorial
FIA	Fluorine ion affinity
FT	Fourier Transform
HAT	Hydrogen Atom Transfer
Hex	Hexyl
HOMO	highest occupied molecular orbital
Hz	Hertz
IR	Infrared
J	scalar coupling constant, in Hz
LED	light-emitting diode
LUMO	lowest unoccupied molecular orbital
mCPBA	3-Chloroperoxybenzoic acid
MO	Molecular orbital
NE	North East
NMR	nuclear magnetic resonance
nN	nanoNewton
ppm	parts per million
PPN	Bis(triphenylphosphine)iminium
PTC	Phase Transfer Catalyst
PTFE	tetrafluoroethylene polymer (Teflon)

r.t.	Room temperature
SCE	saturated calomel electrode
SET	Single electron transfer
Sn2	Bimolecular nucleophilic substitution
Sn2X	halogenophilic SN2
SOMO	Singly Occupied Molecular Orbital
SP	Square pyramidal
Srn1	nucleophilic radical substitution reaction
SW	Southwest
TBA	tetrabutylammonium
TBAB	Tetrabutylammoniumbromide
TBAF	tetrabutylammoniumfluoride
TBP	Trigonal bispyramide
TDAE	Tetrakis(dimethylamino)ethylene
THF	Tetrahydrofuran
TMSCl	Trimethylsilyl chloride
UV	Ultraviolet–visible
XAT	Halogen atom transfer
XB	Halogen bonding
XRD	X-ray diffraction
Å	Ångström
a, b, c	unit cell edge lengths
α, β, γ	unit cell angles
Z	molecules per unit cell
V	unit cell volume
λ	wavelength
δ	chemical shift
ν	stretching mode
cm–1	wavenumber

Chapter I.
Bis(catecholato)silicates, hypercoordinate silicon species

Chapter I.
Bis(catecholato)silicates, hypercoordinate silicon species

This first chapter contains material from two papers in the following peer-reviewed journals:

EJIC for chapter 1.1 and Synlett for 1.3.

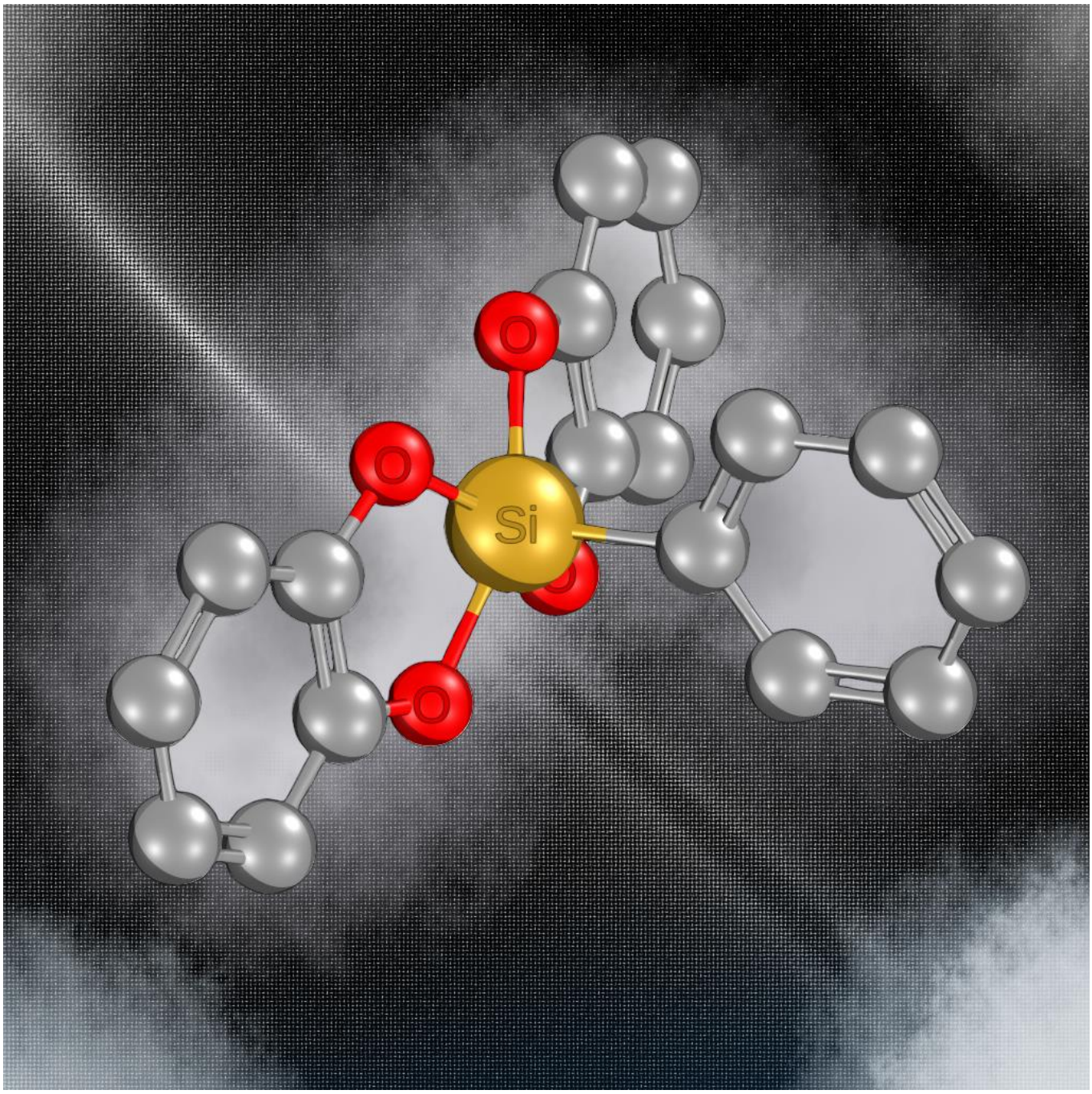

1.1 State of art, Synthesis, Structural Data and application

1.1.1 Introduction

Hypercoordinate silicon compounds have attracted the attention of molecular chemists for decades. While penta- or hexacoordinate species are the most encountered ones, hepta coordination has also been reported.[1] Ease of synthesis and stability, specific geometrical features and reactivities of these compounds are generally the observed properties. Overall, these silicon derivatives have been extensively studied, and several reviews were published,[2a--f] including a comparison between hypercoordinate phosphorus and silicon species.[2e] From these reviews, and in particular that of Rendler and Oestreich,[2g] it can be pointed out that a tetravalent silane with latent Lewis acid character brought by the L ligands can be converted to a hypercoordinate species *via* two main processes.

- First, the direct interaction of the tetravalent silicon center with an additional neutral ligand can occur inter- or intramolecularly to form a weak dative bond. The intermolecular interaction has been observed with a donor compound or solvent (such as MeCN or DMF) leading to the hypercoordinate derivative. The intramolecular interaction has been mainly observed with a bidentate ligand. These derivatives often take advantage of weak N···Si or O···Si dative bonds.

- The second common way to obtain a penta- or hexacoordinate species is by forming a covalent bond between silicon and a negatively charged ligands such as an halide (e.g. F, or Cl) or alkoxy groups (e.g. O-Alkyl or O-Aryl). The case of hexacoordinate silicon species usually requires electronegative substituents such as fluorine as in related pentafluorosilicates,[2f] these attracting groups facilitating polyaddition on the silicon center (Figure 1).

-

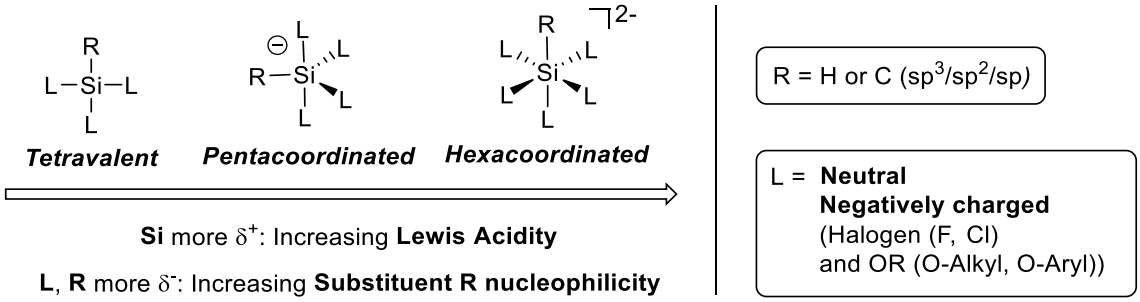

Figure 1. Hypercoordinate silicon species: from tetra- to hexacoordinate[2g]

Hypercoordination induces a modification of the physico-chemical properties, the main one being the Lewis acidity. This property gradually increases as follows, tetravalent<pentavalent<hexavalent. Indeed, the increase of the coordination leads to the decrease of the electron density at silicon and thus to the increase of its Lewis acidity. Moreover, the nucleophilicity of the substituent (R=C or H) is also modified by the coordination of the silicon center. The nucleophilicity of the R substituent and that of the ligands is first increased at the pentavalent state and even more when the silicon reaches the hexacoordination.[2g]

Beyond the well-known pentafluorosilicates,[2f] bis(catecholato) derivatives occupy a particular situation and have recently witnessed intensive use in organic synthesis, particularly as powerful alkyl radical precursors under photooxidative conditions.[3] To accompany these developments, this minireview will focus on the access to this specific class of compounds and will summarize their syntheses, structural and analytical data.

1.1.2 Synthesis of Bis(catecholato)silicates

1.1.2.1 Foreword

Contrary to other pentacoordinate silicates such as those originating from Martin's spirosilane (bearing the dianion of hexafluorocumyl alcohol), alkyl and aryl bis(catecholato)silicates cannot be prepared from the corresponding spirosilane by addition of nucleophiles onto the electrophilic silicon center.[4, 5] Bis(catecholato)silane indeed exists only in solution as an insoluble oligomer.[6] Of note, the tris(catecholato)silicate dianion has also been described but despite a recent highly interesting report by Greb[7a] its chemistry has so far been limited in terms of applications (Figure 2).

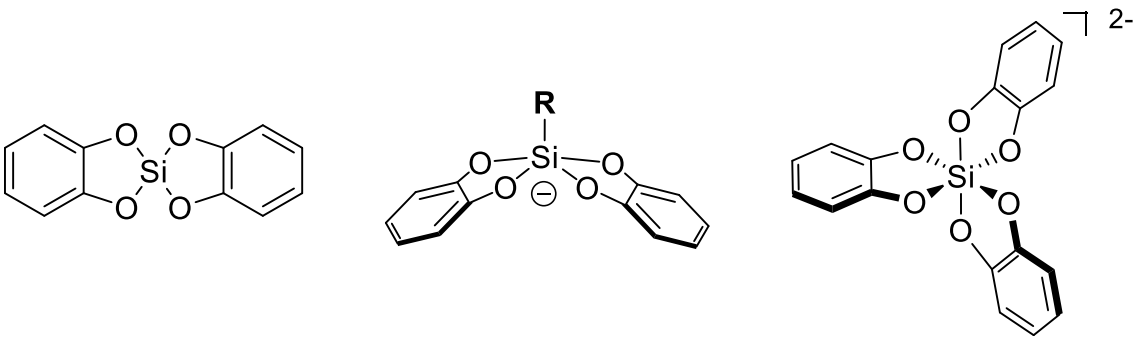

Figure 2. Spirosilane, bis(catecholato) and tris(catecholato) species

We will focus on the bis(catecholato)silicate derivatives[7b] and will not deal with silicates derivatives based on substituted catechols, perhalo and others, as nicely developed by Greb.[7c, 7d] All chemical structures of bis(catecholato)silicates will be numbered in bold and listed in Table 1.

Their synthesis usually occurs under mild conditions. Trichloro- or trialkoxysilanes are often used as starting materials but alkoxysilanes are preferably chosen in order to prevent the in-situ generation of HCl (Scheme 1). A trichlorosilane derivative bearing the desired moiety can be converted into the alkoxysilane on a large scale. In this case, the formation of a trimethoxysilane simplifies the purification by distillation due to the lower boiling point of these silanes compared to the corresponding triethoxy- or triisopropoxysilanes.

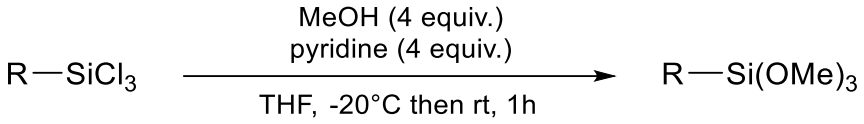

Scheme 1. Synthesis of trimethoxysilanes from trichlorosilanes

By simply mixing two equivalents of catechol in basic conditions with the trichloro- or trialkoxysilanes, the hypercoordinated silicates can be obtained. They are generally purified from the reaction medium by crystallisation using a non-polar solvent. Several protocols will be now discussed (Scheme **2**).

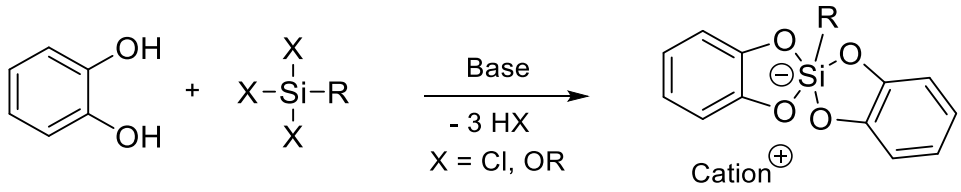

Scheme 2. General synthesis of bis(catecholato)silicates from trichloro- or trialkoxysilanes

Thus, it was also described by Sakurai and coworkers8 that a solution of di-deprotonated catechol (dilithium-catecholate) could be prepared before adding it to a THF solution of allyl(trichloro)silane. The corresponding lithium allyl bis(catecholato)silicate (14 Li) was not isolated but directly engaged to react quantitatively in an allylation reaction (Scheme 3).

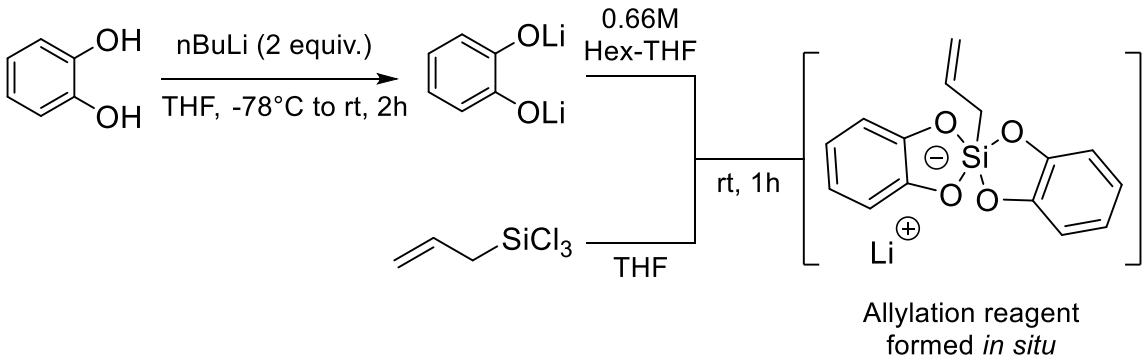

Scheme 3. Formation of lithium allyl bis(catecholato)silicate from allyl(trichloro)silane

Another pathway for the synthesis of bis(catecholato)silicates has been developed by Tacke and coworkers.[9] While the classical reaction is generally based on the elimination of methoxide or chloride anions, Tacke described here the use of less reactive substituents such as a methyl or a phenyl as leaving groups allowing the formation of the desired silicate by the introduction of catechol on the silane (Scheme 4).

Based on this methodology and by the extrusion of methane, benzene and methanol from (dimethylamino)methyl)methoxy(methyl) phenylsilane, (dimethylammonio)methyl bis(catecholato)silicate (79) was obtained in 30 % yield and isolated directly from the reaction medium thanks to the in-situ crystallisation of the zwitterionic species.

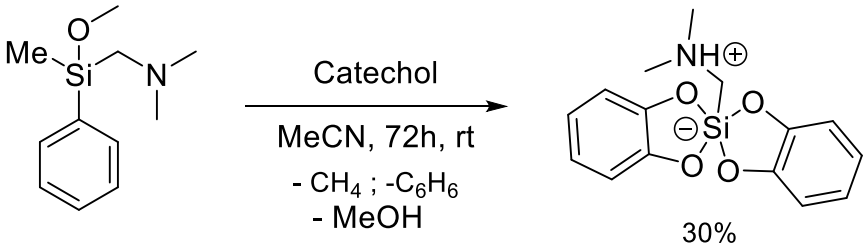

Scheme 4. Synthesis of (dimethylammonio)methyl bis(catecholato)silicate from [(dimethylamino)methyl)]methoxy(methyl)phenylsilane

This type of route remains an exception and we will now present more general methodologies to access various silicates with different cations, recognizing that the counterion can be inorganic or organic.

1.1.2.2 Silicate Synthesis

2.2.1. Alkali-silicate

In this section, we deal with bis(catecholato)silicate flanked with an alkali metal counterion (Figure **3**).

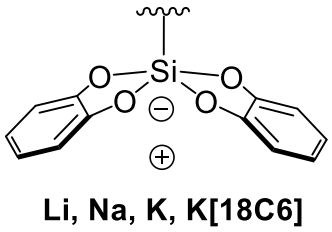

Figure 3. Alkali based bis(catecholato)silicates

As previously reported in Scheme **3**, lithium silicates were mainly described for the synthesis of allyl derivatives by Sakurai (Scheme **5**A).[8] But more recently, our group synthetized lithium benzyl bis(catecholato)silicate (**1 Li**) by addition of a homemade lithium methoxide solution in methanol on benzyltrimethoxysilane and catechol. The silicate was isolated in 64 % yield after recrystallisation from acetone by slow addition of ether.[10] This derivative appears more stable than the previously described lithium allyl bis(catecholato)silicate.

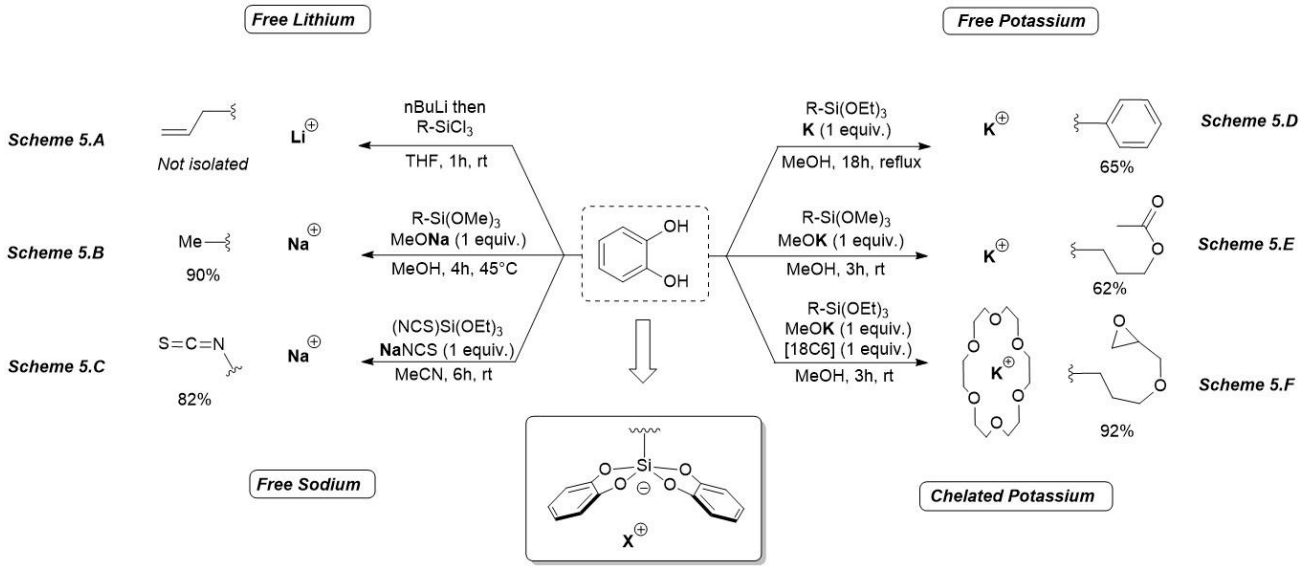

Scheme 5. Synthesis of alkali alkyl and aryl bis(catecholato)silicates

Most of sodium derivatives have been prepared by Corriu and coworkers.[11] The synthesis of sodium methyl bis(catecholato)silicate (**3 Na**) (Scheme **5**B) was reported using a solution of methyltrimethoxysilicate and sodium methoxide in methanol and afforded the silicate in 90 % yield.
Although sodium derivatives are quite rare, an interesting synthesis was achieved by Narula and coworkers.[12] Their methodology cleverly used the cation (K, Na, K[18C6]) of an isothiocyanate salt to easily access to different types of isothiocyanato bis(catecholato)silicate derivatives (**106**) in good yields, including the desired sodium one (**106 Na**) (Scheme **5**C). Recently, new sodium silicates (sodium benzyl-, acetoxypropyl- and cyclohexyl- bis(catecholato)silicates **1 Na**, **10 Na** and **2 Na**) from the corresponding alkyl trimethoxy- and triethoxysilane were synthetized and used in modern organic synthesis by our group.[13] Their synthesis required conventional inert techniques and a homemade sodium methoxide solution from elemental sodium. Once crystallised, this type of hypercoordinated derivatives gains stability and can be stored on the bench.

Several other silicates with a potassium cation are found in the literature. Preparation of these derivatives can be achieved by directly using the potassium metal to generate the alkoxide *in situ* from the alcoholic solvent, in most cases methanol.[14]

This synthesis methodology was applied for instance for the synthesis of potassium phenyl bis(catecholato)silicate (**54 K**) from phenyl triethoxysilicate and catechol (Scheme **5**D). Otherwise, a commercially available alkoxide solution such as potassium methoxide is commonly used for the synthesis of potassium silicates including potassium acetoxypropyl bis(catecholato)silicate (**10 K**) from acetoxypropyl trimethoxysilicate in Scheme **5**E[15] even if the scope is quite broad.

To facilitate the crystallisation of potassium derivatives and stabilise hypercoordinated silicon derivatives, our group, inspired by the work of Hey-Hawkins and Tamao respectively on silicate[16] and organofluorosilicates,[17] has shown the value of using 18-crown-6 as an additive.[15] To the best of our knowledge, crown ethers have only been involved for the synthesis of potassium silicates and there is no example of a 12-crown-4 lithium silicate and only one example of a 15-crown-5 sodium silicate that we recently reported.[13] A representative example consists in the synthesis of potassium [18-crown-6] (3-glycidoxypropylpropyl) bis(catecholato)silicate (**53 K[18C6]**) as shown in Scheme **5**F.

2.2.2. Ammonium-silicate

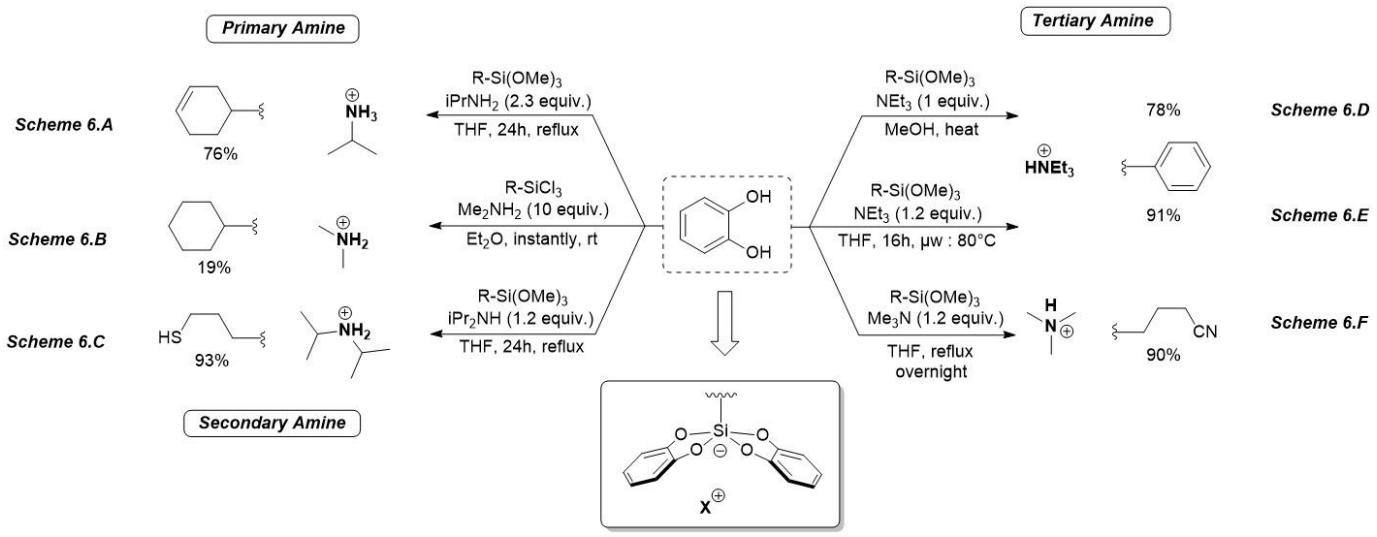

Scheme 6. Synthesis of ammonium alkyl and aryl bis(catecholato)silicates

Ammonium-based silicates are the most commonly encountered. Due to their huge diversity, several methodologies have been developed over the years. Herein, we divide these species in two categories based on their synthetic pathways, by the direct synthesis using the amine as base or by cation metathesis. Compared to the other silicates presented above, the formation of ammonium silicates requires refluxing conditions for 24 h. The crude product has to be completely dried under high vacuum for several hours to facilitate the crystallisation and the purification of these species.

2.2.2.1. Ammonium-silicate (primary, secondary and tertiary)

A special attention will be made on the non-quaternary ammoniums of Scheme **6** that imply a distinct synthetic procedure. To avoid the formation of ammonium hydrochloride salts in the reaction medium, alkoxysilanes are preferable. As shown on Scheme **6**, a great variety of amines could be used for the synthesis of ammonium-based silicates.

Nevado *et al.*[18] have described the only example of isopropylammonium (cyclohex-3-en-1-yl) bis(catecholato)silicate (**74 H_3NiPr**). The synthesis starts with the transformation of cyclohex-3-en-1yl (trichloro)silane to the corresponding trimethoxysilane as described above (Scheme **1**). Then, reaction with catechol and isopropylamine in THF at reflux led to the desired silicate in 76 % yield, after evaporation and cleanse with diethyl ether and pentane (Scheme **6**A).

A dimethylamine ammonium derivative has also been reported only once by Holmes and coworkers.[19] Using a trichlorosilane substrate as a precursor placed in ether with dimethylamine at room temperature, a poor yield of cyclohexyl bis(catecholato)silicate product (**2** H_2NMe_2, 19 %) was obtained due to the difficulty to get rid of the dimethylammonium salt generated during the reaction (Scheme **6**B). On the other hand, diisopropylammonium silicates can be considered as the main derivatives that this family can count.

While several methodologies can be highlighted, a reproducible one was published by Molander in *Organic Synthesis* in 2017.[20] As a representative example, the synthesis of the biisopropylammonium 3-mercaptopropyl bis(catecholato)silicate (**74** $H_2N(iPr)_2$) prepared from the corresponding trimethoxysilane was obtained in 93 % yield (Scheme **6**C).[21]

The last secondary ammonium silicates presented in this review were synthetized by Korlyukov and coworkers in 2008.[22] Following a new methodology that required a higher temperature (130 °C) and a non-polar solvent (xylene), they prepared for the first time dicyclohexylammonium [(N-methyl-acetamido)methyl-C,O] bis(catecholato)silicate (**82** $H_2N(cHex)_2$) in very good yield (94 %) from (N-methyl-acetamido)methyl-C,O trimethoxysilane (Scheme **7**). This study also corresponded to the first use of dicyclohexylamine as a base for its synthesis.

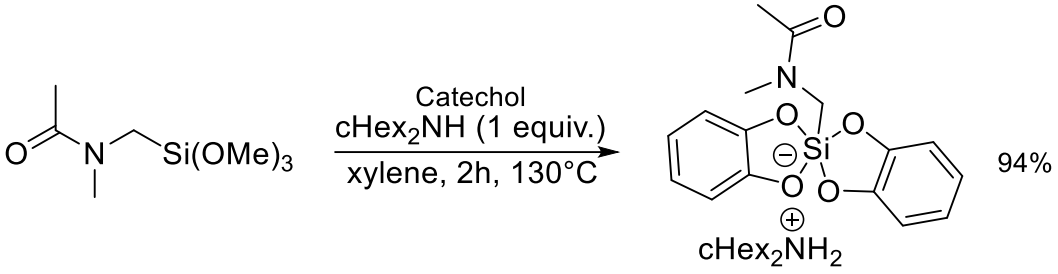

Scheme 7. Synthesis of dicyclohexylammonium [(N-methyl-acetamido)methyl-C,O] bis(catecholato)silicate from (N-methyl-acetamido)methyl-C,O trimethoxysilane

Triethylammonium is the main counterion found for tertiary ammonium silicates. In addition to reporting the first example of bis(catecholato)silicate, C. L. Frye[23] was also the first to use triethylamine as the base for the synthesis of triethylammonium phenyl bis(catecholato)silicate (**54** $HNEt_3$) from the corresponding trimethoxysilane (Scheme **6**D). Hashmi and coworkers showed that the reaction can be run in THF at 80 °C under microwave irradiation for 16 h (Scheme **6**E).[24]

The last example of tertiary ammonium silicate was reported by Molander[25] relying on the same type of methodology based on the use of triethylamine. Herein is presented the synthesis of trimethylammonium 3-cyanopropyl bis(catecholato)silicate (**26 HNMe$_3$**) from the starting trimethoxysilane using a THF solution of Me_3N to afford the silicate in 90 % yield (Scheme **6**F).

2.2.2.2. Ammonium-silicate (quaternary)

Due to the straightforward accessibility of the other ammonium silicates described above, only a few examples of silicates bearing a quaternary ammonium can be found. There are two major ways to produce quaternary ammonium bis(catecholato)silicates:

-*By ammonium exchange*. The usual method for forming quaternary ammonium bis(catecholato) organosilicates is based on a cation exchange reaction. Holmes and coworkers[26b] proposed a synthesis of tetraethylammonium *tert*-butyl bis(catecholato)silicate (**56 NEt$_4$**) from tert-butyl**(**trichloro)silane based on treatment with catechol and Et_3N in refluxing benzene followed by ammonium exchange with Et_4NCl in acetonitrile. They took advantage of the good water solubility of triethylammonium hydrochloride to remove and render complete the cation metathesis with tetraethylammonium chloride (Scheme **8**). From our own experience, efficient drying of the hydrophilic tetraethylammonium salt highly increases the yield of the reaction.

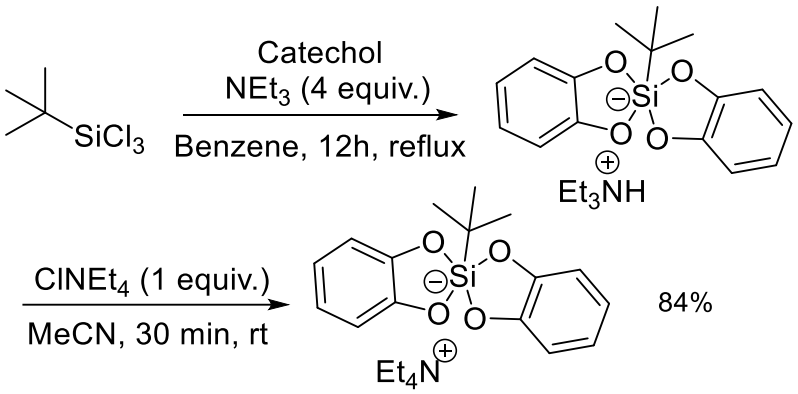

Scheme 8. Synthesis of tetraethylammonium tertbutyl bis(catecholato)silicate from tert-butyl(trichloro)silane

A similar protocol was employed by Nevado et al.18 in Scheme 9 for the synthesis of the tertiary (2,3-dimethylbutan-2-yl) tetraethylammonium bis(catecholato)silicate 75 from 2,3-dimethylbutan-2-yl(trichloro)silane, but the yield of this reaction was not documented.

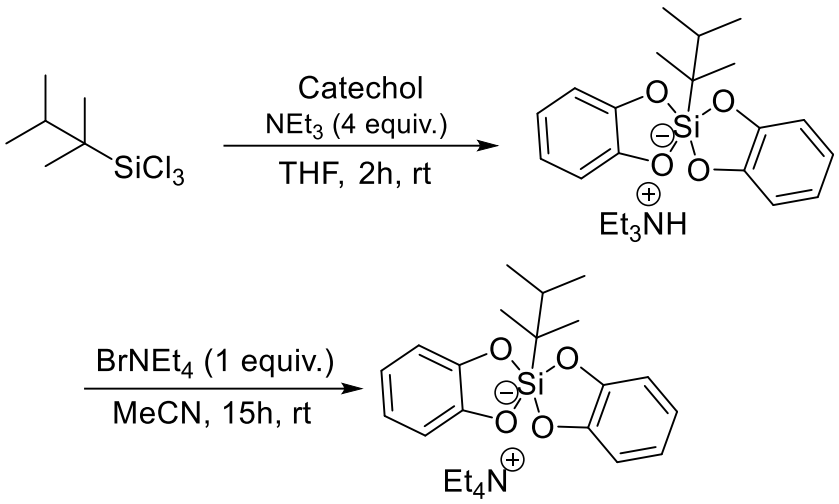

Scheme 9. Synthesis of tetraethylammonium (2,3dimethylbutan-2-yl) bis(catecholato)silicate from 2,3-dimethylbutan-2-yl**(**trichloro)silane

Corriu[27] elegantly circumvented the cation exchange step by performing the synthesis of tetramethyl allyl bis(catecholato)silicate **14 NMe4** from catechol and allyltrimethoxysilane in methanol with 20 wt % Me_4NOH in MeOH (Scheme **10**). This approach avoids the addition of a large amount of water (required before the ammonium exchange) that can lead to the degradation of the intermediate silicate. Here, the reaction was performed on a 50 mmol scale, at low temperature and without water. These reaction conditions and the good miscibility in methanol could explain the almost quantitative yield of this silicate, without degradation of the residue after washing with anhydrous ether.

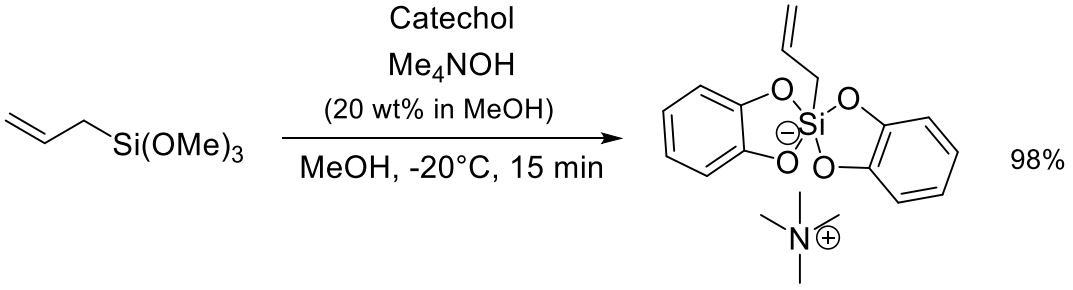

Scheme 10. Synthesis of tetramethyl allyl bis(catecholato)silicate from allyltrimethoxysilane

2.2.3. Phosphonium-silicate

Silicates with a phosphonium counterion can be found essentially in several patents except for the bis(triphenylphosphoranylidene)ammonium (PPN) which has been employed to form highly bulky silicates (Figure 4).

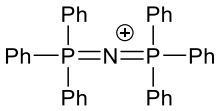

Figure 4. PPN : Bis(triphenylphosphoranylidene)ammonium

Go[28] has reported an efficient synthesis of phosphonium bis(catecholato)silicates (Scheme 11A). The chemistry based on these cations appears restricted; nevertheless they have found their utility in materials.

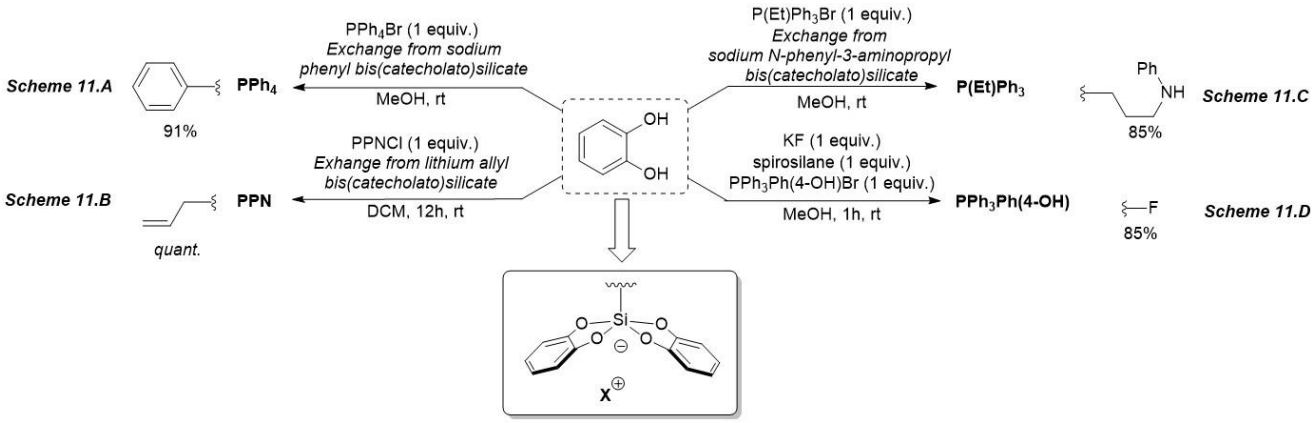

Scheme 11. Synthesis of phosphonium alkyl bis(catecholato)silicates

Due to the bulkiness of the tetraphenylphosphonium, crystallisation is slowly induced *in-situ* by cation exchange with sodium phenyl bis(catecholato)silicate (**54 Na**). The latter is generated from catechol and phenyl trimethoxysilane in the presence of sodium methoxide in methanol[11] and is added directly to a methanol solution of the corresponding phosphonium salt PPh_4Br. Tetraphenylphosphonium phenyl bis(catecholato)silicate (**54 PPh_4**) is effectively obtained in 91 % yield.

In 1988, Sakurai and coworkers[8] took advantage of the good crystallisation properties of phosphonium silicates to characterize an allyl silicate derivative while they were unable to isolate the corresponding lithium allyl bis(catecholato)silicate (**14 Li**). Once again, lithium exchange with bis(triphenylphosphine)iminium chloride (PPNCl) provided a quantitative amount of bis(triphenylphosphoranylidene)ammonium allyl bis(catecholato)silicate (**14 PPN**) (Scheme **11**B). Even with this bulky counter-cation, the silicate remained very sensitive to moisture and air.

Another example of silicate bearing a phosphonium cation was synthetized by Go[27] for materials chemistry. Again, a good yield of ethyltriphenylphosphonium N-phenyl-3-aminopropyl bis(catecholato)silicate was obtained (Scheme **11**C) by cation exchange with sodium silicate using the same methodology developed in Scheme **11**A.

The formation of fluorinated silicate was reported from the corresponding bis(catecholato)spirosilane by Jung and coworkers. Direct addition of fluoride from potassium fluoride and an *in-situ* cation exchange of potassium with the desired phosphonium afforded the desired silicate (**110 $PPh_3Ph(4\text{-}OH)$**) in 85 % yield (Scheme **11**D).[30]

2.2.4. Zwitterionic-silicate

Zwitterionic silicates have the advantage of being cation independent. Their synthesis follows the same methodologies as above. For instance, [2-(dimethylaminomethyl),6-(dimethylammoniomethyl)phenyl] bis(catecholato)silicate (**84 H**) was prepared by Corriu et al.[31] following the steps described in Scheme 5E in 39 % yield starting from 2,6-bis(dimethyl-aminomethyl)phenyl trimethoxysilicate (Scheme **12**).

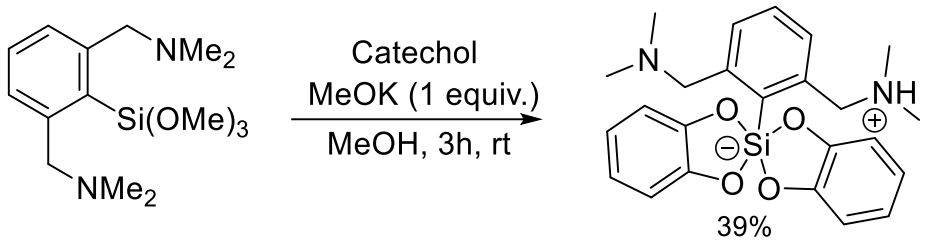

Scheme 12. Synthesis of [2-(dimethylaminomethyl),6-(dimethylammoniomethyl)phenyl] bis(catecholato)silicate from 2,6-bis(dimethyl-aminomethyl)phenyl trimethoxysilicate

Corriu and coworkers also showed the possibility of converting a zwitterionic silicate into potassium and PPN analogs.[31] For instance, treatment of [2-(dimethylaminomethyl),6-(dimethylammoniomethyl)phenyl] bis(catecholato)silicate (**84 H**) with potassium hydride led to the corresponding potassium phenyl silicate (**84 K**) (Scheme 13). This reaction was achieved in 98 % yield and demonstrated the flexibility of zwitterionic silicates. In the same publication, the transformation of this potassium silicate (84 K) to phosphonium silicate **(84 PPN**) was also described by ionic metathesis with PPNCl in 84 % yield.

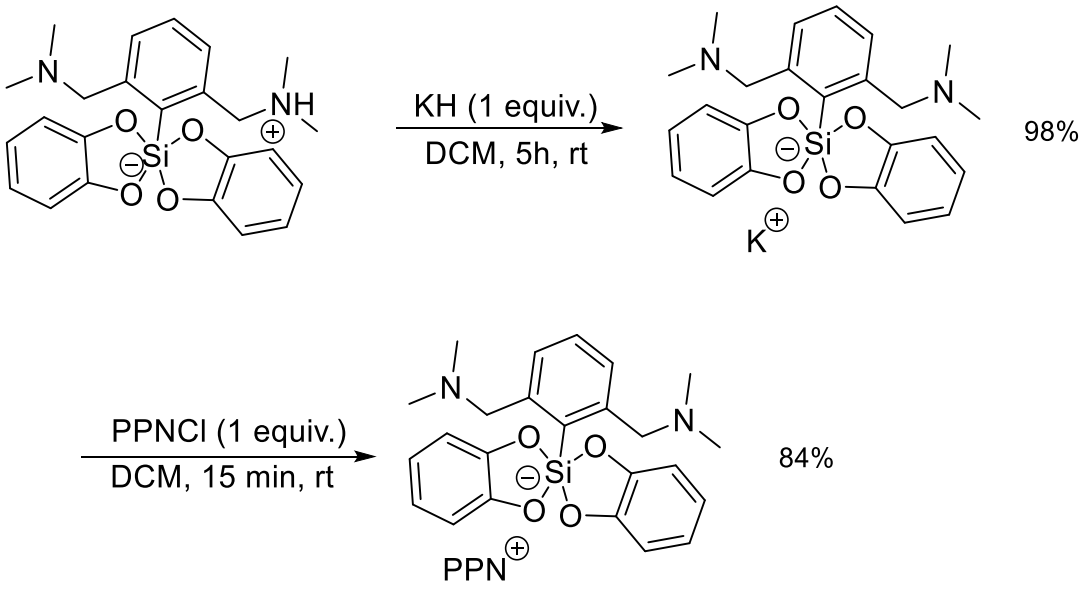

Scheme 13. Synthesis of potassium and bis(triphenylphosphoranylidene)ammonium 2,6-bis(dimethylaminomethyl)phenyl bis(catecholato)silicate from [2(dimethylaminomethyl),6-(dimethylammoniomethyl)phenyl]bis(catecholato)silicate

1.1.3 Silicates diversity

The following Table **1** gives an exhaustive overview of all the synthesized bis(catecholato)silicates, the corresponding synthesis yields as well as their ^{29}Si NMR shifts. The NMR experiments were performed mainly in solution but also in the solid state.

From the ^{29}Si NMR data in Table **1** and the observed diversity, the chemical shifts of the pentavalent bis(catecholato)silicates can be modulated by the relative steric or electronic effect of the substituents, the nature of the counter-cation, and/or the inter- or intramolecular dative interaction (or coordinate covalent bond) leading to hexavalent species. The wide range of chemical shifts in ^{29}Si NMR is consistent with a pentacoordinate configuration of the silicon species and the average is at −80 ppm for a range covering −70 to −110 ppm. The shielded values, from −110 to −200 ppm, can be attributed to hexacoordinate silicon derivatives.

For alkyl bis(catecholato)silicates, ^{29}Si NMR shifts are generally comprised between −70 and −80 ppm and for aromatics slightly upfield from −80 to −90 ppm. Based on the reported value, the

nature of the substituent can lead to a shielding of the ^{29}Si NMR shift as follows: alkyl > benzyl (R=−Me, −74.32 ppm (**3 K**); R=−CH_2Ph, −80.9 ppm (**1 K**))/allyl>phenyl (R=−Allyl, −80.24 ppm (**14 K[18C6]**); R=−Ph, −87.83 ppm (**54 K[18C6]**))/alkyl>cycloalkyl (R=−Hex, −75.6 ppm (**4 K[18C6]**)); R=−Cyclohexyl, −77.93 ppm (**2 K[18C6]**)).

When the length of the carbon chain is increased, a slight shift is observed (R=−Me, −74.32 ppm (**3 K**); R=−Et, −74.77 ppm (**29 K**); R=−Hex, −75.6 ppm (**4 K[18C6]**)). A slight upshield was observed from the arrangement induced from a richer and hindered *tert*-butyl moiety (−76.21 ppm **(56 Et_4N)**). An electronic effect can also be observed if the silicate bears a more or less electron withdrawing substituents in α-position to the silicon (R=−CH_2NHPh, −81.36 ppm, (**52 K[18C6]**); R=−CH_2OMe, −82.2 ppm, (**60 K[18C6]**); R=−CH_2Cl, −85.57 ppm, (**6 K[18C6]**); R=−CH_2OAc, −85.8 ppm, (**35 K[18C6]**)). The effect of substituents is still present in beta position but it is much weaker beyond (R=−CH_2CH_2CN, −80.17 ppm, (**57 K[18C6]**); R=−$CH_2CH_2CH_2$CN, −77.6 ppm, (**26 K[18C6]**)) and also R=−$CH_2CH_2CH_2$OAc, −76.6 ppm, (**10 K[18C6]**); R=−$CH_2CH_2CH_2$Cl, −76.9 ppm, (**58 K[18C6]**) compared to the previous (**35 K[18C6]**) and (**6 K[18C6]**)).

This decrease was also observed with the morpholinium derivatives (R=−CH_2Morph, −85.8 ppm, (**64 K[18C6]**); R=−$CH_2CH_2CH_2$ Morph, −76.9 ppm, (**63 K[18C6]**)). Finally, donor molecules such as 1,8-diazabicyclo[5.4.0]undec-7-ene (DBU), hexamethylphosphoramide (HMPA), and 1,3-dimethyl-2-imidazolidinone (DMI) can interact with the silicon center of the spiro bis(catecholato)silane *via* an intermolecular coordinating covalent bond, and the NMR values of the new pentacoordinate forms shift toward about −100 ppm (R=DBU, −98.7 ppm, (**124**); R=HMPA, −107.3 ppm, (**125**); R=DMI, −104.5 ppm, (**126**)).

A shielding of the ^{29}Si NMR shift was also observed with some heteroatomic residues (R=−NCS, −110.4 ppm, (**106 K[18C6]**); R=−OMe, −99.1 ppm, (**108 K[18C6]**)). ^{29}Si NMR chemical shifts showed a weak influence of the counter-cation with respect to the nature of the substituent. Few silicates can be compared completely by varying the counter cation. For example, the alkaline bis(catecholato)benzyl silicate (**1**) was studied extensively by our group and showed the same value (−80.9 ppm). A difference of 0.1 ppm was observed between free and crown ether chelated (15C5 and 18C6, −80.8 and −80.9 ppm respectively) sodium and potassium silicates.

Higher ^{29}Si NMR shifts were observed and confirmed the formation of a hexavalent species by inter- or intramolecular interaction. A donor solvent such as THF can interact with the spiro bis(catecholato)silane *via* an intermolecular bond and yields the hexacoordinate derivative with a ^{29}Si NMR shift of −134.4 ppm.[68] Interestingly, the NMR shifts for Si-NCS silicate (**106**) reported by Narula are at the extreme of the pentacoordinate region in ^{29}Si NMR (from −110.4 ppm to −112.6 ppm) whatever the counter-cation and in the hexavalent part of the spectrum (from −140.7 ppm to −156.2 ppm) when a secondary amine is coordinated to silicate (**107**).[12] Probably, these corresponding values suggest intermolecular coordination of the amine.

The same observation was made with intramolecular coordination of an amide (N−C(O)) by Korlyukov. A NMR shift of silicate (**82**) was observed at −133.5 ppm, again in the ^{29}Si NMR region expected for hexavalent derivatives. This value related to the O…Si interaction of the hexacoordinate species is comparable to those observed for (**84**) with the intramolecular Si…N interaction. The NMR shift of the zwitterionic ammonium, potassium, and quaternary ammonium (PPN) silicate (**84**) (i. e., −134.9, −129.8, and −127.2 ppm respectively) were reported by Reyé in 1992.[31]

Some structures containing nitrogen moieties, such as silicates (**79**) and (**123**) of Table **1**, have been characterized by solid state NMR (^{29}Si and ^{15}N NMR) by Tacke and coworkers.[9] The solid state ^{29}Si NMR shift is consistent with the expected in solution (for (**123**): −88.6 ppm, close to −80 ppm for the pentavalent silicon species) and rare ^{15}N NMR data have been compiled for two zwitterionic silicate species (for silicate (**79**): −324.7 ppm and for (**123**): −336.9 ppm).

Table 1. Silicate diversity, yield of synthesis and δ ^{29}Si NMR

N°	Silicate	Cation	Yield	^{29}Si
1*	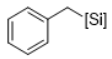	$HNEt_3$ K[18C6] K Na Na[15C5] Li	92 [31] 84 [32] 54 [12] 55 [12] 45 [12] 64 [9]	- *-80.90* *-80.90* *-80.90* *-80.80* -
2*		$HNEt_3$ K[18C6] H_2NMe_2 $H_2N(i\text{-}Pr)_2$ Na	96 [31] 79 [32] 19 [18] 96 [19] 55 [12]	- *-77.93* - - *-77.75*
3		$HNEt_3$ Na K	73 [31] 90 [10] 96 [13]	- *-73.77* *-74.32*
4		$HNEt_3$ K[18C6]	88 [31] 85 [32]	- *-75.6*
5	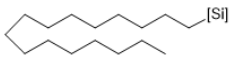	$H_2N(i\text{-}Pr)_2$	71 [20]	-
6		$HNEt_3$ K[18C6]	93 [31] 93 [32]	- *-85.57*
7	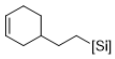	$HNEt_3$	86 [31]	-
8	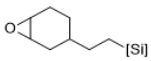	$H_2N(i\text{-}Pr)_2$ K[18C6]	86 [31] 85 [32]	- *-75.75*
9	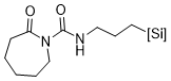	$H_2N(i\text{-}Pr)_2$ $HNMe_3$	83 [31] 73 [24]	- -
10	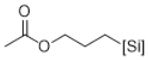	$HNEt_3$ K K[18C6] Na	95 [31] 62 [14] 91 [14] 64 [12]	- - *-76.6* *-76.36*
11	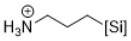	Ø	94 [31] 92 [27]	- -
12	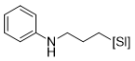	$H_2N(i\text{-}Pr)_2$ $P(Et)PPh_3$	89 [31] 85 [28]	- -
13*		K[18C6] $HNEt_3$ Et_4N	Nd [33] 55 [34] 68 [35] 56 [32]	- *-79.15* *-75.61*
14		$HNEt_3$ K[18C6] PPN Li Me_4N	55 [35] *quant.*[36, 37] 84 [32] *quant.* [7] *nd* [7] 98 [26]	- *-80.24* *-78.8* - -

Table 1. Continuation.

N°	Silicate	Cation	Yield	^{29}Si
15	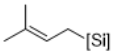	PPN Li $HNEt_3$	*Nd* [7] *Nd* [7] *Quant* [36,37]	*-77.3* - *-76.7*
16	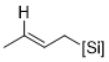	Li $HNEt_3$	*Nd* [7] *quant.*[37]	- *-78.4*
17		Li	*Nd* [7]	-
18		Li	*Nd* [38]	-
19*	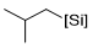	$HNEt_3$ $H_2N(iPr)_2$ K[18C6]	*Nd* [39] 86 [20,35] 91 [32]	- - *-76.14*
20		$HNMe_3$ $H_2N(i\text{-}Pr)_2$	88 [24] 86 [35]	- -
21	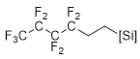	$H_2N(i\text{-}Pr)_2$	92 [31]	-
22	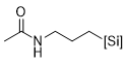	$H_2N(i\text{-}Pr)_2$	66 [35]	-
23	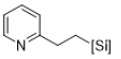	$HNEt_3$ $H_2N(i\text{-}Pr)_2$	91 [31] nd [35]	- -
24	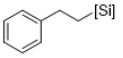	$H_2N(i\text{-}Pr)_2$	93 [40]	-
25	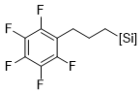	$H_2N(i\text{-}Pr)_2$	89 [40]	-
26		$HNMe_3$ K[18C6] $H_2N(i\text{-}Pr)_2$	90 [24] 90 [14] 95 [40]	- *-77.6* -
27		$H_2N(i\text{-}Pr)_2$ K[18C6] $HNEt_3$	77 [40] 91 [41] nd [39]	- - -
28	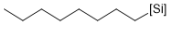	K[18C6]	85 [41]	-
29		K[18C6] K	88 [41] 29 [13]	- *-74.77*
30*		Et_4N	20 [25]	-
31	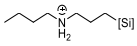	Ø	90 [42] nd [10]	- -

Table 1. Continuation.

N°	Silicate	Cation	Yield	^{29}Si
32		$H_2N(i\text{-}Pr)_2$	55 [43]	-
33		$H_2N(i\text{-}Pr)_2$ Et_4N	81 [31] nd [44]	- -
34	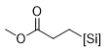	$H_2N(i\text{-}Pr)_2$	77 [43]	-
35		$HNMe_3$ K[18C6] $H_2N(i\text{-}Pr)_2$	60 [24] 94 [14] 76 [42]	- *-85.8* -
36	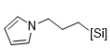	$HNMe_3$	82 [24]	-
37	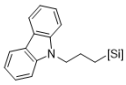	$H_2N(i\text{-}Pr)_2$	68 [45]	-
38	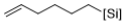	K[18C6] $HNMe_3$	50 [32] 90 [24]	*-75.7* -
39	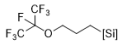	$HNMe_3$	68 [24]	-
40		K[18C6] $HNEt_3$	88 [41] 77 [46]	- -
41		$HNEt_3$	94 [46]	-
42	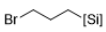	$H_2N(i\text{-}Pr)_2$	97 [47]	-
43	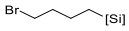	$H_2N(i\text{-}Pr)_2$	82 [47]	-
44	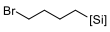	$H_2N(i\text{-}Pr)_2$	86 [47]	-
45	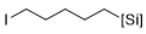	$H_2N(i\text{-}Pr)_2$	nd [48]	-
46	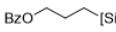	$H_2N(i\text{-}Pr)_2$	nd [48]	-
47	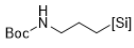	$H_2N(i\text{-}Pr)_2$	44 [43]	-
48	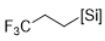	K[18C6] $H_2N(i\text{-}Pr)_2$	80 [14] 92 [42]	*-78.6* -
49	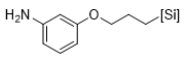	$H_2N(i\text{-}Pr)_2$	67 [45]	-
50		$H_2N(i\text{-}Pr)_2$	93 [20]	-
51	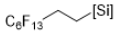	K[18C6]	71 [32]	*-78.51*
52	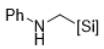	K[18C6]	85 [32]	*-81.36*

Table 1. Continuation.

N°	Silicate	Cation	Yield	^{29}Si
53	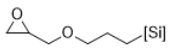	K[18C6]	92 [32]	*-76.13*
54*		$HNEt_3$ K[18C6] PPh_4 Na K H_3NPh H_3NBn ImH 2-Me-ImH DMAP-H Piperidinium $HNEt_3$	93[31] 78 [22] 91[23] 88[49] 54 [50] 50 [13] 87 [32] 91 [27] 90 [10] 65 [13] Nd [51] nd [52] nd [52] nd [52] nd [52] nd [52] 80 [25a]	*-87.53* *-87.83* - *-87.4* *-87.51* - - - - - - *-87.0*
55	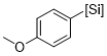	K[18C6] $HNEt_3$	85 [32] 86 [49]	*-87.60* -
56*		Et_4N	39 [32] 84 [25b]	*-76.21* *-75.8*
57*		K[18C6]	83 [32]	*-80.17*
58		K[18C6] $H_2N(i\text{-}Pr)_2$	95 [14] Nd [47]	*-76.9* -
59	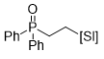	K[18C6]	72 [53]	*-78.10*
60		K[18C6]	64 [44]	*-82.2*
61		K[18C6]	12 [44]	*-80.6*
62*		H PPN	27, 37 [54] 67 [55]	- *-121.2*
63	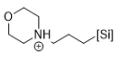	Ø	31,40,94 [56] 65 [57]	*-76.9*
64*	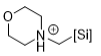	Ø	82, 83 [56] 92 [57]	*-85.8*
65	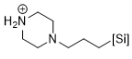	Ø	71 [42]	-
66*	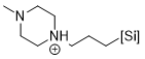	Ø	78 [57]	*-85.8*
67	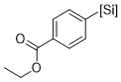	$HNEt_3$	89 [49]	-
68		$HNEt_3$	94 [49]	-
69		$HNEt_3$	82 [49]	-

Table 1. Continuation.

N°	Silicate	Cation	Yield	^{29}Si
70		$HNEt_3$	83 [49]	-
71		$HNEt_3$	90 [49]	-
72	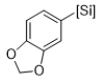	$HNEt_3$	82 [49]	-
73	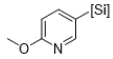	$HNEt_3$	94 [49]	-
74		H_3NiPr	76 [17]	-
75		Et_4N	nd [17]	-
76		2K	81 [58]	*-78.63*
77	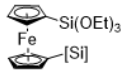	K	81 [58]	*-80.27*
78*		Et_4N $HNEt_3$ PPh_4 Na	87 [25b] 81 [25b] 89 [59] 90 [10]	*-84.9* - - *-84.64*
79*		Ø	98 [8] nd [54]	*-84.8* *-85.9*
80*		Ø	*Quant* [60]	-
81		K	98 [61]	-
82*		$H_2N(C_6H_{11})_2$	94 [21]	*-133.5*
83*	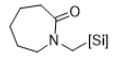	$H_2N(C_6H_{11})_2$	*Quant* [21]	*-132.5*
84*		H K PPN	39 [30] 98 [30] 55 (84) [30]	*-134.9* *-129.8* *-127.2*
85		$HNEt_3$	55 [50]	*-87.0*
86		$HNEt_3$	49 [50]	*-86.7*
87*	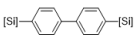	$HNEt_3$	30 [50]	*-87.4*

Table 1. Continuation.

N°	Silicate	Cation	Yield	^{29}Si
88		HNE	69 [50]	*-81.7*
89		$HNEt_3$	75 [50]	*-73.7*
90	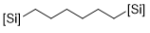	$HNEt_3$	55 [50]	*-71.9*
91	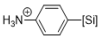	Ø	89 [28]	-
92*		K	99 [62] 65 [63,64]	-
93*	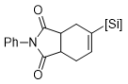	K	99 [62–64]	-
94	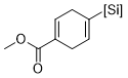	K	nd [62]	-
95	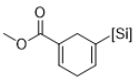	K	nd [62]	-
96	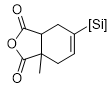	K	78 [63,64]	-
97	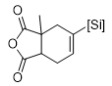	K	78 [63,64]	-
98	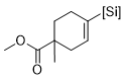	K	Nd [62]	-
99	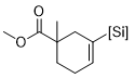	K	nd [62]	-
100	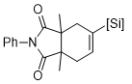	K	nd [62]	-
101	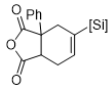	K	Nd [62]	-
102	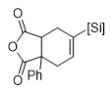	K	Nd [62]	-
103	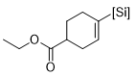	K	94 [63]	-
104	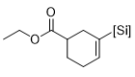	K	94 [63]	-
105	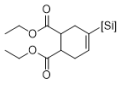	K	70 [63]	-

Table 1. Continuation.

N°	Silicate	Cation	Yield	^{29}Si
106		K Na K[18C6] NH_4	81 [11] 82 [11] 88 [11] 86 [11]	*-110.7* *-112.6* *-110.4* *-111.5*
107	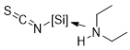	K Na K[18C6] H_2NEt_2	84 [11] 81 [11] 74 [11] 78 [11]	*-142.7* *-140.7* *-156.2* *-141.3*
108		$K.Me_2SO_3$ $Na.Me_2SO_3$ K[18C6] NH_4	53 [11] 51 [11] 75 [11] 86 [11]	*-99.8* *-99.9* *-99.1* -
109		PPh_4	85 [29]	-
110*		$PPh_3Ph(4\text{-}OH)$	85 [29]	-
111		$H_2N(i\text{-}Pr)_2$	nd	-
112		$H_2N(i\text{-}Pr)_2$	nd	-
113	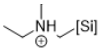	$H_2N(i\text{-}Pr)_2$	nd	-
114	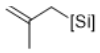	$HNEt_3$	*quant.*[37]	-
115	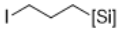	$H_2N(i\text{-}Pr)_2$	nd [47]	-
116	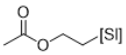	$H_2N(i\text{-}Pr)_2$	nd [48]	-
117		$HNEt_3$	nd [65]	-
118	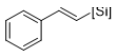	$HNEt_3$	nd [65]	-
119		$HNEt_3$	nd [65]	-
120		$HNEt_3$	nd [65]	-
121	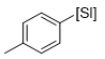	$HNEt_3$	88 [49]	-
122		$H_2N(i\text{-}Pr)_2$	nd [66]	-
123*		Ø	nd [8]	*-88.6* *(Solid NMR)*
124*	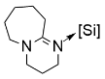	Ø	nd[67]	*-98.7*
125	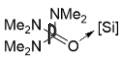	Ø	nd[67]	*-107.3*
126	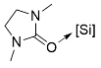	Ø	nd[67]	*-104.5*

1.1.4 X-Ray diffraction analysis

As mentioned by Holmes in 1985, a continuum between a square or rectangular pyramidal geometry (SP) and a trigonal bipyramidal geometry (TBP) involving a structural distortion along the Berry pseudorotational coordinate has been observed for the structure of bis(catecholato)silicates. In such structures, the apical site is always occupied by the R substituent, and the percent displacement from TBP to SP can be quantified using the dihedral angle method initially reported by Holmes in 1977 on cyclic phosphoranes[26c] and extrapolated to the hypercoordinated silicon species.[26a]

The geometry of silicates has been shown to be influenced by the nature of the cation and the substituent.[26a] For example, changing the *t*Bu substituent to *n*Bu with the same cation (i. e. NEt_4) gave a distortion (in % from TBP toward SP) of 91.4 % to 63.8 % respectively. In this case, reducing the steric hindrance disfavours the SP geometry toward TBP. The direct influence of the cation was also highlighted by changing the silicate cation (NEt_4 *versus* HNC_5H_5) with the same substituent (napthyl), the distortion observed (%TBP→SP) was 30.8 % for quaternary ammonium and 58.7 % for pyridinium, respectively. To better illustrate these geometries, we have selected several structures shown in Figure **4**.

Other silicates tend to adopt either a square pyramidal (SP) structure, such as the chelated potassium ether-crown pentacoordinated silicate (**19 K[18C6]**) (CCDC 1403595) in Figure **5**A[33] or a trigonal-bipyramidal (TBP) structure as shown in Figure **5**E, for the silicate flanked by a PPN cation (**62 PPN**) (1280206) stabilised in a hexavalent geometry by the amine coordination to the silicon center.[56] A slight distortion from these two limiting structures can be observed in the silicates (**92 K**) (648236) illustrated in Figure **5**B,[65] (**2 Na**) in Figure **5**C[13] and (**54 $HNEt_3$**) in Figure **5**D[26a] for instance.

In the case of the sodium silicate (**2 Na**) (Figure **5**C), the dihedral angle method resulted in an 89.3 % shift from the TBP structure to the SP structure.[13] Here, a polymeric assembly along the *c*-axis resulting from non-covalent bonds between sodium and oxygen atoms of catechols of two silicates is observed. This interaction of the catechol moieties through the oxygen atoms with the potassium cation was also observed in Figure **5**B with potassium. Moreover, as depicted in the Figure **5**D, hydrogen bonding can be established between the catechol ligand and triethylammonium.[26a]

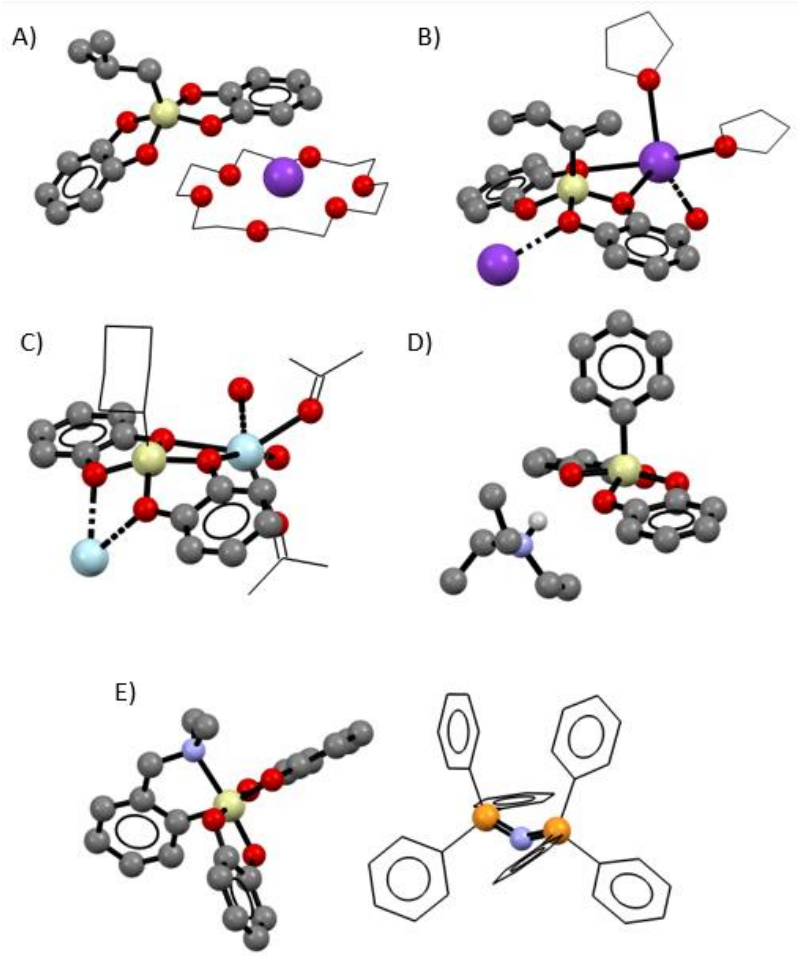

Figure 5. Selected examples of X-ray crystal structures of silicates. Thermal ellipsoids are drawn at 50% probability level. Hydrogen atoms are omitted for clarity. Carbons of cyclohexyl, acetone, THF, crown-ether and phenyl of PPN are drawn as wireframe for clarity Dashed lines denote bonds between neighbouring silicates. Deposit number, A: **19 K[18C6]** (1403595); B : **92 K** (648236); C : **2 Na** (2050302) ; D : **54 HNEt$_3$** (1135883) ; E : **62 PPN** (1280206)

The countercation effect was observed with cyclohexyl bis(catecholato)silicates. Sodium cyclohexyl bis(catecholato)silicates without crown ether (**2 Na**) and the potassium analog[10, 13] (**2 K**) are isostructural Pbca crystals compared to the chelated one (**2 K[18C6]**) (1403596) and the ammonium derivative (**2 H$_2$NMe$_2$**) (1194879). The structural data of these cyclohexyl derivatives are presented in Table 2 For both non-chelated inorganic cations Na and K (Entries 1 and 2), close cell parameters are observed with a slight variation in the length of the a, b, c axis due to the variation of the cation.

As expected, angles and Z-values of these isostructural crystals are identical and chelation of the cation for both species with catechol provides a similar polymeric assembly. Increasing the size of the potassium by chelation with the [18C6] crown ether (Entry 4) led to a reduction in the number of molecules in the asymmetric unit (from Z=8 to Z=2) and prevents chelation of the cation between two silicate catechols.

In the case of the ammonium derivative (Entry 3), hydrogen bonding is observed allowing intermolecular interaction between two distinct silicates resulting in an increase in the number of molecules per unit (Z=8) as for both inorganic cations.

Table 2. Reported crystal details of cyclohexyl bis(catecholato)silicates (**2**)

	Cation	CCDC	SG	Cell parameters (Å | °)		Z
1	Na	2050302	*Pbca*	*a* 20.1599(19) *b* 11.4841(11) *c* 21.738(3)	*α* 90 *β* 90 *γ* 90	**8**
2	K	[9]	*Pbca*	*a* 19.6679(4) *b* 11.6484(3) *c* 22.0285(5)	*α* 90 *β* 90 *γ* 90	8
3	H_2NMe_2	1194879	*P2₁/c*	*a* 13.566(2) *b* 14.962(3) *c* 20.561(4)	*α* 90 *β* 103.56(1) *γ* 90	*8*
4	K[18C6]	1403596	*Pmn2₁*	*a* 17.7244(4) *b* 8.4874(2) *c* 10.6609(2)	*α* 90 *β* 90 *γ* 90	2

1.1.5 Redox potentials

The use of silicates as radical precursors by single-electron transfer, including visible-light photoredox catalysis, requires a good understanding of the redox properties of these species. For this purpose, the oxidation potential (E_{OX}) of each silicate has been measured by cyclic voltammetry (CV) or using a differential pulse voltammetry (DPV) technique, which allows to anticipate their reactivity from a thermodynamic point of view. In this section, all oxidation potentials given are in V vs SCE and correspond to irreversible oxidation waves.

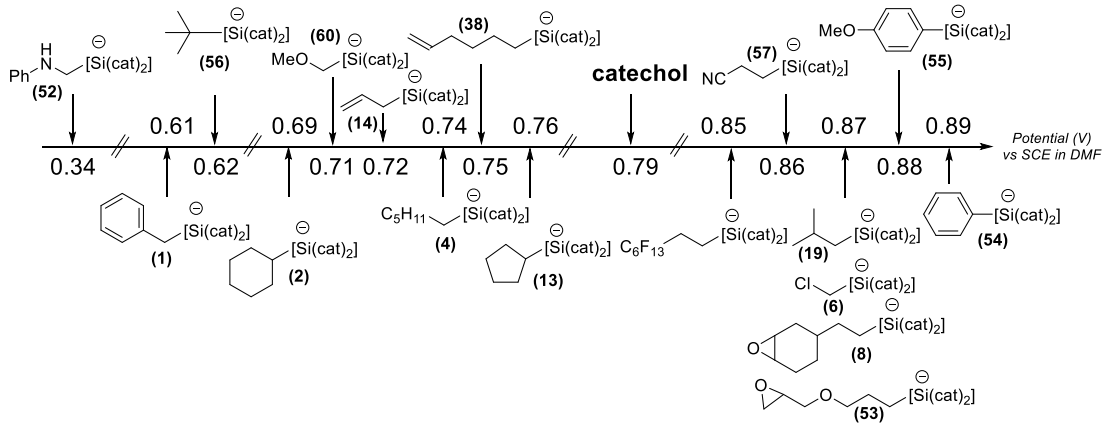

Figure 6. Selected examples of oxidation potentials (in V *vs* SCE) of bis(catecholato)silicates depending of their substituents and solvents

In 2007, Nishigaichi measured the oxidation potential of tetramethylammonium allyl bis(catecholato)silicates (**14 NMe_4**) using a DPV technique in acetonitrile and showed to be +1.12 V (vs SCE). Addition of a donor solvent such as DMF, DMSO or an amine (pyridine, imidazole, *n*-butylamine and piperidine) leads to the formation of a hexacoordinated silicon species and decreases the E_{OX} value to 1.08, 1.06 V or 0.78–0.80 V respectively.[68]

More recently, Molander reported the oxidation potentials of several triethylammonium primary and secondary alkyl species in acetonitrile using CV analysis. The E_{OX} values of triethylammonium benzyl, cyclohexyl and hexyl bis(catecholato)silicates were found to be almost identical (+0.70 V for (**1 $HNEt_3$**), +0.74 V for (**2 $HNEt_3$**) and +0.75 V for (**4 $HNEt_3$**), respectively. The study was extended to triethylammonium phenylbis(catecholato)silicate (**54 $HNEt_3$**) which can be oxidized at a similar potential value (+0.76 V vs SCE).[32]

Meanwhile, Goddard, Ollivier and Fensterbank studied 16 different [18-C-6] crown-ether chelated potassium alkyl and aryl bis(catecholato)silicates.[33] The values of the oxidation potential were determined by CV in DMF and range from 0.34 V for the anilinomethyl silicate (**52 K[18C6]**) to 0.89 V for the phenyl silicate (**54 K[18C6]**). The oxidation potential evolves according to the nature of the substituent, increasing in the order alkyl<aryl; benzylic<tertiary**<**secondary**<**primary; benzylic<allylic; alkyl<aryl and anilinomethyl<methoxymethyl<chloromethyl as shown in Figure **6**.

Modulation of the counter-cation of [18C6]-complexed potassium silicates to its sodium counterpart has been shown to influence their oxidation potential. A noticeable increase is observed with benzyl bis(catecholato)silicates from +0.61 V (**K[18C6]**) to +0.77 V (**Na**) and with cyclohexyl bis(catecholato)silicates from +0.69 V (**K[18C6]**) to +0.81 V (**Na**) *vs* SCE in DMF.

References part 1.1

[1] N. Kano, N. Nakagawa, T. Kawashima, *Angew. Chem. Int. Ed.* **2001**, *40*, 3450–3452.

[2] a) Claude. Chuit, R. J. P. Corriu, Catherine. Reye, J. Colin. Young, *Chem. Rev.* **1993**, *93*, 1371–1448. b) E. P. A. Couzijn, J. C. Slootweg, A. W. Ehlers, K. Lammertsma, *Zeitschrift für anorganische und allgemeine Chemie* **2009**, *635*, 1273–1278. c) D. Kost, I. Kalikhman, *Acc. Chem. Res.* **2009**, *42*, 303–314. d) N. Kano, in *Organosilicon Compounds*, Elsevier, **2017**, pp. 645–716. e) R. R. Holmes, *Chem. Rev.* **1996**, *96*, 927–950. f) D. Schomburg, R. Krebs, *Inorg. Chem.* **1984**, *23*, 1378–1381.

[3] V. Corcé, C. Lévêque, C. Ollivier, L. Fensterbank, *Silicates in Photocatalysis*. In *Science of Synthesis: Photocatalysis in Organic Synthesis* B. König Ed.; Thieme: Stuttgart, 2019, Chap 15, pp 427–466.

[4] E. F. Perozzi, J. C. Martin, *J. Am. Chem. Soc.* **1979**, *101*, 1591–1593.

[5] S. Deerenberg, M. Schakel, A. H. J. F. de Keijzer, M. Kranenburg, M. Lutz, A. L. Spek, K. Lammertsma, *Chem. Commun.* **2002**, 348–349.

[6] R. Maskey, H. Wadepohl, L. Greb, *Angew. Chem. Int. Ed.* **2019**, *58*, 3616–3619.

[7] Mitsuo. Kira, Kazuhiko. Sato, Hideki. Sakurai, *J. Am. Chem. Soc.* **1988**, *110*, 4599–4602.

[8] R. Tacke, A. Lopex-Mras, J. Sperlich, C. Strohmann, W. F. Kuhs, G. Mattern, A. Sebald, *Chem. Ber.* **1993**, *126*, 851–861.

[9] Unpublished results.

[10] A. Boudin, G. Cerveau, C. Chuit, R. J. P. Corriu, C. Reye, *Bull. Chem. Soc. Jpn* **1988**, *61*, 101–106.

[11] S. P. Narula, R. Shankar, Meenu, *Phosphorus Sulfur Silicon Relat. Elem.* **1996**, *113*, 237–243.

[12] M. Abdellaoui, A. Millanvois, E. Levernier, C. Ollivier, L. Fensterbank, *Synlett* **2021**, *32*, 1513–1518.

[13] D. F. Evans, A. M. Z. Slawin, D. J. Williams, C. Y. Wong, J. D. Woollins, *J. Chem. Soc., Dalton Trans.* **1992**, 2383–2387.

[14] C. Lévêque, L. Chenneberg, V. Corcé, J.-P. Goddard, C. Ollivier, L. Fensterbank, *Org. Chem. Front.* **2016**, *3*, 462–465.

[15] U. Dettlaff-Weglikowska, E. Hey-Hawkins, H. G. von Schnering, *Z. Naturforsch., B: J. Chem. Sci.* **1991**, *46*, 609-614.

[16] S. Yamaguchi, S. Akiyama, K. Tamao, *Organometallics* **1999**, *18*, 2851–2854.

[17] A. García-Domínguez, R. Mondal, C. Nevado, *Angew. Chem. Int. Ed.* **2019**, *58*, 12286–12290.

[18] K. C. K. Swamy, V. Chandrasekhar, J. J. Harland, J. M. Holmes, R. O. Day, R. R. Holmes, *J. Am. Chem. Soc.* **1990**, *112*, 2341–2348.

[19] K. Lin, *Org. Synth.* **2017**, *94*, 16–33.

[20] M. Jouffroy, C. B. Kelly, G. A. Molander, *Org. Lett.* **2016**, *18*, 876–879.

[21] A. A. Korlyukov, A. G. Shipov, E. P. Kramarova, Vad. V. Negrebetskii, Yu. I. Baukov, *Russ. Chem. Bull.* **2009**, *57*, 2093–2100.

[22] C. L. Frye, *J. Am. Chem. Soc.* **1964**, *86*, 3170–3171.

[23] S. Witzel, K. Sekine, M. Rudolph, A. S. K. Hashmi, *Chem. Commun.* **2018**, *54*, 13802–13804.

[24] S. Zheng, D. N. Primer, G. A. Molander, *ACS Catal.* **2017**, *7*, 7957–7961.

[25] a) R. R. Holmes, R. O. Day, V. Chandrasekhar, J. M. Holmes, *Inorg. Chem.* **1985**, *24*, 2009–2015. b) R. R. Holmes, R. O. Day, V. Chandrasekhar, J. J. Harland, J. M. Holmes, *Inorg. Chem.* **1985**, *24*, 2016–2020.

[26] G. Cerveau, C. Chuit, R. J. P. Corriu, C. Reye, *J. Organomet. Chem.* **1987**, *328*, C17–C20.

[27] Patent JP2009298975A.

[28] Patent JP2008255322A.

[29] Patent KR20160117871A.

[30] F. Carré, C. Chuit, R. J. P. Corriu, A. Mehdi, C. Reyé, *J. Organomet. Chem.* **1993**, *446*, C6–C8.

[31] M. Jouffroy, D. N. Primer, G. A. Molander, *J. Am. Chem. Soc.* **2016**, *138*, 475–478.

[32] V. Corcé, L.-M. Chamoreau, E. Derat, J.-P. Goddard, C. Ollivier, L. Fensterbank, *Angew. Chem. Int. Ed.* **2015**, *54*, 11414–11418.

[33] A. Cartier, E. Levernier, V. Corcé, T. Fukuyama, A.-L. Dhimane, C. Ollivier, I. Ryu, L. Fensterbank, *Angew. Chem. Int. Ed.* **2019**, *58*, 1789–1793.

[34] C. Lévêque, V. Corcé, L. Chenneberg, C. Ollivier, L. Fensterbank, *Eur. J. Org. Chem.* **2017**, *2017*, 2118–2121.

[35] N. R. Patel, C. B. Kelly, M. Jouffroy, G. A. Molander, *Org. Lett.* **2016**, *18*, 764–767.

[36] A. Hosomi, S. Kohra, Y. Tominaga, *J. Chem. Soc., Chem. Commun.* **1987**, 1517–1518.

[37] A. Hosomi, S. Kohra, K. Ogata, T. Yanagi, Y. Tominaga, *J. Org. Chem.* **1990**, *55*, 2415–2420.

[38] M. Kira, K. Sato, H. Sakurai, *J. Org. Chem.* **1987**, 52, 949–951.

[39] K. D. Raynor, G. D. May, U. K. Bandarage, M. J. Boyd, *J. Org. Chem.* **2018**, *83*, 1551–1557.

[40] N. R. Patel, C. B. Kelly, A. P. Siegenfeld, G. A. Molander, *ACS Catal.* **2017**, *7*, 1766–1770.

[41] W. Luo, Y. Yang, Y. Fang, X. Zhang, X. Jin, G. Zhao, L. Zhang, Y. Li, W. Zhou, T. Xia, B. Chen, *Adv. Synth. Catal.* **2019**, *361*, 4215–4221.

[42] M. Jouffroy, G. H. M. Davies, G. A. Molander, *Org. Lett.* **2016**, *18*, 1606–1609.

[43] K. Lin, R. J. Wiles, C. B. Kelly, G. H. M. Davies, G. A. Molander, *ACS Catal.* **2017**, *7*, 5129–5133.

[44] E. Levernier, V. Corcé, L.-M. Rakotoarison, A. Smith, M. Zhang, S. Ognier, M. Tatoulian, C. Ollivier, L. Fensterbank, *Org. Chem. Front.* **2019**, *6*, 1378–1382.

[45] S. B. Lang, R. J. Wiles, C. B. Kelly, G. A. Molander, *Angew. Chem. Int. Ed.* **2017**, *56*, 15073–15077.

[46] J. P. Phelan, S. B. Lang, J. S. Compton, C. B. Kelly, R. Dykstra, O. Gutierrez, G. A. Molander, *J. Am. Chem. Soc.* **2018**, *140*, 8037–8047.

[47] L. R. E. Pantaine, J. A. Milligan, J. K. Matsui, C. B. Kelly, G. A. Molander, *Org. Lett.* **2019**, *21*, 2317–2321.

[48] J. A. Milligan, K. L. Burns, A. V. Le, V. C. Polites, Z.-J. Wang, G. A. Molander, C. B. Kelly, *Adv. Synth. Catal.* **2020**, *362*, 242–247.

[49] W. M. Seganish, P. DeShong, *J. Org. Chem.* **2004**, *69*, 1137–1143.

[50] D. A. Loy, J. H. Small, K. J. Shea, *Organometallics* **1993**, *12*, 1484–1488.

[51] Patent JP2008189824A.

[52] Patent JPWO2017195822A1.

[53] C. Lévêque, L. Chenneberg, V. Corcé, C. Ollivier, L. Fensterbank, *Chem. Commun.* **2016**, *52*, 9877–9880.

[54] R.-M. L. Mercado, A. Chandrasekaran, R. O. Day, R. R. Holmes, *Organometallics* **1999**, *18*, 1686–1692.

[55] F. Carré, G. Cerveau, C. Chuit, R. J. P. Corriu, C. Réyé, *Angew. Chem. Int. Ed.* **1989**, *28*, 489–491.

[56] J. Sperlich, J. Becht, M. Mühleisen, S. A. Wagner, G. Mattern, R. Tacke, *Z. Naturforsch. B* **1993**, *48*, 1693–1706.

[57] R. Tacke, B. Ulmer, B. Wagner, M. Arlt, *Organometallics* **2000**, *19*, 5297–5309.

[58] G. Cerveau, C. Chuit, E. Colomer, R. J. P. Corriu, C. Reye, *Organometallics* **1990**, *9*, 2415–2417.

[59] Patent JP2007246671A.

[60] I. Richter, M. Penka, R. Tacke, *Organometallics* **2002**, *21*, 3050–3053.

[61] F. Carre, G. Cerveau, R. J. P. Corriu, C. Reye, *New J Chem* **1992**, 63–69.

[62] Patent US20100056801A1.

[63] R. R. Pidaparthi, C. S. Junker, M. E. Welker, C. S. Day, M. W. Wright, *J. Org. Chem.* **2009**, *74*, 8290–8297.

[64] R. R. Pidaparthi, M. E. Welker, C. S. Day, M. W. and Wright, *Org. Lett.* **2007**, 9, 9, 1623–1626.

[65] A. Hosomi, S. Kohra, Y. Tominaga, *Chem. Pharm. Bull.* **1988**, *36*, 4622–4625.

[66] Z.-J. Wang, S. Zheng, J. K. Matsui, Z. Lu, G. A. Molander, *Chem. Sci.* **2019**, *10*, 4389–4393.

[67] D. Hartmann, T. Thorwart, R. Müller, J. Thusek, J. Schwabedissen, A. Mix, J.-H. Lamm, B. Neumann, N. W. Mitzel, L. Greb, *J. Am. Chem. Soc.* **2021**, *143*, 18784–18793.

[68] R. R. Holmes, J. A. Deiters, *Phosphorus Sulfur Silicon Relat. Elem.* **1995**, *98*, 105–124.

[69] E. Levernier, K. Jaouadi, H. R. Zhang, V. Corcé, A. Bernard, G. Gontard, C. Troufflard, L. Grimaud, E. Derat, C. Ollivier, L. Fensterbank, *Chem. Eur. J.* **2021, *27,*** 8782–8790.

[70] K. C. K. Swamy, C. Sreelatha, R. O. Day, J. Holmes, R. R. Holmes, *Phosphorus Sulfur Silicon Relat. Elem.* **1995**, *100*, 107–121.

[71] R. Tacke, C. Burschka, M. Willeke, R. Willeke, *Eur. J. Inorg. Chem.* **2001**, 1671–1674.

[72] F. Riedel, A. Oehlke, S. Spange, *Z. Anorg. Allg. Chem.* **2009**, *635*, 1335–1340.

1.2 Reactivity and perspectives [compendium]

1.2.1 Introduction

The research of greener radical precursors, was motivated to avoid the use of classical stannane initiators. It has positively evolved toward the use of stable anionic radical precursors such as carboxylate, trifluoroborate and silicate. The second ones, readily accessible from a boron derivative and inorganic fluorine source easily react with dye and metal based photocatalyst for the generation of radical. The main drawback of trifluoroborates consists in the difficulty to generate poorly stabilised primary radicals in addition to the generation of toxic but soluble trifluoroborate. This lack of unstabilized radicals was then largely compensated by the discovery and the use of bis(catecholato) silicates as radical precursors, allowing the smooth generation and utilization of primary radicals. The redox properties of bis(catecholato) silicates started to be investigates by Reyé and co-workers in 1989 and 1990 respectively. [2,3] Interestingly, the $1e^-$ reduction of silicate was observed but no synthetic application was found at this time (scheme 1).

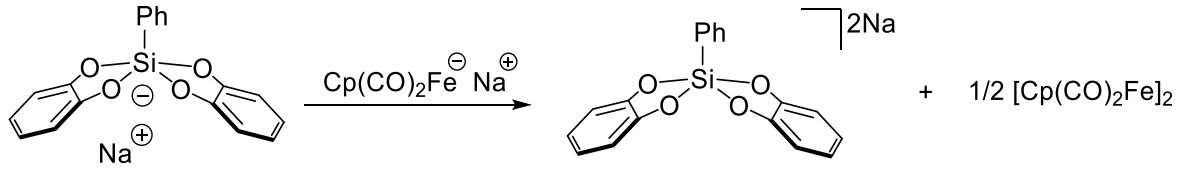

Scheme 1. Reduction of bis-(catecholato) silicate.

It was in 2014 that Nishigaishi reported the first radical reaction under irradiation involving a bis(catecholato) silicate leading to the desired cleavage of the apical substituent using intense irradiation and generation of the desired radicals. [4] Since then, the oxidation has been exploited by our group and Molander's one in 2015 and 2016. The application involving silicate are nowadays in the presence of a photocatalyst under irradiation. [5,6] With their low oxidation potentials compared to the previous precursors (from 0.4 V to 1.0 V vs SCE), numerous dye and metal based photocatalyst can oxidize these species. (Scheme 2) When oxidized, the homolytic cleavage of the apical substituent (mainly alkyl group) permits to generate the desired radical and a spirosilane. Of note, if the fate of the radical species is now well-understood, the one of the spirosilane ([Si(cat)$_2$]) was not until the publication of Greb and co-workers on this subject.[7]

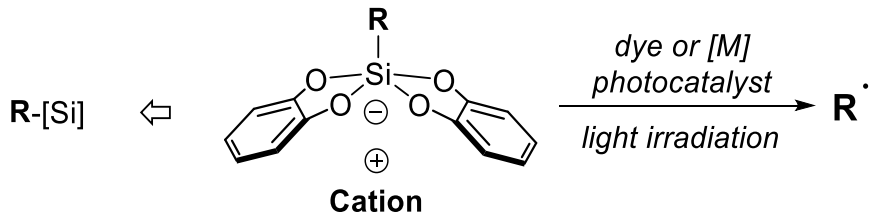

Scheme 2. Structure of bis-(catecholato) silicate.

1.2.2 Table overview

Table 1.

N°	Silicate	Application(s)
1	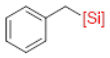	*Photoredox cross coupling,* [5,6,8–12] *Photo-allylation* [5] *Imine alkylation* [13] *Ketone synthesis* [14]
2		*Photoredox cross coupling* [5,6,9–12,15,16] *Photo- allylation* [5,17] *Intermolecular addition* [5] *Photoredox amidation* [18] *Carbonylation* [19] *Flow coupling* [15] *Imine alkylation* [13] *Hydrazone alkylation*[20] *Photoredox cyclopropanation* [21] *Ketone synthesis* [14] *Annulation* [22] *Three component reaction* [23] *Selane sulfane synthesis* [24] Desulfinative alkylation[25] *Amidation*[26]
3		*No application*
4		*Photoredox cross coupling* [5,6,8–10] *Photoredox allylation*[5,17] *Carbonylation*[19] *Flow coupling*[15] *Photoredox cyclopropanation*[21] *Ketone synthesis*[14] *Selane synthesis*[24] *Amidation*[26]
5		*H-Abstractor* [27]
6		*Photoredox cross coupling* [6,9,17] *Photoredoxallylation* [5] *Photoredox cyclopropanation* [21,28]
7	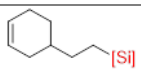	*Photoredox cross coupling*[6,10,11] *Desulfinative alkylation*[25]
8	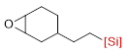	*Photoredox cross coupling* [6,8] *Photoredox allylation* [5] *Carbonylation* [19] *Amidation* [26]
9	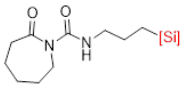	*Photoredox cross coupling*[6,11,16] *Photoredox amidation*[18] *Imine alkylation*[13] *Defluorinative alkylation* [29] *Annulation*[22]
10	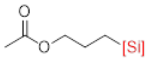	*Photoredox cross coupling* [6,8,10,12,16,17] *Photoredox amidation*[18] *Flow coupling*[15] *Carbonylation*[19] *Imine alkylation*[13] *Defluorinative alkylation*[29] *Photoredox allylation* [17] *Hydrazone alkylation*[20]
11	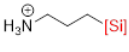	*Photoredox cross coupling*[6,10,16] *Material chemistry*[30]
12	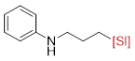	*Photoredox cross coupling* [6,11,16] *Material chemistry* [30] *Selane synthesis* [24] *Amidation* [26]

Table 1. Continuation

N°	Silicate	Application(s)
13		*Photoredox cross coupling* [5,9–11] *Photoredox allylation* [5] *Carbonylation* [19] *Imine alkylation* [13] *Ketone synthesis* [14] *Three component reaction* [23] *Selane, sulfane synthesis* [24] *Desulfinative alkylation*[25] *Amidation*[26]
14		*Photoredox cross coupling* [5,8,10] *Photoredox allylation*[5] *Allylation*[31–34] *Imine alkylation*[13]
15	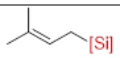	*Allylation* [31,33]
16	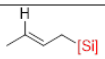	*Allylation*[31]
17	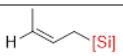	*Allylation* [31]
18		*Reduction* [35]
19		*Photoredox cross coupling* [8,10,11,16] *Intermolecular addition*[5] *Flow coupling* [15] *H-Abstractor* [27] *Carbonylation* [19] *Imine alkylation*[13] *Photoredox cyclopropanation*[21] *Annulation*[22] *Selane synthesis*[24] *Hydrazone alkylation*[20] *Amidation*[26]
20	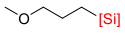	*Photoredox cross coupling* [10,11,16] *Photoredox amidation* [18] *Imine alkylation* [13] *Defluorinative alkylation*[29] *Annulation* [22] *Hydrazone alkylation* [20]
21	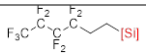	*Photoredox cross coupling* [6]
22	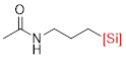	*Photoredox cross coupling* [10,11,16] *Defluorinative alkylation* [29]
23	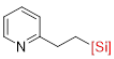	*Photoredox cross coupling* [6,10,11,16] *Photoredox amidation* [18] *Defluorinative alkylation*[29] *Annulation*[22]
24	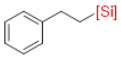	*Photoredox amidation*[18] *Imine alkylation*[13] *Annulation*[22] *Selane, sulfane synthesis* [24] *Desulfinative alkylation*[25]
25	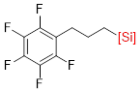	*Photoredox cross coupling* [11] *Photoredox amidation* [18] *Imine alkylation* [13] *Annulation* [22] *Amidation* [26]
26	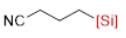	*Photoredox cross coupling* [8,9,11] *Photoredox amidation* [18] *Imine alkylation* [13] *Annulation* [22]

Table 1. Continuation

N°	Silicate	Application(s)
27		*Flow coupling* [15] *Imine alkylation* [13] *Photoredox cyclopropanation* [21] *Selane synthesis* [24] *Hydrazone alkylation* [20]
28	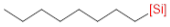	*Photoredox cyclopropanation* [21]
29		*Flow coupling* [15] *Photoredox cyclopropanation* [21] *Selane synthesis* [24]
30		*No application reported*
31	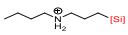	*Photoredox cross coupling*[16j]
32		*Photoredox cross coupling*[11]
33		*Photoredox cross coupling*[6,16] *Ketone synthesis*[14] *Defluorinative alkylation*[29] *Three component reaction*[23]
34	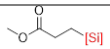	*Photoredox cross coupling*[11] *Desulfinative alkylation*[25]
35		*Photoredox cross coupling*[9,11,16,17] *Photoredox amidation*[18] *Photoredox cyclopropanation*[21] *Ketone synthesis*[14]
36	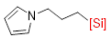	*Photoredox amidation*[18] *Annulation*[22]
37	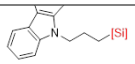	*Defluorinative alkylation* [29]
38	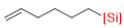	*Photoredox allylation* [5] *Carbonylation*[19] *Photoredox cross coupling*[17] *Amidation*[18]
39	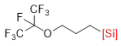	*Photoredox amidation*[18] *Carbonylation*[19] *Desulfinative alkylation*[25]
40		*Photoredox cyclopropanation*[21,28]
41		Photoredox cyclopropanation[28]
42	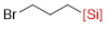	*Annulation*[36]
43	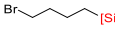	*Annulation*[36]
44		*Annulation*[36]
45	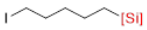	*Annulation*[22]
46		*Annulation*[22]
47	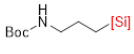	*Photoredox cross coupling*[11] *Defluorinative alkylation*[29] *Annulation*[22] *Selane synthesis* [24]

Table 1. Continuation

N°	Silicate	Application(s)
48	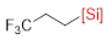	*Photoredox cross coupling*[8,9,16] *Flow coupling*[15] *Photoredox cyclopropanation*[21] *Ketone synthesis*[14] *Annulation*[22]
49	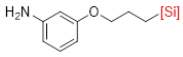	*Defluorinative alkylation* [29] *Annulation* [22]
50		*Photoredox cross coupling*[11] *H-Abstractor* [27]
51	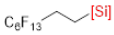	*Photoredox allylation*[5 [2]] *Amidation*[26]
52	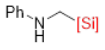	*Photoredox cross coupling*[5,8,9,17] *Photoredox allylation*[5,17] *Photoredox cyclopropanation*[21]
53	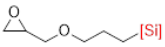	*Photoredox cross coupling*[8,9] *Intermolecular addition*[5] *Carbonylation*[19]
54		*Gold photoredox cross coupling*[37] *Pd cross coupling* [38]
55	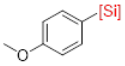	*Pd cross coupling*[38]
56		*Photoredox allylation* [5,17] *Carbonylation*[19] *Ketone synthesis*[14] *Amidation*[26]
57	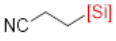	*Photoredox cross coupling* [5,8,9] *Photoredox cyclopropanation*[21] *Ketone synthesis*[14] *Amidation*[26]
58	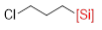	*Photoredox cross coupling*[8,10] *Photoredox cyclopropanation*[21] *Selane, sulfane synthesis*[24] *Annulation*[36]
59	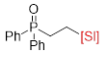	*Photoredox allylation*[17] *Photoredox cross coupling*[17]
60		*Ketone synthesis*[14]
61	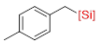	*Ketone synthesis*[14]
62	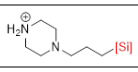	*Photoredox cross coupling* [16]
63	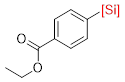	*Pd cross coupling* [38]
64		*Pd cross coupling* [38]
65		*Pd cross coupling* [38]
66		*Pd cross coupling* [38]

Table 1. Continuation

N°	Silicate	Application(s)
67		*Pd cross coupling*[38]
68	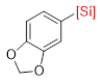	*Pd cross coupling*[38]
69	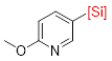	*Pd cross coupling* [38]
70		*Three component reaction*[23]
71		*Three component reaction*[23]
72		*Electrochemical studies*[3]
73	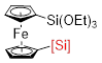	*Electrochemical studies*[3]
74		*Diels-Alder*[39,40,41]
75	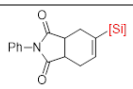	*Pd cross coupling* [39,58]
76	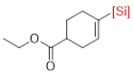	*Pd cross coupling* [40]
77	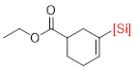	Pd cross coupling[40]
78	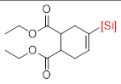	Pd cross coupling[40]
79		*Allylation*[34]
80		*Annulation*[36]
81		Annulation[22]
87		Pd cross coupling[42]
83		Pd cross coupling[42]
84		Pd cross coupling[42]
85		Pd cross coupling[42]
86		Pd cross coupling [38]
87		Desulfinative alkylation[25]

1.2.3 Applications

As highlighted in the previous table, silicates can now be considered as common reagents for the generation of radicals as presented after in this chapter but was firstly known for the Hiyama-type cross coupling reaction. (Y. Hatanaka, T. Hiyama, *J. Org. Chem.* **1988**, *53*, 918–920.)

1.2.1. Palladium cross-coupling

Indeed, Deshong *et al.* firstly reported the use of aryl bis(catecholato) silicates as reagents for the palladium cross-coupling reaction with triflate- or halogeno- aryl substrats. [38] The formation of bis-aryl product such as **2** was achieved in high yield (98%) following some classical palladium methodology (i.e. Buchwald phosphine and Pd(0)$(dba)_2$ as pre-catalyst). The reaction takes place in refluxing dioxane (scheme 3).

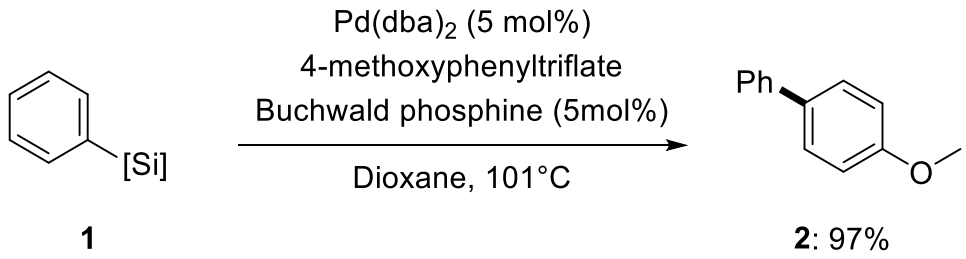

1 **2**: 97%

Scheme 3. Cross coupling of silicate catalysed by Palladium

Welker and co-workers mainly focused their work on the formation of silicate precursors (e.g. secondary vinyl silicate) but also investigated the cross-coupling reaction using the bis(catecholato) vinyl silicate. (Table 1, entry 74-78) These cross-coupling reaction appears highly efficient as described by Deshong.

1.2.2. Diels-Alder

Welker et al. have reported [4+2] cycloaddition between activated dienophile **4** and enriched diene by the silicate **3**.[39] The Diels-Alder reaction proceeds under relatively mild conditions in THF to afford the desired product **5** in 99% yield (scheme 4.a). The intrinsic electron richer nature of the substituent of the hypercoordinated silicon species such as silicate (**3**) was briefly exposed by this Diels-Alder reaction. Indeed, the comparison of the reactivity between diene substituted in position 3 by a potassium bis(catecholato) silicate (**3**) versus a trimethoxy silane (**3'**) led to a quantitative yield for the formal [4+2] with **4** for the silicate (99% yield) (scheme 4.a) and nearly no reaction (2% yield) with the silane (scheme 4.b).

Interestingly, this +I effect of bis(catecholato) silicate was already observed and used in organic synthesis at the end of the eighty as described later in the nucleophilic allylation reaction on aldehyde (see 1.2.8).

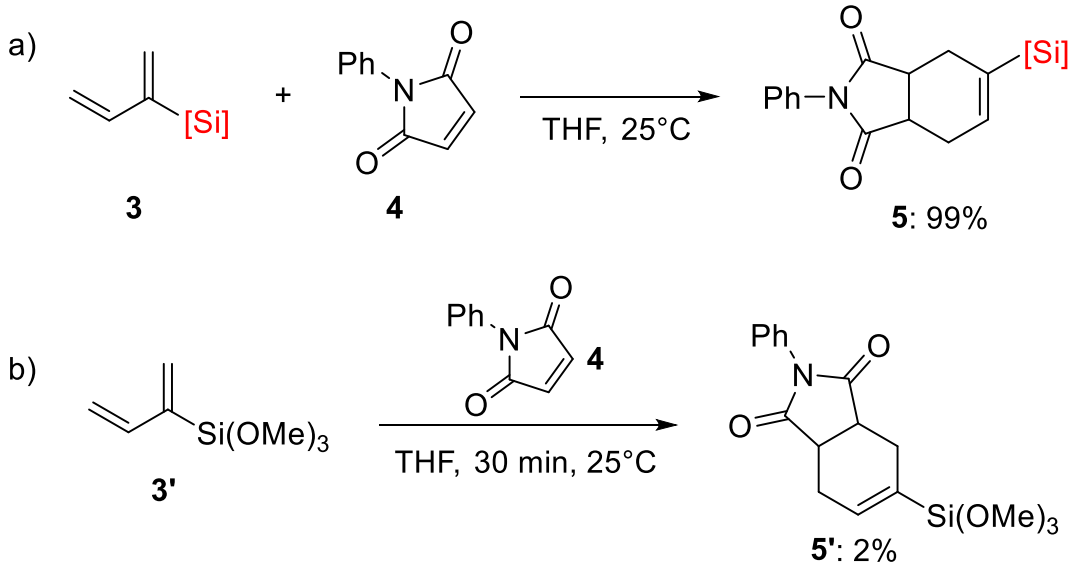

Scheme 4. a) Formation of silicate by D.A. reaction; b) Attempted formation of silane by D.A. reaction

As mentioned before, the resulting vinyl silicate (**3**) was then engaged in palladium catalysed reaction and afford the desired product in quantitative yield.

1.2.3. Gold photoredox cross-coupling

More recently, cross-coupling reaction using silicates was extended using noble metal such as gold for the direct formation of biaryls compound. Compared with the previous cross-couplings described by Deshong working mainly with rich aryls, Hashmi and co-workers have reported a gold catalysed cross-coupling reaction under visible light irradiation afford good result with electron poor aryls such as the chloro **7** in 94% yield (scheme 5). [37] The reaction involved a $Au^{I/III}$ (O.A.), transmetalation and R.E. to obtain the biaryl product. In this work, no photosensitizer was used for the key reductive elimination.

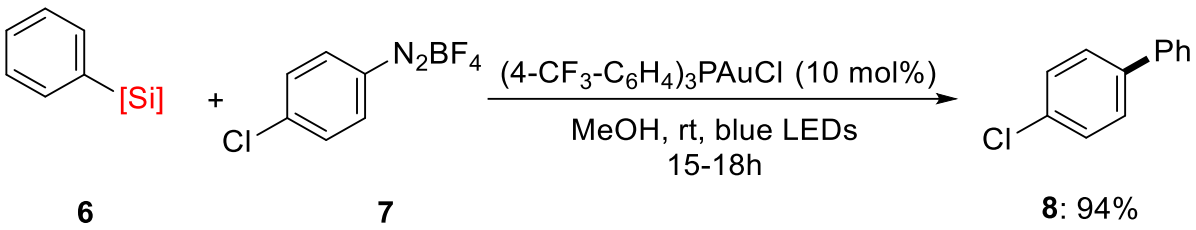

Scheme 5. Gold catalysed cross coupling of aryl silicate

1.2.4. H-Abstractor

An interesting methodology that combined photoredox chemistry and HAT radical chemistry was published by Molander and co-workers in 2016 reported the synthesis of thioether **11** by the reaction of alkyl silicates **9** with bromoaryl **10** (scheme 6).[27]

Under irradiation using $[Ru(bpy)_3](PF_6)_2$ photocatalyst for the generation of the alkyl radical and a $[NiCl_2(dme)]$ catalyst for the cross-coupling reaction, the desired thio-etherification was achieved in 89% yield.

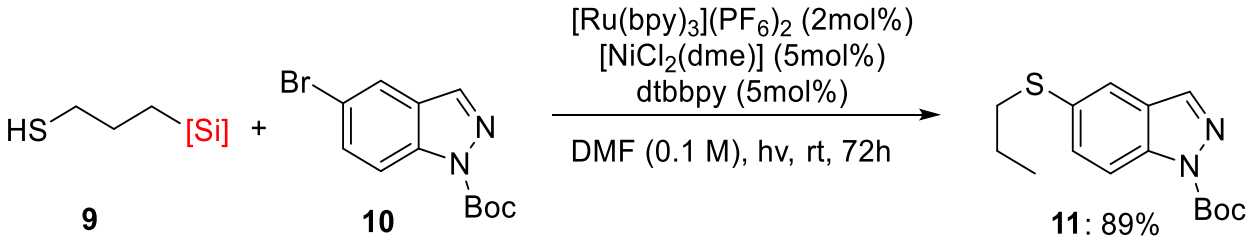

Scheme 6. Cross-coupling promoted by photo-oxidation / HAT

The following mechanism was proposed and feature the use of the radical from the silicate as hydrogen abstractor in intramolecular abstraction (1,4-H transfer) and also in an intermolecular fashion as shown in scheme 7. Firstly, oxidation of the alkyl silicate bearing a thiol (-SH group) led to the formation of a primary *C*-centered radical. 1,4-H atom abstraction occurred and led to the formation of a stable S-centered one. At the same time, oxidative addition (O.A.) of a $[Ni^0]$ catalyst with bromo-aryl occurred and provided a $[Ni^{II}]$ intermediate. Radical addition on the metal led to the $[Ni^{III}]$ species and subsequent reductive elimination (R.E.) occurred allowing the formation of the desired thioether. Finally, reduction of the $[Ni^{I}]$ in $[Ni^0]$ regenerate the reactive Nickel catalyst and ruthenium photocatalyst.

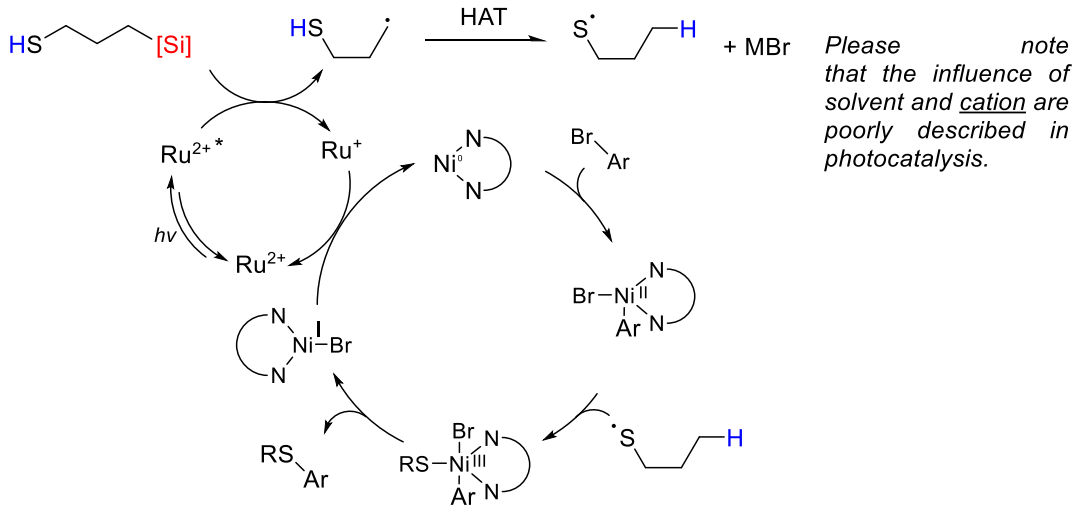

Please note that the influence of solvent and cation are poorly described in photocatalysis.

Scheme 7. Nickel dual photoredox cross-coupling mechanism

1.2.5. Photoredox cross-coupling

Molander and co-workers have reported metal-catalyzed reaction of primary and secondary ammonium alkyl silicates with arylated bromides in good to excellent yields.[6] They performed the reaction of primary ammonium alkyl silicates with bromo-indazole coupling partner in the presence of Ru photocatalyst and Ni cocatalyst. The indazole scaffold **11** was obtained in excellent yields after 16 h (scheme 8).

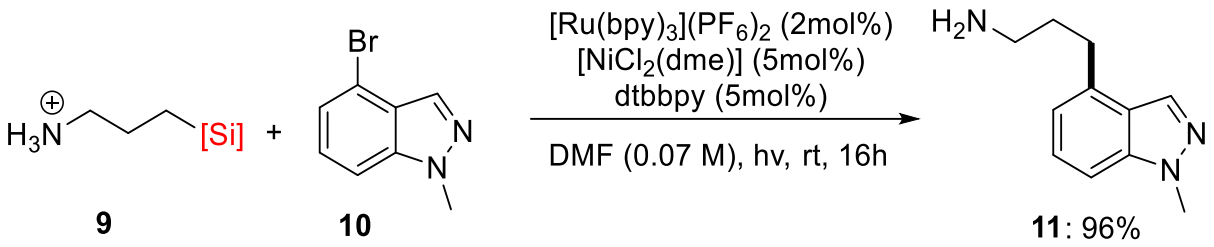

Scheme 8. Nickel dual cross coupling on heteroaryl.

The presumable mechanism proposed for dual cross coupling photoredox reaction that is shown in scheme 7 can be extrapolated in nearly all the Ni/Photoredox dual cross-couplings. Based on these methodologies and the emergence of flow chemistry, the combination of both fields has naturally occurred (see below).

1.2.6. Flow coupling

Indeed, Boyd et al. have reported a continuous flow Csp3−Csp2 cross-coupling for the synthesis of organic moieties by using trifluoroborates and silicate reagents in 2018 (scheme 9). [15]

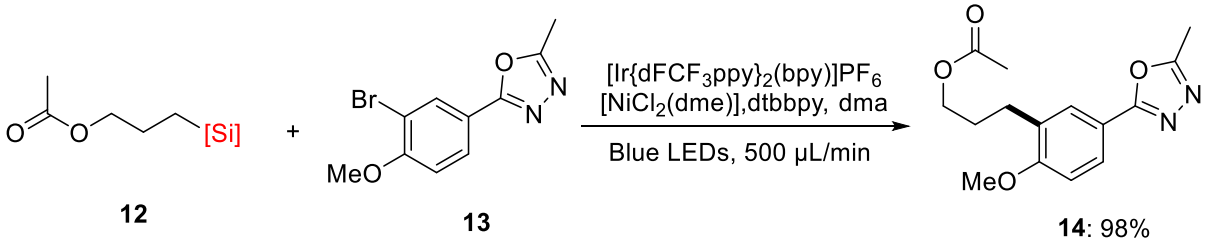

Scheme 9. Effect of continuous flow on silicate couplings

The cross-coupling reaction rate was exhibited to be a significantly faster under flow condition (40 min vs. 24 h) compared to classical batch reactions. In addition, the formation of **14** gave an almost quantitative yield. The same observation was observed with another nickel dual cross coupling between flow and classical bench experiment by Abdellaoui and co-workers in 2021 (our group).[12] In addition to the adaptability of the methodology in continuous flow reaction, the methodology allows the Z-selective cross-coupling reaction of a silicate with dichlorostyrene as coupling partner (scheme 10).

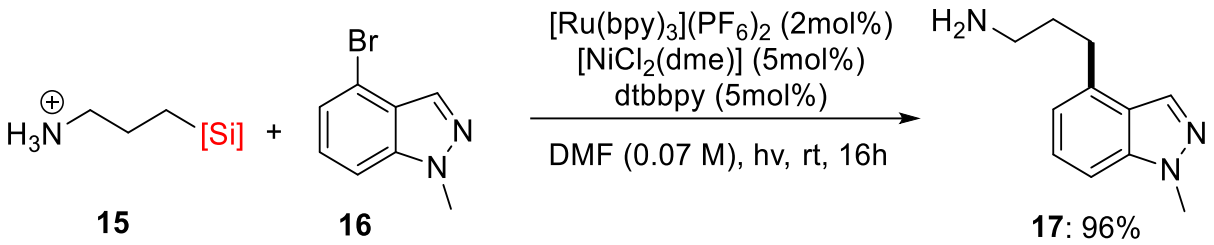

Scheme 10. Cross coupling reaction

1.2.7. Reduction

An uncommon reduction of ketone was developed by Sakurai and co-workers in 1987. The reduction takes place by the *in situ* generation of an unstable hydridosilicates (scheme 11). [35] At first, the hydro intermediate was generated by the reaction of dilithium catecholate in THF with trichlorosilane. *Cyclohexanone* (**21**) reacts with the generated silicate to successfully produce cyclohexanol (**20**) in excellent yields over 5 hours.

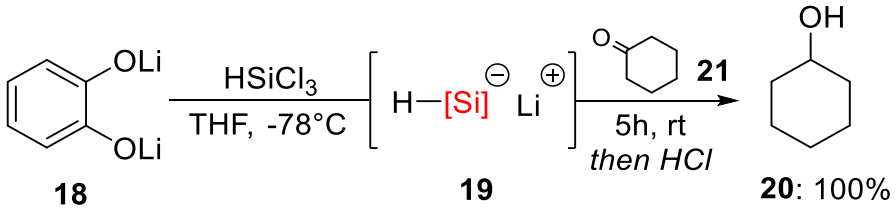

Scheme 11. Reduction of carbonyl using silicate.

1.2.8. Allylation

The same methodology was applied the *in-situ* generation of an unstable allyl silicate. [31] With the allylation reagent in hand, the allylation of several aldehydes was performed allowing the formation of the desired allyl alcohol in high yield. (scheme 12**)**

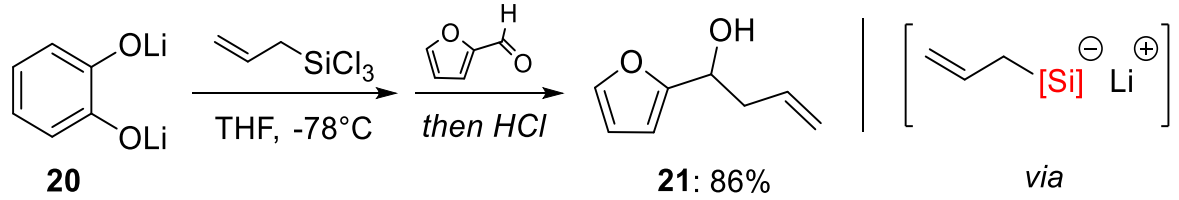

Scheme 12. Reduction of carbonyl using silicate.

In addition to the high yielding reaction for the allylation, crotylation was performed following the same methodology and permitted to reach good yield and stereoselectivity based on a Zimmerman-Traxler chair-like transition state. The same year Hosomi and co-workers also published the same reactivity using a more stable ammonium allyl silicate derivative[33]. In 2001, Hosomi also reported the use of phenyl silicate acting as basic catalyst for the Michael addition of enolate (generate using the silicate) on MVK.[43]

Nowadays, the direct C-C bond formation using silicates is essentially achieved following radical pathways. As example, photoredox allylation reaction was reported recently in 2016 by our group.

1.2.9. Photoredox allylation

The radical allylation can be considered as a classical reaction in radical chemistry. The use of a catalytic amount of photocatalyst such as 4CzIPN, an effective purely organic dye, and of a greener radical precursor have permitted to dramatically simplify this reaction. We published some years ago the combination of these reactants for the addition on allylsulfone and various acceptors as presented hereafter (scheme 13).[17]

Scheme 13. Reaction of silicates with tosyl allyl.

The mechanism involved in this reaction can be considered as a general one for any radical addition involving silicate and photocatalyst (e.g. allylation, 1,2 and 1,4 radical addition). Oxidation of the silicate by the photocatalyst (PC) that can be Ir/Ru/Dye permit to generate the desired radical. Mechanistic insights reveal a non-radical chain pathway as shown by the measured quantum yield (if $\Phi < 1$).[19] In this case (scheme 14) the common radical addition-elimination proceeds to generate the desired product and tosyl radical.

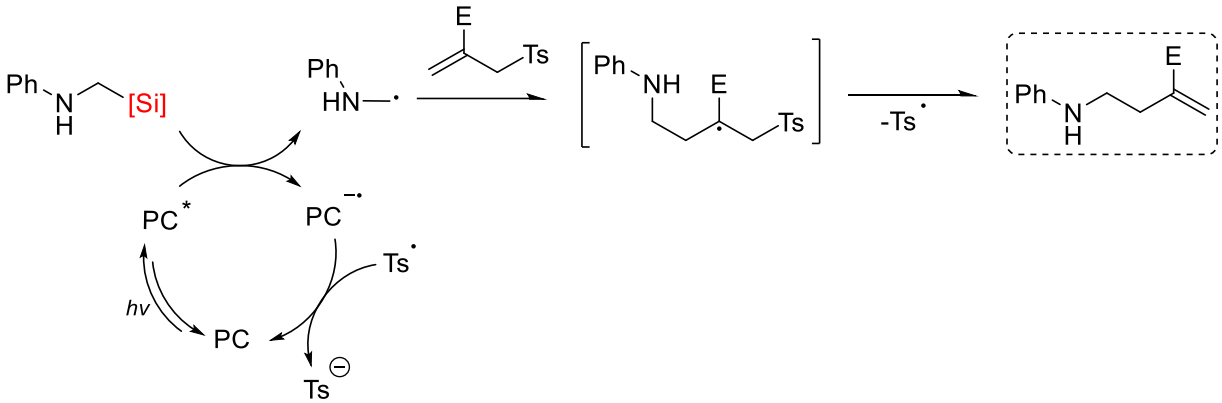

Scheme 14. Reaction of silicates with tosyl allyl.

The mechanism presented above shows the regeneration of the photocatalyst by the reduction of the sulfonyl to form a sulfinate. This is observed with any resulting stabilized radical (as example, N-centered from 1,2 addition or C-centered from 1,4 addition on α, β-unsaturated enone) and led to the generation of stable anion (as example, respectively an amidure or enolate).

1.2.10. Intermolecular addition

The silicates have been many times reported as a versatile source of alkyl radicals for the C-C bond formation coupling upon visible-light photocatalysis. The 1,4 radical addition was for example reported by our group as described in scheme 15.[5] The cyclohexyl radical generated under blue led irradiation reacts on the highly activated acceptor **26** to give the desired product **27** in 80% yield.

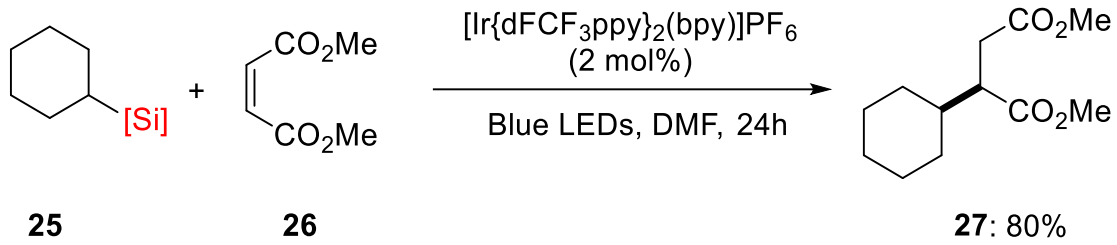

25 **26** **27**: 80%

Scheme 15. Intermolecular 1,4 additions.

1.2.11. Imine alkylation

Patel *et al.* have reported a photoredox alkylation of imines (scheme 16).[13] As for the photoredox allylation or 1,4 radical addition, the reaction elegantly occurs without the need of any additive. The alkylation takes place in high yield and the amine **30** was obtained in 91% yield.

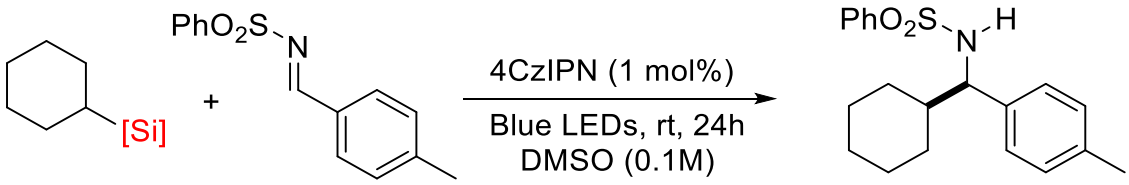

28 **29** **30**: 91%

Scheme 16. Intermolecular 1,2 additions.

The addition on *N*-acylhydrazone was also reported by Cullen and Friestad in 2019 following a relatively close methodology. In their methodology, the use of Lewis acid was necessary to achieve the intermolecular radical addition on these acceptors (scheme 16).[20] The reaction between silicate **31** and hydrazone **32** allowed to obtain **33** in 60% yield after 24h, prolonging the manipulation time from 24h to 48h allowed to reach the product in 88%.

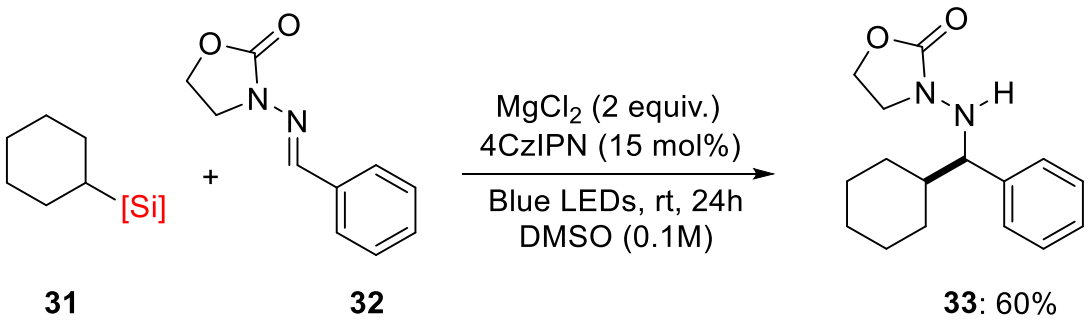

Scheme 16. Intermolecular additions on hydrazone derivative

1.2.12. Defluorinative alkylation

More specific addition has been developed such as the following defluorinative alkylation and was for example used for the formation of a DNA-Encoded library.[44] Before being used as tool for a chemical library, the methodology was reported by Lang et al. for the formation of gem-difluoroalkenes. [29] (scheme 19).

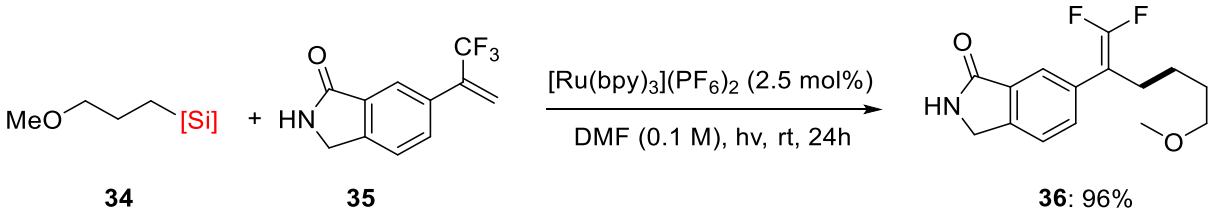

Scheme 19. Defluorinative alkylation.

Mechanistically, the resulting highly stabilized benzyl radical intermediate can be reduced by the reduced photocatalyst. This permits the recovery of the photocatalyst and the generation of a stabilized benzylic anion. E1cB type elimination of fluoride from the trifluoromethyl group provides the desired gem-difluoroalkene **36** in 96% yield.

The formation of C-C bond, by cross coupling reaction or direct radical addition are the important reactions that have given to silicates the opportunity to become a versatile radical precursor. These early reported procedures were then slowly replaced by the development of more challenging methodologies. Firstly, the formation of essential functions for any organic chemist was developed.

1.2.13. Ketone synthesis

The dual nickel cross coupling reaction on acyl chloride was reported by our group in 2019.[14] This methodology gives access in high yield to several ketone derivatives as described in scheme 20.

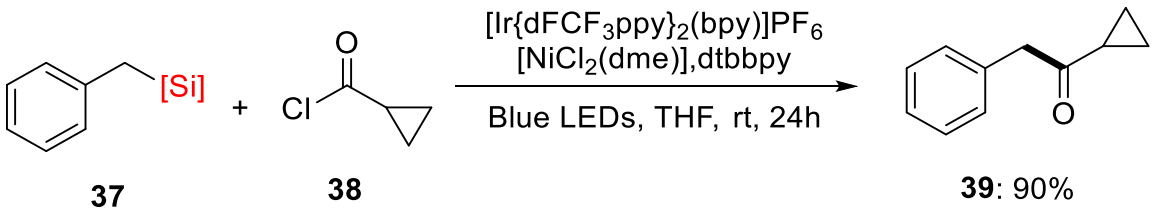

Scheme 20. Ketone synthesis via dual nickel photocatalysis cross coupling.

1.2.14. Carbonylation

The same year, Cartier et al. (our group in collaboration with Ryu's one) have reported a multicomponent reaction becoming the first example of oxidative photoredox catalysis based on a radical carbonylation for the synthesis described in scheme 21.[19] The methodology enables to access to several ketones such as **42** in high yield.

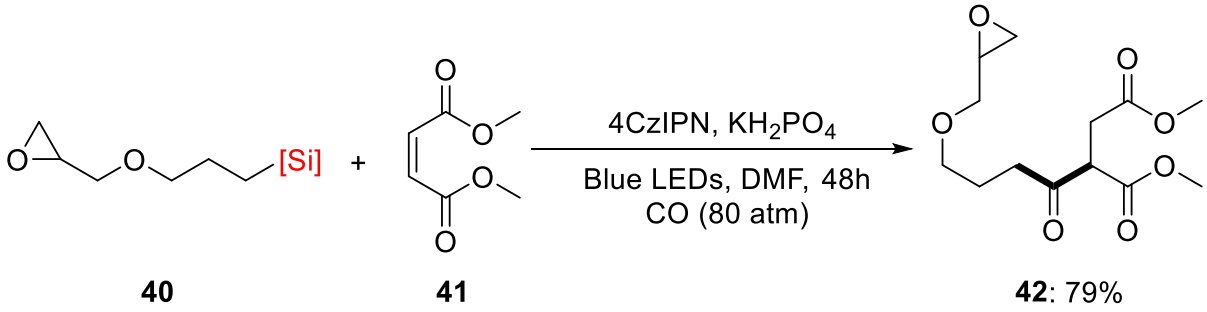

Scheme 21. Ketone synthesis via radical carbonylation.

The key step of that procedure is the formation of the acyl radical, after its regeneration, the radical is directly trapped by the CO. By the use of high pressure of carbon monoxide, the reaction is completely displaced toward the formation of radical acyl intermediate rather than the direct 1,4 radical addition. On year later, the same authors reported the photoredox amidation using a relatively close methodology. (scheme 22).[26]

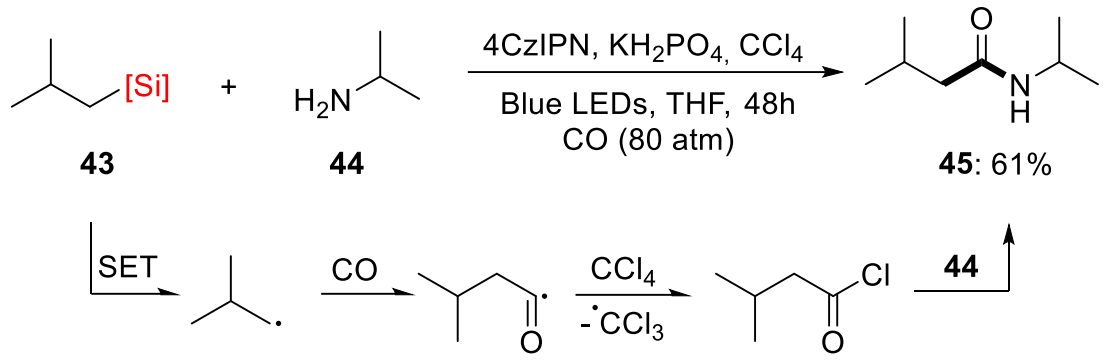

Scheme 22. Amide synthesis via radical carbonylation

As for the ketone synthesis, the amide synthesis required the use of CO gas that enables to generate the desired acyl radical. In comparison to the direct radical addition in scheme 21, the formation of **45** proceeds by the in-situ generation of acyl chloride after the reaction of the radical intermediate with CCl_4. Finally, the reaction between the generated acyl chloride and amine **44** leads to the formation of the desired amide **45** in 61% yield (scheme 22).

1.2.15. Photoredox amidation

The formation of amides was also reported by Molander and co-workers by the direct reaction of silicates to isocyanates derivatives under Nickel dual photoredox catalysis.[18] (Scheme 23)

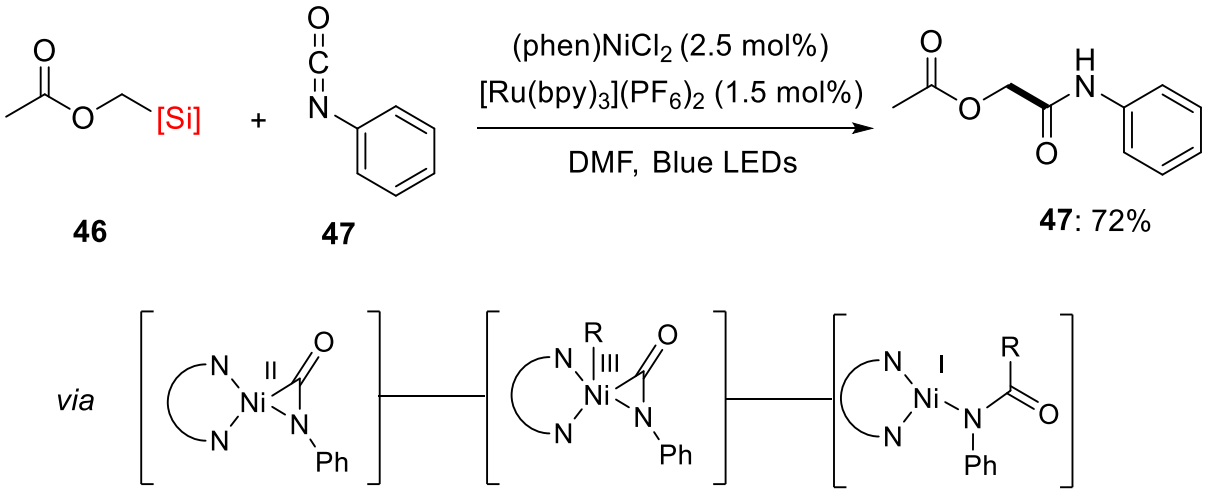

Scheme 23. Amide synthesis via Ni dual photocatalysis

The proposed mechanism starts by the formation of a three-member ring containing the $Ni^{(II)}$ species, radical addition enables to generate an unstabilized $Ni^{(III)}$ followed by a reductive elimination and the formation of a $Ni^{(I)}$ intermediate. Finally, single electron transfer generates a $Ni^{(0)}$ catalyst that will react with the isocyanate and permit the regeneration of the photocatalyst. These conditions afforded **47** in 72% yield with a low loading of catalyst.

1.2.16. Selane / sulfane synthesis

Finally, silicates have been used for the direct synthesis of selane permitting the access of several new alkylselane. (scheme 24).[24]

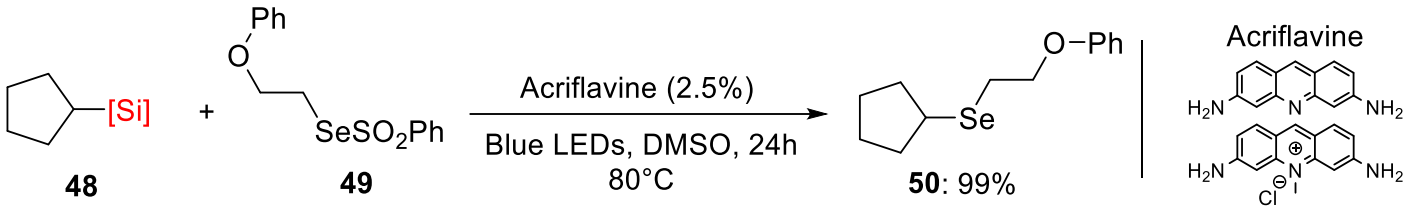

Scheme 24. Selane synthesis promoted by photoredox catalysis.

Several examples such as **50** gave quantitative yields, the methodology was also extended for the direct synthesis of thioethers. The use of sulfone as leaving group was also used by Molander and co-workers in a desulfinative process to achieve a Nickel free alkylation of hetero aryl **52** to afford **53** in 83% yield. (scheme 25).[25]

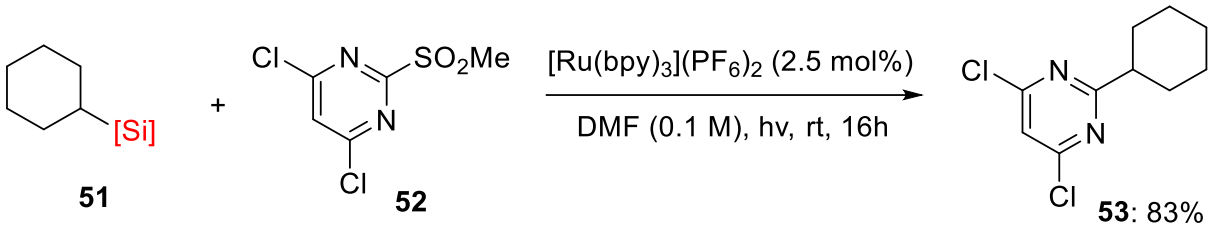

Scheme 25. Alkylation of heterocycle.

In addition to the formation of important functions as building blocks for organic synthesis, several methodologies were designed to access specific structures such as cyclopropane.

1.2.17. Photoredox cyclopropanation

Luo and co-workers have developed, similarly to the defluorinative alkylation presented above, a two-steps reaction considered as "radical-polar crossover". [21] Indeed, the generated radical from **54** does a radical addition on 55 to form a stabilized radical. The carbanion that will undergo a cyclopropanation is generated by reduction of the radical leading to the regeneration of the iridium photocatalyst.

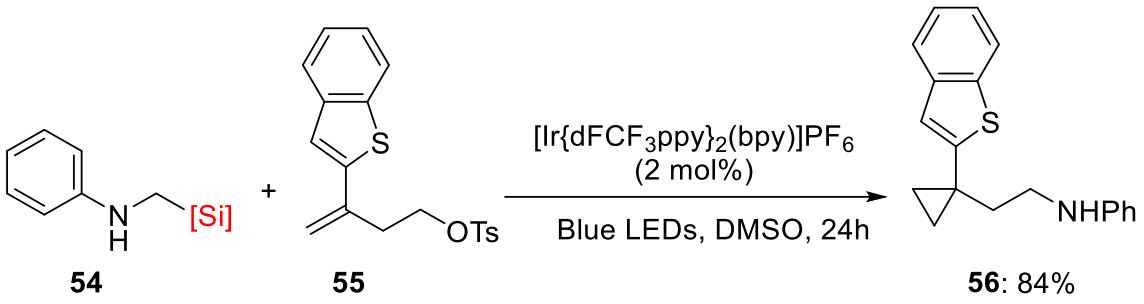

Scheme 26. One pot radical addition – polar cyclopropanation.

Several cyclopropane derivatives were synthesized using different Michael acceptors and some styrene derivatives, as exposed in scheme 27, this methodology gives to access to the benzothiophene analogue **56** in 84% yield.

1.2.18. Annulation

The same approach was reported by Kelly and Molander in 2019 allowing the formation of complex cyclopropane. (scheme 28).[22]

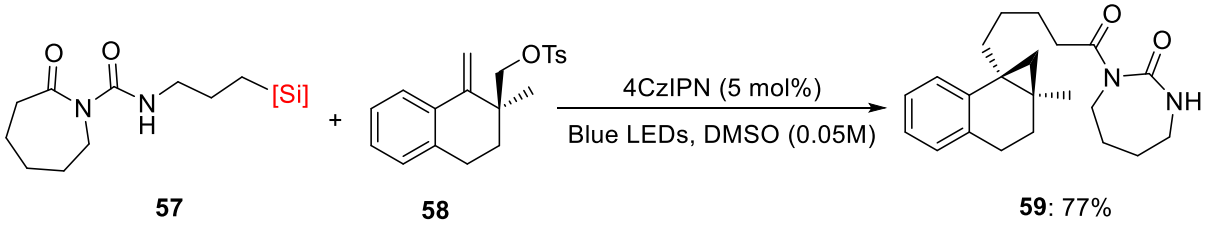

Scheme 28. Synthesis of polycyclic cyclopropane.

The polycyclic cyclopropane **59** was obtained in 77% yield, this methodology was also extended to several other derivatives such as indanone and 7-member ring derivatives.

1.2.19. Three component reaction

To conclude, Nevado and co-workers published in 2019[23] a three component reaction. (scheme 29).

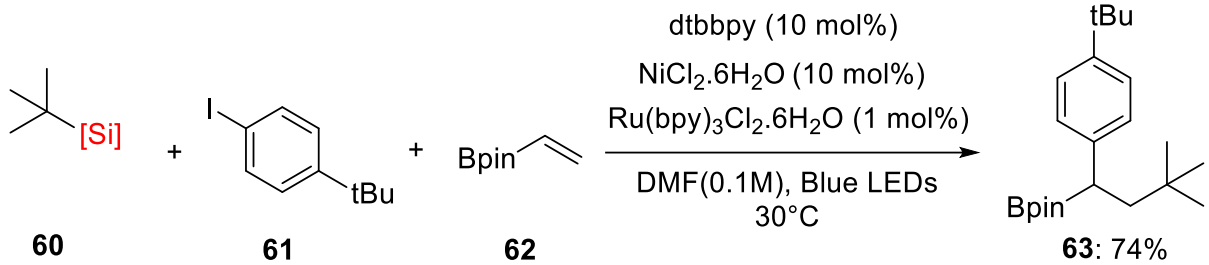

Scheme 29. Dicarbofunctionalization of alkene.

Here, one of the rare tertiary radical precursors (**60**) did a radical addition on the vinyl-borane **62**. The radical intermediate then reacted with the nickel catalyst to perform the cross-coupling reaction with the iodoaryl **61** permitting to access to **63** in 74% yield.

References part 1.2

1 C. L. Frye, *Journal of the American Chemical Society*, 1964, **86**, 3170–3171.

2 G. Cerveau, C. Chuit, R. J. P. Corriu, L. Gerbier and C. Reyé, *Phosphorus, Sulfur, and Silicon and the Related Elements*, 1989, **42**, 115–121.

3 G. Cerveau, C. Chuit, E. Colomer, R. J. P. Corriu and C. Reye, *Organometallics*, 1990, **9**, 2415–2417.

4 D. Matsuoka and Y. Nishigaichi, *Chem. Lett.*, 2014, **43**, 559–561.

5 V. Corcé, L.-M. Chamoreau, E. Derat, J.-P. Goddard, C. Ollivier and L. Fensterbank, *Angewandte Chemie International Edition*, 2015, **54**, 11414–11418.

6 M. Jouffroy, D. N. Primer and G. A. Molander, *J. Am. Chem. Soc.*, 2016, **138**, 475–478.

7 D. Hartmann, T. Thorwart, R. Müller, J. Thusek, J. Schwabedissen, A. Mix, J.-H. Lamm, B. Neumann, N. W. Mitzel and L. Greb, *J. Am. Chem. Soc.*, 2021, **143**, 18784–18793.

8 C. Lévêque, L. Chenneberg, V. Corcé, J.-P. Goddard, C. Ollivier and L. Fensterbank, *Org. Chem. Front.*, 2016, **3**, 462–465.

9 C. Lévêque, V. Corcé, L. Chenneberg, C. Ollivier and L. Fensterbank, *European Journal of Organic Chemistry*, 2017, **2017**, 2118–2121.

10 N. R. Patel, C. B. Kelly, M. Jouffroy and G. A. Molander, *Org. Lett.*, 2016, **18**, 764–767.

11 K. Lin, R. J. Wiles, C. B. Kelly, G. H. M. Davies and G. A. Molander, *ACS Catal.*, 2017, **7**, 5129–5133.

12 M. Abdellaoui, A. Millanvois, E. Levernier, C. Ollivier and L. Fensterbank, *Synlett*, , DOI:10.1055/a-1374-9384.

13 N. R. Patel, C. B. Kelly, A. P. Siegenfeld and G. A. Molander, *ACS Catal.*, 2017, **7**, 1766–1770.

14 E. Levernier, V. Corcé, L.-M. Rakotoarison, A. Smith, M. Zhang, S. Ognier, M. Tatoulian, C. Ollivier and L. Fensterbank, *Org. Chem. Front.*, 2019, **6**, 1378–1382.

15 K. D. Raynor, G. D. May, U. K. Bandarage and M. J. Boyd, *J. Org. Chem.*, 2018, **83**, 1551–1557.

16 M. Jouffroy, G. H. M. Davies and G. A. Molander, *Org. Lett.*, 2016, **18**, 1606–1609.

17 C. Lévêque, L. Chenneberg, V. Corcé, C. Ollivier and L. Fensterbank, *Chem. Commun.*, 2016, **52**, 9877–9880.

18 S. Zheng, D. N. Primer and G. A. Molander, *ACS Catal.*, 2017, **7**, 7957–7961.

19 A. Cartier, E. Levernier, V. Corcé, T. Fukuyama, A.-L. Dhimane, C. Ollivier, I. Ryu and L. Fensterbank, *Angewandte Chemie International Edition*, 2019, **58**, 1789–1793.

20 S. T. J. Cullen and G. K. Friestad, *Org. Lett.*, 2019, **21**, 8290–8294.

21 W. Luo, Y. Yang, Y. Fang, X. Zhang, X. Jin, G. Zhao, L. Zhang, Y. Li, W. Zhou, T. Xia and B. Chen, *Advanced Synthesis & Catalysis*, 2019, **361**, 4215–4221.

22 J. A. Milligan, K. L. Burns, A. V. Le, V. C. Polites, Z.-J. Wang, G. A. Molander and C. B. Kelly, *Advanced Synthesis & Catalysis*, 2020, **362**, 242–247.

23 A. García-Domínguez, R. Mondal and C. Nevado, *Angewandte Chemie International Edition*, 2019, **58**, 12286–12290.

24 F. Wang and S.-Y. Wang, *Org. Chem. Front.*, , DOI:10.1039/D1QO00085C.

25 Z.-J. Wang, S. Zheng, J. K. Matsui, Z. Lu and G. A. Molander, *Chem. Sci.*, 2019, **10**, 4389–4393.

26 A. Cartier, E. Levernier, A.-L. Dhimane, T. Fukuyama, C. Ollivier, I. Ryu and L. Fensterbank, *Advanced Synthesis & Catalysis*, 2020, **362**, 2254–2259.

27 M. Jouffroy, C. B. Kelly and G. A. Molander, *Org. Lett.*, 2016, **18**, 876–879.

28 J. P. Phelan, S. B. Lang, J. S. Compton, C. B. Kelly, R. Dykstra, O. Gutierrez and G. A. Molander, *J. Am. Chem. Soc.*, 2018, **140**, 8037–8047.

29 S. B. Lang, R. J. Wiles, C. B. Kelly and G. A. Molander, *Angewandte Chemie International Edition*, 2017, **56**, 15073–15077.

30 JP2009298975A, 2009.

31 Mitsuo. Kira, Kazuhiko. Sato and Hideki. Sakurai, *J. Am. Chem. Soc.*, 1988, **110**, 4599–4602.

32 G. Cerveau, C. Chuit, R. J. P. Corriu and C. Reye, *Journal of Organometallic Chemistry*, 1987, **328**, C17–C20.

33 A. Hosomi, S. Kohra and Y. Tominaga, *J. Chem. Soc., Chem. Commun.*, 1987, 1517–1518.

34 A. Hosomi, S. Kohra, K. Ogata, T. Yanagi and Y. Tominaga, *J. Org. Chem.*, 1990, **55**, 2415–2420.

35 M. Kira, K. Sato and H. Sakurai, Reduction of carbonyl compounds with pentacoordinate hydridosilicates, https://pubs.acs.org/doi/pdf/10.1021/jo00381a048, (accessed July 25, 2020).

36 L. R. E. Pantaine, J. A. Milligan, J. K. Matsui, C. B. Kelly and G. A. Molander, *Org. Lett.*, 2019, **21**, 2317–2321.

37 S. Witzel, K. Sekine, M. Rudolph and A. S. K. Hashmi, *Chem. Commun.*, 2018, **54**, 13802–13804.

38 W. M. Seganish and P. DeShong, *J. Org. Chem.*, 2004, **69**, 1137–1143.

39 United States, US20100056801A1, 2010.

40 R. R. Pidaparthi, C. S. Junker, M. E. Welker, C. S. Day and M. W. Wright, *J. Org. Chem.*, 2009, **74**, 8290–8297.

41 Ramakrishna R. Pidaparthi, * Mark E. Welker, and Cynthia S. Day and M. W. Wright, Preparation of 2-Trialkylsiloxy- Substituted 1,3-Dienes and Their Diels−Alder/Cross-Coupling Reactions, https://pubs.acs.org/doi/pdf/10.1021/ol070089e, (accessed July 25, 2020).

42 A. Hosomi, S. Kohra and Y. Tominaga, *Chem. Pharm. Bull.*, 1988, **36**, 4622–4625.

43 J. Tateiwa and A. Hosomi, *European Journal of Organic Chemistry*, 2001, **2001**, 1445–1448.

44 J. P. Phelan, S. B. Lang, J. Sim, S. Berritt, A. J. Peat, K. Billings, L. Fan and G. A. Molander, *J. Am. Chem. Soc.*, 2019, **141**, 3723–3732.

1.3 Case of alkali bis(catecholato)silicates

1.3.1 Introduction

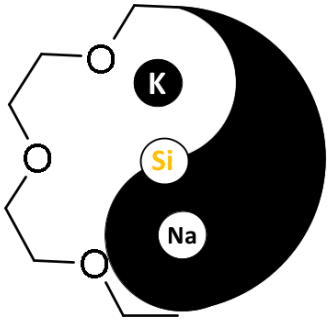

In comparison to ammonium based and chelated potassium silicates, sodium silicates are poorly described as shown in the table 1 of the introduction. In 1988 Reye and co-workers published the first synthesis of sodium bis(catecholato)methylsilicate.[1] (Scheme 1)

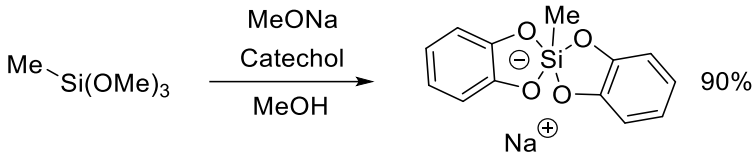

Scheme 1: Synthesis of sodium bis(catecholato)methyl silicate

More examples of free silicates (mainly potassium) were already described and used in organic synthesis (see 1.1) and nowadays, chelated potassium has merge as an efficient radical precursor. Interestingly, these forgotten unchelated sodic derivatives were not used in organic chemistry.[2] Firstly, we began our investigation following the known procedure for the chelated potassium but this time using a prepared solution of sodium methoxide in methanol.[3] Compared to their chelated counterpart, these derivatives such as sodium silicates **2-Na** require the use of the conventional Schlenk techniques for their synthesis (scheme 2). We then also decided to briefly investigate the chelation of sodium silicate as depicted in the general scheme **2** for the synthesis of **2'** derivative.

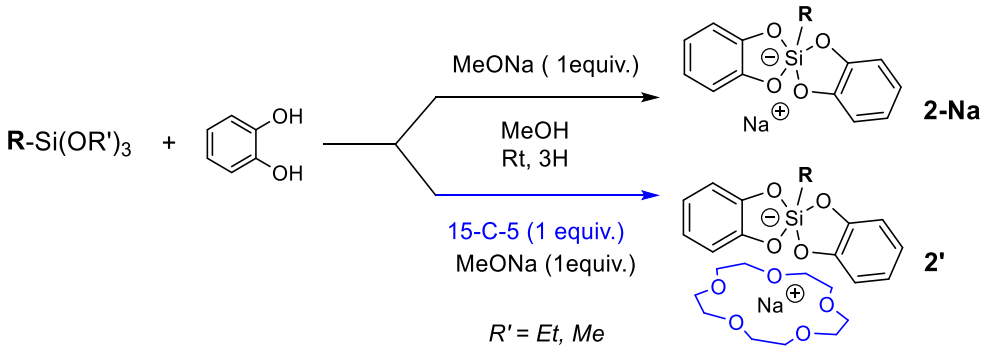

Scheme 2. General path for preparation of sodium and chelated sodium silicates

As for the well-known potassium crown ether derivative, the desired alkoxysilane is dissolved in methanol with pyrocatechol (2 equiv.). If desired, 15-crown-5 (1 equiv.) can be added before the solution of sodium methoxide (1 equiv.) in methanol. Exposition of these unchelated silicates to air before complete drying and precipitation/crystallisation induced degradation and dramatically increased the difficulty of the purification process by precipitation. Derivatives **2a,b,c,-Na** gave 55, 64 and 55% yield and free **2a-K** gave 54% yield. Chelated sodium **2a'** and **2c'** afforded respectively 45 and 50% yield (scheme 3). Gram scale synthesis of these derivatives can be performed (such as **2-Na**, 55% yield, 5 mmol scale), and the silicate can be kept several months without degradation if stored under air and moisture free conditions. In comparison, the immediate stability offered by [18C6] chelation is not observed for sodium silicate chelated by [15-C-5] that remain sensitive.

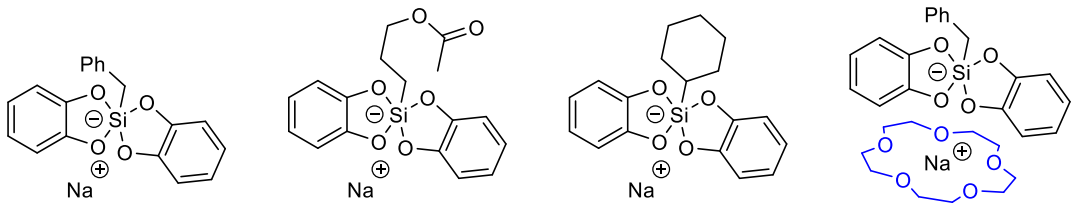

2a-Na 55% **2b-Na** 64% **2c-Na** 55% **2a'** 45%

Scheme 3. Sodium bis(catecholato)alkyl silicates

1.3.2 Crystal structure analysis

To further describe these salts, the crystal structure of **2a-Na** and **2a-K** was determined by X-ray diffraction (Figure 1-3) and the selected informations for each organosilicon salt was reported in table 1. Suitable crystals of the sodium bis(catecholato)benzyl-silicate acetone solvate (**2a-Na**) and potassium bis(catecholato)benzyl-silicate acetone solvate (**2a-K**) were obtained by slow vapor diffusion using acetone and diethyl ether as anti-solvent at 10°C.

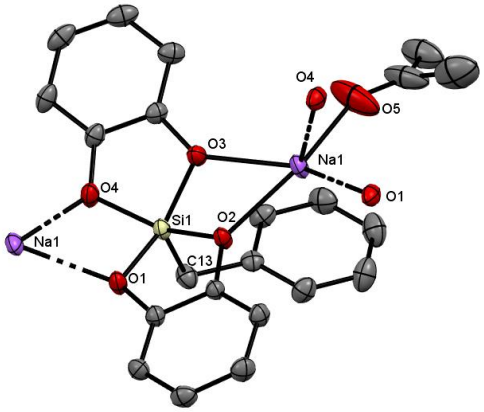

Figure 1. X-ray crystal structure of **2a-Na**, thermal ellipsoids are drawn at 50% probability level. Hydrogen atoms are omitted for clarity. Dashed lines denote bonds between neighbouring silicates.

[$C_{22}H_{21}NaO_5Si$] has crystallized in a tetragonal crystal system with a = 19.0046(7) Å, b = 19.0046(7) Å, c = 11.5788(5) Å; α, β, γ = 90° (Z = 8). In this organosilicon salt, sodium ions are chelated by one oxygen atom of four pyrocatechol ligands, and one acetone molecule completes the coordination sphere. The $O_{1\text{-}5}$-Na_1 bond lengths are going from 2.288(3) Å to 2.355(2) Å. Finally, an intramolecular π-cation interaction between the centroid of the benzyl and Na_1 can be observed with a distance of 3.2712(9) Å with a free sodium cation compared to a chelated potassium silicates (see figure 3).

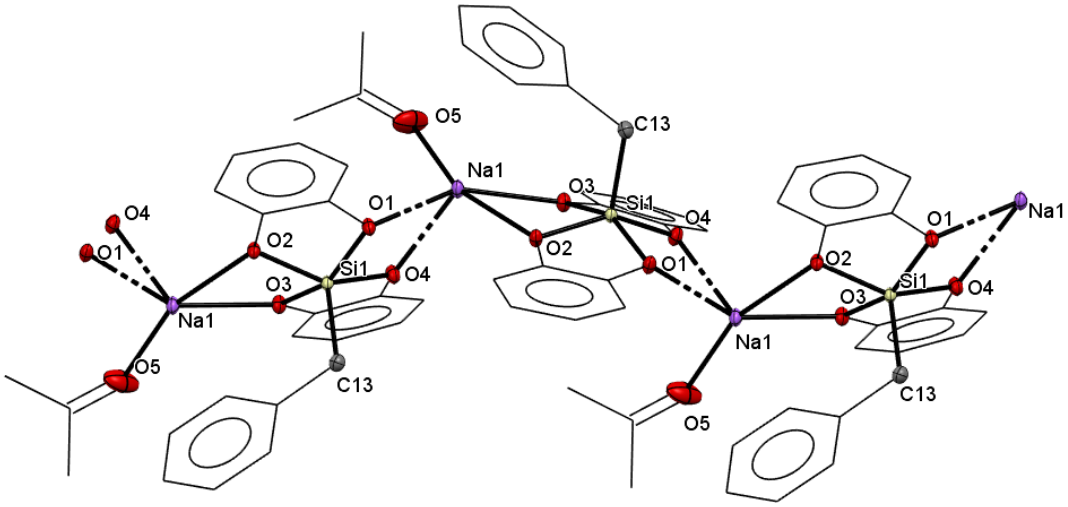

Figure 2. X-ray crystal structure of **2a-Na** (view along the b-axis), thermal ellipsoids are drawn at 25% probability level. Pyrocatechol ligands and acetone's carbons are drawn as wireframe for clarity. Hydrogen atoms are omitted for clarity. Dashed lines denote bonds between neighbouring silicates.

The Si-coordination of **2a-Na** can be described as a slightly distorted SP with the benzyl group occupying the apical site (Si-C_{13} bond length = 1.879(2) Å). The four basal positions are occupied by the two oxygen atoms of two pyrocatechol ligands. We can notice that the Si atom is located just a little above the plane defined by these four atoms (distance Si-plane centroid = 0.4517(6) Å). For **2a-Na**, the dihedral angle method shows a displacement of 89.3% (TBP → SP). This is also underlined by the close length of all the 4 basal bond distances. The Si-$O_{1\text{-}4}$ bond lengths are going from 1.735(2) Å to 1.759(2) Å. In comparison to an idealized SP with four angles of 86°, a slight distortion is observed, the main increased angle is 2.1° when the main decreased one is -2.5°. Interestingly, 2a-Na forms a polymeric assembly along the c-axis, the 1D polymer is built by multiple interactions between Na and oxygen atoms from the pyrocatechol of two silicates. This is represented in the figure 2.

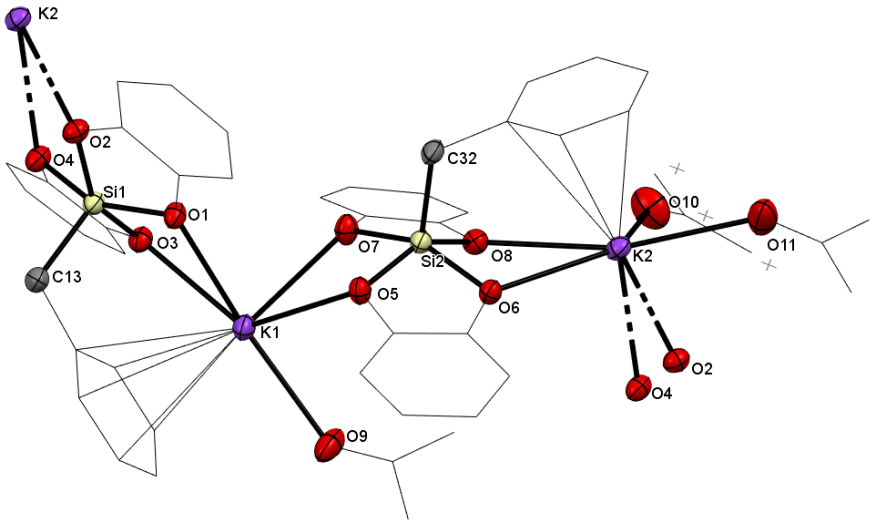

Figure 3. X-ray crystal structure of **2a-K**, thermal ellipsoids are drawn at 25% probability level. Pyrocatechol ligands and acetone's carbons are drawn as wireframe for clarity. Hydrogen atoms are omitted for clarity. Dashed lines denote bonds between neighbouring silicates.

$[C_{23.5}H_{24}KO_{5.5}Si]$ crystallized in $P2_1/c$ crystal system with a = 11.9706(4) Å, b = 18.9194(5) Å, c = 21.4398(6) Å, α, γ = 90° and β = 103.160(2) ° (Z=8). As for **2a-Na,** potassium ions of **2a-K** are chelated by one acetone molecule in addition to the four pyrocatechol ligands. Interestingly, one more acetone molecule can complete the coordination of K_2. For K_1 the O-K_1 bond lengths are going from 2.672 to 2.777 Å, these values are close to the bond length of O-K_2 (2.715 to 2.821 Å). Two intramolecular π-cation interactions between both centroid of each benzyl and $K_{1\text{-}2}$ can be observed with a distance of 3.055 and 3.103 Å respectively.

Both Si-coordination of **2-K** can be described as slightly distorted SP. Both silicates have the apical site occupied by the benzyl group, following the coordination of the previously described 2a-Na. For Si_1-C_{13} and Si_2-C_{13} the distances are 1.881 and 1.870 Å. The four basal positions of each silicates are occupied by the two oxygen atoms of two pyrocatechol ligands. This is once again underlined by the close length of all the 4 basal bond distances. Indeed, the Si_1-$O_{1\text{-}4}$ bond lengths are going from 1.737(3) to 1.757(3) Å and the Si_2-$O_{1\text{-}4}$ from 1.742(2) to 1.758(3) Å. Both Si atoms are located just a little above the plane defined by these four atoms (distance Si-plane centroid = 0.718 Å for Si_1 and 0.451 Å for Si_2), this is highlighted by the angle distortion compared to the idealized SP. With this crystal, the interaction built by multiple interactions between K and oxygen atoms from the pyrocatechol of silicates is along the a-axis.

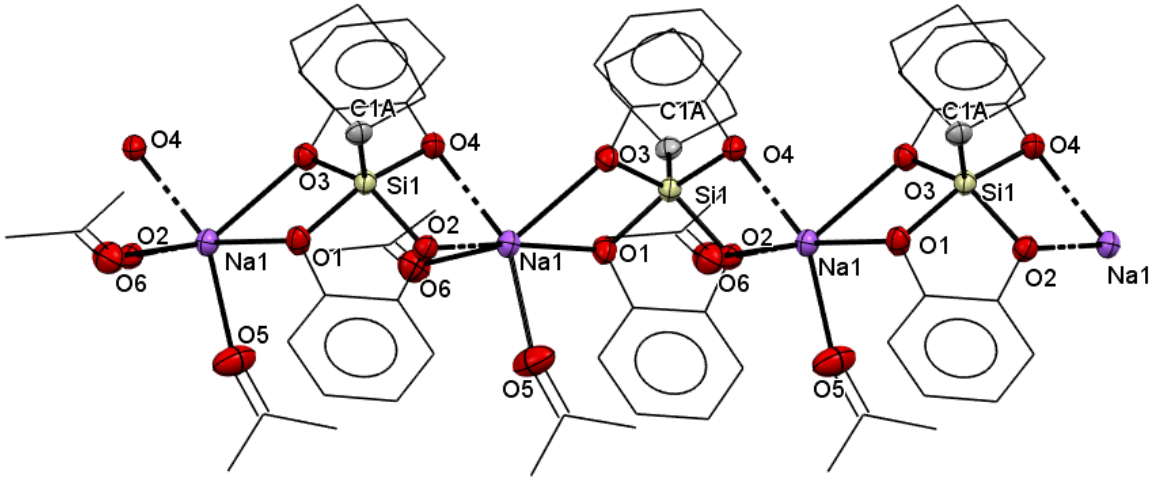

Figure 4. X-ray crystal structure of 2c-Na (view along the a-axis), thermal ellipsoids are drawn at 50% probability level. Hydrogen atoms are omitted for clarity. Dashed lines denote bonds between neighbouring silicates.

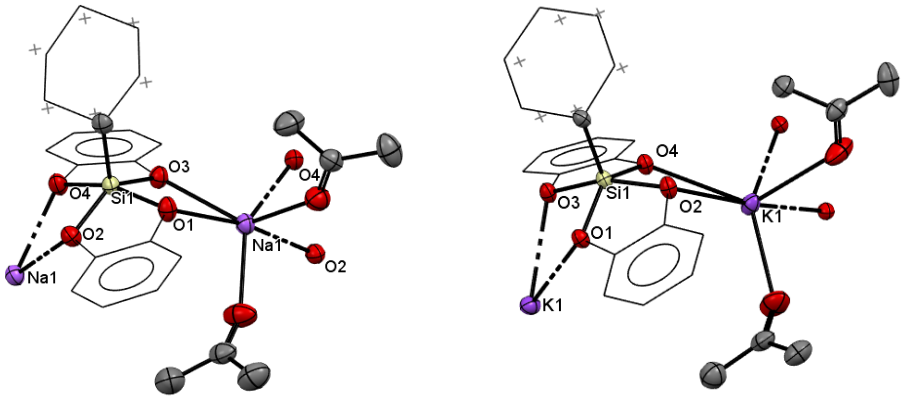

Figure 5. X-ray crystal structure of 2c-Na (left) and 2c-K (right), thermal ellipsoids are drawn at 50% probability level. Pyrocatechol ligands and cyclohexyl's carbons are drawn as wireframe for clarity/Hydrogen atoms are omitted for clarity. Dashed lines denote bonds between neighbouring silicates.

These two structures show way more than few similarities as for both benzyl silicates one. Moreover, in this case the structures seem identical. Compiled data can be found in table 1.

Table 1. Selected bond length and Structural information of benzyl silicates 2a and cyclohexyl 2c.

Structure	**2a -Na**	**2a-K**	**2c-Na**	**2c-K**
Formula	$[C_{22}H_{21}NaO_5Si]$	$C_{23.5}$ H_{24} K $O_{5.5}$ Si	C_{24} H_{31} Na O_6 Si	C_{18} H_{19} O_4 Si K
Space group	P $2_1/c$	P $2_1/c$	P b c a	P b c a
Cell lengths (Å)	a 20.1599(19) b 11.4841(11) c 21.738(3)	a 20.1599(19) b 11.4841(11) c 21.738(3)	a 20.1599(19) b 11.4841(11) c 21.738(3)	a 19.6679(4) b 11.6484(3) c 22.0285(5)
Cell angles (°)	α = β = γ = 90	α = β = γ = 90	α = β = γ = 90	α = β = γ = 90

To conclude this part, several similarities have been observed between each silicates structures depending on the moiety and the cation. The direct comparison of these structures has been possible due to the application of the same crystallisation technique. (vapor diffusion, saturated acetone / diethyl ether, in the same fridge temperature, 10°C) Several interesting properties like the 1D-polymeric unit are observed for all these species. Finally, the most surprising result is the crystallisation in the same space group of the cyclohexyl sodium and potassium.

1.3.3 Electrochemistry

The oxidation potential of these new organosilicon salts was determined in DMF using nBu_4NPF_6 as electrolyte and saturated calomel electrode as reference one. As for the previously described chelated silicates, all these unchelated silicates display an irreversible one electron oxidation of the silicates followed by a second oxidation of the catechol. For the first time, in addition to their utilisation in photoredox catalysis, comparative data on inherent oxidation properties of alkali-silicates has been exposed. (Scheme 3)

	$Na^{\oplus}$	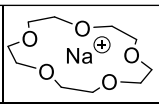	$K^{\oplus}$	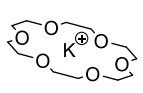
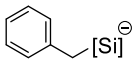	0.77 V	0.77 V	0.78 V	0.61 V
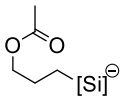	0.88 V	X	X	0.77 V
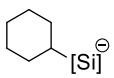	0.81 V	X	X	0.89 V

Scheme 3. Oxidation potentials (in V vs SCE) of bis-catecholato silicates. (Depicted online in the eSI of the article)

Interestingly, variation from our standard chelated potassium silicates toward free potassium or chelated/free sodium led to variation of the E_{ox}.[3] Indeed, benzyl silicate **2a** (E_{Ox} = 0.61 V) bearing the classical chelated potassium have a lower oxidative potential than the other derivatives with an unchanging increasement of 0.1V as well as for free sodium **2a-Na**, potassium **2a-K** and chelated sodium **2a'**. The same observation with 0.1V increasement can be observed with the acetoxypropyl **2b-Na** compared to **2b** (E_{ox} = 0.77 V). Regarding the cyclohexyl silicate **2c** (E_{ox} = 0.89 V), a moderate decrease of the oxidative potential is observed for the chelated sodium **2c'** (0.86V) and the free sodium **2c-Na** (0.81 V). Independently of variation, these modifications of the oxidative potential can be considered as negligible in terms of influence on the reactivity under photocatalytic conditions.

1.3.4 NMR studies

NMR data (^{1}H, ^{13}C and ^{29}Si NMR) displays several information and correlation with crystal structure analysis (exposed previously). NMR shift of all the benzyl silicates derivatives is exposed in Table 2. The ^{13}C NMR data shows the equivalence of both catechol in each of these silicates (compared to the inequivalent catechols in the cyclopropane described in chapter 1.4), resulting in the only observation of 3 distinct peaks. This phenomenon is relatively present in every silicates, arbitrary, the shift of chelated potassium (benzyl bis(catecholato) silicate) is set as reference to determine the chemical shift differences.

Table 2. Chemical shift differences ($\Delta\delta_{\text{Cation-K[18C6]}}$) for Na, K, [15C5]. Value of K[18C6] are given in ppm.

^{13}C			Benzyl	
Cation	K [18-C-6]	K	Na [15-C-5]	Na
Catechols	150.9	-0.2	±0	-0.1
	119.3	+0.1	±0	+0.1
	111.5	±0	±0	+0.1
$^{13}C_{\alpha}$-Si	27.9	-0.4	-0.3	-0.1
^{29}Si			Benzyl	
| Si |	(-) 80.90	±0	-0.1	±0
^{1}H			Benzyl	
Catechol	7.09 – 6.75 (m, 5H)	7.01 – 6.95 (m, 2H) 6.91-6.84 (m, 3H)	6.98 – 6.80 (m, 5H)	7.00 – 6.93 (m, 2H) 6.92-6.83 (m, 3H)

As for the oxidative potential or the relatively close crystal structure, only moderate shift can be observed when changing a sodium by a potassium. It must be highlighted than the signal in ^{1}H NMR of chelated

As for the oxidative potential or the relatively close crystal structure, only a moderate shift can be observed when changing sodium by a potassium. It must be highlighted that the signal in ^{1}H NMR of chelated (K[18-C-6] & Na[15-C-5]) species appears as a unique multiplet, when the non-chelated (K & Na) shows two distinct multiplets. The explanation of this modification is directly given by the X-ray structure. In both unchelated species, the π-cation interaction between the benzyl group and the cation can be observed and results in the modification of the signal. This interaction is not observed for the chelated species. The structure of chelated species shows the direct interaction between the catechol and chelated alkali (with crown-ether) when the unchelated one shows benzyl + cation + solvent interaction. Finally, a correlation with the experimental procedure can also be made. The benzyl unchelated silicate is the only one that does not crystallize in pure acetone, this could be explained by the intramolecular interaction that could complicate the organization of the observed crystallized structure (acetone + two silicates). Finally, the ^{29}Si NMR datas agree with five-coordinate silicon species.

1.3.5 Applications

Before the application of these sodium-based silicates in cross coupling reaction, we first investigated the reactivity of these derivatives in (considered) classical radical reactions.[3] (scheme 4)

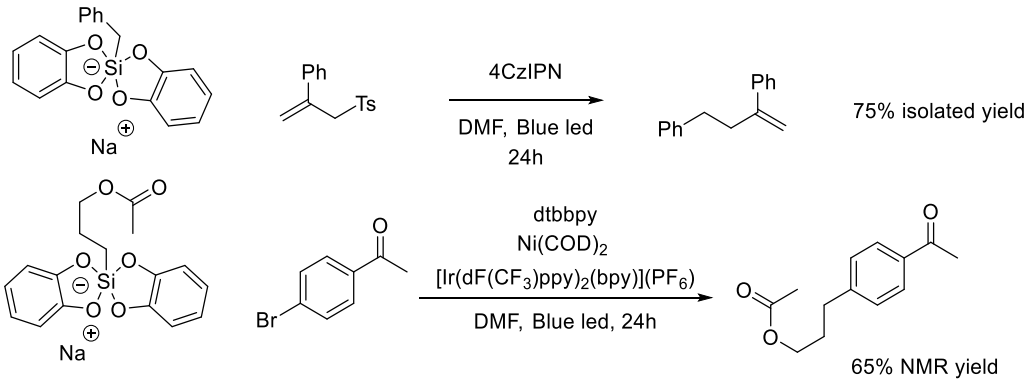

Scheme 4. Radical addition and cross-coupling using sodic silicates

In comparison with the chelated potassium silicates that respectively provided 80% for the allylation and 85% yield for the dual, the sodium derivative honourably gave 75% and 65% yield respectively. Based on these first results, the desired radical generation was established. These silicates were then used in the next methodology to establish the first comparison of alkali silicates depending on their cation.

Photoredox dual Ni catalysis application.

To compare the reactivity between each cation, le chelated free sodium and potassium benzyl silicates were synthetized in addition to the sodium chelated one as described previously. The reaction takes place at room temperature in DMF under moisture and oxygen free conditions during 48H. The photocatalyst use was 4CzIPN (1 mol%) and the nickel partner was $NiCl_2$.dme (2 mol%) wearing a dtbbpy as ligand. (2 mol %; resulting in the complexes prepared *in situ*) This reaction appears to be highly sensitive to impurities but have the main advantages to only provides a (Z) stereoisomer (Table 3).

Table 3. Optimisation of the cross-coupling reaction.

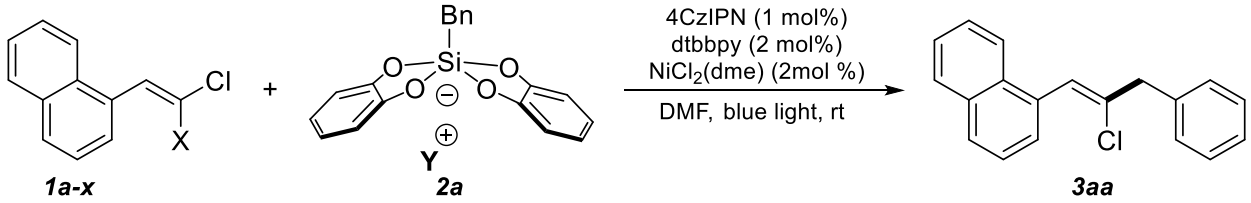

1a-x *2a* *3aa*

Entry	React. time (h)	X	Y	Silicate equiv.	Yield (%), 3aa[a]
1	48	F, **1a-F**	K[18-C-6], **2a**	1.5	NR[b]
2	48	Br, **1a-Br**	K[18-C-6], **2a**	1.5	Mixture
3	48	Cl, **1a**	K[18-C-6], **2a**	1.5	44
4	48	Cl, **1a**	K, **2a-K**	1.5	39
5	48	Cl, **1a**	Na[15-C-5], **2a'**	1.5	39
6	48	Cl, **1a**	Na, **2a-Na**	1.5	42
7	48	Cl, **1a**	K[18-C-6], **2a**	3	47
8[c]	48	Cl, **1a**	K[18-C-6], **2a**	3	51
9	72	Cl, **1a**	K[18-C-6], **2a**	1.5	50
10	72	Cl, **1a**	K[18-C-6], **2a**	3	**70**
11[d]	48	Cl, **1a**	K[18-C-6], **2a**	1.5	0

[a] NMR Yield determined using 1,3,5-trimethoxybenzene as internal standard. [b] NR: no reaction detected. [c] Variation of the concentration (from 0.1 M to 0.2 M). [d] Reaction performed without nickel catalyst.

We began our investigation by delineating the range of dihalogenostyrenes that could handle this approach (Table 3, entries 1–3). The difluorinated reagent **1a-F** did not react despite the presence of silicon on the radical precursor likely to establish a strong interaction with a fluoride. In contrast, the dibrominated reagent 1a-Br led in our conditions to a complex mixture in which only a marginal amount of monoalkylated was detected. Interestingly, only the presumably less reactive dichlorinated substrate 1a positively reacted in this dual catalysis reaction (44% of adduct **3aa**) and was then chosen as model substrate for the optimization of the reaction conditions. To our delight, the alkylation occurred selectively without any formation of side products such as the dialkylated product or the E-stereoisomer. The Z-stereochemistry of **3aa** was assigned by analogy with subsequent findings (vide infra).

We then examined the effect of the cation in this reaction. No improvement of yield was observed from free potassium silicate **2a-K** (39% of **3a**, entry 4), sodium silicates with 15-C-5 (**2a'**, 39%, entry 5) or without 15-C-5 (**2a-Na**, 42%, entry 6). Nevertheless, the fact that the plain sodium silicate **2a-Na** could be engaged successfully opened interesting perspectives. Focusing on silicate 2a, we then investigated other possibilities to increase the yield of **3aa** (Table 3). While doubling the loading in silicate (entry 7) or its concentration (entry 8) did not have a significant impact on the yield, a longer reaction time (72 h) with double amount of 2a provided the best yield of **3a** (70%, entry 10). We also checked that nickel catalysis was necessary for this transformation: no radical addition then elimination of a chlorine radical takes place to deliver **3aa** (entry 11). The nickel catalyst appears essential in the reaction mechanism. The scope was then extended with two others sodium silicate (cHex and acetoxypropyl) due to the result and the atom economy provided by the cation. Based on all the results from Table 3, the standard conditions (48 h and 1.5 equiv. of silicate) appear to be a good compromise in terms of reaction time and cost to reach a decent yield in this cross-coupling reaction. Subsequently, we engaged under those conditions various [18-C-6]-potassium and sodium silicates **2** and **2-Na** with α,α-dichlorostyrenes 1 under the Ni/4CzIPN dual catalysis conditions to explore the scope of this reactivity (Scheme 2).

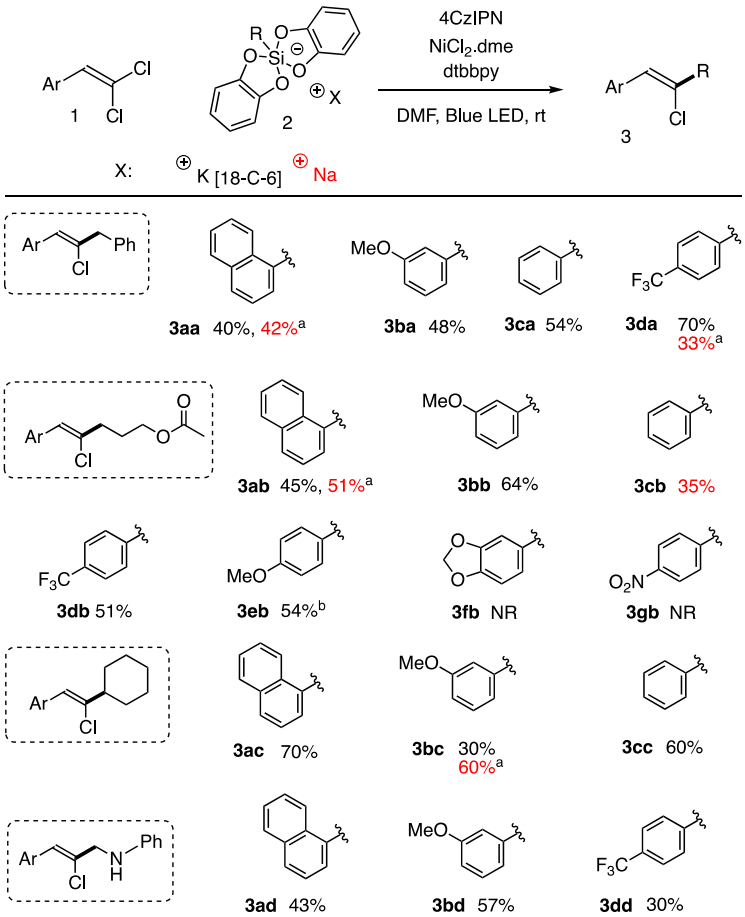

Scheme 5. Reaction scope

Because we know that nickel is necessary in these reactions to obtain products 3 and based on the literature mechanism proposals of related Ni/photoredox dual catalysis reactions,[4-7] it appears reasonable to invoke the trapping by nickel of a C-centered radical originating from the photo-induced oxidation of the silicates 2. The nickel intermediate that would be involved is the nickel(II) complex I that originates from the oxidative addition into the alpha C-Cl bond of the substrates 1 (Scheme 3). The observed (Z)-selectivity might be ascribed to the presence of the bidentate ligand on nickel that would generate a significant steric hindrance around the metallic center and that possibly orients the oxidative addition on the more accessible C-Cl bond, with no aryl group in syn. Even though the effect of the bulkiness around the metallic center seems clear, the insensitivity of the coupling to the substituent on the aryl moiety might appear strange but is reminiscent of previous findings in arylative couplings.[9,10] This would be consistent with a radical addition on nickel(II) that is rather insensitive to electronic effects.[11-14] The resulting nickel(III) complex II then undergoes reductive elimination to provide products 3 and a nickel(I) salt that would be reduced by the photoredox cycle to Ni(0).

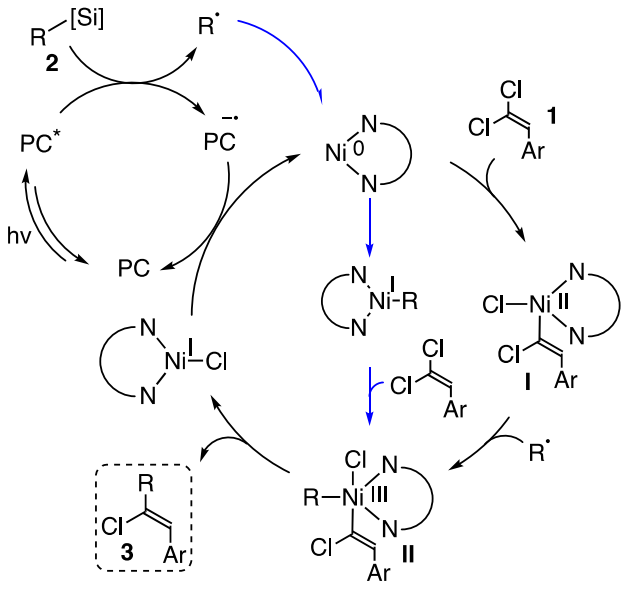

1.3.6 Conclusion

The synthesis of several new silicates derivatives was achieved allowing the comparison of several properties and reactivity depending on the cation. Silicates bearing sodium cation appear as valuable candidates for the use of silicates in a greener fashion, indeed, due to their lower molecular mass and similar reactivity compared to classical chelated bis(catecholato) silicate. These derivatives have been stored without further degradation for over 1 year (dark, argon). These non-volatile powders also appears easy to handle and engage in photochemical reaction.

References part 1.3

[1] A. Boudin, G. Cerveau, C. Chuit, R. J. P. Corriu, C. Reye, *Bull. Chem. Soc. Jpn* **1988**, *61*, 101–106.

[2] *As described in Chapter 1.1*

[3] V. Corcé, L.-M. Chamoreau, E. Derat, J.-P. Goddard, C. Ollivier, L. Fensterbank, *Angew. Chem. Int. Ed.* **2015**, *54*, 11414–11418.

[4] Nacsa, E. D.; MacMillan, D. W. C. *Org. React.* 2019; pp 471–546.

[5] Skubi, K. L.; Blum, T. R.; Yoon, T. P. *Chem. Rev.* **2016**, *116*, 10035

[6] Tellis, J. C.; Kelly, C. B.; Primer, D. N.; Jouffroy, M.; Patel, N. R.; Molander, G. A. *Acc. Chem. Res.* **2016**, *49*, 1429.

[7] Tasker, S. Z.; Jamison, T. F. *J. Am. Chem. Soc.* **2015**, *137*, 9531.

[8] Lévêque, C.; Chenneberg, L.; Corcé, V.; Goddard, J.-P.; Ollivier, C.; Fensterbank, L. *Org. Chem. Front.* 2016, *3*, 462.

[9] Jouffroy, M.; Primer, D. N.; Molander, G. A. *J. Am. Chem. Soc.* **2016**, *138*, 475.

[10] Durandetti, M.; Nédélec, J.-Y.; Périchon, J. *J. Org. Chem.* **1996**, *61*, 1748.

[11] Weix, D. J. *Acc. Chem. Res.* **2015**, *48*, 1767.

[12] Richmond, E.; Moran, J. *Synthesis* **2018**, *50*, 499.

[13] Lévêque, C.; Ollivier, C.; Fensterbank, L. in *Nickel Catalysis in Organic Synthesis* Edt Ogoshi, S. Wiley **2020**, pp 151-181

[14] Goldfogel, M. J.; Huang, L.; Weix, D. J. *ibid*. pp 183-222.

Supporting information

Unless otherwise noted, reactions were carried out under an argon atmosphere in oven-dried glassware. Methanol was distillated over CaH_2 and DMF was dried with a PureSolv solvent purification system from Innovative Technology. Catechol was purchased from commercial source and purified by crystallization from chloroform. Reagents and chemicals were purchased from commercial sources and used as received. Infrared (IR) spectra were recorded on a Bruker Tensor 27 (ATR diamond) spectrophotometer. Melting points were determined on a melting point apparatus SMP3 (Stuart scientific). Electrochemical measurements were carried out an Origaflex (Origalys) electrochemical workstation. ^{1}H, ^{13}C and ^{19}F NMR spectra were recorded at room temperature at 400, 100 and 376 MHz respectively, on 400 MHz Bruker AVANCE I spectrometer and at 300, 75 and 282 MHz respectively, on 300 MHz Bruker AVANCE II spectrometer. ^{29}Si NMR pectra were recorded at room temperature at 79 MHz on 400 MHz Bruker AVANCE I spectrometer. Chemical shifts (δ) are reported in ppm and coupling constants (J) are given in Hertz (Hz). Abbreviations used for peak multiplicity are: s (singlet); bs (broad singlet); d (doublet); t (triplet); q (quartet); quint (quintet); sept (septet); m (multiplet) etc. Thin layer chromatographies (TLC) were performed on Merck silica gel 60 F 254 and revealed with a UV lamp (λ = 254 nm) and $KMnO_4$ staining. Flash Column Chromatographies were conducted on Silica gel 60 M**,** 0.04**–**0.063 mm, from Macherey Nagel. High resolution mass spectrometries were performed on a microTOF (ESI). All the solvents used in flash chromatography (toluene, petroleum ether, pentane and Et_2O) were distillated.

General procedure 1. Synthesis of the silicates

Synthesis of [18-crown-6] bis(catecholato)-alkylsilicate

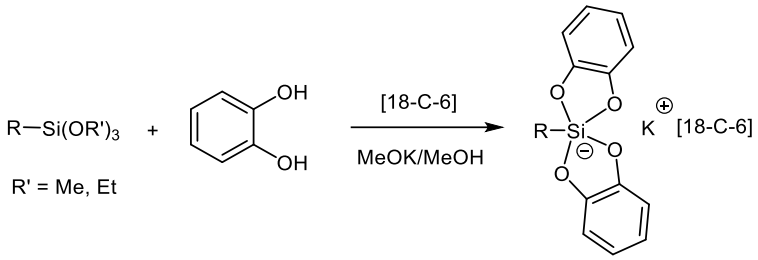

To a stirred solution of catechol (2 equiv.) in dry methanol (0.25 M) was added 18-Crown-6 [18-C-6] (1 equiv.). After dissolution of the crown ether, the trialkoxyorganosilane (1 equiv.) was added followed by a solution of potassium methoxide in methanol (1 equiv.). The reaction mixture was stirred for 3 hours and the solvent was removed under reduced pressure. The residue was dissolved in a minimum volume of acetone and diethyl ether was added until a cloudy solution was obtained (scrapping on the edge of the flask could be done to induce crystallization). The flask was placed at -20°C overnight. The crystals were collected by filtration under air, washed with diethyl ether and dried under vacuum to afford [18-C-6] potassium silicate.[1]

Synthesis of sodium or potassium bis(catecholato)-alkyl silicate

All manipulations were performed following the conventional Schlenk techniques.

In a dry Schlenk tube under argon covered with aluminium fold was added catechol (2 equiv.) and the Schlenk was purged. Degassed MeOH (0.25 M) was added followed by the alkyltriethoxysilane (1 equiv.). A solution of sodium or potassium methoxide in methanol (1 equiv.) was added dropwise and the reaction was stirred 3 hours at room temperature. Solvent was removed directly on the Schlenk line and the crude was dry under high vacuum until a powder was obtained. Silicate was purified by recrystallisation as mentioned for each silicate. The crystals were collected by filtration under argon flux, washed with degassed diethyl ether and dried under vacuum to afford the desired silicate.

[1] Corcé, V.; Chamoreau, L. M.; Derat, E.; Goddard, J.-P.; Ollivier, C.; Fensterbank, L. *Angew. Chem. Int. Ed.* **2015**, *54*, 11414.

General procedure 2. Synthesis of β,β-dihalostyryls

Synthesis of β,β-dichlorostyryl derivatives

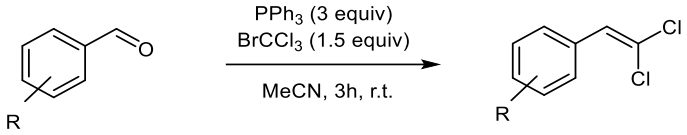

In a round-bottom-flask was added the aldehyde (1.0 equiv.) in MeCN (0.125 M). The reaction mixture was cooled with an ice bath to 0°C and $BrCCl_3$ (1.5 equiv.) was added, followed by addition of a solution of triphenylphosphine (3.0 equiv) in a minimum amount of MeCN. The reaction mixture was stirred at room temperature for 3 hours then the solvent was removed under reduced pressure to afford a crude residue. This residue was dissolved in dichloromethane (0.25 M) and the organic phase was washed with water, brine and dried over $MgSO_4$. The solvent was removed under reduced pressure and the residue purified on a pad of silica (elution with a mixture Et_2O:*n*-pent (1:9)) , giving the pure material.

Synthesis of β,β-dibromostyryl derivatives

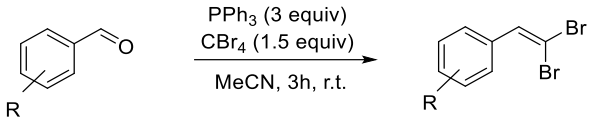

In a round-bottom-flask was added the aldehyde (1.0 equiv.) in MeCN (0.125 M). The reaction mixture was cooled with an ice bath to 0°C and CBr_4 (1.5 equiv.) was added, followed by addition of a solution of triphenylphosphine (3.0 equiv.) in a minimum amount of MeCN. The reaction mixture was stirred at room temperature for 3 hours then the solvent was removed under reduced pressure to afford a crude residue. This residue was dissolved in dichloromethane (0.25 M) and the organic phase was washed with water, brine and dried over $MgSO_4$. The solvent was removed under reduced pressure and the residue purified on a pad of silica (Et_2O:*n*-pentane) , giving the pure material.

Synthesis of β,β-difluorostyryl derivatives

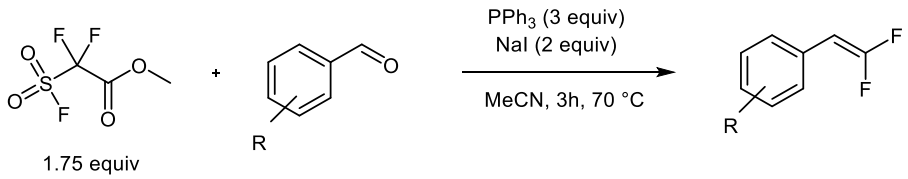

In a two-neck round-bottom-flask was added the aldehyde (1.0 equiv), NaI (2 equiv.) and PPh_3 (3.0 equiv.) in MeCN (0.5 M). The reaction mixture was heated at 70°C for 30 minutes then methyl 2,2-difluoro-2-(fluorosulfonyl)acetate (1.75 equiv.) was added over 10 minutes. The reaction mixture was stirred at 70°C for 3 hours then water was added and the resulting solution was extracted with Et_2O (3 times), dried over $MgSO_4$, filtered and concentrated *in vacuo*. The obtained residue was purified by column chromatography (*n*-pentane).

General procedure 3. Photoredox/nickel cross-coupling dual catalysis with the β,β-dihalogenostyryl derivative

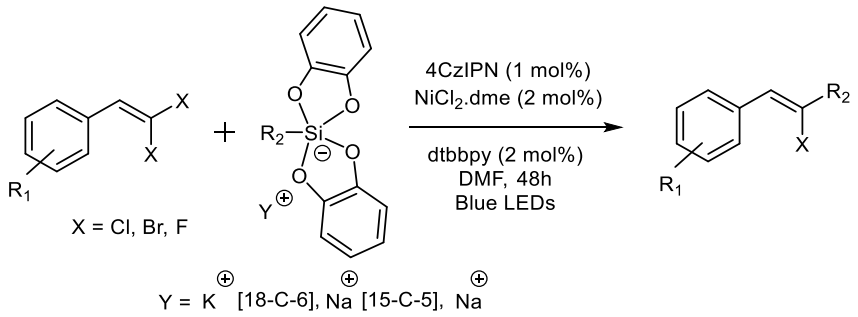

To a Schlenk tube was added the β,β-dihalostyryl derivative (1 equiv.), the appropriate silicate (1.5 equiv.), 4CzIPN (1 mol %) and 4,4′-di-tertbutyl-2,2′-bipyridine (2 mol %). The Schlenk tube was then charged with $NiCl_2$.dme (2 mol %) into a glovebox, sealed with a rubber septum, removed from the glovebox, and evacuated/purged with vacuum/argon three times. Degassed DMF (0.1 M) was introduced (with the β,β-dihalostyryl derivative if it is a liquid) and the reaction mixture was irradiated with blue LEDs (477 nm) for 48 hours. The reaction mixture was diluted with diethyl ether, washed with saturated $NaHCO_3$ (2 times), brine (2 times), dried over $MgSO_4$ and evaporated under reduced pressure. The residue was purified by flash column chromatography on silica gel to afford the cross-coupling product.

General procedure 4. Continuous flow photoredox/nickel cross-coupling dual catalysis

A solution of 1-(2,2-dichlorovinyl)naphthalene 1a (0.21 mmol, 47.3 mg) with potassium [18-C-6] bis(catecholato)-cyclohexylsilicate 2c (0.32 mmol, 193 mg), 4CzIPN (1 mol %, 0.002 mmol, 1.73 mg), 2,2′-di-tert-butyl-bipyridine (2 mol %, 0.004 mmol, 1 mg) and $NiCl_2$.dme (2 mol %, 0.004 mmol, 0.93 mg) prepared in glovebox in degassed DMF (1 mL) was pumped by a syringe pump (KDScience, model KDS-100-CE) with a flow rate of 1.2 mL/h for the experiment with a residence time of 50 min (Experiment in Red) and 0.67 mL/h for a residence time of 90 min (Experiment in Blue). The mixture was mixed within a glass milli-mixer (LTF-MX, 0.2 mL at room temperature, Little Things Factory, Germany) under blue LED irradiation (477 nm) and then flowed through a PTFE tubing (1/16" tubing, 2 m, 1 mL at room temperature) under blue LED irradiation (477 nm). The mixer and the PTFE tubing were rinsed with degassed DMF prior to use. The residence time was calculated with the total reaction volume and the total flow rate. The reaction mixture was then collected, diluted with diethyl ether, washed with an aqueous saturated K_2CO_3 solution (2 times), brine (2 times), dried over $MgSO_4$ and evaporated.

Characterization

Potassium [18-Crown-6] bis(catecholato)-benzylsilicate 2a

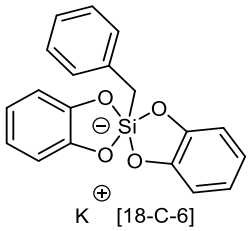

The silicate 2a was synthesized as described in General procedure 1.1. The spectroscopic data are in agreement with those reported in the literature.[1] ^{1}H NMR (400 MHz, Methanol-d4): δ 7.09 – 6.75 (m, 5H), 6.66 – 6.60 (m, 4H), 6.56 – 6.49 (m, 4H), 3.55 (s, 24H), 2.14 (s, 2H). ^{13}C NMR (100 MHz, Methanol-d4): δ 150.9 (4 C), 142.8, 129.8 (2 C), 128.2 (2 C), 123.9, 119.3 (4 C), 111.5 (4 C), 71.3 (12 C), 27.9.

Potassium [18-Crown-6] bis(catecholato)-acetoxypropylsilicate 2b

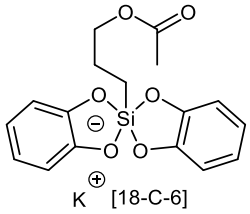

The silicate 2b was synthesized as described in General procedure 1.1. The spectroscopic data are in agreement with those reported in the literature.[2] ^{1}H NMR (400 MHz, Methanol-d4): δ 6.68 (dd, J = 5.6, 3.5 Hz, 4H), 6.56 (dd, J = 5.6, 3.5 Hz, 4H), 3.88 (t, J = 7.0 Hz, 2H), 1.92 (s, 3H), 1.66 – 1.56 (m, 2H), 0.70 – 0.65 (m, 2H). ^{13}C NMR (100 MHz, Methanol-d4): δ 173.1, 150.9 (4 C), 119.3 (4 C), 111.5 (4 C), 71.2 (12 C), 68.6, 24.9, 20.8, 13.9.

Potassium [18-Crown-6] bis(catecholato)-cyclohexylsilicate 2c

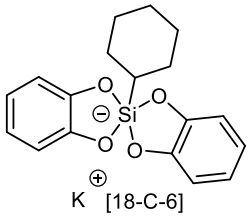

The silicate 2c was synthesized as described in General procedure 1.1. The spectroscopic data are in agreement with those reported in the literature and the X-ray crystal structure was previously determined. ^{1}H NMR (400 MHz, Methanol-d4): δ 6.72 – 6.60 (m, 4H), 6.57 – 6.49 (m, 4H), 3.53 (s, 24H), 1.69 – 1.48 (m, 5H), 1.34 – 1.02 (m, 5H), 0.84 (tt, J = 12.2, 3.1 Hz, 1H). ^{13}C NMR (100 MHz, Methanol-d4): δ 151.5 (4 C), 119.0 (4 C), 111.2 (4 C), 71.2 (12 C), 31.4, 29.6 (2 C), 29.4 (2 C), 28.3.

[2] Lévêque, C.; Chenneberg, L.; Corcé, V.; Goddard, J.-P.; Ollivier, C.; Fensterbank, L. *Org. Chem. Front.* **2016**, *3*, 462.

Potassium [18-Crown-6] bis(catecholato)-anilinomethylsilicate 2d

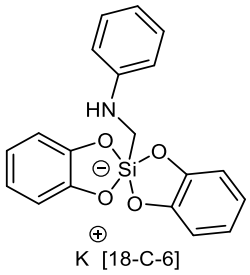

The silicate 2d was synthesized as described in General procedure 1.1. The spectroscopic data are in agreement with those reported in the literature.[1] ^{1}H NMR (400 MHz, Methanol-d4): δ 7.27 – 6.90 (m, 2H), 6.87 – 6.71 (m, 4H), 6.70 – 6.54 (m, 4H), 6.55 – 6.39 (m, 3H), 3.56 (s, 24H), 2.52 (s, 2H), NH is missing. ^{13}C NMR (100 MHz, Methanol-d4): δ 152.2, 150.8 (4 C), 129.8 (2 C), 119.7 (4 C), 117.0, 113.4 (2 C), 111.9 (4 C), 71.3 (12 C), 34.1.

Sodium bis(catecholato)-benzylsilicate 2a-Na

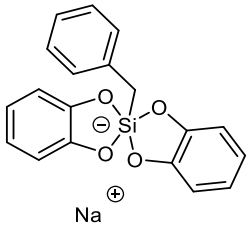

The silicate 2a-Na was synthesized as described in General procedure 1.2 with catechol (5 mmol, 0.55 g), benzyltriethoxysilane (2.5 mmol, 0.64 g), MeOH (10 mL), NaOMe in MeOH (2.5 mmol, 1.66M). Recrystallisation was done from acetone using diethyl ether as anti-solvent affording 1.37 mmol (0.49 g, 55%) of the desired silicate 2a-Na as a white powder. ^{1}H NMR (400 MHz, Methanol-d4): δ 7.00 – 6.93 (m, 2H), 6.92-6.83 (m, 3H), 6.73 – 6.66 (m, 4H), 6.62 – 6.52 (m, 4H), 2.18 (s, 2H). ^{13}C NMR (100 MHz, Methanol-d4): δ 150.6 (4 C), 142.7, 129.7 (2 C), 128.2 (2 C), 123.9, 119.4 (4 C), 111.6 (4 C), 27.5. ^{29}Si NMR (79 MHz, Methanol-d4): δ -80.90. HRMS: calc. for $C_{19}H_{15}O_4SiNa_2$ 381.0530; found 381.0529. M.p. >350°C.

Potassium bis(catecholato)-benzylsilicate 2a-K

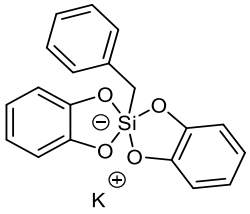

The silicate 2a-K was synthesized as described in General procedure 1.2. with catechol (5 mmol, 0.55 g), benzyltriethoxysilane (2.5 mmol, 0.64 g), MeOH (10 mL), KOMe in MeOH (2.5 mmol, 3.56 M). Recrystallisation was done from acetone using diethyl ether as anti-solvent affording 1.35 mmol (0.5 g, 54%) of the desired silicate 2a-K as a grey powder. *Note: Exposing the silicate to air before drying turn the powder darker.* ^{1}H NMR (400 MHz, Methanol-d4): δ 7.01 – 6.95 (m, 2H), 6.91-6.84 (m, 3H), 6.73 – 6.67 (m, 4H), 6.62 – 6.57 (m, 4H), 2.18 (s, 2H). ^{13}C NMR (100 MHz,

Methanol-d4): δ 150.7 (4 C), 142.9, 129.7 (2 C), 128.2 (2 C), 123.9, 119.4 (4 C), 111.5 (4 C), 71.3 (12 C), 27.5. ^{29}Si NMR (79 MHz, Methanol-d4): δ -80.90. HRMS: calc. for $C_{19}H_{15}O_4Si$ 335.0745; found 335.0741. M.p. >350°C.

Sodium [15-crown-5] bis(catecholato)-benzylsilicate 2a'

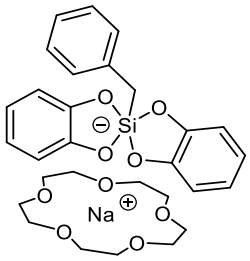

The silicate 2a' was synthesized as described in General procedure 1.2. with catechol (8 mmol, 0.88 g), benzyltriethoxysilane (4 mmol, 1 g), MeOH (16 mL), 15-C-5 (4 mmol, 790 µL) that was added before NaOMe in MeOH (4 mmol, 1.66 M). Recrystallisation was done from acetone affording 1.6 mmol (0.92 g, 45%) of the desired silicate 2a' as a white powder. ^{1}H NMR (400 MHz, Methanol-d4): δ 6.98 – 6.80 (m, 5H), 6.68 – 6.62 (m, 4H), 6.59 – 6.53 (m, 4H), 3.65 (s, 20H), 2.17 (s, 2H). ^{13}C NMR (100 MHz, Methanol-d4): δ 150.9 (4 C), 142.7, 129.8 (2 C), 128.2 (2 C), 123.9, 119.3 (4 C), 111.5 (4 C), 69.9 (10 C), 27.8. ^{29}Si NMR (79 MHz, Methanol-d4): δ -80.80. HRMS: calc. for $C_{19}H_{15}O_4Si$ 335.0745; found 335.0743. M.p. 238°C (decomp.).

Sodium bis(catecholato)-acetoxypropylsilicate 2b-Na

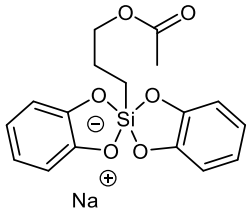

Following general procedure 1.2. with catechol (10 mmol, 1.1 g), acetoxypropyltrimethoxysilane (5 mmol, 1.1 g), MeOH (20 mL), NaOMe in MeOH (5 mmol, 1.66 M). Recrystallisation was done from acetone using diethyl ether as anti-solvent affording 3.2 mmol (1.17 g, 64%) of the desired silicate 2b-Na as a white powder. ^{1}H NMR (400 MHz, Methanol-d4): δ 6.77 – 6.69 (m, 4H), 6.63 – 6.57 (m, 4H), 3.91 (t, J = 7.0 Hz, 2H), 1.95 (s, 3H), 1.69 – 1.59 (m, 2H), 0.73 – 0.65 (m, 2H). ^{13}C NMR (100 MHz, Methanol-d4): δ 173.3, 150.6 (4 C), 119.4 (4 C), 111.6 (4 C), 68.5, 24.7, 20.8, 13.5. ^{29}Si NMR (79 MHz, Methanol-d4): δ -76.36. HRMS: calc. for [$C_{17}H_{17}O_6SiNa_2$] 391.0584; found 345.0584. M.p. 300°C (decomp.).

Sodium bis(catecholato-)cyclohexylsilicate 2c-Na

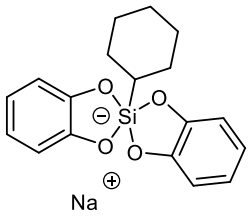

Following general procedure 1.2. with catechol (10 mmol, 1.1 g), cyclohexyltrimethoxysilane (5 mmol, 1.02 g), MeOH (20 mL), NaOMe in MeOH (5 mmol, 1.66 M). Recrystallisation was done from acetone affording 2.75 mmol (0.96 g, 55%) of the desired silicate 2c-Na as a white powder. ^{1}H NMR (300 MHz, Methanol-d4): δ 6.73 – 6.69 (m, 4H), 6.60 – 6.55 (m, 4H), 1.68 – 1.54 (m, 5H), 1.30 – 1.05 (m, 5H), 0.87 (tt, J = 12.0, 3.0 Hz, 1H). ^{13}C NMR (100 MHz, Methanol-d4): δ 151.3 (4 C), 119.1 (4 C), 111.2 (4 C), 31.2, 29.6 (2 C), 29.3 (2 C), 28.2. ^{29}Si NMR (79 MHz, Methanol-d4): δ -77.75. HRMS: calc. for $C_{18}H_{19}O_4SiNa_2$ 373.0843; found 373.0842. M.p. > 350°C.

Synthesis of the dihalostyryl derivatives

1-(2,2-Difluorovinyl)naphthalene (1a-F)

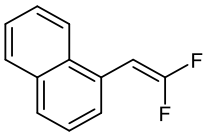

The difluoro-styryl derivative 1a-F was synthesized as described in General procedure 2.3. The spectroscopic data are in agreement with those reported in the literature.[3] ^{1}H NMR (300 MHz, $CDCl_3$): δ 8.01 – 7.76 (m, 3H), 7.64 – 7.44 (m, 4H), 5.88 (dd, J = 24.3, 3.0 Hz, 1H). ^{13}C NMR (75 MHz, $CDCl_3$): δ 156.8 (dd, J= 7.7 and 286.5 Hz), 133.8, 131.6 (d, J = 3.4 Hz), 128.8, 128.1, 126.5–126.7 (m, 2C), 126.4, 125.6, 125.1, 123.9, 78.8 (dd, J= 286.7 and 294.3 Hz). ^{19}F NMR (282 MHz, $CDCl_3$): δ -84.9 – -85.1 (m), -83.1 – -83.3 (m).

1-(2,2-dibromovinyl)naphthalene (1a-Br)

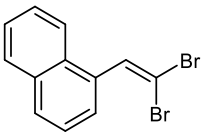

The gem-dibromo-styryl derivative 1a-Br was synthesized as described in General procedure 2.2. The spectroscopic data are in agreement with those reported in the literature.[4] ^{1}H NMR (300 MHz, $CDCl_3$): 7.99-7.84 (m, 4H), 7.64 (d, J =

[3] Zhang, B.; Zhang, X.; Hao, J.; Yang, C. *Eur. J. Org. Chem.* **2018**, 5007.
[4] Ma, X.; Herzon, S. B. *J. Org. Chem.* **2016**, *81*, 8673.

6.9 Hz, 1H), δ 7.60-7.46 (m, 3H). ^{13}C NMR (75 MHz, $CDCl_3$): δ 136.0, 133.6, 133.3, 130.8, 129.0, 128.7, 126.9, 126.7, 126.3, 125.4, 124.3, 93.0.

1-(2,2-dichlorovinyl)naphthalene (1a)

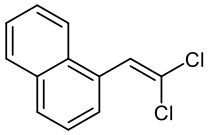

The gem-dichloro-styryl derivative 1a was synthesized as described in General procedure 2.1. The spectroscopic data are in agreement with those reported in the literature.[5] ^{1}H NMR (400 MHz, $CDCl_3$): δ 7.89-7.84 (m, 2H), 7.65-7.63 (m, 1H), 7.54-7.49 (m, 3H), 7.36 (s, 1H). ^{13}C NMR (100 MHz, $CDCl_3$): δ 133.4, 131.1, 130.8, 128.9, 128.6, 127.0, 126.9, 126.6, 126.2, 125.2, 124.0, 123.5.

1-(2,2-dichlorovinyl)-3-methoxybenzene (1b)

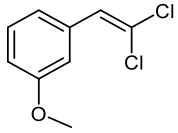

The gem-dichloro-styryl derivative 1b was synthesized as described in General procedure 2.1. The spectroscopic data are in agreement with those reported in the literature.[5] ^{1}H NMR (400 MHz, $CDCl_3$): δ 7.29-7.26 (m, 1H), 7.12-7.08 (m, 2H), 6.89-6.86 (m, 1H), 6.84 (s, 1H), 3.82 (s, 3H). ^{13}C NMR (100 MHz, $CDCl_3$): δ 159.5, 134.6, 129.5, 128.5, 128.5, 121.3, 114.2, 114.0, 55.3.

2,2-dichlorostyrene (1c)

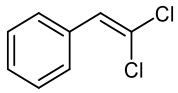

The gem-dichloro-styryl derivative 1c was synthesized as described in General procedure 2.1. The spectroscopic data are in agreement with those reported in the literature.[5] ^{1}H NMR (400 MHz, $CDCl_3$): δ 7.61 – 7.51 (m, 2H), 7.48 – 7.34 (m, 4H), 6.89 (s, 1H). ^{13}C NMR (100 MHz, $CDCl_3$): δ 133.4, 128.6 (2C), 128.6, 128.5, 128.4 (2C).

1-(2,2-dichlorovinyl)-4-(trifluoromethyl)benzene (1d)

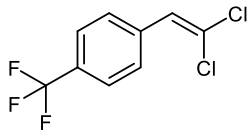

The gem-dichloro-styryl derivative 1d was synthesized as described in General procedure 2.1. The spectroscopic data are in agreement with those reported in the literature.[6] ^{1}H NMR (400 MHz, $CDCl_3$): δ 7.63 (m, 4H), 6.90 (s, 1H). ^{13}C

[5] Ranu, B. C.; Samanta, S.; Das, A. *Tetrahedron Lett.* **2002**, *43*, 5993.
[6] Semba, K.; Kameyama, R.; Nakao, Y. *Chem. Lett.* **2018**, *47*, 213.

NMR (75 MHz, $CDCl_3$): δ 137.0 (q, J =1.5 Hz, 1C), 130.4 (q, J = 32.5 Hz, 1C), 129.0 (2C), 127.5 (1C), 125.5 (q, J = 3.5 Hz, 2C), 123.7 (1C), 123.0 (q, J = 270.4 Hz, 1C). ^{19}F NMR (376 MHz, $CDCl_3$): δ -62.8.

1-(2,2-dichlorovinyl)-4-methoxybenzene (1e)

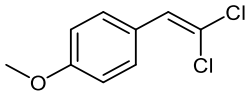

The gem-dichloro-styryl derivative 1e was synthesized as described in General procedure 2.1. The spectroscopic data are in agreement with those reported in the literature.[5] ^1H NMR (400 MHz, $CDCl_3$): δ7.50 (d, J = 8.8 Hz, 2H), 6.90 (d, J = 8.8 Hz, 2H), 6.79 (s, 1H), 3.83 (s, 3H). ^{13}C NMR (100 MHz, $CDCl_3$): δ159.7, 130.2 (2C), 128.2, 126.1, 118.9, 114.0 (2C), 55.4.

5-(2,2-dichlorovinyl)benzo[d][1,3]dioxole (1f)

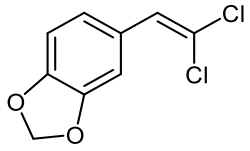

The gem-dichloro-styryl derivative 1f was synthesized as described in General procedure 2.1 The spectroscopic data are in agreement with those reported in the literature.[7]

1-(2,2-dichlorovinyl)-4-nitrobenzene (1g)

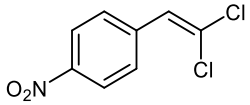

The gem-dichloro-styryl derivative 1g was synthesized as described in General procedure 2.1 The spectroscopic data are in agreement with those reported in the literature.[8] ^1H NMR (400 MHz, $CDCl_3$): δ 6.95 (s, 1H), 7.71 (d, J = 8.0 Hz, 2H), 8.25 (d, J = 8.0 Hz, 2H) ppm. ^{13}C NMR (75 MHz, $CDCl_3$): δ 123.9 (2C), 125.4, 126.9, 129.5 (2C), 139.7, 147.3.

Photoredox/nickel cross-coupling dual catalysis with the β,β-dichlorostyryl

(Z)-1-(2-chloro-2-benzyl)naphthalene (3aa)

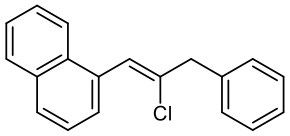

Following General procedure 3 with 1-(2,2-dichlorovinyl)naphthalene (0.32 mmol, 71 mg), potassium [18-Crown-6] bis(catecholato)-benzylsilicate (0.45 mmol, 280 mg). The crude product was purified by flash column chromatography (Et_2O:*n*-pentane From 0/100 to 2/98) to afford (Z)-1-(2-chloro-2-benzyl)naphthalene (3aa) (33.5 mg, 40%) as a colorless oil. ^1H NMR (400 MHz, $CDCl_3$): δ 7.93 -7. 84 (m, 2H), 7.81 (d, J = 8.2 Hz, 1H), 7.67 (dt, J = 7.1 Hz, 1.2

[7] Saputra, M. A.; Ngo, L.; Kartika, R. *J. Org. Chem.* **2015**, *80*, 8815.
[8] Newman, S. G.; Brian, C. S.; Perez, D.; Lautens, M. *Synthesis* **2011**, *2*, 342.

Hz, 1H), 7.53-7.45 (m, 3H), 7.44-7.40 (m, 4H), 7.36-7.30 (m, 1H), 7.00 (s, 1H), 3.95 (s, 2H). ^{13}C NMR ($CDCl_3$, 100 MHz): δ 137.3, 136.3, 133.5, 132.4, 131.5, 129.2 (2C), 128.7 (2C), 128.6, 128.1, 127.2, 127.1, 126.1, 125.8, 125.2, 124.4, 124.3, 46.7. HRMS: calc. for $C_{19}H_{15}Cl$ 279.0935; found 279.0933.

(Z)-4-chloro-5-(3-methoxyphenyl)benzyl (3ba)

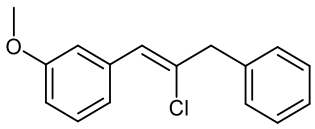

Following General procedure 3 with 1-(2,2-dichlorovinyl)-3-methoxybenzene (0.32 mmol, 64.2 mg) and potassium [18-Crown-6] bis(catecholato)-benzyl silicate (0.45 mmol, 280 mg). The crude product was purified by flash column chromatography (Et_2O:*n*-pentane 2/98) to afford (Z)-4-chloro-5-(3-methoxyphenyl)benzyl (3ba) (38 mg, 48%) as a pale brown oil. ^1H NMR (300 MHz, $CDCl_3$): δ 7.43 – 7.27 (m, 6H), 7.24 (t, J = 2.1 Hz, 1H), 7.18 (d, J = 7.7 Hz, 1H), 6.89 – 6.81 (m, 1H), 6.55 (s, 1H), 3.84 (s, 3H), 3.82 (s, 2H). ^{13}C NMR (75 MHz, $CDCl_3$): δ 159.4, 137.3, 136.2, 133.7, 129.1 (d, J = 1.9 Hz), 128.6, 127.0, 125.8, 121.8, 114.3, 113.6, 55.3, 47.4. HRMS: calc. for $C_{16}H_{15}ClO$ 259.0884; found 259.0883.

Z-[2-chloro-1-propene-1,3-diyl]bisbenzene (3ca)

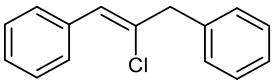

Following General procedure 3 with (2,2-dichlorovinyl)-benzene (0.32 mmol, 55.4 mg) and potassium [18-Crown-6] bis(catecholato)-benzyl silicate (0.45 mmol, 280 mg). The crude product was purified by flash column chromatography (Toluene) to afford the cross-coupling product Z-[2-chloro-1-propene-1,3-diyl]bisbenzene (3ca) (35.7 mg, 54 %). Geometry of the double bond was determined by NOESY experiment. All the spectroscopic data agree with the literature.[7] ^1H NMR (400 MHz, $CDCl_3$): δ 7.62 (dd, J = 7.5, 1.7 Hz, 2H), 7.42 – 7.23 (m, 7H), 6.56 (s, 1H), 3.82 (s, 2H). ^{13}C NMR (100 MHz, $CDCl_3$): δ 137.3, 135.0, 133.4, 129.1 (2C), 129.1 (2C), 128.6 (2C), 128.2 (2C), 127.7, 127.0, 125.9, 47.3. HRMS: Calc. for $C_{15}H_{13}Cl$ 228.0700; found 228.0699.

(Z)-1-(2-chloro-3-phenylprop-1-en-1-yl)-4-(trifluoromethyl)benzene (3da)

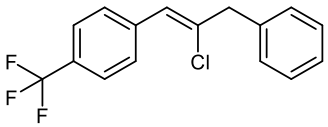

Following General procedure 3 with 1-(2,2-dichlorovinyl)-3-(trifluoromethyl)benzene (0.32 mmol, 76 mg) and potassium [18-Crown-6] bis(catecholato)-benzylsilicate (0.45 mmol, 288 mg). The crude product was purified by flash column chromatography (Toluene:*n*-pentane From 0/100 to 10/90) to afford (Z)-1-(2-chloro-3-phenylprop-1-en-1-yl)-4-(trifluoromethyl)benzene (3ad) (64.3 mg, 70%) as a pale oil. ^1H NMR ($CDCl_3$, 400 MHz): δ 7.70-7.66 (d, J = 8 Hz, 2H), 7.61-7.59 (d, J = 8 Hz, 2H), 7.40-7.35 (m, 2H), 7.32-7.27 (m, 3H), 6.55 (s, 1H), 3.83 (s, 2H). ^{13}C NMR ($CDCl_3$, 100 MHz): δ 138.5, 136.8, 136.0, 129.3 (2C), 129.1 (2C), 128.7 (2C), 128.3, 127.2, 125.1 (q, J = 3.7Hz, 2C), 124.7, 124.2 (q, J = 270.3 Hz), 47.3 ppm. ^{19}F NMR ($CDCl_3$, 376 MHz): δ -62.6 ppm. HRMS: calc for $C_{16}H_{12}ClF_3$: 291.0578; found: 291.2006.

(Z)-4-chloro-5-(naphthalen-1-yl)pent-4-en-1-yl acetate (3ab)

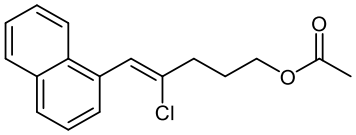

Following General procedure 3 with 1-(2,2-dichlorovinyl)naphthalene (0.30 mmol, 66.7 mg) and potassium [18-Crown-6] bis(catecholato)- acetoxypropylsilicate (0.45 mmol, 231 mg). The crude product was purified by flash column chromatography (Et_2O:*n*-pentane From 2/98 to 10/90) to afford (Z)-4-chloro-5-(naphthalen-1-yl)pent-4-en-1-yl acetate (3ab) (40 mg, 45%) as a pale brown oil. ^1H NMR (400 MHz, $CDCl_3$): δ 7.92-7.79 (m, 3H), 7.65-7.59 (m, 1H), 7.55-7.42 (m, 3H), 6.98 (s, 1H), 4.24 (t, J = 6 Hz, 2H), 2.71 (t, J = 7.5 Hz, 2H), 2.1 (s, 3H), 2.13-2.08 (m, 2H). ^{13}C NMR (100 MHz, $CDCl_3$): δ 171.1, 136.3, 133.5, 132.3, 131.4, 128.6, 128.0, 127.2, 126.1, 125.8, 125.2, 124.3, 123.7, 63.2, 37.0, 26.7, 21.0. HRMS: calc. for $[C_{17}H_{17}ClO_2]Na$ 311.0809; found 311.0811.

(Z)-4-chloro-5-(3-methoxyphenyl)pent-4-en-1-yl acetate (3bb)

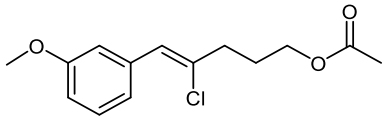

Following General procedure 3 with 1-(2,2-dichlorovinyl)-3-methoxybenzene (0.32 mmol, 64.2 mg) and potassium [18-Crown-6] bis(catecholato)-acetoxypropylsilicate (0.45 mmol, 293 mg). The crude product was purified by flash column chromatography (Et_2O:*n*-pentane 2/98) to afford (Z)-4-chloro-5-(3-methoxyphenyl)pent-4-en-1-yl acetate (3bb) (47.9 mg, 64%) as a pale oil. ^1H NMR (400 MHz, $CDCl_3$): δ 7.24-7.28 (m, 1H), 7.02-7.19 (m, 1H), 7.14-7.12 (m, 1H), 6.85-6.81 (m, 1H), 6.48 (s, 1H), 4.16-4.13 (t, J = 6.4 Hz, 2H), 3.82 (s, 3H), 2.59-2.55 (td, J = 0.52 Hz and 6.7 Hz, 2H), 2.06 (s, 3H), 2.05-1.94 (m, 2H) ppm. ^{13}C NMR (100 MHz, $CDCl_3$): δ 171.1, 159.4, 136.2, 133.7, 129.1, 125.1, 121.7, 114.3, 113.4, 63.2, 55.2, 37.8, 26.7, 20.9 ppm. HRMS: calc for $[C_{14}H_{17}ClO_3]Na$: 291.0759; found: 291.0760.

(Z)-4-chloro-5-phenylpent-4-en-1-yl-acetate (3cb)

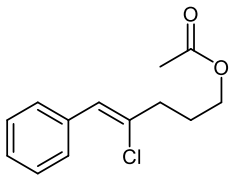

Following General procedure 3 with 1-(2,2-dichlorovinyl)-benzene (0.32 mmol, 55 mg) and sodium bis(catecholato)-acetoxypropylsilicate (0.45 mmol, 166 mg). The crude product was purified by flash column chromatography (Et_2O:*n*-pentane 2/98) to afford (Z)-4-chloro-5-phenylpent-4-en-1-yl acetate (3cb) (25 mg, 35%) as a pale oil. ^1H NMR (400 MHz, $CDCl_3$): δ 7.58 (dd, J = 7.6, 1.7 Hz, 2H), 7.35-7.27 (m, 3H), 6.51 (s, 1H), 4.15 (t, J = 6.4 Hz, 2H), 2.58 (t, J = 7.4 Hz, 2H), 2.07 (s, 3H), 2.04 – 1.97 (m, 2H). ^{13}C NMR (100 MHz, $CDCl_3$): δ 171.0, 134.9, 133.4, 129.0 (2C), 128.1 (2C), 127.6, 125.2, 63.2, 37.7, 26.7, 21.0. HRMS: Calcd for $C_{13}H_{16}O_2Cl$ 239.0834; found 239.0833.

(Z)-4-chloro-5-(4-(trifluoromethyl)phenyl)pent-4-en-1-yl acetate (3db)

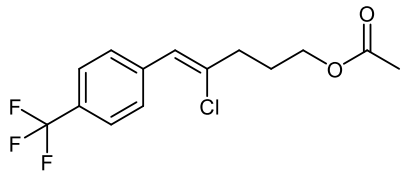

Following General procedure 3 with 1-(2,2-dichlorovinyl)-4-(trifluoromethyl)benzene (0.31 mmol, 72.3 mg) and potassium [18-Crown-6] bis(catecholato)-acetoxypropylsilicate (0.45 mmol, 295 mg). The crude product was purified by flash column chromatography (Et_2O:*n*-pentane 10/90) (Z)-4-chloro-5-(4-(trifluoromethyl)phenyl)pent-4-en-1-yl acetate (3db) (49 mg, 51%) as a pale brown oil. ^{1}H NMR (400 MHz, $CDCl_3$): δ 7.69-7.66 (d, J = 8Hz, 2H), 7.62-7.59 (d, J = 8 Hz, 2H), 6.54 (s, 1H), 4.17-4.13 (t, J = 6.4 Hz, 2H), 2.62-2.58 (td, J = 0.5 Hz and 7 Hz, 2H), 2.06 (s, 3H) , 2.04-1.98 (m, 2H). ^{13}C NMR (100 MHz, $CDCl_3$): δ 171.1, 138.4, 135.9, 129.5, 129.2 (2C), 125.1(q, J=3.7Hz, 2C), 124.3 (q, J = 283.7 Hz), 124.1, 63.1, 37.7, 26.6, 20.9. ^{19}F NMR (376 MHz, $CDCl_3$): δ -62.7 ppm. HRMS: calc for $[C_{14}H_{14}ClF_3O_2]Na$ 329.9527; found 329.9527.

(Z)-1-(2-chloro-2-cyclohexylvinyl)naphthalene (3ac)

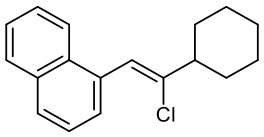

Following General procedure 3 with 1-(2,2-dichlorovinyl)naphthalene (0.32 mmol, 71 mg) and [18-Crown-6] bis(catecholato)-cyclohexylsilicate (0.45 mmol, 290 mg). The crude product was purified by flash column chromatography (Et_2O:*n*-pentane From 0/100 to 2/98) to afford (Z)-1-(2-chloro-2-cyclohexylvinyl)naphthalene (3ac) (58.5 mg, 70%) as a colorless oil. ^{1}H NMR (400 MHz, $CDCl_3$): δ 7.95-7.74 (m, 4H), 7.54-7.45 (m, 3H), 7.62-7.58 (m, 1H), 6.93 (s, 1H), 2.54-.54 (m, 1H), 2.14-2.03 (m, 2H), 1.94-1.85 (m, 2H), 1.62-1.19 (m, 5H). ^{13}C NMR (100 MHz, $CDCl_3$): δ 143.4 133.5, 132.9, 131.5, 128.5, 127.7, 127.1, 125.9, 125.7, 125.2, 124.5, 120.6, 48.2, 31.9 (2C), 26.2 (2C) , 26.0. HRMS: calc for $C_{18}H_{19}Cl$ 273.1174; found 273.6994.

(Z)-4-chloro-5-(3-methoxyphenyl)cyclohexane (3bc)

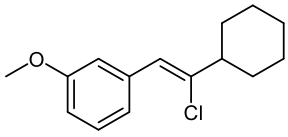

Following general procedure 3 with 1-(2,2-dichlorovinyl)-3-methoxybenzene (0.32 mmol, 60.9 mg) and potassium [18-Crown-6] bis(catecholato)-cyclohexyl silicate (0.45 mmol, 284 mg). The crude product was purified by flash column chromatography (Et_2O:*n*-pentane From 0/100 to 5/95) to afford (Z)-4-chloro-5-(3-methoxyphenyl)benzyl (3bc) as a yellow oil (23 mg, 30%). ^{1}H NMR (400 MHz, $CDCl_3$): δ 7.40 – 7.11 (m, 3H), 6.81 (dd, J = 8.2, 2.6 Hz, 1H), 6.45 (s, 1H), 3.82 (s, 3H), 2.33 (tt, J = 11.6, 3.3 Hz, 1H), 1.94 (d, J = 12.5 Hz, 2H), 1.84 (dt, J = 12.8, 3.1 Hz, 2H), 1.76 – 1.68 (m, 1H), 1.57 – 1.12 (m, 5H).^{13}C NMR (100 MHz, $CDCl_3$): δ 159.3, 140.8, 136.7, 129.0, 122.2, 121.8, 114.4, 113.1, 55.23, 48.8, 31.7(2C), 26.2(2C), 25.9. HRMS: Calc for $C_{15}H_{19}ClO$ 251.1196; found 251.1197.

(Z)-(2-chloro-2-cyclohexylvinyl)benzene (3cc)

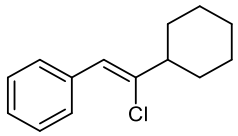

Following General procedure 3 with 1-(2,2-dichlorovinyl)-benzene (0.32 mmol, 55 mg) and potassium [18-Crown-6] bis(catecholato)-cyclohexyl silicate (0.45 mmol, 284 mg). The crude product was purified by flash column chromatography (toluene:cyclohexane From 0/100 to 5/95) to afford (Z)-(2-chloro-2-cyclohexylvinyl)benzene (3cc) (40 mg, 60%) as a pale oil. All the spectroscopic data agree with the literature.[9] ^{1}H NMR (300 MHz, $CDCl_3$): δ 7.61 (d, J = 7.3 Hz, 1H), 7.40 – 7.32 (m, 4H), 6.50 (s, 1H), 2.44 – 2.29 (m, 1H), 2.01 – 1.69 (m, 7H), 1.53 – 1.32 (m, 3H). ^{13}C NMR (75 MHz, $CDCl_3$): δ 129.2 (2C), 128.1 (2C), 127.3, 122.3, 48.8, 31.7 (2C), 29.7 (2C), 26.2, two carbons are missing.

(Z)-N-(2-chloro-3-(naphthalen-1-yl)allyl)aniline (3ad)

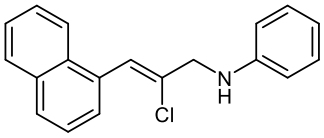

Following General procedure 3 with 1-(2,2-dichlorovinyl)naphthalene (0.32 mmol, 71 mg) and potassium [18-Crown-6] bis(catecholato)-anilinomethylsilicate (0.45 mmol, 294 mg). The crude product was purified by flash column chromatography (Et_2O:*n*-pentane From 2/98 to 10/90) to afford (Z)-N-(2-chloro-3-(naphthalen-1-yl)allyl)aniline (3ad) (39 mg, 43 %) as a pale brown oil. ^{1}H NMR (400 MHz, $CDCl_3$): δ 7.82-7.78 (m, 2H), 7.65-7.59 (m, 2H), 7.49-7.37 (m, 3H), 7.29-7.24 (m, 3H), 6.84-6.75 (m, 3H), 4.23 (s, 2H), NH is missing. ^{13}C NMR (100 MHz, $CDCl_3$): δ 133.7, 133.4, 131.8, 131.5, 129.4 (2C), 128.4, 128.1, 126.9, 126.1, 125.8, 125.2, 124.4, 123.3, 113.4 (2C), 118.5, 113.5, 51.5. HRMS: calc. for $[C_{19}H_{17}ClN]^+$ 294.1044, found: 294.1055.

(Z)-N-(2-chloro-3-(3-methoxyphenyl)allyl)aniline (3bd)

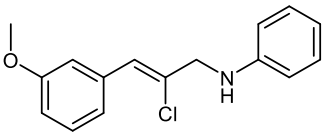

Following General procedure 3 with 1-(2,2-dichlorovinyl)-3-methoxybenzene (0.73 mmol, 149 mg) and potassium [18-Crown-6] bis(catecholato)-anilinomethylsilicate (1.09 mmol, 713 mg). The crude product was purified by flash column chromatography (Et_2O:*n*-pentane From 2/98 to 10/90) to afford (Z)-N-(2-chloro-3-(3-methoxyphenyl)allyl)aniline (3bd) (110 mg, 57 %) as a pale brown oil. ^{1}H NMR (400 MHz, $CDCl_3$): δ 7.19 – 7.05 (m, 5H), 6.77 – 6.58 (m, 5H), 4.15 (m, 1H), 4,01 (d, J = 2.6 Hz, 2H), 3.72 (s, 3H), NH is missing. ^{13}C NMR (100 MHz, $CDCl_3$): δ 159.4, 147.0, 135.7, 131.5, 129.3 (2C), 129.2, 124.4, 121.8, 118.3, 114.4, 113.9, 113.1 (2C), 55.3, 52.1. HRMS: calc. for $[C_{16}H_{17}ClNO]^+$:274.0993, found: 274.099.

(Z)-N-(2-chloro-3-(4-(trifluoromethyl)phenyl)allyl)aniline (3dd)

[9] Adak, T.; Hoffmann, M.; Witzel, S.; Rudolph, M.; Dreuw, A.; Hashmi, S. K. *Chem. Eur. J.* **2020**, *26*, 15573.

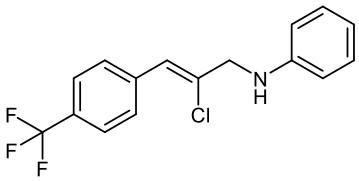

Following General procedure 3 with 1-(2,2-dichlorovinyl)-4-(trifluoromethyl)benzene (0.30 mmol, 72.3 mg) and potassium [18-Crown-6] bis(catecholato)-anilinomethylsilicate (0.45 mmol, 294 mg). The crude product was purified by flash column chromatography (Et_2O:*n*-pentane 10/90) to afford (Z)-N-(2-chloro-3-(4-(trifluoromethyl)phenyl)allyl)aniline (3dd) (28 mg, 30%) as a pale brown oil. ^1H NMR (300 MHz, $CDCl_3$): δ 7.67 (d, J = 8.4 Hz, 2H), 7.58 (d, J = 8.4 Hz, 2H), 7.25 – 7.17 (m, 2H), 6.84 – 6.62 (m, 4H), 4.25 (s, 1H), 4.11 (s, 2H).^{13}C NMR (75 MHz, $CDCl_3$): δ 146.9, 138.1 (d, J = 1.3 Hz, 1C), 133.9, 129.6 (d, J = 58.0 Hz, 1C), 129.5 (2C), 129.4 (2C), 125.2 (q, J = 3.75 Hz, 2C), 124.2 (q, J = 270.3 Hz, 1C), 123.2, 118.6, 113.2 (2C), 52.1. ^{19}F NMR (376 MHz, $CDCl_3$): δ -62.7. HRMS: Calc. for [$C_{16}H_{13}ClF_3N$] 312.0761; found 312.0761.

1.4 Case of cyclopropane hypercoordinated silicon species

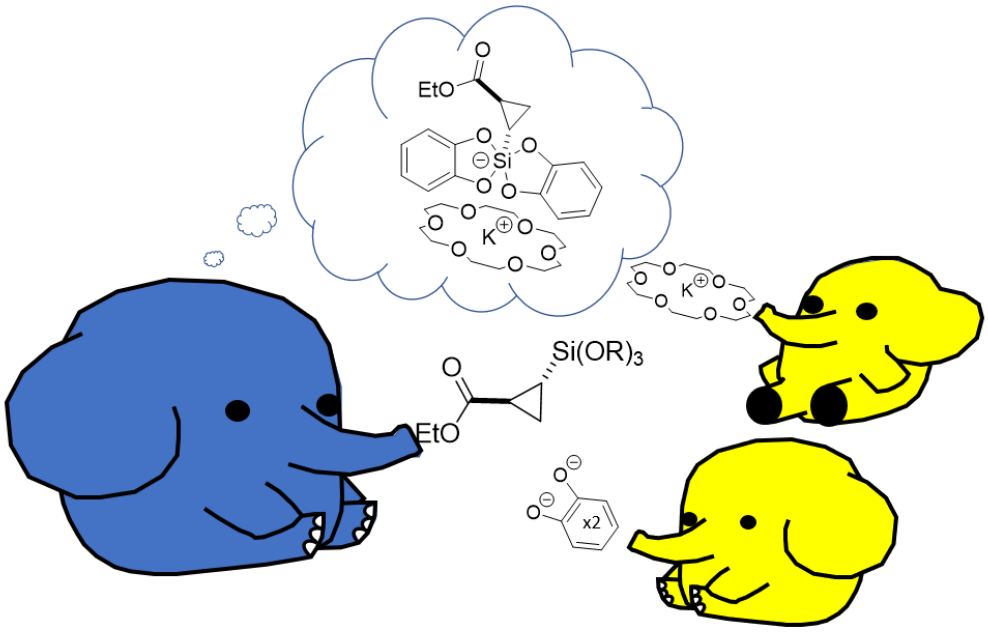

1.4.1 Introduction

The synthesis of silicates depends on the availability of the alkoxysilanes. Their preparation (1.1) and use (1.2) are mainly based on commercially available ones. This has been an advantage regarding the synthesis of the primary radical precursor. However, it also led to a lack of diversity of resulting radical species.[1] To overcome this and investigate new radical precursor, we decided to focus on the synthesis of non-trivial silanes such as cyclopropyl ones.[2] The most efficient known methodology involved diazomethane that was unfortunately not accessible in our laboratory. (scheme 1)

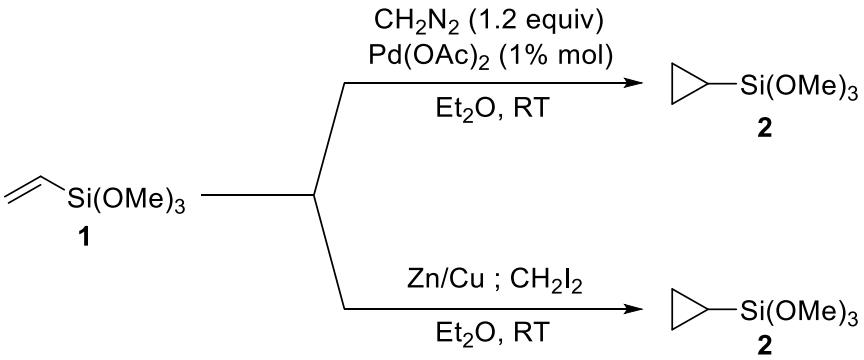

Scheme 1. Synthesis of cyclopropyl trimethoxysilane

Based on the nucleophilicity of the diazo precursor, the reaction on slightly enriched vinyl-silane appears remarkably fast and efficient as described by Nassim in 1992.[2] Another more accessible but undocumented methodology (USSR thesis) was proposed by Plavov's student using the Simmons-Smith reaction.[3] (scheme 1)

More recently, Chawner and co-workers (2017) investigated the nucleophilic behaviour of anionic cyclopropyl generated from the reaction between isopropyl Grignard reagent and chlorotrimethoxysilane.[4] But even if the desired target was obtained, this methodology cannot be used for our silicates synthesis due to numerous amount of synthetic step and reported 50 mg scale.

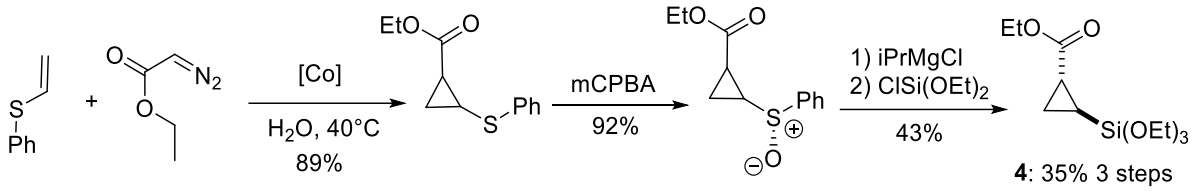

Scheme 2. Synthesis of cyclopropyl trimethoxysilane

From this, to perform the investigation of a potential radical precursor, the preparation of an efficient, scalable and safe methodology must be developed.

1.4.2 Synthesis

Firstly, the Simmons-Smiths (SS) reaction was investigated with no indication of the methodology for the preparation of the Zinc-Copper amalgam (neutral, acid, basic ?, reagent grade…) nor experimental detail. From this, we decided to investigate some classical conditions and variations as described in the scheme 3.[5]

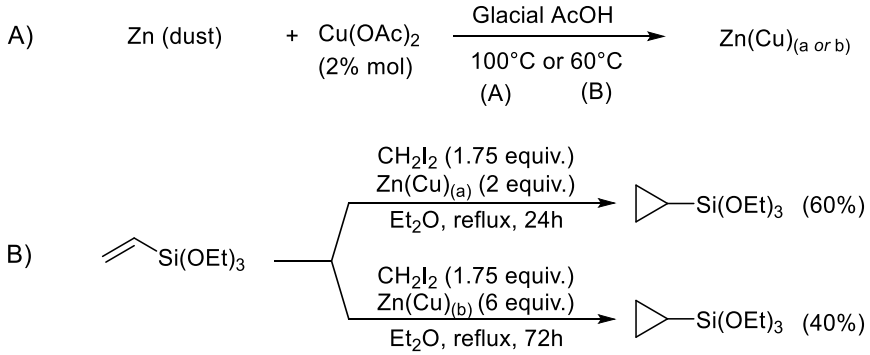

Scheme 3. A) Preparation of Zn/Cu amalgam; B) Simmons-Smith reaction best result

The preparation of the amalgam (Scheme 3.A) was done in hot glacial acetic acid and used directly for the SS (3.B). Compared to the described room temperature experiment, the reaction starts at higher temperature (reflux). Best results gave respectively 60% and 40%. (SM/Prod mixture, impure, NMR yield)

With this methodology, the full conversion of the starting material does not seem possible, and isolation from the starting material by distillation also appears unrealistic because of the similar described boiling points. We then decided to search for a methodology allowing the full conversion of the starting material. This was achieved by the use of commercially available TMS-diazomethane and ethyl diazoacetate (EDA)

by a formal [2+1] cycloaddition catalysed by palladium(II) bis(acetylacetonate). (scheme 3) Both silanes were obtained in gram scale and purified safely as mentioned in the experimental part.

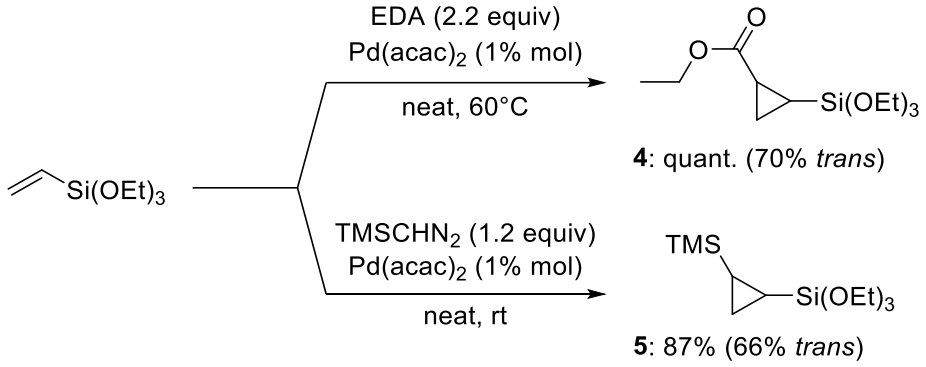

Scheme 3. Synthesis of triethoxycyclopropyl silanes | Isolated yield (trans % determined by ^{1}H nmr)

The synthesis is performed under neat conditions, in both cases, 1% [Pd] catalyst is dissolved in the silane and the desired diazo is then added. For EDA, the reaction takes place at 60°C with slow addition of diazo (0.2 equiv./h) overnight. Each reaction is monitored by the formation of palladium black that indicates the end of the reaction. The purification of the silane from the diazo in reaction medium firstly takes advantages of the EDA melting point (precipitation, m.p. : -21°C) and TMS-diazomethane volatility (purified by vacuum transfer). More information can be found in the supplementary information. For each silane, a cis/trans compound are obtained and cannot be separated by distillation. Short investigation of the modification of the *d.r.* ratio for the silylated diazo toward the *trans* one shows a negative influence of the low temperature. The experiment at higher temperature was not launched to favour the formation of the reactive silane for the next step.

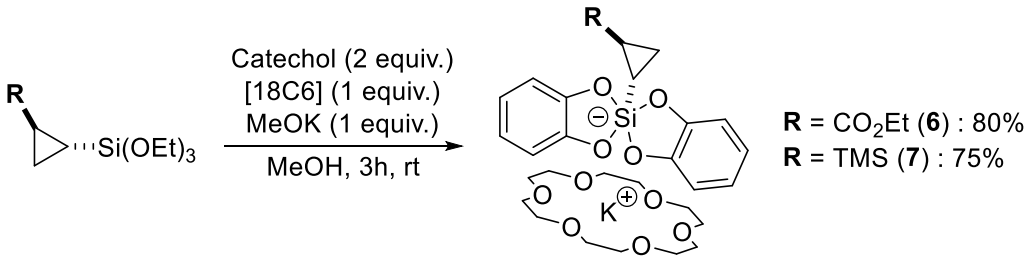

Scheme 4. Synthesis of bis(catecholato)silicates | Isolated yield (based on reactive *trans alkoxysilane*)

When the synthesis of each silane was achieved, we started investigating the synthesis of the corresponding new bis(catecholato) silicates.[6,7] (Scheme 4) For this, we decided to follow, the classical chelated potassium procedure for its ease of crystallisation and stability. To our delight the reaction worked in the same manner that previously described for chelated silicates. The isolated yield is given based on the *trans* silane, indeed recovery of enriched *cis* one can be done from the precipitation filtrate.

The ethyl ester derivative (6) was obtained in 80% yield and the trimethyl silane (7) one in 75% yield. Finally, another hypercoordinated silicon was synthetised in the laboratory by Thomas Deis.[8,9] The reaction involved the use of Martin's spirosilane and lithium cyclopropyl for the direct generation of pentavalent species. Cation exchange in DCM using tetrabutylammonium bromide provided the desired product (8) in 77% yield. (scheme 5)

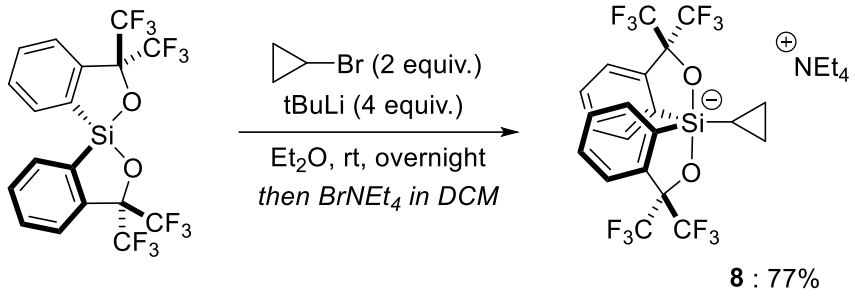

Scheme 5. Synthesis of Martin cyclopropyl-spirosilane.

1.4.3. Structural datas

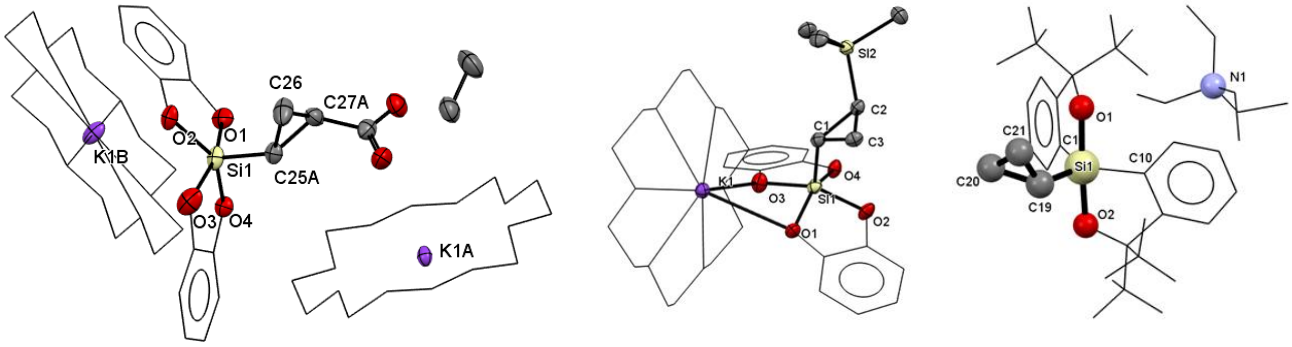

Figure 1. X-ray crystal structures, thermal ellipsoids are drawn at 25% probability level. For clarity in all structure, hydrogen atoms are omitted, pyrocatechol ligands and crown ether are drawn as wireframe in of **6** (left) **7** (middle) as Martin's spirosilane ligand and tetraethylammonium carbons in **8** (right)

The crystal structure of these new silicon derivatives was determined by X-ray diffraction, Suitable crystals were obtained by slow vapor diffusion using acetone and diethyl ether as anti-solvent at 10°C for bis(catecholato)silicates and following the same strategy with DCM/Pentane at -20°C for the Martin spirosilane. (Fig. 1)

Bis(catecholato)cyclopropyl silicate **6** (-CO_2Et) and **7** (-TMS) crystallized respectively in the monoclinic and orthorhombic space group I2/a and Pnma21. The complete structure of the TMS one contains a symmetrical plan, here (Fig. 1) only the half of the structure is represented in order to facilitate the representation. The whole structure is depicted in Figure 2. Both pentavalent silicon "Si_1" are described as a slightly distorted square pyramid with the cyclopropane at the apical site. In the cyclopropyl-ester 6 the Si_1-$C25_A$ distance is 1.848(7) Å. The influence of the silicon (hyper)-coordination is highlighted as shown

by the increased length of the Si-C bond (Si_1-C_1 at 1.863(4) Å in 7) compared with the TMS moiety (Si_2-C_2 distance of 1.629(4) Å). Both oxygen from catechol ligand occupy the 4 basal positions with a distance going from 1.714(3) to 1.771(3) ppm for 6 and 1.7331 to 1.7774 ppm for 7. In the spirosilicate 8, the distance Si_1-C_{19} is 1.875(2) Å. This value appears similar to the one observed for both substituted cyclopropane with pentavalent silicon. The Si_1-O_1 and Si_1-O_2 are respectively 1.826(1) and 1.842(2) Å. These values are longer than the ones in 6 and 7 but in the same range that is known Martin's spirosilicate.[10-11] It has to be mentioned that this Si-O length is directly correlated to the electronic influence of the substituent for Martin's derivative, the cyclopropyl in this case appear as slightly electron-donating substituent. Finally, the Si_1-C_1 is 1.907(2) Å and Si_1-C_2 is 1.904(2) Å.

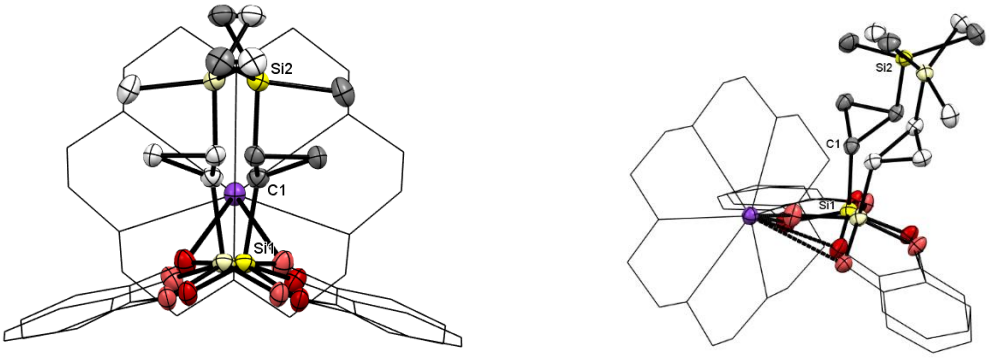

Figure 2. Two different perspectives of TMS cyclopropyl silicate's X-ray crystal structure. Thermal ellipsoids are drawn at 25% probability level. Pyrocatechol ligands and crown ether are drawn as wireframe for clarity. Hydrogen atoms are omitted for clarity.

Table 1. XRD data:

Compound	SG	*a, b, c* (Å)	*α, β, γ* (°)	Z ; Z'
6	*I2/a*	***a*** *18.3838(5)* ***b*** *9.7676(2)* ***c*** *37.4952(10)*	***α*** *90* ***β*** *98.025(2)* ***γ*** *90*	***Z****: 8 ;* ***Z'****: 0*
7	*Pnma2₁*	***a*** *18.0876(6)* ***b*** *8.9711(3)* ***c*** *10.3729(3)*	***α*** *90* ***β*** *90* ***γ*** *90*	***Z****: 2 ;* ***Z'****: 0*
8	*P1*	***a*** *11.3017(2)* ***b*** *14.9959(2)* ***c*** *19.2078(3)*	***α*** *104.6810(10)* ***β*** *98.1160(10)* ***γ*** *101.4000(10)*	***Z****: 4 ;* ***Z'****: 0*

For each species, the ^{29}Si NMR shift is in the expected range of five coordinated silicon species and in the silane one for the one bearing a TMS. Indeed, the spectrum shows the λ^5Si of **7** at δ = -76.9 ppm and λ^4Si at 2.1 ppm (TMS). The silicate obtained bearing an ester shows an expected singlet at δ = -81.4 ppm similar to the previous bis(catecholato) silicate. Interestingly, Martin's silicate shows a singlet at δ = -66 ppm that illustrates the strong influence of the ligand on physical properties of λ^5Si. ^{13}C NMR datas show the non-equivalence of both catechols in **6** and **7**. The phenomenon was previously only highlighted on bis(R-catecholato)silicate bearing functionalized catechols (CN, OMe, halogen...), due to the existence of *cis* and *trans* isomers of the silicate in solution. In this case, catechol's carbons are anisochronous due to the non-symmetrical cyclopropane substituent. This being confirmed in the Martin's silicate bearing an unfunctionalized cyclopropane resulting in the observation of isochronous ^{13}C of the the 2,2,2,2',2',2'-hexafluorocumyl ligand.

The oxidation potential of **6**, **7** and **8** was determined in DMF with saturated calomel electrode as reference electrode. (figure 3)

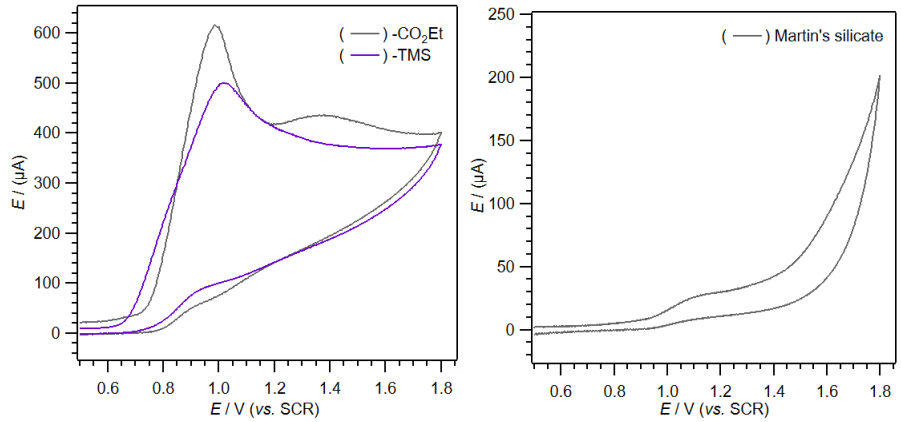

Figure 3. Cyclic voltammetry of bis(catecholato) silicate (left) of **6** (grey) , **7** (purple) and Martin's **8** (right) in DMF with $[Bu_4N][PF_6]$ as supporting electrolyte

Compound **6** displays an irreversible one-electron oxidation of the silicate followed by a second oxidation of free catechol. Interestingly, the $1e^-$ oxidation of **7** shows only one irreversible oxidation of the silicate. The $E_{ox}^{1/2}$ obtained are close, determined as +0.81 and +0.82 V vs SCE. Therefore, we report the most difficult alkyl bis(catecholato) silicates to oxidized. Finally, the Martin's salt gave an $E_{ox}^{1/2}$ (**8**) of +1.05 V vs SCE, situated in the reported range of alkyl Martin's salts.

1.4.4. (*un)*-reactivity and theoretical insights

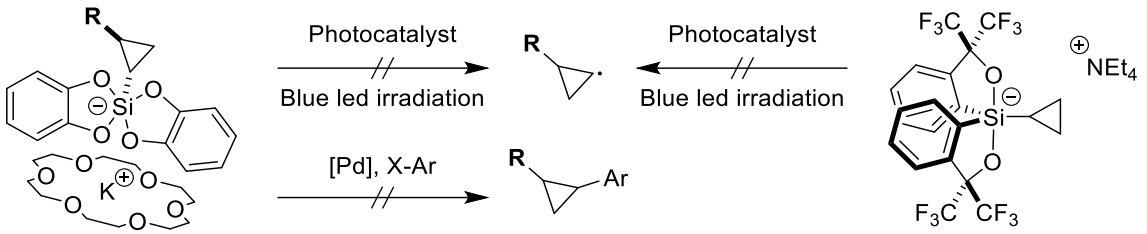

Scheme 6. Overview of investigated reaction type.

The classical methodologies described in the chapter 1.2 was then screened. Firstly, we decided to have a look toward the generation of radical species has expected.[12,13] It must be noted that the generation of this radical is poorly described from a direct bond cleavage following an oxidative pathway. The only related photoredox report was done using trifluoroborate derivative and direct trapping of the intermediate with SO_2 transfer reagent.[14a] (scheme 7) No given details from this report permited to confirm an oxidation of the trifluoroborate and therefore the reaction of the cyclopropyl radical. More exemples of generated radical cyclopropyl (called *"radical leaving group"*) were described for tertiary cyclopropane. This time, the trapping of this radical was performed using Ni catalyst for the preparation of corresponding aryl-cyclopropane. Reported reagents involved N-benzoyl carbamothioate,[14b] iodine,[14c] N-hydroxyphthalimide esters[14d] or pyridinium salts.[14e]

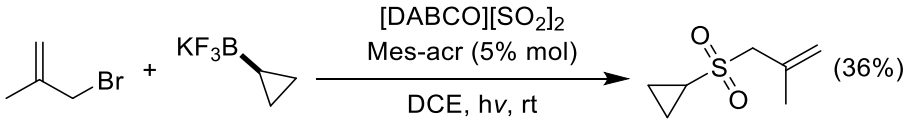

Scheme 7. Example of photoredox/cyclopropyl reactivity

We decided to investigate the generation of the radical species using the most common methodology from our laboratory. Screening of photocatalyst (i.e. 4CzIPN, [Ir], and Fukuzumi's derivative) for each bis(catecholato) silicates and Martin spirosilicate, irradiation apparatus, solvents appear rapidly inefficient for this purpose. Screened reaction involved trapping, allylation, dual Ni/photoredox cross-coupling and few 1,2 addition. We later investigate solid-state oxidation (see chapter 4) without success. Based on the measured oxidative potential (0.9V vs SCE), we conclude that this silicate strangely followed the expected range for these species (see 1.1.5). During our investigation of this radical generation, trapping (allyl, TEMPO) also appeared inefficient. We decided to investigate the generation from electrochemistry in collaboration with Dr. Khaoula Jaouadi.[15] Indeed, she managed to develop a methodology for the desired oxidation/fragmentation of silicates during her PhD. Unfortunately, our bis(catecholato) silicates appears once again un-reactive.

With this lack of reactivity from the radical side observed, we then decided to look into the reported palladium cross-coupling reaction from Deshong and Seganish, but these reactions also did not provide any traces of the desired product. Finally, we wanted to gain theoretical insights for this reaction by performing density functional theory (DFT) to better understand the behaviour of bis(catecholato)cyclopropyl silicate.[16] These calculations illustrated the free energy profile of the generation of the desired cyclopropyl radical from the oxidized silicates as illustrated in scheme 8.

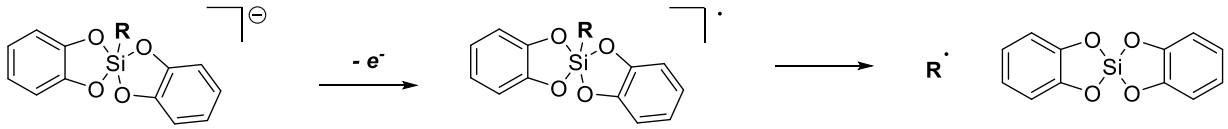

Scheme 8. DFT investigation, generation of radical from the 1e- oxidized silicate. | R = "C_3", Ph, cHex

We mainly focused on the cyclopropyl derivative, but calculations were also performed for the cyclohexyl silicate and phenyl radical for comparison with two well know silicates. It must be noted that the cyclohexyl one is one of the most reactive silicate while the phenyl one appears unreactive following all classical conditions. Geometry optimization of both cyclopropanes starting from a square planar silicate led to a more stable species when a slight distortion occurs affording a TBP type structure.[17] This was not observed with cyclohexyl nor phenyl silicates. These two geometries are well known and often observed in solid state for a wide range of silicates species no matter what their counter cation is. If the TBP is not observed in solid state for each 3 members ring, no rigorous direct comparison can be done. With the optimized anionic silicates in hand, the resulting oxidized silicates were then computed. (Table 2) Concerning each cyclopropane, the distortion toward a TBP shape was slightly exacerbated. Interestingly, and following the previous observation of Kano [18] the oxidation of the cyclohexyl-silicate lead to a distorted BP that should afford a more stable local minimum intermediate. This phenomenon was not observed with the resulting oxidized phenyl silicate.

Table 2. Computed value for the oxidation process *($\Delta G^{\ddagger}_{anion,ox}$)* and decomposition (= BDE, *($\Delta G^{\ddagger}_{ox,rad}$)*

Entry	*($\Delta G^{\ddagger}$) anion → ox*	*Kj/mol*	*Kcal/mol*	*($\Delta G^{\ddagger}$) ox → rad*	*Kj/mol*	*Kcal/mol*
1	TMS-	***339.2***	***81.0***	TMS-	***99.6***	***23.8***
2	EtO_2C-	***346.8***	***82.9***	EtO_2C-	***106.5***	***25.4***
3	cHex	***339.3***	***81.0***	cHex	***40.6***	***9.7***
4	Ph	***345.1***	***82.4***	Ph	***107.2***	***25.6***

The different computed values have been highlighted for the oxidation of each silicate (table 2). No major difference can be observed by direct comparison of the value calculated for the oxidation of each silicate. (Figure 4)

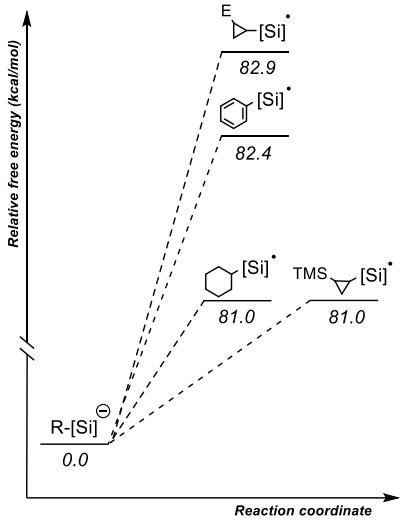

Figure 4. Relative free energy for the 1e- oxidation of anionic bis(catecholato) silicates.

More interestingly, and following the experimental observation, both cyclopropane and phenyl silicates have a much higher energy difference ($\Delta G^{\ddagger}_{ox,rad}$) than the "easily oxidable" cyclohexyl silicate. (Figure 5) These datas are also in consistency with the one calculated by Kano and in the study recently published on phenyl silicates. Here the computed high bond dissociation energy (BDE) matches with the experimental observation and could explain the difficulty on the generation of the desired radical.

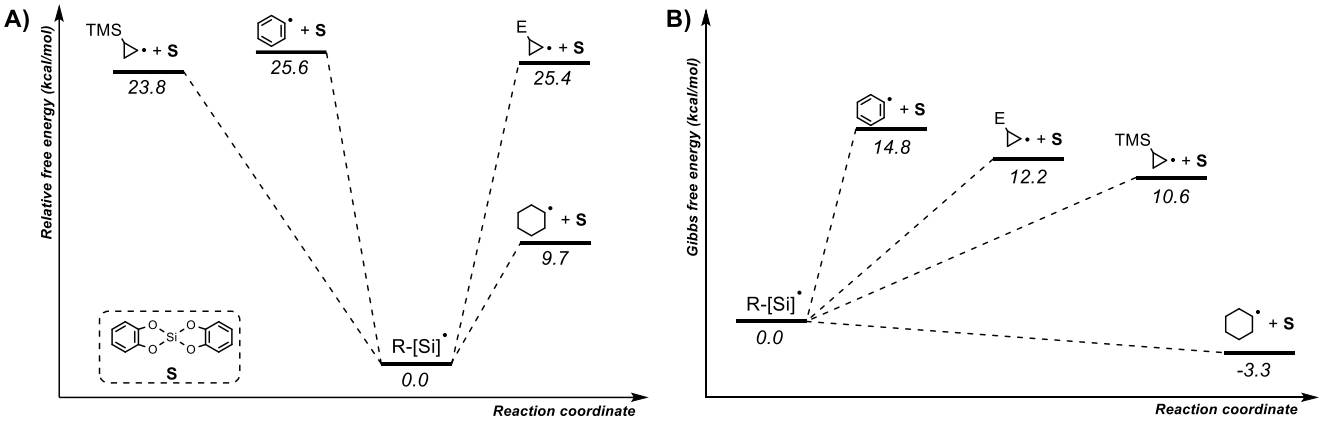

Figure 5. A) Compute BDE of several bis(catecholato) silicates; B) Gibbs free energy.

In addition, the Gibbs free energy result are exposed in figure 5.B, the transition step energy was not determined but according to the previous calculation done on silicates, the reaction with phenyl silicate for the generation of the desired radical is endergonic as for both cyclopropanes. Interestingly, according to the value obtained, the reaction should be exergonic in the case of the cyclohexyl radical formation.

1.4.5. Conclusion and perspective

In summary, we have developed an efficient methodology for the synthesis of alkoxysilane wearing cyclopropyl moiety in gram scale based on a formal [2+1] palladium based cyclopropanation. The silane was then transformed efficiently in the hypercoordinated species bearing bis(catecholato) ligand. The use of this hypercoordinated species as radical precursors unfortunately did not provide the expected reactivity. It appears that the fragmentation of the 1e- oxidized [Si]- is not favourable, theoretically and experimentally like the reported poorly reactive phenyl silicate. We then managed to compare the physical properties and reactivity of both of the most classical radical precursors based on hypercoordinated silicon (Martin's one and bis(catecholato) silicates).

Investigation of other hypercoordinated like Martin spirosilane also confirm the difficulty to obtain the desired radical from *classical* hypercoordinated species. In the meantime, attempt to perform the synthesis of the pentafluorosilicate derivative from the alkoxysilane was ineffective :

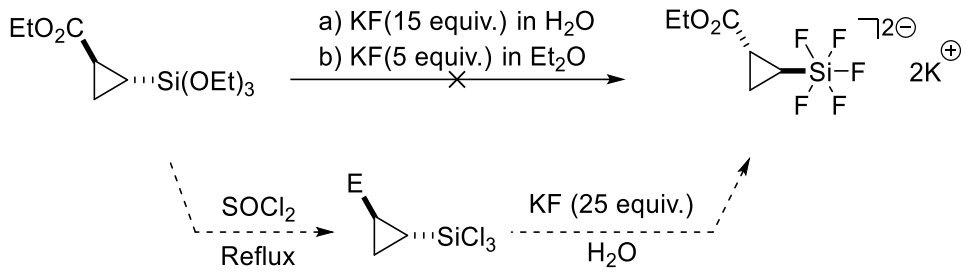

Scheme 9. Unsuccessful hexavalent synthesis & possible synthetic pathway.

A more realistic pathway should involve the trichlorosilane derivative. If no direct efficient synthesis from $SiCl_4$ could be envisaged, the transformation of the alkoxysilane using thionyl chloride appears as a promising synthetic pathway. With the hexavalent silicon species in hand, the generation of the desired radical using [Cu] in solution or organic/inorganic oxidant in solid-state mechanochemistry could be also investigated. (see chapter 4)

References part 1.4

[1] Millanvois, A.; Ollivier, C.; Fensterbank, L. Bis(Catecholato)Silicates: Synthesis and Structural Data. *European Journal of Inorganic Chemistry* **2022**, *2022* (17), e202101109.

[2] *M. Nasim, V. S. Petrosyan, G. S. Zaitseva, J. Lorberth, Journal of Organometallic Chemistry* ***1992****, 430, 269–272.*

[3] Nasim Mokhammed, Ph.D. Thesis, A. N. Nesmeyanov Institute of Organoelement Compounds, Russian Acad. Sci., Moscow, 1991 (in Russian).

[4] S. J. Chawner, M. J. Cases-Thomas, J. A. Bull, *European Journal of Organic Chemistry* **2017**, *2017*, 5015–5024.

[5] S. D. Rychnovsky, J. P. Powers, in *Encyclopedia of Reagents for Organic Synthesis*, John Wiley & Sons, Ltd, **2001**.

[6] *As described in Chapter 1.1*
[7] V. Corcé, L.-M. Chamoreau, E. Derat, J.-P. Goddard, C. Ollivier, L. Fensterbank, *Angew. Chem. Int. Ed.* **2015**, *54*, 11414–11418.
[8] See Thomas Deis, Ph.D. Thesis, Sorbonne Université, équipe MACO
[9] T. Deis, J. Forte, L. Fensterbank, G. Lemière, *Molecules* **2022**, *27*, 1767.
[10] T. Deis, J. Maury, F. Medici, M. Jean, J. Forte, N. Vanthuyne, L. Fensterbank, G. Lemière, *Angewandte Chemie* **2022**, *134*, e202113836.
[11] T. Deis, F. Medici, A. Poussard-Schulz, G. Lemière, L. Fensterbank, *Journal of Organometallic Chemistry* **2021**, *956*, 122120.
[12] See Chapter 1.2
[13] M. Jouffroy, D. N. Primer, G. A. Molander, *J. Am. Chem. Soc.* **2016**, *138*, 475–478.
[14] a) S. Ye, X. Li, W. Xie, J. Wu, *Asian Journal of Organic Chemistry* **2019**, *8*, 893–898. b) L. R. Mills, J. J. Monteith, G. dos Passos Gomes, A. Aspuru-Guzik, S. A. L. Rousseaux, *J. Am. Chem. Soc.* **2020**, *142*, 13246–13254. c) K. Yotsuji, N. Hoshiya, T. Kobayashi, H. Fukuda, H. Abe, M. Arisawa, S. Shuto, *Advanced Synthesis & Catalysis* **2015**, *357*, 1022–1028. d) J. Cornella, J. T. Edwards, T. Qin, S. Kawamura, J. Wang, C.-M. Pan, R. Gianatassio, M. Schmidt, M. D. Eastgate, P. S. Baran, *J. Am. Chem. Soc.* **2016**, *138*, 2174–2177. e) J. Liao, C. H. Basch, M. E. Hoerrner, M. R. Talley, B. P. Boscoe, J. W. Tucker, M. R. Garnsey, M. P. Watson, *Org. Lett.* **2019**, *21*, 2941–2946.
[15] See Khaoula Jaouadi, Ph.D. Thesis, Étude mécanistique de la catalyse duale impliquant des dérivés hypercoordinés du silicium, Sorbonne Université, IPCM (UMR 8232)
[16] F. Neese, F. Wennmohs, U. Becker, C. Riplinger, *J. Chem. Phys.* **2020**, *152*, 224108.
[17] Computed at PBeh-3C/def2-mSVP // PW6B95(D3BJ)/def2-QZVPP level of theory
[18] T. Morofuji, Y. Matsui, M. Ohno, G. Ikarashi, N. Kano, *Chemistry – A European Journal* **2021**, *27*, 6713–6718.

Supporting information

All chemicals were used as received without further purification except for the catechol that was purchased from commercial source and purified by crystallization from chloroform. Standard Schlenk techniques were employed, and all reactions were carried under dry argon atmosphere. Melting points were determined on a melting point apparatus SMP3 (Stuart scientific). Electrochemical measurements were carried out with an Origaflex (Origalys) electrochemical workstation. NMR spectrum (1H, 13C, 29Si) were recorded on 400 MHz Bruker AVANCE II spectrometer at room temperature. Chemical shifts (δ) are reported in ppm and coupling constants (J) are given in Hertz (Hz). Abbreviations used for peak multiplicity are, s (singlet); bs (broad singlet); d (doublet); t (triplet); q (quartet); quint (quintet); sept (septet); m (multiplet) etc. For each bis(catecholato)cyclopropyl silicates, catechol's carbon are anisochronous (non equivalent). The computational work for this ab initio investigation was done on resources of the National Supercomputing Computer, Singapore (NSCC). Density functional theory studies were carried out with Orca 4.1.2. The geometry of each species was optimized using PBeh-3C functionals and def2-mSVP as basis set. The modelling involved a simplified silicate, in which the cation was removed to reduce computational costs. Then, for all silicates and resulting structure, frequency analysis was performed to verify the absence of imaginary frequencies. In case of negative frequencies, the geometries were re-optimized with grid6, Tight OPT and VeryTightSCF settings. Finally, the single point-energy was computed using PW6B95-(D3BJ)/def2-QZVPP.

Caution: TMS-diazomethane and Ethyl diazoacetate (EDA) are highly toxic if inhaled and can lead to explosion.

Synthesis of 4: In a flame dried RBF was added $Pd(acac)_2$ (12 mg, 0.04 mmol), the flask was purged with argon and vinyltriethoxysilane (0.84 ml, 4 mmol) was added. The reaction medium was stirred at 60°C

until all the [Pd] was dissolved. EDA (0.92 ml, 8.8 mmol) was added dropwise at 0.1mL/min (N_2 formation was observed) and the reaction was stirred until completion as indicated by the formation of Pd black (generally 6h). The orange crude was dissolved in hexane (5ml), and the flask was cooled down at -196°C using liquid nitrogen (the palladium black precipitate before the freeze of the crude). The flask was gently warmed to -30°C affording a yellow hexane solution, and unreacted brown EDA crystal (m.p. -21°C). The yellow hexane solution was taken off and hexane was removed by vacuum transfer. Quantitative yield, mixture of cis/trans (30:70) was obtained as a light-yellow oil. NMR data are in accordance with the one from the literature.

Synthesis of 5: In a flame dried RBF was added $Pd(acac)_2$ (12 mg, 0.04 mmol), the flask was purged with argon and vinyltriethoxysilane (0.84 ml, 4 mmol) was added followed by TMS-diazomethane (2M in hexane, 6 mmol) in one time. The reaction was stirred 1h at RT until some Pd black was observed. Excess of TMS-diazomethane was removed by vacuum transfer and the crude was distilled using a kugelrohr under vacuum affording 87% yield of **5** a colorless oil containing 66 % of trans-**5**. Attribution presented hereafter (*) is rescaled to 1 for clarity. (the minor is cis-5 product) Attribution of the minor product was done by recovery of unreacted silane in the filtrate after preparation of the corresponding silicate.

^{1}H NMR (Bruker, 400MHz, $CDCl_3$, rt): δ = 3.8 ppm ($m_{(trans+cis)}$, $^1J(^{13}C\text{-}^1H)$: 142 Hz, $^3J(^1H\text{-}^1H)$: 7Hz, Si-O*CH*$_2$, 6H*$_{(cis)}$+6H$_{(trans)}$); 1.21 ppm$_{(trans)}$, 1.22 ppm$_{(cis)}$ (t, $^1J(^{13}C\text{-}^1H)$: 125 Hz, $^3J(^1H\text{-}^1H)$: 7Hz, Si-OCH$_2$-*Me*, 9H*$_{(cis)}$+9H$_{(trans)}$); 0.9 ppm$_{(cis)}$ (dt, 9.5Hz, 2.5Hz, 1H); 0.7 ppm$_{(trans)}$ (dq, 9.1Hz, 6.2Hz, 2.8Hz, 1H); 0.4 ppm$_{(cis + trans)}$ (m (td$_{(cis)}$ + dd?$_{(trans)}$, 1H*$_{(cis)}$ + 1H$_{(trans)}$); 0.05 ppm$_{(cis)}$ (s, $^2J(^{29}Si\text{-}^1H)$: 6.4 Hz, TMS, 9H); -0.05 ppm$_{(trans)}$ (s, $^2J(^{29}Si\text{-}^1H)$: 6.2 Hz, TMS, 9H); -0.2 ppm$_{(cis)}$ (m, 2H*$_{(cis)}$ + 1H$_{(trans)}$); -0.5 ppm$_{(trans)}$ (m, 1H); **^{13}C NMR** (Bruker, 400MHz, $CDCl_3$, rt): δ = 58.4 ppm$_{(trans)}$ Si-O*C*H$_2$, 58.3 ppm$_{(cis)}$ Si-O*C*H$_2$, 18.2 ppm$_{(trans)}$ Si-OCH$_2$-*Me*, 18.1 ppm$_{(cis)}$ Si-OCH$_2$-*Me*, 6.1 ppm$_{(cis)}$, 5.0 ppm$_{(trans)}$, 1.7 ppm$_{(?)}$,-0.2 ppm$_{(?)}$,-1.0 ppm$_{(cis)}$ TMS, -2.75 ppm$_{(trans)}$ TMS, -4.3 ppm$_{(?)}$, -6.13 ppm$_{(trans)}$

General procedure for the synthesis of silicate: In a dry Schlenk tube under argon covered with aluminum foil was added catechol (2 equiv.), crown ether (1 equiv.) and the Schlenk was purged. Degassed MeOH (0.25 M) solution of the alkyltriethoxysilane (1equiv.) Potassium methoxide in methanol (1 equiv.) was added dropwise and the reaction was stirred 3 hours at room temperature. Solvent was removed

directly on the Schlenk line, and the crude was dry under high vacuum until a powder was obtained. Silicates were purified by recrystallisation as mentioned.

Synthesis of 6: Following the general procedure, catechol (659 mg; MeOH 11ml, MeOK (783 µL, 2.8 mmol), silanes (2.8mmol) and 18C6 (2.8 mmol), gave 80% yield (1.5g) based on the reactive trans-silane. **^{1}H NMR** (Bruker, 400MHz, $CDCl_3$, rt): δ = 6.8 ppm (m, cat, 4H); .6 ppm (m, cat, 4H); 4.0 ppm (m, cat, 2H); 3.5 ppm (m, 18C6, 24H); 1.7 ppm (m, 1H); 1.2 ppm (t, 3H); 0.9 ppm (m, 2H); 0.6 ppm (m, 1H); **^{13}C NMR** (Bruker, 400MHz, $CDCl_3$, rt): δ = 176 ppm, 150.7 (d) ppm, 117.5 (d) ppm, 110.4 (d) ppm, 69.9 ppm, 59.7 ppm, 17.5 ppm, 14.2 ppm, 13.1 ppm, 10.8 ppm. **^{29}Si NMR** (Bruker, 400MHz, $CDCl_3$, rt): δ = -81.4 ppm

Synthesis of 7: Following the general procedure, catechol (3.6mmol) ; MeOH (7ml), MeOK (500 µL, 1.8 mmol), silanes (1.8mmol) and 18C6 (2.8 mmol), gave 75% yield based on the reactive trans-silane. **^{1}H NMR** (Bruker, 400MHz, $CDCl_3$, rt): δ = 6.8 ppm (m, cat, 4H); 6.5 ppm (m, cat, 4H); 3.5 ppm (m, 18C6, 24H); 0.6 ppm (ddd, 1H); 0.2 ppm (ddd, 1H); -0.2 ppm (m, 1H); -0.4 ppm (m, 1H); **^{13}C NMR** (Bruker, 400MHz, $CDCl_3$, rt): δ = 151.1 ppm, 150.8 ppm, 117.5 ppm, 117.0 ppm, 69.1 ppm, 5.8 ppm, 0.5 ppm, -0.1 ppm, -2.6 ppm. **^{29}Si NMR** (Bruker, 400MHz, $CDCl_3$, rt): δ = 2.1 ppm (TMS), -76.9 ppm

Chapter II.
Fluorinated hypercoordinated silicon species

Chapter 2.
Fluorinated hypercoordinated silicon species

This first chapter contains material from two papers in the following peer-reviewed journals; The chemical record and submitted to ACIE. The relevant information (figure, ..) from the eSI are integrated in the chapter 1.2 with numeration from the submitted eSI. (example : Figure S1)

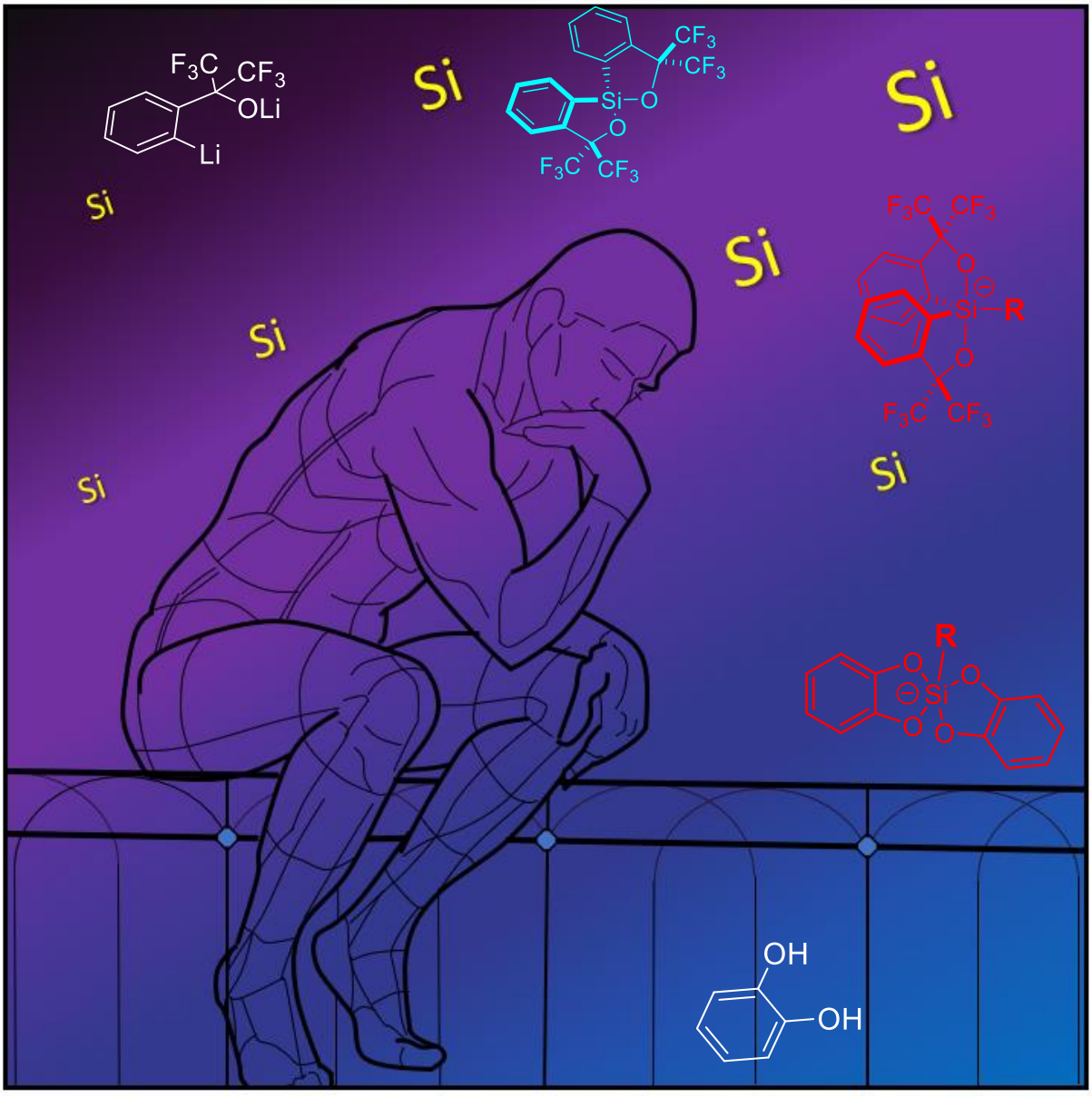

2.1 Introduction

The development of chemicals bearing a trifluoromethyl as essentially find it place in pharmaceutical chemistry due to the strong electron-withdrawing effect, lipophilicity and stability. Methodology developed for the synthesis of R-CF_3 has taken advantages of modern synthetic strategy such as radical/photoredox process. This has been achieved using classical reagents and modern ones, all being commercially available nowadays. (Fig. 1.A) Conceptually, all these reagents involved reducing process for the generation of the desired trifluoromethyl radical species. For example, one of the most common reagentss, *trifluoromethyliodine*,[1] has been directly used for this purpose but also for the synthesis of more friendly reagents. Indeed, F_3CI is gaseous (b.p. -22°C) and relatively toxic if inhaled with potent liberation of strong acid.[2] Solid reagent, such as Langlois'-,[3] Togni's-[4] and Umemoto's[5] one (Respectively, F_3CSO_2Na, hypervalent iodine and sulfonium) were then developed to simplify the handling and experimental procedure.

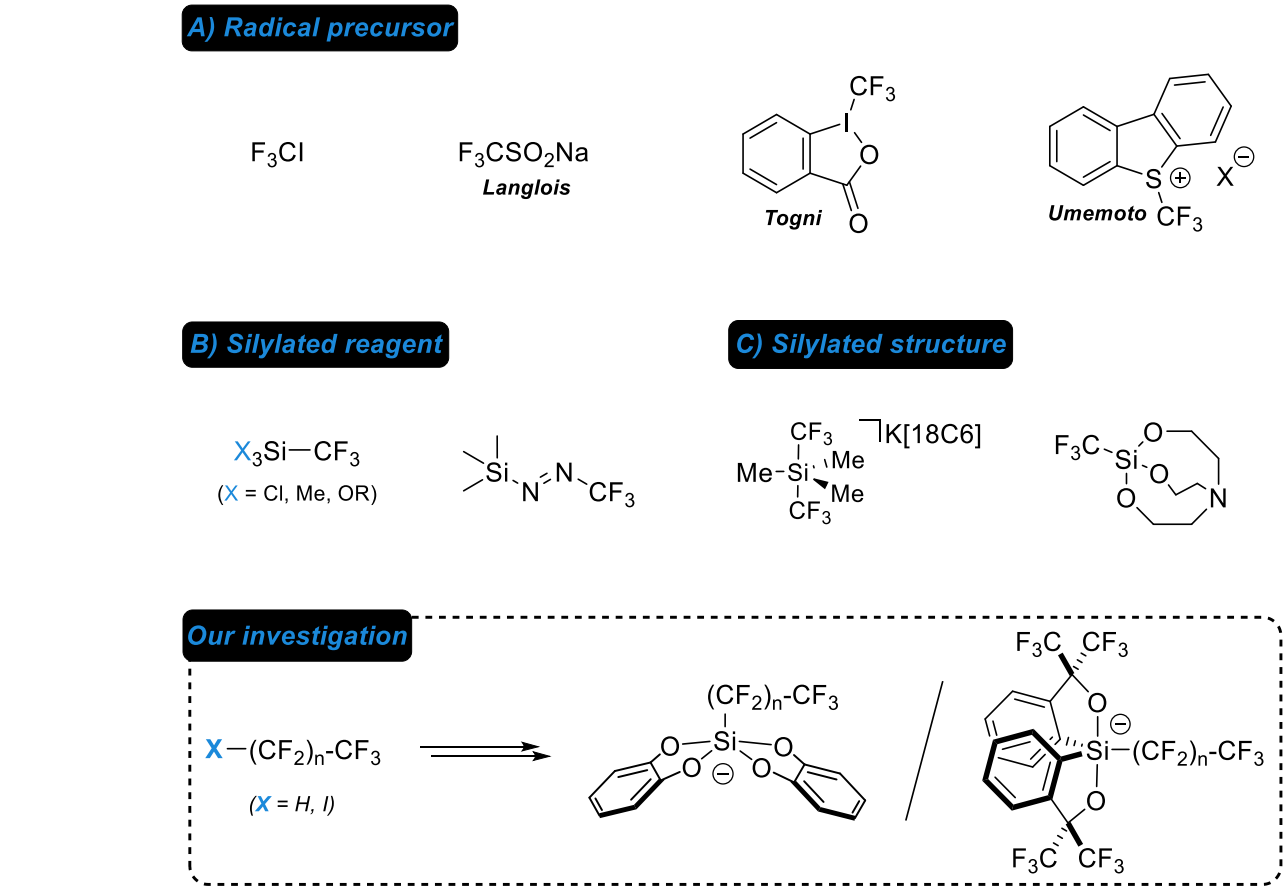

Figure 1. A) Classical radical precursors; B) Nucleophilic reagents and reactive silane; C) Hypercoordinated silicon species

In addition to their ability to act as radical precursors, the Togni and Umemoto's reagents are also acting as electrophilic perfluoroalkylation agents. This behaviour is in contrast with the famous Prakash reagent[6] (Me_3Si-CF_3) and the, now, emerging diazene chemistry[7] (TMS-N=N-CF_3) both known as nucleophilic source of trifluoromethyl anion.[8] (Fig. 1.B) Some non-nucleophilic silane (X_3Si-CF_3, X = Cl, OMe) were also synthesised [9] and then used for the preparation of silatrane (F_3C-$Si(OC_2H_5)_3N$) as described by Eujen and co-workers.[10] (Fig. 1.C) The TMS-CF_3 was also reported to be able to form some hypervalent derivatives as demonstrated by Prakash with the formation of $[K18C6][Si(Me)_3(CF_3)_2]$.[11]

In this context, the preparation of known radical precursors such as Martin's silicates or bis(catecholato) silicates appears as valuable targets to investigate the first possible example of trifluoromethyl radical via an oxidative pathway.

2.2 Hypercoordinated [Si]-CF_3

2.2.1 Bis(catecholato)silicates

To begin our investigation toward the synthesis of the desired hypercoordinated silicon species (bis(catecholato)silicates) or Martin's silicates) bearing the trifluoromethyl substituent, we started by looking into the more accessible methodology for the synthesis of the desired silane. Indeed, the synthesis of bis(catecholato) involved the preparation of the desired alkoxysilane as described in the *chapter 1.1*. Difficulty in the preparation of the desired intermediate appears due to the relative unstability of the trifluoromethyl anion. The decomposition in fluoride plus highly reactive difluorocarbene often results in the formation of strong Si-F and multiple degradation products. The stabilisation of the desired CF_3 anion essentially depends on cation hinderance. In addition, stabilization was reported based on anionic trapping such as a dynamic equilibrium with DMF (F_3C^- + $HC(O)NMe_2$ → $F_3CC(H)(O^-)NMe_2$). Firstly, we started with the developed methodology of Beckers as described in scheme 1.[9]

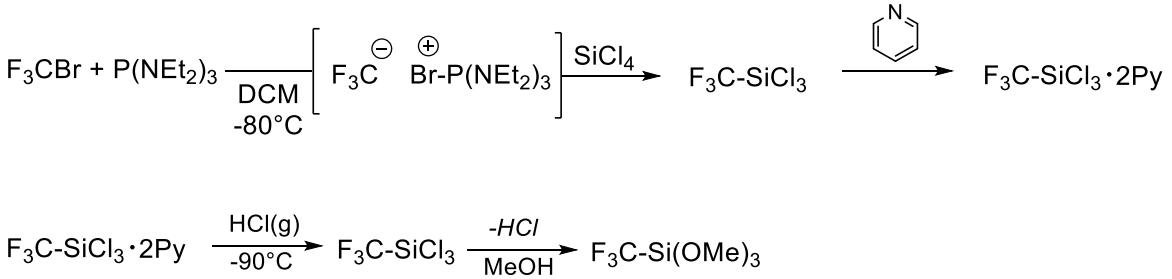

Scheme 1. Preparation of trifluoromethyl silane from CF_3Br

The synthesis begins with the formation of the desired anion from $P(Et_2N)_3$ and CF_3Br in dichloromethane at low temperature. With the anion in hand, the addition on silicon tetrachloride ($SiCl_4$) allows the formation of the desired trichlorotrifluoromethylsilane ($F_3C\text{-}SiCl_3$). Due to the purification difficulty encountered, Beckers *et al.* decided to form the perfectly insoluble $[F_3C\text{-}SiCl_3][Py]_2$ complexes. Filtration of the salt and condensation of anhydrous (gaseous) HCl liberates of the salt and distillation of the volatile products affords the desired trichlorosilane. Then, the silane was transformed into alkoxysilane by addition of methanol and removal of HCl(g).

In our case, only the related $CF_3I_{(g)}$ was available. We then decided to follow the reported methodology and perform the extrapolation with the gas. (Scheme 2) It must be mentioned that the reaction of the anion with $P(Et_2N)_3$ led to the formation of instable phosphine known to decompose violently with air (formation of F_2CO). This sub-reaction is also reported with the phosphonium (X(-) [P](+); X = Br, I) and is unfortunately enhanced in the case of iodide compared to bromide.

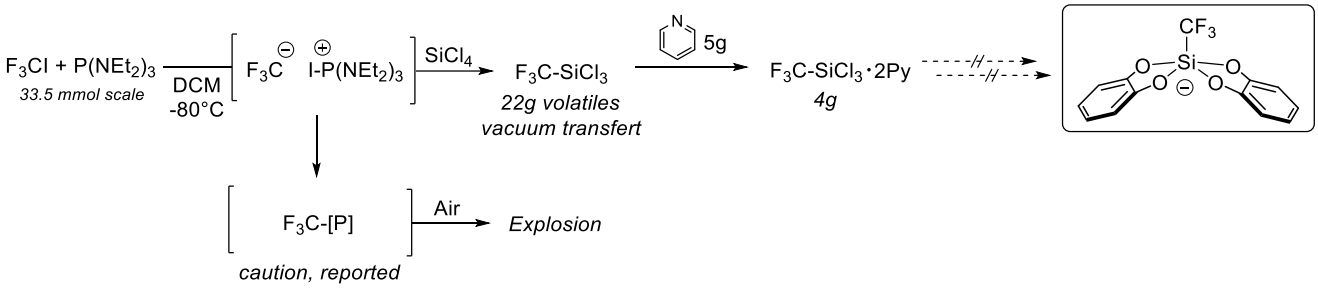

Scheme 2. Preparation of trifluoromethyl silane from CF_3I

To our delight, the formation of the non-soluble intermediate was achieved as reported. ^{19}F NMR of the volatiles isolated by vacuum transfer confirms the presence of the desired silane and multiples degradation products. With the non-soluble intermediate in hand, we then investigated the preparation of anhydrous $HCl_{(g)}$ from the addition of 35% $HCl_{(aq)}$ on $CaCl_2$ and condensation at -90°C. (HCl b.p. -85°C). Unfortunately, distillation of the crude and removal of HCl led to the formation of a colourless liquid with NMR data not relevant compared to the reported one. Different attempts on the non-soluble powder for the direct transformation into the desired pyridinium bis(catecholato)trifluoromethyl silicate were unsuccessful. Due to the experimental difficulty of the starting material preparation, we decided to investigate another *shorter* synthetic route based on the direct formation of an hypercoordinated silicon species (Martin's silicate). For this, Martin's spirosilane was used as electrophile.

2.2.2 Martin's silicates

2.2.2.1 Overview of the corresponding silane/silicates

In 1979, J. C. Martin made a seminal report on the use of the dilithio derivative of hexafluorocumyl alcohol as a bidendate ligand that can be appended twice on heteroatoms such as phosphorus, sulfur and silicon to give the corresponding phosphoranoxide, sulfurane and siliconate.[12] When treated with $SiCl_4$, hexafluorocumyl alcohol dianion provides a direct access to spirosilane **4** that can also be obtained from the treatment of siliconate **3** with triflic acid. (Scheme 3)

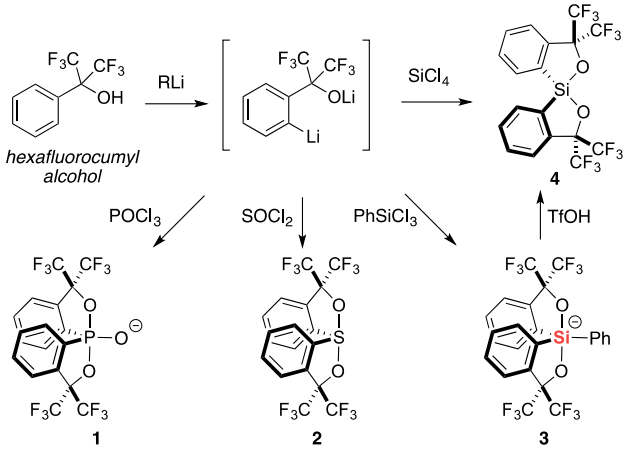

Scheme 3. Access to Martin's spirosilane and valuable derrivative

Martin's spirosilane can act as a Lewis acid allowing the reaction of neutral or charged nucleophiles to obtain original structures. The Lewis acid properties were exploited to easily reach the hypervalent form (pentavalent) that can acts for example as a fluoride probe.[13] very strong Si-F bond warrants selective and quantitative detection of fluoride ions in solution and the structural reorganization of hypervalent silicon structure allows for a diagnostic. (Figure 2)

UV and fluorescence spectroscopies have been used to quantify the fluorosiliconate product attaining detection limits as low as 5 µM, which is close to the residual concentration of fluoride in drinking water. More recently, Greb and coworkers have proposed a bis(alizarinato) spiro silane as chromogenic fluoride sensor which announces further developments in this area.[14]

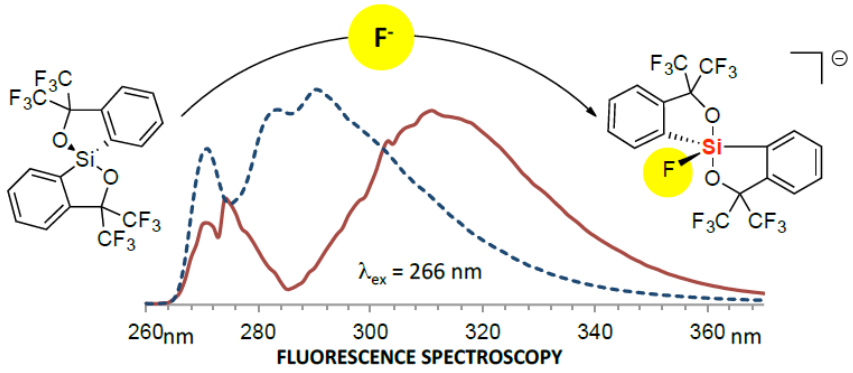

Figure 2. Martin's spirosilane as fluoride sensor.

Martin's spirosilane is able to perform interactions with neutral Lewis bases displaying various strength and steric hindrances. It has been established that the outcome of these interactions was very dependent on both parameters.[15] Indeed, weakly hindered NHCs Lewis base of imidazolylidene type (IMe, IMes) led to the formation of new neutral (zwitterionic) adducts **5** originating from classical Lewis acid-base interactions were obtained in which the pentacoordinated silicon adopts a trigonal bipyramid (TBP) geometry (Scheme 3). Conversely, when the size of the free carbene becomes larger (IPr, ItBu), no direct interaction between the silicon and the divalent carbon of the NHCs can be noticed by ^{1}H NMR monitoring. Considering the strength of the Lewis partners involved, the non-interaction is unambiguously diagnostic of Frustrated Lewis Pair (FLP) behaviors highlighting the bulkiness of the spirosilane to some extent. The mixtures can evolve nonetheless towards the formation of "abnormal adducts" **6** where a covalent bond is created between the silicon atom and one of the two trivalent carbons located on the NHC backbone. As it can be visualized on the X-Ray structure of **6** (R = Dipp), the ligands surrounding the hypervalent silicon are quite distorted due to the steric congestions and deviates from the perfect TBP.

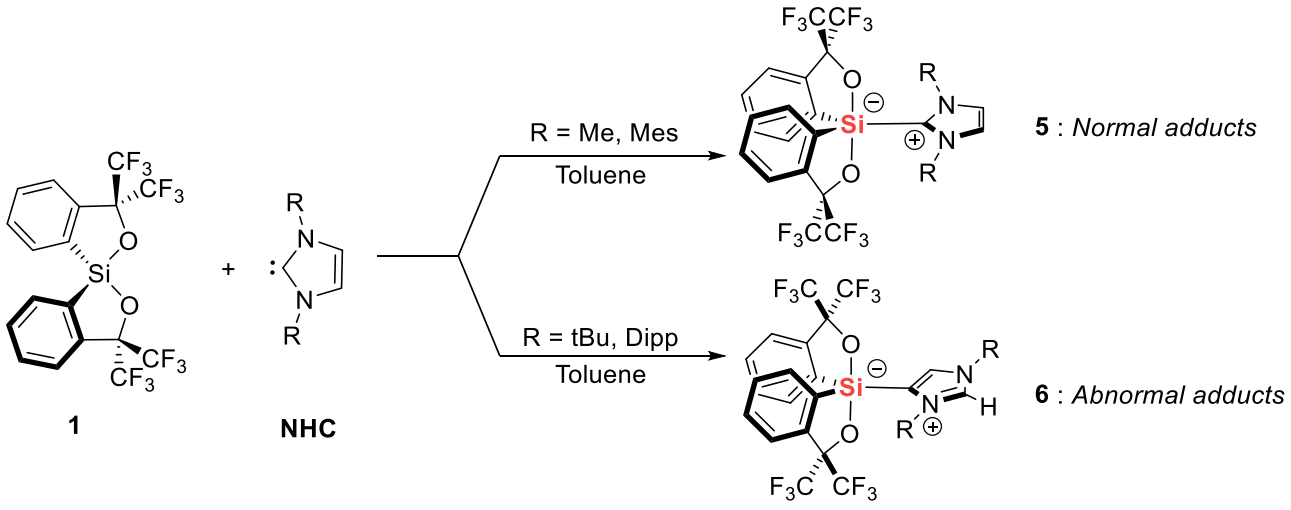

Scheme 3. Silane interaction with NHCs.

The abnormal adducts **6** have been later used as precursors for new anionic NHC carbene ligands possessing within their structure a poorly coordinating anion.[16] As a matter of fact, structures **6** are neutral species that could be seen as imidazolium rings attached to a siliconate anion. Basically, the deprotonation of the positively charged heterocycles by using an appropriate base would lead to a carbene ligands that can interfere with metals to form original organometallic complexes. From this perspective, the abnormal adducts **6** were cleanly deprotonated using n-butyllithium as a base, to be subsequently trapped with gold(I) or Cu(I) species affording complexes of type **7** and **8**, respectively. (Scheme 4) It is noteworthy that the anionic nature of the ligand and the presence of the lithium cation favour the chloride dissociation to provide the corresponding neutral complexes. The strong alpha-donor ability of these new anionic NHC ligands was confirmed by DFT calculations.

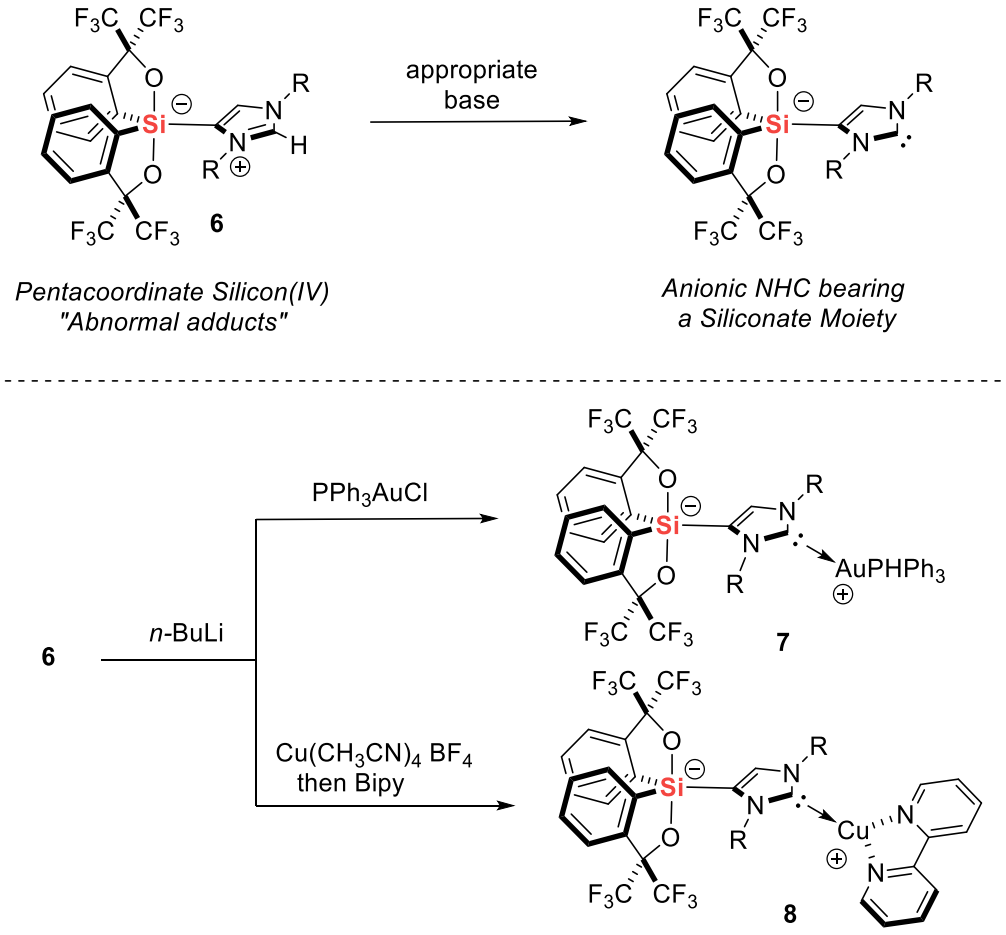

Scheme 4. Siliconate-imidazolium zwitterions as precursors for anionic NHC ligands.

Theoretically, the Lewis acid properties of the Martin's spirosilane **4** can be modulated by introducing substituents on the aromatic rings. For that purpose, a synthesis strategy of analogous structures of spirosilane **4** has been previously developed in our laboratory.[17] It consists in the spirocyclization of functionalized hexafluorocumyl ligands that are readily available from the corresponding 2-brombenzoic acid derivatives. (Scheme 5)

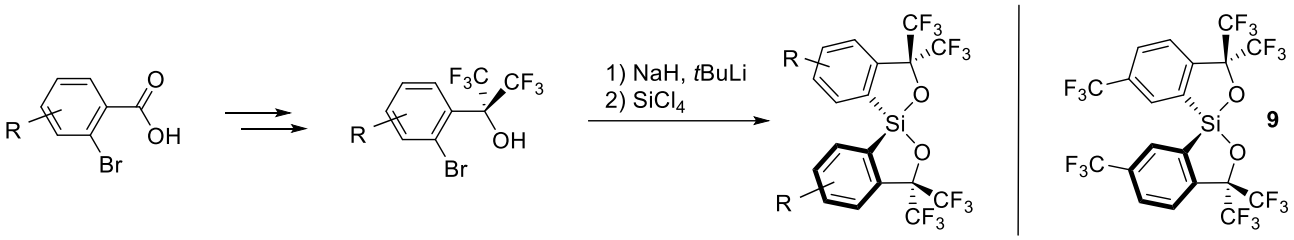

Scheme 5. Synthesis of Martin's spirosilane analogues.

With this method, the synthesis of a spirosilane **9** bearing one trifluoromethyl group on each aromatic ring was achieved. The presence of an electron-withdrawing group has a great effect on the electronic properties of the silicon atom and the acceptor number was calculated with the GB method as AN = 89.2.

That makes spirosilane **9** a Lewis acid prone to reach hypervalency. The high electrophilicity of the CF_3 derivative **9** was confirmed since a classical Lewis adduct **10** was formed in the presence of a bulky NHC (IPr) which has never been observed in the case of simpler spirosilane **4**. (Scheme 6) DFT calculations revealed that the presence of CF_3 groups on the spirosilane increases the Gibbs free enthalpy of formation of the conventional adduct by at least 10 kcal.mol-1.

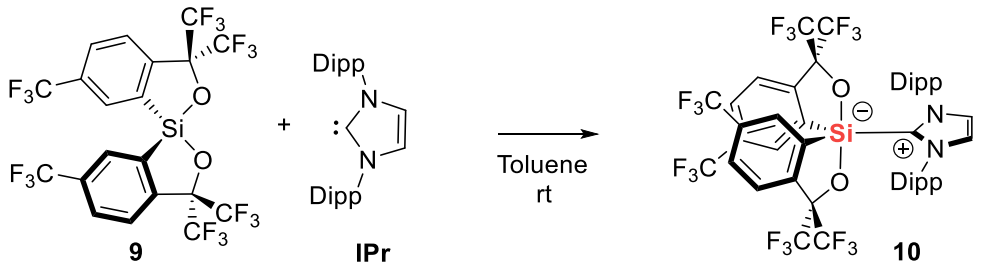

Scheme 6. Formation of classical Lewis adduct by reaction of spirosilane **4** with IPr

Although for the moment, Lewis acid partners **1** and even more acidic **4** proved to be inefficient for the activation of H_2 and CO_2, activation of formaldehyde was possible with the IPr NHC and triisopropylphosphine. In these cases, the zwitterionic adducts of type **11** could be isolated. (Scheme 7)

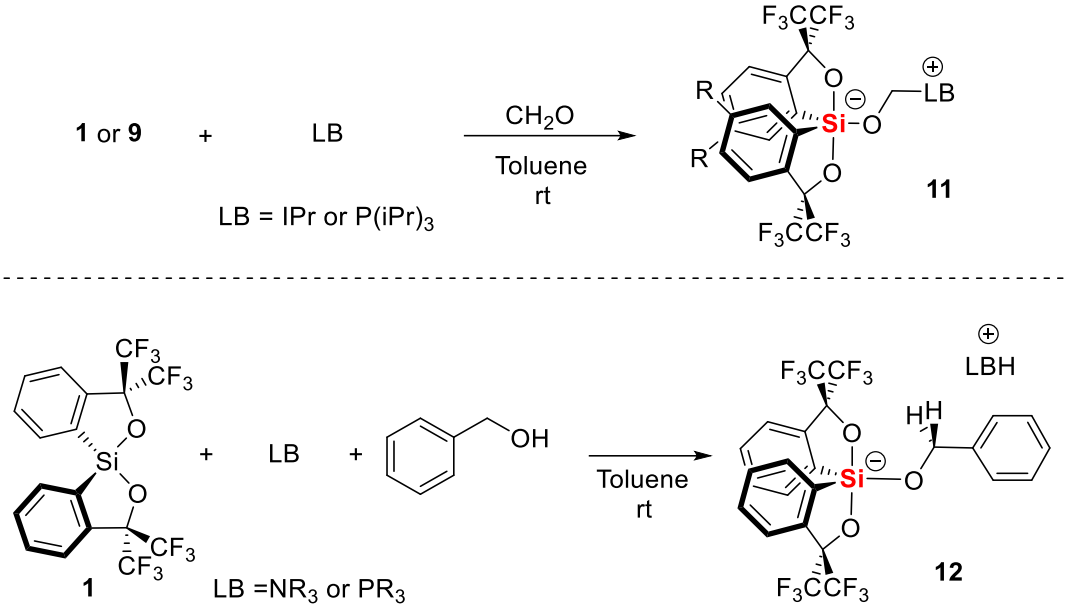

Scheme 7. Use of spirosilanes **1** and **9** in FLP chemistry

Additional

In addition, the Martin's spirosilane **4** could also be used for the activation of alcohols such as benzylic alcohol to form benzyloxysilicates **12** in the presence of hindered phosphines or amines. On the ^{1}H NMR spectrum, adducts **12** displayed AB systems with a large splitting of the two diastereotopic benzylic protons that highlights the intrinsic chirality of the Martin's spirosilane at the NMR timescale. This interesting feature potentially opens the way for further asymmetric FLP transformations using chiral spirosilane analogues. Very recently, Martin's silicates also appeared as a possibility for the generation of radicals species. (Scheme 8) Related use in radical chemistry with *in situ* formation was illustrated by Sakai in 2019. [18]

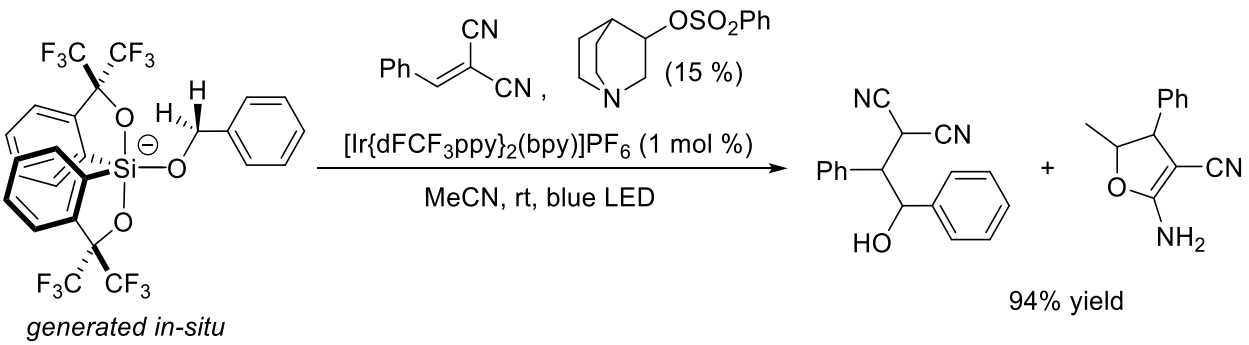

Scheme 8. Spirosilane catalyst for C-H bond-weakening process

The formation of the alkoxy silicates ([Si]-OBn) results in the weakening of the C-H bond dissociation energy (BDE) of the benzylalcohol. With the combination of hydrogen atom transfer catalyst (HAT), the generation of the desired radical was performed and the addition on benzalmalononitrile was achieve. Cyclization was also observed during the purification process due to the silica acidity.

More classically, several Martin's silicates where synthesized from the direct nucleophilic addition of Grignard reagent or from lithium one. With these hypercoordinated species in hand the generation of radicals was allowed by the use of adequate photocatalyst (Mesyl-acridinium derivative). Kano made the first report on the use of these derivatives as radical precursors (Scheme 9).

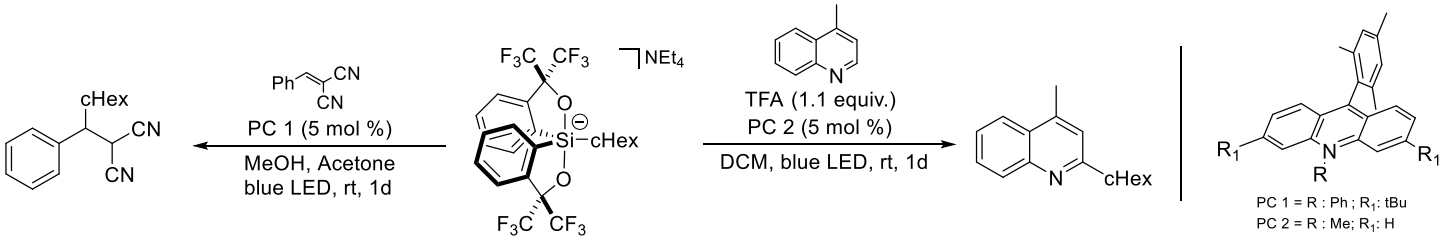

Scheme 9. Martin's silicate as radical precursor

The classical Minisci-type alkylation[19] then allylation reactions[20] were developed respectively in 2020 and 2021. This methodology allowed the generation of a wide range of radicals. Among them the methyl radical appears as remarkabily interesting. Indeed, this nontrivial radical (from the generation point of view) became with this hypercoordinated reagent a new common one.

2.2.2.2 Formation of trifluoromethyl derivative

As illustrated just before, the generation of radicals from hypercoordinated Martin's silicates also appears as a potential solution for the generation of trifluoromethyl radical via an oxidative pathway. Then, the synthesis of the desired silicon salts was investigated via three main pathway for the generation of the trifluoromethyl anion and direct addition on Martin's silane. Our first attempt was once again based on Beckers' work with $P(Et_2N)_3$ and CF_3I.[9] (scheme 10) Compared to the previous silane synthesis with numerous steps, the direct generation on nucleophile and addition for the formation of "stable" pentavalent species appeared as a promising synthetic pathway. To simplify the denomination, Martin's spirosilane will be abbreviated as [SiL_2] with L = α,α-bis(trifluoromethyl) benzenemethanolato-(-2)C2,O).

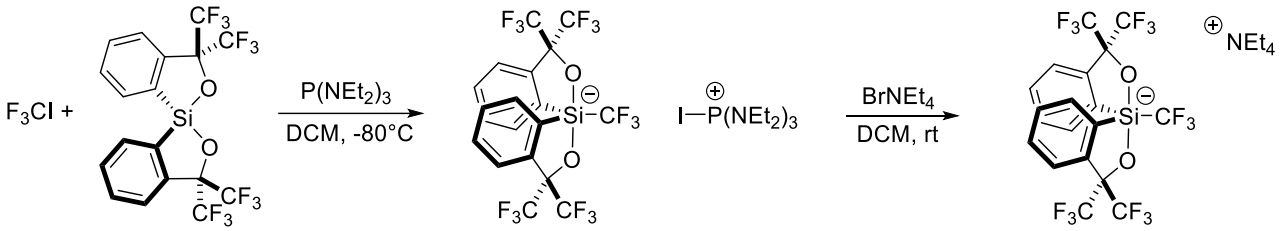

Scheme 10. Expected Martin's trifluoromethyl silicate synthesis

Following the previous methodology, we managed to observe some ^{19}F NMR peaks (-61 ppm, septuplet) that could correspond to the desired -CF_3 coupling with two non-equivalent ligands CF_3. A complex multiplet at -74 ppm corresponding probably to the ligands forming spatial coupling with the other -CF_3 from the ligand (L) and the spatial one with the substituent. These results were observed for all the performed methodologies involving the generation of the desired trifluoromethyl anion, the spectrum is depicted hereafter. (figure 3) The major drawback of this methodology consists in the formation of F_3C-[P] derivative, the formation of $[Si(F)L_2]$- anion due to the decomposition of the anion and probable decomposition of unstable phosphine. Finally, with this methodology, numerous subproducts led to the formation of dirty oil during the precipitation process. At this stage of our investigation, it was not clear yet that the $[Si(CF_3)L_2]$- was unstable in solid-state and degradation was attributed to the different undesired species in the reaction medium. Due to that, we decided to investigate another reported methodology for generation of trifluoromethyl anion as described by Pawelke in 1989.[21] (scheme 10)

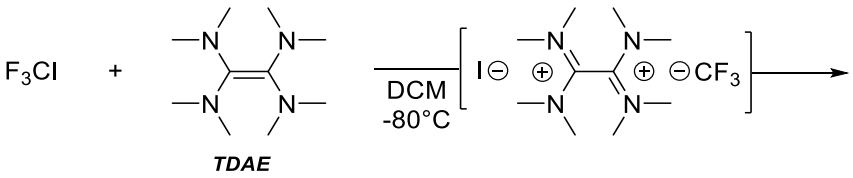

Scheme 10. Preparation of trifluoromethyl anion via TDAE/CF_3I

By analogy with the formation of Prakash reagent described with CF_3I, TMSCl and TDAE, it appears reasonable to investigate the use of this stabilized anion for our synthesis. (scheme 11)

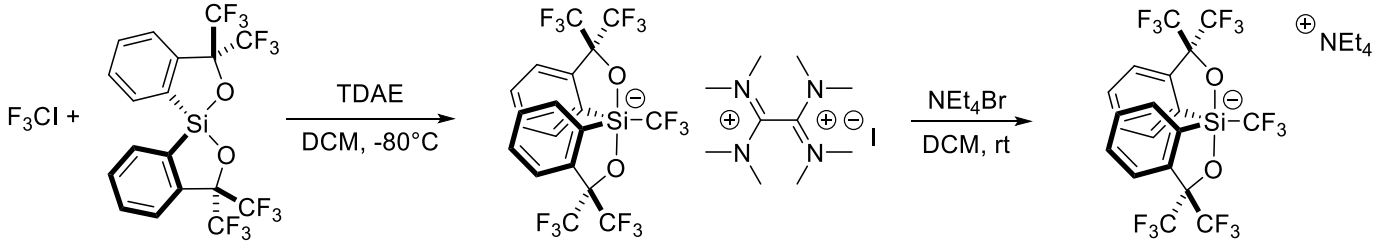

Scheme 11. Expected Martin's trifluoromethyl silicate synthesis

The expected synthetic route is depicted in scheme **11** and was unfortunately less efficient than expected. Indeed, the decomposition of the anion also occurs with the formation of several fluorinated products.

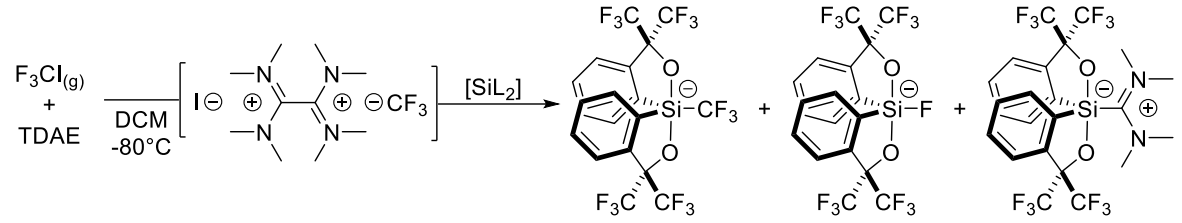

Scheme 12. Observation of several silicates during the nucleophilic addition, cation exchange and cation are not depicted for clarity.

Analysis of the crude (Fig. 3) confirmed that the probable product and Martin's fluoride silicates were obtained. This was also consistent with the previous observations made when using the other procedure.

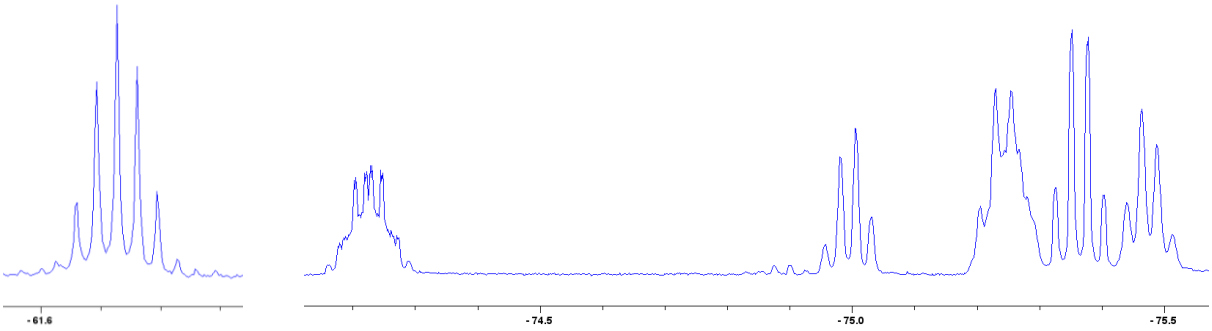

Figure 3. Crude (solution) ^{19}F NMR after cation exchange and extraction (Si-CF_3 at -61.6ppm and ligands -CF_3 with special coupling at -74.2 ppm).

Once again during the isolation process, the desired product was not obtained, $[Si(F)L_2]^-$ was often observed in addition to an unidentified product. The structure was then fully resolved by XRD. It consists in the formation of zwitterionic silicate $[Si(C(NMe_2)_2)L_2]$ (Figure 4). A potential mechanism for the formation of this species is depicted in scheme 13. The tetramethyldiaminocarbene ligands was previously reported.[22] Synthesis of $[Si(C(NMe_2)_2)L_2]$ is currently investigate using the Wanzlick equilibrium (THF-d_8, thermal activation) and from the degradation of [TDAE][2X], X = I, Br, Cl.

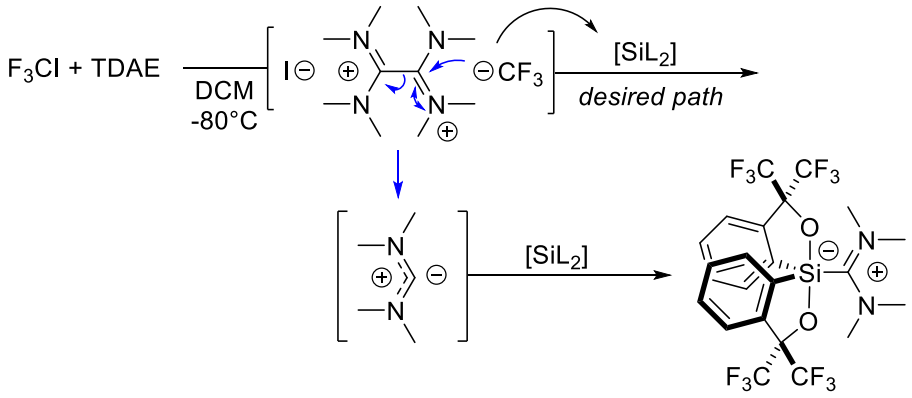

Scheme 13. Proposed mechanism for formation of zwitterionic Martin's carbene

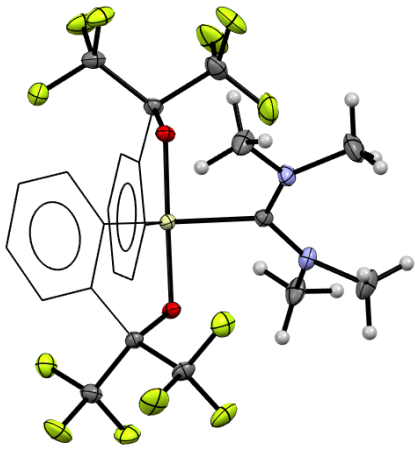

Figure 4. Zwitterionic silicate [Si(C(NMe$_2$)$_2$)L$_2$] molecular structure. Thermal ellipsoids are drawn at 50% probability level. Hydrogen atoms and cation are omitted for clarity. Carbons of Martin's Ligand (L) are drawn as wireframe for clarity.

Suitable crystals of silicate [Si(C(NMe$_2$)$_2$)L$_2$] for an X-ray diffraction analysis were obtained by slow evaporation of a saturated DCM solution. It crystallized in the monoclinic space group P2$_1$/n. (Figure 4). The apical position is occupied by the carbene moiety, Si-C length is 1.968(2) Å. The Si-O$_{ax}$ length is respectively 1.786 Å and 1.788 Å. Both Si-C(—NMe)$_2$ bonds are similar (1.333 and 1.336 Å) and suggest a fast equilibrium of the cation.

Finally, last attempts were performed with a methodology developed by Prakash in 2012.[23] The use of fluoroform (HCF$_3$) permits the generation the desired anion by deprotonation with KHMDS in Toluene. Extrapolation of this methodology with our substrate led to the desired and identified [Si(CF$_3$)L$_2$]-. The crude NMR appeared clean with the only formation of the desired product and the fluoride one. Unfortunately, all the attempts to isolate the desired product only led to the observation of the latter one. From this, we concluded that no strong lattice effect is observed allowing the stabilisation of the desired silicon salt.

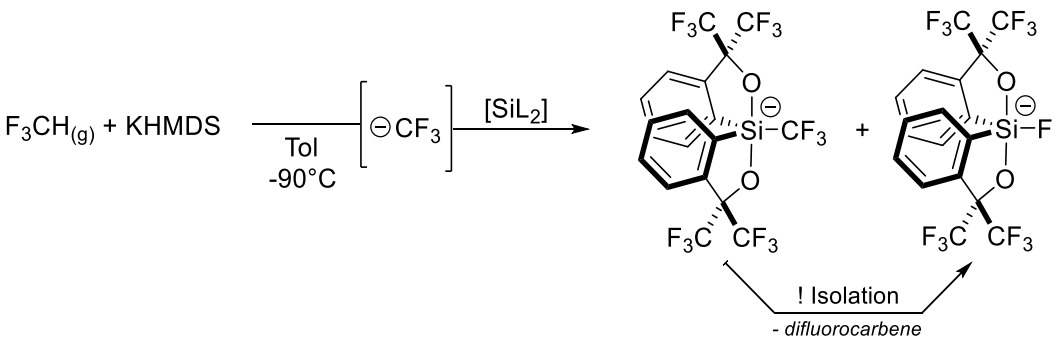

Scheme 14. Synthetic pathway from fluoroform, decomposition during isolation process. Cation and cation exchange reaction are not depicted for clarity.

2.2.3 Conclusion

We investigated the formation of the trifluoromethyl anion and its stabilisation for the synthesis of silane and pentavalent species. These methodologies involved the use of gases such as fluoroform (HCF_3) and CF_3I. The generation of the anion has been done via "SN_2X type" reaction (F_3C-I + [P]) or reduction (F_3C-I + TDAE). For these two examples, the relative stability of the anion is ensured by using hindered cation. The formation of the desired product was observed in addition to multiple undesired ones. In total, three different methodologies allowed the observation of complex multiplet that could be attributed to the spatial interaction between the -CF_3 substituent with Martin's ligand trifluoromethyls.

Unfortunately, the desired silicate appeared unstable in solid-state. Indeed during the isolation process by precipitation, the pure compound was not obtained and degradation leading to the formation of Martin's silicate bearing fluoride was observed. Based on this observation, we proposed a possible decomposition channel of the Si-CF_3 into Si-F + $CF_{2(g)}$ with the carbene being able to decompose from the dimeric structure or directly.
Deeper investigation, from the experimental and chemical points of view, enabled to isolate the desired product. Firstly, slow bubbling of CF_3X (X = I, H) in N_2 with gas dispenser allowed a better control of the temperature and therefore permitted to avoid the potential degradation reaction. Secondly, higher screening of the cation enabled to reach a better lattice effect and potentially stabilized the desired species in solid-state which allowed its isolation.

References chapter 2.1 & 2.2

[1] D. J. Burton, W. Qui, M. Sánchez-Roselló, C. del Pozo Losada, J. Luis Aceña, in *Encyclopedia of Reagents for Organic Synthesis*, John Wiley & Sons, Ltd, **2009**.

[2] N. R. Council, *Iodotrifluoromethane: Toxicity Review*, **2004**.

[3] C. Zhang, *Advanced Synthesis & Catalysis* **2014**, *356*, 2895–2906.

[4] D. K. Yadav, *Synlett* **2010**, *2010*, 2523–2524.

[5] H. Li, *Synlett* **2012**, *23*, 2289–2290.

[6] X. Liu, C. Xu, M. Wang, Q. Liu, *Chem. Rev.* **2015**, *115*, 683–730.

[7] C. Chauvier, L. Finck, E. Irran, M. Oestreich, *Angewandte Chemie International Edition* **2020**, *59*, 12337–12341.

[8] U. Hartkopf, A. de Meijere, *Angewandte Chemie International Edition in English* **1982**, *21*, 443–443.

[9] H. Beckers, H. Bürger, P. Bursch, I. Ruppert, *Journal of Organometallic Chemistry* **1986**, *316*, 41–50.

[10] R. Eujen, A. Roth, D. J. Brauer, in *Silicon Chemistry* (Ed.: U. Schubert), Springer, Vienna, **1999**, pp. 109–115.

[11] G. K. S. Prakash, F. Wang, Z. Zhang, R. Haiges, M. Rahm, K. O. Christe, T. Mathew, G. A. Olah, *Angewandte Chemie International Edition* **2014**, *53*, 11575–11578.

[12] E. F. Perozzi, J. C. Martin, *J. Am. Chem. Soc.* **1979**, *101*, 1591

[13] H. Lenormand, J.-P. Goddard, Louis Fensterbank, *Org. Lett.* **2013**, *15*, 748.

[14] H. Ruppert, L. Greb, *Organometallics* **2020**, 10.1021/acs.organomet.0c00473.

[15] F. Medici, G. Gontard, E. Derat, G. Lemière, L. Fensterbank, *Organometallics* **2018**, *37*, 517

[16] A. Nasr, A. Winkler, M. Tamm *Coord. Chem. Rev.* **2016**, 68.

[17] H. Lenormand, V. Corcé, G. Sorin, C. Chhun, L.-M. Chamoreau, L. Krim, E.-L. Zins, J.-P. Goddard, L. Fensterbank, *J. Org. Chem.* **2015**, *80*, 3280

[18] K. Sakai, K. Oisaki, M. Kanai, *Advanced Synthesis & Catalysis* **2020**, *362*, 337–343.

[19] G. Ikarashi, T. Morofuji, N. Kano, *Chemical Communications* **2020**, *56*, 10006–10009.

[20] T. Morofuji, Y. Matsui, M. Ohno, G. Ikarashi, N. Kano, *Chemistry – A European Journal* **2021**, *27*, 6713–6718.

[21] G. Pawelke, J. Fluorine Chem. **1989**, *42*, 429-433;

[22] a) A. J. Hartshorn, M. F. Lappert, K. Turner, **1978**. b) S. J. Ahmed, Md. I. Hyder, S. E. Kabir, Md. A. Miah, A. J. Deeming, E. Nordlander, *Journal of Organometallic Chemistry* **2006**, *691*, 309–322. c) M. Otto, S. Conejero, Y. Canac, V. D. Romanenko, V. Rudzevitch, G. Bertrand, *J. Am. Chem. Soc.* **2004**, *126*, 1016–1017. d) W. Kantlehner, R. Aichholz, M. Karl, *Zeitschrift für Naturforschung B* **2012**, *67*, 305–319. e) U. Bodensieck, H. Stoeckli-Evans, G. Süss-Fink, *Journal of Organometallic Chemistry* **1992**, *433*, 149–165.

[23] G. K. S. Prakash, P. V. Jog, P. T. D. Batamack, G. A. Olah, *Science* **2012**, *338*, 1324–1327.

Supporting information

All chemicals were used as received without further purification except catechol that was purchased from commercial source and purified by crystallization from chloroform. Standard Schlenk techniques were employed, and all reactions were carried under dry argon atmosphere. NMR spectrum (1H, 13C, 29Si) were recorded on 400 MHz Bruker AVANCE II spectrometer at room temperature. Chemical shifts (δ) are reported in ppm and coupling constants (J) are given in Hertz (Hz). Abbreviations used for peak multiplicity are, s (singlet); bs (broad singlet); d (doublet); t (triplet); q (quartet); quint (quintet); sept (septet); m (multiplet) etc. Note: special care should be taken when working with fluorinated/corrosive gas. Mind the temperature control and oxygen exclusion, violent decomposition and over reaction can occurs.

Typical experiment with CF_3I + $P(NEt_2)_3$:

A sealed, dried 20 mL µw tube was put under vacuum and CF_3I (0.7g, 3.5mmol) was condensed at -196°C. Martin's spirosilane (1g, 2 mmol) in 3 mL of freshly distilled DCM (over CaH_2) was added and the tube allow to warm up to -80 °C. $P(NEt_2)_3$ (0.9 mL, 3.5 mmol) was added dropwise and the reaction medium stirred until reaching rt. Analysis of the crude (^{19}F) permit to observed the attributed peak of $[Si(CF_3)L_2]$-. Direct attempt for precipitation/crystallisation of $[I\text{-}P(NEt_2)_3][Si(CF_3)L_2]$ were unsuccessful such as the different attempt with cation exchange (generally 4 equiv. of NEt_4Br or 1 equiv. of PPNCl in 0.1 M DCM).

Typical experiment with CF_3I + TDAE :

CF_3I (7mmol) was condensed in a flame dried 20 mL µw tube at -90°C, 7 mL of freshly distilled DCM (over CaH_2) was added, the solution was stirred 30 min at this temperature and used directly for the fluorination. Spirosilane (512 mg, 1 mmol) was added in an oven dried 20 mL µw tube, the tube was sealed, purged, and cooled down at -80°C then 2 mL of a 1M solution of CF_3I (2 mmol) was added. Freshly distilled TDAE (1.5 mmol) was added dropwise at -80°C and the following colour change was observed : Yellow → Orange → Deep red corresponding to the generation of the nucleophilic CF_3. The solution was stirred 1h at -80°C and the medium was slowly warm up to rt over 6h. Then the reaction was stirred 10h at RT. The crude was cannulated on a suspension of TEABr (4 mmol) in 4 mL and stirred 4h. The crude was extracted with water/DCM, the organic phase was dried with $MgSO_4$ and concentrated, a powder was obtained by precipitation with DCM/Pentane at -20°C containing 2 hypercoordinated species. $[Si(C(NMe_2)_2)L_2]$ **^{1}H NMR** (Bruker, 400MHz, [D6]acetone, rt): δ = 8.24 ppm (m, 2H); 7.6 (broad s, 2H); 7.4 (broad, 2H); 3.6 (s, 6H); 3.4(s, 6H); **^{13}C{^{1}H} NMR** (Bruker, 600MHz, [D6]acetone, rt): δ = 157.0, 142.2, 138.0, 129.9, 129.4, 124.4, 44.0, 43.1 ppm; **^{19}F NMR** ([D6]acetone, rt): δ = -75.6 ppm (q, 6F); -75.9 (q, 6F); **^{29}Si NMR** (Bruker, 600MHz, [D6]acetone, rt): δ = -78.3 ppm

2.3 Hypercoordinated [Si]-C_2F_5

Figure 0. Pipou (not cited in the paper)

2.3.1 Introduction

The *p*-block elements bearing a strongly electron-withdrawing-C_2F_5 moiety have recently emerged as promising tools for organic synthesis, with novel reactivity from an experimental and theoretical point of view.[1] Due to the strong Lewis acidity induced by the C_2F_5 substituent on the central atom, access to the corresponding stable hypercoordinate phosphorus[2–4] or silicon[5–10] species has been reported. These species have been synthesized by addition of pentafluoroethyllithium [Li][C_2F_5], obtained by metalation of the fluorinated gas HFC-125 (HC_2F_5), onto the chlorinated P or Si substrate (*Fig. 1.a*). To limit the potential hazard (*violent decomposition/explosion*),[11–13] the batch generation of the required organolithium has recently evolved to a safer microflow method (*Fig. 1.b*). [14,15] As an alternative, stabilization of the organolithium in the form of a gas-free tin tank has proven to be a more reliable solution for safer handling of this chemical (*Fig. 1.c*). [16] Other stabilizations of HC_2F_5 as pentafluoroethyl copper[17,18], pentafluoroethyl)galliums[19,20], pentafluoroethyl)bismuthanes[21a] or very recently indate salts[21b] have also been developed.

Following our interest in the derivatization of Martin's spirosilane ([SiL_2], L = α,α-bis(trifluoromethyl) benzenemethanolato-(-2)C_2,O), shown in *Fig.* 1.d) by addition of a nucleophile R, [22–28] we describe here the synthesis, properties and reactivity of the corresponding perfluoroethyl silicate (*Fig 1.e*). Martin's silicates ([Si(R)L_2]$^-$) have been recently used as a source of alkyl radicals,[29–31] as an alternative to their bis(catecholato)silicate counterparts [Si(R)$(cat)_2$]$^-$.[32,33] For both silicon species, the generation of the desired radical R$^\cdot$ is induced by one-electron oxidation and fragmentation of the carbon-silicon bond. To our knowledge, no such route has been described for the generation of a perfluoroalkyl radical, and in particular the pentafluoroethyl radical. On the other hand, the influence of the substituent (R) on Martin's silicate structural properties ([Si(R)L_2]-) has been discussed previously by Holmes but no information on

the potential increase of the Lewis acidity is mentioned.[34] Indeed, the formation of 6-coordinate Martin's silicate has only been mentioned with phenanthroline as ligand.[35] More recently, a mechanism involving a hexacoordinate intermediate was proposed for the ring expansion of a Martin's chloromethylsilicate.[26] Finally, the nucleophilicity of pentavalent perfluoroalkylated silicon species has been previously highlighted by Prakash.[36] We therefore decided to evaluate the destabilisation of the corresponding C_2F_5-silicate bond and to verify a possible nucleophilic behaviour in solution but also in solid-state under mechanochemical conditions.

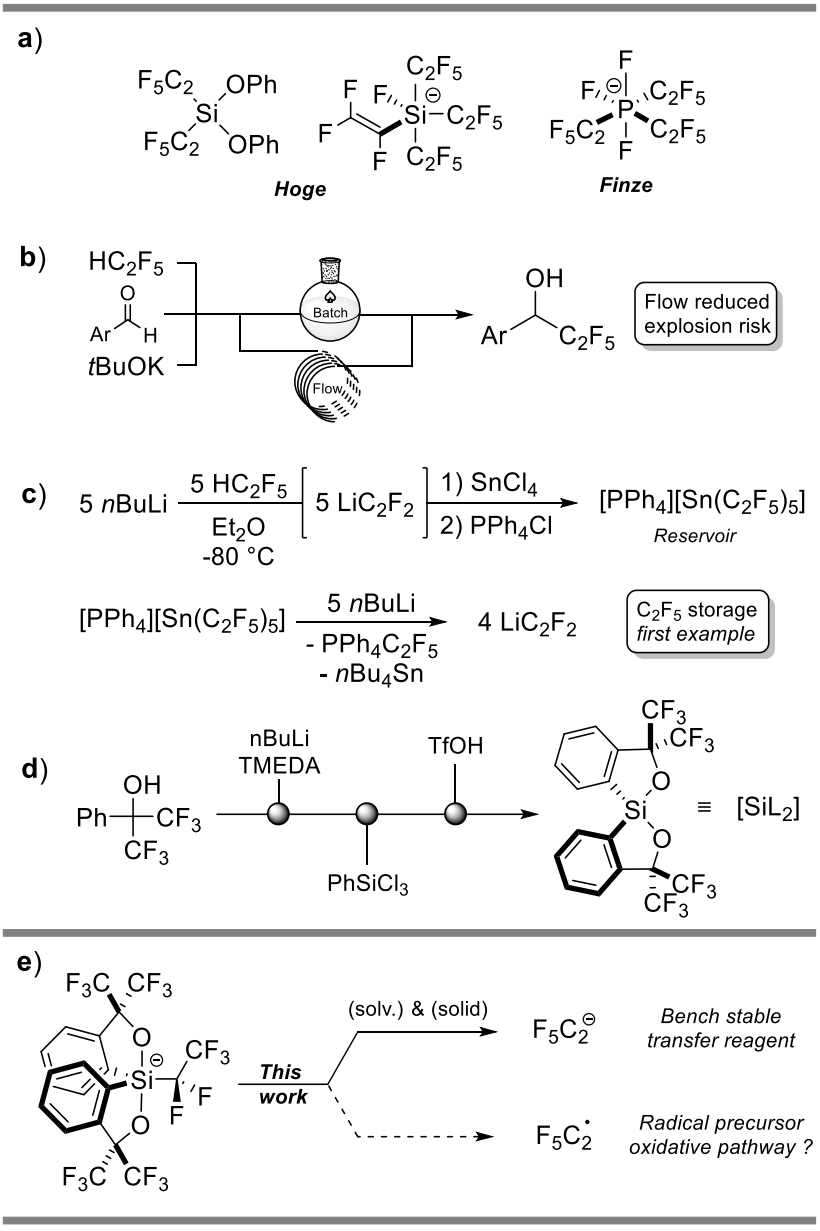

Figure 1. a) Examples of isolated perfluoroethyl hypercoordinated compounds; b) Batch and flow alkylation of aldehyde ; c) Preparation of Tin based reservoir, gas free synthesis of $[Li][C_2F_5]$; d) Martin's spirosilane; e) Our work

2.3.2 Result and discussion

2.3.2.1 Synthesis

Access to the Martin's silicate bearing a pentafluoroethyl chain was performed based on the methodologies described by Hoge and co-workers.[7,13] First, the synthesis of the corresponding lithium silicate salt begins with the preparation of the $C_2F_5^-$ transfer reagent, i.e. pentafluoroethyllithium, by deprotonation of HFC-125 with *n*BuLi. Martin's spirosilane **1** was slowly added at -75 °C to lead to the formation of lithium silicate **2** (Scheme 2, Eq. 1) which shows a good stability in solution but proved unstable in the solid state. To increase its stability, cation exchange using tetratethylammonium bromide (Scheme 2, Eq. 2) after precipitation afforded $[Et_4N][Si(C_2F_5)L_2]$ (**3**) in 78% yield. This type of silicate was also synthesized with a longer 1H-perfluorohexanyl chain (See SI).[37]

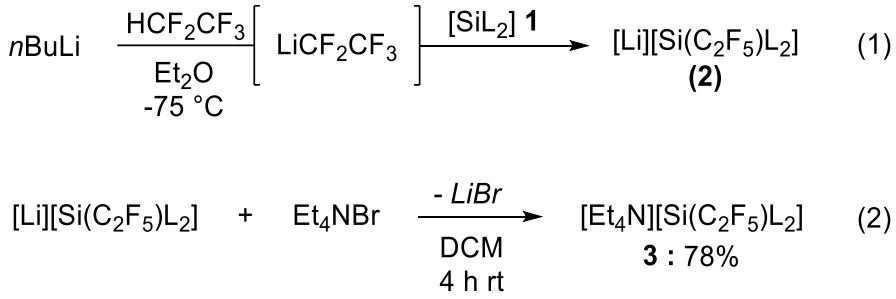

Scheme 2. Preparation of $[Et_4N][Si(C_2F_5)L_2]$

In this study, it was found that pentafluoroethyllithium was also able to act as a fluoride donor to **1**. The corresponding silicate $[Si(F)L_2]^-$ (**4**) was estimated up to ~15% yield, whose structure was confirmed by X-ray analysis (Figure 1). Its formation is mainly depended on the temperature control during the preparation of the reagent (gas condensation) and during the addition of **1**. As reported previously, the formation of a Si-F bond from decomposition of pentafluoroethyllithium (to TFE and LiF) is also depends on the fluorine ion affinity (FIA) of the Lewis acid.[5] Due to the relatively simple formation of this subproduct during the synthesis, we performed computation of the FIA of **1** without solvation correction[38–40] (Computed at PBeh-3C/def2-mSVP // PW6B95(D3BJ)/def2-QZVPP level of theory). The system was anchored by Me_3SiF/Me_3Si^+ and gave a FIA of 248.9 kJ mol^{-1}. This result indicates a relatively low Lewis acidity of this silane, providing a weak effect on fluoride abstraction on $[Li][C_2F_5]$.

2.3.2.2 Structural data

Suitable crystals of silicate **3** for an X-ray diffraction analysis were obtained by slow evaporation of a saturated dichloromethane solution.

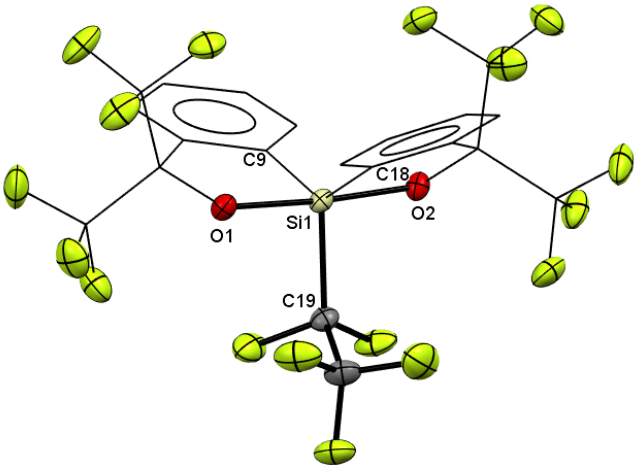

Figure 1. X-Ray crystallographic structure of $[Si(C_2F_5)L_2]$-. Thermal ellipsoids are drawn at 50% probability level. Hydrogen atoms and cation are omitted for clarity. Carbons of Martin's Ligand (L) are drawn as wireframe for clarity.

It crystallised in the monoclinic space group $P2_1/c$ (Figure 2). Slight distortion from an ideal trigonal-bipyramidal (TBP) structure was observed and calculation using the dihedral angle method resulted in an 26.4% shift from the TBP to the ideal square pyramidal (SP) structure.[42] The apical position is occupied by the C_2F_5 moiety, Si-C_{19} length is 1.968(2) Å. The Si-O_{ax} length is respectively 1.787(1) Å and 1.784(1) Å for O_1 and O_2 and influenced by the electronegativity of the substituent.[34]

The distance *d*(Si-O) is close to that of $[(Me_2N)_3S]][Si(F)L_2]$ (Si-O_{ax} = 1.792 Å) and only shows a small difference (~ 1 pm).The electronegativity of the short perfluoroethyl chain had no real impact on the rest of the structure. Finally, the two fluorides of -CF_2- are close but non-equivalent with a C-F distance of 1.392(3) Å and 1.360(2) Å and slightly longer than the one in -CF_3 ranging from 1.309(3) to 1.343(3) Å.

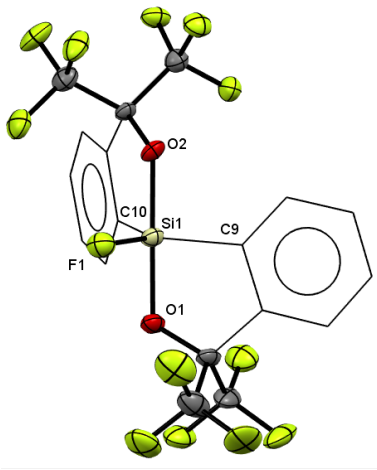

Figure 2. X-Ray crystallographic structure of $[Si(F)L_2]^-$. Thermal ellipsoids are drawn at 50% probability level. Hydrogen atoms are omitted for clarity. Carbons of Martin's Ligand (L) are drawn as wireframe for clarity | Selected bond lengths [Å] and angles [°] : Si_1-F_1 1.62(1), Si_1-O_1 1.789(9), Si_1-O_2 1.780(9), Si_1-C_9 1.89(1), Si_1-C_{10} 1.89(1); C_{10}- Si_1-C_9 124.9(6), O_1-Si_1-O_2 178.8(4), F_1-Si_1-C_9 117.4(5), F_1-Si_1-O_2 91.2(4)

The ^{29}Si NMR shift of -78 ppm is in the expected range of five coordinated silicon species. (Figure 3, left) It shows a doublet of doublet caused by a ^{2}J(Si,F) coupling of 35 Hz with two diastereotopic fluorides in CF_2.

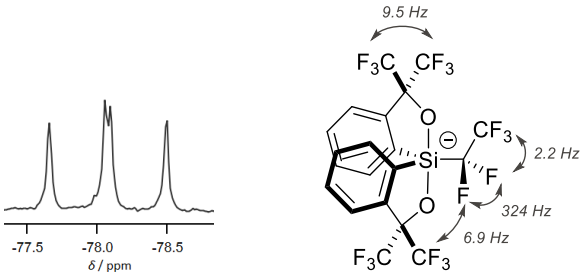

Figure 3. ^{29}Si NMR spectrum (left) and attributed ^{19}F NMR coupling (right)

In the ^{19}F NMR, the diastereotopic fluorides from the CF_2 appear respectively as a d, sept at δ = -119 and a d, sept, d at δ = -127 with the measured ^{2}J(F,F), ^{3}J(F,F) and spatial ^{6}J(F,F) coupling of 324, 2.2 and 6.9 Hz. (Figure 3). As expected, the spatially hindered CF_3 from the bis-trifluoromethyl moiety appears as a quadruplet with a coupling constant of 9.5 Hz, when the other one appears as a complex multiplet due to the numerous couplings with the gem CF_3 and the spatial one with the perfluoro-substituent. The ^{13}C NMR spectrum at 600 MHz shows a quadruplet of triplet and a doublet of quadruplet for C_2F_5 respectively at δ = 122 ppm with the measured couplings ^{1}J(C,F) and ^{2}J(C,F) of 286 Hz and 32 Hz and at δ = 120 ppm with ^{1}J(C,F) and ^{2}J(C,F) of 276 Hz and 37 Hz.

2.3.2.3 Oxidation

The electronic properties of **3** were first evaluated by cyclic voltammetry with a saturated calomel electrode as reference. As usually observed with hypercoordinated Martin's derivatives,[43] a one-electron irreversible oxidation was observed at 1.60 V vs. SCE (Figure 4).

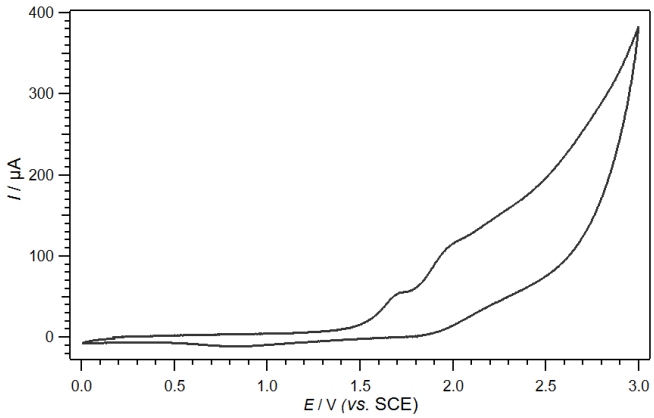

Figure 4. Cyclic voltammetry of **3** in DCM with $[Bu_4N][PF_6]$ as supporting electrolyte

With these data, we tested the ability of the five-coordinate species to act as a radical precursor (Scheme 6). The measured potential value for oxidation (E_{ox}) of Martin's silicate **3** is in the range of highly oxidizing acridinium-based photocatalysts such as tert-butyl-10-phenylacridinium tetrafluoroborate ([Mes-Acr+], Nicewicz's catalyst) used by the Kano group to oxidize Martin's alkylsilicates.[29,31] We first evaluated the reactivity of **3** in solution with the highly oxidizing Nicewicz acridinium photocatalyst.[44] Under these conditions, no desired C_2F_5 pentafluoroethyl radical scavenging product with TEMPO (2,2,6,6-tetramethylpiperidin-1-yl)oxyl) was observed [45,46] and the starting substrate was found to be unchanged (Scheme 6.1).

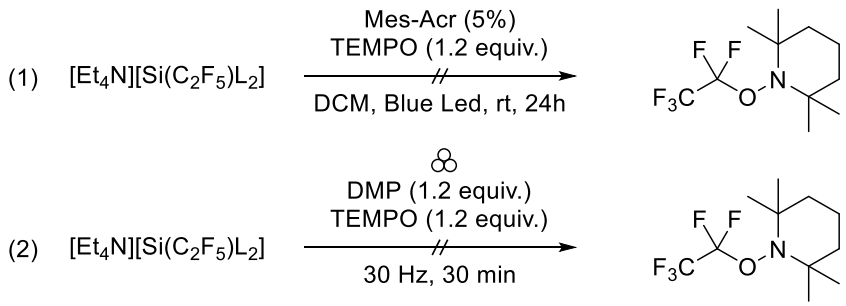

Scheme 6. Investigation of reactivity: (1) TEMPO solution trapping experiment, (2) TEMPO solid-state trapping experiment.

We then performed some unsuccessful solid-state trapping experiments under ball-milling conditions (Scheme 6.2). From these experimental observations, the ability to generate the desired C_2F_5 radical contrasts with the corresponding non-fluorinated alkyl species.[29,31]

These puzzling findings prompted us to perform DFT calculations (Orca 5.0.3, PBeh-3C/def2-mSVP//PW6B95(D3BJ)/def2-QZVPP) to estimate the bond dissociation energy (BDE) of $[Si(C_2F_5)L_2]^-$ and to examine the highest occupied molecular orbital (HOMO) of this substituted silicate (Figure 5). The results suggest that the active orbital for the oxidative event is on the aromatic group of the 2,2,2,2',2',2'-hexafluorocumyl ligand and not on the C-Si bond to provide the formation of the desired radical, which is in sharp contrast with the ethylsilicate $[Si(C_2H_5)L_2]$ reported by Kano.[31] As it was reported, the computational attempts to optimize the one-electron oxidized silicate led to divergence, providing the radical and the spirosilane $[SiL_2]$.

Interestingly, in our case, the optimization of the oxidized pentafluoroethyl silicate also diverged, as we observed the cleavage of a Si-C_{Ar} bond and not the formation of the spirosilane (See SI, Figure S2). We then wondered about the potential reactivity of another interesting fluorinated radical precursor $[Si(CF_3)L_2]^-$. As for the C_2F_5 derivative, the HOMO was mainly localized on the silicate ligand (L). In comparison with previous reports on Martin's silicate as a good radical precursor,[29,31] our experimental results and theoretical view show that Martin's spirosilane bearing a perfluoroalkyl chain might not be suitable candidates for the generation of oxidative radicals.

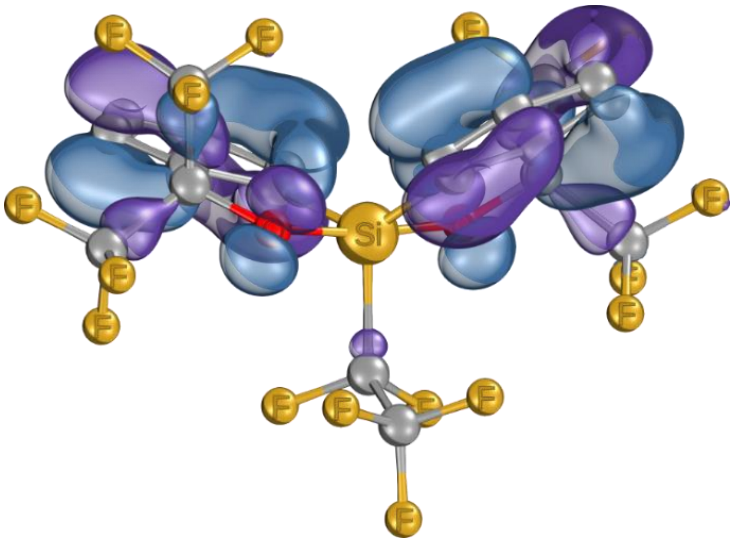

Figure 5. Representation (using iboview[42]) of the HOMO of $[Si(C_2F_5)L_2]$

As described, the HOMO (-5.345 eV, left) of $[Si(C_2F_5)L_2]$- is delocalised mainly over the ligand (L = (α,α-bis(trifluoromethyl) benzenemethanolato-(-2)C2,O) of the silicate (Fig. 5) while the LUMO (2.542 eV, Fig S1.B) results from a contribution of the Si-C σ* orbital (Fig. S1.B, see below).

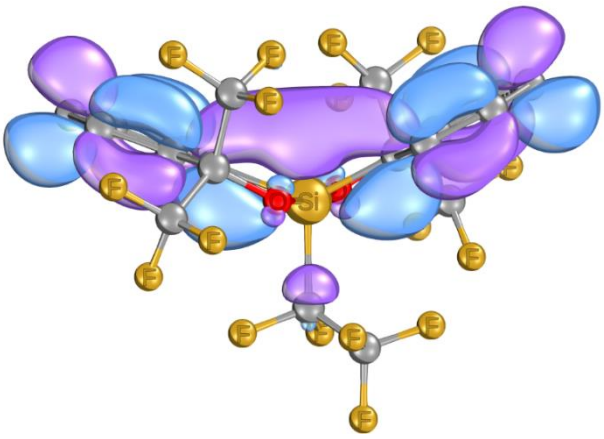

Figure S1.B. $[Si(C_2F_5)L_2]$- representation of LUMO.

During our ab initio investigation, we performed the optimisation of the one electron oxidized intermediate $[Si(C_2F_5)L_2]$• we the main idea to calculate the potential bond dissociation energy (BDE). (Fig. S2.A) During our optimization, the calculation diverges as it was previously reported by Kano. The final structure obtained (bottom left, S2.B) corresponds to the fragmentation of the Si-Ar bond in contrast with the generation of ethyl radical and regeneration of $[SiL_2]$. The orbital suited for describing the spin density of the radical is depicted therefore. (bottom right, S2.C, SOMO -7.955 eV)

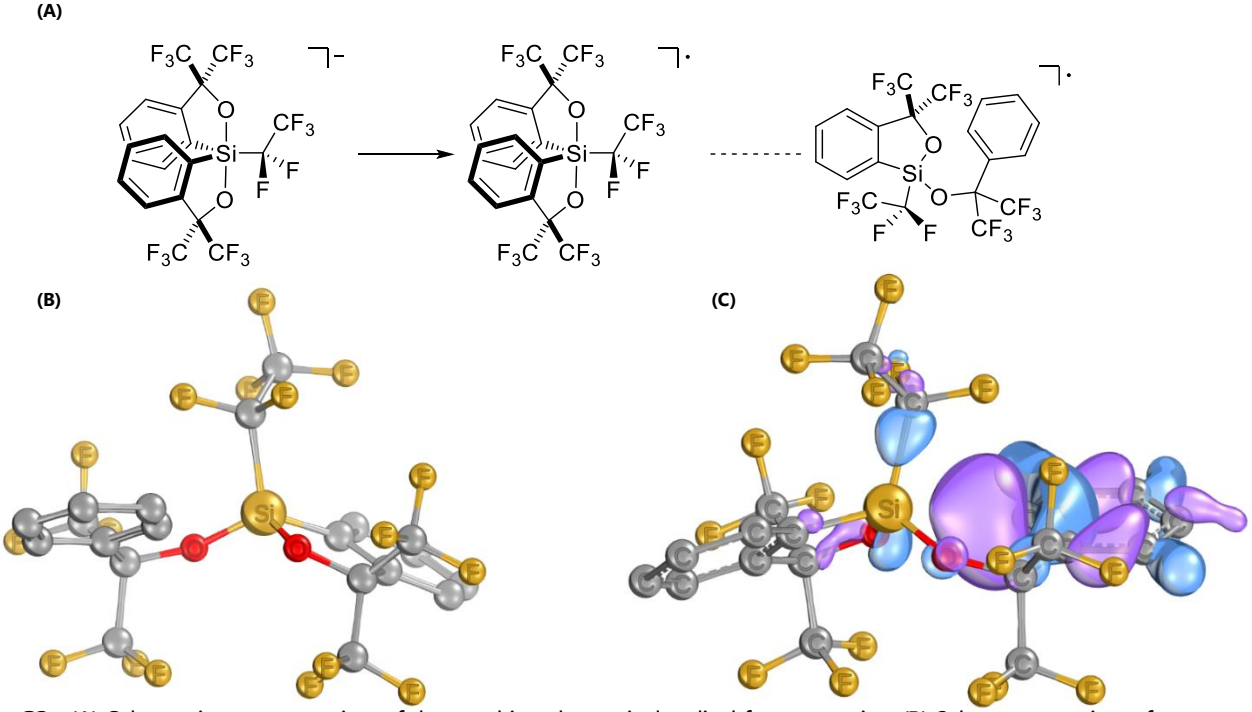

Figure S2. (A) Schematic representation of the resulting theoretical radical fragmentation (B) 3d representation of the calculated fragmented species; (C) SOMO.

2.3.2.4 Nucleophilic behaviour

We then studied the nucleophilic behavior of **3** in different media, in solution and in the solid state (Scheme 7). We first performed the direct 1,2 addition of **3** on benzaldehyde (**5**) without success.

Then, addition of cesium fluoride (CsF) allows the formation of the fluorinated secondary alcohol **6** with an NMR yield of 57% (Scheme 7, eq. 1).[14,15] During the optimization of the process, we observed that a reaction occurs directly on the surface of the CsF (See picture, scheme 7).

From this observation, we wanted to study the possible reactivity in the solid state by mechanochemistry (Scheme 7, eq. 2). To our delight, the extrapolation of the previous conditions in solution to ball-milling conditions (30 min, 30Hz) allows us to obtain **6** with a similar yield (60%, NMR yield).

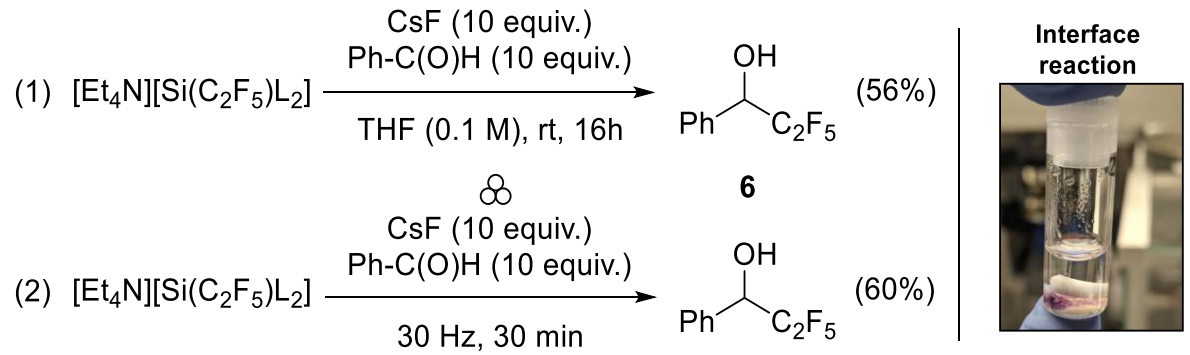

Scheme 7. Nucleophilic behavior of **3** in (1) Solution (2) Solid-state by mechanochemistry | Picture (right) allow the clear observation of an interface reactivity

We then performed control experiments (Scheme 8) and a mechanistic study on this new C_2F_5 transfer reagent. It has recently been shown by theoretical and experimental studies that the influence of C_2F_5 improves the Lewis acidity (LA) of group 14 compounds.[48]

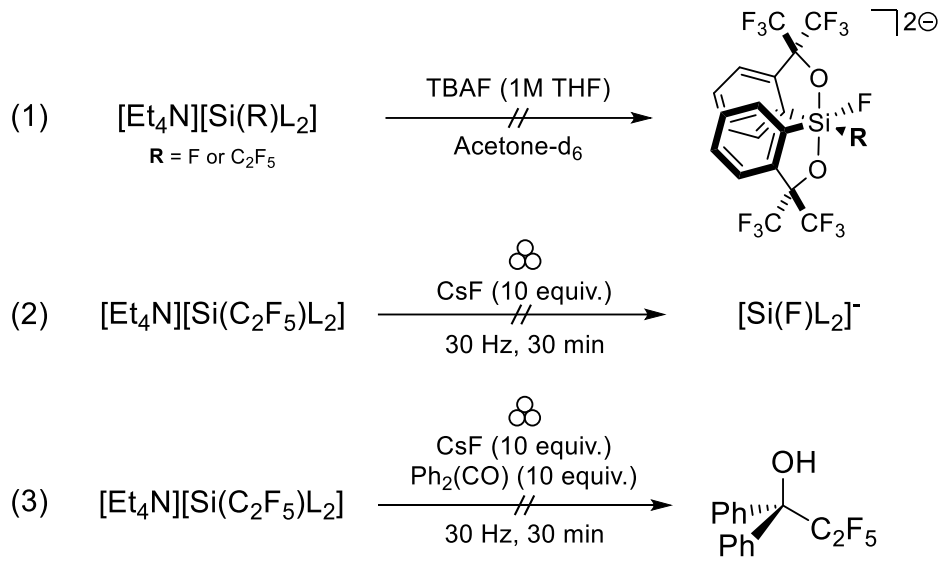

Scheme 8. Control experiment, Equation: (1) Attempt for the synthesis of 6-coordinate species (2) Attempt for the direct fluoride addition and formation of the observed subproduct $[Si(F)L_2]^-$; (3) Modification of the electrophile (benzophenone) for hinderance purpose

To compare the potential influence of the substituent on the L.A., we investigated the potential formation of a covalent 6-coordinate Martin's spirosilane derivative with a fluoride (or a ketone) as a nucleophile (Scheme 8.1). For $[Et_4N][Si(C_2F_5)L_2]$ and $[Et_4N][Si(F)L_2]$, no evidence of a hexavalent intermediate was observed by NMR when mixed in presence of a soluble fluoride donor, the experiment only showed ^{19}F resonance for TBAF (^{19}F: -116 ppm) and each pentacoordinate silicon species (see SI). This indicates similar behaviour of each silicate with the fluoride source in agreement with the physical data (XDR) related to the electronegativity of the substituent ($-C_2F_5$ or -F), demonstrating the absence of a hindering effect of the substituent on direct fluoride addition. We therefore conclude that the direct addition of fluoride to pentavalent silicon species did not occur spontaneously, suggesting the non-participation of the fluoride anion but rather the one of the Cs cation in the reaction mechanism. We then decided to perform the same experiment in solid-state. (Scheme 8.2).

As for the solution experiment, we did not manage to observe traces of hexavalent intermediate nor the formation of $[Si(F)L_2]^-$. We then decided to hinder the system by changing benzaldehyde with benzophenone to possibly prevent chelation of the electrophile partners with the silicate. This modification led to the complete loss of reactivity and full recovery of starting material as observed in ^{19}F NMR, suggesting a steric dependence for chelation of the electrophile on the silicate allowing a potential concerted mechanism between both partners triggered by an electrophilic activation of the silicate with the aldehyde and displacement of the substituent.

2.3.2.5 Mechanistic proposal

2.3.2.5.1 External forces

During the optimisation process, formation of HFC-125 was observed in the crude solution NMR (went from traces amount to complete formation of gas). Due to the solubility induced by the liquid aldehyde, we also observe traces of HFC-125 in solid-state. We did not observe a direct fluoride addition on the silicon atom nor the complete degradation under ball-milling conditions. We assumed that the shock-induced energy did not allow direct bond breaking of the 5-coordinate species and that the most breakable bond is the silicon-perfluoroalkyl one. DFT calculations were performed to rationalize the results obtained under mechanochemical conditions (Figure 6).

We first investigated the influence of external forces on **3** (Figure 6.A). We calculated the influence of an applied force on the Si-C_F bond using the External Force is Explicitly Included (EFEI) approach implemented in Orca (See SI, Figure S3.A).

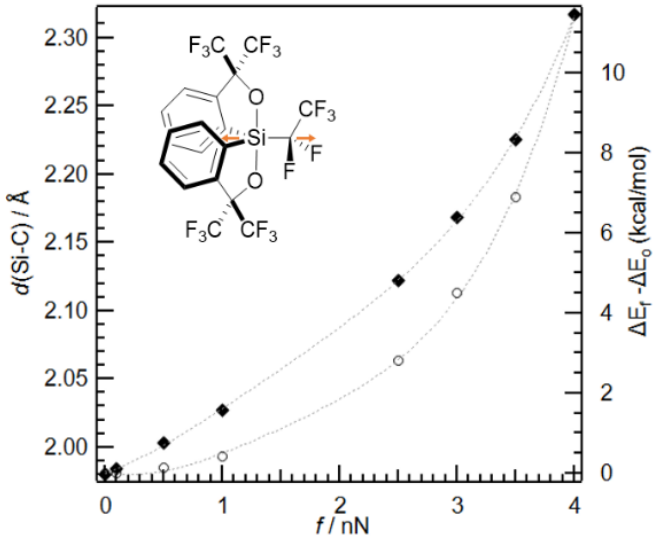

Figure S3.A Force-dependence of the silicon-carbon (♦) bond length in Å (scale at left y-axis) and ΔE_f- ΔE_0 (○) in kcal/mol from DFT calculations (scale at right y-axis) both computed at the PBeh-3C/def2-mSVP // PW6B 95(D3BJ)/def2-QZVPP level of theory

As expected, increasing the force in nanoNewton (nN) whithin the system elongates the Si-C_F bond and thus destabilised the structure. The calculated breaking force for the Si−C bond (F_{max} = 4.2 ± 0.1 nN) is comparable to previous F_{max} value calculated for a silicon-carbon bond.[49] We also showed that our mechanochemical conditions (30Hz, 30 min) did not provide enough strength for direct bond scission of the substituent. Therefore, the proposed mechanism did not involve a direct bond breaking from external force and addition onto our electrophile.

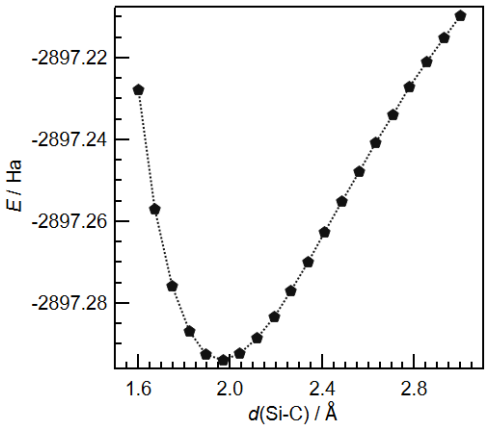

Figure S3.B. B) Morse like function (). Distance dependence at the Si-C bond length indicated in Å and the Energy in Hartree at F0) computed at PBeh-3C/def2-mSVP.

Due to the computational cost/time ratio, we did not investigate the application of oppressing mechanical action that could permit to observe the overall Morse function. In addition, and as indicated previously, using the EFEI method also did not permit to compute and trace energy values for force values overpassing the Si-C bond limit. To overcome this limitation, we decided to plot the Morse function with an external force applied of 0 nN. (Fig. S3.B). As expected, reducing the Si-C_2F_5 bond length directly modifies the overall potential energy of the molecule. Then, we decided to plot the complete Morse function base on the energy obtained in Fig. S3.A. Due to the EFEI approach, and the obtention of 1E/Force, we were not able to compute each Morse function depending on the external force applied.

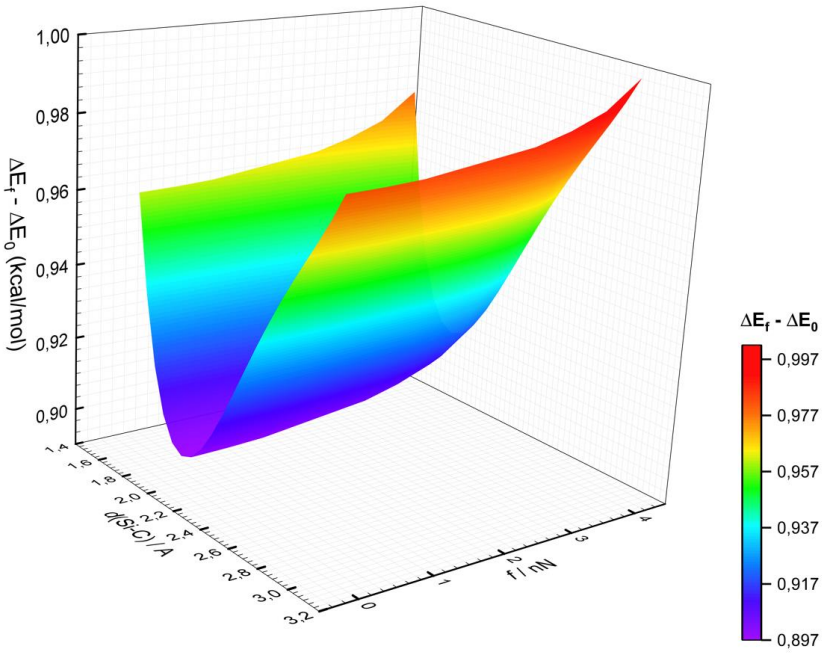

Figure S3.C. Comparative view of the normalized $\Delta E_f - \Delta E_0$ (○) in kcal/mol obtained from the optimized force modified Born-Oppenheimer PES (Fig. S3.A) and DFT calculation of the Potential energy (Fig. S3.B) given the Force-modified potential energy surface

An approximation, in which the local minimum of potential energy (potential well) did not shift depending on the bond length and the force, was realised. Base on this and the calculated value for the force-modified Born–Oppenheimer Potential Energy Scan, we managed to plot the desired 3D map. (Origin, Fig. S3.C) This clearly highlights the higher potential energy obtained which should lead to a change in the geometrical parameter of the molecule.

2.3.2.5.2 Steric map

To better understand the accessibility of the silicon atom, we calculated its steric map by removing the fluorine of terminal CF_3 for clarity (Figure 6.B and S4.B). It appears that two quadrant areas NE and SW are less hindered which could allow the approach of an electrophile or a nucleophile. Moreover, the cation exchange of Et_4N/Cs may destabilise the structure. The influence of the cation for $[Li][Si(C_2F_5)L_2]$ already showed a dramatic effect on its stability in solid state during the isolation process with a complete degradation of the lithium salt in solid-state. This suggests an essential lattice effect on the fate of the silicate. Furthermore, the influence of the surface/cation effect was highlighted at the interface (Scheme 7). This destabilisation may enhance the nucleophilic ability of the silicate. The Cs···F_5C_2 interaction was also reported recently and show close contact between fluorine and Cesium in $Cs[In(C_2F_5)_4]$ (< 360 pm).[21b]

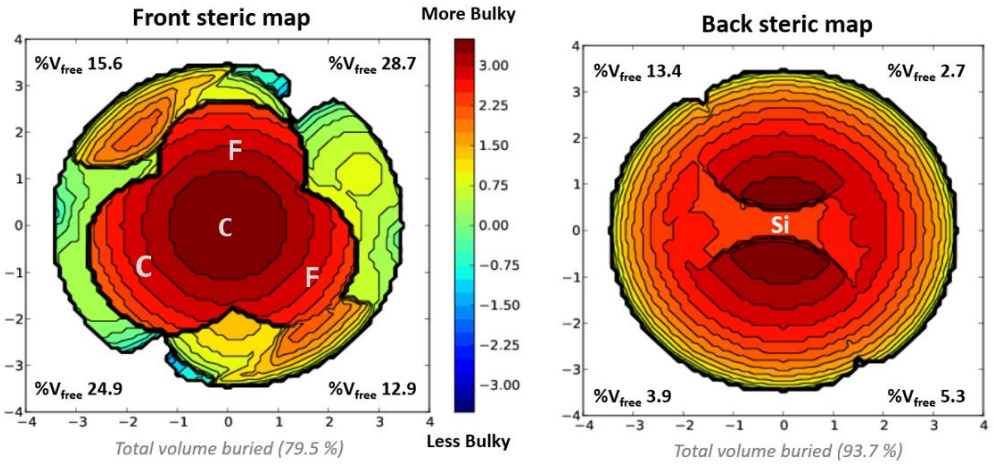

Figure S6.B (left) **and S4.B** (right). Topological steric map of $[Si(C_2F_5)L_2]^-$ from: A) front point of view (Si-C axis) with trifluoromethyl from CF_2CF_3 not displayed for clarity; B) back point of view (C-Si axis). Map generated using SambVCa software and the computed data, value of the free volume ($\%V_{free}$) given according to the quadrant formalism.[8]

Firstly, we represent [Si(C_2F_5)L_2]- along the silicon-carbon bond to observe the availability of the spirosilane from the front view (S6.B) and from the back side as depicted in S4.B. From the first map, it appears that the overall molecule is highly hindered (79.9%) but two area (NE and SW quadrants) appear slightly accessible. This is in contrast with the silicon atom (Fig. B) completely hindered (93.7%) that should not permit any approach of nucleophile nor electrophile. From this mapping, and the previously computed data, the direct bond cleavage via the force applied during the mechanochemical process or the fluoride addition (on the Si-C σ* orbital and formation of hexavalent species) followed by fragmentation of the Si-C σ bond are not the most plausible mechanisms. This matches with the experimental observation of the non-formation of hexacoordinated species using fluoride and still suggest a possible concerted mechanism for the nucleophilic 1,2 addition. Indeed, it seems possible that the electrophile could approach the silicon atom from the front part and could in a concerted manner and with a slight distortion of the structure toward a transitional-hexacoordinated like one allow the transfer of the -C_2F_5 moiety.

2.3.2.5.3 Mechanism pathway

In the following DFT study (Figure 6.C) we considered the transition state (*TS_1*) involving the decoordination of C_2F_5 anion to mimic the observation of HFC-125 resulting in the Si-C bond scission. We first investigated a potential hexacoordinated intermediate (*INT_1*) as already reported experimentally[35] and theoretically[26] on Martin's silicates with other substituents. The *cis* configuration of the ligand's oxygen intermediate appears to be crucial for the stabilisation of the intermediate by reducing the energy of the system. This theoretical observation is coherent with the previous report of hexavalent Martin's silicate. [26,35]

The computational work for this ab initio investigation was done on resources of the National Supercomputing Computer, Singapore (NSCC). Density functional theory studies were carried out with Orca 4.1.2. The geometry of each species was first optimized using PBeh-3C functionals and def2-mSVP as basis set. For all resulting structures, frequency analysis was then performed to verify the absence of imaginary frequencies. In case of negative frequencies, the geometries were re-optimized with grid6, Tight OPT and VeryTightSCF settings. The *External Force is Explicitly Included* approach was used for mechanochemical investigation on starting material and hexacoordinated intermediate. The transition state was found using NEB-TS and OPTTS NUMFREQ as implemented in ORCA. Single Point Energies were computed with PW6B95 D3(BJ) with def2-QZVPP.

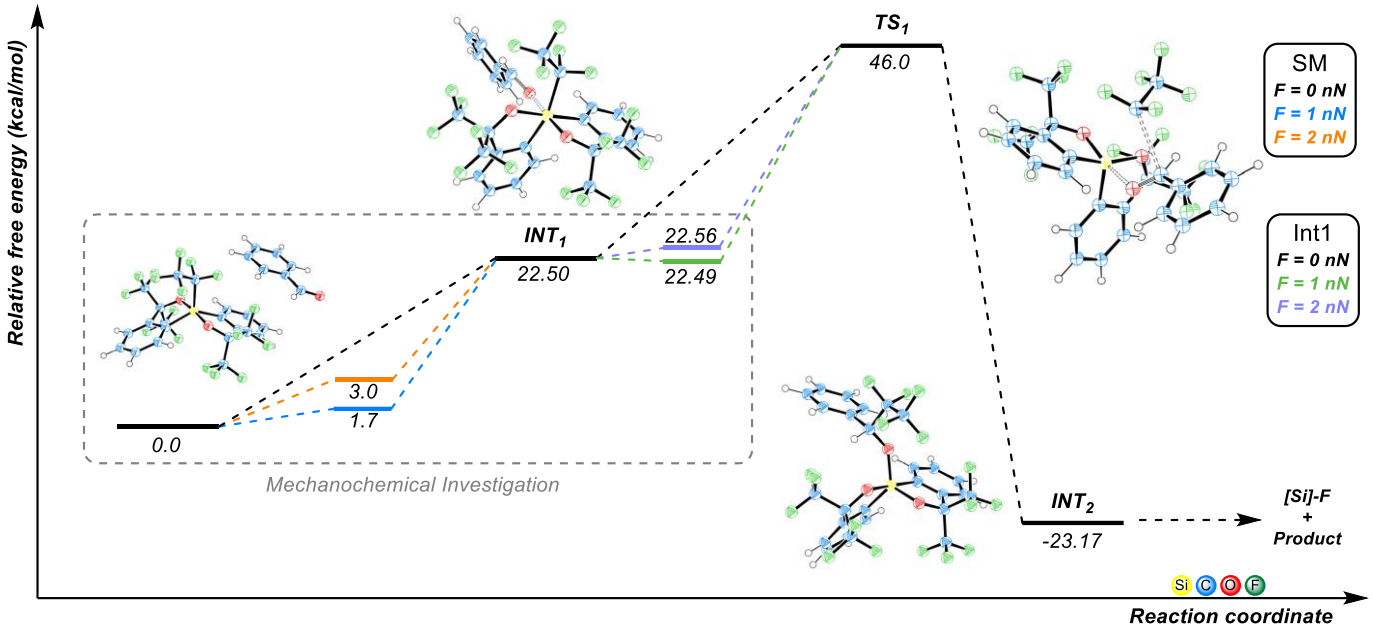

Figure S5. Mechanistic pathways for the mechanochemical influence (using EFEI approach) of 1,2-addition of -C_2F_5 (PBeh-3C/def2-mSVP // PW6B 95(D3BJ)/def2-QZVPP)

The energy barrier for the hexacoordinated species was calculated to be 22.5 kcal.mol^{-1} and is similar our previous computational investigations.[26] A clear beneficial influence of the external force on the starting material allows a reduction of the energy barrier of 3 kcal.mol^{-1} for 2nN applied. This clearly suggests that ball-milling may promote the access to the key intermediate *INT*$_1$. To simplify and reduce the computational cost, we decided to focus on the formation of *INT*$_2$ which was not observed during our work but studied by Sakai and co-workers.[30] The optimised TS$_1$ displays an activation of 23.5 kcal.mol^{-1}, no direct influence of the external force on the intermediate was found yet (See *INT*$_1$ F = 0,1 and 2 nN kcal/mol value).

If no enhancement from applied force has been observed on *INT*$_1$ the energy barrier of each steps appears accessible due to the temperature in the reaction medium (T = ~35 ± 5°C). Here, the positive influence of externals forces in the reaction system was highlighted and clearly simplify the obtention of key intermediate.

2.3.3 Conclusion

In summary, the gram scale synthesis of a new hypercoordinated silicon species bearing a perfluoroethyl chain has been realised by direct nucleophilic addition of pentafluoroethyllithium to the Martin's spirosilane precursor. Full characterization and advanced description are provided by NMR and X-Ray. Its potential use as a precursor of fluoroethyl radicals by photooxidation has led to a better understanding of the reactivity of this species. We have shown that the substitution of an alkyl residue by a C_2F_5 chain in the case of Martin's silicate derivatives led to a change in reactivity leading to the theoretical breaking of the Si-Ar bond and attributed to a displacement of the HOMO of the C-Si bond to the bis(trifluoromethyl) benzenemethanol ligand. The preparation of hypercoordinated silicon species of bis-catecholatosilane type is in progress in our laboratory in order to further study the potential generation of radicals. We then studied the reactivity of the Martin's silicate as a C_2F_5 anion transfer reagent in solution and in the solid state. In this work, we decided to focus on the 1,2 addition to benzaldehyde in the presence of cesium fluoride. The experiment in solution clearly showed a reactivity on the surface of CsF. As in solution in THF, we reported the first mechanochemical addition of the C_2F_5 anion from the hypercoordinated silicon species. DFT calculations clearly demonstrated the ability of external forces to promote the formation of key intermediates. We were able to obtain a key transition state involving the decoordination of the substituent following the experimental observation and we believe that the study of the surface effect could provide deeper mechanistic insight. Finally, we hope that the nucleophilic behaviour of hypercoordinated group 14 compounds will gain interest in the solid state. Mechanochemistry of main group element appears to be a valuable tool for the investigation of new methodologies in this medium.

Article acknowledgements:

This work was supported by Sorbonne University, CNRS and IUF. We thank Thomas Deis for useful discussions, Regina Maruchenko (Plateforme RMN Moléculaire / IPCM - Sorbonne Université) and Imane Senoussaoui (Application Engineer JEOL) for helping with $^{13}C\{^{1}H\}\{^{19}F\}$ NMR experiments-, Jeremy Forté for X-ray diffraction analyses and Gilles Clodic for HRMS analyses.

References part 2.3

[1] M. Wiesemann, B. Hoge, *Chem. Eur. J.* **2018**, *24*, 16457–16471.
[2] J. Bader, B. Neumann, H.-G. Stammler, N. Ignat'ev, B. Hoge, *Chem. Eur. J.* **2018**, *24*, 6975–6982.
[3] S. A. Föhrenbacher, M. J. Krahfuss, L. Zapf, A. Friedrich, N. V. Ignat'ev, M. Finze, U. Radius, *Chem. Eur. J.* **2021**, *27*, 3504–3516.
[4] S. A. Föhrenbacher, V. Zeh, M. J. Krahfuss, N. V. Ignat'ev, M. Finze, U. Radius, *Eur. J. Inorg. Chem.* **2021**, *2021*, 1941–1960.
[5] S. Steinhauer, J. Bader, H.-G. Stammler, N. Ignat'ev, B. Hoge, *Angew. Chem. Int. Ed.* **2014**, *53*, 5206–5209.
[6] S. Steinhauer, T. Böttcher, N. Schwarze, B. Neumann, H.-G. Stammler, B. Hoge, *Angew. Chem. Int. Ed.* **2014**, *53*, 13269–13272.
[7] N. Schwarze, B. Kurscheid, S. Steinhauer, B. Neumann, H.-G. Stammler, N. Ignat'ev, B. Hoge, *Chem. Eur. J.* **2016**, *22*, 17460–17467.
[8] N. Tiessen, M. Keßler, B. Neumann, H.-G. Stammler, B. Hoge, *Angew. Chem. Int. Ed.* **2021**, *60*, 12124–12131.
[9] N. Tiessen, N. Schwarze, H.-G. Stammler, B. Neumann, B. Hoge, *Inorg. Chem.* **2021**, *60*, 15112–15117.
[10] N. Tiessen, M. Keßler, B. Neumann, H.-G. Stammler, B. Hoge, *Angew. Chem. Int. Ed.* **2022**, *61*, e202116468.
[11] D. M. Roddick, *Chem. Eng. News* **1997**, *75*.
[12] D. A. Dixon, Tadamichi. Fukunaga, B. E. Smart, *J. Am. Chem. Soc.* **1986**, *108*, 4027–4031.
[13] B. Waerder, S. Steinhauer, B. Neumann, H.-G. Stammler, A. Mix, Y. V. Vishnevskiy, B. Hoge, N. W. Mitzel, *Angew. Chem. Int. Ed.* **2014**, *53*, 11640–11644.
[14] Y. Fujihira, K. Hirano, M. Ono, H. Mimura, T. Kagawa, D. M. Sedgwick, S. Fustero, N. Shibata, *J. Org. Chem.* **2021**, *86*, 5883–5893.
[15] M. Ono, Y. Sumii, Y. Fujihira, T. Kagawa, H. Mimura, N. Shibata, *J. Org. Chem.* **2021**, *86*, 14044–14053.
[16] M. Wiesemann, J. Klösener, B. Neumann, H.-G. Stammler, B. Hoge, *Chem. Eur. J.* **2018**, *24*, 1838–1843.
[17] A. Lishchynskyi, V. V. Grushin, *J. Am. Chem. Soc.* **2013**, *135*, 12584–12587.
[18] E. D. Kalkman, M. G. Mormino, J. F. Hartwig, *J. Am. Chem. Soc.* **2019**, *141*, 19458–19465.
[19] M. Niemann, B. Neumann, H.-G. Stammler, B. Hoge, *Angew. Chem. Int. Ed.* **2019**, *58*, 8938–8942.
[20] M. Niemann, B. Neumann, H.-G. Stammler, B. Hoge, *Eur. J. Inorg. Chem.* **2019**, *2019*, 3462–3475.
[21] a) S. Solyntjes, J. Bader, B. Neumann, H.-G. Stammler, N. Ignat'ev, B. Hoge, *Chem. Eur. J.* **2017**, *23*, 1557–1567. b) S. Porath, M. Keßler, B. Neumann, H.-G. Stammler, B. Hoge, *Chem. Eur. J.* ***2023****, n/a*, DOI 10.1002/chem.202203278.
[22] F. Medici, G. Gontard, E. Derat, G. Lemière, L. Fensterbank, *Organometallics* **2018**, *37*, 517–520.
[23] F. Medici, J. Maury, G. Lemière, L. Fensterbank, *Chem. Eur. J.* **2019**, *25*, 9438–9442.
[24] T. Deis, F. Medici, A. Poussard-Schulz, G. Lemière, L. Fensterbank, *J. Organomet. Chem.* **2021**, *956*, 122120.
[25] G. Lemière, A. Millanvois, C. Ollivier, L. Fensterbank, *Chem. Rec.* **2021**, *21*, 1119–1129.
[26] T. Deis, J. Forte, L. Fensterbank, G. Lemière, *Molecules* **2022**, *27*, 1767.
[27] T. Deis, J. Maury, F. Medici, M. Jean, J. Forte, N. Vanthuyne, L. Fensterbank, G. Lemière, *Angew. Chem. Int. Ed.* **2022**, *134*, e202113836.
[28] H. Lenormand, V. Corcé, G. Sorin, C. Chhun, L.-M. Chamoreau, L. Krim, E.-L. Zins, J.-P. Goddard, L. Fensterbank, *J. Org. Chem.* **2015**, *80*, 3280–3288.
[29] G. Ikarashi, T. Morofuji, N. Kano, *Chem. Commun.* **2020**, *56*, 10006–10009.
[30] K. Sakai, K. Oisaki, M. Kanai, *Adv. Synth. Cat.* **2020**, *362*, 337–343.
[31] T. Morofuji, Y. Matsui, M. Ohno, G. Ikarashi, N. Kano, *Chem. Eur. J.* **2021**, *27*, 6713–6718.
[32] A. Millanvois, C. Ollivier, L. Fensterbank, *Eur. J. Inorg. Chem.* **2022**, *2022*, e202101109.
[33] V. Corcé, C. Ollivier, L. Fensterbank, *Chem. Soc. Rev.* **2022**, *51*, 1470–1510.
[34] R. R. Holmes, *Chem. Rev.* **1990**, *90*, 17–31.
[35] W. B. Farnham, J. F. Whitney, *J. Am. Chem. Soc.* **1984**, *106*, 3992–3994.
[36] G. K. S. Prakash, F. Wang, Z. Zhang, R. Haiges, M. Rahm, K. O. Christe, T. Mathew, G. A. Olah, *Angew. Chem. Int. Ed.* **2014**, *53*, 11575–11578.
[37] See SI: Preparation of [Li][$C_6F_{12}H$] from $C_6F_{12}H_2$ and addition on Martin's spirosilane.
[38] P. Erdmann, J. Leitner, J. Schwarz, L. Greb, *Chem. Phys. Chem.* **2020**, *21*, 987–994.
[39] P. Erdmann, L. Greb, *Chem. Phys. Chem.* **2021**, *22*, 935–943.
[40] F. Neese, *WIREs Computational Molecular Science* **2022**, *12*, e1606.
[41] *Deposition Number 2223436-2223438, others strucutre has been identified during our investigation (2223436 (a 9.8876(4) b 17.2753(6) c 28.9811(12) P-1) and 2223438 (a 17.6739(8) b 17.4789(9) c 19.7450(10) P21/c)).*
[42] R. R. Holmes, J. A. Deiters, *J. Am. Chem. Soc.* **1977**, *99*, 3318–3326.
[43] *Internal data.*
[44] A. Tlili, S. Lakhdar, *Angew. Chem. Int. Ed.* **2021**, *60*, 19526–19549.
[45] X. Yang, G. C. Tsui, *Org. Lett.* **2020**, *22*, 4562–4567.
[46] Z. Luo, G. C. Tsui, *Org. Chem. Front.* **2022**, *9*, 4969–4974.
[47] G. Knizia, *J. Chem. Theory Comput.* **2013**, *9*, 4834–4843.
[48] L. Greb, *Chem. Eur. J.* **2018**, *24*, 17881–17896.
[49] M. K. Beyer, *J. Chem. Phys.* **2000**, *112*, 7307–7312.

.

Supporting information

General Information

The preparation of Martin's spirosilane (SiL_2, L = (α,α-bis(trifluoromethyl) benzenemethanolato-(-2)C_2,O) was described elsewhere. (see main text) The preparation and handling of (perfluoroethyl)lithium is hazardous. (see main text) All chemicals were commercially available and used directly without further purification. All the experiment were conducted following classical Schlenk techniques under argon atmosphere or nitrogen for the preparation of silicon species. Et_2O and THF were distilled over sodium/benzophenone and DCM over CaH_2. The NMR spectra were recorded on a Bruker AVANCE I NMR 400 spectrometer at room temperature. (^{19}F, ^{1}H), Bruker AVANCE III 600 NMR spectrometer (^{29}Si, ^{13}C), JEOL ECZS 400MHz NMR spectrometer for the $^{13}C\{^{1}H\}\{^{19}F\}$ NMR experiment. All yield were determined by ^{19}F NMR with agreement of the reported experimental data. ATR-FTIR was performed on a Shimadzu IRAffinity-1CE spectrometer . Ball-Milling experiment were performed using a BM-500 apparatus from Anton Paar, 1.5 mL tube in 6*2 tube PTFE adaptator or 5 mL INOX JAR. Balls were purchased from Retsch and InSolido. Melting points were determined on a melting point apparatus SMP3 (Stuart scientific). Electrochemical measurements were carried out an Origaflex (Origalys) electrochemical workstation. High resolution mass spectrometries were performed on a microTOF (ESI).

Synthesis of $[NEt_4][Si(C_2F_5)L_2]$:

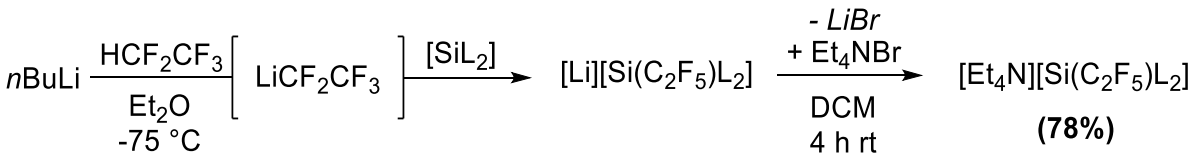

An excess of HC_2F_5 (~90 mL, ~2.5 equiv.) is condensed to a mixture of degassed n-butyllithium solution in hexanes (1 mL, 1.6 mmol, 1.6 M) in Et_2O (3 mL) at -75°C and stirred for 20 min (*The preparation and handling of (perfluoroethyl)lithium is hazardous*). A solution of Martin's spirosilane (SiL_2, L = (α,α-bis(trifluoromethyl) benzenemethanolato-(-2)C_2,O)[28] (800 mg, 1.6 mmol) in Et_2O (4 mL) is added slowly under stirring at -75 °C and slowly warmed up to -30 °C, degassed with nitrogen and warm up to room temperature. A solution of NEt_4Br (2 g, 9.5 mmol) in DCM (0.1M) was added and was stirred overnight at rt. The crude was extracted with DCM/HCl (1M), dry over Na_2SO_4 and the solvent was removed with a rotary evaporator. Precipitation (DCM/pentane) yields 78% of $[NEt_4][Si(C_2F_5)L_2]$ (950 mg, 1.3 mmol) as a white powder over 2 steps.

^{1}H NMR (Bruker, 400MHz, [D6]acetone, rt): δ (ppm) = 8.4 (d, ^{3}J(H-H) = 6.7 Hz, 2H), 7.7 (d, ^{3}J(H-H) = 6.7 Hz, 2H), 7.5 (q, *J* = 8 Hz, 4H), 3.2 (q, *J* = 7 Hz, 8H), 1,2 (tt, br, 12H);

^{13}C{^{1}H} NMR (Bruker, 600MHz, [D6]acetone, rt): δ (ppm) = 141.7 (^{1}J(C,C) = 49.5 Hz, Si*L*$_2$), 140.3 (^{1}J(C,H) = 105.3 Hz,^{1}J(C,C) = 49.9 Hz, Si*L*$_2$), 137.8 (^{1}J(C,C) = 52.2 Hz, Si*L*$_2$), 129.2 (^{1}J(C,C) = 50.3 Hz Si*L*$_2$), 128.5 (^{1}J(C,C) = 59.7 Hz,Si*L*$_2$), 124.4 (q, ^{1}J(C,F) = 288 Hz, C(*C*F$_3$)$_2$), 124.3 (q, (overlap) ^{1}J(C,F) = 288 Hz, C(*C*F$_3$)$_2$), 122.0 (qt, ^{1}J(C,F) = 286 Hz; ^{2}J(C,F) = 32 Hz, -*C*F$_2$CF$_3$), 123.4 (Si*L*$_2$), 120.2 (dq, ^{1}J(C,F) = 276 Hz; ^{2}J(C,F) = 37 Hz, -CF$_2$*C*F$_3$), 81.9 (sept, ^{2}J(C-F) = 28.2 Hz, *C*(CF$_3$)$_2$), 51.9 (t (broad), *J* = 2.6 Hz, N(*C*H$_2$CH$_3$), 6.2 (N(CH$_2$*C*H$_3$);

^{13}C{^{1}H}{^{19}F} NMR (JEOL, 400MHz, [D6]acetone, rt): δ = 143.8, 142.4, 139.9, 131.3, 130.6, 126.4, 126.3, 125.4, 124.0, 122.2, 84.0, 54.0, 8.3;

^{19}F NMR (Bruker, [D6]acetone, rt): δ = -74.3 (m, C(***C*F$_3$***)-CF$_3$, 6F), -75.7 (q, C(CF$_3$)-***C*F$_3$** : ^{4}J(F,F) = 9.5 Hz, 6F), -80.9 m, -CF$_2$-***C*F$_3$***, 3H*), -119 (d, sept, -C(***F***)F-CF$_3$: ^{2}J(F,F) = 324 Hz , ^{6}J(F,F) = 6.9 Hz, 1F), -127 (d, sept, d, -CF(***F***)-CF$_3$: ^{2}J(F,F) = 324 Hz , ^{6}J(F,F) = 6.9 Hz, ^{3}J(F,F) = 2.2 Hz, 1F);

^{29}Si NMR (Bruker, 600MHz, [D6]acetone, rt): δ = -78.0 ppm (dd, ^{2}J(Si, F) = 35 Hz);

IR (ATR): $\tilde{\nu}$ (cm^{-1}) = 1486 (w), 1445 (w), 1396 (w), 1310 (m), 1293 (m), 1268 (m), 1232 (w), 1196 (m), 1177 (s), 1162 (s), 1154 (s), 1136 (s), 1114 (m), 1076 (m), 1038 (m), 1000 (s), 967 (s), 954 (s), 782 (m), 764 (m), 735 (s), 708 (s), 677 (m);

m.p.: 152°C, decomposition (bubbling 175°C)**;**

HRMS: calc. for [$C_{20}H_8F_{17}O_2Si$]$^{-}$ 631.0028 found 631.0024

Reactivity investigations:

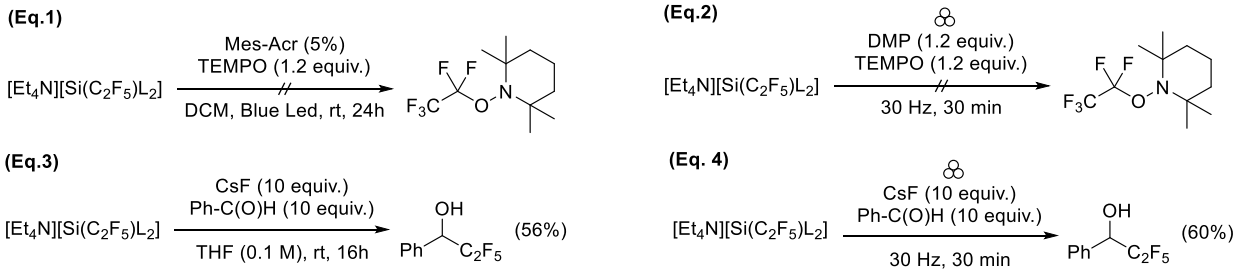

Eq.: (1) TEMPO solution trapping experiment, (2) TEMPO solid-state trapping experiment, (3) Solution nucleophilicity (4) Solid-state nucleophilicity

Note: In the case of radical reactivity, the formation of the correspond radical should not lead to the formation of unstable species. In the case of ionic reactivity, due to the possible generation of TFE violently by anion decomposition and the potent reaction with air forming hazardous peroxide, we decided to scale down the reaction for our investigation in solid state.

Eq.1: In a flame-dried Schlenk tube was added $[NEt_4][Si(C_2F_5)L_2]$ (76 mg, 0.1 mmol), TEMPO (65 mg, 0.4 mmol) and Mes-Acr (2.8 mg, 0.003 mmol). The Schlenk tube was purged with Argon by means of vacuum-refill cycles (3 times) and freshly distilled DCM (0.2M, 500 µL) was added. After 3 cycles of freeze-pump-thaw, the reaction medium was irradiated under blue LEDs and the reaction monitored by ^{19}F NMR. After 48 hours, no reaction proceeded.

Eq.2: In a 5 mL INOX JAR was added $[NEt_4][Si(C_2F_5)L_2]$ (76 mg, 0.1 mmol), one 8 mm INOX ball, TEMPO (20 mg, 0.12 mmol) and (Dess-Martin Periodate) DMP (50 mg, 0.12 mmol). The jar was shaken for 30 min at 30 Hz. The crude was dissolved in d6-Acetone and the reaction monitored by ^{19}F NMR, after 30 min no reaction proceeded.

Eq.3: In a 1.5 mL PP tube was added $[NEt_4][Si(C_2F_5)L_2]$ (7.6 mg, 0.01 mmol), CsF (15 mg, 0.1 mmol) and benzaldehyde (10 µL, 0.1 mmol) in THF (0.1 mL). The reaction was stirred 16h at RT. The crude was filtered, the powder wash with minimum of DCM and then dissolved in d6-Acetone and the reaction yield determined by ^{19}F NMR calibrated with the formed $[Si(F)L_2]$- as internal standard (56% yield).

Eq.4: In a 1.5 mL PP tube was added $[NEt_4][Si(C_2F_5)L_2]$ (7.6 mg, 0.01 mmol), one 5 mm INOX ball, CsF (15 mg, 0.1 mmol) and aldehyde (0.1 mmol). The tube was shaken for 30 min at 30 Hz. The crude was dissolved in d6-Acetone and the yield determined by ^{19}F NMR calibrated with the formed $[Si(R)L_2]^-$ (R = F & OH) as internal standard (60% yield).

Both crude NMR (1H and 19F) peaks of experiment (see Eq. 3 and Eq. 4) are in agreements as reported in the literature.[16] Characteristic peak of 2,2,3,3,3-pentafluoro-1-phenylpropan-1-ol; δ (ppm) ^1H ([D6]acetone, rt) 5.25 (dd, $^3J(H,F)$ = 19.5 Hz; $^3J(H,F)$ = 6.5 Hz, 1H, OC*H*); δ (ppm) ^{19}F ([D6]acetone, rt) –81.5 (s, 3F; CF_3), -119.9 (dd, $^2J(F,F)$ = 273.2 Hz, $^3J(F,H)$ = 6.3 Hz, 1F; CF_2), -130.6 (dd, $^2J(F,F)$ = 272.8 Hz, $^3J(F,H)$ = 19.4 Hz,1F; CF_2).

Synthesis of [Y][Si($C_6F_{12}H)L_2$]:

Early note : all isolation process led to the formation of [Y][Si(F)L_2]

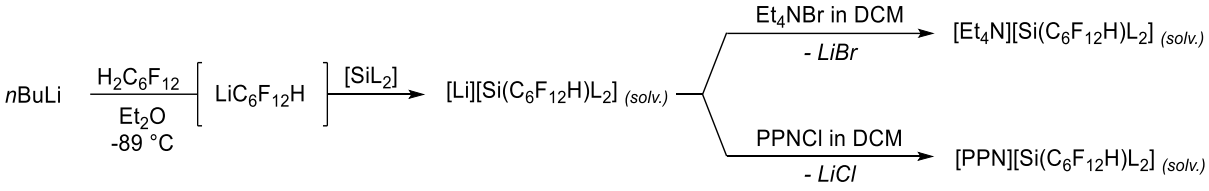

$H_2C_6F_{12}$ (212 µL, 1.1 mmol) is added dropwise to a mixture of degassed solution of n-butyllithium in hexanes (0.68 mL, 1.1 mmol, 1.6 M) in Et_2O (2 ml) at -75°C and stirred for 20 min. A solution of [SiL_2] (512 mg, 1 mmol) in Et_2O (4 mL) is added slowly under stirring at -75 °C and slowly warmed up to -30 °C, degassed with nitrogen and warm up to room temperature. (The ^{19}F NMR shows complete formation of the desired product and traces of degradation.

Characteristic NMR data for characterisation in [D6]acetone: **[Si($C_6F_{12}H)L_2$]$^-$** δ ^{19}F (ppm) -139.1 (d, m, -C**F_2**H : $^2J(F,H)$ = 50.9 Hz , $^3J(F,H)$ = 5.0 Hz, 2F), transformation in s for $^{19}F\{^1H\}$; δ ^1H (ppm) 6.81 (t, t, -CF_2**H** : $^2J(F,H)$ = 50 Hz, $^3J(F,H)$ = 5 Hz, 1H); **[Si($C_6F_{11})L_2$]$^-$** : δ ^{19}F (ppm) -173.2, $^3J(F,F)_{trans}$ = 132 Hz)).

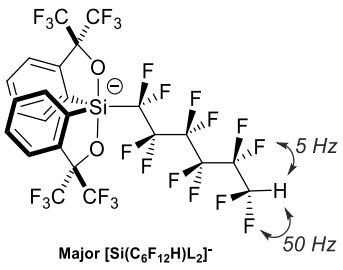

Major [Si($C_6F_{12}H)L_2$]$^-$

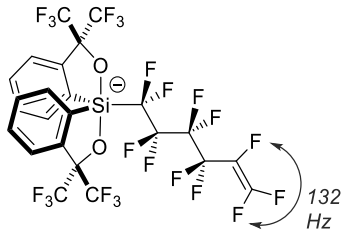

Minor [Si($C_6F_{11})L_2$]$^-$

A solution of NEt_4Br (0.85 g, 4 mmol) or PPNCl (2.3 g, 4 mmol) in DCM (0.1M) was added and was stirred overnight at rt. The crude was extracted with DCM/HCl (1M), dry over Na_2SO_4 and the solvent was removed with a rotary evaporator. Degradation and formation of the Martin's silicate fluoride occurred during the removal of organic solvent and precipitation process (DCM/Pentane). Experimental data agree with the reported one for [Si(F)L_2]$^-$ and confirmed by XRD.

Discussion on the case of [Y][Si($C_6F_{12}H$)L_2]:

We investigated the synthesis of a silicate with a longer fluoroalkyl chain. Following the same methodology, the preparation [Li][Si($C_6F_{12}H$)L_2] from the corresponding lithium reagent Li-$C_6F_{12}H$ was carried out as indicated before.

As for the C_2F_5 derivative, the lithium salt of [Si($C_6F_{12}H$)L_2]$^-$ appears relatively stable in solution but complete degradation into [Li][Si(F)L_2] was observed during the isolation process. We then decided to investigate the cation influence for the possible formation of [Y][Si($C_6F_{12}H$)L_2]$_{(s)}$. We therefore studied the stability with [NEt_4] based on our previous experiment, but this was also unsuccessful such as our last attempt with 1 equivalent of [PPN][Cl] (Bis(triphenylphosphine)iminium chloride).

While each species appears stable in solution, we did not manage to isolate the Martin's spirosilane salt. In the ^{19}F NMR spectrum, full conversion of the spirosilane [SiL_2] into the desired product was observed with the characteristic -CF_2H at δ = -139.1 ppm as a doublet multiplet with a $^2J(F,H)$ and $^3J(F,H)$ coupling of 50.9 Hz and 5.0 Hz in ^{19}F and the expected transformation in a single multiplet at $^{19}F\{^1H\}$. An interesting impurity resulting from the potential deprotonation and subsequent elimination of *Lithium Fluoride* was observed, resulting in generation of polyfluorinated alkene with the characteristic $^3J(F,F)_{trans}$ = 132 Hz at δ = -173.2 ppm.

[Si(C_2F_5)L_2][NEt_4]

^{1}H NMR ([D6]acetone):

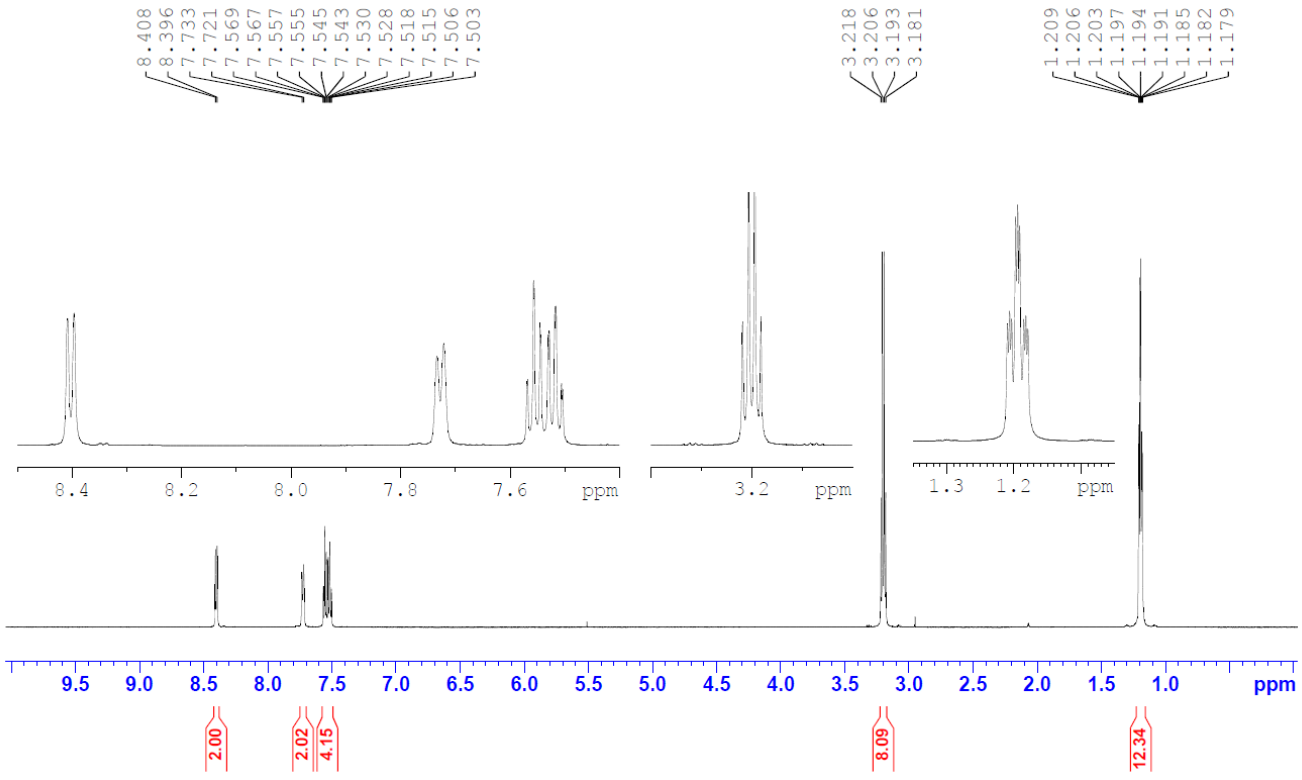

$^{13}C\{^{1}H\}\{^{19}F\}$ NMR ([D6]acetone) :

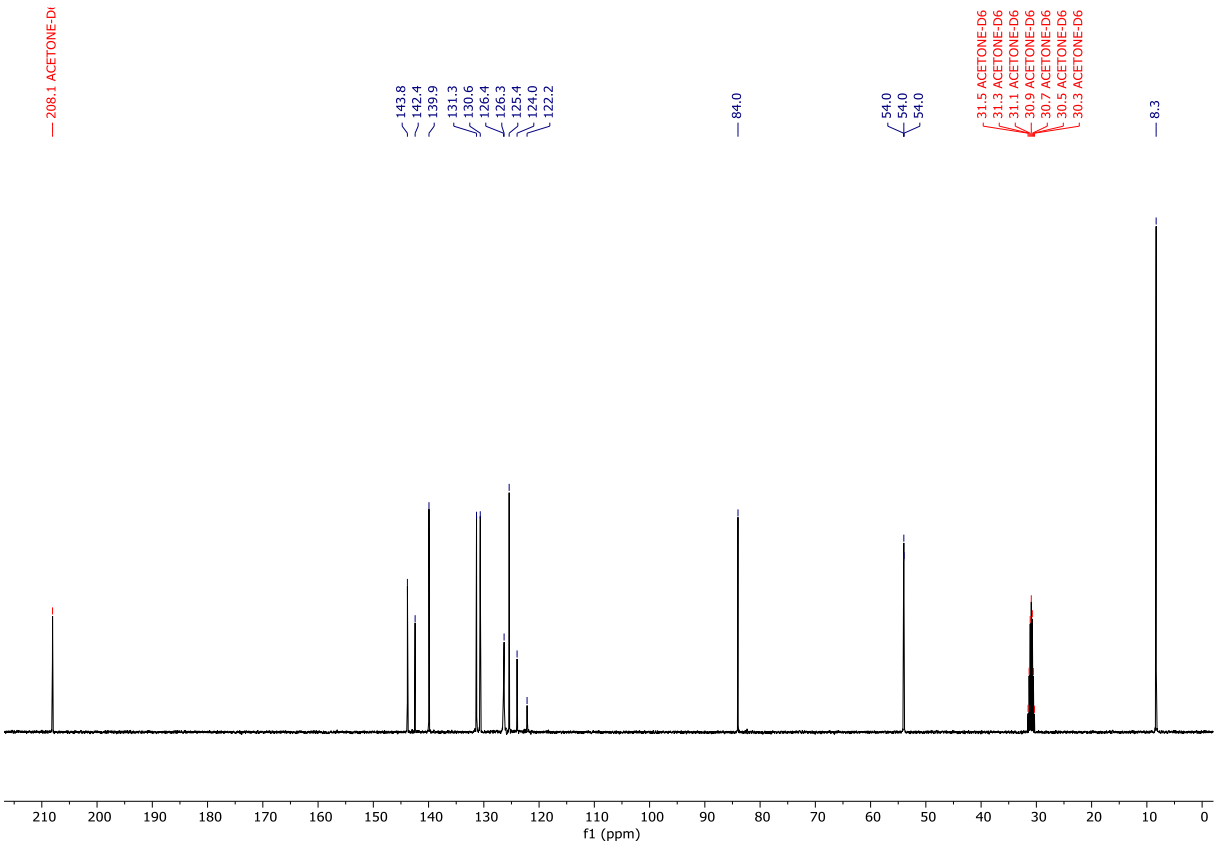

^{19}F NMR ([D6]acetone) :

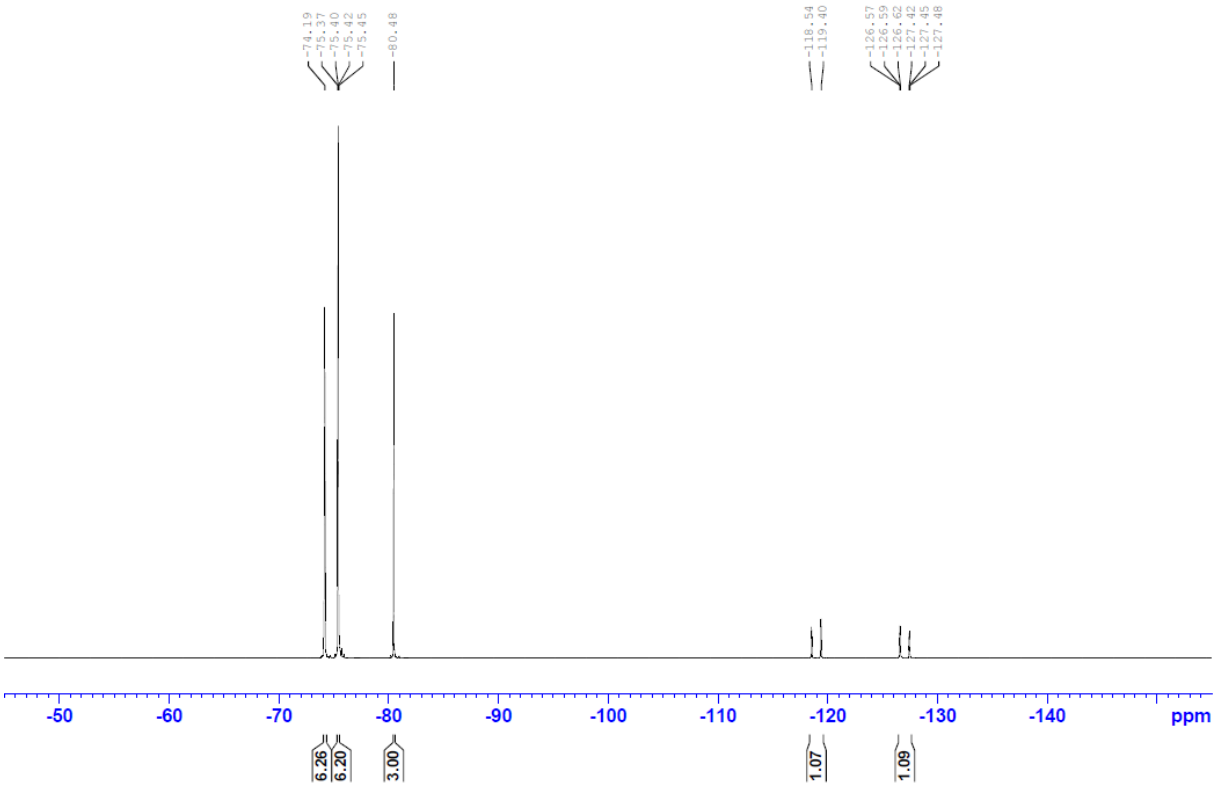

Zoom of ^{19}F NMR ([D6]acetone-wet) plot with Igor. *Note: water in the NMR solvent increased the spectrum resolution.*

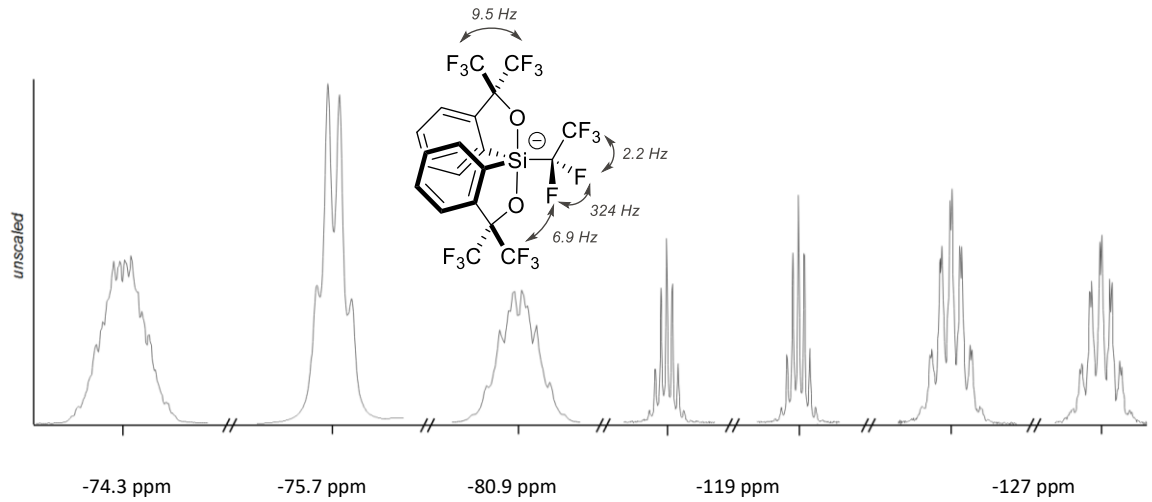

^{19}F NMR ([D6]acetone, rt): δ = -74.3 ppm (m, C(C***F*****$_3$**)-CF_3, 6F); -75.7 (q, C(CF_3)-C***F*****$_3$** : ^{4}J(F,F) = 9.5 Hz, 6F); -80.9 (m, -CF_2-C***F*****$_3$**, *3H*); -119 (d, sept, -C(***F***)F-CF_3 : ^{2}J(F,F) = 324 Hz , ^{6}J(F,F) = 6.9 Hz, 1F); -127.0 (d, sept, d, -CF(***F***)-CF_3 : ^{2}J(F,F) = 324 Hz , ^{6}J(F,F) = 6.9 Hz, ^{3}J(F,F) = 2.2 Hz, 1F);

^{29}Si NMR ([D6]acetone):

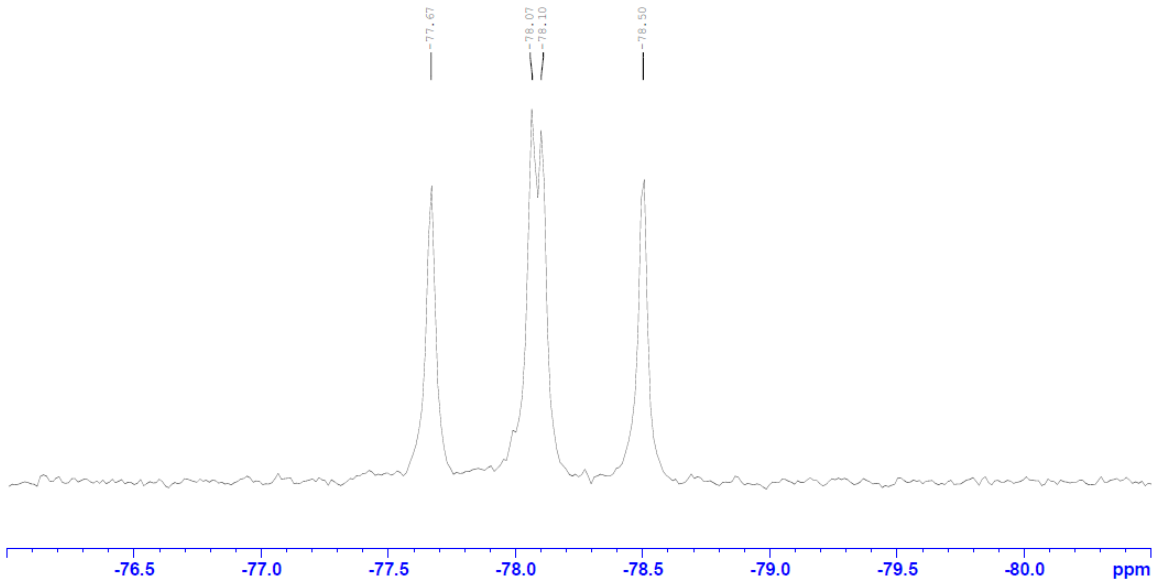

$^{13}C\{^{1}H\}$ NMR ([D6]acetone) :

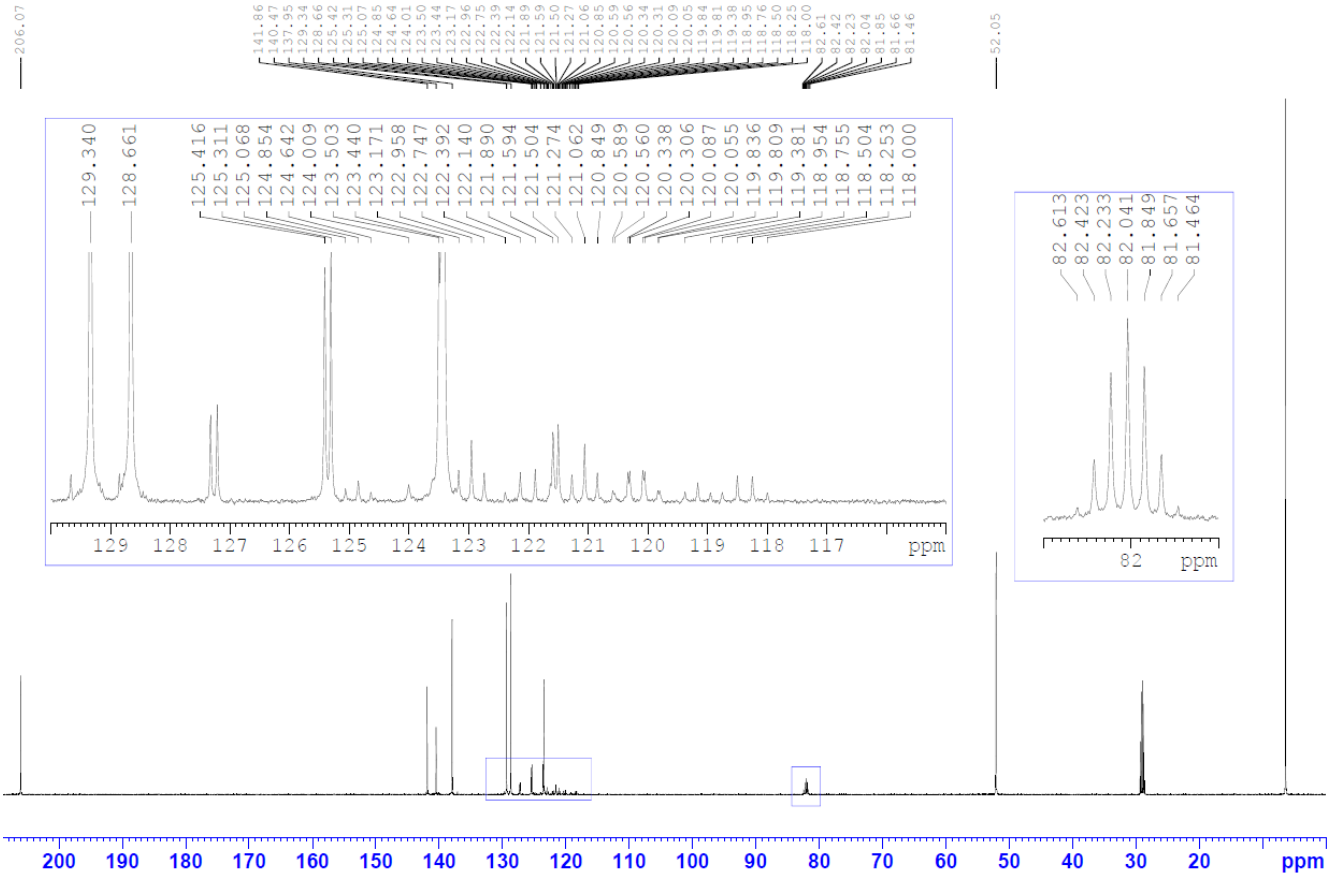

Zoom : $^{13}C\{^{1}H\}$ NMR ([D6]acetone) :

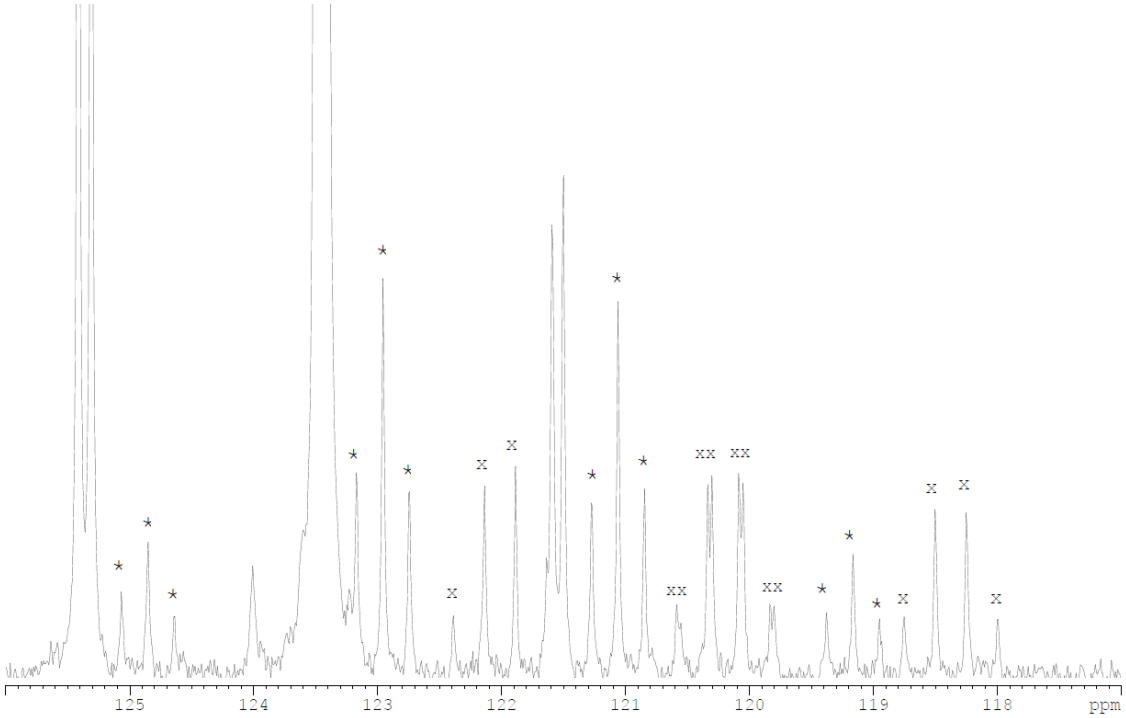

122.0 ppm (*) (qt, $^{1}J(C,F)$ = 286 Hz; $^{2}J(C,F)$ = 32 Hz) | 120.2 ppm (x) (dq, $^{1}J(C,F)$ = 276 Hz; $^{2}J(C,F)$ = 37 Hz)

Zoom $^{13}C\{^{1}H\}$ NMR ([D6]acetone) (Plotted with igor for better resolution**)**

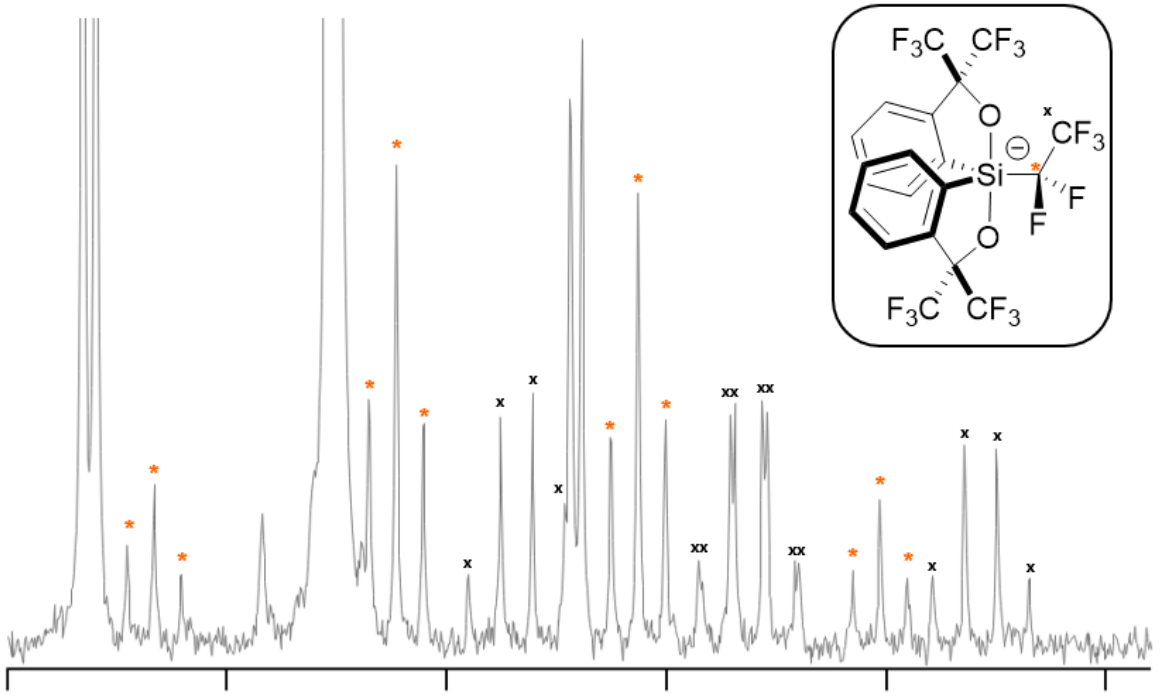

122.0 ppm (*) (qt, $^{1}J(C,F)$ = 286 Hz; $^{2}J(C,F)$ = 32 Hz) | 120.2 ppm (x) (dq, $^{1}J(C,F)$ = 276 Hz; $^{2}J(C,F)$ = 37 Hz)

ATR-FTIR:

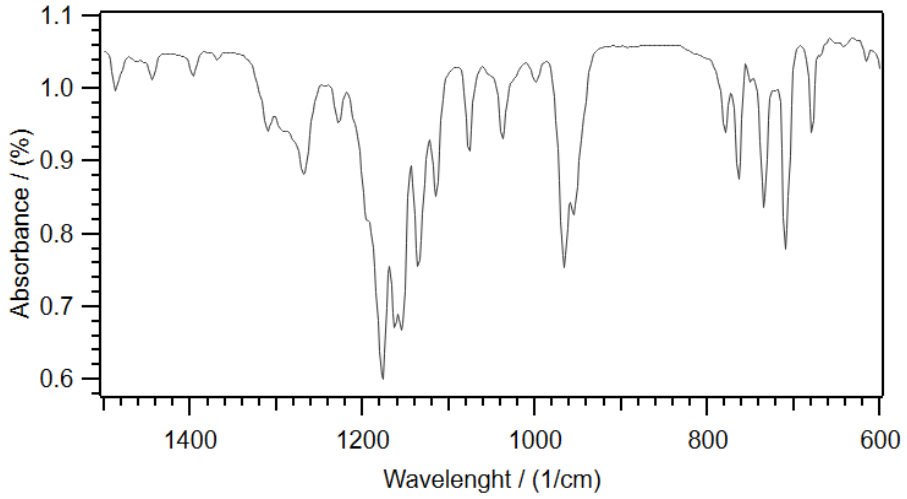

HRMS (631 = $[Si(C_2F_5)L_2]$- & 531 = fragmentation in $[Si(F)L_2]$-) **:**

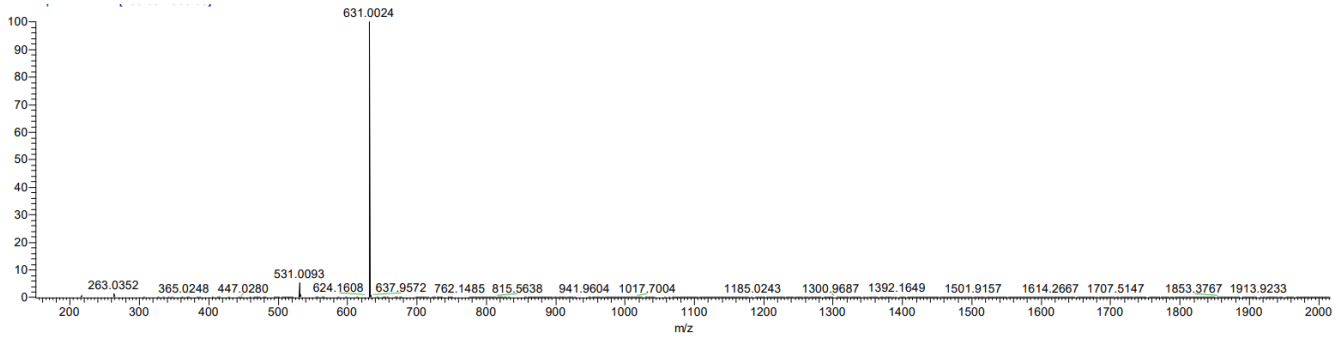

Crude [Si($C_6F_{12}H$)L_2] ^{19}F:

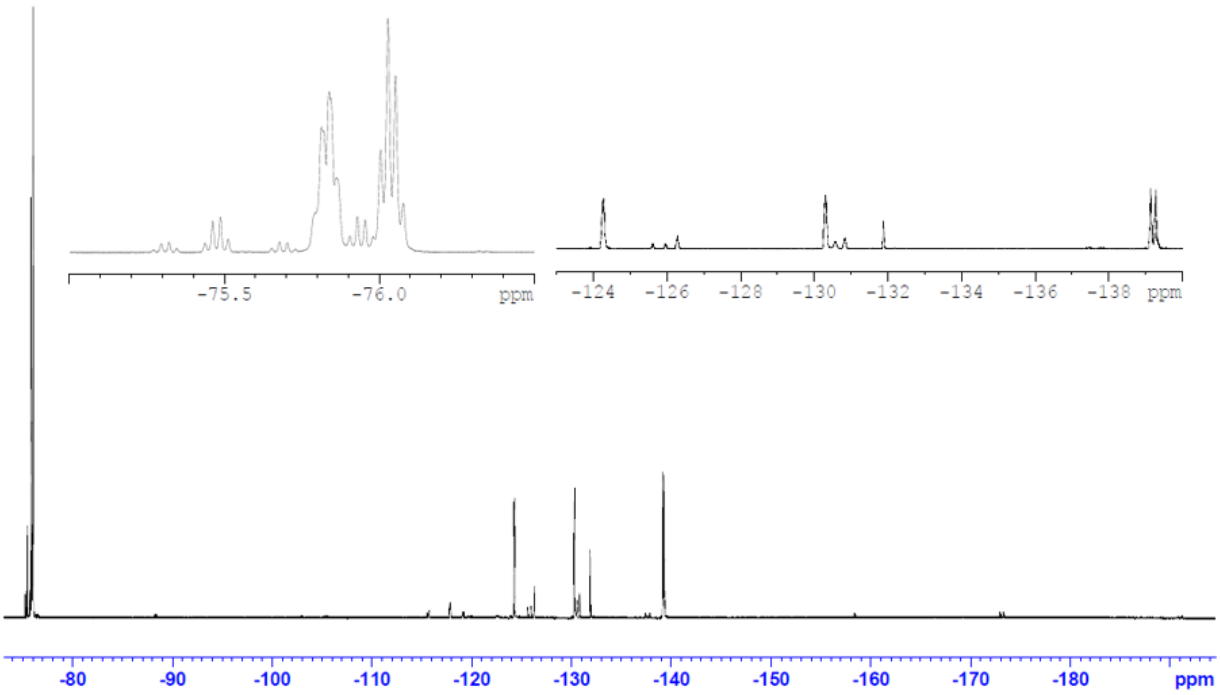

Selected zoom (unscaled, plot with igor, left ^{19}F - ‖ - right $^{19}F\{^1H\}$) :

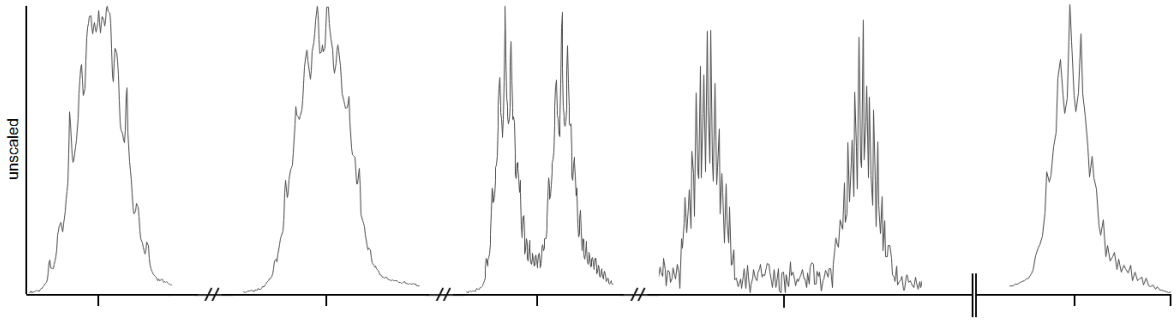

-124 ppm -130 ppm -139 ppm -173 ppm -139 ppm

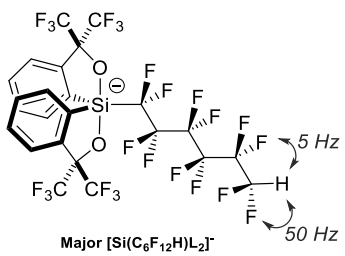

Major [Si($C_6F_{12}H$)L_2]$^-$

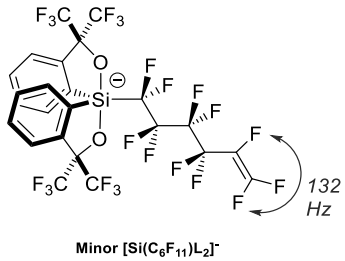

Minor [Si(C_6F_{11})L_2]$^-$

Characteristic NMR data for characterisation in [D6]acetone: **[Si($C_6F_{12}H$)L_2]-** δ ^{19}F -139,1 ppm (d, m, -C***F***$_2$H : $^2J(F,H)$ = 50.9 Hz , $^3J(F,H)$ = 5.0 Hz, 2F), transformation in s for $^{19}F\{^1H\}$; δ ^1H 6.81 ppm (t, t, -CF_2**H** : $^2J(F,H)$ = 50 Hz, $^3J(F,H)$ = 5 Hz, 1H); **[Si(C_6F_{11})L_2]-** : δ ^{19}F -<u>173.2</u> ppm: $^3J(F,F)_{trans}$ = <u>132</u> Hz

Clear observation ($^{19}F\{^{1}H\}$) of HC_2F_5 during the optimisation (solution) process small shift are induced due to the THF solvent:

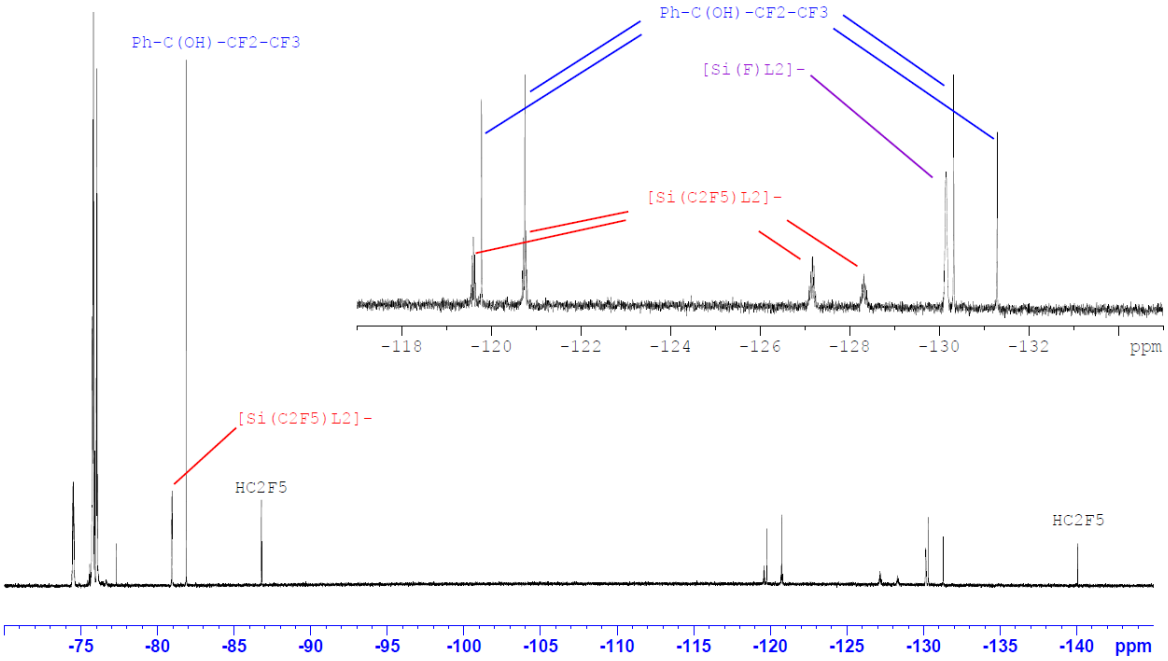

^{19}F NMR yields are calculated with the value as mentioned in the spectral data with:

$n_p = n_i \times \frac{\left(\frac{I_p}{N_p}\right)}{\left(\frac{I_{is}}{N_{is}}\right)}$	Product: *p* n_{is} = 0.01 mmol	Integration: *I* No. of fluorine of chosen peak: *N* Internal Standard: *is*

*Mechanochemical reaction (SiOH + SiF; trace of HC_2F_5; * = $[Et_4N][Si(C_2F_6)L_2]$) (rdt = 60% = 0,01*r *100; r = (1.8/3)/(5.99/6)):*

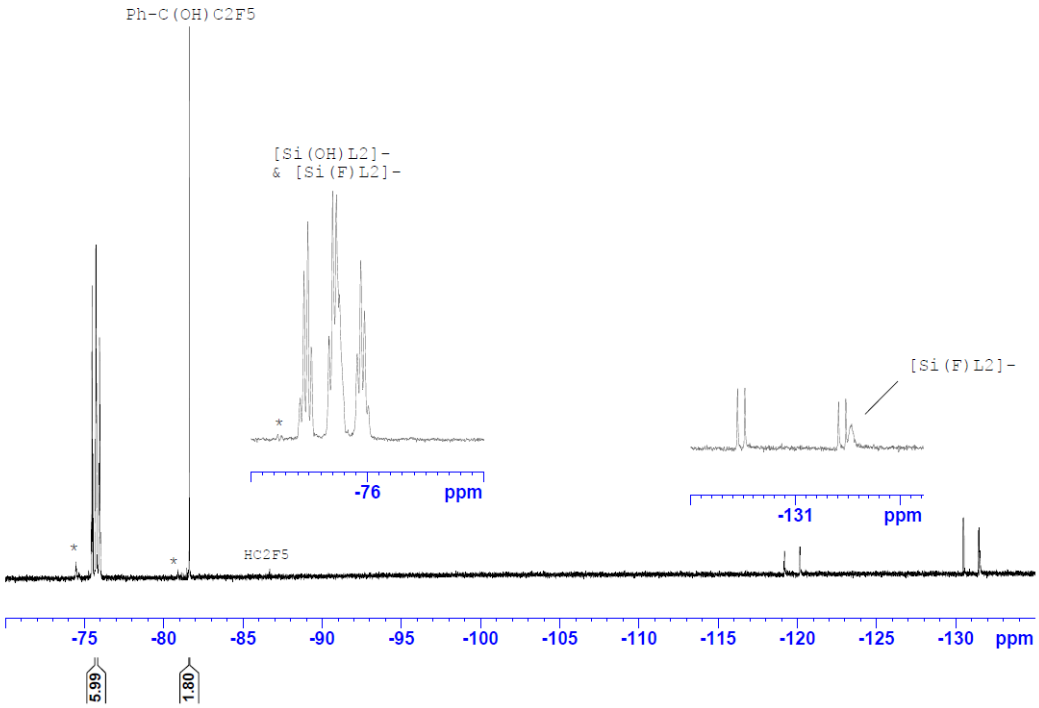

Solution reaction ^{19}F (rdt = 56% = 0,01*r *100; r = (1.4/3)/((6.06-1.02)/6)**):**

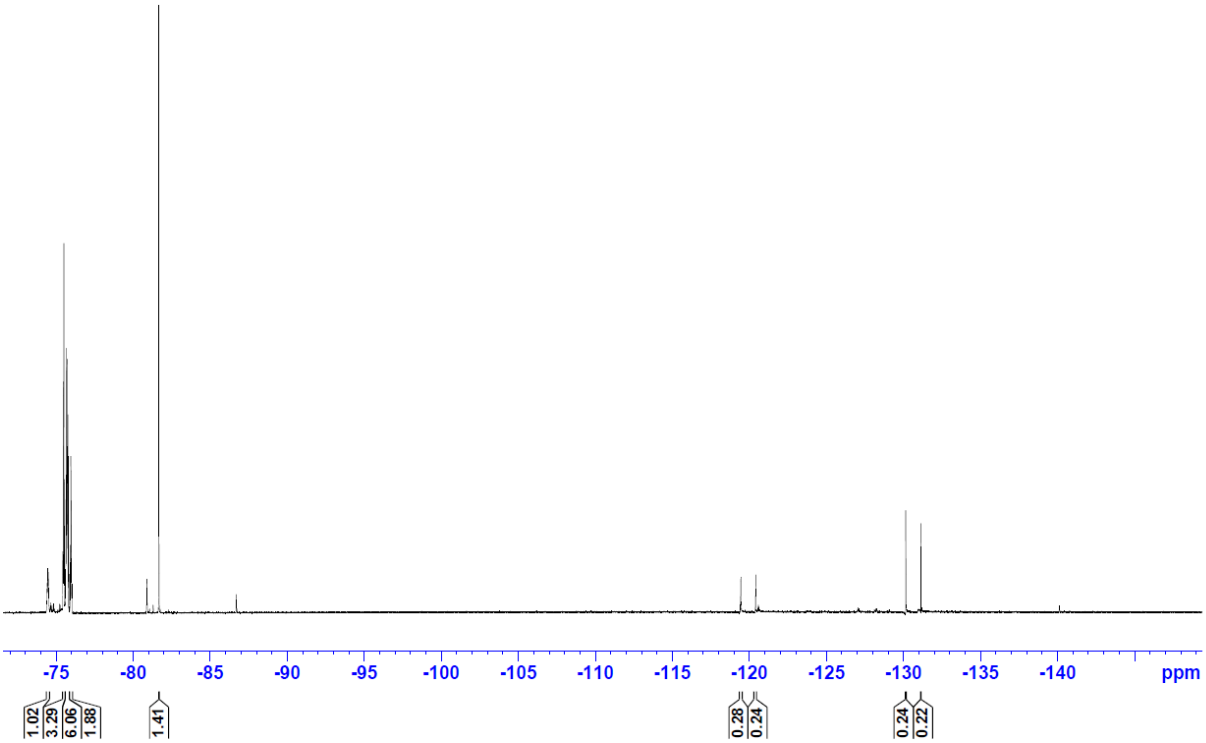

Solution reaction (eq. 3) ^{1}H NMR ([D6]acetone) crude (characteristic peak of 2,2,3,3,3-pentafluoro-1-phenylpropan-1-ol; 5.25 ppm (dd, ^{3}J(H,F)=19.5 Hz; ^{3}J(H,F)= 6.5 Hz, 1H OC**H**):

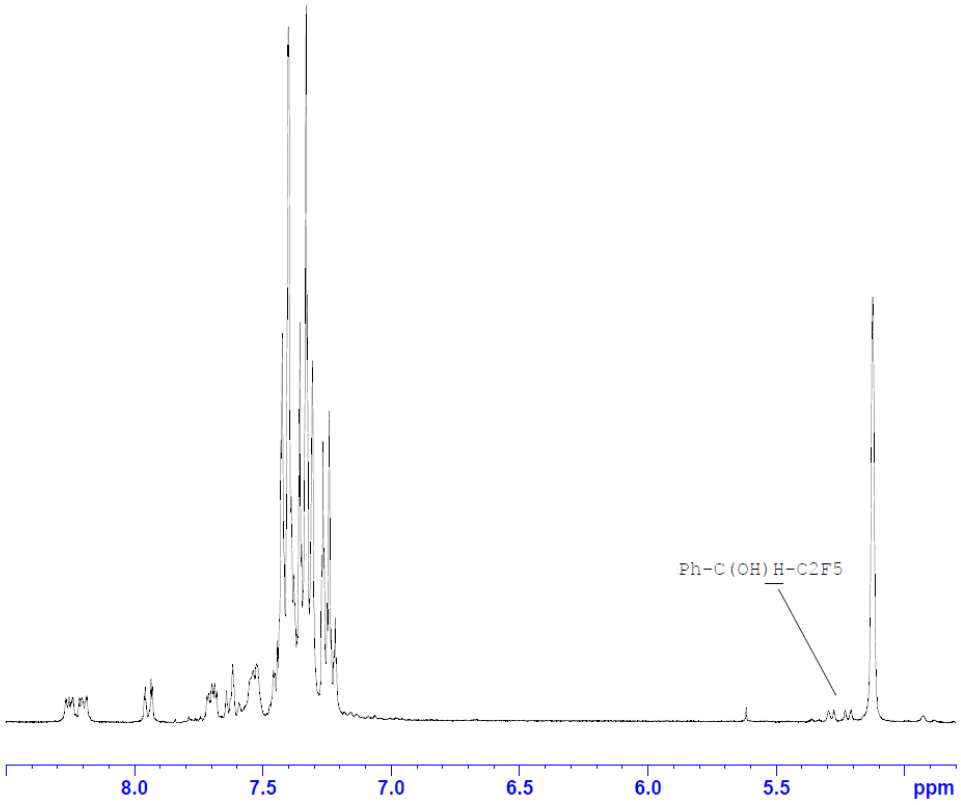

Chapter III.
Asymmetric radical recombination

Chapter 3.
Asymmetric radical recombination

This chapter has been done in direct collaboration with Dr. Ban Xu, here only the mechanistic investigation is presented. All analysis presented hereafter were designed and conducted by A.M.

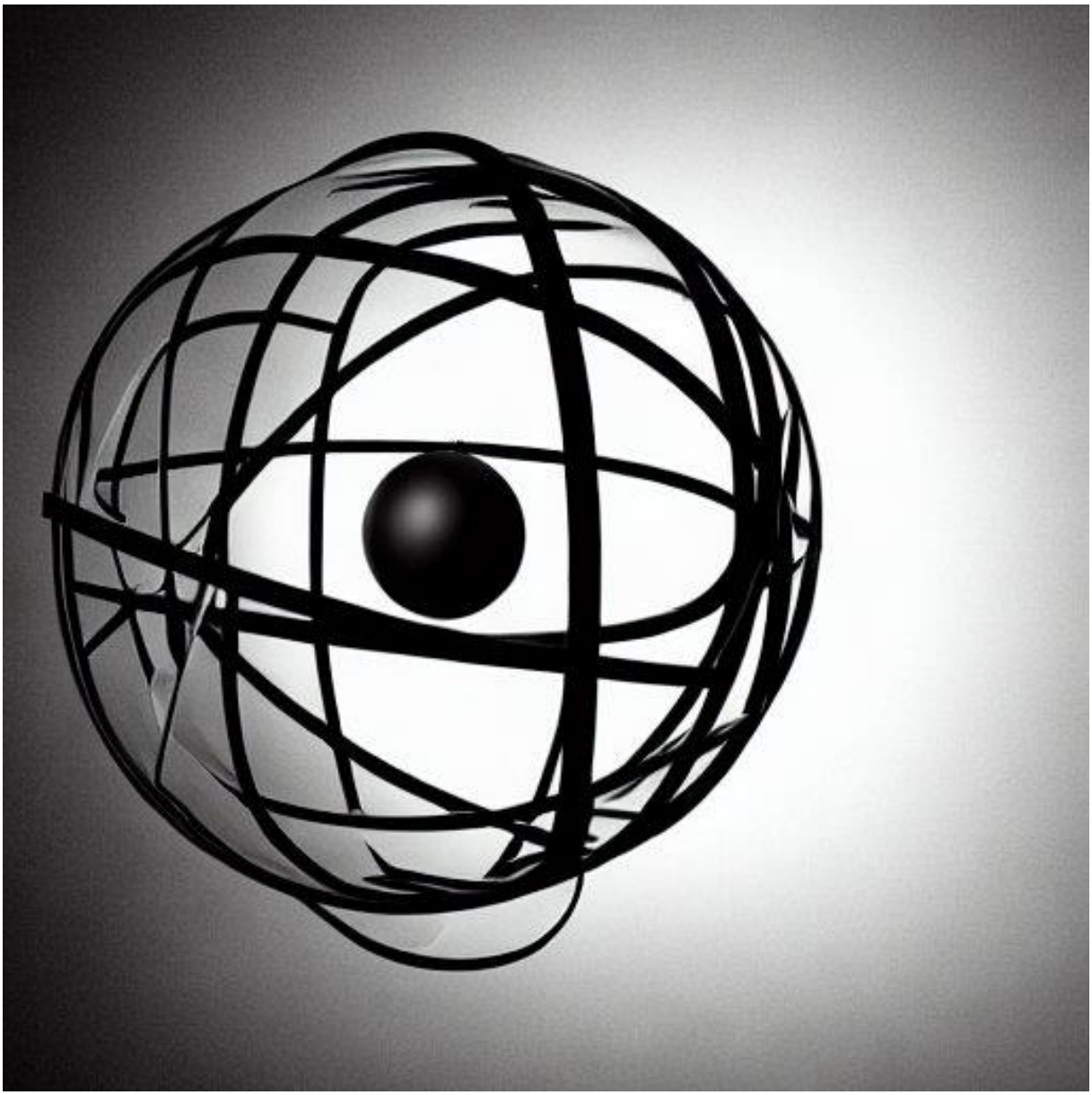

3.1 Introduction

3.1.1 Succinct overview

Numerous strategies for asymmetrical induction in a radical event have been developed over time. As highlighted by the following survey, it is now considered as a hot topic as demonstrated by the publications per year ratio. (Figure 1).[1]

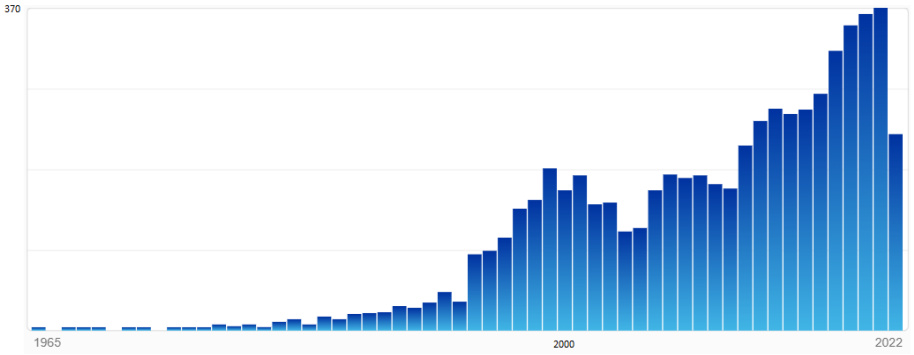

Figure 1. "Asymmetric radical" survey on sci-finder

Nearly 400 papers are now published per year and induction is based on the classical strategies used in organocatalytic chemistry such as hydrogen bond strategies, chiral Lewis or Bronsted acids (Figure 2).[2,3]

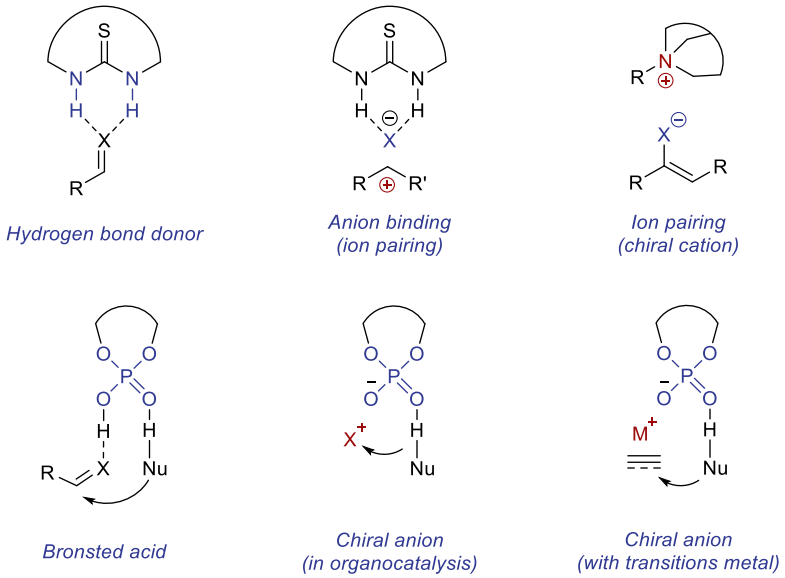

Figure 2. Strategies used for asymmetric induction of radical

During our research and design, we focused on the so called "Ion-Pairing strategies"[4] based on the phase transfer catalyst (PTC) developed in Prof. Tan laboratory.[5] These PTC are based on guanidinium as described in figure 3.

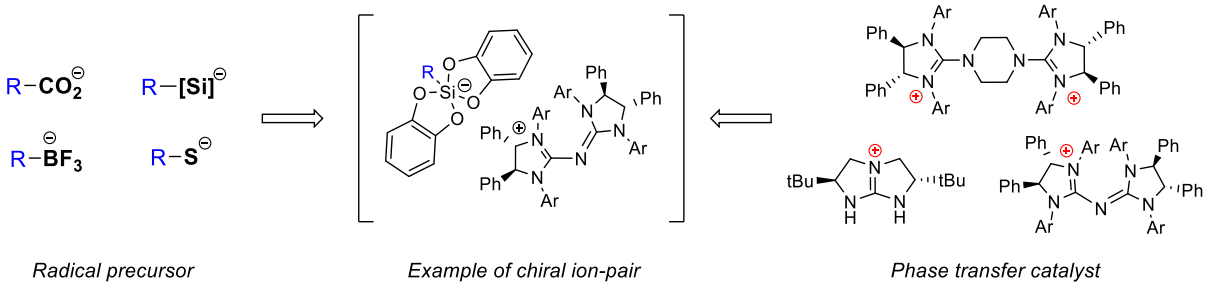

Figure 3. Designed research plan.

The desired reaction involved the formation of strict chiral ion-pair involving chiral cation and radical precursors. In the literature, if the name suggests pur ion-pair, the chiral induction is often en hanced by hydrogen bonding of the cation as reported by Melchiore in 2015 (Figure 4).[6] To the best of our knowledge "strict Ion-pairing" is not yet known. Indeed the difficulty being on the tuning of catalyst leading to it final ability of controling radical with weak or in the best case scenario no interactions.[7]

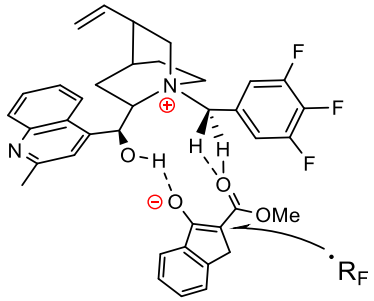

Figure 4. Synergetic ion-pairing and hydrogen bonding

In this project, the resulting radicals obtained from the oxidation of the precursors should not have direct interaction with our PTC. Due to that, the *pre*-organisation of the system inside the chiral pocket between the substrate and the radical precursor is mandatory. Firstly, we have investigated the potential Lewis-acidity of the bis(catecholato) silicate to perform some interaction with acceptor. Unfortunately, this potential interaction was not sufficient for observation of the desired chiral induction in a radical addition. (described in scheme 1).

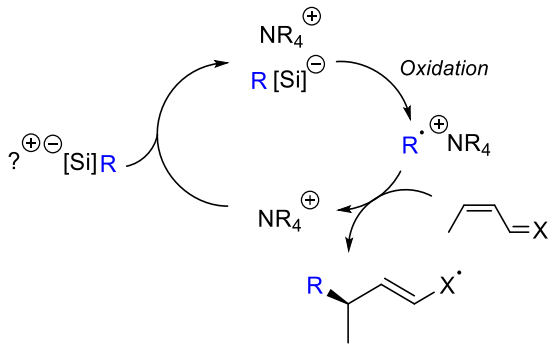

Scheme 1. Possible asymmetric radical addition via the *chiral cage* induction strategy

3.1.2 Concerning our project

Numerous modern strategies for the control of radical intermediates were recently achieved taking advantages of classical interactions as previously mentioned in 3.1.1; performing asymmetric radical-radical recombination is still considered as a modern synthetic challenge when both neutral species must be controlled. In addition, few remaining gaps such as purely/strict ion-pairing or chiral confined space were recently highlighted due to the difficulties to control the generated neutral radical species or the radical acceptor during the reaction without additional interactions or covalent bond.[8,9] It was reported that anions can perform a single-electron transfer (SET) event in the process of a nucleophilic radical substitution reaction (Srn1, scheme 2).

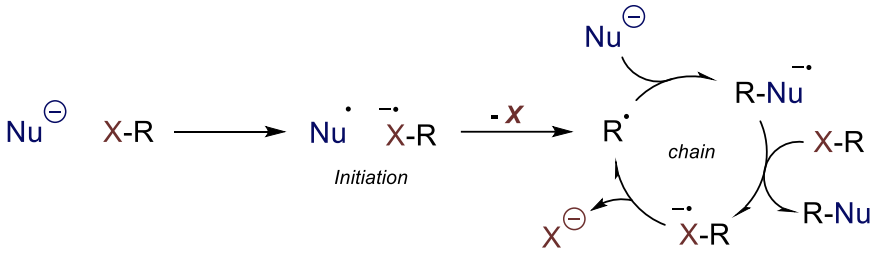

Scheme 2. Reported Srn1 mechanism

The reported radical substitution mechanism involves a chain radical pathway induced by a SET event from the nucleophile as initiation step. Fragmentation of the resulting radical anion leads to the formation of a neutral *C*-centred radical able to react with the nucleophile. The formation of this second anionic radical species permits a second SET with the halogen derivative and is responsible of the chain radical process. More recently in an anionic fashion, the halogen bond has also been described by our group (TCH) an intermediate for the Sn2X reactivity (scheme 3). [10]

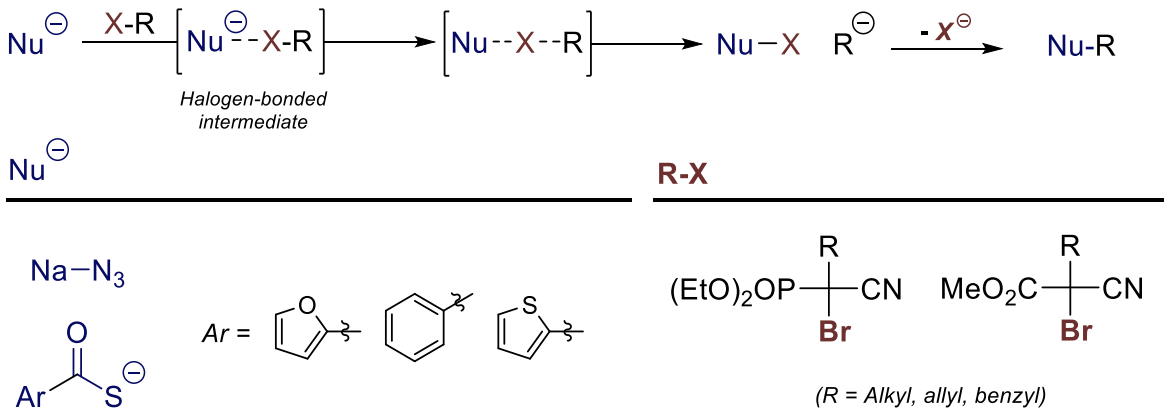

Scheme 3. Proposed mechanism for the Sn2X reaction

This reactivity permits to access quaternary stereocenters in high yield and high *ee* from an activated tertiary bromide. In the case of classical S_N2 reaction attacking the anti-bonding orbital behind the C-X bond is not possible due to the steric hinderance of a tertiary halogenated compound. In the case of the S_N2X, an intermediate involving halogen bonding between the nucleophile (azide or thiocarboxylate) with the tertiary bromine was proposed and supported by DFT calculation. Moderate halogen bonding (S···B distance of 3.04 Å) was calculated with an expected elongation of the C-Br bond. The activation of this bond (XB) is currently under investigation in every area of organic chemistry. In addition of XB activation, modern application involving radical/C-I bond activation via halogen atom transfer (XAT, scheme 4) strategy[11] or asymmetric transition metal/photoactivation[12] were investigated recently to overcome respectively unactivated halide radical precursor reactivity or hinderance issue of tertiary leaving group.

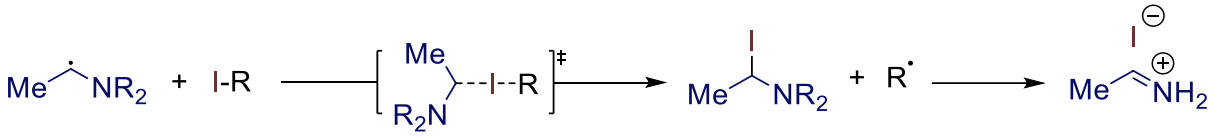

Scheme 4. Halogen atom transfer (XAT) reaction involving a proposed radical-halogen interaction

To the best of our knowledge, the asymmetric variation using ion-pairing/confined space strategies for accessing chiral C-sp^3 via control of neutral radical was not described. Due to the ability of our chiral phase transfer catalyst to perform asymmetric reaction, we firstly questioned the possibility to force the generation of these radicals from the transferred anions from the solid phase to solution. Indeed, the reported radical substitution mechanism involve an interaction between the single electron donor and an iodo-derivative that could takes place inside the catalyst chiral cavity formed via the arms of the catalyst (figure 5).[13] In addition, supramolecular chemistry calls attention to the notion of confined radical control[14] that could be extrapolated to large single system such as bisguanidium (BG).

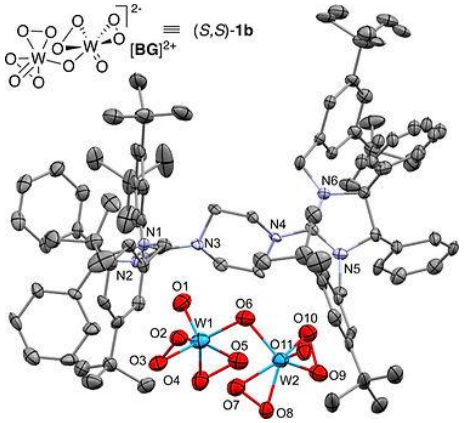

Figure 5. X-Ray of bis(guanidnium) (BG) catalyst (1868566) with Tungsten anion in the chiral pocket.

3.2 Summary of the mechanistic investigation

Here, some results obtained by Dr. Ban Xu are slightly depicted in scheme 5. The reaction was developed in solution under blue light irradiation and in solid-state under mechanochemical one. We aimed to better understand the mechanism involved for each media and compare the difference between each one. More details for each part can respectively be found in chapter 3.3 for solution experiment and 3.4 for solid one.

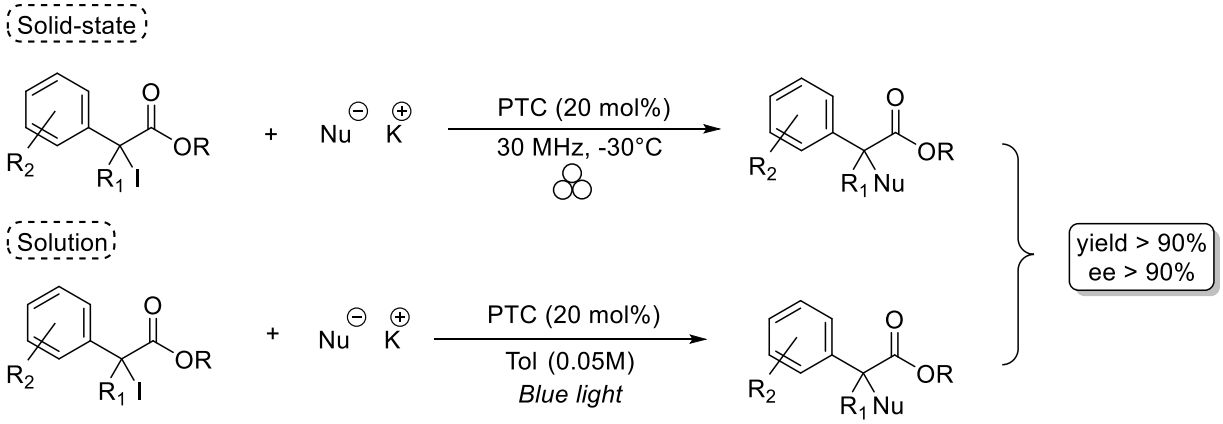

Scheme 5. Overview of the developed reaction | PTC = bis(guanidinium) (BG) catalyst bearing benzyl or alkyl chain.

The design of the reaction was based on the reported Srn1 reactivity as depicted in scheme 6. The ability of nucleophilic anions to perform a single-electron transfer (SET) event in the process of a nucleophilic radical substitution reaction (Srn1) was firstly highlighted in 1970 and was therefore extend to highly activated iodo-perfluoroalkane (scheme 6).[15,16]

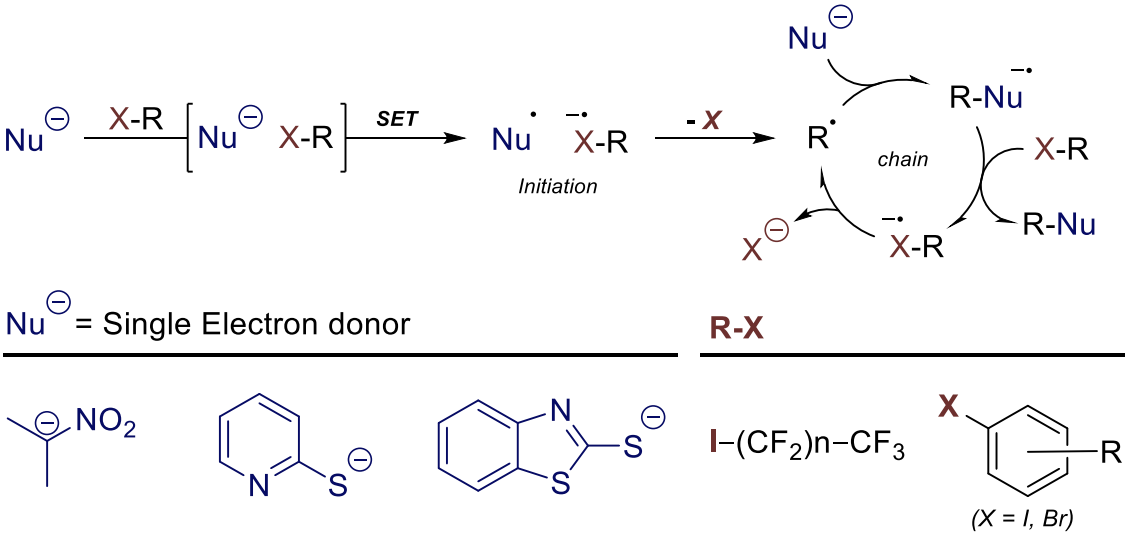

Scheme 6. Detailed mechanism of Srn1.

The reported radical substitution mechanism involves a chain radical pathway induced by a SET event from the nucleophile as initiation step. Fragmentation of the resulting radical anion led to the formation of a neutral *C*-centred radical species and the use of polar solvent allowed the complete solubilisation of the nucleophile and therefore permited the reaction of the radical species with the nucleophile. The formation of this second anionic radical species permits a second SET with the halogen derivative and is responsible of the chain radical process. If the Srn1 mechanism appears as a plausible initial proposition based on the experimental design, we also recently discovered the ability of our phase transfer catalyst to allow the Sn_2X reactivity.[10] Early investigations (control experiments) presented hereafter in scheme 6 were performed to dismiss this reactivity for this new system :

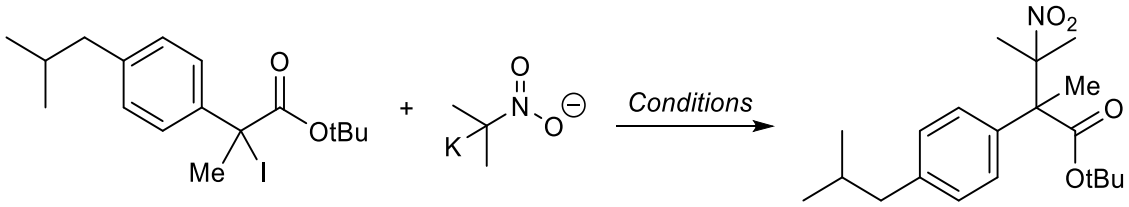

Entry		Conditions	result
1	**Solution**	a) PTC $_{(BG\ or\ TBAB)}$, Toluene, Blue light	✓
		b) PTC $_{(BG\ or\ TBAB)}$, Toluene, Blue light, O_2	✓
		c) PTC $_{(BG\ or\ TBAB)}$, Toluene, ~~Blue light~~	✗
		d) ~~PTC$_{(BG\ or\ TBAB)}$~~, Toluene, Blue light	✗
2	**Solid-state**	a) PTC $_{(BG\ or\ TBAB)}$, O_2	✓
		b) PTC $_{(BG\ or\ TBAB)}$, ~~O_2~~	✓
		~~c) PTC$_{(BG\ or\ TBAB)}$~~, O_2	✗
		~~d) PTC$_{(BG\ or\ TBAB)}$~~, ~~O_2~~	✗

Scheme 7. Control experiment for solution and mechanochemical experiment.

The main difference with the Sn_2X was highlighted by an on/off experiment showing the mandatory activation of the reaction by light in solution to perform the reaction. (Scheme 7, 1.a, 1.c) As expected, the presence of phase transfer catalyst (PTC) is also mandatory for the reaction being able to process, no interface reaction occurs. The main difference with light suggests a different mechanism and the idea of an essential interaction such as halogen bonding involved in this methodology emerged. In the case of the ball-milling (mechanochemical reaction) it also appears that the reaction does not proceed without the use of phase transfer catalyst showing a non-direct reactivity between the nucleophile and electrophile. (Scheme 7, 2.c and 2.d) The last orientation toward a Srn1 based mechanism and by consequent SET instead of energy transfer event (EnT) was done by observation of the non-influence of oxygen for this experiment in both cases. (scheme 7, 1.a-b, 2.a-b)

These control experiments allowed to propose an initial slightly modified Srn1 reaction mechanism for our reaction in solution and solid-state medium. To study this proposed mechanism, a possible research plan was designed and the possible analysis to investigate each steps were indicated as depicted in scheme 8.

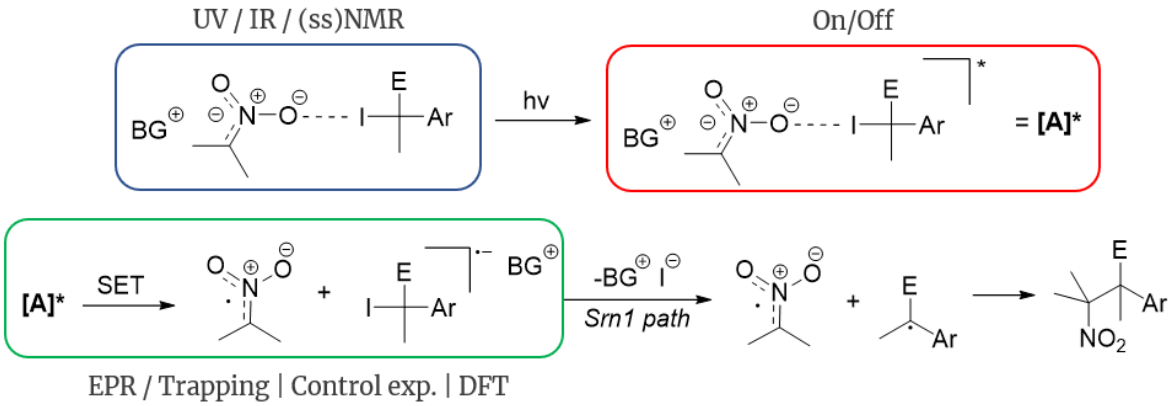

Scheme 8. Overview of one possible mechanism and possible analysis being relevant to the project.

The proposed mechanism (scheme 9) involved a halogen bond (XB) activated respectively by visible light irradiation or ball milling, this activation allows the SET event and resulting fragmentation-recombination inside the chiral pocket form by the arm of the catalyst as suggested by the observed *ee*. Compared to the Srn1, the use of non-polar solvent and therefore the catalytic amount of nucleophile transferred in solution by the phase transfer catalyst permits to avoid the background radical chain reaction and favour the asymmetric behaviour.

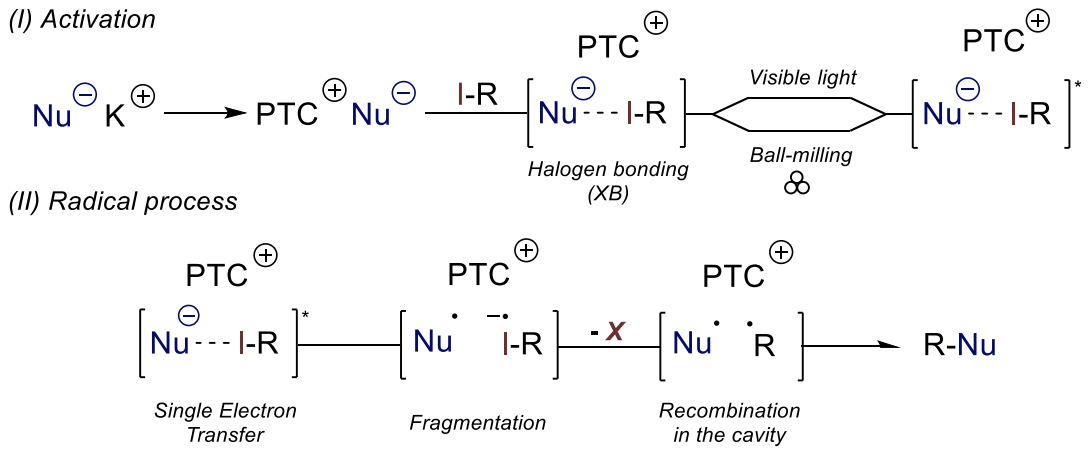

Scheme 9. Overview of the mechanism.

With this Srn1 hypothesis in hand, we firstly investigated the ability of the iodo-ester to be involved in an interaction with the nucleophile in solution. The observation of a shift in UV-Vis at low concentration (Figure 6, left) confirmed the interaction between both reactant and the presence of C-I bond let us envisage the formation of a halogen bond that was supported by density functional theory (DFT) calculation.

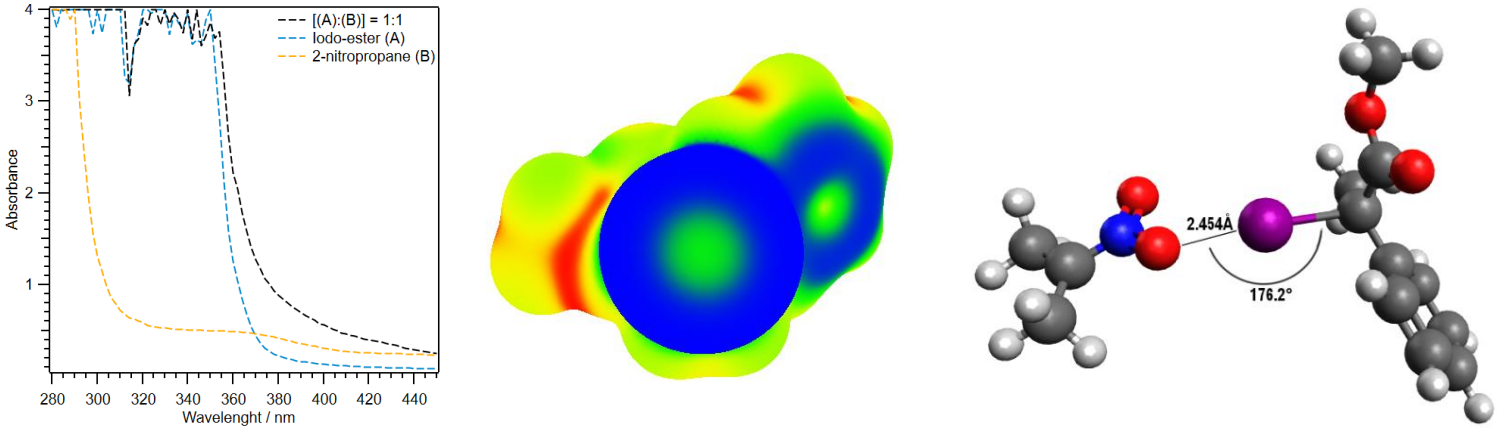

Figure 6. UV-Vis spectrum (left) of halogen bond donor (blue, iodo-ester) and halogen bond acceptor (yellow, nitropropane salt) and stoichiometric mixture (black); Electronic map of simplified halogen bond donor (middle); Interaction between the halogen bond donor/acceptor (right, DFT calculation, computed at PBeh-3C/def2-mSVP).

First, mapping of the halogen bond acceptor confirmed the presence of the σ-hole and the ability of this position to react with radicals and nucleophiles.[17,18] (Figure 6, middle) Secondly, intermolecular halogen bond with a calculated O···I distance of 2.454 Å and an angle of 176.2° that is in the range for strong halogen bond was obtained with an expected slight elongation of the C-I bond. (Figure 6, right)

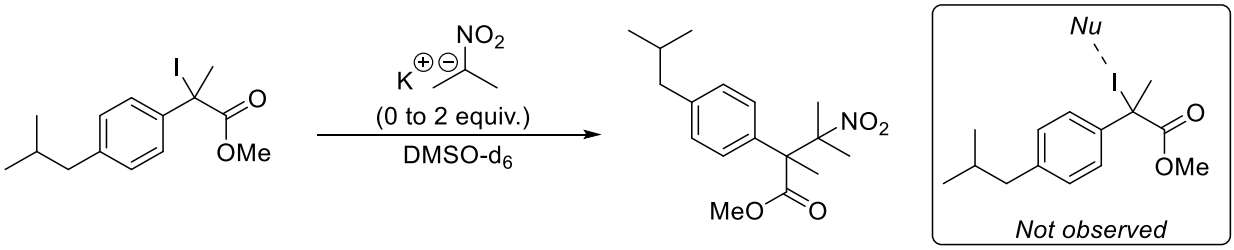

Scheme 10. Example of NMR titration experiment.

To gain experimental data and overcome the low solubility issue of the nucleophilic salt, attempt of nmr titration was done in DMSO-d6 with our halogen bond donor (activated iodo-ester). (scheme 10) Unfortunately, performing the titration with our halogen bond acceptor (e.g. the nitro-salt as depicted or thiopyridone salt) led to the formation of the coupling product. (see 3.3.4)

To overcome this reactivity issue and to support experimentally the ability of our starting material to participate in XB, we performed a titration using deuterated pyridine acting as a non-reactive partner. (scheme 11)

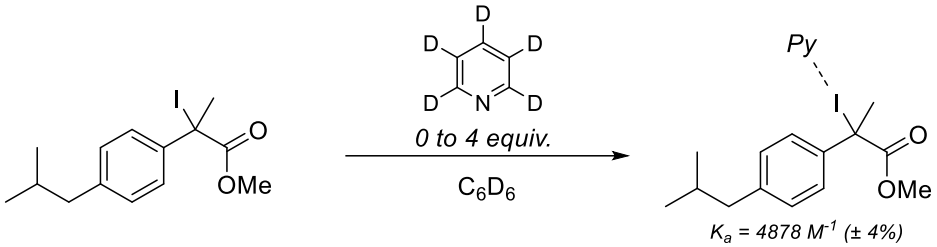

Scheme 11. Example of NMR titration experiment.

This titration permitted to observe characteristic shifts of the alkyl substituent and few modifications in the aromatic moiety confirming the XB capacity of this system. The affinity constant (K_a) was obtained using Stoddard's website (supramolecular.com) and the resulting value obtained as $K_a = 4878\ M^{-1}$ that is consistent with the strong halogen bond determined by DFT. (see 3.3.4)

Then, to support the previous report on the ability of 2-nitropropane anion to undergo a SET event to generate the corresponding nitroxide radical and anionic one. We firstly investigated the stability of the expected anionic radical intermediate by cyclic voltammetry. (Figure 7, left)

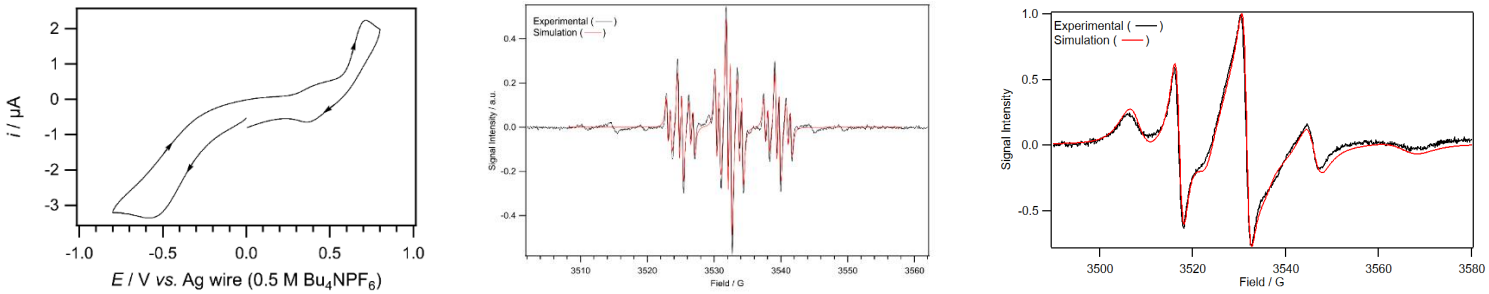

Figure 7. UV-Vis spectrum (left) of halogen bond donor (blue, iodo-ester) and halogen bond acceptor (yellow, nitropropane salt) and stoichiometric mixture (black); Electronic map of simplified halogen bond donor (middle); Interaction between the halogen bond donor/acceptor (right, DFT calculation).

Reduction of the iodo-ibuprofen derivative show an irreversible wave obtained at -0.5 V (Figure 7, left) confirming the short lifetime and lack of stability of this anionic radical intermediates as reported during Srn1 process. The presence of radical species for each media and therefore support of the Srn1 based mechanism (solution and solid-state) was done by electron paramagnetic resonance (EPR).

EPR experiments conducted after performing for a shorter amount of time the ball milling experiment at room temperature enabled us to observe some radical species. As EPR depends on molecular motion, the resulting spectrum from the oily crude medium was in contrast with the well-defined EPR spectrum obtained at isotropic limit from investigation in solution experiments. (figure 7, middle) Analysis of the ball milling slow-motion EPR spectrum (Figure 7, right) allowed us to determine the presence of nitroxide radical generated from the SET of 2-nitropropane salt. With radicals observed in both media and previous report on the ability of these nucleophiles to performe SET. We then conducted some complementary analysis to see if a solid-state halogen bonding was involved in this reaction. Allowing to observe more similarity between both media to get better insight of the reaction mechanism. Solid state halogen bonding was investigated by performing ATR-FTIR spectroscopy:

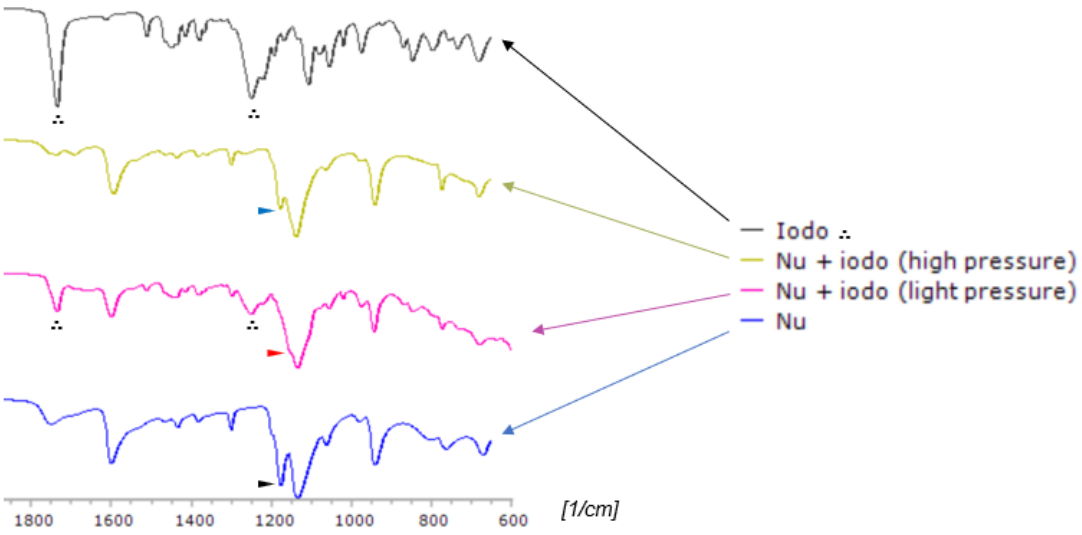

Figure 8. ATR-FTIR of the iodo ester (black, top); potassium 2-nitropropane salt (bottom, blue); and stoichiometric analysis at light (pink) and high (yellow) pressure.

Firstly, analysis of potassium 2-nitropropane salt (XB acceptor, figure 8, bottom) shows the expected stabilisation of the anion on the oxygen of the nitro with a characteristic [ν(C=N)] at 1593 cm^{-1} and two asymmetric stretching band [$\nu_{as}(NO_2)$] at 1176 & 1133 cm^{-1}.[19] By preparing a stoichiometric mixture of donor-acceptor and performing the analysis in ATR-FTIR (figure 8, pink and yellow, middle) we managed to observe a clear shift and a strong decrease of the signal intensity variation at 1176 cm^{-1} that is expected as result of an interaction between O···I.

To conclude, the observation of halogen bonding and radical species in solution and solid-state led us to suggest a similar mechanism for the reaction in each media. In the proposed mechanism, the cation exchange is mandatory in both media as show in control experiment. In solution to solubilise the nucleophile and in solid-state, the cation metathesis could permit to modify the structure and is directly responsible of the reactivity of the species. (The reported [TBA][$C_3H_6NO_2$] is a dimeric structure as depicted in figure 9) Attempt for the obtention of [BG][$C_3H_6NO_2$] or [BG][$C_3H_6NO_2$]•[I-R] were unsuccessful.

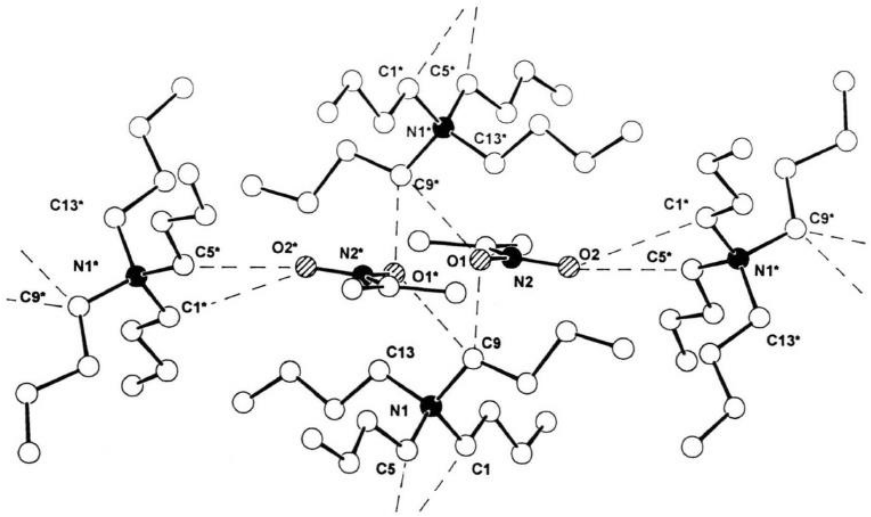

Figure 9. Cristal structure of [TBA][$C_3H_6NO_2$].[20]

In the proposed mechanism, the XB permits to place both substrate inside the chiral pocket as suggested by the *ee* observation. (Note, BX also report some high *d.r.* induction when using non-symmetrical nitro-anion) The interaction of both substrates and the induced radical event observed in each media was triggered via light irradiation or external force. The proposed mechanism involved a non-chain radical process in contrast with the classical Srn1 reaction because of the low concentration of nucleophile able to react respectively due to the low amount of PTC in each media.

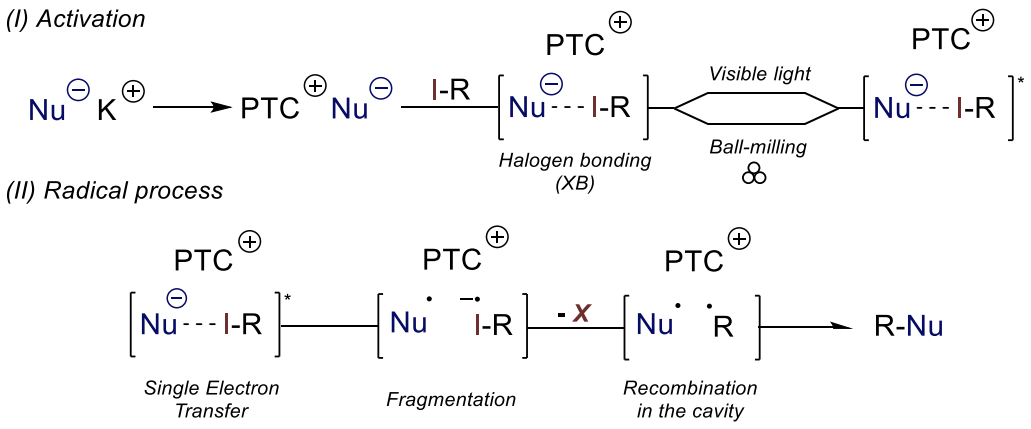

Scheme 12. Proposed mechanism.

Complementary information

3.3 Mechanistic investigation in solution

3.3.1 Control experiment

We firstly controlled several parameters to delimit this system and dismiss the Sn2X reactivity in solution (scheme 13) Indeed, the Sn2X reacts without light irradiation and this main difference was highlighted by an on/off experiment showing the mandatory activation of the reaction by light in solution to perform the reaction (entry 1 and 3). The observation of the desired product takes place under blue LED irradiation.

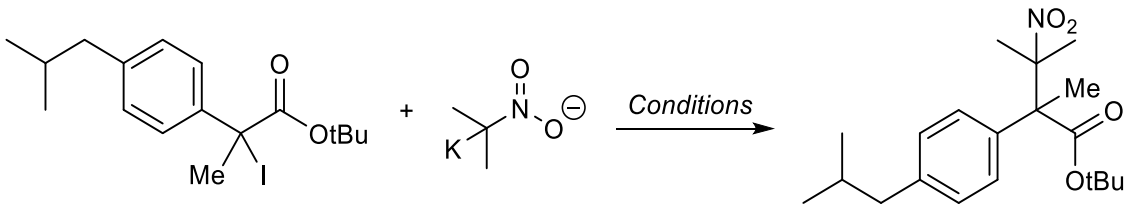

Entry	Conditions	result
1	PTC (BG or TBAB), Toluene, Blue light	✓
2	PTC (BG or TBAB), Toluene, Blue light, O_2	✓
3	PTC (BG or TBAB), Toluene, ~~Blue light~~	X
~~4~~	~~PTC (BG or TBAB),~~ Toluene, Blue light	X

Scheme 13. Control experiment for solution and mechanochemical experiment.

The Srn1 mechanism appears as a plausible initial proposition based on the experimental design and the observed results for this control experiment. Indeed, no difference are observed between inert (argon, setup in a glovebox) conditions and open air one, the reaction proceeds the same way and afford similar result.

Due to the necessity of light two main pathways appear reasonable. The first one, based on Srn1 reactivity with single electron transfer and the second one, with energy transfer (EnT). The second possibility was dismissed due to the presence of oxygen able to be activated (quenching of the activated pair) to generate some triplet state oxygen $^3O_2$.

3.3.2 UV-visible

The absorption spectra of several samples and combinations were recorded in DMSO on an Infinite 200 PRO apparatus. The total volume was fixed to 200 µL and the analysis was performed using a 96-Well plate.

We firstly started our mechanistic investigation by looking for an interaction between our nucleophile (e.g. potassium 2-nitropropane salt) and electrophile (e.g. iodo-ester). Due to the very low solubility of the salt in organic solvent and to approach the experimental conditions, we firstly investigated the preparation of ammonium salt derivative such as tetrabutylammonium, but these attempts remained unsuccessful.

We then decided to perform these experiments in DMSO, this solvent being the only one able to full dissolve the potassium salt. With this solubility issue resolved, we prepared several stock solutions and started recording. (Figure 10)

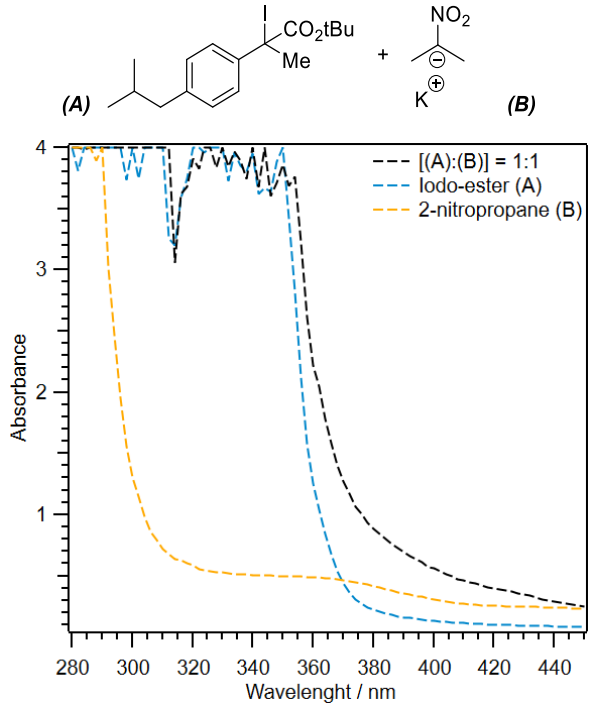

Figure 10. Absorption spectra of a stoichiometric mixture in DMSO of potassium 2-nitropropane (yellow), iodo-ester (blue) and a stoichiometric mixture (iodo-ester:2-nitropropane salt) at 50 µM (black).

As expected, the nucleophile displays a poor ability to absorb the blue light as for the iodo-ester. To our delight, the preparation of a stoichiometric mixture led to a significative shift. To ensure that this result was not an artifact, we then performed again this absorbance at different concentration (figure 11)

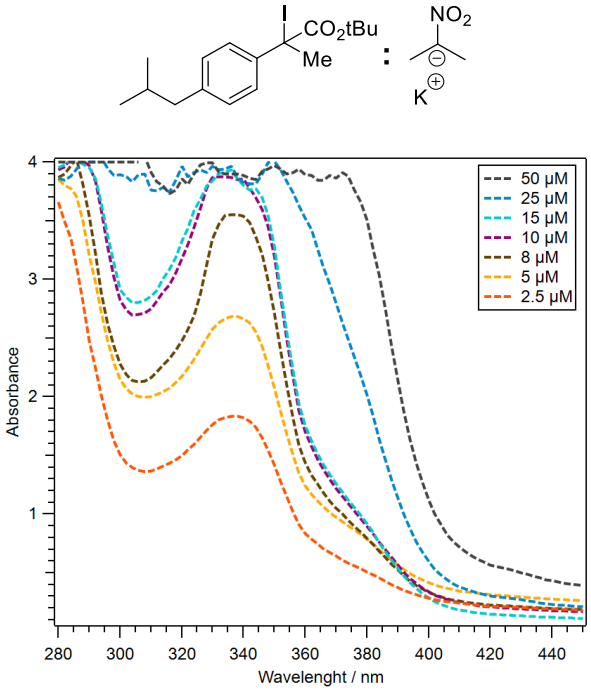

Figure 11. Stacked absorption spectra of a stoichiometric mixture (iodo-ester:2-nitropropane salt) in DMSO at different concentration.

Different concentrations of the stoichiometric mixture (from 2.5 µM to 50 µM) were prepared and the absorbance spectra recorded. From very low concentration (2.5 µM) to 5 until 15 µM, the formation of a new peak was observed at 380 nm and could correspond to an excimer. By increasing the concentration to 25 and 50 µM, the previous result was confirmed with the observation of this main shift.

Based on these observations, it appears reasonable to propose an interaction between the salt and the activated iodo-ester. Based on the observed new shift, this pair could be able to be excited by light. The nature of this interaction of the possible activated species induced by light has been respectively studied hereafter.

3.3.3 DFT calculations

The observation of a shift in UV-Vis at low concentration (figure 11) confirmed the interaction between both reactant and the presence of C-I bond let us envisage the formation of a halogen bond that was supported by density functional theory (DFT) calculation as shown just after. We investigated several "simplified" model substrate with iodine and bromine as activated halogen and ester or phosphor-ester (table 1). With the optimisation performed, we start to look at the charge distributions of these derivatives.

If the sigma hole and the resulting reactivity is a known principle for sp and sp2 halogen, the tertiary compound's sigma holes are far less described from the theoretical and experimental point of view. To confirm its presence in this system, the ESP mapping was performed (figure 12-15, right). Then the ALIE map was performed as depicted in figures 12-15, left. To better understand the result from an ALIE map and according to the WFA-SAS team developer: « *The average local ionization energy is the energy necessary to remove an electron from the point r in the space of a system. Its lowest values reveal the locations of the least tightly-held electrons, and thus the favoured sites for reaction with electrophiles or radicals.* » | WFA-SAS : software used for the generation of ESP and ALIE map after optimisation using orca 4.1 of the desired compound.

Here, the blue sphere (corresponding to the iodide) represents well the ability of halogen to interact with electrophile (with an average angle know between 90 and 120°). Interestingly, the middle of the iodine (green spot) is therefore less able to interact with an electrophile and is situated in the sigma hole area of this tertiary iodine (angle of 180°). We also decided to perform these theoretical investigation using phosphonate derivative. The next figures display the average local ionization energy (ALIE) $\bar{I}(r)$ on 0.001 a.u. electron density isosurface (*left*) and ESP map (*right*) of several electron acceptor.

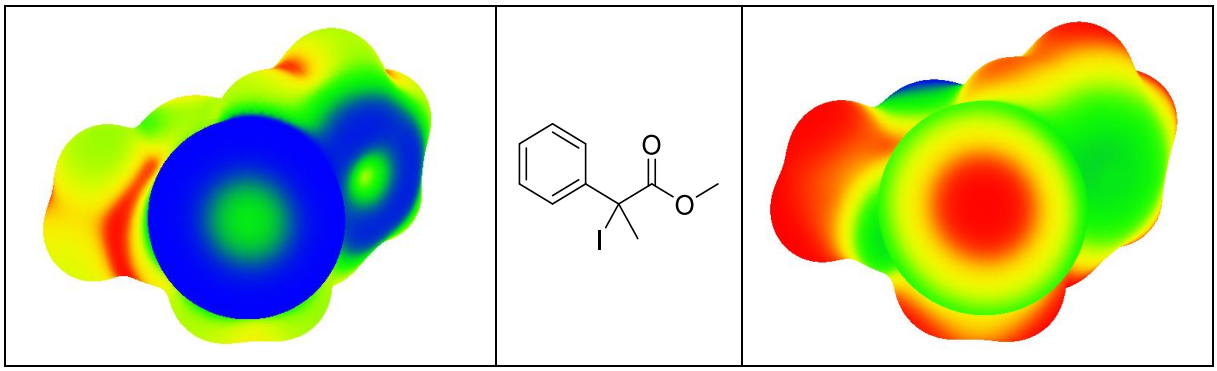

Figure 12. Alie (left) and ESP (right) map of model iodo-ester

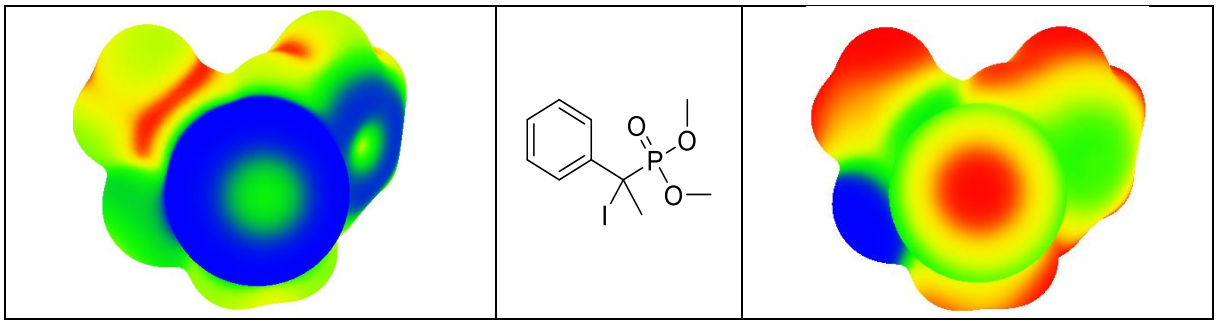

Figure 13. Alie (left) and ESP (right) map of model iodo-phosphonate

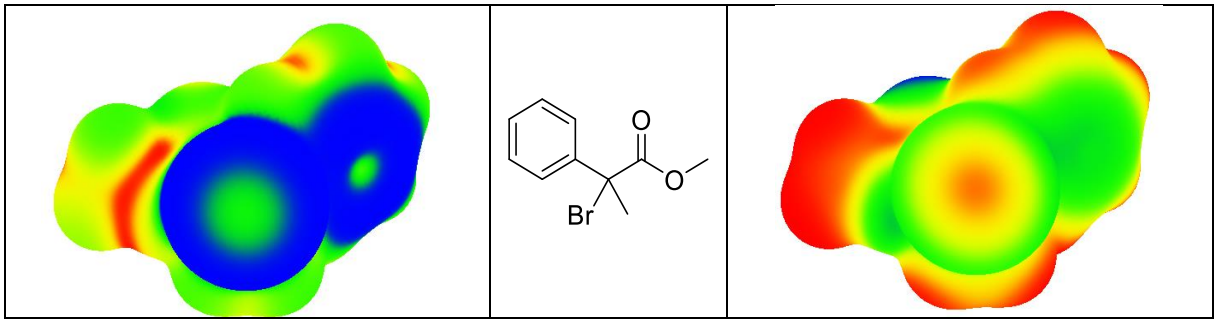

Figure 14. Alie (left) and ESP (right) map of model bromo-ester

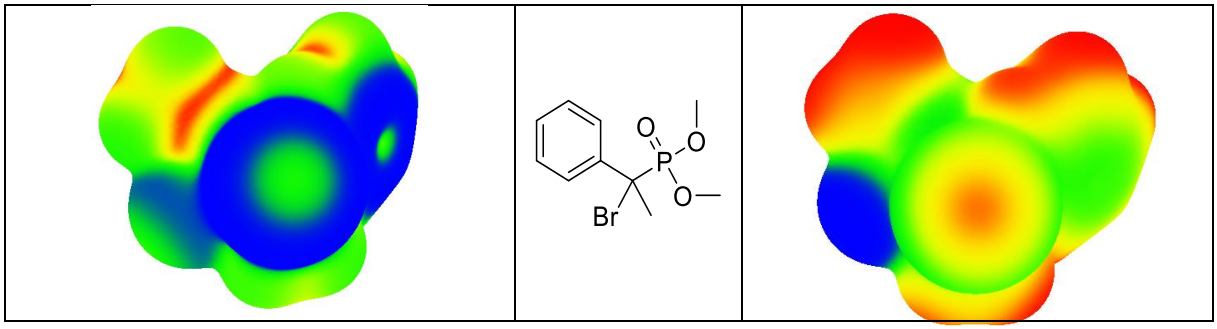

Figure 15. Alie (left) and ESP (right) map of model bromo-phosphonate

First, mapping of the halogen bond acceptor confirmed the presence of the σ-hole and the ability of this position to react with radical and nucleophile. (figure 12-15)

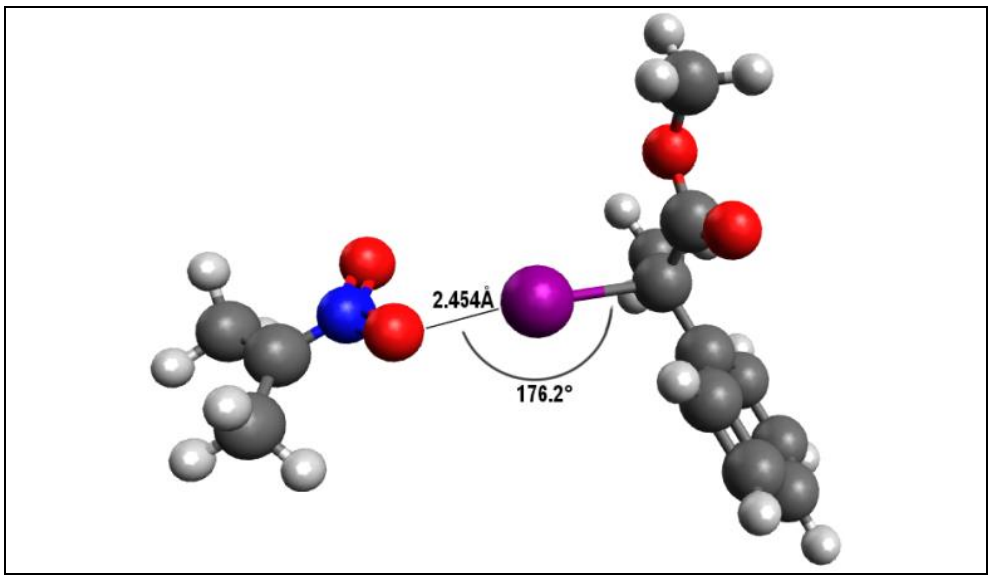

Figure 16. Optimized geometry between 2-nitropropane anion and iodo-ester

As expected, the nucleophile (2-nitropropane) interacts with both tertiary iodo- ester (figure 16), and phosphonate (figure 17). Concerning the ester, the distance and angle are in the range of a strong halogen bond. For the phosphonate, in addition the XB a second interaction (hydrogen bonding) is observed. This follows the observation of Reetz (X-Ray figure 9) with a hydrogen bond in solid state between the anion and TBA cation. Secondly, intermolecular halogen bond with a calculated O···I distance of 2.454 Å and an angle of 176.2° that is in the range for strong halogen bond was obtained with an expected slight elongation of the C-I bond. (figure 17)

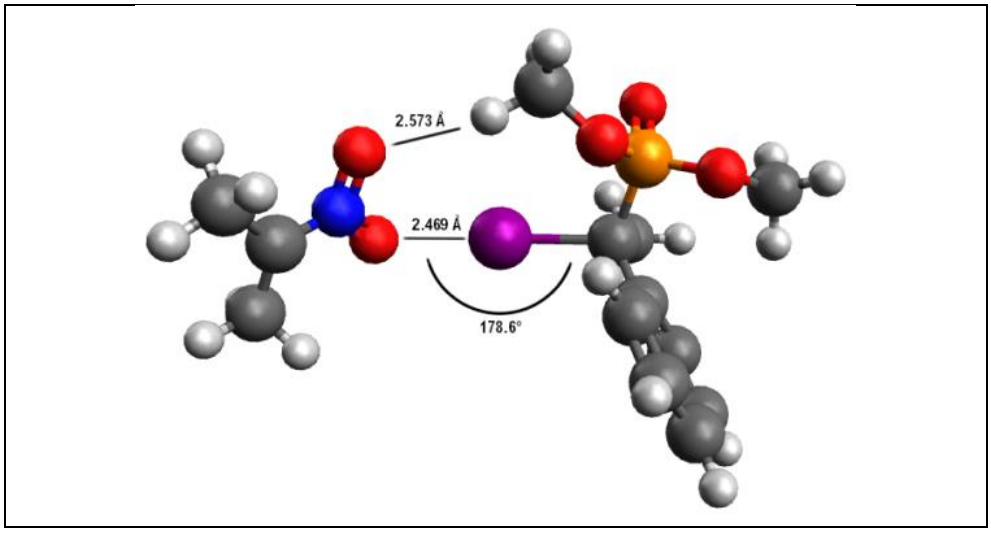

Figure 17. Optimized geometry between 2-nitropropane anion and iodo-phosphonate

3.3.4 Solution NMR experiments

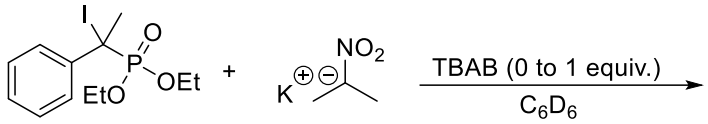

Scheme 14. Attempted titration of iodo-phosphonate by nitropropane anion.

The NMR titration was carried out using a J. Young NMR tube in 0.5 mL of deuterated benzene. The preparation was conducted in a glovebox filled with argon and the nmr tube was protected from light using an aluminium foil. The ^{1}H NMR and ^{31}P NMR and 13C of pure phosphonate (50 mM) was recorded. Potassium 2-nitropropane anion (1 equiv.) was added inside the glovebox and NMR spectrum recorded. After addition of the nucleophile, TBAB was added in 4 portions of respectively (4 * 0.25 equiv.) and each spectrum was recorded after each addition of the PTC. No shift was observed after addition of the nucleophile due to his poor solubility; adding a phase transfer catalyst, TBAB, also lead to the result due to the same solubility parameter.

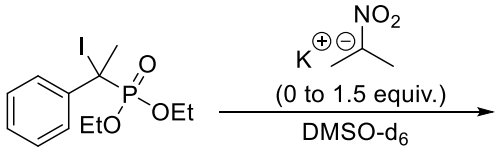

Scheme 15. Titration of iodo-phosphonate in DMSO-d_6

The titration (scheme 15) was carried out using normal NMR tubes with deuterated DMSO, the preparation was conducted in a glovebox filled with argon and all the NMR tubes were protected from light using an aluminium foil. A stock solution of iodo-phosphonate (0.1 mmol in 160 µL DMSO-d6) and potassium 2-nitropropane (0.X mmol in 0.5 ml of DMSO-d6) were prepared. The final volume of the NMR tube was fixed at 0.4 mL with a concentration of iodo-phosphonate set at 40 mM.

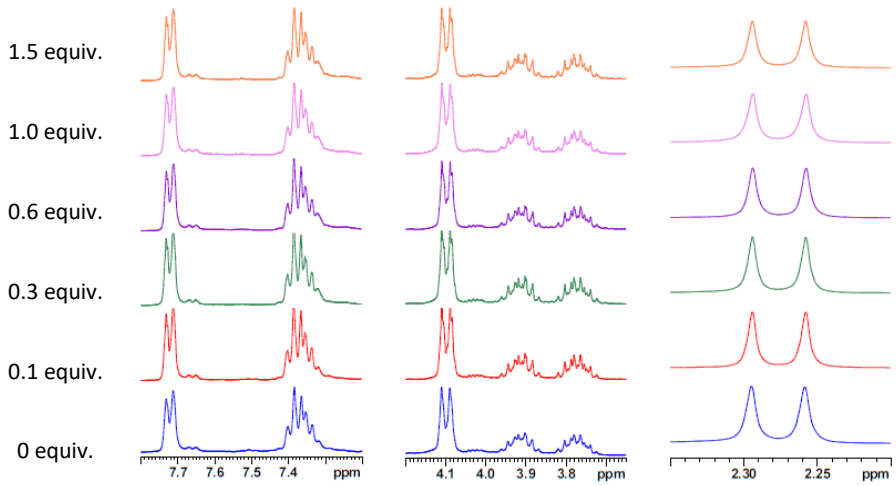

Figure 18. Stacked relevant region of ^{1}H NMR spectra in DMSO-d6 of phosphonate with different equivalent of 2-nitropropane anion.

No shift was observed when the concentration of nucleophile increased. (figure 18) This observation "*follows*" the experimental one, in which the phosphonate being less activated compared to the iodo-ester. In addition, the use of DMSO-d6 is not favourable for the observation of the interaction due to his ability to perform an XB, this could lead to a possible competition (solvent vs Nu). Finally, according to the DFT study and X-ray report by Reetz, hydrogen bonding is possible with this salt and a second competition between H-bonding and XB could occur.

Due to the poor solubility of the nitropropane anion, the titration has been performed in deuterated DMSO and the concentration was fixed at 40 mM with a total volume of 400µL.

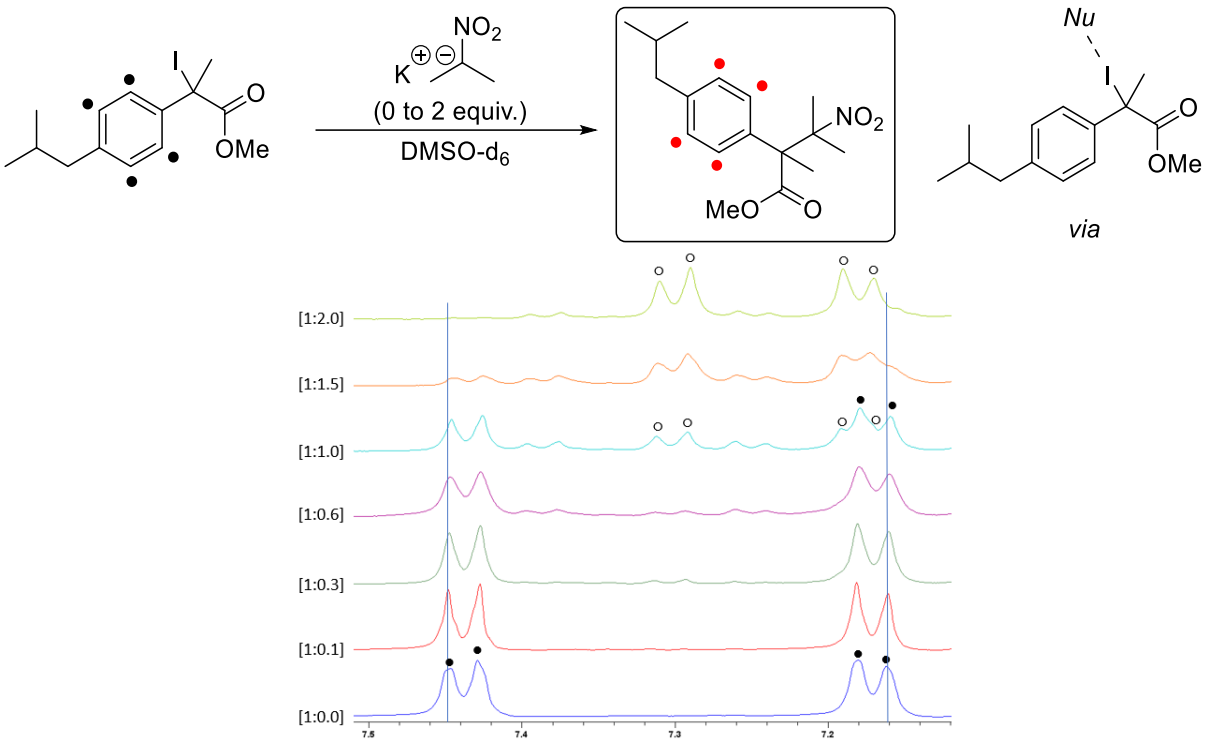

Figure 19. 1H NMR spectra in DMSO-d6 at 40mM [I] with different concentration of nucleophile of relevant region; (●) correspond to the starting material, (○) correspond to the unexpected resulting product.

Unfortunately, during the titration (figure 19) the reaction proceeded even without irradiation (setup in glovebox in the dark and cover with aluminium foil; few light exposures during before the acquisition of the spectrum) which is in contrast with the results obtained in non-polar solvent (on/off experiment in non-polar solvent). Nevertheless, a small shift of the starting material can be observed when increasing the concentration of the nucleophile. Due to the modification of the concentration of the iodo-ester during the NMR titration, the association constant couldn't be determined (Ka) and this observation must be handle carefully to avoid hasty conclusion.

To support the previous DFT calculation on the feasibility of XB with this substrate and with the lack of clear evidence in the previous solution experiment, the titration of the iodo-ester with deuterated pyridine in deuterated benzene was performed. (figure 20) The NMR titration was carried out using a J. Young NMR tube in 0.4 mL of deuterated benzene, the preparation was conducted in a glovebox filled with argon and the NMR tube was protected from light using aluminium foil. The NMR of pure iodo-ester (39 mM in 400µL C_6D_6) was recorded and successive addition of pyridine-d5 (from 0 to 4 equiv.) was done prior to acquisition of the desired NMR spectra.

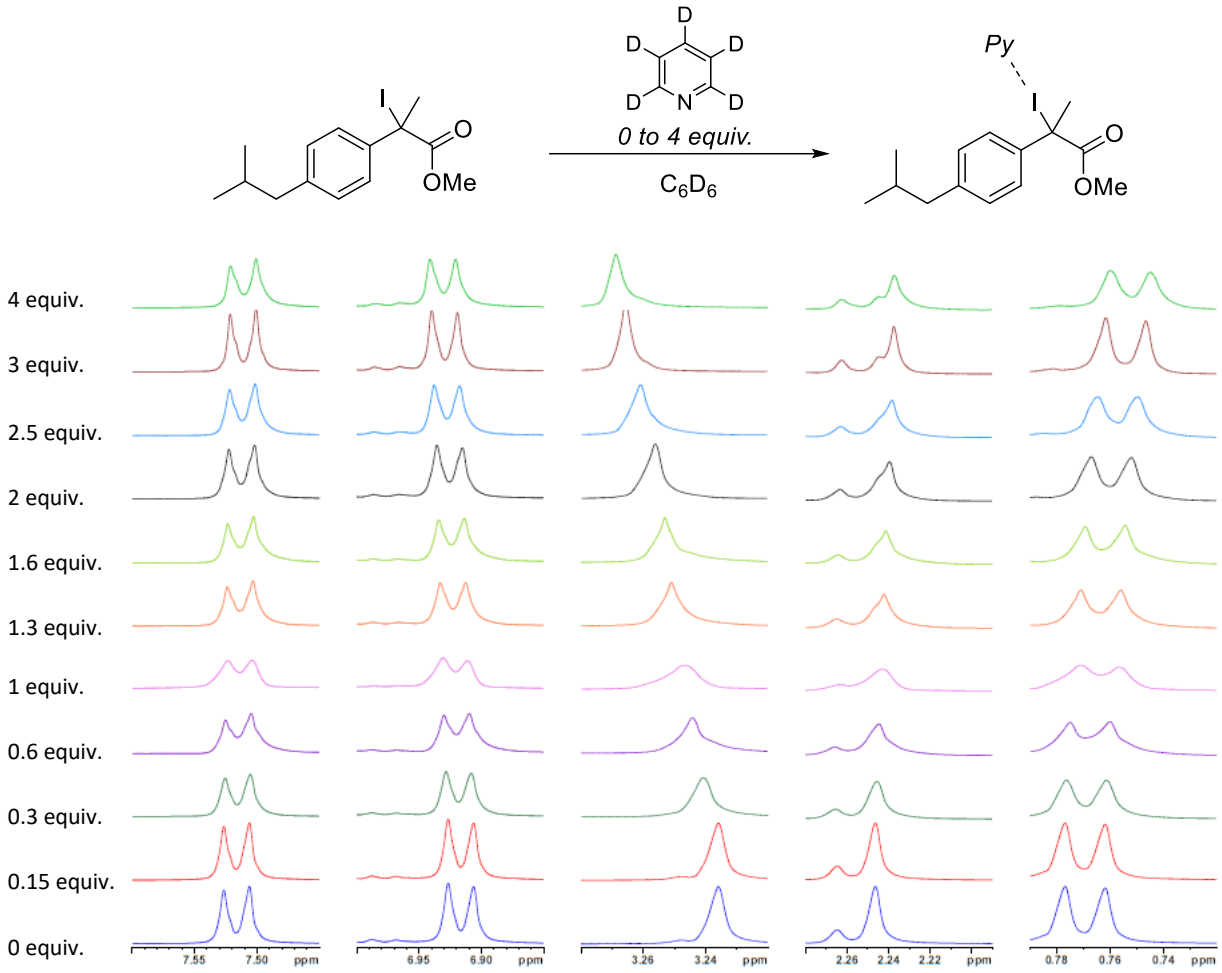

Figure 20. ^1H NMR spectra in C_6D_6 of relevant regions upon addition of deuterated pyridine fixed iodo-ester concentration at 39mM.

The introduction of pyridine led to notable shifts of the iodo-ester. The weak shift of aromatic ones and strong ones in the aliphatic area seems to confirm the expected XB formation better than a possible stacking. Using the freely accessible site *supramolecular.org* the association constant was determined as $K_a = 4878\ M^{-1}$ (± 4%).

Based on the good affinity of pyridine with our halogen bonding acceptor, NMR titration was conducted with the pyridinethione salt. (figure 21) Each solution was prepared in a glovebox under argon atmosphere in the dark and the NMR tube were protected from the light using aluminium foil.

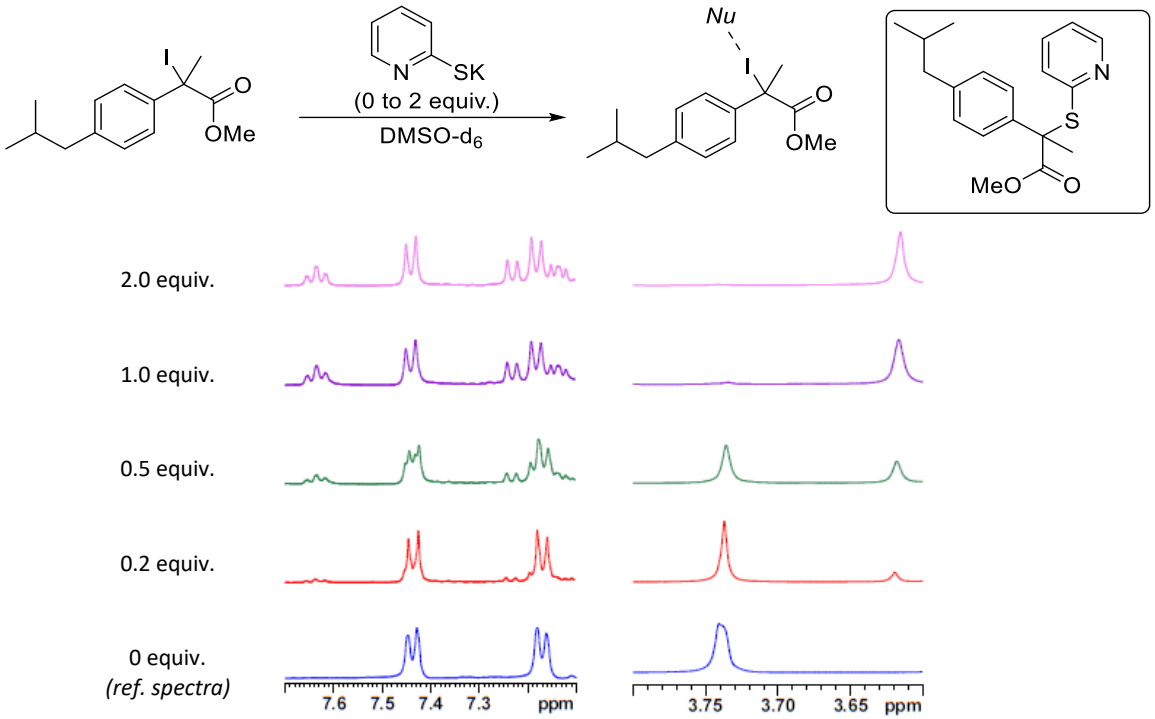

Figure 21. ^{1}H NMR spectra in DMSO-d_6 of relevant regions upon addition of deuterated pyridine fixed iodo-ester concentration at 39mM.

As for the previous system with 2-nitropropane as halogen bond donor, the reaction proceeds immediately and the desired XB was not observed. The last attempt, done to reduce the possible reaction rate, was done following the same conditions at a lower concentration. The titration was then conduct at 4 mM but afford the same observation (figure 22).

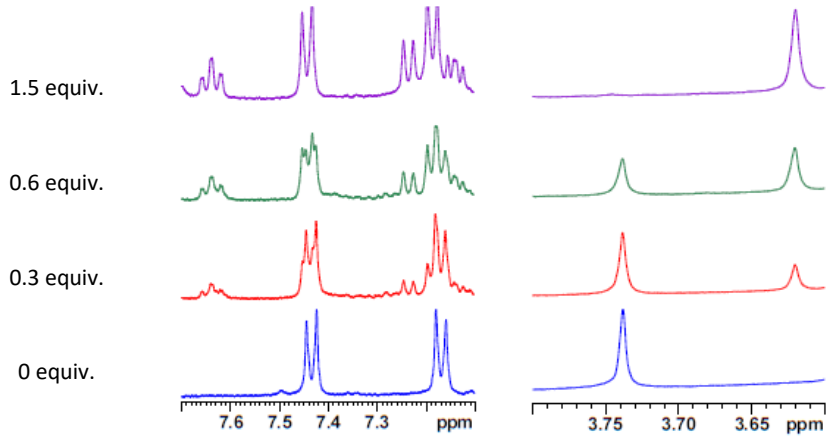

Figure 22. ^{1}H NMR spectra in DMSO-d_6 of relevant regions upon addition of deuterated pyridine fixed iodo-ester concentration at 4mM.

3.3.5 Solution EPR experiment

EPR spectrum were recorded at room temperature under irradiation using Blue LED, the experimental procedure was slightly modified to avoid the poor diffusion in the EPR tube and to facilitate the observation of radical. TBAB was use in 40 mol % instead of 20 and the concentration used was 0.1M instead of 0.05M. The tube was vigorously shaken under light irradiation before recording the spectrum under blue light irradiation. All analysis were performed at room temperature and all simulations were performed on a laptop computer running EasySpin 5.2 and Matlab 9.1 (The Mathworks Inc., Natick, MA).

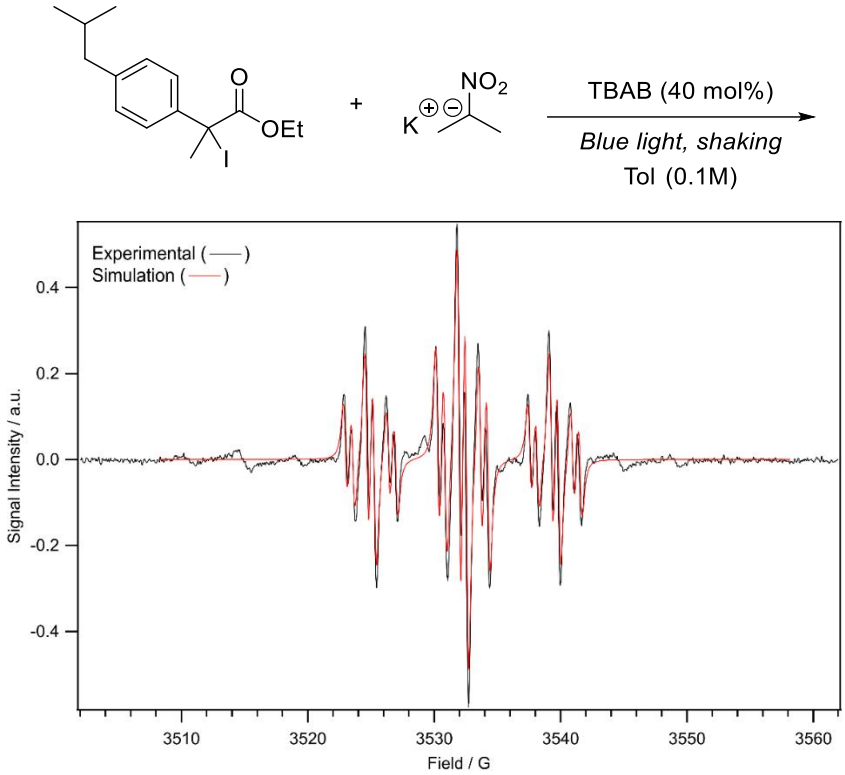

Figure 23. Solution EPR experiments.

In figure 23, the slightly modified experimental conditions using the iodo-ester led to the observation of an organic radical with clear hyperfine coupling. The simulation of the desired spectra was achieved by investigation of a delocalised radical inside the aromatic part. To investigate the source of radical (from the anion or iodo) the same reaction was performed using the naphthyl derivative in figure 24 and another radical species was observed after agitation under light. Compared to the previous iodo-ester, the generation of the radical was more complicated, but we successfully simulated the radical species. A large hyperfine coupling was observed for this radical, this hyperfine suggests a radical essentially located to one site of the molecule and interaction strongly with two different protons, this could correspond to a radical delocalized inside the naphthalene moiety.

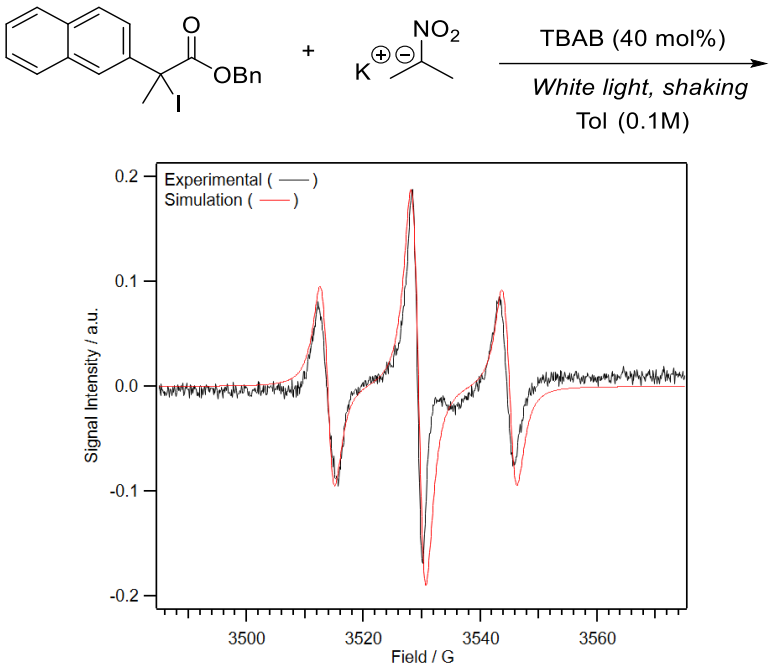

Figure 24. EPR experiment of naphthyl derrivative.

Observation of radical species agrees with previous report on Srn1 radical pathway mechanism. Using the same conditions with another XB donor led to the observation of two different radical species, this suggests that the observed radical results from the XB donor. Few hyperfine couplings were also observed when the poorly reactive iodo-phosphonate was engaged under the same experimental conditions. A suitable resolution of this spectrum is yet unsuccessful but confirms the presence of radicals also for these substrates. The generation of radical using the phosphonate under irradiation with the same condition takes place at a much lower rate, this follow the experimental observation in which this compound is less reactive and the lack of NMR shift observed in figure 18.

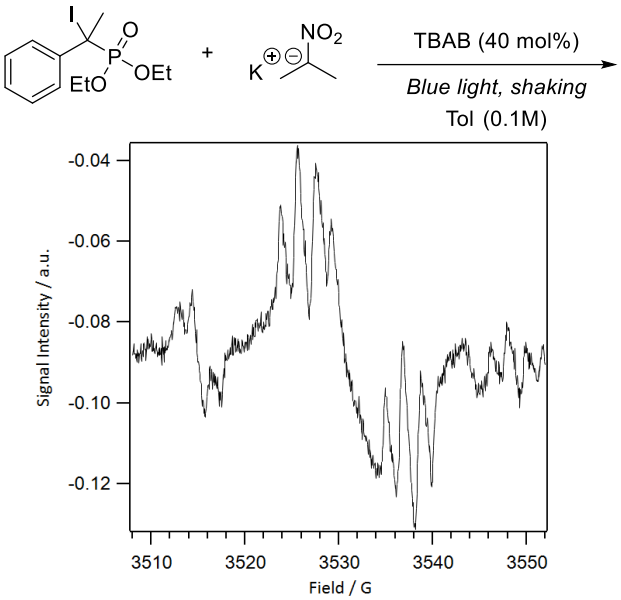

Figure 25. EPR experiment of iodo-phosphonate.

3.4 Mechanistic investigation in solid-state

3.4.1 Control experiment

In the case of the ball-milling (scheme 16) it appears that the reaction did not proceed without the use of phase transfer catalyst showing a non-interface reactivity between the nucleophile and electrophile. Last orientation toward a Srn1 based mechanism and by consequent SET instead of energy transfer event (EnT) was done by observation of the non-influence of oxygen for this experiment in both cases.

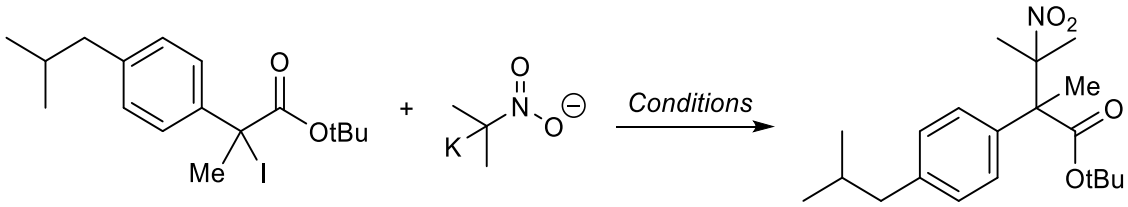

	Conditions	result
Solid-state	PTC (BG or TBAB), O_2	✓
	PTC (BG or TBAB), ~~O_2~~	✓
	~~PTC (BG or TBAB),~~ O_2	X
	~~PTC (BG or TBAB),~~ ~~O_2~~	X

Scheme 16. Control experiment for solution and mechanochemical experiment.

3.4.2 ssEPR experiment

EPR spectrum were recorded at room temperature after launching the ball milling experiment. The experimental procedure was slightly modified to increase the generation of the radical species to facilitate the observation of radical in which TBAB was use in 40 mol % instead of 20 with two equivalents of 2-nitropropane potassium salt and the reaction time was reduced to 30s compared to 20 min at room temperature. As for the solution EPR experiment, the spectrum was recorded at room temperature.

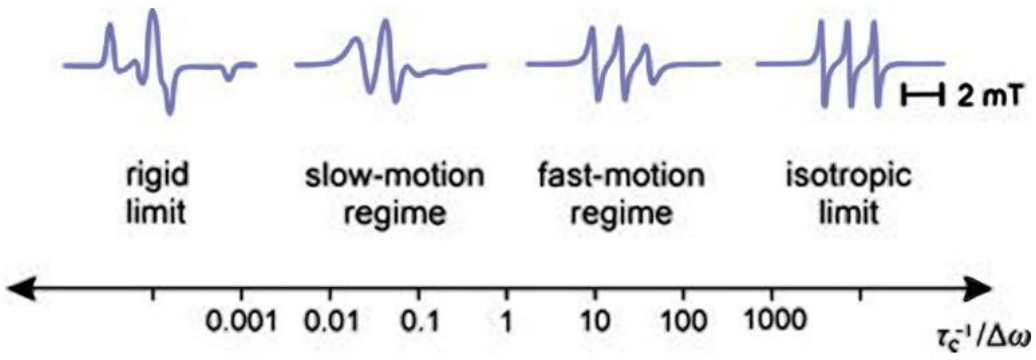

Figure 26. Motion effect on resolution of EPR signal

The main difference between the two media can be found in the shape of the hyperfine when radicals are observed. (figure 26) Indeed in solution, the motion of the radical is called at *isotropic limit* and corresponds to well define hyperfine. This is in contrast with frozen or crystal EPR analysis (*rigid limit*), one of the parameter responsible of this is the correlation time (in s). An interesting area, oscillating between the isotropic and rigid limit is called the fast and slow-motion regime. Depending of the motion on the radical species, influence by the medium and temperature, a EPR spectrum could tend from one to the other or being a mixture of both. (figure 27)

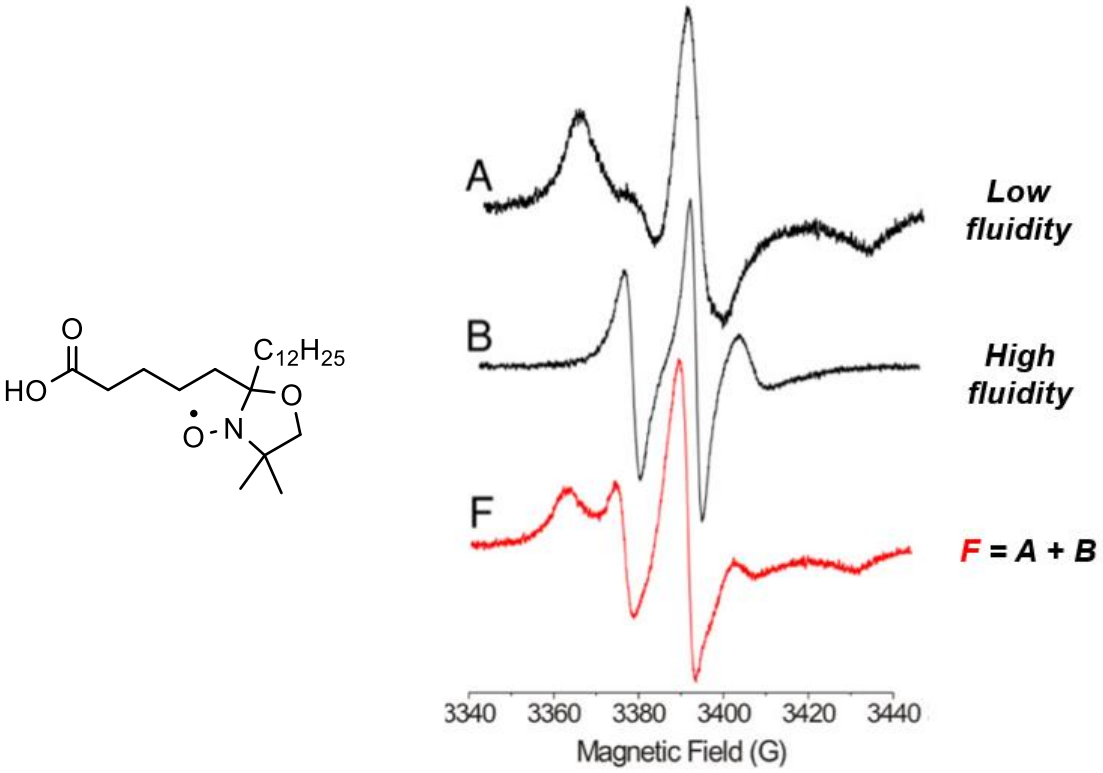

Figure 27. Reported EPR signal of 5-DSA (left) based on the viscosity of the solvent (right)

In this example, the influence of the solvent's viscosity on the radical species was observed. This study was made in order to observe the diffusion of a nitroxide radical. (figure 27 left) The EPR signal of 5-DSA was recorded in a low fluidity and a high fluidity oil. In the low one, the signal can be considered as a slow-motion regime when the high fluidity medium as a fast-motion one. Finally, the diffusion of the radical between two medium led to a mixture of both motion type radical, deconvolution gave the % of the radical in each media.

We then investigated our reaction by ssEPR, the first attempt was done with the thiopyridone salt but was unsuccessful. The second attempt was done using the 2-nitropropane anion. (figure 28)

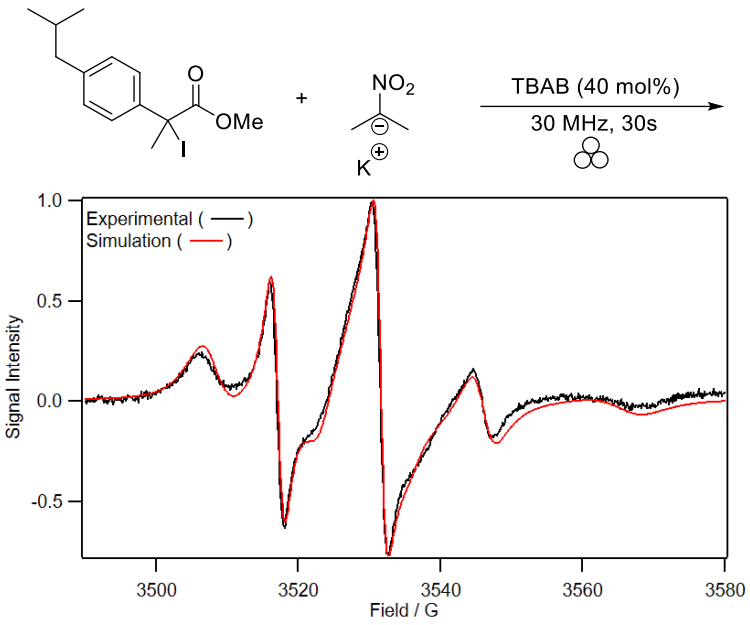

Figure 28. Normalised EPR spectra of nitroxide obtain from the resulting oil after ball milling experiment

The nature of the crude (oil) is observed via the low resolution hyperfine compared to the expected one for a powder/crystal or the well resolved one at isotropic limit. More precisely, due to nature in this crude medium, the spectrum obtained correspond to the slow motion EPR of radical derivative constrained in space/with different motion. Attempts to fit only one radical species were unsuccessful and suggest a multicomponent spectrum. The generation of the resulting spectrum has been made using EasySpin (MATLAB) and SimLabel for the final tuning. The strong signal was fitted, and the resulting spectrum appears to be composed of two nitroxides species which is coherent with the expected mechanism.

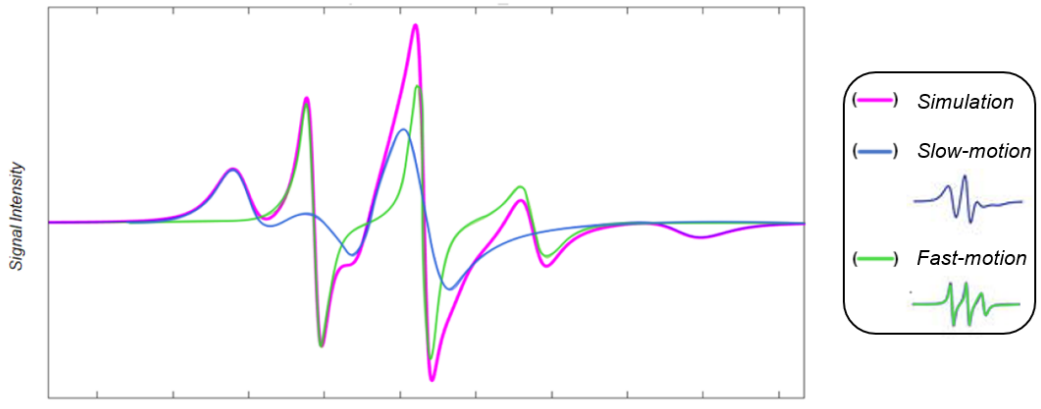

Figure 29. Deconvolution of the EPR spectrum

4 The parameter for the radical combination is g(2.00492 2.00739 2.00044), A(4.9 5.7 34.4) with a correlation time of 1.31 e-08 s and a spin concentration of 79% and g(2.00325 2.00918 2.00076), A(3.8 0.6 39.2) with a correlation time of 5.59 e-10 s for a spin concentration of 21%.

4.1.1 ATR-FTIR

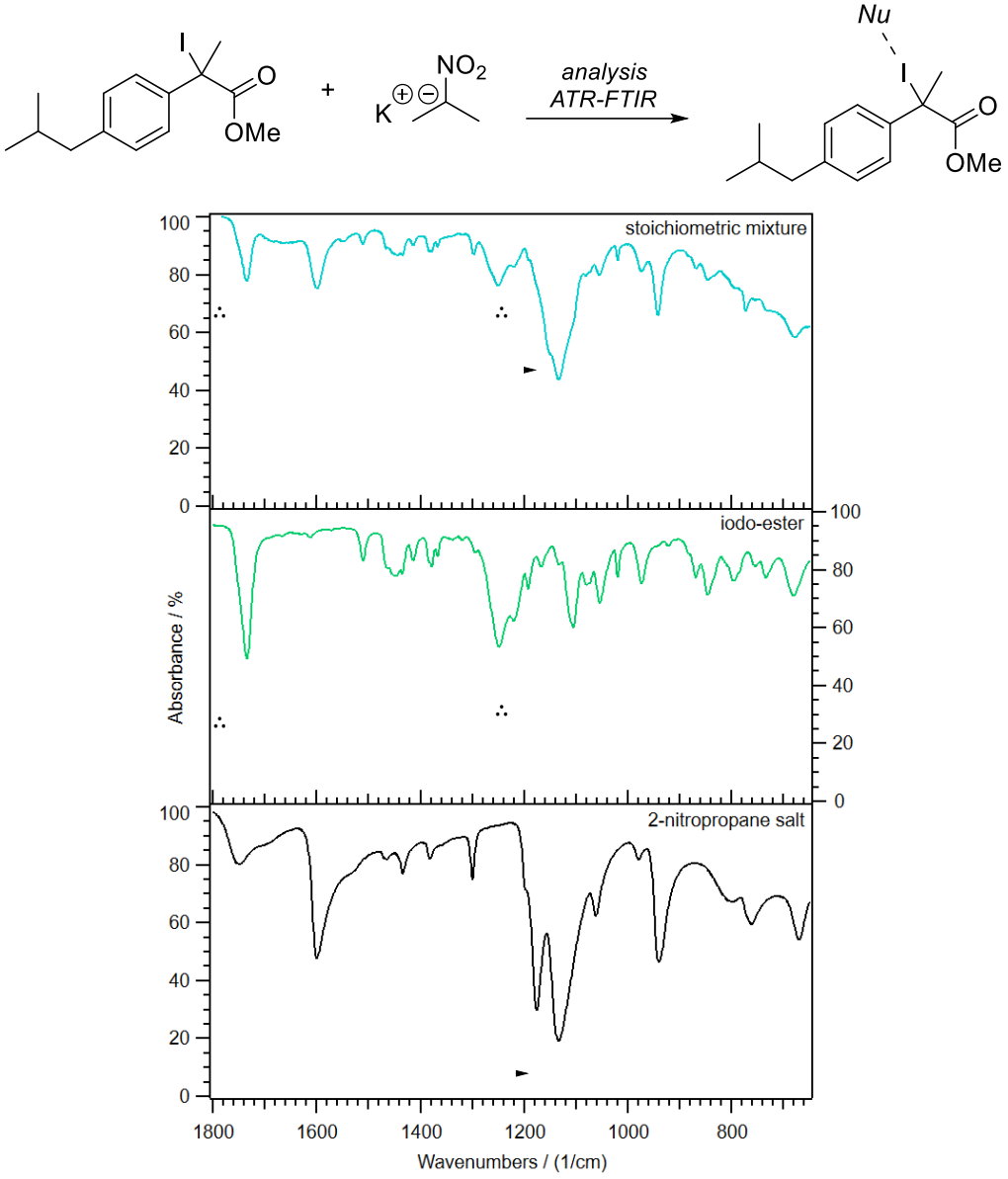

Figure 30. Selected region of ATR-FTIR spectra of potassium 2-nitropropane salt (bottom, black), iodo-ester (middle, green), stoichiometric amount of salt and iodo-ester (top, blue). ∴ : correspond to major signal of iodo-ester. ► : major modification observed.

Comparison with the reported values of potassium 2-nitropropane anion (KBr, *major*: 1605; 1154; 1135; 945 cm^{-1}) with the one obtained with ATR-FTIR show a small shift and band distortion (often observed between these two techniques). Based on the report from Kaizer, analysis of the IR spectra shows a band at 1593 [ν(C=N)] (*note: the value is close to the classical imine C=N signal confirming in solid-state that the potassium salt, as the TBA one reported before by Reetz)* ; 1176 & 1133 [ν_{as}(NO2)] and 939 [ν_{s}(NO2)]. Strong signal intensity decreases and shift for the asymmetric NO_2 at 1176 is observed (blue spectrum).

4.2 Conclusion

In summary, we focused on the mechanistic study of asymmetrical control of radicals by coupling DFT calculations and spectroscopy methods. Following the developed methodology by Dr. Ban Xu, the study was performed in solution and solid-state.

We delimited our investigation toward single electron transfer event as suggested by some control experiments. In addition to this radical event, halogen-bonding was proposed based on the analysis performed in solution (UV-Vis) and solid-state (ATR-FTIR) and supported by DFT calculation. The radical species were then confirmed for each media as observed with EPR. The resulting signals were fitted in solution by proposing an observed radical in the aromatic system and a nitroxide one in solid-state. Finally, the radical-radical recombination pathway was proposed to proceed inside the chiral PTC cavity as suggested by the *ee* observed.

Here, the first mechanistic proposal implying a direct comparison between the solution and solid experiment was made. Based on the collected data, we proposed a similar pathway for each media and this result in the first Srn1 asymmetric radical reaction in solution, and the first asymmetric radical one in solid-state.

References Chapter 3

[1] https://scifinder-n.cas.org/
[2] R. S. J. Proctor, A. C. Colgan, R. J. Phipps, Exploiting attractive non-covalent interactions for the enantioselective catalysis of reactions involving radical intermediates. *Nat. Chem.* **12**, 990–1004 (2020). b) S. Mondal, F. Dumur, D. Gigmes, M. P. Sibi, M. P. Bertrand, M. Nechab, *Chem. Rev.* **2022**, *122*, 5842–5976.
[3] S. Mondal, F. Dumur, D. Gigmes, M. P. Sibi, M. P. Bertrand, M. Nechab, Enantioselective Radical Reactions Using Chiral Catalysts. *Chem. Rev.* (**2022**), doi:10.1021/acs.chemrev.1c00582.
[4] T. E. Schirmer, B. König, *J. Am. Chem. Soc.* **2022**, *144*, 19207–19218.
[5] https://tanchoonhong.wixsite.com/tchlab
[6] Ł. Woźniak, J. J. Murphy, P. Melchiorre, *J. Am. Chem. Soc.* **2015**, *137*, 5678–5681.
[7] Internal data
[8] R. S. J. Proctor, A. C. Colgan, R. J. Phipps, Exploiting attractive non-covalent interactions for the enantioselective catalysis of reactions involving radical intermediates. *Nat. Chem.* **12**, 990–1004 (2020).
[9] S. Mondal, F. Dumur, D. Gigmes, M. P. Sibi, M. P. Bertrand, M. Nechab, Enantioselective Radical Reactions Using Chiral Catalysts. *Chem. Rev.* (2022), doi:10.1021/acs.chemrev.1c00582.
[10] X. Zhang, J. Ren, S. M. Tan, D. Tan, R. Lee, C.-H. Tan, An enantioconvergent halogenophilic nucleophilic substitution (SN2X) reaction. *Science* (2019), doi:10.1126/science.aau7797.
[11] T. Constantin, M. Zanini, A. Regni, N. S. Sheikh, F. Juliá, D. Leonori, Aminoalkyl radicals as halogen-atom transfer agents for activation of alkyl and aryl halides. *Science* (2020), doi:10.1126/science.aba2419.
[12] G. C. Fu, Transition-Metal Catalysis of Nucleophilic Substitution Reactions: A Radical Alternative to SN1 and SN2 Processes. *ACS Cent. Sci.* **3**, 692–700 (2017).
[13] L. Zong, C. Wang, A. M. P. Moeljadi, X. Ye, R. Ganguly, Y. Li, H. Hirao, C.-H. Tan, Bisguanidinium dinuclear oxodiperoxomolybdosulfate ion pair-catalyzed enantioselective sulfoxidation. *Nat Commun*. **7**, 13455 (2016).
[14] R. Wang, J. Rebek, Y. Yu, Organic radical reactions confined to containers in supramolecular systems. *Chem. Commun.* (2022), doi:10.1039/D1CC06851B.
[15] J. F. Bunnett, J. K. Kim, Evidence for a radical mechanism of aromatic "nucleophilic" substitution. *J. Am. Chem. Soc.* **92**, 7463–7464 (1970).
[16] A. E. Feiring, Perfluoroalkylation of the 2-nitropropyl anion. Evidence for an SRN1 process. *J. Org. Chem.* **48**, 347–354 (1983).
[17] Bulat, F.A.; Toro-Labbé, A.; Brinck, T.; Murray, J.S.; Politzer, P. Quantitative Analysis of Molecular Surfaces: Volumes, Electrostatic Potentials and Average Local Ionization Energies. J. Mol. Model. 2010, 16, 1679–1691.
[18] G. Cavallo, P. Metrangolo, R. Milani, T. Pilati, A. Priimagi, G. Resnati, G. Terraneo, *Chem. Rev.* **2016**, *116*, 2478–2601.
[19] J. Kaizer, N. Durkó, M. Czaun, G. Speier, *React Kinet Catal Lett* **2006**, *88*, 193–202.
[20] M. T. Reetz, S. Hütte, R. Goddard, *Zeitschrift für Naturforschung B* **1995**, *50*, 415–422.

Chapter IV.
Radicals via oxidative mechanochemistry

Chapter 4.
Radicals via oxidative mechanochemistry

This short chapter is based on unpublished result and act as an opening for future work, interesting early result and research orientation is depicted.

1. Introduction

Ball milling is now commonly accepted as tool for organic synthesis.[1,2] The activation of radical precursor has recently evolved with the merge of ball milling with reductive catalyst (Fig. 1).[3,4] Indeed, Ito and co-workers firstly took advantage of barium titanate ($BaTiO_3$, piezoelectric material) to trigger a single electron transfer (SET) process with diazonium salt. (Fig. 1.a) With this discovery, the generation of aryl radicals was achieved, and the reactivity investigated. It appears that solid state mechanoredox can achieve subsequent radical precursors reduction allowing a radical arylation or a borylation.[4] Diazonium was also activated in solid state by combining mechanochemistry with photoredox chemistry using transparent ball-milling jar.[5] Under green light irradiation, eosin appears able in this medium to be activated and to perform the SET for the generation of the desired aryl radical species. The radical chemistry in solid-state has already allowed to reach several reactivities previously developed in solution, such as alcohol oxidation with hypervalent iodine species.[6] Hypervalent Iodide (III) is currently a hot topic.[7-12] Currently, all the chemistry developped before is extended to the solid-medium. And until now, no report of solid-state oxidative generation of radical was published.

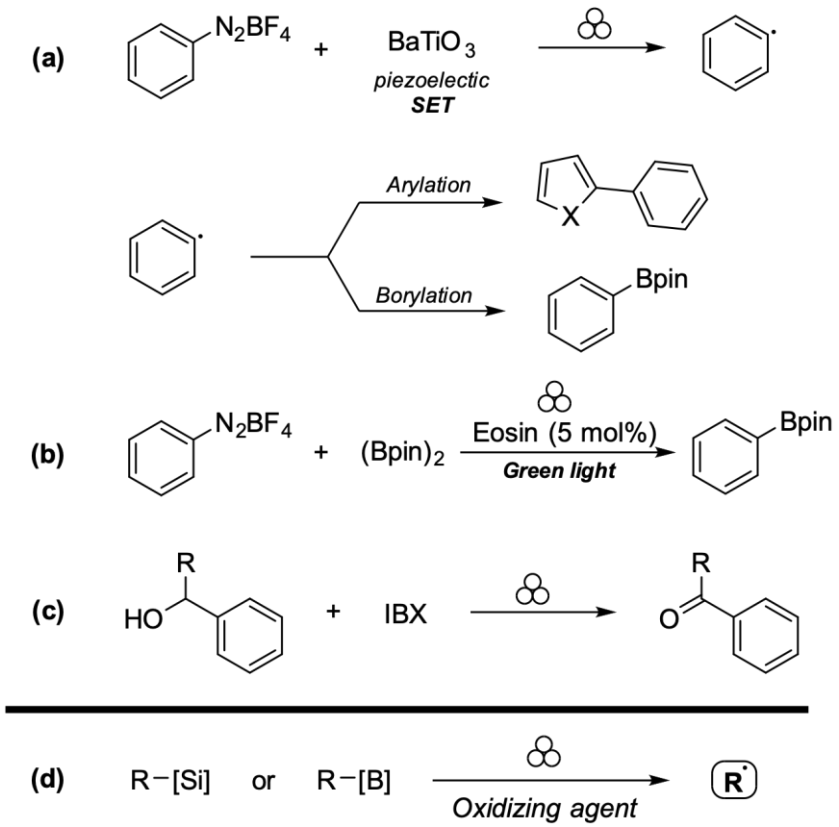

Figure 1. (a) Generation of radical via reductive process; (b) Synergetic (reductive) Ball-Milling/Light irradiation process; (c); Solid state oxidation using hypervalent iodine (d) This works, generation of radical via oxidative pathway

2. Results and discussion

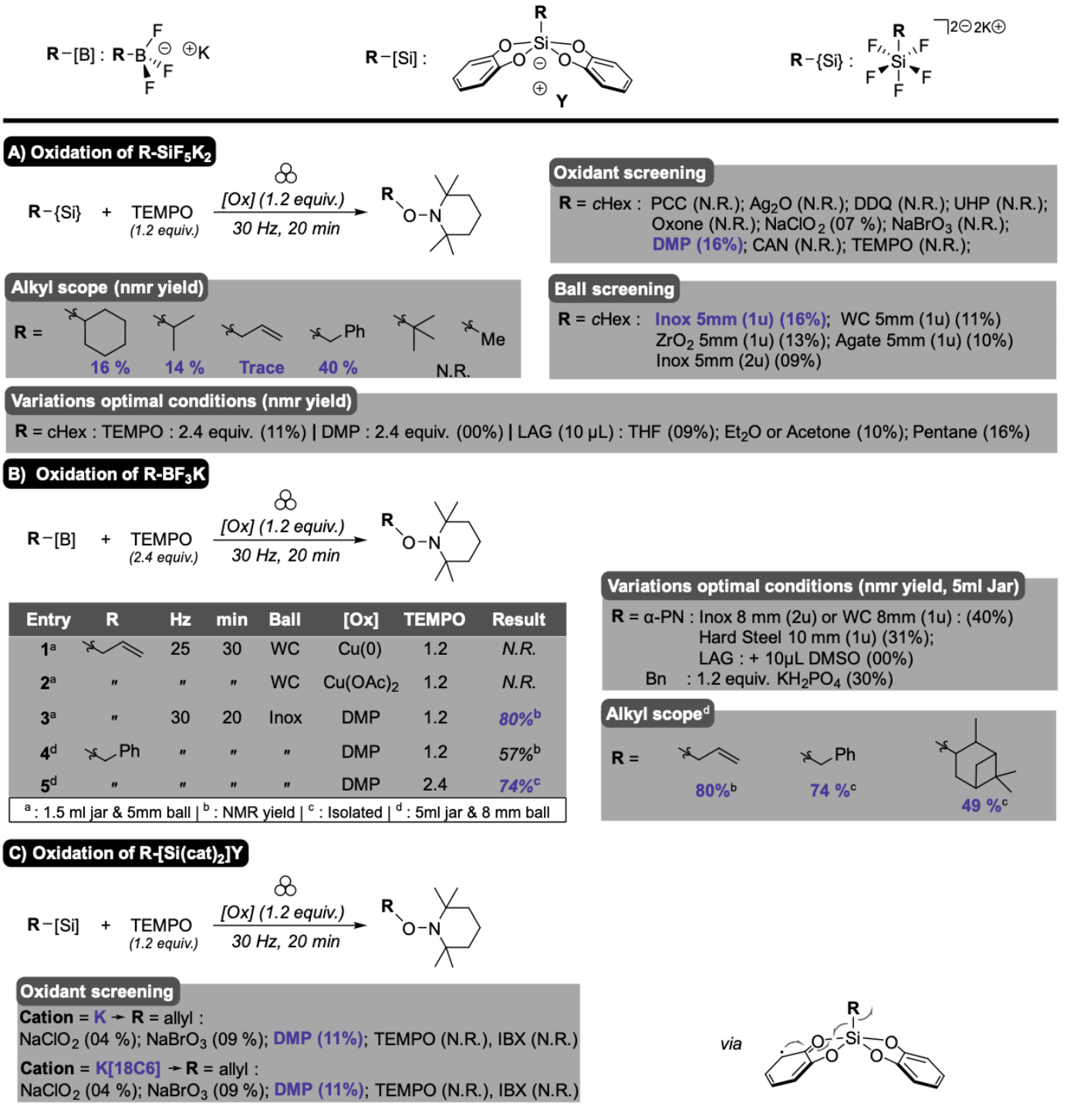

Scheme 1. Investigation/development of the oxidation & trapping of (a) pentafluorosilicate, (b) trifluoroborate, (c) bis(catecholato) silicate

Here, the investigation of solid-state oxidation of anionic radical precursors is highlighted. The investigation of our solid-state generation of radical started with the oxidation/trapping using TEMPO ((2,2,6,6-tetramethylpiperidin-1-yl)oxyl) of alkylpentafluorosilicate. (Scheme 1.a) Indeed, their utilisation in synthetic chemistry is scarce due to the poor solubility of this bis-anionic silicon species. Based on that, we were keen to study the solid-state behaviour of this species as radical precursor.

For this purpose, several organic and inorganic oxidants were screened. To our delight, sodium chlorite ($NaOCl_2$) firstly afforded the desired trapped radical with TEMPO in 7% yield and was increased using Dess-Martin Periodinane (DMP) affording 16% nmr yield. In order to increase this yield, we then screened the ball density and number inside the milling jar. Unfortunately, these physical parameters (the energy induced inside the jar) did not permit to push the generation of the desired radical. We then investigated the influence of the quantity of oxidant and TEMPO then the addition of organic solvent following the reported Liquid Assisted Grinding technics (LAG).[13] Unfortunately, no amelioration was observed. Finally, we screened the nature of the radical involved and it appeared that similar results can be obtained with the isopropyl radical and only trace for the allyl one. The tertiary or primary ones (respectively *t*Bu and Me) cannot be generated from this methodology. Finally, the benzyl radical was observed in at least 40 % nmr yield but needed to be confirmed again. This interesting result was promising concerning these {Si} species and it is the first solid-state example of the solid-state oxidative generation of radicals with this precursor.

We then questioned the ability of alkyltrifluoroborates, another commonly reported radical precursor, to generate via an oxidation the desired radical. (Scheme 1.a) We first started our investigation using the copper(II)/TEMPO system and potassium allyltrifluoroborate as reported in the literature previously in solution[14,15] but without success

The use of our previous oxidant (DMP) used for [R-SiF_5][2K] also led in this case to the formation and trapping of the desired radical in 80% yield when 1.2 equivalent were used (nmr yield). To confirm the nature of the radical event we used benzyltrifluoroborate that afforded 57% yield and we managed to increase this yield by using more TEMPO (from 1.2 to 2.4 equiv.) up to 74% yield (isolated). The scope was then investigated using several known trifluoroborate salts. The sterically hindered α-PN (alpha-pinene) gave the trapped radical in 49% yield. Extension of the scope hasn't been done yet but the desired experimental plan is detailed in conclusion.

From these observed results, they appear similar to the previously reported oxidation of R-BF_3K in solution (DMSO or Et_2O) with the major interest to be solvent-free and faster (20 min) than these in solution (reflux, 6 to 24h). One attempt using DMSO for LAG process and mimic the previous experimental observation was performed but unfortunately led to the complete degradation of the reaction medium.

Finally, the beginning of investigation of bis(catecholato) allyl silicate was performed. It rapidly appeared that chelated potassic salt allyl silicate was unreactive compared to the unchelated. To our delight, the oxidation and trapping of the desired radical was achieved in an initial satisfactory yield. Indeed, based on the mechanism involved for the oxidation of silicates (scheme 1.C) the observation of 9 to 11% at the beginning of our optimisation is an important result.

From a mechanical point of view, the generation of the desired radical is carried out according to a sequential pathway including the oxidation of the silicate ligand (catechol, "cat"), intramolecular electronic event, extrusion of the desired radical (substituent) and formation of spirosilane ([$Si(cat)_2$]). The behavior of bis(catecholato)silane in the solid state is still poorly understood,. but this super Lewis acid tends to degrade, and the possible oxidation of de-coordinate catechol from bis(catecholato)silane, could have dramatical effect on the ability to generate and trap radicals with this precursor.

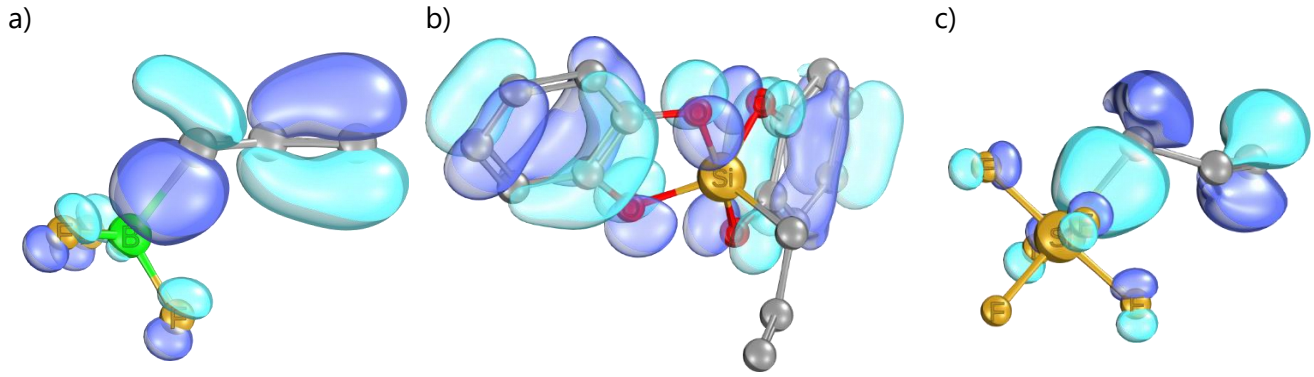

Figure 2. Computation (Orca 5.0.3, PBeh-3C/def2-mSVP // PW6B95(D3BJ)/def2-QZVPP) of HOMO: A) Allyltrifluoroborate; B) Bis(catecholato) allyl silicate; C) Allylpentafluorosilicate; Graphical representation performed using IboView

To better understand the reaction, a computational study was performed using Orca 5 with a special attention on each precursor bearing an allyl substituent. As for the previous study of Martin's silicate (see chapter 2), the HOMO of each precursor can be calculated as depicted in figure 2. Firstly, the known

trifluoroborate (2.a) and silicate (2.b) were calculated. As expected, the HOMO of trifluoroborate is located on the F_3B-C_{allyl} bond and shared on the allyl (-C_3H_5) substituent and the one of silicate is mainly positioned on the catechol ligand. Mechanistically, this described a possible direct oxidation of the B-C bond or a sequential alkene oxidation and fragmentation of the allyl for the trifluoroborate. Concerning the bis(catecholato)allyl silicate, the oxidation of the ligand takes place and leads to the fragmentation of the substituent and generation of bis(catecholato) silane. Interestingly, the pentafluorosilicate's HOMO is mainly located on the F_5Si-C_{allyl} bond and poorly on the π-system of the allyl. In comparison with the trifluoroborate, the generation of the desired radical is inclined to be done following a single pathway with the direct bond oxidation and could result in a loss of reactivity of this precursor. Hypothetically, other starting material such as a non-conjugated one could suffer from steric hinderance of this moiety compared with trifluoroborate.

The limitation of the radical activation was then explored using benzophenone as oxidant. (Scheme 3) Indeed previously, in presence of UV-light irradiation, the generation of triplet state radical allowed the sequential oxidation of a silicate, fragmentation, and a radical-radical recombination. In addition, the nucleophilic character of each anionic radical precursor must be taken in consideration. Indeed, the hypercoordinated silicon species was described in by Sakurai in 1987 for diverse allylation.

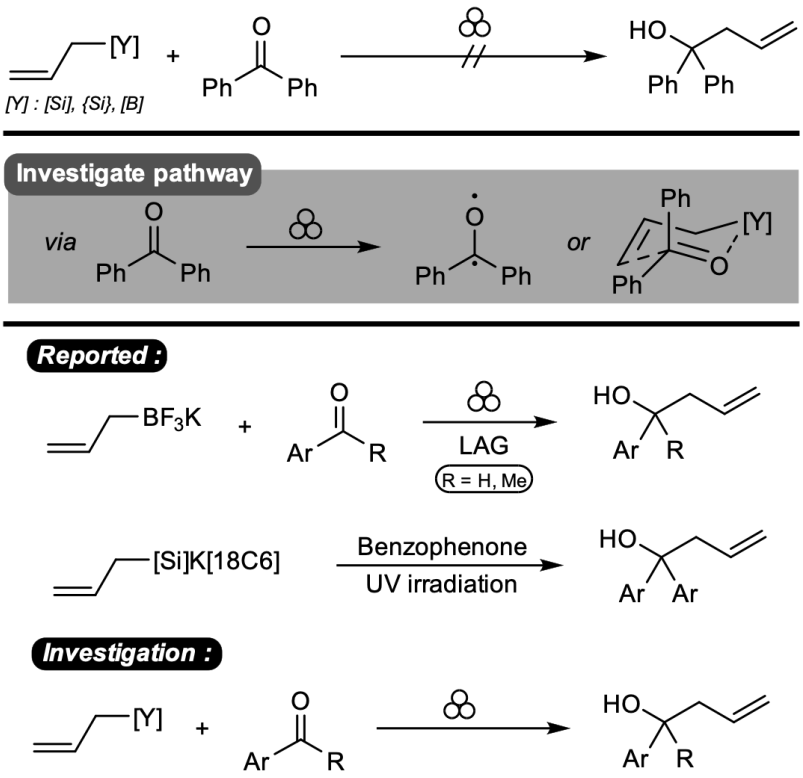

Entry[a]	Y	R	Ar	Hz	min	Ball	Result[b]
1	BF_3K	H	4-NO_2	30	60	Inox	*87%[c]*
2	[Si]K[18C6]	〃	〃	〃	〃	〃	*N.R.*
3	[Si]K	〃	〃	〃	〃	〃	*46%*
4	〃	〃	〃	〃	〃	WC	*55%*
5	BF_3K	Ph	Ph	〃	〃	〃	*N.R.*
6	[Si]K[18C6]	〃	〃	〃	〃	〃	*N.R.*
7	[Si]K	〃	〃	〃	〃	〃	*N.R.*

[a] : 1.5 ml jar & 5mm ball | [b] : NMR yield | [c] : Reported

Scheme 2. Attempted oxidation using benzophenone and nucleophilic character of allyl anion precursor

In solid-state, Malvestiti engaged the trifluoroborate salt in nucleophilic allylation with various aldehyde and ketone, but no example was reported with benzophenone. Here we firstly verified the nucleophilic behaviour of our radical precursor (entry 1-3). It appears that non-chelated potassium silicates can also be used in solid-state for the allylation of aldehyde with a moderate 46% yield obtained, short optimisation shows that tungsten carbine ball (WC) permit to generate more energy inside the reaction jar and increased the yield to 55%. We then engaged them with Ph_2CO with the idea to trigger the oxidation and performing the recombination.

Interestingly, we were unable to observe the allylation product for each radical precursor. This clearly indicates the non-mechanoredox process using benzophenone under milling conditions. Secondly, the ability of non-chelated silicates [R-Si][K] to act as a Lewis acid for the activation of aldehyde did not permit to induce a ketone activation resulting in a possible allylation of Ph_2CO following a Zimmerman-Traxler chair-like transition state.

Finally, we were keen to explore the extrapolation of known dual Ni-photoredox catalysis in an original Ni-mechanoredox one (scheme 3). For this, the trifluoroborate/DMP system was chosen for the generation of the radical species. The desired reaction involved the use of [$NiCl_2$(dtbbpy)] catalyst generally generated in solution (*in-situ*) or engaged already prepared. Here we quickly decided to explore the reaction with the prepared one. To mimic the solution experiment, we firstly attempted a one pot experiment with 4-bromoacetophenone but was unsuccessful using benzyl or allyl trifluoroborate (entry 1-3). Two attempts were done with the idea to trigger the oxidative addition on the bromo-aryl in a stoichiometric manner and later the radical addition & reductive elimination to afford the desired product. These two attempts were unsuccessful but further investigation should be able to develop this Ni-mechanoredox reactivity as several organometallic reactions have already successfully developed in solid-state.

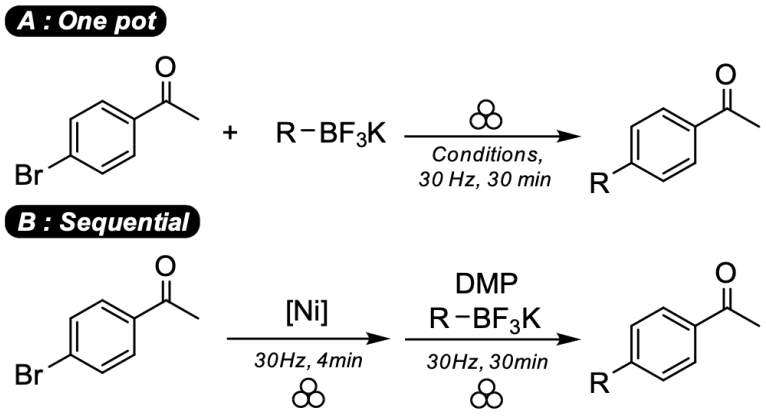

Entry[a]	Condition	R	[Ni]	Add	Result[b]
1	A	Bn	$NiCl_2$.dme	dtbbpy	*N.R.*
2	A	〃	[$NiCl_2$-dtbbpy]	/	*N.R.*
3	A	Allyl	〃	/	*N.R.*
4	B	〃	〃	/	*N.R.*
5	B	Bn	〃	/	*N.R.*

[a] : 1.5 ml jar & 5mm ball; [b] : NMR yield

Scheme 3. Attempted dual Ni-mechanoredox catalysis.

3. Conclusion

In conclusion, we observed the first generation of radical via an oxidative pathway in solid-state. In this early study we focused on two well-known radical precursors (e.g. bis(catecholato)silicates or trifluoroborates) and also an uncommon one with pentafluorosilicates. To perform the one electron transfer event and generate radicals, a wide range of oxidizing reagents were screened and if few results have been obtained for inorganic ones, DMP appeared as the most valuable reagent for the generation of radicals in solid-state.

From these initial results, it appears that mechanoredox chemistry improves drastically the reaction time in comparison with the solution experiments previously reported by our group concerning alkyl trifluoroborates. The isolated yields are slightly lower but similar to the previous system, and the very diverse nature of radicals is consistent between each media.

The use of silicon-based precursors appears more complex than the boron counterpart. As mentioned previously, low yields were obtained for pentafluorosilicates. If optimal conditions have not being found yet, the optimisation appears more delicate for our desired model reaction. The same observation has been made with bis(catecholato)silicates. The influence of the cation seems to be one of the most essential parameters for the possible generation of radicals with this precursor.

The influence of the scale will also be investigated, the α-PN radical precursor was indeed scaled up to 14g. With this starting in hand and several jars available (1, 5 and 25 mL), we aimed to scale up this reaction and be able to rapidly obtain some valuable R-OTMP compound. Concerning the trifluoroborate scope, we will focus on the following example as depicted in the next scheme:

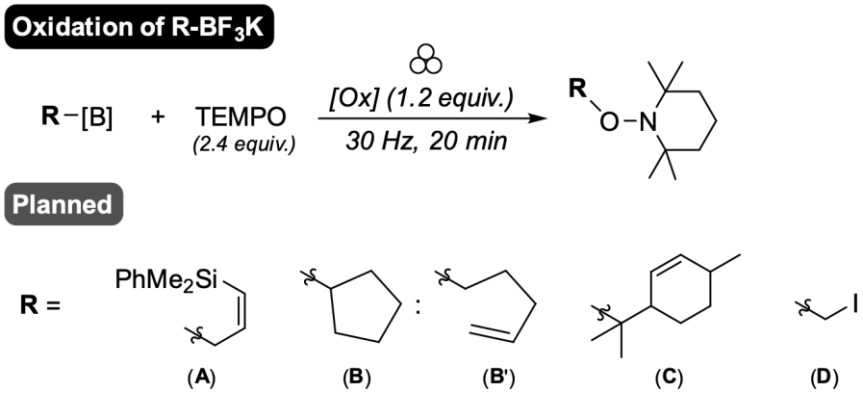

Firstly, from the reaction with the allyl-BF_3K (**A**) substituted with silicon, a primary or a secondary radical will be trapped for the formation of the R-OTMP. If the expected results should lead to the formation of the "primary" trapped radical, the α-Si radical or γ-Si position ratio will be determined such as the Z/E one.

Then, in the same manner, it will be very interesting to know if there is modification of the cyclised (B) : linear (B') ratio from the hexenyl radical precursor. Indeed, it was previously described that modification of the concentration and oxidant led to different ratio of linear or cyclised adducts (as example, 100% linear with DMP in Et_2O was obtained) Here, the reactivity in solid-state is completely unknown, rationalisation of these future findings will be valuable. Then, from *2-carene* (**C**), the resulting trifluoroborate should led to a sequential radical-clock and trapping (as depicted in scheme 1.B). Based on the rate of the ring opening, it will be interesting to know when the trapping happens and the comparison with the solution experiment. Finally, the mechanical and chemical stability of primary iodo-methyl radical precursor and product (**D**) will be investigated.

Finally, with the generation of radical in hand as demonstrated with the TEMPO trapping, the formation of C-C bonds via this mechanistic pathway seems reasonable as depicted in the last scheme hereafter.

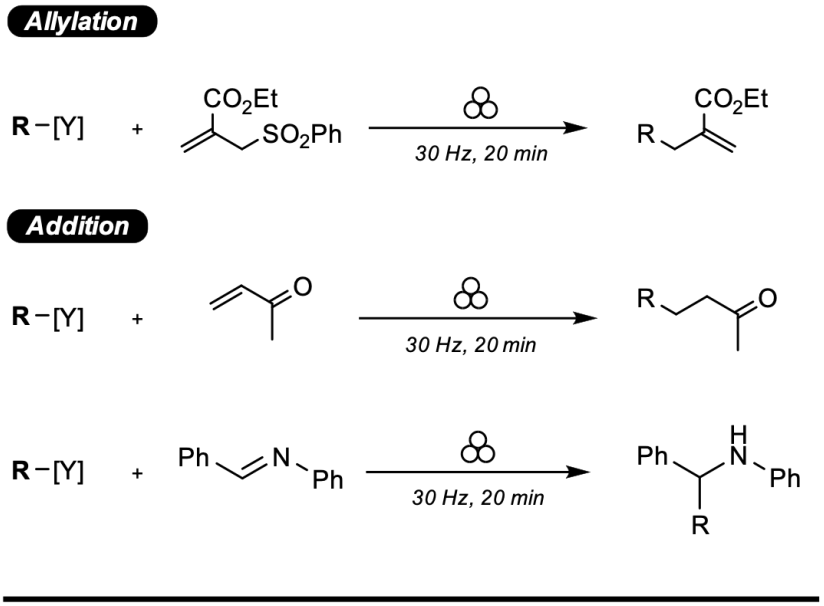

References Chapter 4

[1] Margetić, D.; Štrukil, V. Recent Advances in Mechanochemical Organic Synthesis; IntechOpen, 2020.
[2] Howard, J. L.; Cao, Q.; Browne, D. L. Mechanochemistry as an Emerging Tool for Molecular Synthesis: What Can It Offer? Chem. Sci. **2018**, 9 (12), 3080–3094.
[3] Xia, H.; Wang, Z. Piezoelectricity Drives Organic Synthesis. Science **2019**.
[4] Kubota, K.; Pang, Y.; Miura, A.; Ito, H. Redox Reactions of Small Organic Molecules Using Ball Milling and Piezoelectric Materials. Science **2019**, 366 (6472), 1500–1504.
[5] Hernández, J. G. Mechanochemical Borylation of Aryldiazonium Salts; Merging Light and Ball Milling. Beilstein J. Org. Chem. **2017**, 13 (1), 1463–1469.
[6] Kumar Achar, T.; Maiti, S.; Mal, P. IBX Works Efficiently under Solvent Free Conditions in Ball Milling. RSC Advances **2014**, 4 (25), 12834–12839.
[7] Wu, X.-L.; Xia, J.-J.; Wang, G.-W. Aminobromination of Olefins with TsNH2 and NBS as the Nitrogen and Bromine Sources Mediated by Hypervalent Iodine in a Ball Mill. Org. Biomol. Chem. **2008**, 6 (3), 548–553.
[8] Kumar Achar, T.; Mal, P. Transformation of Contact-Explosives Primary Amines and Iodine(III) into a Successful Chemical Reaction under Solvent-Free Ball Milling Conditions. Advanced Synthesis & Catalysis **2015**, 357 (18), 3977–3985.
[9] Pan, L.; Zheng, L.; Chen, Y.; Ke, Z.; Yeung, Y.-Y. A Mechanochemical, Catalyst-Free Cascade Synthesis of 1,3-Diols and 1,4-Iodoalcohols Using Styrenes and Hypervalent Iodine Reagents. Angewandte Chemie International Edition **2022**, 61 (36), e202207926.
[10] Riley, W.; C. Jones, A.; Singh, K.; L. Browne, D.; M. Stuart, A. Accessing Novel Fluorinated Heterocycles with the Hypervalent Fluoroiodane Reagent by Solution and Mechanochemical Synthesis. Chemical Communications **2021**, 57 (60), 7406–7409.
[11] Hermann, G. N.; Unruh, M. T.; Jung, S.-H.; Krings, M.; Bolm, C. Mechanochemical Rhodium(III)- and Gold(I)-Catalyzed C−H Bond Alkynylations of Indoles under Solventless Conditions in Mixer Mills. Angewandte Chemie International Edition **2018**, 57 (33), 10723–10727.
[12] P. Ying, J. Yu, W. Su, *Advanced Synthesis & Catalysis* **2021**, *363*, 1246–1271.
[13] Bal, A.; Kumar Dinda, T.; Mal, P. Mechanochemical Aliphatic Iodination (and Bromination) by Cascaded Cyclization. Asian Journal of Organic Chemistry 2022, 11 (3), e202200046.
[14] G. Sorin, R. Martinez Mallorquin, Y. Contie, A. Baralle, M. Malacria, J.-P. Goddard, L. Fensterbank, Angewandte Chemie International Edition 2010, 49, 8721–8723.
[15] L. Chenneberg, C. Lévêque, V. Corcé, A. Baralle, J.-P. Goddard, C. Ollivier, L. Fensterbank, Synlett 2016, 27, 731–735.

Supplementary.
DFT

Computational study

Density functional theory studies were carried out with Orca 4.2.1. [1] The geometry of each species was first optimized using PBEh-3c functionals and def2-mSVP. For all resulting structure, frequency analysis was then performed to verify the absence of imaginary frequencies. In case of negative frequencies, the geometries were re-optimized. Single Point Energies were computed with PW6B95[3] D3(BJ) with def2-QZVPP.[4]

Table X. List of coordinates

$Ph[Si]^-$	$Ph[Si]^\cdot$	$Ph^\cdot$
O 1.61138 -4.79526 -2.67644	O 1.67804 -4.75173 -2.56909	C -0.75589 1.16860 0.01716
Si 2.56472 -3.79526 -3.76353	Si 2.62584 -3.71206 -3.54786	C 0.63350 1.23375 0.03269
O 1.39567 -2.51291 -3.47343	O 1.45972 -2.46850 -3.37281	C 1.39767 0.07146 0.03217
C 0.67271 -4.11798 -2.03276	C 0.64050 -4.10812 -2.01410	C 0.77609 -1.17847 0.01612
C 0.54743 -2.79284 -2.49613	C 0.51462 -2.79176 -2.47765	C -0.59533 -1.17948 0.00132
C -0.39591 -1.94347 -1.94663	C -0.50967 -1.97747 -2.03480	C -1.40083 -0.06939 0.00097
C -1.21975 -2.42222 -0.92083	C -1.41148 -2.49975 -1.10644	H -1.34636 2.08480 0.01764
C -1.09620 -3.72500 -0.46489	C -1.28742 -3.80472 -0.64774	H 1.12784 2.20404 0.04548
C -0.14521 -4.58867 -1.02150	C -0.25691 -4.62900 -1.10190	H 2.48567 0.13387 0.04419
O 2.86458 -3.02040 -5.31312	O 2.96158 -2.96562 -5.20042	H 1.36026 -2.09842 0.01555
C 4.05126 -3.28595 -2.71662	C 4.18498 -3.24800 -2.64795	H -2.48819 -0.13866 -0.01105
C 4.53717 -1.97607 -2.74001	C 4.67640 -1.93993 -2.69649	
H -0.48564 -0.92141 -2.31275	H -0.60078 -0.95711 -2.40274	
H -1.96267 -1.75951 -0.47696	H -2.22064 -1.87202 -0.73647	
H -1.74183 -4.08478 0.33651	H -2.00130 -4.19339 0.07694	
C 3.50655 -3.80133 -6.16903	C 3.49836 -3.74249 -6.05368	
C 3.63494 -5.12528 -5.70279	C 3.62476 -5.10364 -5.57463	
C 4.01081 -3.43939 -7.40505	C 3.94346 -3.39672 -7.34406	
C 4.26667 -6.08279 -6.47595	C 4.19268 -6.09755 -6.39478	
C 4.65308 -4.41024 -8.18287	C 4.49269 -4.38743 -8.11500	
C 4.77895 -5.71214 -7.72506	C 4.61568 -5.72719 -7.64424	
H 4.35910 -7.10408 -6.10793	H 4.28356 -7.11845 -6.03015	
H 5.28375 -6.45810 -8.33916	H 5.06087 -6.47182 -8.30227	
H 3.90530 -2.41290 -7.75489	H 3.84664 -2.37219 -7.69697	
O 3.08758 -5.30006 -4.50991	O 3.17592 -5.25597 -4.39388	
C 4.70624 -4.20581 -1.89377	C 4.87524 -4.19025 -1.87953	
C 5.63342 -1.59716 -1.97416	C 5.82801 -1.58605 -2.00625	
C 5.80282 -3.83509 -1.12433	C 6.02704 -3.83844 -1.18847	
C 6.27111 -2.52754 -1.16292	C 6.50653 -2.53623 -1.25353	
H -0.04050 -5.61535 -0.67235	H -0.15220 -5.65418 -0.75115	
H 5.05875 -4.13441 -9.15624	H 4.84919 -4.15233 -9.11650	
H 4.04767 -1.23523 -3.37270	H 4.15079 -1.17992 -3.27480	
H 5.99305 -0.56825 -2.01074	H 6.19551 -0.56158 -2.05193	
H 7.13251 -2.23411 -0.56192	H 7.41003 -2.25939 -0.71126	
H 4.35151 -5.23597 -1.85278	H 4.50776 -5.21412 -1.80918	
H 6.29569 -4.57125 -0.48835	H 6.55073 -4.58311 -0.59022	

cHex[Si]$^-$	cHex[Si]$^\cdot$	cHex$^\cdot$
O -0.47899 -1.12498 2.99448	O 0.08868 -0.69001 3.56240	C 2.14674 0.38102 2.87335
Si 0.47475 -0.13834 1.88421	Si 1.00994 0.03104 2.29116	C 2.24165 1.83956 3.15625
O -0.68579 1.15744 2.20231	O -0.19590 1.19001 2.03578	C 2.51353 -0.59284 3.93795
C -1.40440 -0.44228 3.64871	C -1.08404 -0.06689 3.73288	C 3.51732 2.19792 3.91973
C -1.52403 0.88531 3.18779	C -1.25083 1.01855 2.86411	C 3.78642 -0.18338 4.68042
C -2.45065 1.74296 3.75357	C -2.39269 1.79139 2.89042	C 3.73342 1.27637 5.11397
C -3.26310 1.27113 4.79215	C -3.38683 1.46381 3.81517	H 2.17046 2.42210 2.22789
C -3.14544 -0.03315 5.24458	C -3.22583 0.38908 4.67803	H 3.48313 3.24746 4.24185
C -2.21136 -0.90572 4.67215	C -2.06914 -0.39226 4.64633	H 4.65794 1.55007 5.64020
O 0.69276 0.60944 0.30020	O 1.79164 0.78128 0.65534	H 3.94659 -0.83966 5.54639
C 2.05625 0.34861 2.82093	C 2.61302 0.30401 3.17813	H 2.61563 -1.60414 3.52159
C 2.11407 1.82215 3.23348	C 2.57216 0.80237 4.61426	H 1.57537 0.03902 2.00991
H -2.53649 2.76605 3.38890	H -2.50563 2.63183 2.20775	H 2.91708 1.41660 5.84180
H -3.99332 1.94055 5.24711	H -4.29631 2.06086 3.85664	H 1.68788 -0.66649 4.67568
H -3.78322 -0.38739 6.05455	H -4.01143 0.14834 5.39267	H 4.65378 -0.32912 4.01817
C 1.27475 -0.19024 -0.57882	C 1.90315 -0.07102 -0.26098	H 1.36903 2.15856 3.76209
C 1.42212 -1.50959 -0.10016	C 1.41791 -1.38682 0.11105	H 4.38010 2.11250 3.24155
C 1.70724 0.14749 -1.84884	C 2.44367 0.14481 -1.55718	
C 2.00124 -2.48246 -0.89587	C 1.47222 -2.44740 -0.79551	
C 2.29622 -0.83955 -2.64876	C 2.48175 -0.91234 -2.41999	
C 2.44097 -2.13506 -2.17913	C 2.00039 -2.19858 -2.04373	
H 2.10766 -3.49888 -0.51806	H 1.10571 -3.43131 -0.51101	
H 2.90222 -2.89421 -2.81105	H 2.05448 -3.00790 -2.77018	
H 1.58588 1.16864 -2.20901	H 2.80637 1.13385 -1.82930	
O 0.94680 -1.66426 1.12392	O 0.96023 -1.44092 1.31552	
C 2.36861 -0.55256 4.01929	C 3.03172 -0.58409 4.30726	
C 3.44800 2.18164 3.88176	H -1.93664 -1.23718 5.31985	
C 3.70277 -0.19696 4.66904	H 2.88786 -0.77865 -3.42114	
C 3.76129 1.27366 5.06516	H 3.44411 0.71899 2.60501	
H 1.93088 2.46916 2.36526	H 4.09787 -0.79000 4.39815	
H 3.45014 3.23511 4.20049	H 2.37697 -1.39741 4.61631	
H 4.74486 1.52068 5.49301	C 3.59646 1.80976 5.00176	
H 3.88541 -0.83432 5.54760	H 1.60068 0.91705 5.09495	
H 2.36768 -1.60728 3.71360	O 4.71677 1.84736 4.57768	
H -2.11167 -1.93385 5.01870	O 3.11685 2.67013 5.88941	
H 2.64381 -0.58153 -3.64922	C 3.97564 3.69769 6.36377	
H 2.86641 0.19104 2.08268	H 4.33805 4.30396 5.51955	
H 3.02662 1.45997 5.86580	H 4.86679 3.25547 6.83502	
H 1.56893 -0.46208 4.77203	C 3.20859 4.54589 7.34765	
H 4.52029 -0.41406 3.96155	H 2.33272 5.01247 6.88265	
H 1.30048 2.04316 3.94312	H 3.85369 5.34676 7.72575	
H 4.25182 2.08962 3.13249	H 2.86523 3.95879 8.20706	

TMS-[Si]$^-$			TMS-[Si]$^\cdot$			TMS$^\cdot$		
O	-0.00148	-0.67297 3.27247	O	0.01093	-0.55915 3.46908	C	-5.84111	0.75619 0.81549
Si	0.91564	0.02022 1.89050	Si	0.92415	0.07777 2.14747	C	-4.75999	-0.13057 0.19545
O	-0.35871	1.18612 1.73985	O	-0.33915	1.13233 1.74418	H	-4.41622	0.10388 -0.81646

C	-1.08138	0.01993	3.56493	C	-1.18964	0.02432	3.56101	H	-4.78465	-1.20532	0.39648
C	-1.29306	1.10259	2.68478	C	-1.39484	1.00063	2.57731	Si	-6.56052	2.20290	-0.14859
C	-2.37518	1.94567	2.84246	C	-2.57142	1.71700	2.51023	H	-6.56816	0.25079	1.46646
C	-3.26648	1.71128	3.89784	C	-3.56240	1.44569	3.45666	C	-7.09374	3.52426	1.07718
C	-3.06284	0.65033	4.76521	C	-3.36366	0.47980	4.43278	H	-7.55040	4.38434	0.57124
C	-1.96741	-0.20684	4.60651	C	-2.17145	-0.24476	4.49627	H	-6.23524	3.89332	1.65182
O	1.57998	0.62215	0.33489	O	1.68882	0.68562	0.42853	H	-7.82743	3.13415	1.79368
C	2.40095	0.55002	2.90963	C	2.47761	0.57218	3.01358	C	-5.25870	2.89945	-1.31034
C	2.24299	1.12992	4.30692	C	2.37587	1.19661	4.40077	H	-5.62587	3.81163	-1.79782
H	-2.52017	2.77533	2.15107	H	-2.71265	2.47232	1.73887	H	-4.99329	2.19272	-2.10640
H	-4.12325	2.37128	4.03312	H	-4.49888	2.00026	3.42501	H	-4.33817	3.15864	-0.77264
H	-3.76292	0.47768	5.58300	H	-4.14733	0.28051	5.16225	C	-8.04703	1.60537	-1.13191
C	1.83246	-0.34448	-0.51992	C	1.84071	-0.25617	-0.38776	H	-7.76491	0.82259	-1.84703
C	1.47702	-1.61831	-0.02813	C	1.42062	-1.54557	0.12903	H	-8.50747	2.42294	-1.70125
C	2.38551	-0.22328	-1.78553	C	2.36974	-0.15985	-1.70349	H	-8.82059	1.18644	-0.47595
C	1.67273	-2.75427	-0.78785	C	1.52987	-2.69613	-0.65558	C	-4.45907	0.78759	1.28579
C	2.58506	-1.37655	-2.55333	C	2.46117	-1.30261	-2.44489	H	-4.00717	0.65247	2.26500
C	2.23513	-2.62500	-2.06474	C	2.04584	-2.56165	-1.92606				
H	1.39237	-3.72889	-0.38955	H	1.21398	-3.65952	-0.26135				
H	2.39676	-3.51467	-2.67324	H	2.14209	-3.44280	-2.55848				
H	2.65560	0.76139	-2.16584	H	2.68011	0.81016	-2.08643				
O	0.95496	-1.56746	1.19652	O	0.96391	-1.49129	1.33265				
C	2.87213	-0.21302	4.11130	C	2.95148	-0.16690	4.23655				
H	-1.80393	-1.04257	5.28612	H	-2.01011	-1.00450	5.25900				
H	3.02291	-1.28644	-3.54798	H	2.85972	-1.26026	-3.45722				
H	3.20368	0.99684	2.31472	H	3.27483	0.97835	2.38651				
H	3.94989	-0.31843	4.25530	H	4.02915	-0.30482	4.33919				
H	2.30227	-1.08875	4.42154	H	2.36677	-1.01475	4.59309				
Si	3.20006	2.64875	4.78178	Si	3.39513	2.70858	4.82481				
H	1.22525	1.10581	4.70944	H	1.36997	1.21235	4.83264				
C	5.01977	2.47424	4.31250	C	5.13260	2.54168	4.11810				
C	3.09347	2.92705	6.64725	C	3.49313	2.87352	6.69506				
C	2.46693	4.14037	3.89787	C	2.55565	4.21777	4.08505				
H	5.50251	1.66883	4.88049	H	5.64871	1.65235	4.50134				
H	5.57081	3.40054	4.52107	H	5.74024	3.41279	4.39477				
H	5.14427	2.24879	3.24600	H	5.13348	2.48373	3.02241				
H	2.52370	4.00524	2.81044	H	2.46642	4.12135	2.99570				
H	2.98067	5.07589	4.15517	H	3.11322	5.13915	4.29551				
H	1.40518	4.25751	4.14987	H	1.54191	4.34683	4.48477				
H	3.50671	2.07163	7.19727	H	3.96606	1.99318	7.14807				
H	2.04960	3.04754	6.96478	H	2.49419	2.97525	7.13769				
H	3.64148	3.82508	6.96182	H	4.07507	3.75474	6.99367				

$E\text{-}[Si]^-$				$E\text{-}[Si]^\cdot$				$E^\cdot$			
O	0.10016	-0.75213	3.37377	O	0.08868	-0.69001	3.56240	C	2.66106	0.31323	3.23905
Si	1.05051	0.00420	2.04916	Si	1.00994	0.03104	2.29116	C	2.60138	0.80566	4.62406
O	-0.12548	1.27428	2.04356	O	-0.19590	1.19001	2.03578	C	3.07425	-0.60507	4.27704
C	-0.93559	-0.02438	3.73753	C	-1.08404	-0.06689	3.73288	H	3.16260	0.71286	2.36192

C	-1.07131	1.15364	2.97446	C -1.25083 1.01855 2.86411	H 4.13799 -0.83340 4.38707
C	-2.10001	2.04226	3.21525	C -2.39269 1.79139 2.89042	H 2.40862 -1.41846 4.57677
C	-3.01213	1.75698	4.23930	C -3.38683 1.46381 3.81517	C 3.62547 1.79679 5.05502
C	-2.88225	0.60194	4.99345	C -3.22583 0.38908 4.67803	H 1.62264 0.89709 5.10221
C	-1.84186	-0.30167	4.74891	C -2.06914 -0.39226 4.64633	O 4.76166 1.80337 4.67512
O	1.75990	0.71003	0.56444	O 1.79164 0.78128 0.65534	O 3.12497 2.68221 5.90595
C	2.59363	0.27767	3.09529	C 2.61302 0.30401 3.17813	C 3.98470 3.70254 6.39710
C	2.48063	0.70723	4.55251	C 2.57216 0.80237 4.61426	H 4.38928 4.28871 5.55792
H	-2.18881	2.94618	2.61359	H -2.50563 2.63183 2.20775	H 4.84927 3.25163 6.90767
H	-3.82732	2.45153	4.44130	H -4.29631 2.06086 3.85664	C 3.19792 4.57954 7.33904
H	-3.59737	0.39036	5.78864	H -4.01143 0.14834 5.39267	H 2.34925 5.05623 6.83536
C	1.91761	-0.17569	-0.39599	C 1.90315 -0.07102 -0.26098	H 3.84396 5.37380 7.72913
C	1.45626	-1.45951	-0.03866	C 1.41791 -1.38682 0.11105	H 2.81230 4.01246 8.19397
C	2.46617	0.03546	-1.65153	C 2.44367 0.14481 -1.55718	
C	1.53977	-2.51800	-0.92058	C 1.47222 -2.44740 -0.79551	
C	2.55204	-1.03922	-2.54374	C 2.48175 -0.91234 -2.41999	
C	2.09657	-2.29836	-2.18714	C 2.00039 -2.19858 -2.04373	
H	1.17603	-3.50161	-0.62504	H 1.10571 -3.43131 -0.51101	
H	2.17036	-3.12566	-2.89276	H 2.05448 -3.00790 -2.77018	
H	2.82156	1.02772	-1.92725	H 2.80637 1.13385 -1.82930	
O	0.95434	-1.49831	1.19603	O 0.96023 -1.44092 1.31552	
C	2.99525	-0.65149	4.18759	C 3.03172 -0.58409 4.30726	
H	-1.73584	-1.21269	5.33698	H -1.93664 -1.23718 5.31985	
H	2.98427	-0.87904	-3.53176	H 2.88786 -0.77865 -3.42114	
H	3.43429	0.74241	2.57552	H 3.44411 0.71899 2.60501	
H	4.06059	-0.83293	4.33189	H 4.09787 -0.79000 4.39815	
H	2.34575	-1.49330	4.42376	H 2.37697 -1.39741 4.61631	
C	3.44598	1.71303	5.04303	C 3.59646 1.80976 5.00176	
H	1.48444	0.77855	4.98840	H 1.60068 0.91705 5.09495	
O	4.61527	1.76679	4.77582	O 4.71677 1.84736 4.57768	
O	2.85821	2.60062	5.85344	O 3.11685 2.67013 5.88941	
C	3.64804	3.64649	6.37742	C 3.97564 3.69769 6.36377	
H	4.10609	4.22789	5.56154	H 4.33805 4.30396 5.51955	
H	4.48354	3.23945	6.96971	H 4.86679 3.25547 6.83502	
C	2.76707	4.52797	7.23089	C 3.20859 4.54589 7.34765	
H	1.94615	4.95969	6.64680	H 2.33272 5.01247 6.88265	
H	3.35567	5.35351	7.64816	H 3.85369 5.34676 7.72575	
H	2.32787	3.97086	8.06675	H 2.86523 3.95879 8.20706	
Spiro					
C	-2.38871	-0.01458	0.70641		
C	-3.56159	-0.06194	1.42700		
C	-4.75874	-0.05680	0.70369		
C	-4.75910	-0.00509	-0.70685		
C	-3.56233	0.04275	-1.42922		
C	-2.38908	0.03726	-0.70770		
O	-1.11879	0.08011	-1.25670		
Si	-0.00237	0.05410	0.00031		

O	1.09109	1.33055	0.04681		
C	2.37142	0.80401	0.02717		
C	3.53148	1.54607	0.05407		
C	4.74147	0.84490	0.02805		
C	4.76688	-0.56541	-0.02365		
C	3.58295	-1.30969	-0.05062		
C	2.39690	-0.60988	-0.02466		
O	1.13636	-1.18216	-0.04531		
O	-1.11813	-0.01201	1.25642		
H	-3.55587	-0.10153	2.50998		
H	-5.70719	-0.09324	1.23605		
H	-5.70783	-0.00248	-1.23996		
H	-3.55717	0.08256	-2.51218		
H	3.50653	2.62876	0.09376		
H	5.68045	1.39463	0.04796		
H	5.72507	-1.08098	-0.04280		
H	3.59703	-2.39258	-0.09032		

Fig.S1: Example of computed distortion observed from oxidation (SP → TBP)

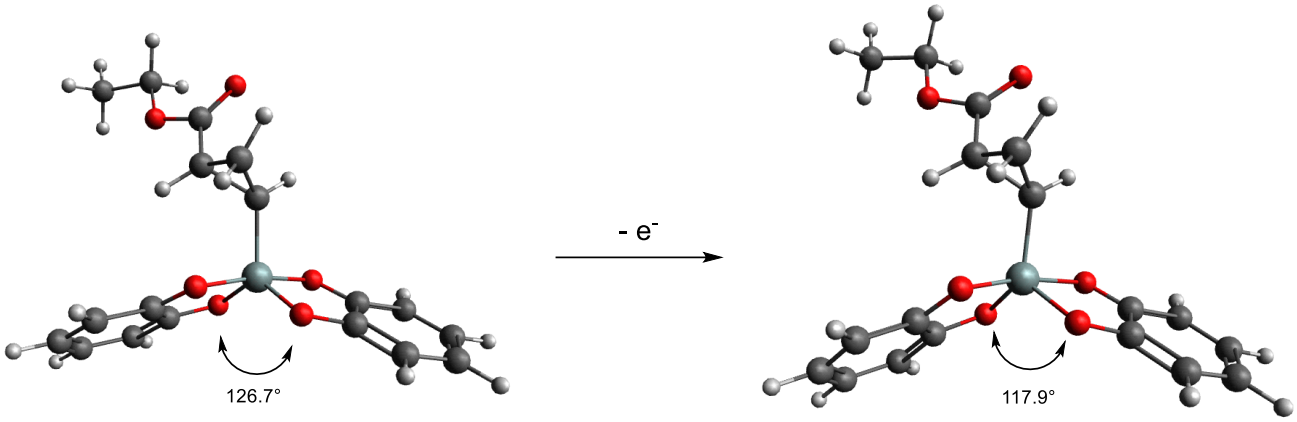

Martin's silicate (Chapter 2)

Density functional theory studies were carried out with Orca 5.0.3 using an Intel(R) Core(TM) i7-7740X CPU @ 4.30GHz processor. Firstly, the geometry of each species was optimized using PBeh-3C functionals and def2-mSVP. Then for all resulting structure, frequency analysis was performed to verify the absence of imaginary frequencies. In case of negative frequencies, the geometries were re-optimized. iboView visualization program was used to describe the 3-dimenstional structure. Single Point Energies were computed with PW6B95 D3(BJ) with def2-QZVPP.

Cartesian Coordinates

$[SiL_2]$

F -9.84583 -2.31319 1.35716
C -10.03483 -3.08728 0.30501
C -9.65001 -2.30443 -0.97901
C -9.86679 -3.12073 -2.28329
F -9.19695 -4.25226 -2.28686
F -11.14187 -3.40177 -2.48940
F -9.44574 -2.39508 -3.30923
O -8.28838 -2.05629 -0.89601
Si -7.83614 -0.45093 -0.93627
O -7.01274 0.05027 0.42556
C -5.72744 0.52494 0.21499
C -4.77568 -0.41759 1.00119
F -3.50891 -0.05014 0.89074
F -5.07309 -0.46610 2.28143
F -4.88673 -1.63727 0.50782
C -5.71626 1.99125 0.72707
F -6.51555 2.71985 -0.03952
F -6.14725 2.08875 1.96443
F -4.50854 2.52733 0.67046
C -5.40552 0.48465 -1.28029
C -6.44853 -0.01896 -2.06108
C -6.30471 -0.11426 -3.44216
C -5.11993 0.29305 -4.03563
C -4.08552 0.79322 -3.25126
C -4.21534 0.89391 -1.87279
C -9.56846 0.14056 -1.08464
C -10.40717 -0.97600 -1.06801
C -11.78773 -0.81892 -1.14469
C -12.31135 0.46326 -1.24479
C -11.48072 1.57935 -1.26631
C -10.10629 1.42040 -1.18294
F -9.30423 -4.16923 0.45973
F -11.30624 -3.45566 0.29337
H -7.11410 -0.50956 -4.05456
H -4.99636 0.22153 -5.11498
H -3.15665 1.11236 -3.72148
H -3.38691 1.28963 -1.29109
H -12.46562 -1.66824 -1.12992
H -13.39077 0.59277 -1.30709
H -11.91241 2.57583 -1.34507
H -9.45381 2.29285 -1.19040

$[Si(F)L_2]$-

F 2.77542 2.05707 0.25038
Si 2.80630 0.42068 0.17718
O 3.14701 0.22977 1.93519
C 2.20223 -0.28240 2.75523
C 1.81318 0.80328 3.79551
F 0.94347 0.36418 4.70905
F 2.86355 1.25833 4.45935
F 1.24657 1.82792 3.18839
C 2.81338 -1.53747 3.43657
F 3.07711 -2.45536 2.52261
F 3.94837 -1.26620 4.06504
F 2.00801 -2.10084 4.33616
C 0.97503 -0.67927 1.93474
C 1.13784 -0.39761 0.58149
C 0.09448 -0.70682 -0.29152
C -1.07806 -1.27692 0.18456
C -1.22081 -1.55113 1.54027
C -0.19433 -1.25457 2.42549
O 2.46697 0.38411 -1.59121
C 3.44746 0.04806 -2.45866
C 2.94652 -1.18010 -3.27134
F 1.82580 -0.92432 -3.93188
F 3.82523 -1.62084 -4.17083
F 2.69935 -2.18510 -2.45015
C 3.71748 1.27192 -3.37778
F 4.19851 2.27658 -2.67242
F 4.60511 1.01620 -4.34284
F 2.61730 1.69586 -3.97820
C 4.70852 -0.33106 -1.68052
C 5.92460 -0.73619 -2.22527
C 6.96783 -1.06689 -1.37210
C 6.79717 -0.99303 0.00577
C 5.58199 -0.58217 0.53590
C 4.52137 -0.24223 -0.30399
H 0.20450 -0.49368 -1.35266
H -1.88907 -1.51116 -0.50514
H -2.14036 -2.00147 1.91449
H -0.32449 -1.47708 3.48196
H 6.07688 -0.80278 -3.29965
H 7.92234 -1.38782 -1.78927
H 7.62042 -1.25673 0.66993
H 5.45282 -0.51831 1.61416

F_5C_2•

C -0.85014 -2.37002 -0.74979
F 0.41597 -2.08743 -0.86473
C -1.15678 -3.66314 -0.01908
F -1.50273 -2.18356 -1.85983
F -0.60150 -4.71202 -0.60801
F -2.45865 -3.85103 0.02156
F -0.69354 -3.59561 1.21203

$[Si(C_2F_5)L_2]$-

F -5.93447 -0.40085 -2.28105
C -4.96164 -1.09467 -1.68223
C -4.12924 -0.23514 -0.69099
C -5.04932 0.51461 0.32157
F -5.84116 1.41900 -0.24815
F -5.83698 -0.30645 1.00358
F -4.29793 1.15908 1.19644
C -3.26724 0.80006 -1.41257
C -3.70222 1.73486 -2.34776
C -2.78503 2.62981 -2.88114
C -1.45517 2.59762 -2.47760
C -1.03533 1.66800 -1.53655
C -1.93994 0.75665 -0.99469
Si -1.59350 -0.61390 0.27467
O 0.05669 0.00962 0.62802
C 0.42571 0.26242 1.90602
C 1.73626 -0.52215 2.19379
F 2.68336 -0.26373 1.30923
F 2.24857 -0.24811 3.39612
F 1.50347 -1.81936 2.16163
C 0.62915 1.79922 2.03699
F -0.50978 2.41913 1.78389
F 1.02251 2.18323 3.24905
F 1.52855 2.26403 1.18057
C -0.67842 -0.21094 2.85239
C -1.77169 -0.72721 2.16380
C -2.83894 -1.24970 2.89363
C -2.80963 -1.24672 4.28044
C -1.72010 -0.70464 4.95302
C -0.64752 -0.18133 4.24461
C -0.92923 -2.23631 -0.64530
F 0.40676 -2.19785 -0.83496
C -1.21439 -3.59805 0.02678
F -1.47403 -2.29823 -1.88321
O -3.32370 -1.06836 0.01186
F -5.54448 -2.11649 -1.08036
F -4.19424 -1.57693 -2.63840
H -4.73975 1.78189 -2.67071
H -3.11477 3.36239 -3.61760
H -0.74207 3.30611 -2.89937
H 0.00494 1.64574 -1.21857
H -3.69623 -1.66538 2.36849
H -3.64431 -1.66476 4.84330
H -1.70226 -0.69217 6.04272
H 0.19614 0.23343 4.79126
F -0.64580 -4.60417 -0.63238
F -2.50720 -3.85294 0.09373
F -0.73468 -3.61867 1.25983

$[Si(C_2F_5)L_2]$•

F -5.92907 -0.06314 -1.92977
C -5.01491 -0.64518 -1.17107
C -3.96769 0.37922 -0.63477
C -4.64841 1.58542 0.08631
F -5.37171 2.31499 -0.74442
F -5.43473 1.18824 1.06470
F -3.71229 2.35954 0.59380
C -3.06200 0.90958 -1.73107
C -3.46315 1.47710 -2.94511
C -2.50719 1.96820 -3.82672
C -1.14923 1.92181 -3.52648
C -0.71958 1.36920 -2.32078
C -1.70904 0.89026 -1.51200
Si -1.73479 -0.77882 0.73154
O -0.54049 0.36319 0.96692
C -0.05584 0.48086 2.26592
C 1.46843 0.18588 2.19152
F 2.05469 0.87086 1.23309
F 2.08105 0.46749 3.32980
F 1.65131 -1.09736 1.94338
C -0.38108 1.92966 2.72598
F -1.69084 2.08610 2.74283
F 0.06888 2.17941 3.94424
F 0.12828 2.83001 1.91155
C -0.76732 -0.53196 3.16239
C -1.72432 -1.30177 2.49590
C -2.48714 -2.22583 3.20399
C -2.27711 -2.39122 4.56352
C -1.30724 -1.63704 5.21531
C -0.54858 -0.70151 4.52574
C -1.06990 -2.09985 -0.54910
F 0.25277 -1.93688 -0.70010
C -1.32221 -3.55627 -0.09298
F -1.63216 -1.96918 -1.75844
O -3.24959 -0.28203 0.33948
F -5.63621 -1.25606 -0.18446
F -4.41149 -1.56300 -1.89698
H -4.51455 1.54576 -3.21587
H -2.83333 2.40437 -4.76906
H -0.41945 2.32173 -4.22956
H 0.33132 1.32036 -2.04030
H -3.25013 -2.81718 2.70068
H -2.87173 -3.11189 5.12240
H -1.14232 -1.77407 6.28280
H 0.19440 -0.11960 5.06505
F -1.00297 -4.43045 -1.01991
F -2.61199 -3.69932 0.18949
F -0.62958 -3.82793 0.99446

$[Si(CF_3)L_2]$-

F -5.75888 -0.55634 -2.38575
C -4.83379 -1.19167 -1.66286
C -4.10087 -0.26031 -0.66244
C -5.08930 0.50287 0.26546
F -5.91945 1.30802 -0.39368
F -5.84354 -0.30980 0.99243
F -4.40121 1.25815 1.10360
C -3.22938 0.75669 -1.39907
C -3.65152 1.66324 -2.36843
C -2.72232 2.52626 -2.93180
C -1.39268 2.48787 -2.52703
C -0.98728 1.58761 -1.55223
C -1.90516 0.70999 -0.97630
Si -1.57910 -0.61846 0.34760
O 0.07908 0.01573 0.66037
C 0.44918 0.30664 1.93006
C 1.86159 -0.29597 2.16660
F 2.66497 -0.07273 1.14377
F 2.46508 0.20623 3.24846
F 1.78980 -1.60148 2.34426
C 0.45413 1.85685 2.08591
F -0.72806 2.33313 1.73727
F 0.68544 2.26412 3.33089
F 1.36244 2.44244 1.31557
C -0.57942 -0.27171 2.89947
C -1.71044 -0.74044 2.23939
C -2.75100 -1.28152 2.99329
C -2.65021 -1.35382 4.37549
C -1.51182 -0.87970 5.01878
C -0.47008 -0.32889 4.28584
C -0.95532 -2.31000 -0.41845
F 0.25324 -2.69059 0.00709
F -1.76574 -3.33971 -0.14736
F -0.86860 -2.24655 -1.75670
O -3.31690 -1.03873 0.11942
F -5.44857 -2.19201 -1.05557
F -3.96826 -1.70894 -2.51433
H -4.68746 1.71184 -2.69601
H -3.04149 3.23692 -3.69404
H -0.66865 3.16881 -2.97502
H 0.05249 1.56235 -1.23273
H -3.64154 -1.65167 2.48930
H -3.46425 -1.78428 4.95889
H -1.43415 -0.93769 6.10437
H 0.41088 0.04060 4.80687

List of coordinates depending of the external force (x nN)

0 nN

F	-5.93457	-0.40137	-2.28116
C	-4.96144	-1.09490	-1.68246
C	-4.12934	-0.23514	-0.69113
C	-5.04986	0.51441	0.32115
F	-5.84118	1.41914	-0.24873
F	-5.83812	-0.30684	1.00226
F	-4.29898	1.15837	1.19683
C	-3.26735	0.80014	-1.41263
C	-3.70228	1.73475	-2.34804
C	-2.78512	2.62978	-2.88134
C	-1.45533	2.59785	-2.47752
C	-1.03553	1.66837	-1.53633
C	-1.94010	0.75693	-0.99455
Si	-1.59364	-0.61364	0.27477
O	0.05659	0.00980	0.62806
C	0.42584	0.26223	1.90606
C	1.73633	-0.52261	2.19334
F	2.68332	-0.26394	1.30872
F	2.24891	-0.24910	3.39568
F	1.50338	-1.81977	2.16070
C	0.62958	1.79895	2.03743
F	-0.50930	2.41915	1.78477
F	1.02325	2.18247	3.24954
F	1.52890	2.26387	1.18098
C	-0.67825	-0.21111	2.85247
C	-1.77172	-0.72703	2.16393
C	-2.83907	-1.24923	2.89381
C	-2.80967	-1.24629	4.28063
C	-1.71994	-0.70456	4.95315
C	-0.64724	-0.18156	4.24470
C	-0.92943	-2.23607	-0.64522
F	0.40647	-2.19742	-0.83543
C	-1.21409	-3.59775	0.02721
F	-1.47474	-2.29834	-1.88289
O	-3.32382	-1.06817	0.01196
F	-5.54388	-2.11699	-1.08070
F	-4.19388	-1.57675	-2.63872
H	-4.73974	1.78154	-2.67125
H	-3.11482	3.36221	-3.61797
H	-0.74226	3.30641	-2.89923
H	0.00471	1.64626	-1.21820
H	-3.69656	-1.66454	2.36873
H	-3.64447	-1.66403	4.84354
H	-1.70205	-0.69207	6.04286
H	0.19650	0.23307	4.79130
F	-0.64565	-4.60387	-0.63206
F	-2.50684	-3.85281	0.09478
F	-0.73382	-3.61813	1.26005

0.1 nN

F	-5.93277	-0.40405	-2.28414
C	-4.95985	-1.09631	-1.68355
C	-4.13003	-0.23502	-0.69161
C	-5.05292	0.51406	0.31875
F	-5.84397	1.41788	-0.25287
F	-5.84166	-0.30783	0.99856
F	-4.30436	1.15898	1.19568
C	-3.26823	0.80066	-1.41268
C	-3.70313	1.73450	-2.34888
C	-2.78631	2.63021	-2.88159
C	-1.45688	2.59966	-2.47646
C	-1.03706	1.67079	-1.53470
C	-1.94133	0.75872	-0.99345
Si	-1.59474	-0.61154	0.27600
O	0.05579	0.01126	0.62843
C	0.42632	0.26211	1.90639
C	1.73597	-0.52477	2.19193
F	2.68266	-0.26636	1.30692
F	2.24976	-0.25327	3.39418
F	1.50123	-1.82155	2.15799
C	0.63236	1.79845	2.03890
F	-0.50569	2.42063	1.78742
F	1.02732	2.18033	3.25111
F	1.53185	2.26277	1.18233
C	-0.67770	-0.21055	2.85324
C	-1.77211	-0.72511	2.16516
C	-2.83965	-1.24636	2.89546
C	-2.80946	-1.24389	4.28227
C	-1.71868	-0.70372	4.95436
C	-0.64580	-0.18168	4.24547
C	-0.92875	-2.23772	-0.64603
F	0.40707	-2.19832	-0.83616
C	-1.21324	-3.59895	0.02692
F	-1.47424	-2.30015	-1.88351
O	-3.32463	-1.06672	0.01320
F	-5.54214	-2.11855	-1.08200
F	-4.19034	-1.57799	-2.63833
H	-4.74031	1.78015	-2.67316
H	-3.11599	3.36206	-3.61880
H	-0.74408	3.30876	-2.89771
H	0.00293	1.64960	-1.21572
H	-3.69789	-1.66055	2.37072
H	-3.64440	-1.66087	4.84553
H	-1.70012	-0.69169	6.04405
H	0.19877	0.23172	4.79173
F	-0.64501	-4.60547	-0.63199
F	-2.50604	-3.85381	0.09478
F	-0.73280	-3.61883	1.25969

0.5 nN

F	-5.92944	-0.40776	-2.28867
C	-4.95784	-1.09802	-1.68369
C	-4.13161	-0.23401	-0.69125
C	-5.05742	0.51499	0.31645
F	-5.85026	1.41543	-0.25798
F	-5.84468	-0.30733	0.99741
F	-4.31127	1.16388	1.19253
C	-3.27027	0.80218	-1.41216
C	-3.70506	1.73437	-2.35002
C	-2.78873	2.63093	-2.88215
C	-1.45991	2.60291	-2.47478
C	-1.04017	1.67560	-1.53148
C	-1.94401	0.76277	-0.99081
Si	-1.59731	-0.60650	0.27917
O	0.05386	0.01450	0.62969
C	0.42655	0.26265	1.90764
C	1.73433	-0.52819	2.19066
F	2.68083	-0.27106	1.30510
F	2.25003	-0.25979	3.39278
F	1.49583	-1.82421	2.15505
C	0.63682	1.79831	2.04170
F	-0.49973	2.42392	1.79197
F	1.03395	2.17770	3.25397
F	1.53673	2.26118	1.18482
C	-0.67756	-0.20829	2.85536
C	-1.77342	-0.72085	2.16812
C	-2.84127	-1.24054	2.89905
C	-2.81006	-1.23823	4.28584
C	-1.71781	-0.70008	4.95717
C	-0.64447	-0.17991	4.24756
C	-0.92362	-2.24652	-0.65186
F	0.41221	-2.20459	-0.83904
C	-1.20950	-3.60667	0.02066
F	-1.46768	-2.30719	-1.88965
O	-3.32624	-1.06360	0.01614
F	-5.54107	-2.11945	-1.08171
F	-4.18482	-1.58099	-2.63496
H	-4.74176	1.77802	-2.67613
H	-3.11830	3.36142	-3.62074
H	-0.74750	3.31260	-2.89568
H	-0.00061	1.65606	-1.21101
H	-3.70059	-1.65319	2.37485
H	-3.64534	-1.65375	4.84968
H	-1.69845	-0.68818	6.04685
H	0.20127	0.23182	4.79327
F	-0.64172	-4.61439	-0.63708
F	-2.50278	-3.85986	0.08721
F	-0.73040	-3.62637	1.25396

1 nN

F	-5.93272	-0.40489	-2.28227
C	-4.96197	-1.09632	-1.67752
C	-4.13245	-0.23259	-0.68802
C	-5.05283	0.51917	0.32293
F	-5.85243	1.41490	-0.24960
F	-5.83282	-0.30062	1.01500
F	-4.30026	1.17431	1.18915
C	-3.27165	0.80244	-1.41166
C	-3.70624	1.73238	-2.35179
C	-2.78961	2.62764	-2.88584
C	-1.46100	2.60105	-2.47778
C	-1.04156	1.67649	-1.53163
C	-1.94563	0.76497	-0.98932
Si	-1.59990	-0.60124	0.28297
O	0.05205	0.01612	0.63220
C	0.42475	0.26402	1.91041
C	1.73137	-0.52840	2.19417
F	2.67918	-0.27167	1.30997
F	2.24585	-0.26112	3.39709
F	1.49138	-1.82402	2.15750
C	0.63649	1.79950	2.04425
F	-0.49951	2.42610	1.79412
F	1.03357	2.17874	3.25657
F	1.53691	2.26145	1.18749
C	-0.68002	-0.20566	2.85813
C	-1.77589	-0.71791	2.17075
C	-2.84414	-1.23769	2.90092
C	-2.81384	-1.23473	4.28771
C	-1.72204	-0.69613	4.95939
C	-0.64794	-0.17667	4.25033
C	-0.91317	-2.25636	-0.66344
F	0.42293	-2.21005	-0.84388
C	-1.20210	-3.61677	0.00406
F	-1.45281	-2.31107	-1.90302
O	-3.32574	-1.06293	0.01745
F	-5.54681	-2.11545	-1.07290
F	-4.19129	-1.58258	-2.62891
H	-4.74278	1.77517	-2.67847
H	-3.11884	3.35599	-3.62670
H	-0.74848	3.30964	-2.90036
H	-0.00223	1.65796	-1.21036
H	-3.70282	-1.65085	2.37613
H	-3.64950	-1.64995	4.85119
H	-1.70357	-0.68350	6.04908
H	0.19747	0.23503	4.79656
F	-0.63228	-4.62509	-0.65185
F	-2.49619	-3.86848	0.06384
F	-0.72917	-3.63863	1.23978

2.5 nN

F	-5.91702	-0.41610	-2.29882
C	-4.95500	-1.10090	-1.67349
C	-4.13927	-0.22606	-0.68343
C	-5.06748	0.52781	0.31890
F	-5.88658	1.39853	-0.26460
F	-5.82877	-0.29151	1.03144
F	-4.31996	1.21241	1.16726
C	-3.28061	0.80956	-1.40911
C	-3.71434	1.73082	-2.35807
C	-2.79872	2.62683	-2.89279
C	-1.47246	2.61017	-2.47654
C	-1.05398	1.69467	-1.52128
C	-1.95724	0.78293	-0.97829
Si	-1.61414	-0.57392	0.30103
O	0.04160	0.03005	0.63955
C	0.42347	0.26786	1.91766
C	1.72353	-0.53857	2.19128
F	2.66933	-0.28816	1.30336
F	2.24634	-0.27963	3.39245
F	1.46984	-1.83116	2.15184
C	0.64974	1.80085	2.05710
F	-0.48130	2.43892	1.81281
F	1.05340	2.17137	3.26985
F	1.55151	2.25828	1.19956
C	-0.68075	-0.19539	2.86961
C	-1.78412	-0.69642	2.18616
C	-2.85358	-1.21053	2.91834
C	-2.81778	-1.21119	4.30499
C	-1.71877	-0.68337	4.97347
C	-0.64276	-0.17124	4.26173
C	-0.88324	-2.30010	-0.69403
F	0.45382	-2.24388	-0.85094
C	-1.18647	-3.65600	-0.03433
F	-1.40722	-2.34224	-1.93902
O	-3.33172	-1.04778	0.03223
F	-5.54775	-2.11374	-1.06577
F	-4.16997	-1.59630	-2.60803
H	-4.74890	1.76592	-2.69173
H	-3.12694	3.34773	-3.64131
H	-0.76093	3.31897	-2.90035
H	-0.01643	1.68280	-1.19413
H	-3.71665	-1.61663	2.39536
H	-3.65444	-1.62124	4.87076
H	-1.69603	-0.67383	6.06310
H	0.20842	0.23105	4.80595
F	-0.61763	-4.67157	-0.68264
F	-2.48385	-3.89656	0.00972
F	-0.72848	-3.68180	1.20704

3 nN

F	-5.90523	-0.42924	-2.31237
C	-4.94713	-1.10794	-1.67456
C	-4.14306	-0.22468	-0.68283
C	-5.08033	0.52890	0.31103
F	-5.90826	1.38469	-0.28179
F	-5.83334	-0.29128	1.03117
F	-4.34066	1.23003	1.15297
C	-3.28621	0.81246	-1.40833
C	-3.71971	1.72782	-2.36309
C	-2.80586	2.62652	-2.89630
C	-1.48174	2.61849	-2.47296
C	-1.06332	1.70842	-1.51256
C	-1.96496	0.79427	-0.97103
Si	-1.62188	-0.55795	0.31131
O	0.03562	0.04027	0.64363
C	0.42479	0.26867	1.92156
C	1.72028	-0.54834	2.18540
F	2.66351	-0.30089	1.29399
F	2.25070	-0.29782	3.38491
F	1.45670	-1.83863	2.14196
C	0.66246	1.79943	2.06734
F	-0.46462	2.44698	1.82961
F	1.07234	2.16113	3.28068
F	1.56465	2.25460	1.20916
C	-0.67891	-0.19059	2.87626
C	-1.78816	-0.68220	2.19552
C	-2.85922	-1.19016	2.92958
C	-2.81934	-1.19357	4.31609
C	-1.71405	-0.67595	4.98220
C	-0.63617	-0.17062	4.26829
C	-0.86952	-2.31852	-0.70674
F	0.46812	-2.25906	-0.85071
C	-1.18157	-3.67247	-0.05188
F	-1.38399	-2.35410	-1.95498
O	-3.33553	-1.03894	0.04180
F	-5.54233	-2.11905	-1.06652
F	-4.15152	-1.60561	-2.59882
H	-4.75255	1.75606	-2.70262
H	-3.13381	3.34269	-3.64945
H	-0.77173	3.32944	-2.89568
H	-0.02733	1.70247	-1.18045
H	-3.72634	-1.58963	2.40824
H	-3.65735	-1.59839	4.88362
H	-1.68782	-0.66919	6.07176
H	0.21995	0.22331	4.81080
F	-0.61237	-4.69126	-0.69618
F	-2.48050	-3.90755	-0.01807
F	-0.73301	-3.70130	1.19291

3.5 nN

F	-5.88625	-0.43590	-2.33080
C	-4.93522	-1.11002	-1.67820
C	-4.14583	-0.22038	-0.68139
C	-5.09371	0.53030	0.30395
F	-5.92772	1.37373	-0.29790
F	-5.84101	-0.29177	1.02731
F	-4.36339	1.24453	1.14348
C	-3.28980	0.81930	-1.40429
C	-3.72295	1.73376	-2.36012
C	-2.80921	2.63338	-2.89192
C	-1.48557	2.62660	-2.46704
C	-1.06766	1.71772	-1.50539
C	-1.96963	0.80363	-0.96429
Si	-1.63112	-0.54305	0.32303
O	0.02967	0.04260	0.64658
C	0.42365	0.27176	1.92312
C	1.71887	-0.54596	2.18412
F	2.65170	-0.31789	1.27718
F	2.26411	-0.27573	3.37284
F	1.44961	-1.83576	2.16731
C	0.66124	1.80296	2.06561
F	-0.46564	2.44917	1.82242
F	1.06688	2.16890	3.27877
F	1.56581	2.25537	1.20845
C	-0.67726	-0.18469	2.88223
C	-1.79286	-0.66768	2.20583
C	-2.86309	-1.17240	2.94313
C	-2.81568	-1.18158	4.32942
C	-1.70335	-0.67396	4.99149
C	-0.62645	-0.17156	4.27391
C	-0.85524	-2.34941	-0.71810
F	0.48431	-2.29360	-0.84058
C	-1.18534	-3.70112	-0.07237
F	-1.35293	-2.37515	-1.97289
O	-3.33941	-1.02893	0.05168
F	-5.53575	-2.11964	-1.07271
F	-4.12622	-1.60935	-2.58962
H	-4.75515	1.76090	-2.70155
H	-3.13692	3.34898	-3.64569
H	-0.77563	3.33773	-2.88951
H	-0.03200	1.71232	-1.17239
H	-3.73468	-1.56582	2.42467
H	-3.65288	-1.58399	4.89983
H	-1.67072	-0.67322	6.08089
H	0.23571	0.21351	4.81330
F	-0.61492	-4.72408	-0.71080
F	-2.48649	-3.92672	-0.05769
F	-0.75415	-3.73608	1.17857

4 nN

F	-5.85267	-0.46557	-2.36483
C	-4.90983	-1.12397	-1.68497
C	-4.15195	-0.21520	-0.68169
C	-5.12567	0.53114	0.28026
F	-5.96468	1.35167	-0.34539
F	-5.86887	-0.29387	1.00418
F	-4.41951	1.26852	1.12050
C	-3.29873	0.82908	-1.40091
C	-3.73072	1.73469	-2.36581
C	-2.81956	2.63891	-2.89402
C	-1.49932	2.64447	-2.45832
C	-1.08235	1.74365	-1.48893
C	-1.98270	0.82686	-0.94959
Si	-1.64758	-0.50986	0.34597
O	0.01846	0.05745	0.65366
C	0.42541	0.27736	1.92807
C	1.71935	-0.54692	2.17267
F	2.62855	-0.34597	1.23703
F	2.29671	-0.25495	3.34145
F	1.43963	-1.83479	2.19294
C	0.67021	1.80723	2.07491
F	-0.45378	2.45849	1.83091
F	1.07480	2.16973	3.28876
F	1.57801	2.25670	1.21920
C	-0.66949	-0.17633	2.89508
C	-1.80051	-0.63467	2.22745
C	-2.87013	-1.13018	2.97159
C	-2.80518	-1.15676	4.35693
C	-1.67533	-0.67768	5.01072
C	-0.59988	-0.18264	4.28575
C	-0.82733	-2.39288	-0.72599
F	0.51582	-2.35140	-0.79222
C	-1.20632	-3.74022	-0.10656
F	-1.27742	-2.39476	-1.99768
O	-3.34814	-1.00627	0.07383
F	-5.51334	-2.13297	-1.08208
F	-4.07469	-1.62298	-2.57267
H	-4.75972	1.75127	-2.71727
H	-3.14642	3.34810	-3.65417
H	-0.79124	3.35848	-2.87897
H	-0.04897	1.74618	-1.14916
H	-3.75386	-1.50445	2.45947
H	-3.64115	-1.55324	4.93323
H	-1.62780	-0.69405	6.09942
H	0.27621	0.18027	4.81807
F	-0.62558	-4.77048	-0.72639
F	-2.51055	-3.94372	-0.15323
F	-0.83247	-3.79173	1.16271

Example of relaxed optimisation input with external force :

```
!PBeh-3c def2-SVP OPT FREQ normalprint

%geom
POTENTIALS
{ C 13 30 4 }
end
end

%output
Print[P_basis] 2
Print[P_MOs] 1
END
* xyz -1 1
```

List of coordinates for the mechanistic investigation

SM

F	-5.17507672274728	-3.12982697918878	1.62817544753357
C	-3.91764636468160	-3.11923651237342	1.18291380792079
C	-3.26893535990462	-1.70957168867002	1.24543345357907
C	-3.42539754202615	-1.07850352948374	2.66288803707935
F	-4.68932682411959	-0.83877883873425	2.99702931910490
F	-2.91285963175744	-1.84239927980167	3.61839281904605
F	-2.78811387750864	0.07848243013485	2.69800091066726
C	-3.88203537123721	-0.75619033089115	0.22042276524054
C	-5.23602172434232	-0.47705121680797	0.05076882584506
C	-5.61660979794966	0.45122812104728	-0.90949323548191
C	-4.65753486217249	1.09946446367659	-1.67870361364453
C	-3.31138760544630	0.81944496492968	-1.49384337663496
C	-2.90857546109015	-0.11837628680066	-0.54293517707391
Si	-1.14110149391269	-0.68119630424046	-0.13060348103713
O	-0.41297314834537	0.62032205876301	-1.13208770888975
C	0.52333176760497	1.43858296212993	-0.59396733978431
C	1.71615022082303	1.50575366266969	-1.58512726573296
F	1.32755225440437	1.81187902683460	-2.81040669827904
F	2.63202333714224	2.41201848342318	-1.23581766280742
F	2.33031197461052	0.34018514185658	-1.64071536281901
C	-0.12949073680599	2.83584972769121	-0.38268016555400
F	-1.17392393833402	2.71592698785448	0.41743887581126
F	0.69160915443099	3.72218693894410	0.17442035541680
F	-0.55981230886808	3.37197307585711	-1.51652082106179
C	0.95437986321724	0.88157568802232	0.76213796881346
C	0.17066821189015	-0.19912233116628	1.15611529428723
C	0.43794260962510	-0.80921283614554	2.38101702921989
C	1.46797900433729	-0.34383818314566	3.18587071256779
C	2.23505634956813	0.74262607181007	2.78067686318687
C	1.98080122037243	1.36684188250252	1.56760717516499
C	-0.56783134108904	-2.13247370746801	-1.34874828294798
F	-0.14381853874309	-1.66122519718620	-2.54405829122646
C	0.55348438746495	-3.06640308078229	-0.84237734972079
F	-1.62258873069146	-2.93765817077686	-1.63319105757456
O	-1.94405979662319	-1.84291393935797	0.99185899574812
F	-3.24976782522178	-4.00530382025599	1.89668241287224
F	-3.95428025752704	-3.56266219632045	-0.06322324497603
H	-6.00222975771108	-0.96675303601252	0.64786983989598
H	-6.67456357176347	0.66488932495086	-1.05985615600002
H	-4.96488504926947	1.81838234778345	-2.43767646742840
H	-2.56377411964836	1.32906035414132	-2.09813705617144
H	-0.16044272301267	-1.65842623776127	2.70479392440700
H	1.67519707647688	-0.82847627445953	4.13998085741165
H	3.03980399045760	1.11173867265431	3.41628871426858
H	2.58652635136586	2.21955796049635	1.27010771430373
F	0.85642703305036	-3.99983882784821	-1.73965912215380
F	0.20423390615995	-3.68702313092865	0.26865761387120
F	1.65710480467032	-2.38264063618538	-0.59621941849478
H	-5.65788522282486	0.31431920187773	-6.39079905376808
H	-7.27864651315831	-0.75281691001392	-4.82889942752034
C	-5.30095517384108	-0.29148686876581	-5.55840238142808
C	-6.20549717878983	-0.88401606973222	-4.69480901286841
O	-7.87951151242903	-2.18568318511338	-2.73925401155969
C	-3.93149113350048	-0.46514395312319	-5.36169415566709
H	-3.22189152024358	0.01224725501307	-6.03691722541454
C	-5.74039456524128	-1.65606487242952	-3.62779664775628
C	-6.68382752331148	-2.27302222319800	-2.67314365455227
C	-3.46543618696544	-1.23346702074540	-4.30448772002204
C	-4.37278274279743	-1.82997894994969	-3.43881514967100
H	-6.19031933592930	-2.84771356169701	-1.85339989888653
H	-2.39786773642160	-1.35291520164642	-4.13235921006775
H	-4.00951268966433	-2.41067541558855	-2.59236382228693

SM + 1nN

F	-5.15955053513071	-3.17818395487899	2.03781538656458
C	-3.94581554284050	-3.16287795769304	1.48349589033549
C	-3.28891558877207	-1.75468682925982	1.52130721989950
C	-3.34818778272230	-1.13654954390285	2.95086381228015
F	-4.58480065760770	-0.89421590382047	3.37371046386147
F	-2.77476398079930	-1.91140476306956	3.86188944147904
F	-2.70504299333038	0.01826875476493	2.95260083220550
C	-3.97151535427257	-0.79800345938647	0.54515560911800
C	-5.33297363859812	-0.51695002865942	0.47721887288894
C	-5.78531161740227	0.39694385751614	-0.46587817404079
C	-4.88688684449241	1.02976791090311	-1.31698603986834
C	-3.52979762661945	0.75209651234944	-1.22949707775425
C	-3.05751676173280	-0.17242271114173	-0.29861987417467
Si	-1.26720041486970	-0.73946540166641	-0.01410393588096
O	-0.61410067796626	0.51764922709485	-1.11683950075079
C	0.36734442317695	1.34567216878183	-0.68380170262048
C	1.48222737273825	1.36263330446037	-1.76376933540111
F	1.00401715911121	1.62604418536380	-2.96771360628814
F	2.42807909036451	2.27270137642495	-1.51970720619052
F	2.08227600400082	0.19009256683499	-1.82018588770643
C	-0.25585083571134	2.75717621770637	-0.47570590520338
F	-1.22686096093934	2.68012816798797	0.41725013078023
F	0.61577563763811	3.65754139099016	-0.02990573642752
F	-0.78063901276540	3.25008167564187	-1.58881310342950
C	0.89615254721879	0.83648432470669	0.65644362752233
C	0.13618661116104	-0.21903034779425	1.15239259320847
C	0.49180281764922	-0.78411975738735	2.37619903592390
C	1.58358847910289	-0.29832729952999	3.08160337698083
C	2.32597047876502	0.76291076540332	2.57589657876204
C	1.98481510069832	1.34144834130088	1.36140214033083
C	-0.76065791180419	-2.26185518786049	-1.25337719249313
F	-0.40361325908625	-1.82248123050798	-2.48112744540152
C	0.38511229880771	-3.18053157076731	-0.78006034472037
F	-1.83254150570364	-3.06890818098696	-1.45198040327141
O	-1.98287092328519	-1.88303618872881	1.17961065383886
F	-3.22257230007191	-4.06524480226733	2.11823825953745
F	-4.09361781247649	-3.57588213340033	0.23646950802052
H	-6.05205391476840	-0.99871766096911	1.13568167657905
H	-6.85117449186392	0.60964072822009	-0.53992106394262
H	-5.25014262048129	1.73934344311809	-2.05977449732917
H	-2.83139452435534	1.25151530028913	-1.89734307415058
H	-0.08753628899842	-1.61434454440742	2.77484778122950
H	1.85907201463989	-0.74830507434157	4.03534447902314
H	3.18019560118373	1.14695255686358	3.13334649814690
H	2.57374568808276	2.17405260704565	0.98390300864896
F	0.65408317359295	-4.13158087083788	-1.67070497320978
F	0.08870633913600	-3.77930238076597	0.35765516340264
F	1.49532677686565	-2.48729404056164	-0.59692986842065
H	-5.52131364121399	0.13720698800350	-6.92245959934074
H	-7.02555255416417	-0.80257586585717	-5.17174387748530
C	-5.10316147854227	-0.30870485668536	-6.02066438665288
C	-5.94307935580318	-0.83008567081324	-5.05121148455368
O	-7.46497676762468	-1.97081445620365	-2.87158055045120
C	-3.72116116669047	-0.34892973254178	-5.84216921255235
H	-3.06468485829937	0.06881959357073	-6.60539072286624
C	-5.39931150966485	-1.39486659821966	-3.89604018927229
C	-6.26574748840508	-1.93838083758839	-2.82826789242712
C	-3.17607924433422	-0.91293421408245	-4.69658979382125
C	-4.01852831320127	-1.43697474654969	-3.72533256010354
H	-5.69873968777839	-2.32308314507461	-1.94828642625356
H	-2.09904233080718	-0.93751697502386	-4.54333049100759
H	-3.59969283793865	-1.87011311470919	-2.81820445510414

SM + 2nN

F	-4.45463506482324	-4.19560850176222	0.57140527441297
C	-3.22470354280708	-3.78748568787964	0.24992757533710
C	-2.91550886768059	-2.34957852184810	0.74643755778666
C	-3.20007402103513	-2.20478673068775	2.27205523308645
F	-4.48129929223934	-2.37342098471725	2.58669241015000
F	-2.50783478183210	-3.06742855862692	3.00305519682899
F	-2.85867924036742	-0.99116574474001	2.66700094858214
C	-3.73367485390787	-1.29717175028925	-0.00212285941023
C	-5.11644348567283	-1.27639704400489	-0.16232575823754
C	-5.69963002061141	-0.21953679801306	-0.84791760586074
C	-4.91357865976732	0.80995354553315	-1.35112402498410
C	-3.53690706349914	0.78610289203930	-1.17369688974951
C	-2.93132791648513	-0.27384565142612	-0.49911750423337
Si	-1.08350159835815	-0.53375877808027	-0.15202111332401
O	-0.66505263912105	1.11243685783511	-0.71398503121250
C	0.09156116385572	1.91670708081655	0.07286595499518
C	1.21594170926551	2.51993713117192	-0.81092238443609
F	0.74037669474790	3.06302894785163	-1.91577637030035
F	1.91274959430623	3.47136623406716	-0.18359201321283
F	2.07451482078176	1.58291677127959	-1.16183305235514
C	-0.83958346581435	3.02053566983325	0.65480554939010
F	-1.82373224495209	2.45115709895617	1.32883698139533
F	-0.21834576898823	3.84637818517184	1.49249394517141
F	-1.38896208407407	3.77159338495951	-0.28861374851256
C	0.66397210946537	1.09337839004251	1.22544344306847
C	0.12417433631708	-0.18871358337615	1.27045224168638
C	0.54150812738583	-1.05909456274558	2.27636375545469
F	0.27451482078176	1.58291677127959	-1.16183305235514
C	-0.83958346581435	3.02053566983325	0.65480554939010
F	-1.82373224495209	2.45115709895617	1.32883698139533
F	-0.21834576898823	3.84637818517184	1.49249394517141
F	-1.38896208407407	3.77159338495951	-0.28861374851256
C	0.66397210946537	1.09337839004251	1.22544344306847
C	0.12417433631708	-0.18871358337615	1.27045224168638
C	0.54150812738583	-1.05909456274558	2.27636375545469
F	0.10578476269192	-0.56563611016700	-2.76486203193706
C	-0.17553928009696	-1.45300637427921	-1.78811503733642
F	0.10578476269192	-0.56563611016700	-2.76486203193706
C	1.12753923224687	-2.21743105972281	-1.49289916475698
F	-1.02693027472394	-2.35258882895412	-2.34164247582062
O	-1.59597189430901	-2.11412158230027	0.54308819327434
F	-2.38531429046646	-4.67595476156115	0.74776370570953
F	-3.13537514996645	-3.85588301269315	-1.06717155173084
H	-5.74992884185007	-2.06649741494532	0.23461850208343
H	-6.77889981185764	-0.20370245849423	-0.99565989917486
H	-5.37764166384774	1.63400359722212	-1.89214648882968
H	-2.92535570620246	1.59724283115879	-1.56486812320514
H	0.13500949502417	-2.06712216375289	2.32180301057996
H	1.80979770609882	-1.33552522605699	3.99088586984689
H	2.73864832088710	0.96100013275542	3.58429403175319
H	2.01492661644581	2.52419115321248	2.14366561574439
F	1.63753687058039	-2.78262330610747	-2.58429442470119
F	0.92788276340983	-3.17952619214907	-0.60996085428430
F	2.04654846915623	-1.40279602922216	-1.00482809706570
H	-7.81896694644954	-0.98397432035431	-5.14396209619803
H	-5.93685132776430	0.60780662209111	-5.50394482489235
C	-6.83360165109506	-1.19558266271319	-4.72952644691268
C	-5.79061914887577	-0.30840966881112	-4.93296038818086
O	-3.49759799381686	1.39274779657538	-5.20380452635991
C	-6.62374422518461	-2.35890866855823	-3.99160891266122
H	-7.44750026221250	-3.05351327179716	-3.82828318044202
C	-4.53076971098728	-0.58217889983975	-4.39715326617366
C	-4.81032866603865	0.36806472901720	-4.58556338863276
C	-5.37221004685132	-2.63442807984502	-3.45887396542381
C	-4.32481376177150	-1.74541364569127	-3.66186366351065
H	-4.45392065887475	0.05931020346490	-4.61309837478266
H	-5.20887493276537	-3.53509755933756	-2.87075323508431
H	-3.34453740740372	-1.94711238669259	-3.23295879874838

Int1

F	1.43769418251217	-3.64635109429338	4.23373315068356
C	1.27048832476660	-3.45180124602111	2.91899759922687
C	1.07277204266674	-1.93593818761172	2.57068696104631
C	2.05383522940836	-1.08611241441835	3.44515015777357
F	1.72461970267019	-1.07135644279155	4.73692358416869
F	3.30122721382541	-1.53030743753333	3.37386379207753
F	2.05942044863583	0.16845412867168	3.04815981800723
C	-0.37748248428775	-1.50628168425333	2.80536432308386
C	-1.07616135998640	-1.66100237860630	4.00029163540418
C	-2.40272647851299	-1.26046593156099	4.07091962997952
C	-3.02227926752513	-0.71544973108490	2.95300875695534
C	-2.31379656823447	-0.56859244621933	1.76715201013170
C	-0.97765249449570	-0.95672952091490	1.66991324677390
Si	0.30259165412557	-0.84518504596120	0.21252242519500
O	1.43993393478172	-0.75642015648292	-1.16630972299011
C	2.32040083158453	0.27517347884609	-1.27594783009039
C	3.75930044436955	-0.25559957615036	-1.00176626710275
F	4.09116107589875	-1.23738747873087	-1.82616026206336
F	4.68719638996856	0.69527043793747	-1.14821854798784
F	3.86595459599486	-0.70487302771734	0.22569353047919
C	2.21022835779506	0.82890285090244	-2.72537686944707
F	1.03185029428665	1.42676450642854	-2.90173407661926
F	3.13176133965856	1.74047547764190	-3.02264501018755
F	2.29782008642990	-0.11815532057824	-3.64091649395458
C	1.94202422186207	1.36915210204813	-0.27328736631114
C	0.87426216559234	0.98968025781352	0.53100455011589
C	0.36038725444680	1.92778776116330	1.42509378965262
C	0.91823250377800	3.19438497459682	1.52773514515813
C	2.01073181981726	3.54082211790629	0.73925607134313
C	2.53014941504405	2.62818486917875	-0.16778531362457
C	-0.53949848702010	-2.53473252800437	-0.70743056130099
F	-1.77277682641401	-2.28675037139482	-1.25986742965578
C	0.22066432705593	-3.31715822004062	-1.79826772418576
F	-0.78396434908232	-3.44193214832816	0.26263860591192
O	1.39324344882352	-1.74314374801336	1.26290813976515
F	2.32707107353857	-3.95908890033780	2.31787052702445
F	0.22729574216167	-4.18055525982065	2.57658808843054
H	-0.60967281123211	-2.09816319002943	4.88060386939450
H	-2.95614936067717	-1.38175903360420	5.00212073892214
H	-4.06739228562440	-0.40804253560852	3.00733106111608
H	-2.82316516279615	-0.14413843644203	0.90236525943349
H	-0.48368319467055	1.66178076345652	2.06341552093500
H	0.50712334255521	3.91640871934404	2.23422719533859

Int1 + 1nN

F	1.43961649826348	-3.64789316599325	4.23294707972126
C	1.27213926330617	-3.45261814150670	2.91829622222631
C	1.07398776153454	-1.93663014940253	2.57077616176748
C	2.05572050409834	-1.08708796338057	3.44481300874029
F	1.72760809036624	-1.07305860966128	4.73691220270602
F	3.30309599781468	-1.53108323513686	3.37224800311708
F	2.06080185998807	0.16766865080392	3.04852515432622
C	-0.37610285462957	-1.50720934531204	2.80706563546542
C	-1.07382217744137	-1.66251494385284	4.00247119425179
C	-2.40028445578906	-1.26186968139763	4.07442161950580
C	-3.02076225143396	-0.71616030767649	2.95733938355429
C	-2.31325953288710	-0.56873336902936	1.77094455623863
C	-0.97720988789736	-0.95691314334722	1.67250251129029
Si	0.30111778533308	-0.84450310421393	0.21395778007419
O	1.43818668163193	-0.75561497614674	-1.16542098576440
C	2.31875265745633	0.27584628573866	-1.27290203200252
C	3.75775287080993	-0.25543642977730	-1.00212535047405
F	4.08835942401981	-1.23771005338460	-1.82643052854672
F	4.68606784237432	0.69491918691282	-1.14986610881470
F	3.86556026631717	-0.70421128408184	0.22541858838964
C	2.20799377237463	0.83024472577904	-2.72424642303726
F	1.02934594942898	1.42765573180488	-2.90030181891331
F	3.12905638107437	1.74225805253892	-3.02138281559601
F	2.29569966715833	-0.11641664485476	-3.64036872443046
C	1.94128480735759	1.36941163045507	-0.27171981770461
C	0.87384588681041	0.98993464544040	0.53304068569448
C	0.36108810431363	1.92770000615102	1.42811902875258
C	0.91972808809729	3.19392631888392	1.53133298851680
C	2.01189903824693	3.54031017167365	0.74239502854282
C	2.53019424339529	2.62801448378042	-0.16565572982967
C	-0.54157907532330	-2.53362530106551	-0.70622058989966
F	-1.77495432854151	-2.28515604835016	-1.25813985857768
C	0.21788419778355	-3.31569304990875	-1.79783939434304
F	-0.78604558936124	-3.44143702550083	0.26337009394247
O	1.39326888536505	-1.74331564734991	1.26280421608262
F	2.32874686377064	-3.95939698928172	2.31672389329158
F	0.22910642392215	-4.18149016390269	2.57569928147182
H	-0.60665637027315	-2.10027011181940	4.88212865247878
H	-2.95289714008643	-1.38356970786181	5.00605470480537
H	-4.06579758445241	-0.40867703729965	3.01277929203652
H	-2.82308442496857	-0.14381027159278	0.90667666939368
H	-0.48272692698988	1.66175178996588	2.06679693072174
H	0.50946002063224	3.91560497498150	2.23866932522949

Int1 + 2nN

F	1.44303903220788	-3.65164929217929	4.22835507730148
C	1.27486486405602	-3.45405017967234	2.91413798773966
C	1.07569086163269	-1.93763067520235	2.56945040001943
C	2.05916153733214	-1.08938979407395	3.44282634700135
F	1.73361184522340	-1.07732943231112	4.73561307160697
F	3.30644422033735	-1.53323319794705	3.36726774228170
F	2.06352051811757	0.16594827867604	3.04842622355617
C	-0.37392683031532	-1.50867532476233	2.80956943895975
C	-1.06926259889113	-1.66590642153316	4.00613471248413
C	-2.39558214523987	-1.26540411031532	4.08137141422998
C	-3.01830124811435	-0.71784901142797	2.96643339795768
C	-2.31319920759871	-0.56847426383847	1.77886420773747
C	-0.97735880869984	-0.95658184583618	1.67715002210228
Si	0.29708971529588	-0.84219890170104	0.21554531790630
O	1.43209010127797	-0.75219597974546	-1.16615919709931
C	2.31415965810304	0.27805678544662	-1.27279367063302
C	3.75268870869598	-0.25610063338436	-1.00501432427172
F	4.08039677184248	-1.23739755504901	-1.83167185706065
F	4.68238135220752	0.69299456212751	-1.15245121700400
F	3.86167300179936	-0.70724415320487	0.22152296816251
C	2.20268475160750	0.83556861123621	-2.72295785699393
F	1.02520760389664	1.43624247417399	-2.89627216502759
F	3.12539153612811	1.74587410888887	-3.01995685961590
F	2.28654952504215	-0.10964977087460	-3.64101375301423
C	1.93970822427336	1.37036460322197	-0.26912091544306
C	0.87252929551140	0.99123905860371	0.53615909382327
C	0.36222507297366	1.92838428263980	1.43329129489764
C	0.92308067899753	3.19349487661112	1.53806671379841
C	2.02068475160750	0.83556861123621	-2.72295785699393
F	1.02520760389664	1.43624247417399	-2.89627216502759
F	3.12539153612811	1.74587410888887	-3.01995685961590
F	2.28654952504215	-0.10964977087460	-3.64101375301423
C	1.93970822427336	1.37036460322197	-0.26912091544306
C	0.87252929551140	0.99123905860371	0.53615909382327
C	0.36222507297366	1.92838428263980	1.43329129489764
C	0.92308067899753	3.19349487661112	1.53806671379841
C	2.01503585096220	3.53941106368726	0.74861283535448
C	2.53082286051835	2.62779228766182	-0.16155389345694
C	-0.54673481553225	-2.53057686498935	-0.70496541614904
F	-1.77812016581110	-2.28099193589200	-1.26089612686737
C	0.21446378656776	-3.31534482722213	-1.79350932041600
F	-0.79550785928417	-3.43674301098189	0.26506430153787
O	1.39214877967391	-1.74232241214536	1.26110751076953
F	2.33153741458751	-3.95920265786804	2.31121214801562
F	0.23215982963620	-4.18289141388750	2.57051592286300
H	-0.60033866928090	-2.10504606447804	4.88415877277505
H	-2.94629274777181	-1.38865143428248	5.01393254481588
H	-4.06321791757417	-0.41043341119269	3.02456100707787
H	-2.82445017919303	-0.14211282046078	0.91616758285574
H	-0.48140565371824	1.66282205425597	2.07237473595234
H	0.51472173071074	3.91464977570334	2.24704708117588

H 2.45900645290645 4.53047796437069 0.82656100521336 H 3.38089732430446 2.91990943843625 -0.78027068421162 F -0.40750694383610 -4.45771157690062 -2.10523149892612 F 1.43741220300879 -3.64196688090037 -1.41992696032878 F 0.30003446783651 -2.63021024931499 -2.93355993898112 H -0.89999776861556 -0.37872838876557 -2.79744505822140 H -2.13285424775499 0.55264206377347 -4.60718860489681 C -1.34940198890014 0.32272998564909 -2.07191902502653 O -1.12880913454460 0.22790827762663 -0.88727869242656 C -2.54254892237677 1.34093503740725 -3.97506839402616 C -2.22470473622662 1.36501468996883 -2.61882162713280 H -3.62503672410397 2.29354747828425 -5.57133148921989 C -3.37199175718571 2.31432137631415 -4.51252336916093 C -2.72628210610759 2.37826136281018 -1.79861750869822 C -3.87334953806852 3.31818593156216 -3.69359333898030 H -2.45126237907160 2.39818125470663 -0.74454669411266 C -3.54820095511393 3.35194249540469 -2.34004543488151 H -4.52024791913806 4.08742162541735 -4.11440630777708 H -3.93820566050724 4.14739916076851 -1.70684308621181	H 2.46090159945908 4.52959629573344 0.83019277161599 H 3.38081301428074 2.91969811302974 -0.77834062495214 F -0.41070943791101 -4.45591471260851 -2.10500451620232 F 1.43484464001465 -3.64093279113234 -1.42065930028335 F 0.29655554284331 -2.62818679180669 -2.93298741592286 H -0.90032696732287 -0.37944065263729 -2.79797127059698 H -2.12968439035552 0.55337470623887 -4.61202606867019 C -1.35106062356114 0.32396881357999 -2.07601957963598 O -1.13050685441414 0.23067658575229 -0.88351181969100 C -2.54050556565948 1.34131211297162 -3.98023778546975 C -2.22508772546943 1.36524640175156 -2.62316773905936 H -3.62019559422289 2.29398235502416 -5.57822184660411 C -3.36932917062718 2.31450666001306 -4.51890835053260 C -2.72868736603308 2.37826214056741 -1.80365497923871 C -3.87269855675441 3.31787684861200 -3.70056781416866 H -2.45547142066871 2.39792833098315 -0.74916400478056 C -3.55015273955108 3.35154409522988 -2.34634758447032 H -4.51915483961329 4.08687907192482 -4.12248926150003 H -3.94174079530380 4.14651166395187 -1.71355760923843	H 2.46580540299111 4.52778785163871 0.83762995305452 H 3.38126279557174 2.91911566536203 -0.77467555870848 F -0.41402689627021 -4.45593684601540 -2.09941385364392 F 1.43066065152131 -3.64012961515976 -1.41366297853278 F 0.29533218178939 -2.63025750707825 -2.93008022479472 H -0.89646519788069 -0.37838314973984 -2.79191860674518 H -2.11772139191336 0.55362407012813 -4.61628470366130 C -1.35270977579755 0.32742874811195 -2.07682839221610 O -1.13714024765972 0.23658256319378 -0.87496601244095 C -2.53307915910713 1.34105956874770 -3.98688917825803 C -2.22461038407385 1.36618269491101 -2.62801934183673 H -3.60620121412835 2.29103980530009 -5.59077238136017 C -3.36078554299744 2.31251528744600 -4.53021333900476 C -2.73426296799221 2.37888410461351 -1.81158003001893 C -3.87006123097147 3.31540576099748 -3.71491467985298 H -2.46643061853118 2.39917913925802 -0.75577533497988 C -3.55454801462767 3.35034770462003 -2.35904559065023 H -4.51568337185815 4.08306199324976 -4.14053901326279 H -3.95072530025597 4.14495627794166 -1.72868403479331
TS F 0.80770 -4.03916 3.53784 C 0.97906 -3.49571 2.32644 C 0.89179 -1.93967 2.36882 C 1.79012 -1.39138 3.52421 F 1.34683 -1.72962 4.73294 F 3.04097 -1.81285 3.44090 F 1.81478 -0.07196 3.48753 C -0.53529 -1.43370 2.56118 C -1.40707 -1.82949 3.57034 C -2.67163 -1.26370 3.63472 C -3.05290 -0.30453 2.70499 C -2.17502 0.08346 1.70326 C -0.90219 -0.47780 1.61356 Si 0.51976 -0.16224 0.38506 O 1.54067 -0.31054 -1.02049 C 2.59376 0.56119 -1.12813 C 3.91191 -0.25861 -0.99589 F 3.97623 -1.24365 -1.87288 F 4.99632 0.49820 -1.18321 F 4.01000 -0.77399 0.20765 C 2.48581 1.23592 -2.52704 F 1.42314 2.02934 -2.57039 F 3.53586 1.99290 -2.82995 F 2.35183 0.35303 -3.50052 C 2.51791 1.62330 -0.02681 C 1.46411 1.40808 0.85615 C 1.23586 2.33414 1.86876 C 2.06084 3.44125 2.00854 C 3.12842 3.62767 1.13667 C 3.36451 2.72105 0.11244 C -1.25690 -2.02572 -1.11247 F -2.42279 -1.82895 -1.85224 C -0.44699 -2.99532 -1.96579 F -1.69643 -2.72698 -0.03220 O 1.37231 -1.45548 1.19186 F 2.15460 -3.90349 1.88891 F 0.05729 -4.01230 1.54937 H -1.12527 -2.57890 4.30675 H -3.36461 -1.57819 4.41462 H -4.04825 0.13681 2.75550 H -2.50098 0.82498 0.97797 H 0.40502 2.18840 2.55999 H 1.87799 4.16421 2.80373 H 3.78360 4.49106 1.25022 H 4.20033 2.88765 -0.56312 F -1.07570 -4.13921 -2.27805 F 0.68781 -3.33824 -1.38488 F -0.13786 -2.42254 -3.13819 H -0.37816 -0.07684 -2.38591 H -1.98334 -0.20489 -4.13765 C -1.03998 0.54455 -1.77399 O -0.69727 0.93736 -0.65513 C -2.60288 0.55986 -3.67126 C -2.25491 1.04693 -2.41131 H -4.01601 0.64052 -5.28668 C -3.74169 1.02855 -4.30712 C -3.05498 2.01020 -1.79275 C -4.53337 1.98884 -3.68893 H -2.77576 2.39331 -0.81244 C -4.18862 2.48091 -2.43358 H -5.42880 2.35774 -4.18863 H -4.81151 3.23422 -1.95327	Int2 F -2.37772759345955 -4.41269599461044 3.09835573529078 C -1.91408233841028 -3.78833699257514 2.01344786637626 C -1.66146359589013 -2.27692569417210 2.25805313494080 C -0.73881748283964 -2.03030326127641 3.48348071958171 F -1.28398623410588 -2.43770456527538 4.62874393815201 F 0.42803842302818 -2.64192470345391 3.37721696618620 F -0.50571333672597 -0.73641901265801 3.60694775759178 C -2.98608993858429 -1.53733474510310 2.44840052860813 C -3.95941028483897 -1.80819772082967 3.40948711380951 C -5.11814787518673 -1.04544186127034 3.42383059062633 C -5.29907781800337 -0.02788833810757 2.49084225197456 C -4.31728840046460 0.22584105440543 1.54367242354920 C -3.14238062442879 -0.52532775361563 1.51220161801368 Si -1.61702296231024 -0.39332463787843 0.33098903594304 O -0.17361301705350 -0.40961871783736 -0.73225649664347 C 0.79467709971502 0.52490742288227 -0.57069723615284 C 2.09020972401773 -0.19222741133089 -0.09716472859280 F 2.44621261083554 -1.16596556937853 -0.91684309775814 F 3.13621939840205 0.63370081471388 -0.00572826501267 F 1.91002943752353 -0.71381665294696 1.09805937916614 C 0.99873397822543 1.23556853561710 -1.93943534420188 F -0.09514215421257 1.91472257402329 -2.25321471558646 F 2.00466026507469 2.10560904255550 -1.94610138681485 F 1.22482815321966 0.38133439964626 -2.92574746634301 C 0.34148912302266 1.55948766552017 0.45992212798251 C -0.92828430452623 1.27774713472901 0.95360909842101 C -1.47813104060289 2.14358478743339 1.89741096858974 C -0.78248576229571 3.26847689450746 2.31866204999668 C 0.48602071143714 3.52988297290654 1.81434763116328 C 1.05976097199320 2.67376598413398 0.88420204625133 C -3.01657283102298 -1.73163120101969 -3.07055106915006 F -3.10528218013067 -1.50868956141821 -4.39679151421367 C -2.09173375083781 -2.96861813994090 -2.91728961464335 F -4.23632434106850 -2.07663250210314 -2.64620002306658 O -1.01190340486098 -1.79155407540224 1.15862823135668 F -0.82239802185063 -4.42994571859936 1.64121946519580 F -2.81733972945649 -3.94703736558877 1.06449364775070 H -3.84008037503631 -2.60301450862414 4.14221295548053 H -5.88918183698472 -1.24949427839093 4.16652301637023 H -6.21454853349323 0.56466193233725 2.50499845608568 H -4.46534619456553 1.02501130728299 0.81476155040759 H -2.45853790758361 1.92891331695281 2.32172115213003 H -1.22566632835478 3.94023345869542 3.05394867468988 H 1.03933436224017 4.40576829035335 2.15304699497239 H 2.05758225765685 2.88997365013679 0.51031440538325 F -2.60339750854851 -4.00044421983215 -3.57918816213686 F -1.93598371783185 -3.32996507186030 -1.66860225687952 F -0.90270062610868 -2.71223745269678 -3.43638477861106 H -1.48005323457741 -0.31032842268264 -2.69589943048729 H -1.90468323891141 1.29025537811891 -4.37072585519513 C -2.52311920989815 -0.44874763034362 -2.36791359243389 O -2.65403649881930 -0.59814717026025 -1.01178112889337 C -2.87471877421062 1.50892575557056 -3.92577657710452 C -3.33923298519692 0.72498963072372 -2.87421858991058 H -3.24317455950190 3.18318909409047 -5.22075431661700 C -3.62619674339659 2.57498428749885 -4.40183894179837 C -4.57192147292578 1.02800036809009 -2.29952423203533 C -4.85578214410163 2.86961341849716 -3.82833739227813 H -4.93981083069869 0.42826167765743 -1.46872300143682 C -5.32428229849957 2.09323027689419 -2.77558245673810 H -5.44648275266453 3.70742016119043 -4.19819462223888 H -6.28688972131472 2.32011966391827 -2.31789523906282	

List of coordinates for the cation overview

[Cs][Si(C$_2$F$_5$)L$_2$]

F	-5.68233835103709	-0.61569250955607	-2.50368727001748
C	-4.72664756926034	-1.24945920151939	-1.82932149349762
C	-4.05855770007357	-0.34698655624309	-0.75553187732954
C	-5.10819699053426	0.28345007352093	0.20897526873161
F	-5.96710783028479	1.08233356716231	-0.40846121165501
F	-5.81015850554190	-0.63361065076362	0.85051438988968
F	-4.47654689007828	1.01193668344703	1.11520688421331
C	-3.25150449371288	0.77701378485354	-1.39798923792592
C	-3.73273206211876	1.69927367541181	-2.32303679990706
C	-2.89704359983818	2.71108389323968	-2.77269767601772
C	-1.60439934563028	2.81936584837729	-2.27680305574549
C	-1.14080219773158	1.89806682527925	-1.34688353531805
C	-1.94665717065477	0.84540174985025	-0.90992581427603
Si	-1.56723984162726	-0.56910165117587	0.30974440692910
O	0.14830224193029	0.05194264689431	0.59728997710126
C	0.55286119182838	0.29197221016198	1.87800951211764
C	1.83272778547935	-0.55141762305912	2.15931943464479
F	2.71361167416404	-0.44547544374485	1.14674166927768
F	2.47630205301939	-0.18691072818692	3.25322965364010
F	1.53826804462863	-1.82576337490902	2.27262403073793
C	0.83126135223777	1.81724542889599	1.98654096148383
F	-0.27914142494140	2.48631492905638	1.75846660791399
F	1.29830264673853	2.19967638835685	3.15972577265714
F	1.72372796362101	2.20654882697613	1.06448994563283
C	-0.55352532818202	-0.12367200424724	2.83926727178473
C	-1.67949313536657	-0.61860579505733	2.18692938251360
C	-2.74870252207857	-1.08022423938369	2.95302519901956
C	-2.68833840994626	-1.03323743332517	4.33804007235464
C	-1.56265173498145	-0.52054977787839	4.97188689159016
C	-0.48456839366174	-0.06290762121750	4.22742752967997
C	-0.81251851108379	-2.17950357386991	-0.59708058877153
F	0.51233906665387	-2.36988506778061	-0.32271897051485
C	-1.46088649069527	-3.56063063459087	-0.31868279906188
F	-0.83626193621309	-1.96752019268301	-1.94769900756810
O	-3.22077764456022	-1.11907587530613	-0.00809252171451
F	-5.27233550710625	-2.32372109568955	-1.30070346569030
F	-3.82315227744568	-1.63774195077515	-2.71192248683834
H	-4.75076468420381	1.65124258063024	-2.70058987939620
H	-3.26815482887322	3.43259632966261	-3.49921380070265
H	-0.96354926988950	3.63861300138096	-2.60205552709140
H	-0.14684486044389	2.04663115524206	-0.92955348601432
H	-3.63092993384402	-1.48728929975325	2.46494764056031
H	-3.52634574797165	-1.39878832676177	4.92996838972163
H	-1.51961037413628	-0.47968317100386	6.05944252548155
H	0.38912781282026	0.32677560992554	4.74516236594879
F	-0.65926640766930	-4.54219918887627	-0.71506036224305
F	-2.60346968972244	-3.71730591691882	-0.93900979134919
F	-1.65222679003462	-3.69991477104901	0.98132935927300
Cs	1.81103661805376	-0.12611153299962	-1.74104448425271

[NEt$_4$][Si(C$_2$F$_5$)L$_2$]

F	-5.13889691510632	-0.08735172159425	-2.66585752386848
C	-4.25994786842786	-0.73437455993796	-1.90255696772848
C	-3.75534629257385	0.12741175118081	-0.71172243206743
C	-4.93380315971190	0.68629071505447	0.14138216010745
F	-5.74057339685221	1.48801238337057	-0.54215901416490
F	-5.67971538246558	-0.27791669707876	0.65289356809030
F	-4.44256751299292	1.39004397260390	1.14726944825009
C	-2.90778554697886	1.29833137516776	-1.20213534543193
C	-3.30919249153041	2.27185365769027	-2.11358840459978
C	-2.45048307040220	3.32039814797019	-2.40885336532500
C	-1.21314907558005	3.40450695573771	-1.78153542769703
C	-0.82668327931637	2.42601568197954	-0.87625173627852
C	-1.65896347144145	1.34496206568189	-0.58483270994542
Si	-1.37671906399433	-0.11103694213806	0.61770220086727
O	0.25665227741055	0.53250591846970	1.12376923835223
C	0.49318252780994	0.74174104869991	2.44945352704826
C	1.79723203704773	-0.00908237860106	2.83880447688968
F	2.80585934999848	0.28927966839431	2.01675333033797
F	2.21951606540491	0.27263478684075	4.06407787185222
F	1.61549210926912	-1.31058842250709	2.77233113881077
C	0.62308367210771	2.27620291921469	2.67665150708474
F	-0.50107679955787	2.87165194372120	2.33035432397879
F	0.88141339633786	2.60910862441840	3.93064245535059
F	1.59630115129798	2.81184209707514	1.93322816866079
C	-0.68487192232994	0.21263282966924	3.26423432496831
C	-1.72297450750177	-0.25364555811415	2.46376510714322
C	-2.86000910467530	-0.77937981039757	3.07548726170813
C	-2.95224083434573	-0.82561448346527	4.45837782279568
C	-1.91185370540788	-0.34321980977556	5.24370999049207
C	-0.77023810104186	0.17988026340558	4.65351723801317
C	-0.57190979669447	-1.73597053247844	-0.20450090291828
F	0.75418410242062	-1.85816470521256	0.06121987592785
C	-1.16357806080746	-3.11955708165537	0.17236941683236
F	-0.64627493236706	-1.64181927064779	-1.56325309892772
O	-2.99540195779824	-0.65708306594566	0.09534769870005
F	-4.83905267010591	-1.84693745916026	-1.50329379504488
F	-3.24417681346344	-1.06144906531406	-2.68394793371700
H	-4.28339752872286	2.23812259711220	-2.59444805865653
H	-2.76028226589976	4.08817353410628	-3.11682068554974
H	-0.55556286922223	4.25020700424787	-1.98625675211248
H	0.13733521291922	2.51526653302847	-0.38259646576526
H	-3.67526038636406	-1.16732881457383	2.46901641655639
H	-3.84158203051727	-1.24180547273121	4.92985154579896
H	-1.98692862473436	-0.37695545782908	6.32993440717931
H	0.03066186194198	0.54896744297504	5.28956409619477
F	-0.35843315167943	-4.09468064859475	-0.24080445340445
F	-2.34011838786533	-3.33399814845252	-0.36677945373811
F	-1.27417346338159	-3.22509002024298	1.48494807165442
N	2.89607679246640	0.75498867243206	-2.12040109114813
C	3.83128786319390	1.02635692774404	-3.25463539614760
C	2.94322985013339	1.85745569488243	-1.08488118977274
C	3.26747775387404	-0.50093577013938	-1.36890411896933
C	1.46172416801465	0.67784695251160	-2.61299771901959
H	1.08289134272815	1.70235153054468	-2.65062395448080
H	0.90670931440609	0.18358035076058	-1.81444734443752
C	1.18383551485446	0.01795058361047	-3.94389936807268
C	2.85132461684573	3.27267040093987	-1.60828437710316
H	3.86760772348773	1.72515764128444	-0.51182619647269
H	2.12309404793076	1.64262496267371	-0.38958188358689
H	3.73852961114738	3.58951254814941	-2.16720567567660
H	2.76524784283068	3.93438803679414	-0.74027272100719
H	1.96787923008970	3.45405424139939	-2.22953790485290
C	3.21294505928981	-1.80460311684533	-2.12760938981982
H	4.27246412949879	-0.33031728140199	-0.96791906074450
H	2.58976852565181	-0.53702309514263	-0.51189900789713
H	3.83473930744935	-1.82065090755664	-3.03018618695250
H	2.19393542781336	-2.10415841468888	-2.38232565763533
H	3.60239196227543	-2.57881431522325	-1.45871286561256
C	5.28606785875208	1.19766667143128	-2.87426968834315
H	3.72540927564683	0.20534136486369	-3.96891272691251
H	3.45955830015333	1.92554304771301	-3.75895170663514
H	5.73921535169075	0.27894298732372	-2.48792386392299
H	5.45002380794578	1.99743796205824	-2.14435171163332
H	5.84251863072458	1.46973875889590	-3.77726904757303
H	1.59255448218555	0.57035886251007	-4.79636818018414
H	0.09425964791803	0.01676620259997	-4.05712566285728
H	1.50517323889352	-1.02348529149252	-4.01116846522577

Cs

Cs	1.81103661805376	-0.12611153299962	-1.74104448425271

NEt$_4$

N	2.87856599178367	0.75126977749263	-2.10833679258688
C	3.81942400006085	1.01988437301152	-3.25108187996992
C	2.93882982803151	1.86651378529680	-1.08411696667895
C	3.25787475877023	-0.50596778284479	-1.36074291880301
C	1.44321984824404	0.67271699662017	-2.60010822313087
H	1.06964781259134	1.70119949702275	-2.63093274723527
H	0.88477855349257	0.16157168003282	-1.80646588347903
C	1.17740254873911	0.03077910775879	-3.94465323961538
C	2.86003675101168	3.27931055835385	-1.61771130891930
H	3.86524549825248	1.73181001901975	-0.51445418379730
H	2.11466257724158	1.67072823168937	-0.38696365954634
H	3.74877942508313	3.57620595822852	-2.18319218141977
H	2.79486067339231	3.95246893052405	-0.75666252985101
H	1.97643814686692	3.47496833056331	-2.23413226506427
C	3.24110919453759	-1.80682279371051	-2.12864372517555
H	4.25634724198814	-0.32595000214722	-0.94795713330715
H	2.57378496367024	-0.55914103881869	-0.50507875116562
H	3.88154481143271	-1.80208584021931	-3.01717640958186
H	2.23733437146688	-2.12954520170397	-2.41659647222000
H	3.63879338979660	-2.57983371304348	-1.46269417282711
C	5.27451197022436	1.18300131690943	-2.87102262233918
H	3.70766780371359	0.19921514210667	-3.96435251941584
H	3.44892339921383	1.92045077359274	-3.75328178192560
H	5.72848867922998	0.26246030088762	-2.48992449719861
H	5.45058712524070	1.98498184511492	-2.14645113350430
H	5.82686287900602	1.45055944697449	-3.77788605164457
H	1.59341154823750	0.59900658172658	-4.78182627395318
H	0.09072511652740	0.02787229816737	-4.08316162725689
H	1.50809109215303	-1.00687857860620	-4.02689204838723

Mechanistic study (Chapter 3)

Mol.	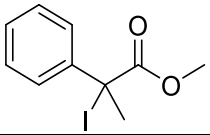	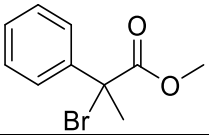	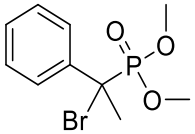	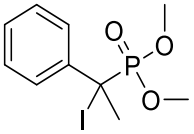	
Coord.	C -5.08498 0.68359 0.04827 C -3.61680 1.00728 -0.18121 C -2.70333 0.18790 0.73615 O -3.13279 -1.05622 0.86996 C -2.35625 -1.94177 1.65173 O -1.73107 0.61334 1.28038 I -3.12025 0.25023 -2.21475 C -3.27826 2.47769 -0.12775 C -4.24212 3.41765 0.23455 C -3.93147 4.77067 0.31589 C -2.64909 5.21005 0.03449 C -1.67882 4.28378 -0.33210 C -1.98807 2.93753 -0.41364 H -5.29248 -0.38089 -0.07754 H -5.72316 1.23594 -0.64819 H -5.37672 0.96092 1.07083 H -2.88415 -2.89920 1.65558 H -2.24423 -1.58534 2.68384 H -1.35521 -2.08522 1.22420 H -5.25835 3.11102 0.46775 H -4.70574 5.48160 0.60089 H -2.40442 6.26958 0.09455 H -0.66714 4.61381 -0.56311 H -1.21040 2.24053 -0.71795	C -5.10004 0.68938 0.07168 C -3.63315 1.00163 -0.18576 C -2.72277 0.19159 0.75098 O -3.10612 -1.07067 0.83343 C -2.33055 -1.94507 1.62891 O -1.79248 0.64292 1.34441 Br -3.19846 0.31507 -2.00540 C -3.28583 2.47387 -0.13772 C -4.23078 3.42094 0.24972 C -3.90648 4.77171 0.31698 C -2.62896 5.19833 -0.00331 C -1.67714 4.26273 -0.39375 C -2.00004 2.91867 -0.46092 H -5.31139 -0.37567 -0.04683 H -5.74428 1.24220 -0.61931 H -5.37475 0.97315 1.09621 H -2.80204 -2.92910 1.56151 H -2.30533 -1.62701 2.67931 H -1.29763 -2.01515 1.26389 H -5.24229 3.12265 0.51265 H -4.66583 5.49064 0.62145 H -2.37314 6.25578 0.04638 H -0.66929 4.58387 -0.65234 H -1.23656 2.21205 -0.77930	C -0.87825 -2.37790 2.07829 C 0.34381 -1.73508 1.42933 P 0.83298 -0.31945 2.49952 O 2.15254 0.21347 1.78990 C 2.97196 1.20269 2.37959 O -0.25605 0.80216 2.13073 C -1.23810 1.28034 3.02506 O 0.92693 -0.60710 3.94061 Br 1.81545 -3.04206 1.56547 C 0.14103 -1.31144 -0.01263 C -1.14708 -1.16845 -0.52917 C -1.35296 -0.73350 -1.83237 C -0.27440 -0.43318 -2.64845 C 1.01336 -0.57329 -2.14696 C 1.22000 -1.00532 -0.84682 H -0.65627 -2.70064 3.09946 H -1.21077 -3.24553 1.49797 H -1.71415 -1.66987 2.13460 H 3.92854 1.20272 1.84784 H 3.15889 0.99466 3.44139 H 2.52142 2.20054 2.28526 H -1.25738 2.37562 2.97693 H -1.03780 0.97654 4.06060 H -2.23010 0.90908 2.73409 H -2.01976 -1.39266 0.07858 H -2.37019 -0.63271 -2.20789 H -0.43471 -0.09560 -3.67137 H 1.87287 -0.34729 -2.77644 H 2.24019 -1.10950 -0.48649	C -0.86694 -2.37343 2.11691 C 0.34406 -1.73491 1.44286 P 0.87849 -0.34382 2.51958 O 2.26903 0.09695 1.88767 C 3.03816 1.14729 2.43957 O -0.08131 0.86921 2.08507 C -1.19671 1.29972 2.83379 O 0.86069 -0.62956 3.96394 I 1.94668 -3.24126 1.52385 C 0.11094 -1.29429 0.01400 C -1.18255 -1.24799 -0.50831 C -1.41957 -0.79355 -1.80009 C -0.36815 -0.37749 -2.59988 C 0.92572 -0.42473 -2.09513 C 1.16280 -0.87709 -0.80792 H -0.62868 -2.69904 3.13280 H -1.21918 -3.23798 1.54427 H -1.69796 -1.65947 2.19124 H 4.05801 1.05140 2.05398 H 3.07320 1.09225 3.53580 H 2.64058 2.12725 2.14228 H -1.26547 2.39076 2.75634 H -1.11313 1.02625 3.89380 H -2.12493 0.87148 2.43016 H -2.03515 -1.56763 0.08523 H -2.44040 -0.76992 -2.17887 H -0.55315 -0.02377 -3.61308 H 1.76568 -0.11058 -2.71316 H 2.18745 -0.91419 -0.44603	O 2.60652 0.08243 -0.06375 N 3.85829 0.08613 -0.07639 O 4.47383 -0.56437 0.79836 C 4.52948 0.77545 -1.01329 C 3.80281 1.55793 -2.04973 C 6.01748 0.78847 -1.02879 H 7.72144 1.44950 -1.93277 H 4.06345 1.24287 -3.07965 H 4.03829 2.64060 -2.01065 H 6.41984 0.16316 -0.22792 H 6.43682 1.80684 -0.90173 H 6.43595 0.42054 -1.98669

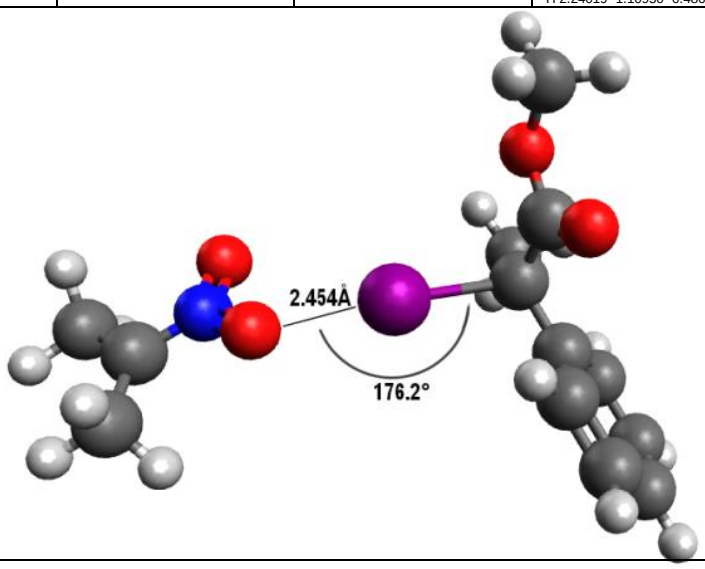

C 2.06311 3.82528 -3.05947
C 3.42582 3.27827 -3.46298
C 4.53577 3.72853 -2.55630
O 4.11374 3.91913 -1.30079
C 5.08421 4.19833 -0.32620
O 5.68217 3.90221 -2.86567
I 3.32857 1.03221 -3.05519
C 3.77743 3.50509 -4.90999
C 2.99066 4.31424 -5.73225
C 3.31775 4.53489 -7.06654
C 4.44672 3.95082 -7.61601
C 5.24066 3.13839 -6.81287
C 4.91103 2.91597 -5.48682
H 1.80291 3.54319 -2.03668
H 1.28243 3.41792 -3.71180
H 2.01876 4.92404 -3.12376
H 4.55389 4.30558 0.62571
H 5.63481 5.12655 -0.53608
H 5.81758 3.38495 -0.23069
H 2.09912 4.79438 -5.33566
H 2.67718 5.17223 -7.67624
H 4.70449 4.11800 -8.66156
H 6.12723 2.65975 -7.22818
H 5.53524 2.25605 -4.89000
O 3.29808 -1.40382 -2.76209
N 2.22935 -1.91926 -2.26414
O 1.50121 -1.23278 -1.52717
C 1.95107 -3.17710 -2.55048
C 2.86198 -3.94065 -3.45284
C 0.73825 -3.76846 -1.91420
H 3.05348 -3.41540 -4.39975
H 2.42162 -4.91634 -3.69443
H 3.85529 -4.13258 -3.01379
H -0.18659 -3.23510 -2.18677
H 0.77743 -3.74208 -0.81300
H 0.61945 -4.81635 -2.21695

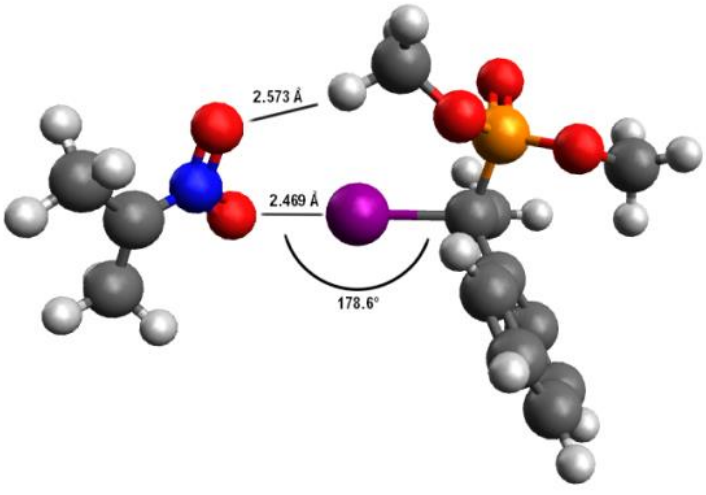

C -4.57800 1.82799 1.59832
C -4.32247 0.68012 0.62517
P -4.05578 1.37837 -1.04855
O -3.26116 0.32801 -1.94369
C -1.88217 0.44103 -2.26853
O -5.46884 1.24868 -1.83050
C -6.57249 2.01973 -1.44425
O -3.51251 2.75276 -1.02657
I -2.33841 -0.22638 1.21536
C -5.36653 -0.40225 0.64822
C -6.45479 -0.34847 1.52388
C -7.41919 -1.35102 1.54791
C -7.32500 -2.43578 0.69195
C -6.24712 -2.50651 -0.18490
C -5.28436 -1.51231 -0.20492
H -3.78169 2.57339 1.53154
H -4.60376 1.45851 2.63066
H -5.52935 2.34770 1.40676
H -1.77261 0.24839 -3.34315
H -1.28802 -0.28562 -1.70047
H -1.49774 1.44558 -2.05198
H -7.27738 2.05735 -2.28403
H -6.29204 3.05364 -1.19095
H -7.10011 1.57741 -0.58431
H -6.56001 0.48432 2.21512
H -8.24976 -1.27654 2.24991
H -8.07722 -3.22367 0.70993
H -6.14824 -3.35519 -0.86117
H -4.44351 -1.60660 -0.88884
O -0.20084 -1.26200 1.89010
N 0.44773 -1.81449 0.92771
O 0.55147 -1.22497 -0.16694
C 1.00408 -2.99050 1.13904
C 0.84090 -3.64379 2.47103
C 1.80592 -3.58001 0.02820
H -0.21271 -3.71075 2.77774
H 1.35494 -3.10671 3.28522
H 1.24883 -4.66198 2.44465
H 1.21951 -3.69864 -0.89612
H 2.18809 -4.56806 0.31312
H 2.67198 -2.95820 -0.25195

The end

EurJIC
European Journal of Inorganic Chemistry

Review
doi.org/10.1002/ejic.202101109

Chemistry Europe
European Chemical Societies Publishing

www.eurjic.org

Special Collection

Bis(catecholato)silicates: Synthesis and Structural Data

Alexandre Millanvois,[a] Cyril Ollivier,*[a] and Louis Fensterbank*[a]

Dedicated to Professor Rinaldo Poli on the occasion of his 65th birthday.

This minireview provides an overview of the synthesized bis(catecholato)silicates based on the nature of the alkyl or aryl residues and associated cations as well as the methods developed for this purpose. Structural and analytical data such as the ^{29}Si NMR shift of silicon penta- and hexacoordinate derivatives, selected examples of crystal structures by X-ray diffraction analysis and oxidation potentials of silicates are reported. Some aspects of reactivity are also mentioned.

1. Introduction

Hypercoordinate silicon compounds have attracted the attention of molecular chemists for decades. While penta- or hexacoordinate species are the most encountered ones, hepta coordination has also been reported.[1] Ease of synthesis and stability, specific geometrical features and reactivities of these compounds are generally the observed properties.

Overall, these derivatives have been extensively studied, and several reviews were published,[2a–f] including a comparison between hypercoordinate phosphorus and silicon species.[2e] From these reviews, and in particular that of Rendler and Oestreich,[2g] it can be pointed out that a tetravalent silane with latent Lewis acid character brought by the L ligands can be converted to a hypercoordinate species *via* two main processes. First, the direct interaction of the tetravalent silicon center with an additional neutral ligand can occur inter- or intramolecularly to form a weak dative bond. The intermolecular interaction has been observed with a donor compound or solvent (such as MeCN or DMF) leading to the hypercoordinate derivative. The intramolecular interaction has been mainly observed with a bidentate ligand. These derivatives often take advantage of weak N···Si or O···Si dative bonds. The second common way to obtain a penta- or hexacoordinate species is by forming a covalent bond between silicon and a negatively charged ligands such as an halide (e.g. F, or Cl) or alkoxy groups (e.g. O-Alkyl or O-Aryl). The case of hexacoordinate silicon species usually requires electronegative substituents such as fluorine as in related pentafluorosilicates,[2f] these attracting groups facilitating polyaddition on the silicon center (Figure 1).

Hypercoordination induces a modification of the physicochemical properties, the main one being the Lewis acidity. This property gradually increases as follows, tetravalent < pentavalent < hexavalent. Indeed, the increase of the coordination leads to the decrease of the electron density at silicon and thus to the increase of its Lewis acidity. Moreover, the nucleophilicity of the substituent (R=C or H) is also modified by the coordination of the silicon center. The nucleophilicity of the R substituent and that of the ligands is first increased at the pentavalent state and even more when the silicon reaches the hexacoordination.[2g]

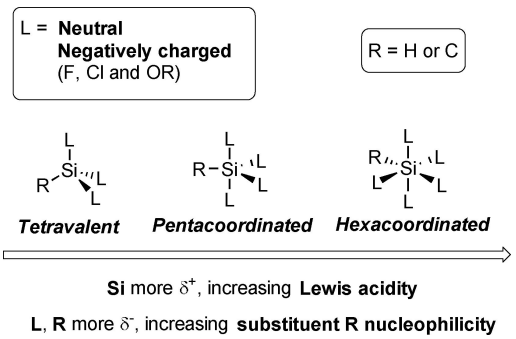

Figure 1. Hypercoordinate silicon species: from tetra- to hexacoordinate.[2g]

Beyond the well-known pentafluorosilicates,[2f] bis(catecholato) derivatives occupy a particular situation and have recently witnessed intensive use in organic synthesis, particularly as powerful alkyl radical precursors under photo-oxidative conditions.[3] To accompany these developments, this minireview will focus on the access to this specific class of compounds and will summarize their syntheses, structural and analytical data. Few aspects of reactivity will be also mentioned.

2. Synthesis of bis(catecholato)silicates

2.1. Foreword

Contrary to other pentacoordinate silicates such as those originating from Martin's spirosilane (bearing the dianion of hexafluorocumyl alcohol), alkyl and aryl bis(catecholato)silicates cannot be prepared from the corresponding spirosilane by addition of nucleophiles onto the electrophilic silicon center.[4,5] Bis(catecholato)silane indeed exists only in solution as an insoluble oligomer.[6] Of note, the tris(catecholato)silicate dianion has also been described but despite a recent highly

[a] A. Millanvois, Dr. C. Ollivier, Prof. L. Fensterbank
Sorbonne Université, CNRS, Institut Parisien de Chimie Moléculaire
4 Place Jussieu, CC 229, F-75252 Paris Cedex 05, France
E-mail: cyril.ollivier@sorbonne-universite.fr
louis.fensterbank@sorbonne-universite.fr

Special Collection *Part of the "Celebratory Collection for Rinaldo Poli".*

Review
doi.org/10.1002/ejic.202101109

interesting report by Greb[7a] its chemistry has so far been limited in terms of applications (Figure 2).

We will focus on the bis(catecholato)silicate derivatives[7b] and will not deal with silicates derivatives based on substituted catechols, perhalo and others, as nicely developed by Greb.[7c–d] All chemical structures of bis(catecholato)silicates will be numbered in bold and listed in Table 1. Their synthesis usually occurs under mild conditions. Trichloro- or trialkoxysilanes are often used as starting materials but alkoxysilanes are preferably chosen in order to prevent the *in-situ* generation of HCl (Scheme 1). A trichlorosilane derivative bearing the desired moiety can be converted into the alkoxysilane on a large scale. In this case, the formation of a trimethoxysilane simplifies the purification by distillation due to the lower boiling point of these silanes compared to the corresponding triethoxy- or triisopropoxysilanes.

By simply mixing two equivalents of catechol in basic conditions with the trichloro- or trialkoxysilanes, the hypercoordinated silicates can be obtained. They are generally purified from the reaction medium by crystallisation using a non-polar solvent. Several protocols will be now discussed (Scheme 2).

Thus, it was also described by Sakurai and coworkers[8] that a solution of di-deprotonated catechol (dilithium-catecholate) could be prepared before adding it to a THF solution of allyl(trichloro)silane. The corresponding lithium allyl bis(catecholato)silicate (**14 Li**) was not isolated but directly engaged to react quantitatively in an allylation reaction (Scheme 3).

Another pathway for the synthesis of bis(catecholato)silicates has been developed by Tacke and coworkers.[9] While the classical reaction is generally based on the elimination of methoxide or chloride anions, Tacke described here the use of less reactive substituents such as a methyl or a phenyl as leaving groups allowing the formation of the desired silicate by the introduction of catechol on the silane (Scheme 4). Based on this methodology and by the extrusion of methane, benzene and methanol from (dimethylamino)methyl)methoxy(methyl) phenylsilane, (dimethylammonio)methyl

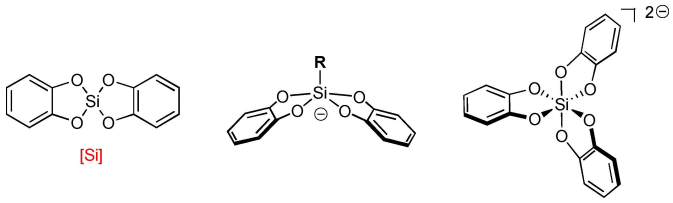

Figure 2. Spirosilane, bis(catecholato) and tris(catecholato) species.

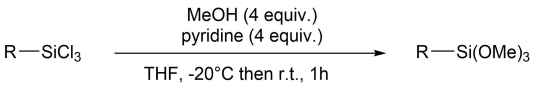

Scheme 1. Synthesis of trimethoxysilanes from trichlorosilanes.

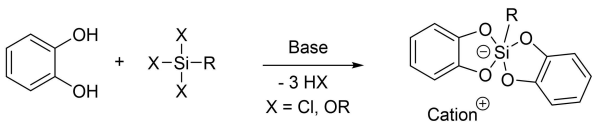

Scheme 2. General synthesis of bis(catecholato)silicates from trichloro- or trialkoxysilanes.

Louis Fensterbank obtained his PhD in 1993 at SUNY Stony Brook under the guidance of Scott Sieburth. After a lecturer position at the Université Pierre & Marie Curie (UPMC), he was appointed in 1995 as a CNRS Chargé de Recherche with Max Malacria. In 2004, he became Professor at UPMC, now Sorbonne Université. His research interests concern the discovery of new molecular transformations relying on radical or organometallic processes and their applications to the synthesis of substrates with relevant properties. Co-author of more than 220 publications, he has received several awards, notably the Silver Medal of CNRS in 2017. He is also Fellow of the Royal Society of Chemistry and senior member of Institut Universitaire de France.

Cyril Ollivier obtained his PhD in 2000 from the University of Fribourg (Switzerland) and UPMC under the guidance of Philippe Renaud in collaboration with Max Malacria. He was awarded a Swiss National Foundation Fellowship to work with Philippe Magnus at the University of Texas at Austin. In 2002, he was appointed Chargé de Recherche CNRS at Aix-Marseille University and in 2007, he moved to UPMC/Sorbonne University where he is now Directeur de Recherche to develop new directions for research on synthetic radical and organometallic chemistry including photocatalytic processes.

Alexandre Millanvois received his Bachelor (UPMC) and master's degree at Sorbonne Université (ex UPMC) with honour. He is currently conducting his joint PhD under the supervision of Prof. Louis Fensterbank, Prof. Tan Choon Hong and Dr. Cyril Ollivier between Sorbonne Université and Nanyang Technological University (NTU). His current research interests are focused on the synthesis of new silicon based radical precursor and their application in asymmetric radical chemistry.

Table 1. Silicate diversity, yield of synthesis and δ ^{29}Si NMR.

N°	Silicate	Cation	Yield	^{29}Si
1[a]	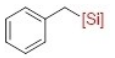	$HNEt_3$	92[32]	–
		K[18C6]	84[33]	*−80.90*
		K	54[13]	*−80.90*
		Na	55[13]	*−80.90*
		Na[15C5]	45[13]	*−80.80*
		Li	64[10]	–
2[a]		$HNEt_3$	96[32]	–
		K[18C6]	79[33]	*−77.93*
		H_2NMe_2	19[19]	–
		$H_2N(i\text{-}Pr)_2$	96[20]	–
		Na	55[13]	*−77.75*
3		$HNEt_3$	73[32]	–
		Na	90[11]	*−73.77*
		K	96[14]	*−74.32*
4	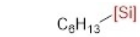	$HNEt_3$	88[32]	–
		K[18C6]	85[33]	*−75.6*
5	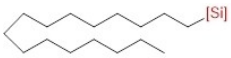	$H_2N(i\text{-}Pr)_2$	71[21]	–
6		$HNEt_3$	93[32]	–
		K[18C6]	93[33]	*−85.57*
7	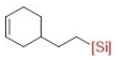	$HNEt_3$	86[32]	–
8	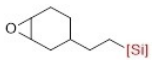	$H_2N(i\text{-}Pr)_2$	86[32]	–
		K[18C6]	85[33]	*−75.75*
9	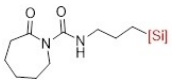	$H_2N(i\text{-}Pr)_2$	83[32]	–
		$HNMe_3$	73[25]	–
10	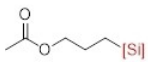	$HNEt_3$	95[32]	–
		K	62[15]	–
		K[18C6]	91[15]	*−76.6*
		Na	64[13]	*−76.36*
11	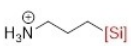	Ø	94[32]	–
			92[28]	–
12	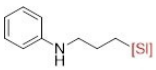	$H_2N(i\text{-}Pr)_2$	89[32]	–
		$P(Et)PPh_3$	85[29]	–
13[a]		K[18C6]	nd[34]	–
		$HNEt_3$	55[35]	*−79.15*
		Et_4N	68[36]	*−75.61*
			56[33]	
14		$HNEt_3$	55[36]	–
		K[18C6]	*quant.*[37,38]	*−80.24*
		PPN	84[33]	*−78.8*
		Li	*quant.*[8]	–
		Me_4N	*nd*[8]	–
15	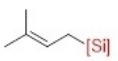	PPN	98[27]	*−77.3*
		Li	*nd*[8]	–
		$HNEt_3$	*nd*[8]	*−76.7*
16	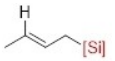	Li	*quant.*[37,38]	*−78.4*
		$HNEt_3$	*nd*[8]	–
17	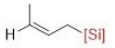	Li	*quant.*[38]	–
18		Li	*nd*[39]	–
19[a]		$HNEt_3$	*nd*[40]	–
		$H_2N(iPr)_2$	86[21,36]	–
		K[18C6]	91[33]	*−76.14*
20	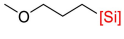	$HNMe_3$	88[25]	–
		$H_2N(i\text{-}Pr)_2$	86[36]	–
21	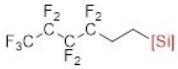	$H_2N(i\text{-}Pr)_2$	92[32]	–
22	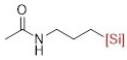	$H_2N(i\text{-}Pr)_2$	66[36]	–
23	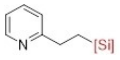	$HNEt_3$	91[32]	–
		$H_2N(i\text{-}Pr)_2$	nd[36]	–

Table 1. continued

N°	Silicate	Cation	Yield	^{29}Si
24	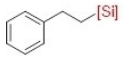	$H_2N(i\text{-}Pr)_2$	93[41]	–
25	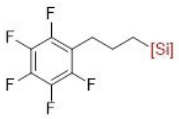	$H_2N(i\text{-}Pr)_2$	89[41]	–
26		$HNMe_3$	90[25]	–
		K[18C6]	90[15]	*−77.6*
		$H_2N(i\text{-}Pr)_2$	95[41]	–
		$H_2N(i\text{-}Pr)_2$	77[41]	–
27	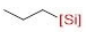	K[18C6]	91[42]	–
		$HNEt_3$	nd[40]	–
28	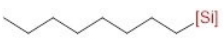	K[18C6]	85[42]	–
29		K[18C6]	88[42]	–
		K	29[14]	*−74.77*
30[a]	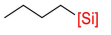	Et_4N	20[26]	–
31	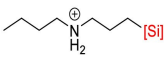	Ø	90[43]	–
			nd[11]	–
32		$H_2N(i\text{-}Pr)_2$	55[44]	–
33	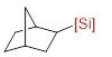	$H_2N(i\text{-}Pr)_2$	81[32]	–
		Et_4N	nd[45]	–
34	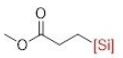	$H_2N(i\text{-}Pr)_2$	77[44]	–
35	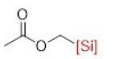	$HNMe_3$	60[25]	–
		K[18C6]	94[15]	*−85.8*
		$H_2N(i\text{-}Pr)_2$	76[43]	–
36	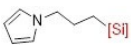	$HNMe_3$	82[25]	–
37	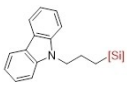	$H_2N(i\text{-}Pr)_2$	68[46]	–
38	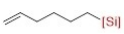	K[18C6]	50[33]	*−75.7*
		$HNMe_3$	90[25]	–
39	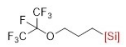	$HNMe_3$	68[25]	–
40	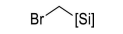	K[18C6]	88[42]	–
		$HNEt_3$	77[47]	–
41		$HNEt_3$	94[47]	–
42		$H_2N(i\text{-}Pr)_2$	97[48]	–
43		$H_2N(i\text{-}Pr)_2$	82[48]	–
44		$H_2N(i\text{-}Pr)_2$	86[48]	–
45		$H_2N(i\text{-}Pr)_2$	nd[49]	–
46		$H_2N(i\text{-}Pr)_2$	nd[49]	–
47		$H_2N(i\text{-}Pr)_2$	44[44]	–
48		K[18C6]	80[15]	*−78.6*
		$H_2N(i\text{-}Pr)_2$	92[43]	–
49		$H_2N(i\text{-}Pr)_2$	67[46]	–
50		$H_2N(i\text{-}Pr)_2$	93[21]	–
51		K[18C6]	71[33]	*−78.51*
52		K[18C6]	85[33]	*−81.36*
53		K[18C6]	92[33]	*−76.13*
54[a]		$HNEt_3$	93[32] 78[23] 91[24] 88[50]	*−87.53*
		K[18C6]	54[51] 50[14]	*−87.83*
		PPh_4	87[33]	–
		Na	91[28]	*−87.4*
		K	90[11]	*−87.51*

Review
doi.org/10.1002/ejic.202101109

Table 1. continued

N°	Silicate	Cation	Yield	^{29}Si
		H_3NPh	65[14]	–
		H_3NBn	nd[52]	–
		ImH	nd[53]	–
		2-Me-ImH	nd[53]	–
		DMAP-H	nd[53]	–
		Piperidinium	nd[53]	–
		$HNEt_3$	nd[53]	*−87.0*
			80[26a]	
55	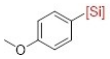	K[18C6]	85[33]	*−87.60*
		$HNEt_3$	86[50]	–
56[a]		Et_4N	39[33]	*−76.21*
			84[26b]	*−75.8*
57[a]	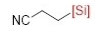	K[18C6]	83[33]	*−80.17*
58		K[18C6]	95[15]	*−76.9*
		$H_2N(i\text{-}Pr)_2$	nd[48]	–
59	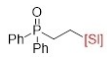	K[18C6]	72[54]	*−78.10*
60	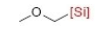	K[18C6]	64[45]	*−82.2*
61	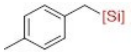	K[18C6]	12[45]	*−80.6*
62[a]	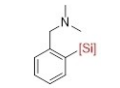	H	27, 37[55]	–
		PPN	67[56]	*−121.2*
63	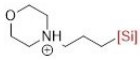	Ø	31,40,94[57]	*−76.9*
			65[58]	
64[a]		Ø	82, 83[57]	*−85.8*
			92[58]	
65	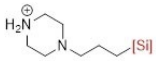	Ø	71[43]	–
66[a]	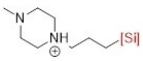	Ø	78[58]	*−85.8*
67	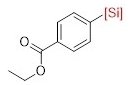	$HNEt_3$	89[50]	–
68	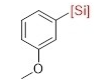	$HNEt_3$	94[50]	–
69	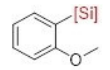	$HNEt_3$	82[50]	–
70	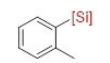	$HNEt_3$	83[50]	–
71	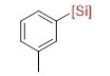	$HNEt_3$	90[50]	–
72	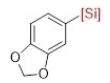	$HNEt_3$	82[50]	–
73	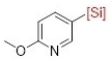	$HNEt_3$	94[50]	–
74	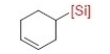	H_3NiPr	76[18]	–
75	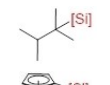	Et_4N	nd[18]	–
76	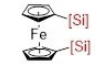	2 K	81[59]	*−78.63*
77	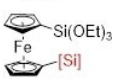	K	81[59]	*−80.27*

Table 1. continued

N°	Silicate	Cation	Yield	^{29}Si
78[a]	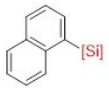	Et_4N	87[26b]	*−84.9*
		$HNEt_3$	81[26b]	–
		PPh_4	89[60]	–
		Na	90[11]	*−84.64*
79[a]		Ø	98[9]	*−84.8*
			nd[55]	*−85.9*
80[a]		Ø	*quant.*[61]	–
81		K	98[62]	–
82[a]		$H_2N(C_6H_{11})_2$	94[22]	*−133.5*
83[a]	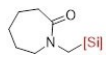	$H_2N(C_6H_{11})_2$	*quant.*[22]	*−132.5*
84[a]	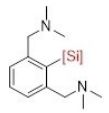	H	39[31]	*−134.9*
		K	98[31]	*−129.8*
		PPN	55 (84)[31]	*−127.2*
85	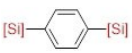	$HNEt_3$	55[51]	*−87.0*
86	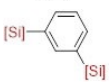	$HNEt_3$	49[51]	*−86.7*
87[a]	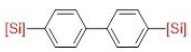	$HNEt_3$	30[51]	*−87.4*
88		HNE	69[51]	*−81.7*
89	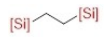	$HNEt_3$	75[51]	*−73.7*
90	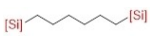	$HNEt_3$	55[51]	*−71.9*
91	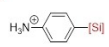	Ø	89[29]	–
92[a]		K	99[63]	–
			65[64,65]	
93[a]	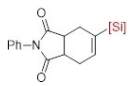	K	99[63–65]	–
94	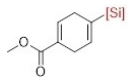	K	nd[63]	–
95		K	nd[63]	–
96		K	78[64,65]	–
97		K	78[64,65]	–
98		K	nd[63]	–
99		K	nd[63]	–
100		K	nd[63]	–

Table 1. continued

N°	Silicate	Cation	Yield	^{29}Si
101	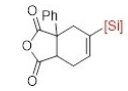	K	nd[63]	–
102	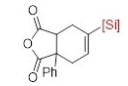	K	nd[63]	–
103	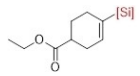	K	94[64]	–
104	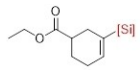	K	94[64]	–
105	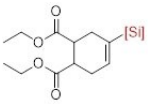	K	70[64]	–
106		K Na K[18C6] NH_4	81[12] 82[12] 88[12] 86[12]	*−110.7* *−112.6* *−110.4* *−111.5*
107	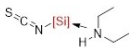	K Na K[18C6] H_2NEt_2 $K.Me_2SO_3$ $Na.Me_2SO_3$ K[18C6] NH_4	84[12] 81[12] 74[12] 78[12] 53[12] 51[12] 75[12] 86[12]	*−142.7* *−140.7* *−156.2* *−141.3* *−99.8* *−99.9* *−99.1* –
108				
109		PPh_4	85[30]	–
110[a]		$PPh_3Ph(4\text{-}OH)$	85[30]	–
111		$H_2N(i\text{-}Pr)_2$	nd	–
112		$H_2N(i\text{-}Pr)_2$	nd	–
113	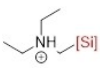	$H_2N(i\text{-}Pr)_2$	nd	–
114		$HNEt_3$	*quant.*[38]	–
115		$H_2N(i\text{-}Pr)_2$	nd[48]	–
116	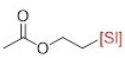	$H_2N(i\text{-}Pr)_2$	nd[49]	–
117		$HNEt_3$	nd[66]	–
118	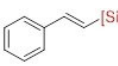	$HNEt_3$	nd[66]	–
119		$HNEt_3$	nd[66]	–
120	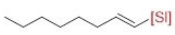	$HNEt_3$	nd[66]	–
121		$HNEt_3$	88[50]	–
122		$H_2N(i\text{-}Pr)_2$	nd[67]	–
123[a]	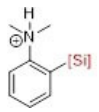	Ø	nd[9]	*−88.6 (Solid NMR)*
124[a]	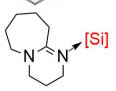	Ø	nd[68]	*−98.7*
125	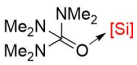	Ø	nd[68]	*−107.3*

Table 1. continued

N°	Silicate	Cation	Yield	^{29}Si
126	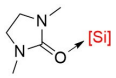	Ø	nd[68]	*−104.5*

[a]: X-Ray crystal structures are reported.

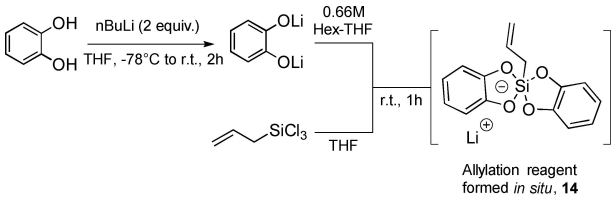

Scheme 3. Formation of lithium allyl bis(catecholato)silicate from allyl(trichloro)silane.

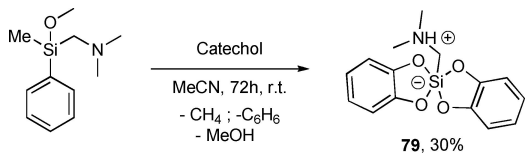

Scheme 4. Synthesis of (dimethylammonio)methyl bis(catecholato)silicate from [(dimethylamino)methyl)]methoxy(methyl)phenylsilane.

bis(catecholato)silicate (**79**) was obtained in 30% yield and isolated directly from the reaction medium thanks to the *in-situ* crystallisation of the zwitterionic species.

This type of route remains an exception and we will now present more general methodologies to access various silicates with different cations, recognizing that the counterion can be inorganic or organic.

2.2. Silicate Synthesis

2.2.1. Alkali-Silicate

In this section, we deal with bis(catecholato)silicate flanked with an alkali metal counterion (Figure 3).

As previously reported in Scheme 3, lithium silicates were mainly described for the synthesis of allyl derivatives by Sakurai (Scheme 5A).[8] But more recently, our group synthetized lithium benzyl bis(catecholato)silicate (**1 Li**) by addition of a homemade lithium methoxide solution in methanol on benzyltrimeth-

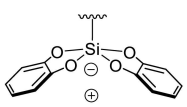

Figure 3. Alkali based bis(catecholato)silicates.

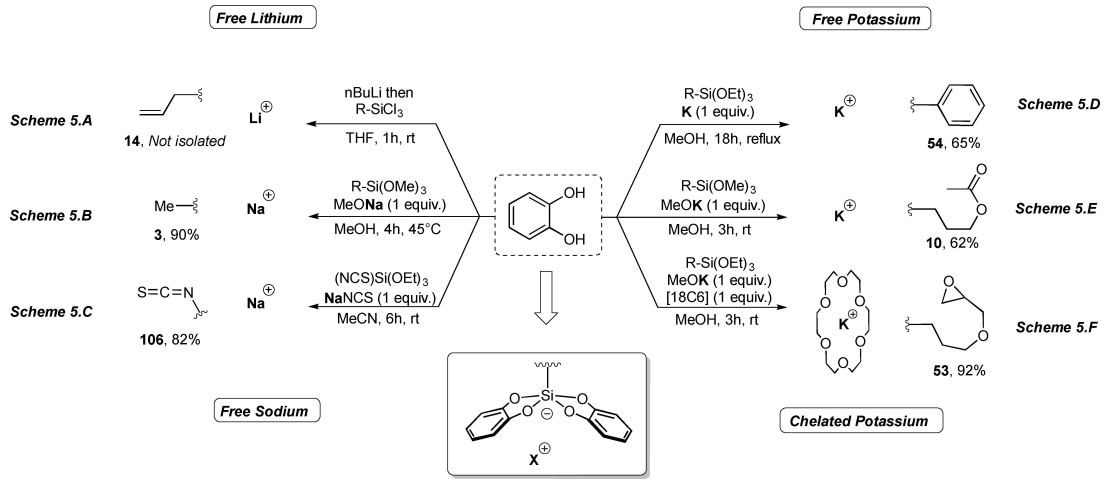

Scheme 5. Synthesis of alkali alkyl and aryl bis(catecholato)silicates.

oxysilane and catechol. The silicate was isolated in 64% yield after recrystallisation from acetone by slow addition of ether.[10] This derivative appears more stable than the previously described lithium allyl bis(catecholato)silicate.

Most of sodium derivatives have been prepared by Corriu and coworkers.[11] The synthesis of sodium methyl bis(catecholato)silicate (**3 Na**) (Scheme 5B) was reported using a solution of methyltrimethoxysilicate and sodium methoxide in methanol and afforded the silicate in 90% yield. Although sodium derivatives are quite rare, an interesting synthesis was achieved by Narula and coworkers.[12] Their methodology cleverly used the cation (K, Na, K[18C6]) of an isothiocyanate salt to easily access to different types of isothiocyanato bis(catecholato)silicate derivatives (**106**) in good yields, including the desired sodium one (**106 Na**) (Scheme 5C). Recently, new sodium silicates (sodium benzyl-, acetoxypropyl- and cyclohexyl- bis(catecholato)silicates **1 Na**, **10 Na** and **2 Na**) from the corresponding alkyl trimethoxy- and triethoxysilane were synthetized and used in modern organic synthesis by our group.[13] Their synthesis required conventional inert techniques and a homemade sodium methoxide solution from elemental sodium. Once crystallised, this type of hypercoordinated derivatives gains stability and can be stored on the bench.

Several other silicates with a potassium cation are found in the literature. Preparation of these derivatives can be achieved by directly using the potassium metal to generate the alkoxide *in situ* from the alcoholic solvent, in most cases methanol.[14]

This synthesis methodology was applied for instance for the synthesis of potassium phenyl bis(catecholato)silicate (**54 K**) from phenyl triethoxysilicate and catechol (Scheme 5D). Otherwise, a commercially available alkoxide solution such as potassium methoxide is commonly used for the synthesis of potassium silicates including potassium acetoxypropyl bis(catecholato)silicate (**10 K**) from acetoxypropyl trimethoxysilicate in Scheme 5E[15] even if the scope is quite broad.

To facilitate the crystallisation of potassium derivatives and stabilise hypercoordinated silicon derivatives, our group, inspired by the work of Hey-Hawkins and Tamao respectively on silicate[16] and organofluorosilicates,[17] has shown the value of using 18-crown-6 as an additive.[15] To the best of our knowledge, crown ethers have only been involved for the synthesis of potassium silicates and there is no example of a 12-crown-4 lithium silicate and only one example of a 15-crown-5 sodium silicate that we recently reported.[13] A representative example consists in the synthesis of potassium [18-crown-6] (3-glycidoxypropylpropyl) bis(catecholato)silicate (**53 K[18C6]**) as shown in Scheme 5F.

2.2.2. Ammonium-Silicate

Ammonium-based silicates are the most commonly encountered. Due to their huge diversity, several methodologies have been developed over the years. Herein, we divide these species in two categories based on their synthetic pathways, by the direct synthesis using the amine as base or by cation metathesis. Compared to the other silicates presented above, the formation of ammonium silicates requires refluxing conditions for 24 h. The crude product has to be completely dried under high vacuum for several hours to facilitate the crystallisation and the purification of these species.

2.2.2.1. Ammonium-Silicate (Primary, Secondary and Tertiary)

A special attention will be made on the non-quaternary ammoniums of Scheme 6 that imply a distinct synthetic procedure. To avoid the formation of ammonium hydrochloride salts in the reaction medium, alkoxysilanes are preferable. As shown on Scheme 6, a great variety of amines could be used for the synthesis of ammonium-based silicates.

Nevado *et al.*[18] have described the only example of isopropylammonium (cyclohex-3-en-1-yl) bis(catecholato)silicate (**74 H_3NiPr**). The synthesis starts with the transformation of

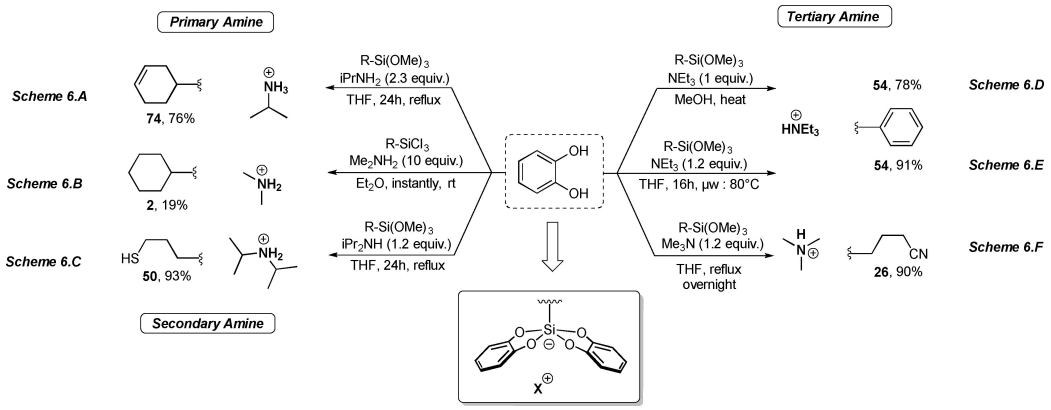

Scheme 6. Synthesis of ammonium alkyl and aryl bis(catecholato)silicates.

cyclohex-3-en-1yl (trichloro)silane to the corresponding trimethoxysilane as described above (Scheme 1). Then, reaction with catechol and isopropylamine in THF at reflux led to the desired silicate in 76% yield, after evaporation and cleanse with diethyl ether and pentane (Scheme 6A).

A dimethylamine ammonium derivative has also been reported only once by Holmes and coworkers.[19] Using a trichlorosilane substrate as a precursor placed in ether with dimethylamine at room temperature, a poor yield of cyclohexyl bis(catecholato)silicate product (**2 H_2NMe_2**, 19%) was obtained due to the difficulty to get rid of the dimethylammonium salt generated during the reaction (Scheme 6B). On the other hand, diisopropylammonium silicates can be considered as the main derivatives that this family can count.

While several methodologies can be highlighted, a reproducible one was published by Molander in *Organic Synthesis* in 2017.[20] As a representative example, the synthesis of the biisopropylammonium 3-mercaptopropyl bis(catecholato)silicate (**74 $H_2N(iPr)_2$**) prepared from the corresponding trimethoxysilane was obtained in 93% yield (Scheme 6C).[21]

The last secondary ammonium silicates presented in this review were synthetized by Korlyukov and coworkers in 2008.[22] Following a new methodology that required a higher temperature (130 °C) and a non-polar solvent (xylene), they prepared for the first time dicyclohexylammonium [(N-methyl-acetamido)methyl-C,O] bis(catecholato)silicate (**82 $H_2N(cHex)_2$**) in very good yield (94%) from (N-methyl-acetamido)methyl-C,O trimethoxysilane (Scheme 7). This study also corresponded to the first use of dicyclohexylamine as a base for its synthesis.

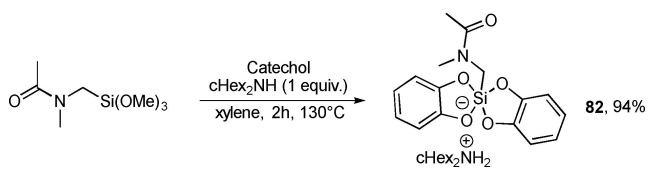

Scheme 7. Synthesis of dicyclohexylammonium [(N-methyl-acetamido)methyl-C,O] bis(catecholato)silicate from (N-methyl-acetamido)methyl-C,O trimethoxysilane.

Triethylammonium is the main counterion found for tertiary ammonium silicates. In addition to reporting the first example of bis(catecholato)silicate, C. L. Frye[23] was also the first to use triethylamine as the base for the synthesis of triethylammonium phenyl bis(catecholato)silicate (**54 $HNEt_3$**] from the corresponding trimethoxysilane (Scheme 6D). Hashmi and coworkers showed that the reaction can be run in THF at 80 °C under microwave irradiation for 16 h (Scheme 6E).[24]

The last example of tertiary ammonium silicate was reported by Molander[25] relying on the same type of methodology based on the use of triethylamine. Herein is presented the synthesis of trimethylammonium 3-cyanopropyl bis(catecholato)silicate (**26 $HNMe_3$**) from the starting trimethoxysilane using a THF solution of Me_3N to afford the silicate in 90% yield (Scheme 6F).

2.2.2.2. Ammonium-Silicate (Quaternary)

Due to the straightforward accessibility of the other ammonium silicates described above, only a few examples of silicates bearing a quaternary ammonium can be found. There are two major ways to produce quaternary ammonium bis(catecholato)silicates:

By ammonium exchange. The usual method for forming quaternary ammonium bis(catecholato) organosilicates is based on a cation exchange reaction. Holmes and coworkers[26b] proposed a synthesis of tetraethylammonium *tert*-butyl bis(catecholato)silicate (**56 NEt_4**) from tert-butyl(trichloro)silane based on treatment with catechol and Et_3N in refluxing benzene followed by ammonium exchange with Et_4NCl in acetonitrile. They took advantage of the good water solubility of triethylammonium hydrochloride to remove and render complete the cation metathesis with tetraethylammonium chloride (Scheme 8). From our own experience, efficient drying of the hydrophilic tetraethylammonium salt highly increases the yield of the reaction.

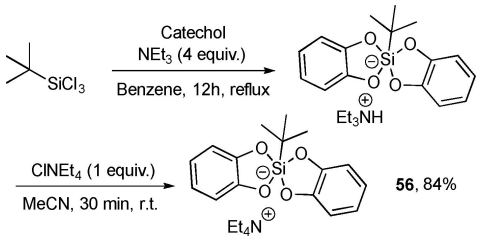

Scheme 8. Synthesis of tetraethylammonium tertbutyl bis(catecholato)silicate from tert-butyl(trichloro)silane.

A similar protocol was employed by Nevado *et al.*[18] in Scheme 9 for the synthesis of the tertiary (2,3-dimethylbutan-2-yl) tetraethylammonium bis(catecholato)silicate **75** from 2,3-dimethylbutan-2-yl(trichloro)silane, but the yield of this reaction was not documented.

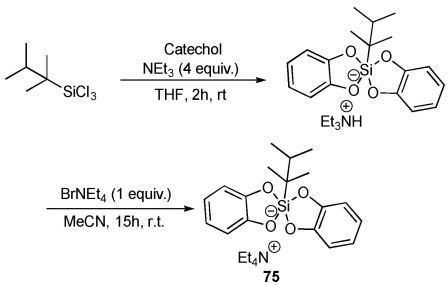

Scheme 9. Synthesis of tetraethylammonium (2,3dimethylbutan-2-yl) bis(catecholato)silicate from 2,3-dimethylbutan-2-yl(trichloro)silane.

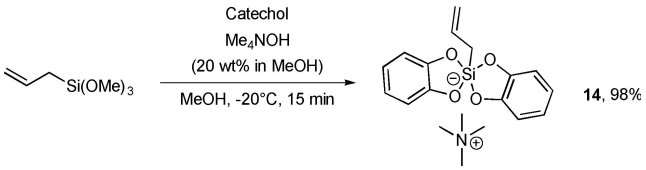

Scheme 10. Synthesis of tetramethyl allyl bis(catecholato)silicate from allyltrimethoxysilane.

Corriu[27] elegantly circumvented the cation exchange step by performing the synthesis of tetramethyl allyl bis(catecholato)silicate **14 NMe$_4$** from catechol and allyltrimethoxysilane in methanol with 20 wt% Me_4NOH in MeOH (Scheme 10). This approach avoids the addition of a large amount of water (required before the ammonium exchange) that can lead to the degradation of the intermediate silicate. Here, the reaction was performed on a 50 mmol scale, at low temperature and without water. These reaction conditions and the good miscibility in methanol could explain the almost quantitative yield of this silicate, without degradation of the residue after washing with anhydrous ether.

2.2.3. Phosphonium-Silicate

Silicates with a phosphonium counterion can be found essentially in several patents except for the bis-(triphenylphosphoranylidene)ammonium (PPN) which has been employed to form highly bulky silicates (Figure 4).

Go[28] has reported an efficient synthesis of phosphonium bis(catecholato)silicates (Scheme 11A). The chemistry based on these cations appears restricted; nevertheless they have found their utility in materials.

Due to the bulkiness of the tetraphenylphosphonium, crystallisation is slowly induced *in-situ* by cation exchange with sodium phenyl bis(catecholato)silicate (**54 Na**). The latter is generated from catechol and phenyl trimethoxysilane in the presence of sodium methoxide in methanol[11] and is added directly to a methanol solution of the corresponding phosphonium salt PPh_4Br. Tetraphenylphosphonium phenyl bis(catecholato)silicate (**54 PPh$_4$**) is effectively obtained in 91% yield.

In 1988, Sakurai and coworkers[8] took advantage of the good crystallisation properties of phosphonium silicates to characterize an allyl silicate derivative while they were unable

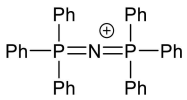

Figure 4. PPN : Bis(triphenylphosphoranylidene)ammonium.

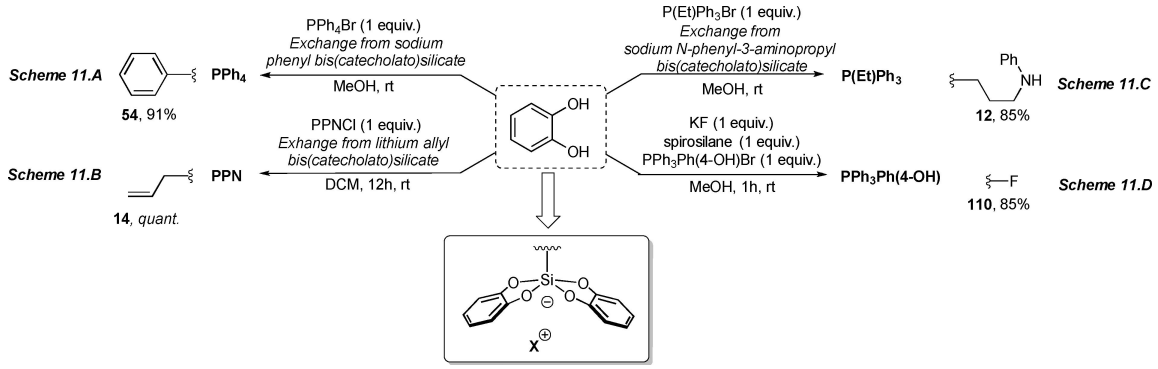

Scheme 11. Synthesis of phosphonium alkyl bis(catecholato)silicates.

to isolate the corresponding lithium allyl bis(catecholato)silicate (**14 Li**). Once again, lithium exchange with bis(triphenylphosphine)iminium chloride (PPNCl) provided a quantitative amount of bis(triphenylphosphoranylidene)ammonium allyl bis(catecholato)silicate (**14 PPN**) (Scheme 11B). Even with this bulky counter-cation, the silicate remained very sensitive to moisture and air.

Another example of silicate bearing a phosphonium cation was synthetized by Go[27] for materials chemistry. Again, a good yield of ethyltriphenylphosphonium N-phenyl-3-aminopropyl bis(catecholato)silicate was obtained (Scheme 11C) by cation exchange with sodium silicate using the same methodology developed in Scheme 11A.

The formation of fluorinated silicate was reported from the corresponding bis(catecholato)spirosilane by Jung and co-workers. Direct addition of fluoride from potassium fluoride and an in situ cation exchange of potassium with the desired phosphonium afforded the desired silicate (**110 PPh_3Ph(4-OH)**) in 85% yield (Scheme 11D).[30]

2.2.4. Zwitterionic-Silicate

Zwitterionic silicates have the advantage of being cation independent. Their synthesis follows the same methodologies as above. For instance, [2-(dimethylaminomethyl),6-(dimethylammoniomethyl)phenyl] bis(catecholato)silicate (**84 H**) was prepared by Corriu et al.[31] following the steps described in Scheme 5E in 39% yield starting from 2,6-bis(dimethylaminomethyl)phenyl trimethoxysilicate (Scheme 12).

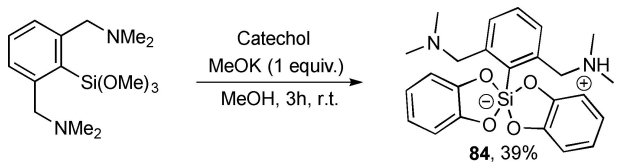

Scheme 12. Synthesis of [2-(dimethylaminomethyl),6-(dimethylammoniomethyl)phenyl] bis(catecholato)silicate from 2,6-bis(dimethylaminomethyl)phenyl trimethoxysilicate.

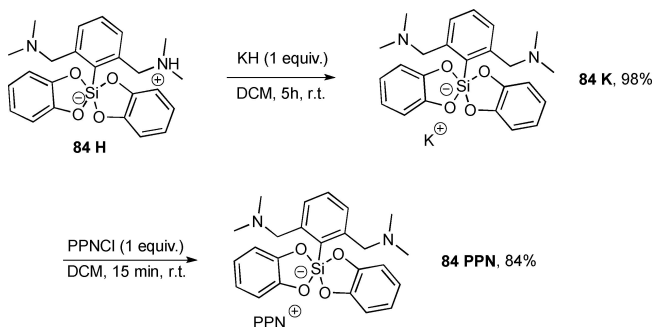

Scheme 13. Synthesis of potassium and bis(triphenylphosphoranylidene)ammonium 2,6-bis(dimethyl-aminomethyl)phenyl bis(catecholato)silicate from [2(dimethylaminomethyl),6-(dimethylammoniomethyl)phenyl]bis(catecholato)silicate.

Corriu and coworkers also showed the possibility of converting a zwitterionic silicate into potassium and PPN analogs.[31] For instance, treatment of [2-(dimethylaminomethyl),6-(dimethylammoniomethyl)phenyl] bis(catecholato)silicate (**84 H**) with potassium hydride led to the corresponding potassium phenyl silicate (**84 K**) (Scheme 13). This reaction was achieved in 98% yield and demonstrated the flexibility of zwitterionic silicates. In the same publication, the transformation of this potassium silicate (**84 K**) to phosphonium silicate (**84 PPN**) was also described by ionic metathesis with PPNCl in 84% yield.

3. Silicate Diversity

The following Table 1 gives an exhaustive overview of all the synthesized bis(catecholato)silicates, the corresponding synthesis yields as well as their ^{29}Si NMR shifts. The NMR experiments were performed mainly in solution but also in the solid state.

From the ^{29}Si NMR data in Table 1 and the observed diversity, the chemical shifts of the pentavalent bis(catecholato)silicates can be modulated by the relative steric or electronic effect of the substituents, the nature of the counter-cation, and/or the inter- or intramolecular dative interaction (or coordinate covalent bond) leading to hexavalent species. The wide range of chemical shifts in ^{29}Si NMR is consistent with a pentacoordinate configuration of the silicon species and the average is at −80 ppm for a range covering −70 to −110 ppm. The shielded values, from −110 to −200 ppm, can be attributed to hexacoordinate silicon derivatives.

For alkyl bis(catecholato)silicates, ^{29}Si NMR shifts are generally comprised between −70 and −80 ppm and for aromatics slightly upfield from −80 to −90 ppm. Based on the reported value, the nature of the substituent can lead to a shielding of the ^{29}Si NMR shift as follows: alkyl > benzyl (R=–Me, −74.32 ppm (**3 K**); R=$-CH_2Ph$, −80.9 ppm (**1 K**))/allyl > phenyl (R=–Allyl, −80.24 ppm (**14 K[18C6]**); R=–Ph, −87.83 ppm (**54 K[18C6]**))/alkyl > cycloalkyl (R=–Hex, −75.6 ppm (**4 K[18C6]**)); R=–Cyclohexyl, −77.93 ppm (**2 K[18C6]**)). When the length of the carbon chain is increased, a slight shift is observed (R=–Me, −74.32 ppm (**3 K**); R=–Et, −74.77 ppm (**29 K**); R=–Hex, −75.6 ppm (**4 K[18C6]**)). A slight upshield was observed from the arrangement induced from a richer and hindered *tert*-butyl moiety (−76.21 ppm (**56 Et_4N**)). An electronic effect can also be observed if the silicate bears a more or less electron withdrawing substituents in α-position to the silicon (R=$-CH_2NHPh$, −81.36 ppm, (**52 K[18C6]**); R=$-CH_2OMe$, −82.2 ppm, (**60 K[18C6]**); R=$-CH_2Cl$, −85.57 ppm, (**6 K[18C6]**); R=$-CH_2OAc$, −85.8 ppm, (**35 K[18C6]**)). The effect of substituents is still present in beta position but it is much weaker beyond (R=$-CH_2CH_2CN$, −80.17 ppm, (**57 K[18C6]**); R=$-CH_2CH_2CH_2CN$, −77.6 ppm, (**26 K[18C6]**)) and also R=$-CH_2CH_2CH_2OAc$, −76.6 ppm, (**10 K[18C6]**); R=$-CH_2CH_2CH_2Cl$, −76.9 ppm, (**58 K-[18C6]**) compared to the previous (**35 K[18C6]**) and (**6 K[18C6]**)). This decrease was also observed with the morpholinium derivatives (R=$-CH_2$Morph, −85.8 ppm, (**64 K[18C6]**); R=$-CH_2CH_2CH_2$ Morph, −76.9 ppm, (**63 K[18C6]**)). Finally, donor molecules such as

1,8-diazabicyclo[5.4.0]undec-7-ene (DBU), hexamethylphosphoramide (HMPA), and 1,3-dimethyl-2-imidazolidinone (DMI) can interact with the silicon center of the spiro bis(catecholato)silane *via* an intermolecular coordinating covalent bond, and the NMR values of the new pentacoordinate forms shift toward about −100 ppm (R = DBU, −98.7 ppm, (**124**); R = HMPA, −107.3 ppm, (**125**); R = DMI, −104.5 ppm, (**126**)). A shielding of the ^{29}Si NMR shift was also observed with some heteroatomic residues (R = –NCS, −110.4 ppm, (**106 K[18C6]**); R = –OMe, −99.1 ppm, (**108 K[18C6]**)). ^{29}Si NMR chemical shifts showed a weak influence of the counter-cation with respect to the nature of the substituent. Few silicates can be compared completely by varying the counter cation. For example, the alkaline bis(catecholato)benzyl silicate (**1**) was studied extensively by our group and showed the same value (−80.9 ppm). A difference of 0.1 ppm was observed between free and crown ether chelated (15C5 and 18C6, −80.8 and −80.9 ppm respectively) sodium and potassium silicates.

Higher ^{29}Si NMR shifts were observed and confirmed the formation of a hexavalent species by inter- or intramolecular interaction. A donor solvent such as THF can interact with the spiro bis(catecholato)silane *via* an intermolecular bond and yields the hexacoordinate derivative with a ^{29}Si NMR shift of −134.4 ppm.[68] Interestingly, the NMR shifts for Si-NCS silicate (**106**) reported by Narula are at the extreme of the pentacoordinate region in ^{29}Si NMR (from −110.4 ppm to −112.6 ppm) whatever the counter-cation and in the hexavalent part of the spectrum (from −140.7 ppm to −156.2 ppm) when a secondary amine is coordinated to silicate (**107**).[12] Probably, these corresponding values suggest intermolecular coordination of the amine.

The same observation was made with intramolecular coordination of an amide (N–C(O)) by Korlyukov. A NMR shift of silicate (**82**) was observed at −133.5 ppm, again in the ^{29}Si NMR region expected for hexavalent derivatives. This value related to the O…Si interaction of the hexacoordinate species is comparable to those observed for (**84**) with the intramolecular Si…N interaction. The NMR shift of the zwitterionic ammonium, potassium, and quaternary ammonium (PPN) silicate (**84**) (i.e., −134.9, −129.8, and −127.2 ppm respectively) were reported by Reyé in 1992.[31]

Some structures containing nitrogen moieties, such as silicates (**79**) and (**123**) of Table 1, have been characterized by solid state NMR (^{29}Si and ^{15}N NMR) by Tacke and coworkers.[9] The solid state ^{29}Si NMR shift is consistent with the expected in solution (for (**123**): −88.6 ppm, close to −80 ppm for the pentavalent silicon species) and rare ^{15}N NMR data have been compiled for two zwitterionic silicate species (for silicate (**79**): −324.7 ppm and for (**123**): −336.9 ppm).

4. X-ray Diffraction Analysis

As mentioned by Holmes in 1985, a continuum between a square or rectangular pyramidal geometry (SP) and a trigonal bipyramidal geometry (TBP) involving a structural distortion along the Berry pseudorotational coordinate has been observed for the structure of bis(catecholato)silicates. In such structures, the apical site is always occupied by the R substituent, and the percent displacement from TBP to SP can be quantified using the dihedral angle method initially reported by Holmes in 1977 on cyclic phosphoranes[26c] and extrapolated to the hypercoordinated silicon species.[26a] The geometry of silicates has been shown to be influenced by the nature of the cation and the substituent.[26a] For example, changing the *t*Bu substituent to *n*Bu with the same cation (i.e. NEt_4) gave a distortion (in % from TBP toward SP) of 91.4% to 63.8% respectively. In this case, reducing the steric hindrance disfavours the SP geometry toward TBP. The direct influence of the cation was also highlighted by changing the silicate cation (NEt_4 *versus* HNC_5H_5) with the same substituent (napthyl), the distortion observed (% TBP→SP) was 30.8% for quaternary ammonium and 58.7% for pyridinium, respectively. To better illustrate these geometries, we have selected several structures shown in Figure 4.

Other silicates tend to adopt either a square pyramidal (SP) structure, such as the chelated potassium ether-crown pentacoordinated silicate (**19 K[18C6]**) (CCDC 1403595) in Figure 5A[33] or a trigonal-bipyramidal (TBP) structure as shown in Figure 5E, for the silicate flanked by a PPN cation (**62 PPN**) (1280206) stabilised in a hexavalent geometry by the amine coordination to the silicon center.[56] A slight distortion from these two limiting structures can be observed in the silicates (**92 K**) (648236) illustrated in Figure 5B,[65] (**2 Na**) in Figure 5C[13] and (**54 $HNEt_3$**) in Figure 5D[26a] for instance. In the case of the

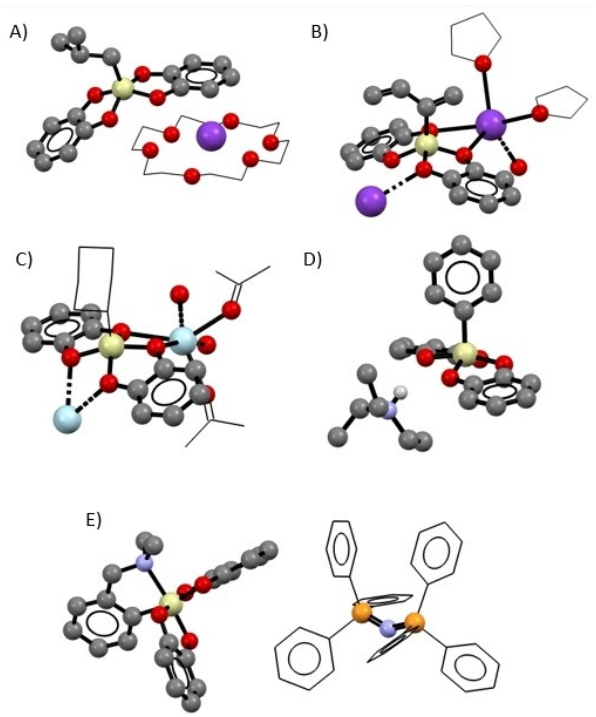

Figure 5. Selected examples of X-ray crystal structures of silicates. Thermal ellipsoids are drawn at 50% probability level. Hydrogen atoms are omitted for clarity. Carbons of cyclohexyl, acetone, THF, crown-ether and phenyl of PPN are drawn as wireframe for clarity Dashed lines denote bonds between neighbouring silicates. Deposit number, A: **19 K[18C6]** (1403595); B: **92 K** (648236); C: **2 Na** (2050302); D: **54 $HNEt_3$** (1135883); E: **62 PPN** (1280206).

sodium silicate (**2 Na**) (Figure 5C), the dihedral angle method resulted in an 89.3% shift from the TBP structure to the SP structure.[13] Here, a polymeric assembly along the *c*-axis resulting from non-covalent bonds between sodium and oxygen atoms of catechols of two silicates is observed. This interaction of the catechol moieties through the oxygen atoms with the potassium cation was also observed in Figure 5B with potassium. Moreover, as depicted in the Figure 5D, hydrogen bonding can be established between the catechol ligand and triethylammonium.[26a]

The countercation effect was observed with cyclohexyl bis(catecholato)silicates. Sodium cyclohexyl bis(catecholato)silicates without crown ether (**2 Na**) and the potassium analog[10,13] (**2 K**) are isostructural *Pbca* crystals compared to the chelated one (**2 K[18C6]**) (1403596) and the ammonium derivative (**2 H_2NMe_2**) (1194879). The structural data of these cyclohexyl derivatives are presented in Table 2 For both non-chelated inorganic cations Na and K (Entries 1 and 2), close cell parameters are observed with a slight variation in the length of the a, b, c axis due to the variation of the cation. As expected, angles and Z-values of these isostructural crystals are identical and chelation of the cation for both species with catechol provides a similar polymeric assembly. Increasing the size of the potassium by chelation with the [18C6] crown ether (Entry 4) led to a reduction in the number of molecules in the asymmetric unit (from Z = 8 to Z = 2) and prevents chelation of the cation between two silicate catechols. In the case of the ammonium derivative (Entry 3), hydrogen bonding is observed allowing intermolecular interaction between two distinct silicates resulting in an increase in the number of molecules per unit (Z = 8) as for both inorganic cations.

5. Redox Potentials

The use of silicates as radical precursors by single-electron transfer, including visible-light photoredox catalysis, requires a good understanding of the redox properties of these species. For this purpose, the oxidation potential (E_{OX}) of each silicate has been measured by Cyclic Voltammetry (CV) or using a Differential Pulse Voltammetry (DPV) technique, which allows to anticipate their reactivity from a thermodynamic point of view.

Table 2. Reported crystal details of cyclohexyl bis(catecholato)silicates (**2**).

	Cation	CCDC	SG	Cell parameters (Å | °)		Z
1	Na	2050302	*Pbca*	*a* 20.1599(19)	α 90	8
				b 11.4841(11)	β 90	
				c 21.738(3)	γ 90	
2	K	[10]	*Pbca*	*a* 19.6679(4)	α 90	8
				b 11.6484(3)	β 90	
				c 22.0285(5)	γ 90	
3	H_2NMe_2	1194879	$P2_1/c$	*a* 13.566(2)	α 90	8
				b 14.962(3)	β 103.56(1)	
				c 20.561(4)	γ 90	
4	K[18C6]	1403596	$Pmn2_1$	*a* 17.7244(4)	α 90	2
				b 8.4874(2)	β 90	
				c 10.6609(2)	γ 90	

In this section, all oxidation potentials given are in V vs SCE and correspond to irreversible oxidation waves.

In 2007, Nishigaichi measured the oxidation potential of tetramethylammonium allyl bis(catecholato)silicates (**14 NMe_4**) using a DPV technique in acetonitrile and showed to be +1.12 V (vs SCE). Addition of a donor solvent such as DMF, DMSO or an amine (pyridine, imidazole, *n*-butylamine and piperidine) leads to the formation of a hexacoordinated silicon species and decreases the E_{OX} value to 1.08, 1.06 V or 0.78–0.80 V respectively.[68] More recently, Molander reported the oxidation potentials of several triethylammonium primary and secondary alkyl species in acetonitrile using CV analysis. The E_{OX} values of triethylammonium benzyl, cyclohexyl and hexyl bis(catecholato)silicates were found to be almost identical (+0.70 V for (**1 $HNEt_3$**), +0.74 V for (**2 $HNEt_3$**) and +0.75 V for (**4 $HNEt_3$**), respectively. The study was extended to triethylammonium phenylbis(catecholato)silicate (**54 $HNEt_3$**) which can be oxidized at a similar potential value (+0.76 V vs SCE).[32]

Meanwhile, Goddard, Ollivier and Fenterbank studied 16 different [18-C-6] crown-ether chelated potassium alkyl and aryl bis(catecholato)silicates.[33] The values of the oxidation potential were determined by CV in DMF and range from 0.34 V for the anilinomethyl silicate (**52 K[18C6]**) to 0.89 V for the phenyl silicate (**54 K[18C6]**). The oxidation potential evolves according to the nature of the substituent, increasing in the order alkyl < aryl; benzylic < tertiary < secondary < primary; benzylic < allylic; alkyl < aryl and anilinomethyl < methoxymethyl < chloromethyl as shown in Figure 6.

Modulation of the counter-cation of [18C6]-complexed potassium silicates to its sodium counterpart has been shown to influence their oxidation potential. A noticeable increase is observed with benzyl bis(catecholato)silicates from +0.61 V (K[18C6]) to +0.77 V (Na) and with cyclohexyl bis(catecholato)silicates from +0.69 V (K[18C6]) to +0.81 V (Na) *vs* SCE in DMF.

6. Reactivity and Perspectives

Bis(catecholato)silicates have recently been involved in a wide spectrum of synthetic applications. Only the most representative transformations are mentioned here in a concise manner way.

The first example of reactivity of these silicates took advantage of its nucleophilicity. For example, Sakurai and coworkers used in 1987 an *in situ* generated lithium hydrido bis(catecholato)silicate for the reduction of various carbonyl compounds.[39] One year later, following the same methodology, the *in situ* generation of a hypercoordinated lithium allyl bis(catecholato)silicate (**14 Li**) allowed the allylation of furfural giving the desired allyl alcohol in 86% yield (Scheme 14).[8]

While silicate can act as a nucleophile, the influence of hypercoordination was clearly demonstrated by Wright in Diels-Alder reactions (Scheme 15). In contrast to the silane precursor, which did not show good reactivity, the diene silicate (**92 K**) reacted almost quantitatively with N-phenylphthalamide to form new cycloadducts which were then engaged in the cross-coupling reaction described below.

Review
doi.org/10.1002/ejic.202101109

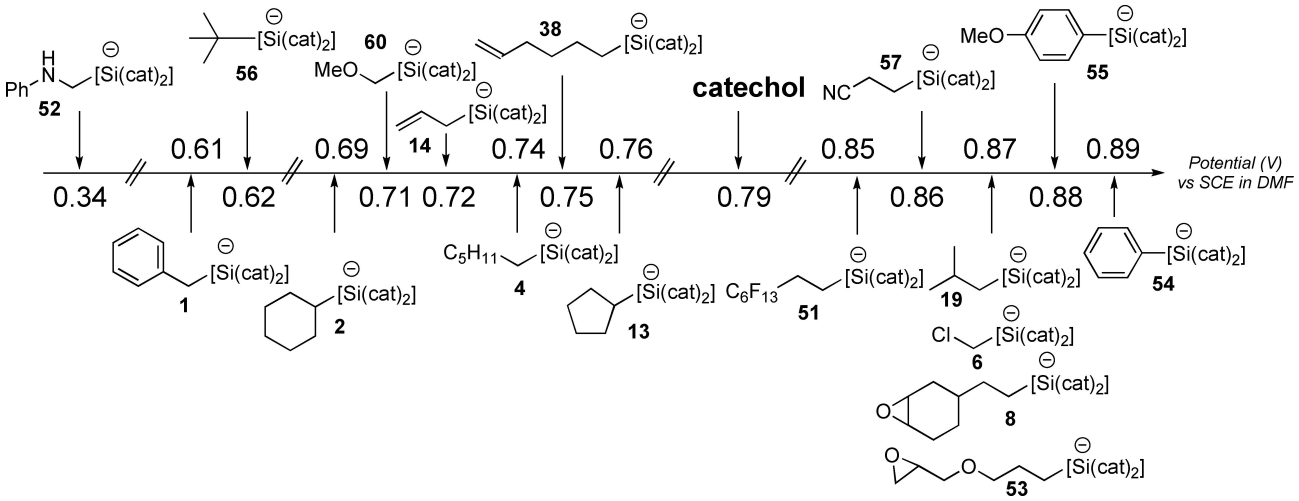

Figure 6. Selected examples of oxidation potentials (in V *vs* SCE) of bis(catecholato)silicates depending on their substituents.

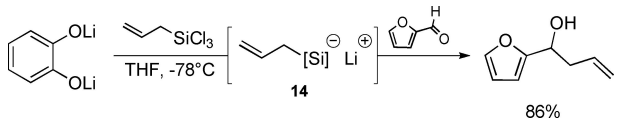

Scheme 14. Allylation of furfural using lithium allyl bis(catecholato)silicate.

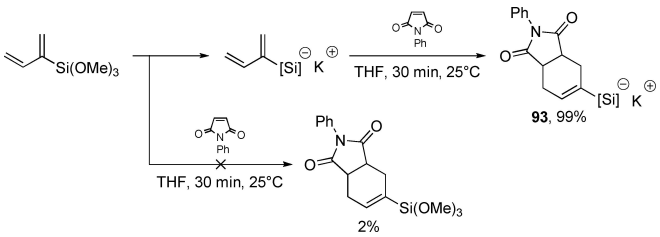

Scheme 15. Reactivity of diene silicate (**92 K**) in Diels-Alder reactions with N-phenylphthalamide.

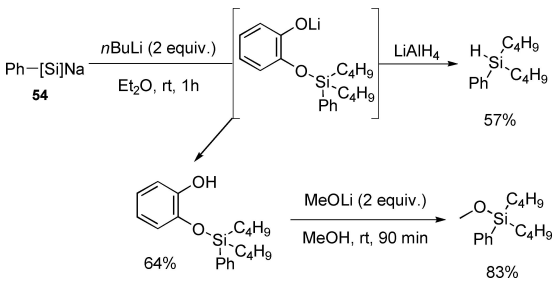

Scheme 16. Electrophilicity of silicate for the synthesis of polysubstituted silanes.

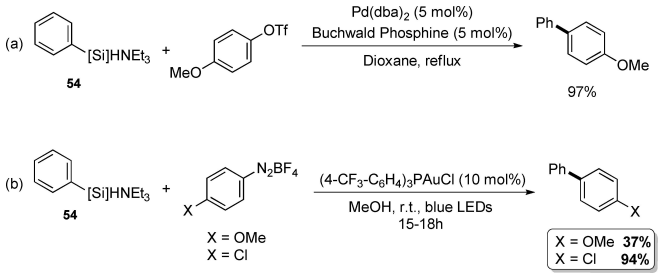

Scheme 17. Palladium (a) and gold (b) catalysed cross-coupling of ammonium aryl bis(catecholato)silicates.

In addition to reactions using silicates as nucleophile, the electrophilicity of these derivatives has been studied by Corriu to access different silanes from the same intermediate.[69] Silicates appear to be efficient substrates for the synthesis of polysubstituted silanes. The methodology takes advantage of the controlled addition of two strong nucleophiles such as nBuLi or a Grignard reagent by displacement of the catechol ligand. The resulting intermediate can be reduced by $LiAlH_4$ or reacted with a third equivalent nucleophile allowing the formation of a $R_2SiR'R''$-type derivative. In addition, the intermediate can be cooled and isolated to allow further transformation such as the formation of alkoxy- or chlorosilanes in high yields (Scheme 16).

While aryl silicates, such as triethylammonium phenyl bis(catecholato)silicate (**54 HNEt$_3$**), can be engaged in palladium-catalyzed cross-coupling reactions, as reported by Deshong (Scheme 17a)[50] or using a gold catalyst under light irradiation, as shown by Hashmi (Scheme 17b),[24] the main interest today lies in the intrinsic properties of the silicon species, their ligand-dependent modulation, and its reactivity as a precursor of alkyl or aryl radicals.

Bis(catecholato)silicates are now considered common reagents for the generation of alkyl radicals by visible-light photocatalytic oxidation and their use for carbon-carbon bond formation.[33] Radical allylation is a versatile synthetic process. Using a catalytic amount of the organic photocatalyst 4CzIPN, potassium [18-Crown-6] anilinomethyl bis(catecholato)silicate (**52 K[18C6]**) placed in the presence of tosyl allylsulfone under visible light irradiation gave the corresponding allylic product in

a nearly quantitative manner. This illustrates the efficiency of photocatalytic reactions employing bis(catecholato)silicates (Scheme 18).

Unlike alkyl silicates, the generation of aryl radicals from aryl bis(catecholato)silicates, such as potassium [18-Crown-6] phenyl bis(catecholato)silicate (**54 K[18C6]**), could not be achieved under these photooxidation conditions. Modulation of the catechol ligand, as shown in Scheme 19, has recently emerged as an attractive solution to the reactivity problem of these species. For instance, this strategy provided the phenyl radical from the corresponding potassium [18-Crown-6] phenyl bis(3-cyanocatechol)silicate.[70]

In the same vein, other original structures of bis(catecholato)silicates are reported in Scheme 18. For example, Holmes prepared 2,2′-biphenolate silicates in 1990 (Scheme 20A),[71] Tacke replaced the catechol ligand with a 1-hydroxy-2-pyridone ligand allowing the formation of a hexacoordinate silicon compound (Scheme 20B),[72] and Spange published an interesting silicate bearing coumarin ligands (Scheme 20C).[73] Studies on the reactivity of such structures would be of particular interest.

7. Conclusion

Recent applications in anionic bis(catecholato) hypercoordinate silicon species in photoredox and organometallic catalysis has led to a second wave of synthesis of these derivatives allowing for a broader structural diversity of the silicates. In this review, we have summarized various approaches to the synthesis of bis(catecholato)silicates based on the nature of the countercation and the substituent R, from the bis(catecholato) aryl silicates to the more recent alkyl derivatives over the 1964 to 2021 period. In addition, the results of ^{29}Si NMR studies, X-ray diffraction analyses, and oxidation potential measurements have been compiled, providing a comprehensive overview of the influence of the cations and the substituents on these hypercoordinated species as well as the potential reactivity of these systems. Recent solutions tend to extend their scope of application but the limitation of silicates comes from the initial silanes commercial availability or the synthetic methods to generate them. Future research should focus on the tuning of the silicon ligand. Recently, the use of Martin's spirosilane (bearing the dianion of hexafluorocumyl alcohol) has emerged as an interesting solution to activate molecules or to deliver new transferable moieties in a practical way.[74] Thus, it is expected that other hypercoordinated silicon species will find their place and become a tool for increasing structural diversity in applied organic chemistry. We hope that this review will facilitate the knowledge of these derivatives and stimulate their research and applications in contemporary synthetic chemistry.

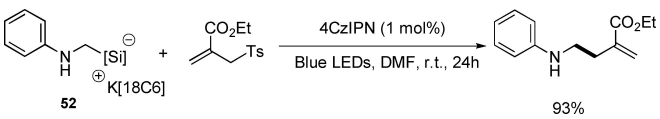

Scheme 18. Visible-light photocatalytic oxidation of the anilinomethyl bis(catecholato)silicate with an allylsulfone.

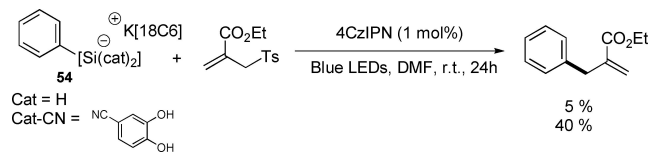

Scheme 19. Radical allylation of phenyl potassium [18-Crown-6] bis(3-cyanocatechol)silicate.

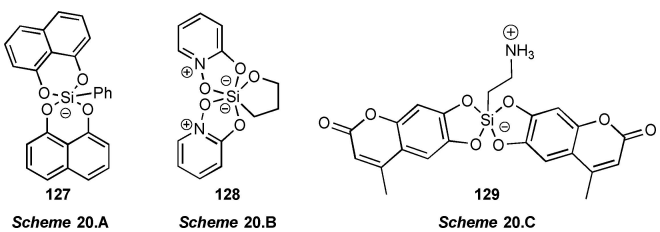

Scheme 20. Other original structures of hypercoordinated silicon species.

Acknowledgements

The authors thank CNRS, Sorbonne Université and IUF for financial support. We thank the Knizia Research group for the development of IboView, used for the graphical abstract.

Conflict of Interest

The authors declare no conflict of interest.

Keywords: Bis(catecholo)silicate · Hypercoordinated silicon · Silicon NMR · Oxidation potential · X-ray analysis

[1] N. Kano, N. Nakagawa, T. Kawashima, *Angew. Chem. Int. Ed.* **2001**, *40*, 3450–3452; *Angew. Chem.* **2001**, *113*, 3558–3560.
[2] a) C. Chuit, R. J. P. Corriu, C. Reye, J. C. Young, *Chem. Rev.* **1993**, *93*, 1371–1448; b) E. P. A. Couzijn, J. C. Slootweg, A. W. Ehlers, K. Lammertsma, *Z. Anorg. Allg. Chem.* **2009**, *635*, 1273–1278; c) D. Kost, I. Kalikhman, *Acc. Chem. Res.* **2009**, *42*, 303–314; d) N. Kano, in *Organosilicon Compounds*, Elsevier, **2017**, pp. 645–716; e) R. R. Holmes, *Chem. Rev.* **1996**, *96*, 927–950; f) D. Schomburg, R. Krebs, *Inorg. Chem.* **1984**, *23*, 1378–1381; g) S. Rendler, M. Oestreich, *Synthesis* **2005**, *11*, 1727–1747.
[3] V. Corcé, C. Lévêque, C. Ollivier, L. Fensterbank, *Silicates in Photocatalysis. In Science of Synthesis: Photocatalysis in Organic Synthesis* (Ed.: B. König), Thieme, Stuttgart, **2019**, Chap 15, pp 427–466.
[4] E. F. Perozzi, J. C. Martin, *J. Am. Chem. Soc.* **1979**, *101*, 1591–1593.
[5] S. Deerenberg, M. Schakel, A. H. J. F. de Keijzer, M. Kranenburg, M. Lutz, A. L. Spek, K. Lammertsma, *Chem. Commun.* **2002**, 348–349.
[6] D. Hartmann, T. Thorwart, R. Müller, J. Thusek, J. Schwabedissen, A. Mix, J.-H. Lamm, B. Neumann, N. W. Mitzel, L. Greb, *J. Am. Chem. Soc.* **2021**, *143*, 18784–18793.
[7] a) R. Maskey, H. Wadepohl, L. Greb, *Angew. Chem. Int. Ed.* **2019**, *58*, 3616–3619; *Angew. Chem.* **2019**, *131*, 3655–3658; b) C. Y. Wong, J. D. Woollins, *Coord. Chem. Rev.* **1994**, *130*, 175–241; c) D. Hartmann, M. Schädler, L. Greb, *Chem. Sci.* **2019**, *10*, 7379–7388; d) T. Thorwart, D. Roth, L. Greb, *Chem. Eur. J.* **2021**, *27*, 10422–10427.

[8] K. Mitsuo, S. Kazuhiko, S. Hideki, *J. Am. Chem. Soc.* **1988**, *110*, 4599–4602.
[9] R. Tacke, A. Lopex-Mras, J. Sperlich, C. Strohmann, W. F. Kuhs, G. Mattern, A. Sebald, *Chem. Ber.* **1993**, *126*, 851–861.
[10] Unpublished results.
[11] A. Boudin, G. Cerveau, C. Chuit, R. J. P. Corriu, C. Reye, *Bull. Chem. Soc. Jpn.* **1988**, *61*, 101–106.
[12] S. P. Narula, R. Shankar, Meenu, *Phosphorus Sulfur Silicon Relat. Elem.* **1996**, *113*, 237–243.
[13] M. Abdellaoui, A. Millanvois, E. Levernier, C. Ollivier, L. Fensterbank, *Synlett* **2021**, *32*, 1513–1518.
[14] D. F. Evans, A. M. Z. Slawin, D. J. Williams, C. Y. Wong, J. D. Woollins, *J. Chem. Soc. Dalton Trans.* **1992**, 2383–2387.
[15] C. Lévêque, L. Chenneberg, V. Corcé, J.-P. Goddard, C. Ollivier, L. Fensterbank, *Org. Chem. Front.* **2016**, *3*, 462–465.
[16] U. Dettlaff-Weglikowska, E. Hey-Hawkins, H. G. von Schnering, *Z. Naturforsch., B: J. Chem. Sci.* **1991**, *46*, 609–614.
[17] S. Yamaguchi, S. Akiyama, K. Tamao, *Organometallics* **1999**, *18*, 2851–2854.
[18] A. García-Domínguez, R. Mondal, C. Nevado, *Angew. Chem. Int. Ed.* **2019**, *58*, 12286–12290; *Angew. Chem.* **2019**, *131*, 12414–12418.
[19] K. C. K. Swamy, V. Chandrasekhar, J. J. Harland, J. M. Holmes, R. O. Day, R. R. Holmes, *J. Am. Chem. Soc.* **1990**, *112*, 2341–2348.
[20] K. Lin, *Org. Synth.* **2017**, *94*, 16–33.
[21] M. Jouffroy, C. B. Kelly, G. A. Molander, *Org. Lett.* **2016**, *18*, 876–879.
[22] A. A. Korlyukov, A. G. Shipov, E. P. Kramarova, Vad. V. Negrebetskii, Yu. I. Baukov, *Russ. Chem. Bull.* **2009**, *57*, 2093–2100.
[23] C. L. Frye, *J. Am. Chem. Soc.* **1964**, *86*, 3170–3171.
[24] S. Witzel, K. Sekine, M. Rudolph, A. S. K. Hashmi, *Chem. Commun.* **2018**, *54*, 13802–13804.
[25] S. Zheng, D. N. Primer, G. A. Molander, *ACS Catal.* **2017**, *7*, 7957–7961.
[26] a) R. R. Holmes, R. O. Day, V. Chandrasekhar, J. M. Holmes, *Inorg. Chem.* **1985**, *24*, 2009–2015; b) R. R. Holmes, R. O. Day, V. Chandrasekhar, J. J. Harland, J. M. Holmes, *Inorg. Chem.* **1985**, *24*, 2016–2020; c) R. R. Holmes, J. A. Deiters, *J. Am. Chem. Soc.* **1977**, *99*, 3318–3326.
[27] G. Cerveau, C. Chuit, R. J. P. Corriu, C. Reye, *J. Organomet. Chem.* **1987**, *328*, C17–C20.
[28] Patent *JP2009298975A*.
[29] Patent *JP2008255322A*.
[30] Patent *KR20160117871A*.
[31] F. Carré, C. Chuit, R. J. P. Corriu, A. Mehdi, C. Reyé, *J. Organomet. Chem.* **1993**, *446*, C6–C8.
[32] M. Jouffroy, D. N. Primer, G. A. Molander, *J. Am. Chem. Soc.* **2016**, *138*, 475–478.
[33] V. Corcé, L.-M. Chamoreau, E. Derat, J.-P. Goddard, C. Ollivier, L. Fensterbank, *Angew. Chem. Int. Ed.* **2015**, *54*, 11414–11418; *Angew. Chem.* **2015**, *127*, 11576–11580.
[34] A. Cartier, E. Levernier, V. Corcé, T. Fukuyama, A.-L. Dhimane, C. Ollivier, I. Ryu, L. Fensterbank, *Angew. Chem. Int. Ed.* **2019**, *58*, 1789–1793; *Angew. Chem.* **2019**, *131*, 1803–1807.
[35] C. Lévêque, V. Corcé, L. Chenneberg, C. Ollivier, L. Fensterbank, *Eur. J. Org. Chem.* **2017**, *2017*, 2118–2121.
[36] N. R. Patel, C. B. Kelly, M. Jouffroy, G. A. Molander, *Org. Lett.* **2016**, *18*, 764–767.
[37] A. Hosomi, S. Kohra, Y. Tominaga, *J. Chem. Soc. Chem. Commun.* **1987**, 1517–1518.
[38] A. Hosomi, S. Kohra, K. Ogata, T. Yanagi, Y. Tominaga, *J. Org. Chem.* **1990**, *55*, 2415–2420.
[39] M. Kira, K. Sato, H. Sakurai, *J. Org. Chem.* **1987**, *52*, 949–951.
[40] K. D. Raynor, G. D. May, U. K. Bandarage, M. J. Boyd, *J. Org. Chem.* **2018**, *83*, 1551–1557.
[41] N. R. Patel, C. B. Kelly, A. P. Siegenfeld, G. A. Molander, *ACS Catal.* **2017**, *7*, 1766–1770.
[42] W. Luo, Y. Yang, Y. Fang, X. Zhang, X. Jin, G. Zhao, L. Zhang, Y. Li, W. Zhou, T. Xia, B. Chen, *Adv. Synth. Catal.* **2019**, *361*, 4215–4221.
[43] M. Jouffroy, G. H. M. Davies, G. A. Molander, *Org. Lett.* **2016**, *18*, 1606–1609.
[44] K. Lin, R. J. Wiles, C. B. Kelly, G. H. M. Davies, G. A. Molander, *ACS Catal.* **2017**, *7*, 5129–5133.
[45] E. Levernier, V. Corcé, L.-M. Rakotoarison, A. Smith, M. Zhang, S. Ognier, M. Tatoulian, C. Ollivier, L. Fensterbank, *Org. Chem. Front.* **2019**, *6*, 1378–1382.
[46] S. B. Lang, R. J. Wiles, C. B. Kelly, G. A. Molander, *Angew. Chem. Int. Ed.* **2017**, *56*, 15073–15077; *Angew. Chem.* **2017**, *129*, 15269–15273.
[47] J. P. Phelan, S. B. Lang, J. S. Compton, C. B. Kelly, R. Dykstra, O. Gutierrez, G. A. Molander, *J. Am. Chem. Soc.* **2018**, *140*, 8037–8047.
[48] L. R. E. Pantaine, J. A. Milligan, J. K. Matsui, C. B. Kelly, G. A. Molander, *Org. Lett.* **2019**, *21*, 2317–2321.
[49] J. A. Milligan, K. L. Burns, A. V. Le, V. C. Polites, Z.-J. Wang, G. A. Molander, C. B. Kelly, *Adv. Synth. Catal.* **2020**, *362*, 242–247.
[50] W. M. Seganish, P. DeShong, *J. Org. Chem.* **2004**, *69*, 1137–1143.
[51] D. A. Loy, J. H. Small, K. J. Shea, *Organometallics* **1993**, *12*, 1484–1488.
[52] Patent *JP2008189824A*.
[53] Patent *JPWO2017195822A1*.
[54] C. Lévêque, L. Chenneberg, V. Corcé, C. Ollivier, L. Fensterbank, *Chem. Commun.* **2016**, *52*, 9877–9880.
[55] R.-M. L. Mercado, A. Chandrasekaran, R. O. Day, R. R. Holmes, *Organometallics* **1999**, *18*, 1686–1692.
[56] F. Carré, G. Cerveau, C. Chuit, R. J. P. Corriu, C. Réyé, *Angew. Chem. Int. Ed.* **1989**, *28*, 489–491; *Angew. Chem.* **1989**, *101*, 474–476.
[57] J. Sperlich, J. Becht, M. Mühleisen, S. A. Wagner, G. Mattern, R. Tacke, *Z. Naturforsch. B* **1993**, *48*, 1693–1706.
[58] R. Tacke, B. Ulmer, B. Wagner, M. Arlt, *Organometallics* **2000**, *19*, 5297–5309.
[59] G. Cerveau, C. Chuit, E. Colomer, R. J. P. Corriu, C. Reye, *Organometallics* **1990**, *9*, 2415–2417.
[60] Patent *JP2007246671A*.
[61] I. Richter, M. Penka, R. Tacke, *Organometallics* **2002**, *21*, 3050–3053.
[62] F. Carre, G. Cerveau, R. J. P. Corriu, C. Reye, *New J. Chem.* **1992**, *16*, 63–69.
[63] Patent *US20100056801A1*.
[64] R. R. Pidaparthi, C. S. Junker, M. E. Welker, C. S. Day, M. W. Wright, *J. Org. Chem.* **2009**, *74*, 8290–8297.
[65] R. R. Pidaparthi, M. E. Welker, C. S. Day, M. W. Wright, *Org. Lett.* **2007**, *9*, 1623–1626.
[66] A. Hosomi, S. Kohra, Y. Tominaga, *Chem. Pharm. Bull.* **1988**, *36*, 4622–4625.
[67] Z.-J. Wang, S. Zheng, J. K. Matsui, Z. Lu, G. A. Molander, *Chem. Sci.* **2019**, *10*, 4389–4393.
[68] a) Y. Nishigaichi, A. Suzuki, T. Saito, A. Takuwa, *Tetrahedron Lett.* **2005**, *46*, 5149–5151; b) Y. Nishigaichi, A. Suzuki, A. Takuwa, *Tetrahedron Lett.* **2007**, *48*, 211–214; c) D. Matsuoka, Y. Nishigaishi, *Chem. Lett.* **2014**, *43*, 559–561.
[69] A. Boudin, G. Cerveau, C. Chuit, R. J. P. Corriu, C. Reye, *Bull. Chem. Soc. Jpn.* **1988**, *61*, 101–106.
[70] E. Levernier, K. Jaouadi, H. R. Zhang, V. Corcé, A. Bernard, G. Gontard, C. Troufflard, L. Grimaud, E. Derat, C. Ollivier, L. Fensterbank, *Chem. Eur. J.* **2021**, *27*, 8782–8790.
[71] K. C. K. Swamy, C. Sreelatha, R. O. Day, J. Holmes, R. R. Holmes, *Phosphorus Sulfur Silicon Relat. Elem.* **1995**, *100*, 107–121.
[72] R. Tacke, C. Burschka, M. Willeke, R. Willeke, *Eur. J. Inorg. Chem.* **2001**, *2001*, 1671–1674.
[73] F. Riedel, A. Oehlke, S. Spange, *Z. Anorg. Allg. Chem.* **2009**, *635*, 1335–1340.
[74] G. Lemière, A. Millanvois, C. Ollivier, L. Fensterbank, *Chem. Rec.* **2021**, *21*, 1119–1129.

Manuscript received: December 28, 2021
Revised manuscript received: April 1, 2022
Accepted manuscript online: April 20, 2022

Synlett M. Abdellaoui et al. Cluster

Visible-Light-Mediated *Z*-Stereoselective Monoalkylation of β,β-Dichlorostyrenes by Photoredox/Nickel Dual Catalysis

Mehdi Abdellaoui
Alexandre Millanvois
Etienne Levernier
Cyril Ollivier*
Louis Fensterbank*

Institut Parisien de Chimie Moléculaire, Sorbonne Université, UMR CNRS 8232, 4 Place Jussieu, Paris Cedex 05, France
cyril.ollivier@sorbonne-universite.fr
louis.fensterbank@sorbonne-universite.fr

Published as part of the Cluster
Modern Nickel-Catalyzed Reactions

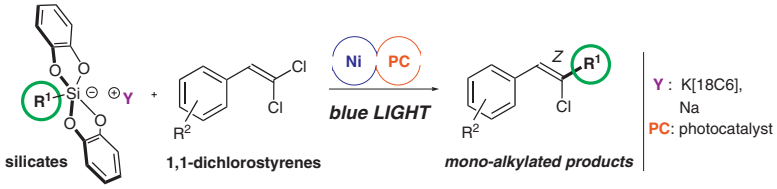

Received: 18.12.2020
Accepted after revision: 26.01.2021
Published online: 27.01.2021
DOI: 10.1055/a-1374-9384; Art ID: St-2020-k0632-c

Abstract Metal-catalyzed alkylation of 1,1-dihalovinyl moiety commonly suffers from both a lack of stereoselectivity and the overreaction leading to the dialkylation product. The methodology described herein features a new pathway to alkylate stereoselectively β,β-dichlorostyryl substrates to provide the *Z*-trisubstituted olefin only with fair to good yields. This cross-coupling reaction bears on the smooth and photoinduced formation of a C-centered radical that engages in a nickel-catalyzed organometallic cycle to form the key C_{sp2}–C_{sp3} bond.

Key words cross-coupling, stereoselective alkylation, radical, dichlorostyrenes, bis(catecholato)silicates, dual catalysis, counterion, nickel

The substitution of the carbon–chlorine bond of β,β-dichlorostyryl derivatives[1,2] was firstly approached by Minato and Tamao[3,4] who developed a palladium-catalyzed arylation that advantageously provided the *Z*-monoarylated product (Scheme 1, eq. a). Later, Negishi and co-workers developed a palladium-catalyzed alkynylation[5,6] employing zinc acetylides as nucleophilic partners to afford the *Z*-monosubstituted products with high yields and stereoselectively (Scheme 1, eq. b). However, the formation of the side dialkynylated product remains the main weakness of this methodology. Concerning the alkylation attempts of β,β-dichlorostyryl substrates, they also suffered from overreaction and the disubstituted products were often observed.[7,8] An alternative was considered by Figadère and Alami and consisted in the iron-catalyzed version of the Kumada cross-coupling but the formation of the dialkylated compound remained competitive (Scheme 1, eq. c).[9] It was not until the work of Roulland and co-workers[10] that a promising answer to the problem of a stereoselective monoalkylation was provided. Indeed, Roulland designed a Suzuki-type reaction with 9-BBN alkyl boranes that relies on the use of a bidentate phosphine ligand for palladium with a large bite angle to achieve the monoalkylation with high stereoselectivity and in excellent yields. However, once again, they observed traces of the *E*-stereoisomer and/or of the dialkylated side product that proved difficult to separate (Scheme 1, eq. d).

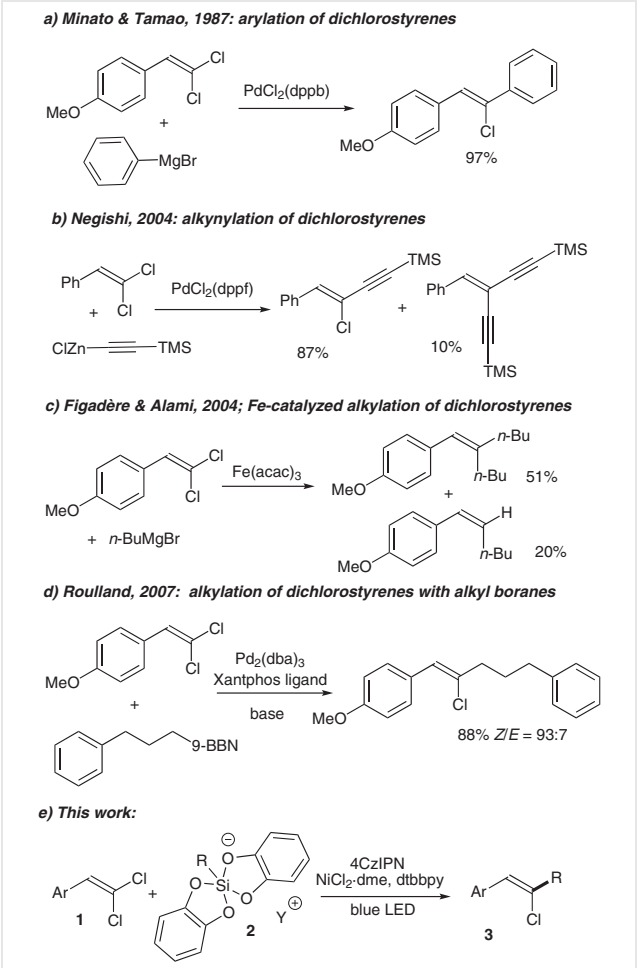

Scheme 1 Literature on metal-catalyzed arylation, alkynylation, and alkylation of β,β-dichlorostyrenes

Georg Thieme Verlag KG, Rüdigerstraße 14, 70469 Stuttgart, Germany

In contrast, to the best of our knowledge, nickel-catalyzed monoalkylation of such electrophiles has not yet been reported in the literature. Indeed, the closest example was the enantioselective alkylation of (*Z*)-β-bromo-styryl derivatives developed by Reisman[11] to afford the *Z*-trisubstituted alkenes with retention of the stereochemistry of the double bond. However, this methodology did not involve the substitution of dihalogenated styryl derivatives.

Considering those elements and based on our continuing interest in photoredox catalysis[12–15] and in photoredox/Ni dual catalysis,[16–20] we considered involving bis(catecholato)silicates in a photoredox/Ni-catalyzed vinylation reaction.[21] Indeed, thanks to their low oxidation potential (between 0.3 and 0.9 V vs SCE) bis(catecholato)silicates are known as efficient radical precursors.[22] Their uses in dual catalysis were investigated by our group[22,23] and the group of Molander for the alkylation of aryl and alkenyl halides.[24,25] To illustrate the versatility of this methodology, our group also investigated the C_{sp3}–C_{sp3} bond formation,[26] the formation of ketones through cross-coupling with acyl chlorides,[27] and the alkylation of alkenyl halides including one preliminary example of alkylation of *p*-methoxy β,β-dichlorostyrene.[28] We wished to further investigate this valuable transformation and examined the reactivity of various dichlorostyryl substrates **1** towards silicates **2** to furnish cross-coupling (*Z*)-styrylchloride products **3** (Scheme 1, eq. e).[29]

[18-C-6]-Potassium silicates **2a** (R = Bn), **2b** (R = –$(CH_2)_2$OAc), **2c** (R = cyclohexyl), and **2d** (R = –CH_2NHPh) were prepared as in previously described procedures.[22,30] At the occasion of this study, we also introduced the previously unknown sodium silicates **2-Na** since they could result in altered reactivity. Sodium salts as additives have indeed resulted in optimized reactivity in some nickel-catalyzed cross-coupling reactions.[11,31]

Sodium silicates **2-Na** were prepared as previously for potassium silicates (Scheme 2).[22] The desired alkoxysilane is reacted with catechol (2 equiv.) and with 1 equiv. of sodium methoxide in methanol. 15-Crown-5 (1 equiv.) can also be added in the reaction mixture to provide sodium silicates **2′**. Gram quantities of **2a-Na** (55% yield), **2b-Na** (64%), and **2c-Na** (55%) were obtained. Similarly, 15-C-5-chelated sodium silicates **2a′** were isolated in 45% yield. All these sodium silicates can be kept several months without degradation if stored under air- and moisture-free conditions.

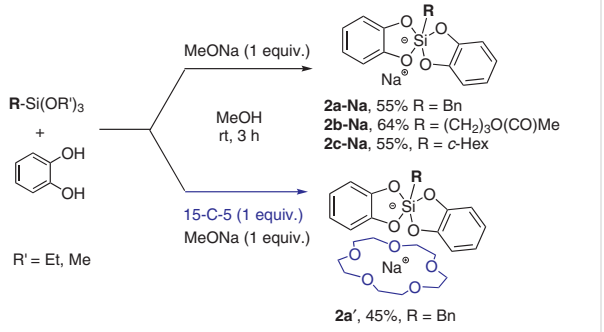

Scheme 2 Synthesis of sodium silicate **2-Na** and **2′**

Suitable crystals of the sodium bis(catecholato)benzyl silicate **2a-Na** were obtained by vapor diffusion using an acetone/diethyl ether mixture (Figure 1). [$C_{22}H_{21}NaO_5Si$] crystallized in a tetragonal crystal system with a = 19.0046(7) Å, b = 19.0046(7) Å, c = 11.5788(5) Å, $\alpha = \beta = \gamma = 90°$ (Z = 8).[32] Sodium ions are coordinated to one oxygen atom of four catechol ligands and one acetone molecule completes the coordination sphere. The O_{1-5}–Na_1 bond lengths are spanning from 2.288(3) Å to 2.355(2) Å. Finally, an intramolecular π-cation interaction between the centroid of the benzyl and Na_1 can be observed with a distance of 3.2712(9) Å.

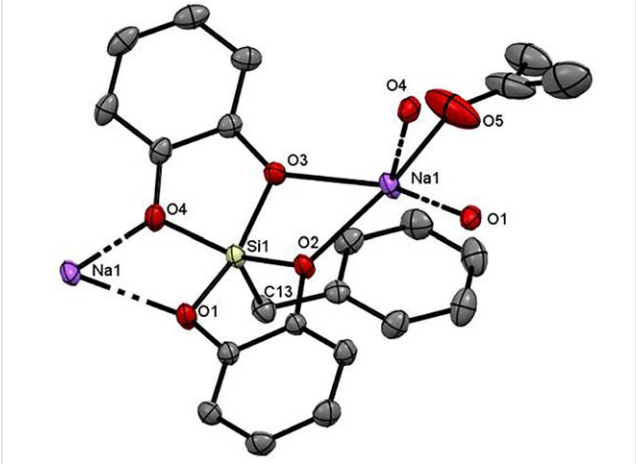

Figure 1 X-ray crystal structure of **2a-Na**, thermal ellipsoids are drawn at 50% probability level. Hydrogen atoms are omitted for clarity. Dashed lines denote bonds between neighboring silicates.

The Si coordination of **2a-Na** can be described as a slightly distorted square pyramid (SP) structure with the benzyl group occupying the apical site (Si–C_{13} bond length = 1.879(2) Å). The four basal positions are occupied by the two oxygen atoms of two catechol ligands. We can notice that the Si atom is located just a little above the plane defined by these fourth atoms (distance Si–plane centroid = 0.4517(6) Å). For **2a-Na,** the dihedral angle method permits to calculate a displacement of 89.3% (TBP → SP, TBP: trigonal bipyramidal).[33] This is also underlined by the close values of all the 4 basal bond Si–O distances from 1.735(2) to 1.759(2) Å. Compared to an idealized SP with four angles of 86°, a slight distortion is observed with angle deviations from –2.5° to 2.1°. Interestingly, **2a-Na** forms a polymeric assembly along the *c*-axis that originates from multiple interactions between Na and oxygen atoms of the catechols of two silicates (see Supporting Information). Sodium cyclohexyl silicate **2c-Na** also crystallized, and an XRD structure

analysis was obtained[34] and proved to be very similar to the corresponding potassium one.[22]

Finally, oxidation potentials of sodium silicates were determined by cyclic voltammetry and proved consistent with the low values we already observed for the potassium ones[22] i.e., E_{ox} = +0.77 V vs SCE for **2a-Na**, +0.88 V for **2b-Na**, and +0.81 V for **2c-Na**.

All β,β-dichlorostyrenes **1** were synthesized by a common Corey–Fuchs–Ramirez olefination from the corresponding aldehydes[35] and were obtained with good yields. For our catalytic system, we considered the same as in our previous studies,[28] namely nickel(II)·dme in the presence of 2,6-di-*tert*-butyl bipyridine as catalytic system and 1,2,3,5-tetrakis(carbazol-9-yl)-4,6-dicyanobenzene (4CzIPN)[36] as photocatalyst. 4CzIPN is endowed with a very high reduction potential after photoexcitation (+1.59 V vs SCE)[37] and a long-lived excited state (5.1 µs) which enables the efficient oxidation of the silicate (E_{ox} < 0.9 V vs SCE) to afford the corresponding C-centered radical.

We first concentrated on the cross-coupling of 1-vinylnaphthalene derivatives **1a** as electrophiles with benzyl silicates **2a** (see Table 1). We began our investigation by delineating the range of dihalogenostyrenes that could handle this approach (Table 1, entries 1–3). The difluorinated reagent **1a-F** did not react despite the presence of silicon on the radical precursor likely to establish a strong interaction with a fluoride. In contrast, the dibrominated reagent **1a-Br** led in our conditions to a complex mixture in which only a marginal amount of monoalkylated was detected. Interestingly, only the presumably less reactive dichlorinated substrate **1a** positively reacted in this dual catalysis reaction (44% of adduct **3aa**) and was then chosen as model substrate for the optimization of the reaction conditions. To our delight, the alkylation occurred selectively without any formation of side products such as the dialkylated product or the *E*-stereoisomer. The *Z*-stereochemistry of **3aa** was assigned by analogy with subsequent findings (vide infra).

We then examined the effect of the cation in this reaction. No improvement of yield was observed from free potassium silicate **2a-K** (39% of **3a**, entry 4), sodium silicates with 15-C-5 (**2a′**, 39%, entry 5) or without 15-C-5 (**2a-Na**, 42%, entry 6). Nevertheless, the fact that the plain sodium silicate **2a-Na** could be engaged successfully opened interesting perspectives. Focusing on silicate **2a**, we then investigated other possibilities to increase the yield of **3aa** (Table 1). While doubling the loading in silicate (entry 7) or its concentration (entry 8) did not have a significant impact on the yield, a longer reaction time (72 h) with double amount of **2a** provided the best yield of **3a** (70%, entry 10). We also checked that nickel catalysis was necessary for this transformation: no radical addition – β-elimination of a chlorine radical takes place[22] to deliver **3aa** (entry 11)

Table 1 Optimization of the Cross-Coupling Reaction

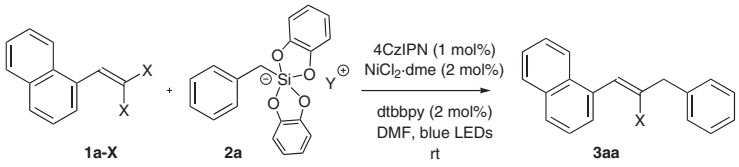

Entry	Reaction time (h)	X	[Si] counterion Y	Silicate (equiv.)	Yield of **3aa** (%)[a]
1	48	F, **1a-F**	K[18-C-6], **2a**	1.5	NR[b]
2	48	Br, **1a-Br**	K[18-C-6], **2a**	1.5	mixture
3	48	Cl, **1a**	K[18-C-6], **2a**	1.5	44
4	48	Cl, **1a**	K, **2a-K**	1.5	39
5	48	Cl, **1a**	Na[15-C-5], **2a′**	1.5	39
6	48	Cl, **1a**	Na, **2a-Na**	1.5	42
7	48	Cl, **1a**	K[18-C-6], **2a**	3	47
8[c]	48	Cl, **1a**	K[18-C-6], **2a**	3	51
9	72	Cl, **1a**	K[18-C-6], **2a**	1.5	50
10	72	Cl, **1a**	K[18-C-6], **2a**	3	70
11[d]	48	Cl, **1a**	K[18-C-6], **2a**	1.5	0

[a] NMR yield was determined using 1,3,5-trimethoxybenzene as internal standard.
[b] NR: no reaction detected.
[c] Variation of the concentration (0.1–0.2 M)
[d] Reaction performed without nickel catalyst.

Based on all the results from Table 1, the standard conditions (48 h and 1.5 equiv. of silicate) appear to be a good compromise in terms of reaction time and cost to reach a decent yield in this cross-coupling reaction. Subsequently, we engaged under those conditions various [18-C-6]-potassium and sodium silicates **2** and **2-Na** with β,β-dichlorostyrenes **1** under the Ni/4CzIPN dual catalysis conditions to explore the scope of this reactivity (Scheme 2).

The results of Scheme 3 illustrate a certain versatility of this cross-coupling reaction between the *gem*-dichlorostyryl precursors **1** and the silicates **2**. Indeed, the reaction occurs with an alkyl silicate (primary and secondary), a benzylic one, and even the α-methyl-anilino-silicate with various dichlorostyrenes **1**, and provides previously unknown coupling products with fair to good yields. In some cases, the use of the sodium silicates **2-Na** compared to the potassium ones **2** proved more rewarding in terms of yields for coupling products **3** (products **3ab** and **3bc**). The coupling does not depend on the electron-withdrawing or electron-donating character of the substituent of the dichlorostyrene. Indeed, substrates that own a methoxy group or a trifluoromethyl group in *para* position react similarly with the primary alkyl acetoxypropyl radical (**2b**) or the more nucleophilic α-methyl-aniline one (**2d**) (Scheme 3).

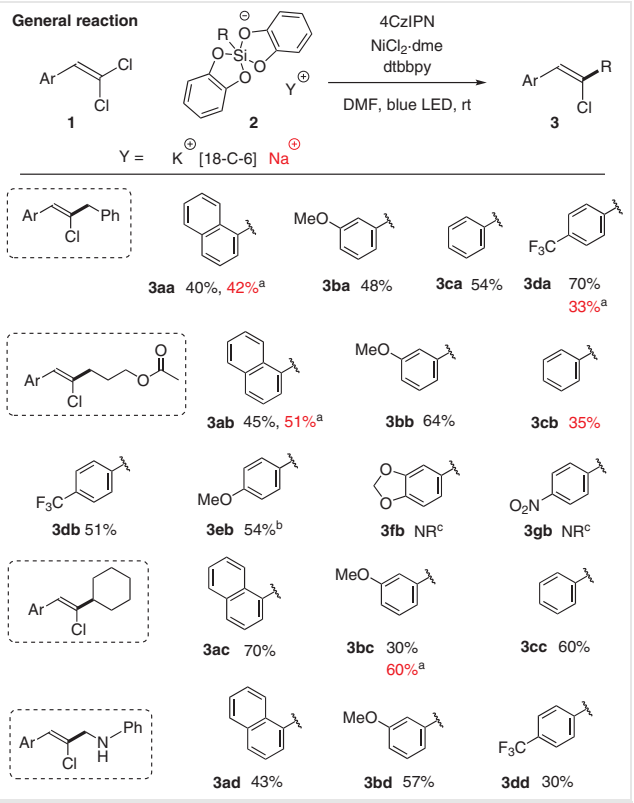

Scheme 3 Reaction of *gem*-dichlorostyrenes **1** with various silicates **2** (isolated yieds). *Reagents and conditions*: **1** (1 equiv), **2** (1.5 equiv), 4CzIPN (1 mol%), $NiCl_2$·dme/dtbbpy (2 mol%), rt for 48 h. [a] NMR yield was determined using 1,3,5-trimethoxybenzene as internal standard. [b] See also ref. 28. [c] NR: no reaction detected, starting material was recovered.

Of note, the more sensitive precursors, piperonal and nitro substrates failed to give any adducts (**3fb** and **3gb**) and it is also important to specify that only the *Z*-isomer, as determined by NOESY experiments, of each adduct **3** was isolated and that no dialkylation product was observed. In the reactions of amino silicate **2d**, some (*Z*)-chlorostyrene was formed as side product in 15–20% yield that was highly suggestive of a protodenickelation based on the proposed mechanism of Scheme 4.

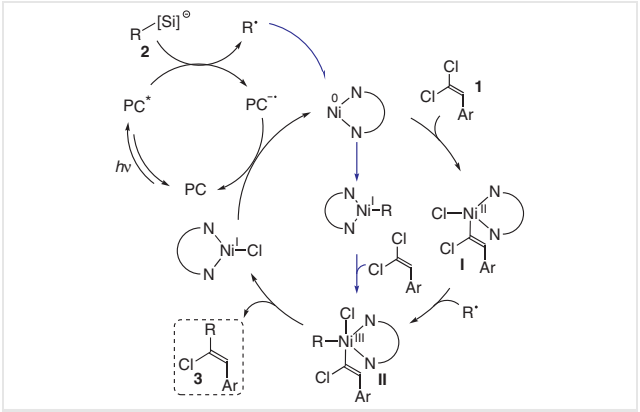

Scheme 4 Plausible mechanism for the cross-coupling reaction

Because we know that nickel is necessary in these reactions to obtain products **3** and based on the literature mechanism proposals of related Ni/photoredox dual catalysis reactions,[18–20,38] it appears reasonable to invoke the trapping by nickel of a C-centered radical originating from the photoinduced oxidation of the silicates **2**. The nickel intermediate that would be involved is the nickel(II) complex **I** that originates from the oxidative addition into the C–Cl bond of the substrates **1** (Scheme 4). The observed *Z*-selectivity might be ascribed to the presence of the bidentate ligand on nickel that would generate a significant steric hindrance around the metallic center and that possibly orients the oxidative addition on the more accessible C–Cl bond, with no aryl group in *syn*. Even though the effect of the bulkiness around the metallic center seems clear, the insensitivity of the coupling to the substituent on the aryl moiety might appear strange but is reminiscent of previous findings in arylative couplings.[23,24] This would be consistent with a radical addition on nickel(II) that is rather insensitive to electronic effects.[39–42] The resulting nickel(III) complex **II** then undergoes reductive elimination to provide products **3** and a nickel(I) salt that would be reduced by the photoredox cycle to Ni(0).

Based on the clean but inefficient conversion of some of these reactions, we also wished to explore other conditions to run them. Notably we used an in-house flow setting[43,44] (see the Supporting Information for details) in order to re-

duce the reaction times. We tested silicate **2c** and naphthyl electrophile **1a** as a model reaction based on its efficiency in batch after 48 h of irradiation (70% of **3ac**, Scheme 3). Interestingly, within a residence time of 50 min, we reached 32% yield in **3ac** and 50% within 90 min (Scheme 5). Therefore, the flow conditions open promising perspectives for this methodology.

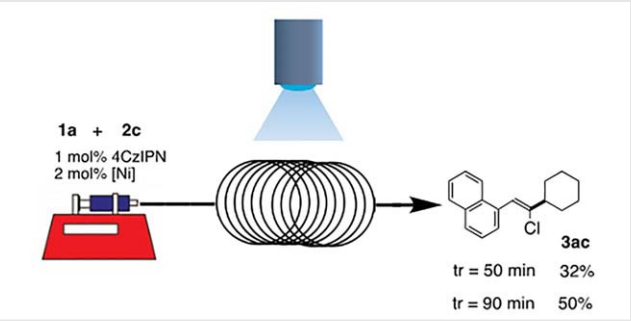

Scheme 5 Continuous-flow conditions

Finally, we investigated the possibility of the postfunctionalization of the alkylated adducts **3** by using our methodology. We engaged different monoalkylated products **3** with silicates **2** (**3bb** with benzyl silicate and **3bd** with acetoxypropyl silicate) and we only recovered the starting material after 2 days of irradiation. All in all, this absence of reactivity confirms that our methodology is inoperative to achieve the substitution of the two C–Cl bonds. Nevertheless, Roulland's and Tamao's works showed that the postfunctionalization of the monosubstituted product was effective by engaging them in their palladium-catalyzed alkylation or arylation sequences.[2,3]

To conclude, we have developed an innovative way to alkylate *gem*-dichlorostyrenes with fair to good yields. Contrary to most of the previous methodologies employing palladium catalysts, this cross-coupling reaction advantageously combines the earth-abundant nickel metal with a cheap organic dye to achieve smoothly the substitution at room temperature (where all the previous methods mentioned are performed under reflux). Furthermore, the main advantages of this reaction are its total *Z*-stereoselectivity and the absence of overreaction to widen the scope of this methodology. Otherwise, one of the aims of the study was the approach of the silicate's counterion and its effect on the photoredox catalysis. The second interest of this study is the introduction of sodium silicates **2-Na** that improves the atom economy compared to the [18-C-6]-chelated potassium silicate analogues **2**. If this work provided interesting and promising insights, the influence of the counterion remains nonexhaustive and will be pursued by our group.

Funding Information

The authors thank the Agence Nationale de la Recherche (Grant No. ANR-17-CE07-0018, HyperSilight (PhD grant to EL)), the Centre National de la Recherche Scientifique (CNRS), and Sorbonne Université for financial support.

Acknowledgment

We are grateful to J. Forté, G. Gontard and Lise-Marie Chamoreau for X-ray diffraction analyses and helpful discussions.

Supporting Information

Supporting information for this article is available online at https://doi.org/10.1055/a-1374-9384.

References and Notes

(1) Chelucci, G. *Chem. Rev.* **2012**, *112*, 1344.
(2) Arthuis, M.; Lecup, A.; Roulland, E. *Chem. Commun.* **2010**, *46*, 7810.
(3) Minato, A.; Suzuki, K.; Tamao, K. A. *J. Am. Chem. Soc.* **1987**, *109*, 1257.
(4) Minato, A. *J. Org. Chem.* **1991**, *56*, 4052.
(5) Shi, J.; Zeng, X.; Negishi, E. *Org. Lett.* **2003**, *5*, 1825.
(6) Negishi, E.; Shi, J.; Zeng, X. *Tetrahedron* **2005**, *61*, 9886.
(7) Andrei, D.; Wnuk, S. F. *J. Org. Chem.* **2006**, *71*, 405.
(8) Tan, Z.; Negishi, E. *Angew. Chem. Int. Ed.* **2006**, *45*, 762.
(9) Dos Santos, M.; Franck, X.; Hocquemiller, R.; Figadère, B.; Peyrat, J.-F.; Provot, O.; Brion, J.-D.; Alami, M. *Synlett* **2004**, 2697.
(10) Liron, F.; Fosse, C.; Pernolet, A.; Roulland, E. *J. Org. Chem.* **2007**, *72*, 2220.
(11) DeLano, T. J.; Reisman, S. E. *ACS Catal.* **2019**, *9*, 6751.
(12) McAtee, R. C.; McClain, E. J.; Stephenson, C. R. J. *Trends Chem.* **2019**, *1*, 111.
(13) Marzo, L.; Pagire, S. K.; Reiser, O.; König, B. *Angew. Chem. Int. Ed.* **2018**, *57*, 10034.
(14) Crespi, S.; Fagnoni, M. *Chem. Rev.* **2020**, *120*, 9790.
(15) Xuan, J.; Zang, Z.-G.; Xiao, W.-J. *Angew. Chem. Int. Ed.* **2015**, *54*, 15632.
(16) Levin, M. D.; Kim, S.; Toste, F. D. *ACS Cent. Sci.* **2016**, *2*, 293.
(17) Hopkinson, M. N.; Sahoo, B.; Li, J.-L.; Glorius, F. *Chem. Eur. J.* **2014**, *20*, 3874.
(18) Nacsa, E. D.; MacMillan, D. W. C. *Org. React.* **2019**, 471.
(19) Skubi, K. L.; Blum, T. R.; Yoon, T. P. *Chem. Rev.* **2016**, *116*, 10035.
(20) Tellis, J. C.; Kelly, C. B.; Primer, D. N.; Jouffroy, M.; Patel, N. R.; Molander, G. A. *Acc. Chem. Res.* **2016**, *49*, 1429.
(21) Goddard, J.-P.; Ollivier, C.; Fensterbank, L. *Acc. Chem. Res.* **2016**, *49*, 1924.
(22) Corcé, V.; Chamoreau, L. M.; Derat, E.; Goddard, J.-P.; Ollivier, C.; Fensterbank, L. *Angew. Chem. Int. Ed.* **2015**, *54*, 11414.
(23) Lévêque, C.; Chenneberg, L.; Corcé, V.; Goddard, J.-P.; Ollivier, C.; Fensterbank, L. *Org. Chem. Front.* **2016**, *3*, 462.
(24) Jouffroy, M.; Primer, D. N.; Molander, G. A. *J. Am. Chem. Soc.* **2016**, *138*, 475.
(25) Patel, N. R.; Kelly, C. B.; Jouffroy, M.; Molander, G. A. *Org. Lett.* **2016**, *18*, 764.
(26) Lévêque, C.; Corcé, V.; Chenneberg, L.; Ollivier, C.; Fensterbank, L. *Eur. J. Org. Chem.* **2017**, 2118.

(27) Levernier, E.; Corcé, V.; Rakotoarison, L.-M.; Smith, A.; Zhang, M.; Ognier, S.; Tatoulian, M.; Ollivier, C.; Fensterbank, L. *Org. Chem. Front.* **2019**, *6*, 1378.
(28) Lévêque, C.; Chenneberg, L.; Corcé, V.; Ollivier, C.; Fensterbank, L. *Chem. Commun.* **2016**, *52*, 9877.
(29) For a recent access to vinylchlorides, see: Adak, T.; Hoffmann, M.; Witzel, S.; Rudolph, M.; Dreuw, A.; Hashmi, A. S. K. *Chem. Eur. J.* **2020**, *26*, 15573.
(30) Corcé, V.; Lévêque, C.; Ollivier, C.; Fensterbank, L. In *Science of Synthesis: Photocatalysis in Organic Synthesis*; König, B., Ed.; Thieme: Stuttgart, **2019**, 427–466.
(31) Prinsell, M. R.; Everson, D. A.; Weix, D. J. *Chem. Commun.* **2010**, *46*, 573.
(32) CCDC 2048159 contains the supplementary crystallographic data for compound **2a-Na**. The data can be obtained free of charge from The Cambridge Crystallographic Data Centre via www.ccdc.cam.ac.uk/structures.
(33) Holmes, R. R.; Deiters, J. A. *Phosphorus, Sulfur Silicon Relat. Elem.* **1995**, *98*, 105.
(34) CCDC 2050302 contains the supplementary crystallographic data for compound **2c-Na**. The data can be obtained free of charge from The Cambridge Crystallographic Data Centre via www.ccdc.cam.ac.uk/structures.
(35) Burton, G.; Elder, J. S.; Fell, S. C. M.; Stachulski, A. V. *Tetrahedron Lett.* **1988**, *29*, 3003.
(36) Shang, T.-Y.; Lu, L.-H.; Cao, Z.; Liu, Y.; He, W.-M.; Yu, B. *Chem. Commun.* **2019**, *55*, 5408.
(37) Le Vaillant, F.; Garreau, M.; Nicolai, S.; Gryn'ova, G.; Corminboeuf, C.; Waser, J. *Chem. Sci.* **2018**, *9*, 5883.
(38) Tasker, S. Z.; Jamison, T. F. *J. Am. Chem. Soc.* **2015**, *137*, 9531.
(39) Durandetti, M.; Nédélec, J.-Y.; Périchon, J. *J. Org. Chem.* **1996**, *61*, 1748.
(40) Weix, D. J. *Acc. Chem. Res.* **2015**, *48*, 1767.
(41) Richmond, E.; Moran, J. *Synthesis* **2018**, *50*, 499.
(42) (a) Lévêque, C.; Ollivier, C.; Fensterbank, L. In *Nickel Catalysis in Organic Synthesis*; Ogoshi, S., Ed.; Wiley-VCH: Weinheim, **2020**, 151–181. (b) Goldfogel, M. J.; Huang, L.; Weix, D. J. In *Nickel Catalysis in Organic Synthesis*; Ogoshi, S., Ed.; Wiley-VCH: Weinheim, **2020**, 183–222.
(43) Cambié, D.; Bottecchia, C.; Straathof, N. J. W.; Hessel, V.; Noël, T. *Chem. Rev.* **2016**, *116*, 10276.
(44) Garlets, Z. J.; Nguyen, J. D.; Stephenson, C. R. J. *Isr. J. Chem.* **2014**, *54*, 351.

Personal Account

DOI: 10.1002/tcr.202100049

THE CHEMICAL RECORD

A Parisian Vision of the Chemistry of Hypercoordinated Silicon Derivatives

Gilles Lemière,* Alexandre Millanvois, Cyril Ollivier,* and Louis Fensterbank*[a]

Dedicated to Scott Sieburth, a visionary of silicon chemistry

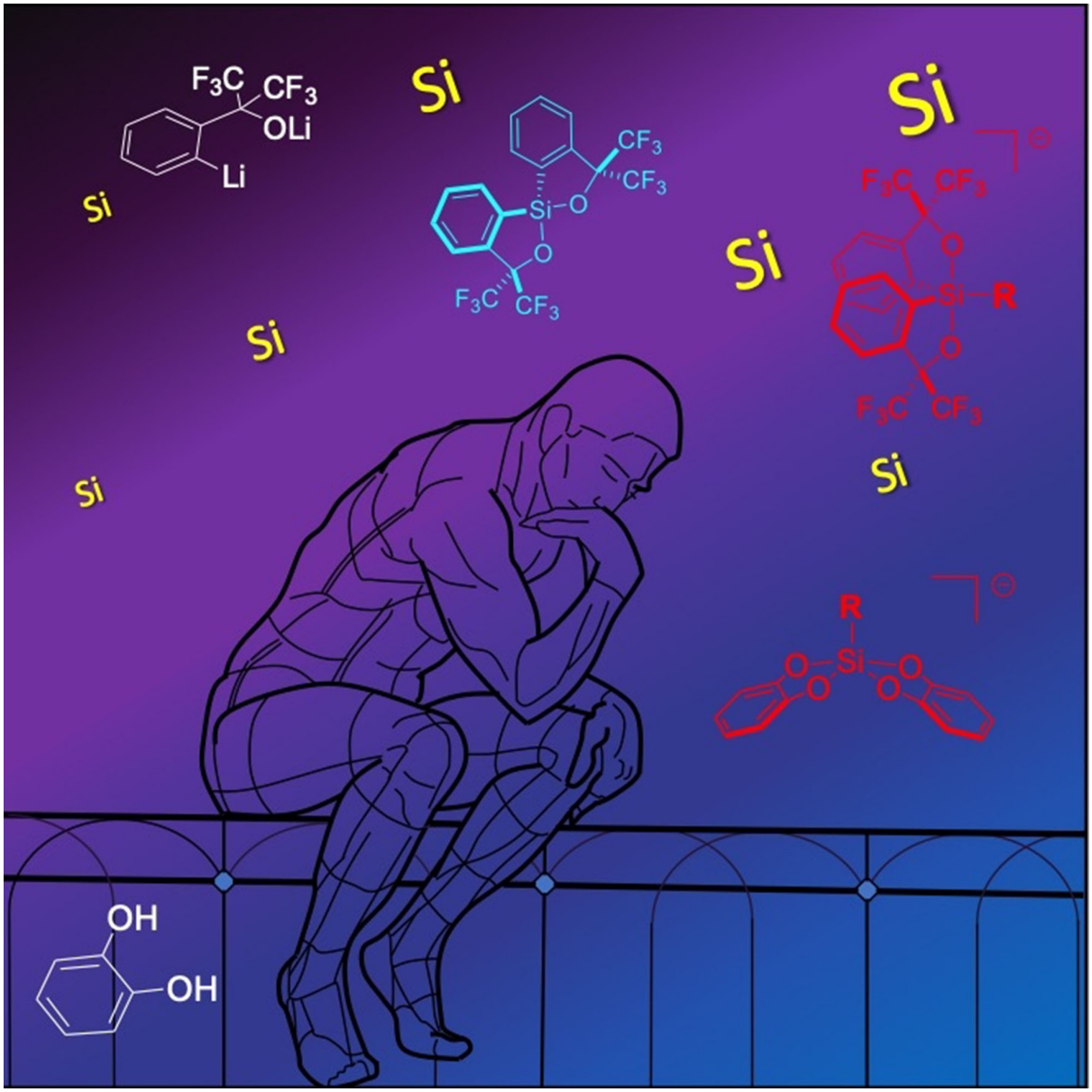

Abstract: Less than ten years of acquaintance with hypercoordinated silicon derivatives in our lab is described in this account. Martin's spirosilane derivatives open new opportunities as ligands and as agents for the activation of small molecules and bis-catecholato silicates have proven to be exquisite radical precursors in photoredox conditions for broad synthetic applications.

Keywords: Silicon, Lewis acid, silicate, photoredox, radical

1. Introduction: Why Hypercoordinated Silicon Derivatives?

Just below carbon in the periodic table, silicon is much more than a pale imitation of carbon. While organosilicon compounds featuring a C–Si bond are very common, silicon, due to its lower electronegativity compared to carbon, the longer bonds by which it connects to neighboring atoms, its high affinity for fluoride and alkoxy ligands and its propensity to form hypercoordinated derivatives offers unique opportunities in organic chemistry. The first example of a hexavalent silicon derivative ($SiF_4 \cdot 2NH_3$) was reported at the beginning of the 19th century by Gay-Lussac and Davy.[1] But it was the following century that saw the major discoveries that laid the foundations for the modern chemistry of hypercoordinated organosilicon compounds as conceptualized in the 1980s by Voronkov,[1] Holmes[2] and Corriu[3] just to name a few.[4] As nicely highlighted in 2005 by Oestreich,[5] the hypercoordinated mode can be transiently generated to trigger valuable reactivities such as the Brook rearrangement, the Tamao-Fleming oxidation or the Hiyama cross coupling just to name a few. But stable adducts can also be prepared, isolated and fully characterized.[6] Our acquaintance with organosilicon compounds has a long history featuring arylsilanolates as metalation directing groups,[7] silicon tethered Diels-Alder reactions,[8] bromomethylsilyl ethers as precursors of radical cascades,[9] epoxysilanes,[10] silapiperidines.[11] In this story, we will focus on two more recent stories. The first one deals with the use of Martin's spirosilane and derivatives as Lewis acids and their reactions toward various nucleophiles. The second one focuses on the introduction of bis-catecholato silicates as precursors of radicals in photooxidative conditions.

[a] *Dr. G. Lemière, A. Millanvois, Dr. C. Ollivier, Prof. L. Fensterbank*
Institut Parisien de Chimie Moléculaire
Sorbonne Université, CNRS
4 place Jussieu, 75005 Paris
E-mail: gillles.lemiere@sorbonne-universite.fr
cyril.ollivier@sorbonne-universite.fr
louis.fensterbank@sorbonne-universite.fr

2. Martin's Spirosilanes as an Entry for Stable Peculiar Silicates

2.1. Martin's Spirosilane, a Valuable Lewis Acid

James Cullen Martin a.k.a. J. C. Martin is mainly known for his invention of the Dess-Martin reagent. Nevertheless in 1979, he made a seminal report on the use of the dilithio derivative of hexafluorocumyl alcohol as a bidendate ligand that can be appended twice on heteroatoms such as phosphorus, sulfur and silicon to give the corresponding phosphoranoxide **1**, sulfurane **2** and silicate **3**.[12] When treated with $SiCl_4$, hexafluorocumyl alcohol dianion provides a direct access to spirosilane **4** that can also be obtained from the treatment of silicate **3** with triflic acid (Scheme 1). Due to the presence of the highly electronegative bis-trifluoro alkoxy ligand, spirosilane **4** is a very strong Lewis acid that can react with a variety of charged and neutral nucleophiles.[13]

2.2. Martin's Spirosilane as a Fluoride Sensor

For several years, our laboratory has been interested in the reactivity of Martin's spirosilanes **4** towards neutral or charged nucleophiles in order to obtain original structures. In particular, it was possible to exploit the Lewis acid properties and its ability to easily reach the hypercoordinated form, to use it as a fluoride probe (Scheme 2).[14] The very strong Si–F bond warrants selective and quantitative detection of fluoride

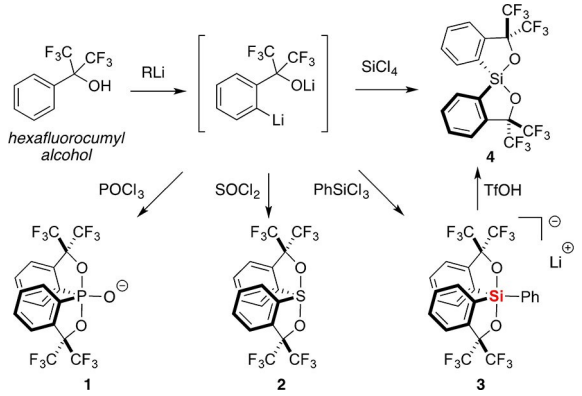

Scheme 1. Attachment of Martin's ligand on phosphorus, sulfur and silicon. Access to spirosilane **4.**

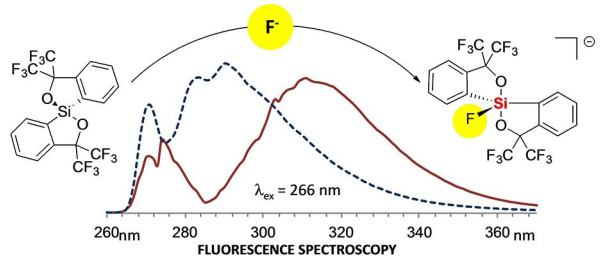

Scheme 2. Martin's spirosilane **4** as a fluoride sensor.

ions in solution and the structural reorganization of hypercoordinated silicon structure allows for a diagnostic.

UV and fluorescence spectroscopy have been used to quantify the fluorosilicate product attaining detection limits as low as 5 μM which is close to the residual concentration of fluoride in some drinking waters. Recently, Greb and coworkers have proposed a bis(alizarinato) spirosilane as chromogenic fluoride sensor which announces further developments in this area.[15]

2.3. Interaction of Martin's Spirosilane with N-heterocyclic Carbenes (NHCs)

Recently, we have studied the interactions of the Martin's spirosilane with neutral Lewis bases displaying various strength and steric hindrances. It has been established that the outcome

Louis Fensterbank obtained his PhD in 1993 at SUNY Stony Brook under the guidance of Scott Sieburth. After a lecturer position at the Université Pierre & Marie Curie (UPMC), he was appointed in 1995 as a CNRS Chargé de Recherche with Max Malacria. In 2004, he became Professor at UPMC, now Sorbonne Université. His research interests concern the discovery of new molecular transformations relying on radical or organometallic processes and their applications to the synthesis of substrates with relevant properties. Co-author of more than 220 publications, he has received several awards, notably the Silver Medal of CNRS in 2017. He is also Fellow of the Royal Society of Chemistry.

Gilles Lemière studied chemistry in Paris at the Université Pierre et Marie Curie (UPMC), where he obtained his PhD in 2008 under the supervision of Profs. Louis Fensterbank and Max Malacria. After his PhD on gold-catalysed new organic reactions, he joined the group of Prof. Jonathan Clayden in Manchester as a postdoctoral fellow to work on the total synthesis of natural compounds. In 2010, he was appointed CNRS Researcher at the University of Nice in the group of Elisabet Dunach and moved in 2015 to Sorbonne Université, Paris. His research interests deal with the development of new metal- and acid-catalysed cycloisomerisation processes and silicon chemistry.

Alexandre Millanvois received his Bachelor (UPMC) and master's degree at Sorbonne Université (ex UPMC) with honour. He is currently conducting his joint PhD under the supervision of Prof. Louis Fensterbank, Prof. Tan Choon Hong and Dr. Cyril Ollivier between Sorbonne Université and Nanyang Technological University (NTU). His current research interests are focused on the synthesis of new silicon based radical precursor and their application in asymmetric radical chemistry.

Cyril Ollivier obtained his PhD in 2000 from the University of Fribourg (Switzerland) and UPMC under the guidance of Philippe Renaud in collaboration with Max Malacria. He was awarded a Swiss National Foundation Fellowship to work with Philippe Magnus at the University of Texas at Austin. In 2002, he was appointed Chargé de Recherche CNRS at Aix-Marseille University and in 2007, he moved to UPMC/Sorbonne University where he is now Directeur de Recherche to develop new directions for research on synthetic radical and organometallic chemistry including photocatalytic processes.

of these interactions was very dependent on both parameters.[16] Indeed, in the presence of weakly hindered NHCs Lewis base of imidazolylidene type (IMe, IMes), new neutral adducts **5** originating from classical Lewis acid-base interactions were obtained in which the pentacoordinated silicon adopts a trigonal bipyramid (TBP) geometry (Scheme 3), as highlighted by their X-ray diffraction (XRD) analyses. Conversely, when the size of the free carbene becomes larger (IPr, ItBu), no direct interaction between the silicon and the divalent carbon of the NHCs can be noticed by ^{1}H NMR monitoring. Considering the strength of the Lewis partners involved, the non-interaction is unambiguously diagnostic of Frustrated Lewis Pair (FLP) behaviors highlighting the bulkiness of the spirosilane to some extent. After some time, the mixtures evolves nonetheless towards the formation of an "abnormal adduct" **6** where a covalent bond is created between the silicon atom and one of the two trivalent carbons located on the NHC backbone. As it can be visualized on the XRD structure of **6** (R = Dipp), the ligands surrounding the hypercoordinated silicon are quite distorted due to the steric congestions and deviates from the perfect TBP.

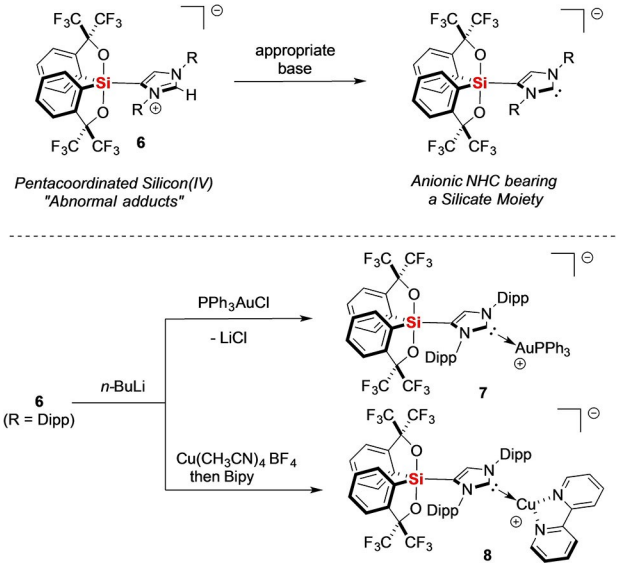

Scheme 4. Silicate-imidazolium zwitterions as precursors for anionic NHC ligands.

2.4. Anionic NHC Ligand Featuring Hypercoordinated Silicon

The abnormal adducts **6** have been later used as precursors for new anionic NHC carbene ligands possessing within their backbone a poorly coordinating anion.[17] As a matter of fact, structures **6** are neutral species that could be seen as imidazolium rings attached to a silicate anion. Basically, the deprotonation of the positively charged heterocycles by using an appropriate base would lead to carbene ligands that can interfere with metals to form original organometallic complexes. From this perspective, the abnormal adducts **6** were cleanly deprotonated using *n*-butyllithium as a base, to be subsequently trapped with Au(I) or Cu(I) species affording complexes of type **7** and **8**, respectively (Scheme 4). It is noteworthy that the anionic nature of the ligand and the presence of the lithium cation presumably favors the chloride dissociation from $ClAuPPh_3$ to provide the corresponding neutral complexes. The strong σ-donor ability of these new anionic NHC ligands was confirmed by density-functional theory (DFT) calculations.

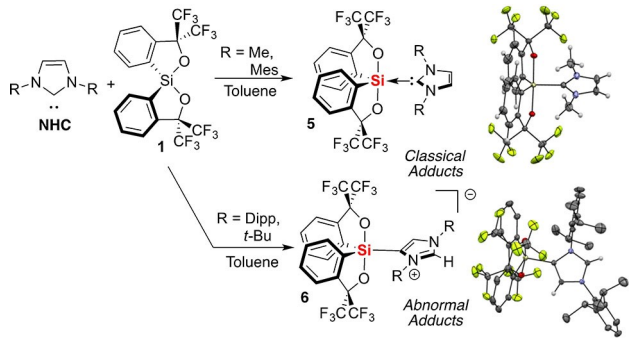

Scheme 3. Interaction between Martin's spirosilane **1** and NHCs.

2.5. Spirosilanes as Lewis Acid Partners in FLP Chemistry

As previously mentioned, the Martin's spirosilane **4** exhibits a FLP character when confronted to encumbered NHCs. The same trend was also observed with other hindered bases such as *tert*-butylphosphine and 2,2,6,6-tetramethylpiperidine since in both cases, no adducts are formed when they are in presence of silane **4**.[18] This behavior is similar to that of $B(C_6F_5)_3$, the most employed Lewis acid in FLP chemistry.[19] For the sake of comparison, the Lewis acidity of Martin's spirosilane **4** was assessed using the Gutmann-Beckett parameter.[20] Although the understanding of the Lewis acidity is very complex and depends on many parameters, this method based on the shift of triethylphopshine oxide in ^{31}P NMR spectroscopy represents a convenient way to roughly compare the electrophilicity of various species. The acceptor number of **4** was evaluated as AN = 84.4 which is slightly higher than the one calculated for $B(C_6F_5)_3$ (AN = 81.4).[21]

Theoretically, the Lewis acid properties of the Martin's spirosilane **4** can be modulated by introducing substituents on the aromatic rings. For that purpose, a synthesis strategy of analogous structures of spirosilane **4** has been previously developed in our laboratory.[22] It consists in the spirocyclization of functionalized hexafluorocumyl ligands that are readily

available from the corresponding 2-bromobenzoic acid derivatives (Scheme 5).

With this method, the synthesis of a spirosilane **9** bearing one trifluoromethyl group on each aromatic ring was achieved. The presence of an electron-withdrawing group has a great effect on the electronic properties of the silicon atom and the acceptor number was calculated as AN = 89.2. That makes spirosilane **9** a remarkable Lewis acid particularly prone to reach hypercoordination. The high electrophilicity of the CF_3 derivative **9** was confirmed since a classical Lewis adduct **10** was formed in the presence of a bulky NHC (IPr) which has never been observed in the case of the simpler spirosilane **4** (Scheme 6). DFT calculations revealed that the presence of CF_3 groups on the spirosilane increases the Gibbs free enthalpy of formation of the conventional adduct by at least 10 kcal.mol^{-1}.

Although for the moment, Lewis acid partners **4** and even more Lewis acidic **9** proved to be inefficient for the activation of H_2 and CO_2, activation of formaldehyde was possible with

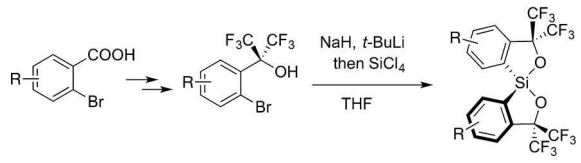

Scheme 5. Synthesis of Martin's spirosilane analogues.

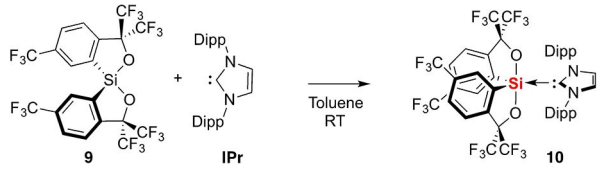

Scheme 6. Formation of classical Lewis adduct by reaction of spirosilane **9** with IPr.

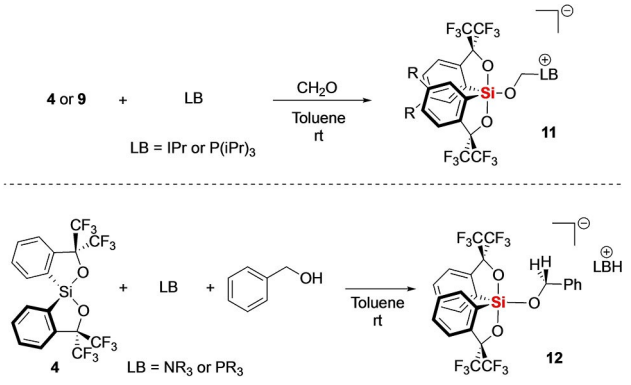

Scheme 7. Use of spirosilanes **4** and **9** in FLP chemistry.

the IPr NHC and tri-isopropylphosphine. In these cases, the zwitterionic adducts of type **11** could be isolated (Scheme 7).

In addition, the Martin's spirosilane **4** could also be used for the activation of alcohols such as benzylic alcohol to form benzyloxysilicates **12** in the presence hindered phosphines or amines. On the ^{1}H NMR spectrum, adducts **12** displayed AB systems with a large splitting of the two diastereotopic benzylic protons that highlights the intrinsic chirality of the Martin's spirosilane at the NMR timescale. This interesting feature potentially opens the way for further asymmetric FLP transformations using chiral spirosilane analogues.

3. Bis-catecholato Silicates as Radical Precursors

3.1. Oxidation of Soft Carbanions

In the quest for new radical precursors, we engaged in the exploration of the oxidation of ate and hypercoordinated derivatives. The idea of such an approach originated from the very inspiring works of Kumada as PI, featuring also the two prominent chemists: Kohei Tamao and the late Jun-ichi Yoshida, on the oxidation of pentafluorosilicates with copper (II) and some organic oxidants.[23] We first tested this idea on alkyltrifluroborates and showed they could be smoothly oxidized by copper(II) salts or Dess-Martin periodinane to give alkyl radicals including primary ones.[24] We then examined the reactivity of more soluble and user friendly bis-catecholato silicates synthesized by Cecil Frye[25] and Robert Corriu.[26] We were encouraged to do so based on a series of works of Nishigaichi who reported the photoallylation of benzil-type derivatives and dicyanobenzene in moderate yields, but these reactions were limited to the generation of stabilized allyl and benzyl radicals.[27] We therefore decided to prepare a series of bench stable alkyl bis-catecholato silicates **13** and to test them in photooxidative conditions under visible-light irradiation in order to generate functionalized alkyl radicals and particularly unstabilized primary ones (Scheme 8).[28]

3.2. Oxidation of Alkyl Bis-catecholato Silicates through Visible Light Photoredox Catalysis: Preliminary Screenings

Potassium alkyl bis-catecholato silicates **13** can be easily obtained by reaction of trialkoxysilanes with catechol and

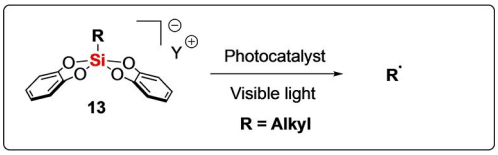

Scheme 8. Generation of alkyl radicals by photooxidation of alkyl bis-catecholato silicates **13** under visible light irradiation.

potassium methoxide in methanol. The presence of crown ether 18-crown-6 (18-C-6) stabilizes the hypercoordinated species[3] so that a series of primary and secondary alkylsilicates with various functions can be prepared on a large scale and stored for a long time at room temperature with no significant degradation. Sodium silicates **13** are also accessible under the same conditions (MeONa/MeOH) but have shown a reduced stability, even in the presence of 15-crown-5.[29] For cyclopentyl and tert-butyl silicates, the corresponding tetraethylammonium salts were obtained from trichlorosilanes (Scheme 9).[30]

The structures of the silicates **13** were studied by X-ray crystallography and showed a continuum between a quasi-square planar pyramidal (SP) geometry (R = cyclohexyl, K^+[18C6]) and a trigonal bipyramidal (TBP) (R = cyclopentyl, Et_4N^+), as already observed by Holmes[31] (Scheme 10). The oxidation potentials of these silicates were determined by cyclic voltammetry that provided values $< +1.0$ V vs. saturated calomel electrode (SCE) for both activated and non-activated alkylsilicates **13**. These values were found to be lower than those of the corresponding carboxylates[32] and trifluoroborates[33,34] and suggest that some photoexcited ruthenium or iridium-based photocatalysts can oxidize all the alkylsilicates.

Initially, benzylsilicate **14** was found to be capable of generating benzyl radical **15** under photooxidation conditions

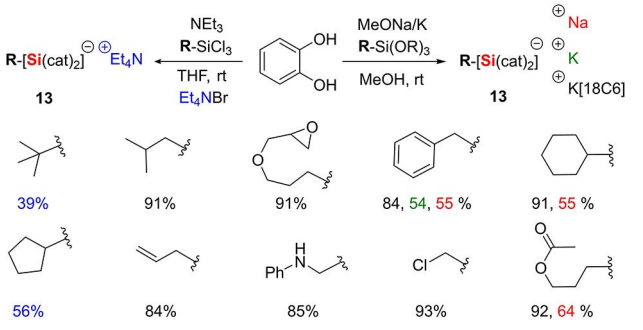

Scheme 9. Synthesis of functionalized sodium, potassium, ammonium and potassium[18-C-6] alkyl bis-catecholato silicates **13.**

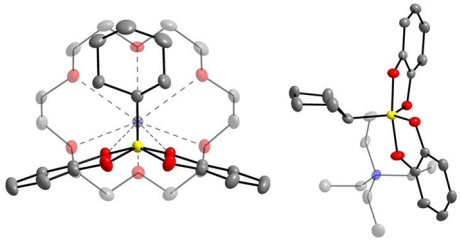

Scheme 10. X-ray crystallography of cyclohexyl (SP) and cyclopentyl (TBP) bis-catecholato silicates.

(Scheme 11).[29] Based on a screening of photocatalysts including $Ru(bpy)_3(PF_6)_2$ (bpy = bipyridine) as well as $Ir[(dF(CF_3)ppy)_2(bpy)]PF_6$ (dF-(CF_3)ppy = 2-(2,4-difluorophenyl)-5-trifluoromethylpyridine), the latter revealed to be the most effective under blue light-emitting diodes (LEDs) irradiation leading to the 2,2,6,6-tetramethylpiperidinyl-oxide (TEMPO) adduct **16** in good yield. The low value of the oxidation potential of the benzylsilicate (**14**, $Eox = +0.61$ V vs. SCE) fitted with the potential of the photoactivated catalyst ($Ru^{II*}/Ru^{I} = +0.77$ V vs. SCE in CH_3CN, $Ir^{III*}/Ir^{II} = +1.32$ V vs. SCE in CH_3CN) and suggests that this one can oxidize the silicate. Stern-Volmer plot showed a linear relation between the intensity of the fluorescence and the concentration of quencher. Based on these experiments, a mechanism, where the photoactivated catalyst oxidizes the silicate and the benzyl radical **15** is trapped by TEMPO, was proposed (Scheme 11). The photocatalyst would be regenerated by the reduction of TEMPO (present in excess).

3.3. Carbon-Carbon Bond Formation by Radical Addition from Alkyl Bis-catecholato Silicates

The formation of carbon-carbon bond was explored by focusing mainly on the allylation of alkyl bis-catecholato silicates **13** with allylsulfones (Scheme 12).[29] The range of substrates proved to be quite wide, from primary to tertiary alkylsilicates. We can mention in particular the generation of non-activated primary radicals, as well as new examples of aminomethylation and chloromethylation. A similar mechanism was proposed except that the radical adds to allylsulfone and after fragmentation, the sulfonyl radical participates to the regeneration of the photocatalyst, as already proved by MacMillan.[35] As detailed below, radical chain mechanism in

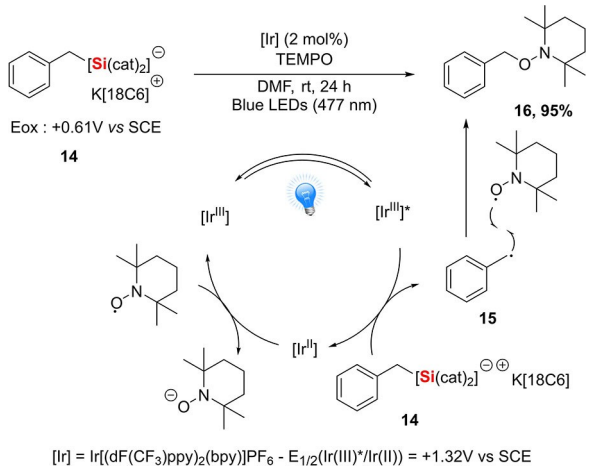

Scheme 11. Visible-light photooxidation of benzyl bis-catecholato silicate **14**, spin-trapping experiments with TEMPO and proposed mechanism.

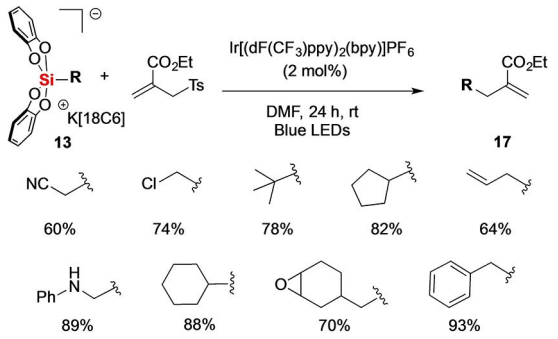

Scheme 12. Allylation reactions of a variety of functionalized silicates **13.**

these allylations was excluded based on light/dark experiments and the determination of quantum yields.[36]

We next examined the reactivity of cyclohexyl silicate **18** toward various radical acceptors. The cyclohexyl radical **19** generated was then engaged in Giese-type reactions with various activated olefins. Vinylation can be reached by addition/fragmentation with vinylsulfones, bromides or chlorides, and alkynylation using an alkynylsulfone (Scheme 13).

Computational studies on the oxidation of cyclohexyl bis-catecholato silicate by the triplet state of Ir(III)-dF(CF_3) (triplet state) were carried out by Etienne Derat and showed a single-electron transfer (SET) process from the catecholate ligand of the silicate to the metallic center of the photocatalyst. Comparison of the bond dissociation energy (BDE) of the substrates before and after electron transfer indicates that oxidation significantly weakens the Si–C bond that undergoes cleavage.[29] These DFT calculations fully validated the proposed mechanism.

As previously mentioned, the oxidation of the bis-catecholato silicates **13** has been accomplished using metal-based photocatalysts, and particularly rare and expensive polypyridine complexes of ruthenium or iridium. In order to provide greener reaction conditions, the reactivity of organic dyes as an alternative to metal complexes was explored.[33,37] First, we found that only the more oxidant Fukuzumi acridinium photocatalyst revealed to be the most efficient in spin trapping experiments with benzylsilicate **14** and no reaction was observed with Eosin and Fluorescein even if their oxidation potentials at the excited state also match with the silicate.[33] In 2012, Adachi described a new carbazoyl dicyanobenzene complex, 1,2,3,5-tetrakis(carbazol-9-yl)-4,6-dicyanobenzene (4CzIPN), which demonstrated a high photoluminescence quantum yield (94.6%) and a long life-time (5.1 μs) at the excited state.[38] Later, Zhang measured the oxidative potentials of 4CzIPN and of related structures. He was also the first one to apply these carbazole derivatives as photocatalysts for the photooxidation of stabilized carboxylate and trifluoroborate.[39] The potential of 4CzIPN at the excited state was recently revised by Waser at +1.59 V vs. SCE.[40] Based on these physico-chemical data and not surprisingly, benzylsilicate **14** gave the TEMPO adduct **16** in 94% yield with a catalytic loading in 4CzIPN of only 1 mol% (Scheme 14). Vinylation, allylation, alkynylation and Giese-type adducts **21** were also obtained in good yields with a variety of alkylsilicates (Scheme 15).

A new methodology of radical carbonylation of alkyl bis-catecholato silicates **13** under photocatalyzed oxidation conditions was developed in collaboration with the group of Illhong Ryu and Takahide Fukuyama from Osaka Prefecture University and could be implemented in multicomponent

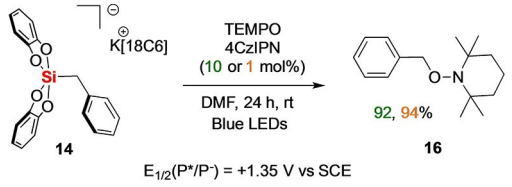

Scheme 14. Photooxidation of benzyl bis-catecholato silicate **14** with the organic dye 4CzIPN.

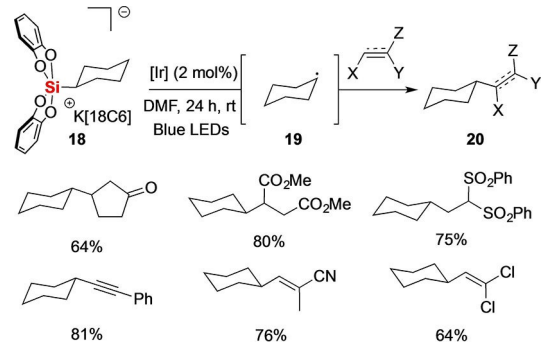

Scheme 13. Reactivity of cyclohexyl silicate **18** towards various radical acceptors.

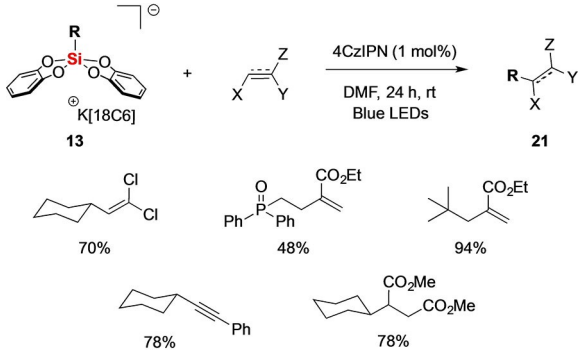

Scheme 15. Photooxidation of alkylsilicates **13** by 4CzIPN with various C-radical acceptors.

reactions. Thus, alkyl radicals generated by photooxidation of the corresponding organosilicates with 4CzIPN, participate in radical carbonylation with carbon monoxide (CO) in the presence of electron-deficient alkenes as radical acceptors, providing a series of unsymmetrical ketones **22** and **23** *via* an acyl radical intermediate. These optimized conditions were applied to a variety of alkylsilicates. The carbonylation of primary, secondary and tertiary radicals worked well and led to the corresponding ketones in good yields (Scheme 16). Gratifyingly, we tested different alkenes as radical acceptors. For instance, α,β-unsaturated ketones participated in these three-component to afford 1,4-diketones. Transformations with *N,N*-dimethyl acrylamide and acrylonitrile were equally effective as well as those carried out with an allylsulfone.

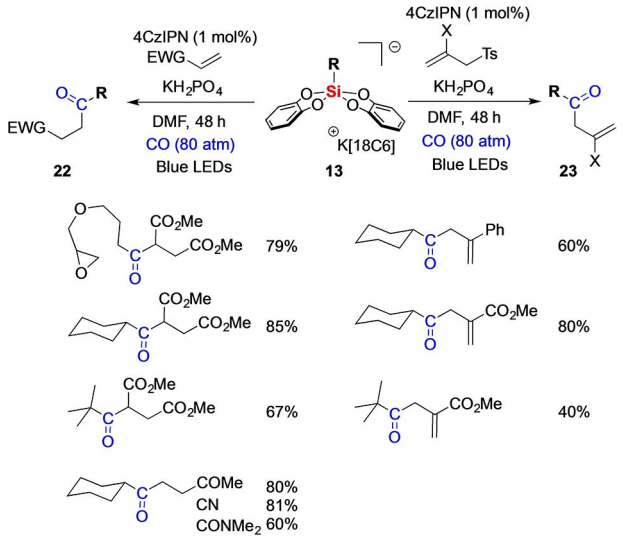

Scheme 16. Three-component radical carbonylation reactions of alkyl bis-catecholato silicates **13** for the synthesis of unsymmetrical ketones **22** and **23.**

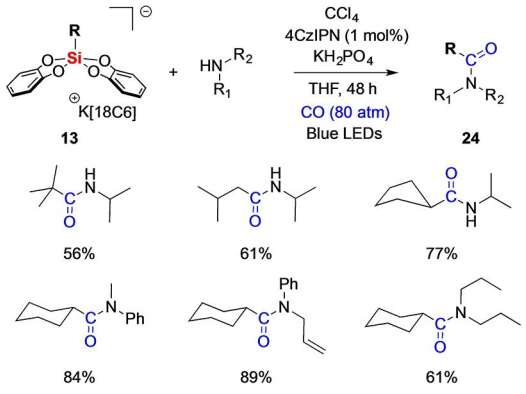

Scheme 17. Synthesis of aliphatic amides **24** by radical carbonylation starting from alkyl bis-catecholato silicates **13.**

"Light-dark" experiments conducted in the absence of CO and quantum yield measurements supported a catalytic photoredox process and not a radical chain pathway. In this case, a SET oxidation of the silicate by the excited photocatalyst results in the formation of the alkyl radical that adds to CO to form an acyl radical. The latter then adds to the radical acceptor.

In the presence of an amine and carbon tetrachloride, the transient acyl radical generates an acyl chloride through chlorine abstraction from CCl_4 and leads this time to a variety of amides **24** with yields ranging from 34 to 89%. An amine with a potentially reactive alcohol only furnishes the corresponding amide and no trace of ester was observed (Scheme 17).[41]

3.4. Cross-coupling Reactions by Dual Photoredox/Nickel Catalysis

A particularly attractive field concerns dual photoredox/organometallic catalysis. Initially developed through photoreductive processes,[42] the possibility of coupling aromatic electrophiles with radicals, generated by photooxidation, thanks to nickel complexes was recently demonstrated.[43] This type of coupling was first reported by the groups of Molander, MacMillan and Doyle with a primary or a secondary radical obtained respectively from activated trifluoroborates or carboxylic acid derivatives or methylamines as easy oxidation substrates.[44,45] We wished to examine the possibility of introducing silicates in these cross couplings and notably what would be the benefits of their use (Scheme 18).[36,46] When treated with $Ni(COD)_2$/iridium photocatalyst or $NiCl_2$.dme/4CzIPN catalytic systems, silicates **13** could be coupled with

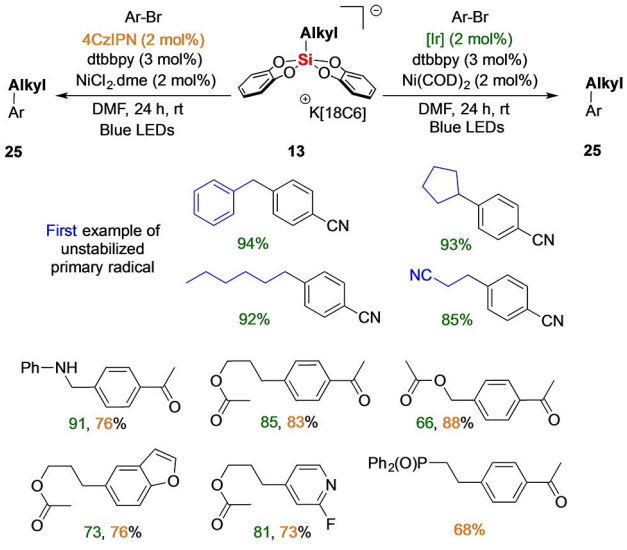

Scheme 18. Cross coupling reactions of silicates **13** with various arylbromides.

electron poor and electron rich (hetero)arylbromides and gave the cross-coupling product **25** with benzyl, allyl, α-amino methyl and secondary radicals as well as proved successful with unstabilized primary radicals. These results revealed that silicates are partners of choice in the dual catalysis processes, as shown also by the Molander group.[47] The scope of the transformation is broad and the process is tolerant with various functions, such as a pinacol alkylboronate function on the aryl ring. The $NiCl_2$/4CzIPN dual catalysis conditions allowed to couple both ethylenic bromides and chlorides with acetoxypropyl bis-catecholato silicate **26** with a high diastereoselectivity (Scheme 19, Eq. 1).[36] Finally, gem-dichlorostyrenes were reacted with primary and secondary (non-)activated alkylsilicates **13** (such as **14**, R = benzyl) and provided exclusively the corresponding monoalkylated cross coupling (*Z*)-styrylchloride products (**28**) (Scheme 19, Eq. 2).[36,28]

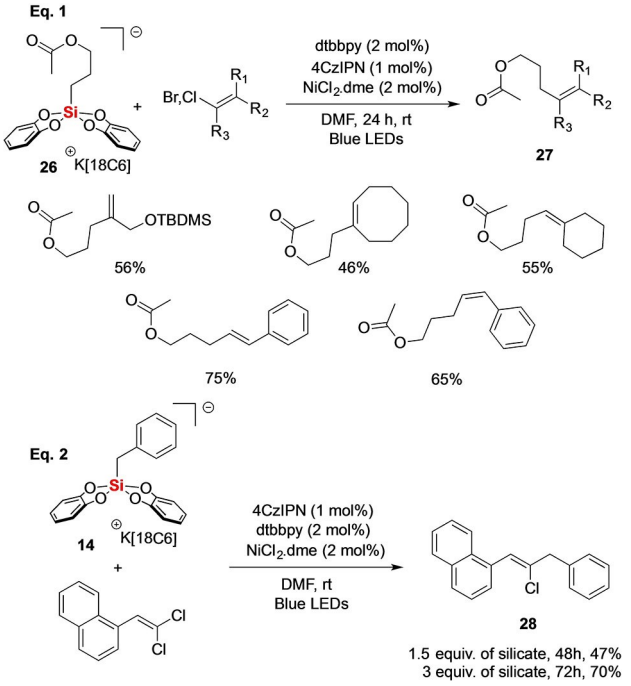

Scheme 19. Reaction of bis-catecholato silicates **26** and **14** with alkenyl halides.

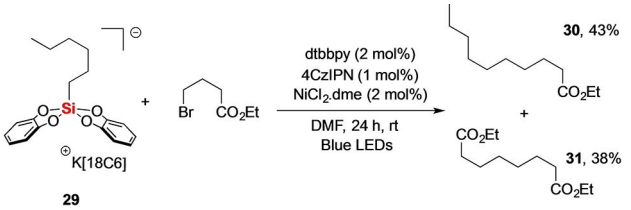

Scheme 20. Cross-coupling reactions between *n*-hexyl bis-catecholato silicate **29** and 4-bromobutyrate.

After developing an efficient photoredox/nickel dual catalytic process for C(sp^3)-C(sp^2) coupling, alkylsilicates **13** (such as **29**, R = n-hexyl) were involved in cross-coupling reactions with alkyl halides such as 4-bromobutyrate to create C(sp^3)-C(sp^3) bonds.[48] The corresponding products (**30**) were obtained in moderate yields, either from primary and also secondary alkylsilicates, along with the homocoupling product (**31**) of the alkyl halide. The mechanism is still under discussion and needs to be clarified (Scheme 20).

Finally, we were interested in the reactivity of silicates **13** towards acyl chlorides in order to obtain benzyl and alkyl ketones **32**, which are of great interest in fragrance and flavors industry, and more generally, as synthetic intermediates.[49] Upon treatment with a complex of iridium as photocatalyst and $NiCl_2$.dme under irradiation with blue LEDs, an alkylsilicate **13** can be coupled to an acyl chloride as electrophile to give the expected ketones **32** (Scheme 21). Several silicates **13** were then tested under these conditions. Cyclohexyl, norbornyl and mainly the activated silicates such as the methoxymethylene and benzyl derivatives were able to provide the desired product and notably highly enolizable ketones. The nature of the acyl chloride partner also influenced this coupling since both electron-rich benzoyl chlorides and alkyl ones afforded the corresponding ketones in good yields, including variously substituted dibenzyl ketones (Scheme 21). In collaboration with Michaël Tatoulian, Stéphanie Ognier and Mengxue Zhang from Institut Pierre-Gilles de Gennes in Paris, we used miniaturized flow reactors to accelerate this photooxidative process, without increasing the yield though. Only 20 minutes are necessary to obtain the cross-coupling product **33** from benzylsilicate **14** and benzoyl chloride whereas 24 hours are necessary under normal circumstances (Scheme 22).

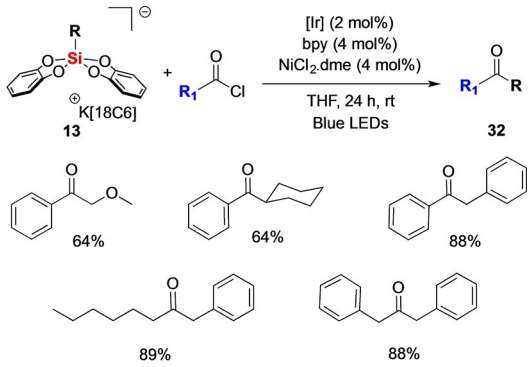

Scheme 21. Acylation of alkyl bis-catecholato silicates **13** *via* dual nickel photocatalysis.

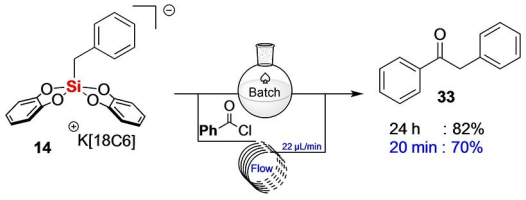

Scheme 22. Continuous flow vs. batch processing.

4. Perspectives

This survey of our recent works involving hypercoordinated silicon derivatives illustrates, if it was still necessary, that this class of intriguing compounds offer unique opportunities in organic synthesis. At the origin of the described reactivities in this account, lays the Lewis acidity of a silicon center bearing electronegative ligands such as a catecholate[50] or the dianion of hexafluorocumyl alcohol, Martin's, which formally welcomes a nucleophilic addition to generate selectively pentavalent species. The formally resulting bis-catecholato silicates have proven to be excellent precursors of unstabilized alkyl radicals in a series of radical sequences. They position therefore themselves as reagents of choice for the introduction of Csp^3-rich fragments on (hetero)aryl platforms through dual Ni/photoredox catalysis which is highly praised in medicinal chemistry ("escape from the flatland"). The realm of applications of these reagents is rapidly expanding as illustrated by the contributions of several groups.[51]

Martin's spirosilane **4** has been known for more than 40 years but rarely considered as an alternative to the highly encountered $B(C_6F_5)_3$ Lewis acids. Our preliminary works have delivered valuable elements of reactivity that augur well for more sophisticated applications. Interestingly, alkylsilicates obtained by Kano's group from **4** also proved to be sources of radicals. Despite their higher oxidation potentials (>1.0 V), they also give an access to C-centered alkyl radicals, including the methyl radical.[52] The oxidation mechanism in that case is distinct since it is the C–Si bond that is directly oxidized.

Future research directions along these lines will involve the tuning of the silicon ligands[22] and the study of their effects. Notably, how can their modification by the substitution of the aromatic groups can improve the oxidation process and give access to sp^2-radicals[53] for instance. Application to radical cascades that open a straightforward access to molecular complexity are envisioned.

Acknowledgements

We wish to warmly acknowledge all our collaborators whose works were cited in this manuscript. We also thank Sorbonne Université, CNRS, PSL University, ANR-17-CE07-0018 HyperSiLight.

References

[1] S. N. Tandura, M. G. Voronkov, N. V. Alekseev, *Top. Curr. Chem.* **1986**, *131*, 99–189.
[2] R. R. Holmes, *Chem. Rev.* **1996**, *96*, 927–950.
[3] C. Chuit, R. J. P. Corriu, C. Reye, J. C. Young, *Chem. Rev.* **1993**, *93*, 1371–1448.
[4] For recent articles on the chemistry of hypercoordinated organosilicon compounds, see: a) G. Singh, G. Kaur, J. Singh, *Inorg. Chem. Commun.* **2018**, *88*, 11–20; b) A. S. Soldatenko, I. V. Sterkhova, N. F. Lazareva, *J. Organomet. Chem.* **2019**, *903*, 120997–121004; c) D. Mu, W. Yuan, S. Chen, N. Wang, B. Yang, L. You, B. Zu, P. Yu, C. He, *J. Am. Chem. Soc.* **2020**, *142*, 13459–1348.
[5] S. Rendler, M. Oestreich, *Synthesis* **2005**, 1727–1747.
[6] D. Kost, I. Kalikhman, in PATAI's Chemistry of Functional Groups, John Wiley & Sons **2009**, 1–107.
[7] S. M. Sieburth, L. Fensterbank, *J. Org. Chem.* **1993**, *58*, 6314–6318.
[8] S. M. Sieburth, L. Fensterbank, *J. Org. Chem.* **1992**, *57*, 5279–5281.
[9] S. Bogen, M. Gulea, L. Fensterbank, M. Malacria, *J. Org. Chem.* **1999**, *64*, 4920–4925 and references therein.
[10] N. Puljic, M. Albert, A.-L. Dhimane, L. Fensterbank, E. Lacôte, M. Malacria, *Helv. Chim. Acta* **2006**, *89*, 2297–2305.
[11] C. Blaszykowski, C. Brancour, A.-L. Dhimane, L. Fensterbank, M. Malacria, *Eur. J. Org. Chem.* **2009**, 1674–1678.
[12] E. F. Perozzi, J. C. Martin, *J. Am. Chem. Soc.* **1979**, *101*, 1591–1593.
[13] a) W. H. Stevenson III, S. Wilson, J. C. Martin, W. B. Farnham, *J. Am. Chem. Soc.* **1985**, *107*, 6340–6352; b) D. A. Dixon, W. R. Hertler, D. B. Chase, W. B. Farnham, F. Davidson, *Inorg. Chem.* **1988**, *27*, 4012–4018; c) S. K. Chopra, J. C. Martin, *J. Am. Chem. Soc.* **1990**, *112*, 5342–5343; d) N. Kano, H. Miyake, K. Sasaki, T. Kawashima, N. Mizorogi, S. Nagase, *Nat. Chem.* **2010**, *2*, 112–116.
[14] H. Lenormand, J.-P. Goddard, L. Fensterbank, *Org. Lett.* **2013**, *15*, 748–751.
[15] H. Ruppert, L. Greb, *Organometallics* **2020**,*39*, 4340–4349.
[16] F. Medici, G. Gontard, E. Derat, G. Lemière, L. Fensterbank, *Organometallics* **2018**, *37*, 517–520.
[17] For review on anionic *N*-Heterocyclic Carbenes, see: A. Nasr, A. Winkler, M. Tamm, *Coord. Chem. Rev.* **2016**, *316*, 68–124.
[18] F. Medici, J. Maury, G. Lemière, L. Fensterbank, *Chem. Eur. J.* **2019**, 25, 9438–9442.
[19] For leading reviews, see: a) D. W. Stephan, *Acc. Chem. Res.* **2015**, *48*, 306–316; b) D. W. Stephan, G. Erker, *Angew. Chem. Int. Ed.* **2015**, *54*, 6400–6441; *Angew. Chem.* **2015**, *127*, 6498–6541; c) D. W. Stephan, *J. Am. Chem. Soc.* **2015**, *137*, 10018–10032; d) J. Paradies, *Angew. Chem. Int. Ed.* **2014**, *53*, 3552–3557; *Angew. Chem.* **2014**, *126*, 3624–3629.

[20] a) M. A. Beckett, G. C. Strickland, J. R. Holland, K. S. Varma, *Polymer* **1996**, *37*, 4629–4631; b) V. Gutmann, *Coord. Chem. Rev.* **1976**, *18*, 225–255.
[21] A. Ashley, T. J. Herrington, G. G. Wildgoose, H. Zaher, A. L. Thompson, N. H. Rees, T. Krämer, D. O'Hare, *J. Am. Chem. Soc.* **2011**, *133*, 14727–14740.
[22] H. Lenormand, V. Corcé, G. Sorin, C. Chhun, L.-M. Chamoreau, L. Krim, E.-L. Zins, J.-P. Goddard, L. Fensterbank, *J. Org. Chem.* **2015**, *80*, 3280–3288.
[23] J.-i. Yoshida, K. Tamao, H. Yamamoto, T. Kakui, H. Matsumoto, M. Takahashi, A. Kurita, M. Murata, M. Kumada, *Organometallics* **1982**, *1*, 355–368.
[24] G. Sorin, R. Martinez Mallorquin, Y. Contie, A. Baralle, M. Malacria, J.-P. Goddard, L. Fensterbank, *Angew. Chem. Int. Ed.* **2010**, *49*, 8721–8723; *Angew. Chem.* **2010**, *122*, 8903–8905.
[25] C. L. Frye, *J. Am. Chem. Soc.* **1964**, *86*, 3170–3171.
[26] A. Boudin, G. Cerveau, C. Chuit, R. J. P. Corriu, C. Reye, *Bull. Chem. Soc. Jpn.* **1988**, *61*, 101–106.
[27] a) Y. Nishigaichi, A. Suzuki, T. Saito, A. Takuwa, *Tetrahedron Lett.* **2005**, *46*, 5149–5151; b) Y. Nishigaichi, A. Suzuki, A. Takuwa, *Tetrahedron Lett.* **2007**, *48*, 211–214; c) D. Matsuoka, Y. Nishigaichi, *Chem. Lett.* **2014**, *43*, 559–561; d) D. Matsuoka, Y. Nishigaichi, *Chem. Lett.* **2015**, *44*, 163–165.
[28] V. Corcé, C. Lévêque, C. Ollivier, L. Fensterbank in *Science of Synthesis: Photocatalysis in Organic Synthesis* (Ed.: B. König), Thieme Stuttgart, **2019**, pp. 427–466.
[29] M. Abdellaoui, A. Millanvois, E. Levernier, C. Ollivier, L. Fensterbank, *Synlett* **2021**, *32*, doi: https://doi.org/10.1055/a-1374-9384.
[30] V. Corcé, L.-M. Chamoreau, E. Derat, J.-P. Goddard, C. Ollivier, L. Fensterbank, *Angew. Chem. Int. Ed.* **2015**, *54*, 11414–11418; *Angew. Chem.* **2015**, *127*, 11576–11580.
[31] R. R. Holmes, *Chem. Rev.* **1990**, *90*, 17–31.
[32] H. G. Roth, N. A. Romero, D. A. Nicewicz, *Synlett* **2016**, *27*, 714–723.
[33] J. Suzuki, M. Tanigawa, S. Inagi, T. Fuchigami, *ChemElectroChem* **2016**, *3*, 2078–2083.
[34] L. Chenneberg, C. Lévêque, V. Corcé, A. Baralle, J.-P. Goddard, C. Ollivier, L. Fensterbank, *Synlett* **2016**, *27*, 731–735.
[35] A. Noble, D. W. C. MacMillan, *J. Am. Chem. Soc.* **2014**, *136*,11602–11605.
[36] A. Cartier, E. Levernier, V. Corcé, T. Fukuyama, A.-L. Dhimane, C. Ollivier, I. Ryu, L. Fensterbank, *Angew. Chem. Int. Ed.* **2019**, *58*, 1789–1793; *Angew. Chem. Int. Ed.* **2019**, *131*, 1803–1807.
[37] C. Lévêque, L. Chenneberg, V. Corcé, C. Ollivier, L. Fensterbank, *Chem. Commun.* **2016**, *52*, 9877–9880.
[38] H. Uoyama, K. Goushi, K. Shizu, H. Nomura, C. Adachi, *Nature* **2012**, *492*, 234–240.
[39] J. Luo, J. Zhang, *ACS Catal.* **2016**, *6*, 873–877.
[40] F. Le Vaillant, M. Garreau, S. Nicolai, G. Gryn'ova, C. Corminboeuf, J. Waser, *Chem. Sci.* **2018**, *9*, 5883–5889.
[41] A. Cartier, E. Levernier, A.-L. Dhimane, T. Fukuyama, C. Ollivier, I. Ryu, L. Fensterbank, *Adv. Synth. Catal.* **2020**, *362*, 2254–2259.
[42] a) D. Kalyani, K. B. McMurtrey, S. R. Neufeldt, M. S. Sanford, *J. Am. Chem. Soc.* **2011**, *133*, 18566–18569; b) J. Twilton, C. C. Le, P. Zhang, M. H. Shaw, R. W. Evans, D. W. C. MacMillan, *Nat. Chem. Rev.* **2017**, *1*, 1–19.
[43] C. Lévêque, C. Ollivier, F. Fensterbank, in *Nickel Catalysis in Organic Synthesis* (Ed.: S. Ogoshi), Wiley **2020**, pp 151–181.
[44] J. C. Tellis, D. N. Primer, G. A. Molander, *Science* **2014**, *345*, 433–436.
[45] Z. Zuo, D. Ahneman, L. Chu, J. Terrett, A. G. Doyle, D. W. C. MacMillan, *Science* **2014**, *345*, 437–440.
[46] C. Lévêque, L. Chennenberg, V. Corcé, J.-P. Goddard, C. Ollivier, L. Fensterbank, *Org. Chem. Front.* **2016**, *3*, 462–465.
[47] a) M. Jouffroy, D. N. Primer, G. A. Molander, *J. Am. Chem. Soc.* **2016**, *138*, 475–478; b) J. K. Matsui, S. B. Lang, D. R. Heitz, G. A. Molander, *ACS Catal.* **2017**, *7*, 2563–2575.
[48] C. Lévêque, V. Corcé, L. Chenneberg, C. Ollivier, L. Fensterbank, *Eur. J. Org. Chem.* **2017**, 2118–2121.
[49] E. Levernier, V. Corcé, L.-M. Rakotoarison, A. Smith, M. Zhang, S. Ognier, M. Tatoulian, C. Ollivier, L. Fensterbank, *Org. Chem. Front.* **2019**, *6*, 1378–1382.
[50] a) A. L. Liberman-Martin, R. G. Bergman, T. D. Tilley, *J. Am. Chem. Soc.* **2015**, *137*, 5328–5331; b) R. Maskey, M. Schädler, C. Legler, L. Greb, *Angew. Chem. Int. Ed.* **2018**, *57*, 1717–1720, *Angew. Chem.* **2018**, *130*, 1733–1736; c) D. Hartmann, M. Schadler, L. Greb, *Chem. Sci.* **2019**, *10*, 7379–7388.
[51] a) K. D. Raynor, G. D. May, U. K. Bandarage, M. J. Boyd, *J. Org. Chem.* **2018**, *83*, 1551–1557; b) T. Guo, X. Liu, Y. Fang, X. Jin, Y. Yang, Y. Li, B. Chen, M. Ouyang, *Adv. Synth. Catal.* **2018**, *360*, 4457–4650; c) A. García-Domínguez, R. Mondal, C. Nevado, *Angew. Chem. Int. Ed.* **2019**, *58*, 2–7; *Angew. Chem.* **2019**, *131*, 12414–12418; d) S. T. J. Cullen, G. K. Friestad, *Org. Lett.* **2019**, *21*, 8290–8294; e) Z.-J. Wang, S. Zheng, J. K. Matsui, Z. Lu, G. A. Molander, *Chem. Sci.* **2019**, *10*, 4389–4393.
[52] a) G. Ikarashi, T. Morofuji, N. Kano, *Chem. Commun.* **2020**, *56*, 10006–10009; b) T. Morofuji, Y. Matsui, M. Ohno, G. Ikarashi, N. Kano, *Chem. Eur. J.* **2021**, DOI: https://doi.org/10.1002/chem.202005300.
[53] E. Levernier, K. Jaoudi, H.-R. Zhang, V. Corcé, A. Bernard, G. Gontard, C. Troufflard, L. Grimaud, E. Derat, C. Ollivier, *submitted*.

Manuscript received: February 16, 2021
Revised manuscript received: March 5, 2021
Version of record online: March 18, 2021

EurJOC
European Journal of Organic Chemistry

Research Article
doi.org/10.1002/ejoc.202300223

Chemistry Europe
European Chemical Societies Publishing

www.eurjoc.org

Synthesis and Properties of the Perfluoroethyl Martin Silicate: Reactivity in Solution and Solid-State Mechanochemistry

Alexandre Millanvois,[a, b] Choon-Hong Tan,[b] Cyril Ollivier,*[a] and Louis Fensterbank*[a]

We herein report the first synthesis of a Martin silicate bearing a pentafluoroethyl chain. The full characterisation of this new pentacoordinated silicon species is detailed. Insights on its electronic properties based on structural, physicochemical and computational data are provided. A comparative study of reactivity in solution and in solid state by mechanochemistry has been performed in order to assess the ability of this bench-stable salt to act as a safe C_2F_5-alkylation reagent in a nucleophilic or radical manner.

Introduction

The *p*-block elements-based derivatives bearing a strongly electron-withdrawing-C_2F_5 moiety have recently emerged as promising tools for organic synthesis, with novel reactivities from an experimental and theoretical point of view.[1] Due to the strong Lewis acidity induced by the C_2F_5 substituent on the central atom, access to the corresponding stable hypercoordinate phosphorus[2–4] or silicon[5–10] species has been reported. These species have been synthesized by addition of pentafluoroethyllithium [Li][C_2F_5], obtained by metalation of the fluorinated gas HFC-125 (HC_2F_5), onto the chlorinated P or Si substrate (Figure 1.a). To limit the potential hazard (*violent decomposition/explosion*),[11–13] the batch generation of the required organolithium reagent has recently evolved to a safer microflow method (Figure 1.b).[14,15] As an alternative, stabilization of the organolithium in the form of a stannate reagent reservoir has proven to be a more reliable solution for safer handling of this chemical (Figure 1.c).[16] Other stabilizations of HFC-125 as pentafluoroethyl -cuprates,[17,18] -gallanes,[19,20] -bismuthanes[21a] or very recently -indates salts[21b] have also been developed.

[a] Dr. A. Millanvois, Dr. C. Ollivier, Prof. L. Fensterbank
Sorbonne Université
CNRS, Institut Parisien de Chimie Moléculaire
4 Place Jussieu, CC 229
75252 Paris Cedex 05 (France)
E-mail: cyril.ollivier@sorbonne-universite.fr
louis.fensterbank@sorbonne-universite.fr
[b] Dr. A. Millanvois, Prof. C.-H. Tan
Division of Chemistry and Biological Chemistry
School of Physical and Mathematical Sciences
Nanyang Technological University
21 Nanyang Link, 637371 Singapore (Singapore)

Supporting information for this article is available on the WWW under https://doi.org/10.1002/ejoc.202300223

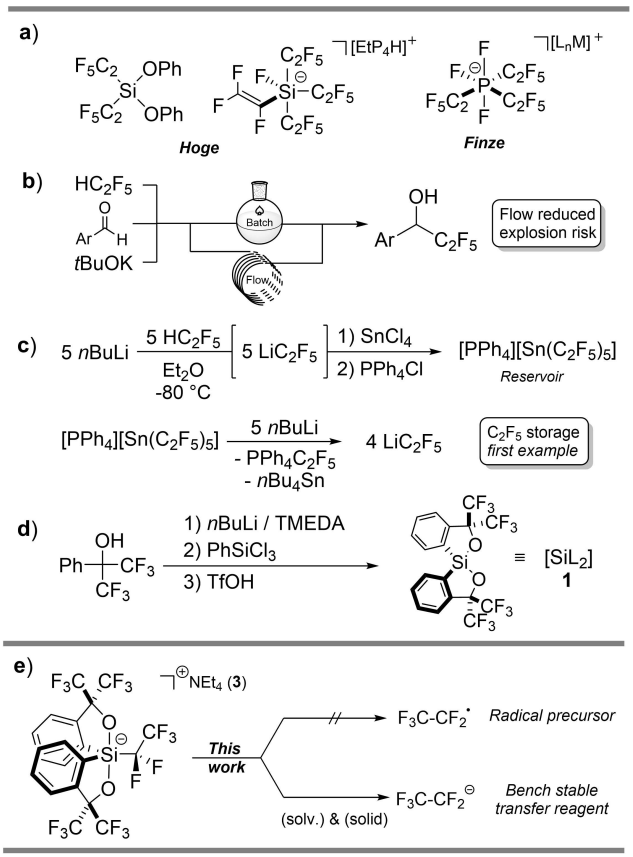

Figure 1. a) Examples of isolated perfluoroethyl hypercoordinate compounds; b) Batch vs flow alkylation of aldehyde with pentafluoroethyllithium; c) In solution preparation of [Li][C_2F_5] from a stannate; d) Martin spirosilane synthesis; e) This work: potential destabilisation of the corresponding C_2F_5-silicon of the silicate bond to generate the perfluoroethyl radical/anion.

Pursuing our interest on the derivatization of the Martin spirosilane ([SiL_2] **1**, L = α,α-bis(trifluoromethyl) benzenemethanolato-(−2)C_2,O), shown in Figure 1.d),[22–28] we herein report an alternative reagent for the storage and introduction of the C_2F_5 anion based on the use of **1**. Spirosilane **1** is easily obtained from the sequential bis-deprotonation of hexafluorocumyl

Research Article
doi.org/10.1002/ejoc.202300223

alcohol and reaction with phenyltrichlorosilane to afford a phenylsilicate intermediate. Protonation by TFA allows the formation of the desired silane **1**. Upon addition of the $C_2F_5^-$ anion to **1**, the synthesis of the corresponding perfluoroethylsilicate **3** is described as well as some properties and preliminary reactivity of **3** (Figure 1.e). Martin silicates ($[Si(R)L_2]^-$) have been recently used as a source of alkyl radicals,[29–31] as an alternative to their bis(catecholato)silicate counterparts $[Si(R)(cat)_2]^-$.[32,33] For both silicon species, the generation of the desired radical R· is induced by one-electron oxidation and fragmentation of the carbon-silicon bond. To our knowledge, no such route has been described for the generation of a perfluoroalkyl radical, and in particular the pentafluoroethyl radical.

On the other hand, the influence of the substituent (R) on the Martin silicate structural properties ($[Si(R)L_2]^-$) has been discussed previously by Holmes but no information on the potential increase of the Lewis acidity through this lever is mentioned.[34] Indeed, the formation of 6-coordinate Martin silicate has only been disclosed with phenanthroline as ligand.[35] Finally, the nucleophilicity of pentavalent perfluoroalkylated silicon species has been previously highlighted by Prakash.[36] We therefore decided to evaluate the destabilisation of the corresponding C_2F_5-silicon bond of the silicate and to verify a possible nucleophilic behaviour in solution but also in solid-state under mechanochemical conditions.

Results and Discussion

Access to the Martin silicate bearing a pentafluoroethyl chain was performed based on the methodologies described by Hoge and co-workers.[7,13] First, the synthesis of the corresponding lithium silicate salt begins with the preparation of the $C_2F_5^-$ transfer reagent, i.e. pentafluoroethyllithium, by deprotonation of HFC-125 with *n*-BuLi. Martin spirosilane **1** was slowly added at −75 °C to lead to the formation of lithium silicate **2** (Scheme 1, reaction 1) which shows a good stability in solution but proved unstable in the solid state. To increase its stability, cation exchange using tetratethylammonium bromide (Scheme 1, reaction 2) after precipitation afforded $[Et_4N][Si(C_2F_5)L_2]$ (**3**) in 78% yield.

In this study, it was also found that pentafluoroethyllithium was also able to act as a fluoride donor to **1**. The yield of the corresponding side-product $[Si(F)L_2]^-$ (**4**) was estimated up to ~15% by ^{19}F NMR (inseparable mixture of **3** and **4**), whose structure was confirmed by X-ray analysis (Figure 2). A perfluorinated derivative was also synthesized with a longer 1H-perfluorohexanyl chain following the same methodology using $[Li][C_6F_{12}H]$ (Scheme 2 and Supporting Information).[37]

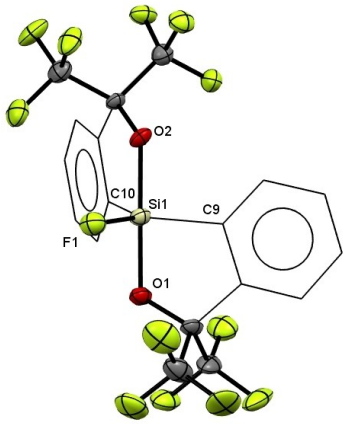

Figure 2. X-ray crystallographic structure of **4**. CCDC (2208664). Thermal ellipsoids are drawn at 50% probability level. Hydrogen atoms are omitted for clarity. Carbons of Martin Ligand (L) are drawn as wireframe for clarity | Selected bond lengths [Å] and angles [°]: Si_1–F_1 1.62(1), Si_1–O_1 1.789(9), Si_1–O_2 1.780(9), Si_1–C_9 1.89(1), Si_1–C_{10} 1.89(1); C_{10}– Si_1–C_9 124.9(6), O_1–Si_1–O_2 178.8(4), F_1–Si_1–C_9 117.4(5), F_1–Si_1–O_2 91.2(4).

Slow addition of silane (**1**) at −90 °C on the lithium anion provide the lithium silicate (**5**) and cation exchange with tetratethylammonium bromide gave the ammonium silicate (**6**). In this case, both silicates appear to be unstable in solid state; their decomposition results in the total formation of $[Si(F)L_2]^-$ (**4**).

The amount of **4** generated as side product during the preparation of **3** is mainly dependent on the temperature control during the preparation of the reagent (gas condensation) and during the addition of **1**. As reported previously, the formation of a Si–F bond from decomposition of pentafluoroethyllithium (to C_2F_4 and LiF) also depends on the fluorine ion affinity (FIA) of the Lewis acid.[5] Due to the relatively simple formation of this side-product during the synthesis, we performed computations on the FIA of **1** without solvation correction[38–40] (Computed at PW6B95-D3(BJ)/def2-QZVPP//PBEh-3c/def2-mSVP) level of theory). The system was referenced to Me_3SiF/Me_3Si^+ and gave a FIA of 248.9 kJ mol^{-1}. This result indicates a relatively low Lewis acidity of **1** ($SiMe_4$: 140, SiF_4: 310, BCF: 448; in kJ.mol^{-1}),[38] rationalizing the minor fluoride abstraction on $[Li][C_2F_5]$ by **1**.

Suitable crystals of silicate **3** for an X-ray diffraction analysis were obtained by slow evaporation of a saturated dichloromethane solution. It crystallised in the monoclinic space group $P2_1/c$ (Figure 3). Slight distortion from an ideal trigonal-bipyramidal (TBP) to a square-pyramidal (SP) structure was observed and quantified to 26.4% using the dihedral angle method.[42]

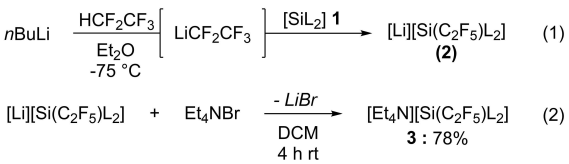

Scheme 1. Preparation of $[Et_4N][Si(C_2F_5)L_2]$ from HFC-125.

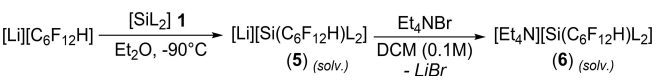

Scheme 2. Preparation of $[Si(C_6F_{12})L_2]^-$.

Research Article
doi.org/10.1002/ejoc.202300223

Chemistry Europe
European Chemical Societies Publishing

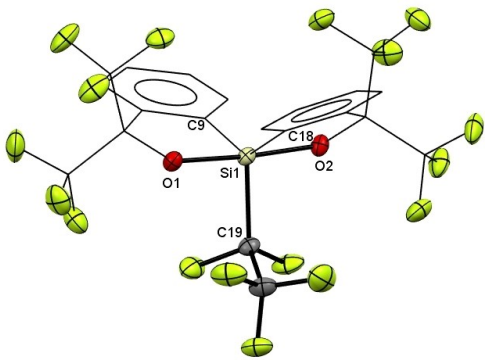

Figure 3. X-ray crystallographic structure (CCDC 2223437) of **3**.[41] Thermal ellipsoids are drawn at 50% probability level. Hydrogen atoms and cation are omitted for clarity. Carbons of Martin Ligand (L) are drawn as wireframe for clarity.

One of the equatorial positions is occupied by the C_2F_5 moiety, the Si–C19 length is 1.968(2) Å. For the axial oxygen atoms, similar lengths are observed with *d*(Si–O1) = 1.787(1) Å and *d*(Si–O2) = 1.784(1) Å, which are shortened and typical of a Martin silicate bearing an electronegative substituent at the equatorial position.[34] Indeed, the observed *d*(Si–O) on **3** is similar to that of $[(Me_2N)_3S][Si(F)L_2]$ ($Si–O_{ax}$ = 1.792 Å).

The electronegativity of the short perfluoroethyl chain had no real impact on the rest of the structure. Finally, the two fluorides of $–CF_2–$ are non-equivalent with a C–F distance of 1.392(3) Å and 1.360(2) Å and slightly longer than the one in $–CF_3$ ranging from 1.309(3) to 1.343(3) Å.

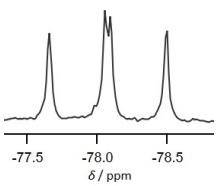

Figure 4. ^{29}Si NMR spectrum of **3** ($[Et_4N][Si(C_2F_5)L_2]$).

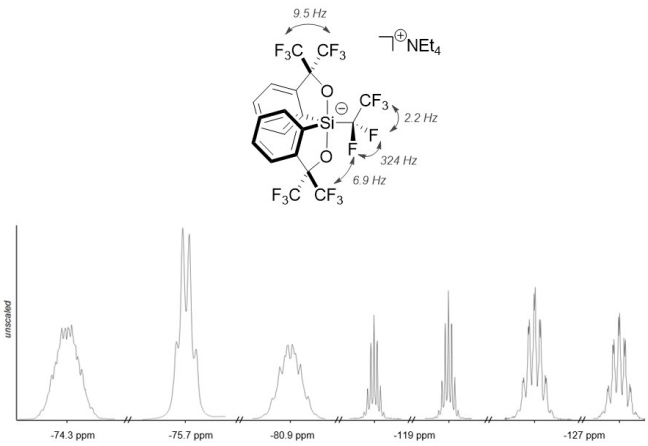

Figure 5. Attributed ^{19}F NMR coupling from ^{19}F NMR spectrum (bottom) of **3**.

The ^{29}Si NMR (119 MHz) shift of **3** at −78 ppm is in the expected range of a five coordinated silicon species (Figure 4). It shows a doublet of doublet caused by a $^2J(Si,F)$ coupling of 35 Hz with two diastereotopic fluorides in $–CF_2–$.

In the ^{19}F NMR (564 MHz) spectrum, the diastereotopic fluorine atoms from the CF_2 group appear respectively as a doublet of septet at δ = −119 and a doublet of septet of doublet at δ = −127 with the measured $^2J(F,F)$, $^3J(F,F)$ and spatial $^6J(F,F)$ coupling of 324, 2.2 and 6.9 Hz. (Figure 5). As expected, the spatially hindered CF_3 (δ = −75.7) from the bis-trifluoromethyl moiety appears as a quadruplet with a coupling constant of 9.5 Hz, while the other one (δ = −74.3) appears as a complex multiplet due to the numerous couplings with the gem CF_3 and the spatial one with the perfluoro-substituent.

Finally, the ^{13}C NMR spectrum at 150.9 MHz shows a quadruplet of triplet and a doublet of doublet of quadruplet for C_2F_5 respectively at δ = 122 ppm with the measured couplings $^1J(C,F)$ and $^2J(C,F)$ of 286 Hz and 32 Hz and at δ = 120 ppm with $^1J(C,F)$ and $^2J(C,F)$ of 276 Hz and 37 Hz (see Supporting Information).

The electronic properties of **3** were first evaluated by cyclic voltammetry with a saturated calomel electrode as reference. As usually observed with hypercoordinated Martin derivatives, a one-electron irreversible oxidation was observed at 1.60 V vs. SCE (Figure 6).

This appeared indeed in the same range as for classical alkyl Martin silicates (for instance, butyl: 1.64 V vs SCE) as described previously by Morofuji and Kano.[29,43]

With these data in hands, we tested the ability of the five-coordinate species to act as a radical precursor (Scheme 3). The measured potential value for oxidation (E_{ox}) of Martin silicate **3**

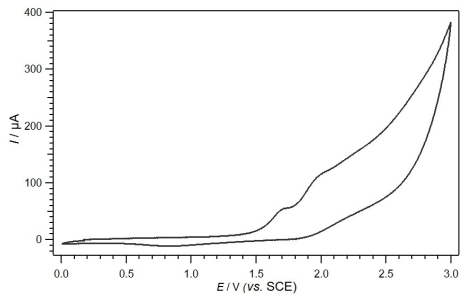

Figure 6. Cyclic voltammetry of **3** in DCM with $[Bu_4N][PF_6]$ as supporting electrolyte.

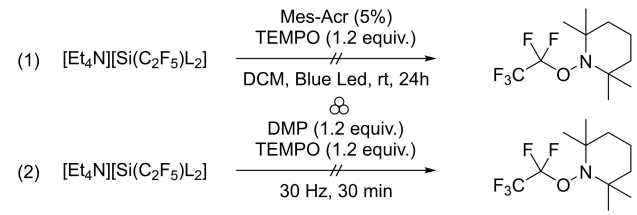

Scheme 3. Investigation of reactivity of **3** under oxidative conditions: (1) TEMPO solution trapping experiment. (2) TEMPO solid-state trapping experiment.

is in the range of the highly oxidizing acridinium-based photocatalysts such as tert-butyl-10-phenylacridinium tetrafluoroborate ([Mes-Acr+], (Nicewicz's catalyst) used by the Kano group to oxidize Martin alkylsilicates.[29,31] We thus evaluated the reactivity of **3** in solution with Nicewicz acridinium photocatalyst.[44] Under these conditions, no desired C_2F_5 pentafluoroethyl radical scavenging product with TEMPO (2,2,6,6-tetramethylpiperidin-1-yl)oxyl) was observed[45,46] and the starting substrate was fully recovered (Scheme 3.1). Solid-state trapping experiments under ball-milling conditions proved to be also unsuccessful using Dess-Martin periodinane (DMP) as oxidant. (Scheme 3.2). This series of findings marks a sharp contrast with the recently reported smooth photooxidation of Martin alkylsilicates.[29,31]

These puzzling findings prompted us to perform DFT calculations (Orca 5.0.3, PW6B95-D3(BJ)/def2-QZVPP//PBEh-3c/def2-mSVP) to examine the highest occupied molecular orbital (HOMO) (Figure 7) of **3**. The results suggest that the orbital susceptible of undergoing an oxidative event is on the aromatic group of the 2,2,2,2′,2′,2′-hexafluorocumyl ligand and not on the C–Si bond to provide the formation of the desired radical, which is in sharp contrast with the ethylsilicate $[Si(C_2H_5)L_2]^-$ reported by Morofuji and Kano.[31] As reported, the computational attempts to optimize the one-electron oxidized silicate led to divergence providing the ethyl radical and **1**.

Interestingly, in our case, the optimization of the oxidized pentafluoroethyl silicate also diverged, as we observed the cleavage of a $Si–C_{Ar}$ bond and not the formation of the spirosilane (See Supporting Information, Figure S2). We then wondered about the potential reactivity of the related fluorinated radical precursor $[Si(CF_3)L_2]^-$. As for the C_2F_5 derivative, the HOMO was mainly localized on the silicate ligand (L). In comparison with previous reports on Martin silicates,[29,31] our experimental results and theoretical analysis suggest **3** might not a be suitable candidate for the oxidative generation of radicals.

The nucleophilic behavior of **3** in solution and in solid state was then studied (Scheme 4). No direct 1,2-addition of **3** on benzaldehyde (**7**) was observed. However, addition of cesium fluoride (CsF) allowed the formation of the fluorinated secondary alcohol **8** with an NMR yield of 57% (Scheme 4, reaction 1).[14,15]

During the optimization of the process, we observed that the reaction seems to occur on the surface of the CsF, and we also observed the formation of HC_2F_5 presumably occurring via the decoordination of the ligand. This observation drove us to study the possible reactivity in solid state by mechanochemistry (Scheme 4, reaction 2). To our delight, the extrapolation of the previous conditions in solution to ball-milling conditions (30 min, 30 Hz) allowed us to obtain **8** with a similar yield (60%, NMR yield).

We then performed control experiments (Scheme 5) and a mechanistic study on this new C_2F_5 transfer reagent. It has recently been shown by theoretical and experimental studies that the presence of a C_2F_5 group enhances the Lewis acidity (LA) of group 14 (e.g. Si, Ge, Sn) compounds.[48]

To gauge the potential influence of this substituent on the LA, we investigated the potential formation of a covalent 6-coordinate Martin's spirosilane (**9a** or **9b**) derivative from **3** and **4** with fluoride as nucleophile (Scheme 5). No evidence of a hexavalent intermediate was observed by NMR in both cases. These experiments only showed ^{19}F resonance for TBAF (^{19}F: −116 ppm) and the recovered pentacoordinate silicon species (see Supporting Information). This indicates similar behaviour of each silicate with the fluoride source in agreement with the physical data (XRD) related to the electronegativity of the substituent (–C_2F_5 or –F), demonstrating the absence of a hindering effect of the substituent on direct fluoride addition (see topological map, Figure S4).

We then decided to perform the same experiment in solid-state. (Scheme 6.1).

As for the solution experiment, we did not observe traces of hexavalent intermediate nor the formation of $[Si(F)L_2]^-$. We also examined the effect of the steric hindrance on the electrophile by using benzophenone (**10**) (scheme 6.2). Complete loss of reactivity without formation of the tertiary alcohol **11** and full recovery of **3** were observed by ^{19}F NMR.

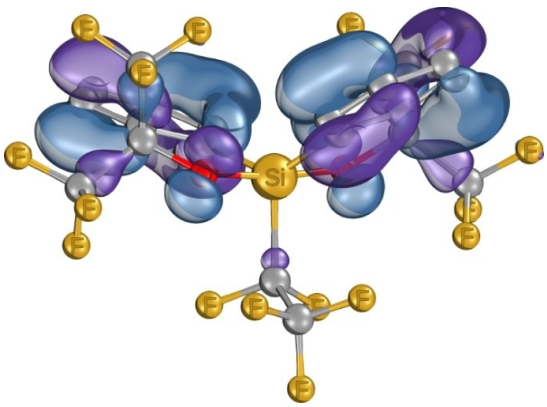

Figure 7. Representation (using IboView[47]) of the HOMO of **3**.

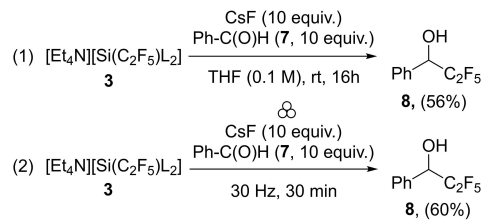

Scheme 4. Nucleophilic behavior of **3** in (1) solution and in the solid-state (2) by mechanochemistry.

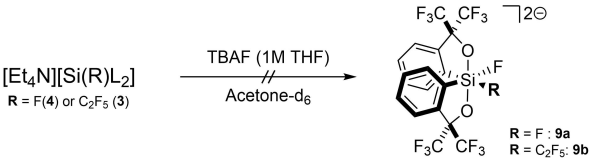

Scheme 5. Attempt for the synthesis of 6-coordinate species.

Research Article
doi.org/10.1002/ejoc.202300223

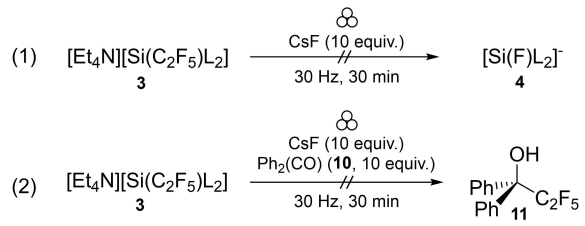

Scheme 6. Control experiments, (1) Attempt for the direct fluoride addition and formation of the observed subproduct $[Si(F)L_2]^-$; (2) Modification of the electrophile (benzophenone).

DFT calculations were performed to rationalize the results obtained under mechanochemical conditions (Figure 8). The influence of external forces on **3** were first investigated notably the influence of an applied force on the Si–C_F bond using the External Force is Explicitly Included (EFEI) approach implemented in Orca (See Supporting Information, Figure S3). As expected, increasing the force in nanoNewton (nN) within the system elongated the Si–C_F bond and thus destabilised the structure. The calculated breaking force for the Si–C bond ($F_{max} = 4.2 \pm 0.1$ nN) was comparable to a previous F_{max} value calculated for a silicon-carbon bond (4.78 nN, $H_3Si\text{-}CH_2CH_3$).[49]

We also showed experimentally that the mechanochemical conditions (30 Hz, 30 min) did not provide enough strength for direct bond scission of the substituent. Therefore, a direct bond breaking by an external force and addition onto the aldehyde electrophile appears unlikely. Currently, no realistic mechanism has been found by performing DFT calculations, this theoretical study is still ongoing in our laboratory.

Conclusion

In summary, the gram scale synthesis of a new hypercoordinated silicon species bearing a perfluoroethyl chain has been accomplished by direct nucleophilic addition of pentafluoroethyllithium to the Martin spirosilane as electrophile. Full characterizations are provided by NMR and X-ray diffraction analyses. Its potential use as a precursor of the fluoroethyl radical by photooxidation has proved unsuccessful so far but has led to a better understanding of the reactivity of this species. It was thus calculated that the substitution of an alkyl residue by the C_2F_5 group on the corresponding Martin silicate resulted in altered reactivity leading to the theoretical cleavage of the Si–Ar bond. This was attributed to a displacement of the HOMO to the bis(trifluoromethyl)benzenemethanol ligand. The reactivity of the Martin silicate as a C_2F_5 anion transfer reagent in solution and in the solid state was also assessed. In this work, we decided to focus on the addition to benzaldehyde in the presence of cesium fluoride. The experiment in solution indicates a potential reactivity on the surface of CsF. Also, the first mechanochemical addition of the C_2F_5 moiety from the hypercoordinated silicon species was observed. We demonstrated herein the use of mechanochemistry to transfer in solid state a reported explosive anion.

Finally, we surmise that the mechanochemistry of main group elements and notably the nucleophilic behaviour of hypercoordinate species will strongly gain scrutiny to develop new methodologies.

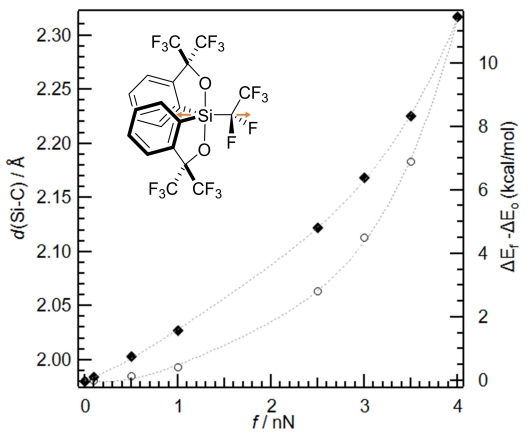

Figure 8. Solid-state theoretical investigations: force-dependence of the silicon-carbon (♦) bond length in Å (scale at left y-axis) and ΔE_f- ΔE_0 (°) in kcal/mol from DFT calculations (scale at right y-axis) both computed at the PW6B95-D3(BJ)/def2-QZVPP//PBEh-3c/def2-mSVP level of theory.

Experimental Section

Synthesis of $[NEt_4][Si(C_2F_5)L_2]$ (**3**): An excess of HC_2F_5 (~90 mL, ~2.5 equiv.) is condensed to a mixture of degassed n-butyllithium solution in hexanes (1 mL, 1.6 mmol, 1.6 M) in Et_2O (3 mL) at −75 °C and stirred for 20 min (*The preparation and handling of perfluoroethyllithium is hazardous, this anion being explosive*). A solution of Martin spirosilane (**1**) (SiL_2, L = (α,α-bis(trifluoromethyl) benzenemethanolato-(−2)C_2,O)[28] (800 mg, 1.6 mmol) in Et_2O (4 mL) is added slowly under stirring at −75 °C and slowly warmed up to −30 °C, degassed with nitrogen and warm up to room temperature. A solution of NEt_4Br (2 g, 9.5 mmol) in DCM (0.1 M) was added and was stirred overnight at rt. The crude was extracted with DCM/HCl (1 M), dry over Na_2SO_4 and the solvent was removed with a rotary evaporator. Precipitation (DCM/pentane) yields 78% of $[NEt_4][Si(C_2F_5)L_2]$ (**3**) (950 mg, 1.3 mmol) as a white powder over 2 steps. ^{1}H NMR (400 MHz on Bruker 400 MHz, [D6]acetone, rt): δ (ppm) = 8.4 (d, ^3J(H–H) = 6.7 Hz, 2H), 7.7 (d, ^3J(H–H) = 6.7 Hz, 2H), 7.5 (q, J = 8 Hz, 4H), 3.2 (q, J = 7 Hz, 8H), 1,2 (tt, br, 12H); $^{13}C\{^1H\}$ NMR (150.9 MHz on Bruker 600 MHz, [D6]acetone, rt): δ (ppm) = 141.7 (^1J(C,C) = 49.5 Hz, SiL_2), 140.3 (^1J(C,H) = 105.3 Hz,^1J(C,C) = 49.9 Hz, SiL_2), 137.8 (^1J(C,C) = 52.2 Hz, SiL_2), 129.2 (^1J(C,C) = 50.3 Hz SiL_2), 128.5 (^1J(C,C) = 59.7 Hz, SiL_2), 124.4 (q, ^1J(C,F) = 288 Hz, $C(CF_3)_2$), 124.3 (q, (overlap) ^1J(C,F) = 288 Hz, $C(CF_3)_2$), 122.0 (qt, ^1J(C,F) = 286 Hz; ^2J(C,F) = 32 Hz, -CF_2CF_3), 123.4 (SiL_2), 120.2 (ddq, ^1J(C,F) = 276 Hz; ^2J(C,F) = 37 Hz, -CF_2CF_3), 81.9 (sept, ^2J(C–F) = 28.2 Hz, $C(CF_3)_2$), 51.9 (t (broad), J = 2.6 Hz, N(CH_2CH_3), 6.2 (N(CH_2CH_3); $^{13}C\{^1H\}\{^{19}F\}$ NMR (100.6 MHz on JEOL 400 MHz, [D6]acetone, rt): δ = 143.8, 142.4, 139.9, 131.3, 130.6, 126.4, 126.3, 125.4, 124.0, 122.2, 84.0, 54.0, 8.3; ^{19}F NMR (564.6 MHz on Bruker 600 MHz, [D6]acetone, rt): δ = −74.3 (m, C(CF_3)-CF_3, 6F), −75.7 (q, C(CF_3)-CF_3:^{4}J(F,F) = 9.5 Hz, 6F), −80.9 m, -CF_2-CF_3, *3H*), −119 (d, sept, -C(***F***)F-CF_3:^{2}J(F,F) = 324 Hz, ^{6}J(F,F) = 6.9 Hz, 1F), −127 (d, sept, d, -CF(***F***)-CF_3:^{2}J(F,F) = 324 Hz, ^{6}J(F,F) = 6.9 Hz, ^{3}J(F,F) = 2.2 Hz, 1F); ^{29}Si NMR (119.2 MHz on Bruker 600 MHz, [D6]acetone, rt): δ = −78.0 ppm (dd, ^{2}J(Si, F) = 35 Hz); IR (ATR): $\tilde{\nu}$ (cm^{-1}) = 1486 (w), 1445 (w), 1396 (w), 1310 (m), 1293 (m),

1268 (m), 1232 (w), 1196 (m), 1177 (s), 1162 (s), 1154 (s), 1136 (s), 1114 (m), 1076 (m), 1038 (m), 1000 (s), 967 (s), 954 (s), 782 (m), 764 (m), 735 (s), 708 (s), 677 (m); m.p.: 152 °C, decomposition (bubbling 175 °C); HRMS: calc. for $[C_{20}H_8F_{17}O_2Si]^-$ 631.0028 found 631.0024.

Deposition Numbers href = "https://www.ccdc.cam.ac.uk/services/structures?id = doi:10.1002/ejoc.202300223"2208664 (for **4**) and 2223437 (for **3**) contain the supplementary crystallographic data for this paper. These data are provided free of charge by the joint Cambridge Crystallographic Data Centre and Fachinformationszentrum Karlsruhe url href = "https://www.ccdc.cam.ac.uk/structures"Access Structures service.

Acknowledgements

This work was supported by Sorbonne University, CNRS and IUF. We thank Thomas Deis for helpful discussions, Regina Maruchenko (Plateforme RMN Moléculaire/IPCM - Sorbonne Université) and Imane Senoussaoui (Application Engineer JEOL) for helping with $^{13}C\{^1H\}\{^{19}F\}$ NMR experiments, Jeremy Forté for X-ray diffraction analyses and Gilles Clodic for HRMS analyses.

Conflict of Interest

The authors declare no conflict of interest.

Data Availability Statement

The data that support the findings of this study are available from the corresponding author upon reasonable request.

Keywords: martin spirosilane · mechanochemistry · pentafluoroethyl anion · silicon · solid-state

[1] M. Wiesemann, B. Hoge, *Chem. Eur. J.* **2018**, *24*, 16457–16471.
[2] J. Bader, B. Neumann, H.-G. Stammler, N. Ignat'ev, B. Hoge, *Chem. Eur. J.* **2018**, *24*, 6975–6982.
[3] S. A. Föhrenbacher, M. J. Krahfuss, L. Zapf, A. Friedrich, N. V. Ignat'ev, M. Finze, U. Radius, *Chem. Eur. J.* **2021**, *27*, 3504–3516.
[4] S. A. Föhrenbacher, V. Zeh, M. J. Krahfuss, N. V. Ignat'ev, M. Finze, U. Radius, *Eur. J. Inorg. Chem.* **2021**, *2021*, 1941–1960.
[5] a) S. Steinhauer, J. Bader, H.-G. Stammler, N. Ignat'ev, B. Hoge, *Angew. Chem. Int. Ed.* **2014**, *53*, 5206–5209; *Angew. Chem.* **2014**, *126*, 5307–5310; b) S. Steinhauer, J. Bader, H.-G. Stammler, N. Ignat'ev, B. Hoge, *Angew. Chem.* **2014**, *126*, 5307–5310; *Angew. Chem. Int. Ed.* **2014**, *53*, 5206–5209.
[6] a) S. Steinhauer, T. Böttcher, N. Schwarze, B. Neumann, H.-G. Stammler, B. Hoge, *Angew. Chem. Int. Ed.* **2014**, *53*, 13269–13272; *Angew. Chem.* **2014**, *126*, 13485–13488; b) S. Steinhauer, T. Böttcher, N. Schwarze, B. Neumann, H.-G. Stammler, B. Hoge, *Angew. Chem.* **2014**, *126*, 13485–13488; *Angew. Chem. Int. Ed.* **2014**, *53*, 13269–13272.
[7] N. Schwarze, B. Kurscheid, S. Steinhauer, B. Neumann, H.-G. Stammler, N. Ignat'ev, B. Hoge, *Chem. Eur. J.* **2016**, *22*, 17460–17467.
[8] a) N. Tiessen, M. Keßler, B. Neumann, H.-G. Stammler, B. Hoge, *Angew. Chem. Int. Ed.* **2021**, *60*, 12124–12131; *Angew. Chem.* **2021**, *133*, 12231–12238; b) N. Tiessen, M. Keßler, B. Neumann, H.-G. Stammer, B. Hoge, *Angew. Chem.* **2021**, *133*, 12231–12238; *Angew. Chem. Int. Ed.* **2021**, *60*, 12124–12131.
[9] N. Tiessen, N. Schwarze, H.-G. Stammler, B. Neumann, B. Hoge, *Inorg. Chem.* **2021**, *60*, 15112–15117.
[10] a) N. Tiessen, M. Keßler, B. Neumann, H.-G. Stammler, B. Hoge, *Angew. Chem. Int. Ed.* **2022**, *61*, e202116468; b) N. Tiessen, M. Keßler, B. Neumann, H.-G. Stammler, B. Hoge, *Angew. Chem.* **2022**, *134*, e202116468.
[11] D. M. Roddick, *Chem. Eng. News* **1997**, *75*.
[12] D. A. Dixon, Tadamichi. Fukunaga, B. E. Smart, *J. Am. Chem. Soc.* **1986**, *108*, 4027–4031.
[13] a) B. Waerder, S. Steinhauer, B. Neumann, H.-G. Stammler, A. Mix, Y. V. Vishnevskiy, B. Hoge, N. W. Mitzel, *Angew. Chem. Int. Ed.* **2014**, *53*, 11640–11644; *Angew. Chem.* **2014**, *126*, 11824–11828; b) B. Waerder, S. Steinhauer, B. Neumann, H.-G. Stammler, A. Mix, Y. V. Vishnevskiy, B. Hoge, N. W. Mitzel, *Angew. Chem.* **2014**, *126*, 11824–11828; *Angew. Chem. Int. Ed.* **2014**, *53*, 11640–11644.
[14] Y. Fujihira, K. Hirano, M. Ono, H. Mimura, T. Kagawa, D. M. Sedgwick, S. Fustero, N. Shibata, *J. Org. Chem.* **2021**, *86*, 5883–5893.
[15] M. Ono, Y. Sumii, Y. Fujihira, T. Kagawa, H. Mimura, N. Shibata, *J. Org. Chem.* **2021**, *86*, 14044–14053.
[16] M. Wiesemann, J. Klösener, B. Neumann, H.-G. Stammler, B. Hoge, *Chem. Eur. J.* **2018**, *24*, 1838–1843.
[17] A. Lishchynskyi, V. V. Grushin, *J. Am. Chem. Soc.* **2013**, *135*, 12584–12587.
[18] E. D. Kalkman, M. G. Mormino, J. F. Hartwig, *J. Am. Chem. Soc.* **2019**, *141*, 19458–19465.
[19] a) M. Niemann, B. Neumann, H.-G. Stammler, B. Hoge, *Angew. Chem. Int. Ed.* **2019**, *58*, 8938–8942; *Angew. Chem.* **2019**, *131*, 9033–9038; b) M. Niemann, B. Neumann, H.-G. Stammler, B. Hoge, *Angew. Chem.* **2019**, *131*, 9033–9038; *Angew. Chem. Int. Ed.* **2019**, *58*, 8938–8942.
[20] M. Niemann, B. Neumann, H.-G. Stammler, B. Hoge, *Eur. J. Inorg. Chem.* **2019**, *2019*, 3462–3475.
[21] a) S. Solyntjes, J. Bader, B. Neumann, H.-G. Stammler, N. Ignat'ev, B. Hoge, *Chem. Eur. J.* **2017**, *23*, 1557–1567; b) S. Porath, M. Keßler, B. Neumann, H.-G. Stammler, B. Hoge, *Chem. Eur. J.* **2023**, *n/a*, 10.1002/chem.202203278.
[22] F. Medici, G. Gontard, E. Derat, G. Lemière, L. Fensterbank, *Organometallics* **2018**, *37*, 517–520.
[23] F. Medici, J. Maury, G. Lemière, L. Fensterbank, *Chem. Eur. J.* **2019**, *25*, 9438–9442.
[24] T. Deis, F. Medici, A. Poussard-Schulz, G. Lemière, L. Fensterbank, *J. Organomet. Chem.* **2021**, *956*, 122120.
[25] G. Lemière, A. Millanvois, C. Ollivier, L. Fensterbank, *Chem. Rec.* **2021**, *21*, 1119–1129.
[26] T. Deis, J. Forte, L. Fensterbank, G. Lemière, *Molecules* **2022**, *27*, 1767.
[27] a) T. Deis, J. Maury, F. Medici, M. Jean, J. Forte, N. Vanthuyne, L. Fensterbank, G. Lemière, *Angew. Chem. Int. Ed.* **2022**, *134*, e202113836; b) T. Deis, J. Maury, F. Medici, M. Jean, J. Forte, N. Vanthuyne, L. Fensterbank, G. Lemière, *Angew. Chem.* **2022**, *134*, e202113836.
[28] H. Lenormand, V. Corcé, G. Sorin, C. Chhun, L.-M. Chamoreau, L. Krim, E.-L. Zins, J.-P. Goddard, L. Fensterbank, *J. Org. Chem.* **2015**, *80*, 3280–3288.
[29] G. Ikarashi, T. Morofuji, N. Kano, *Chem. Commun.* **2020**, *56*, 10006–10009.
[30] T. Morofuji, Y. Matsui, M. Ohno, G. Ikarashi, N. Kano, *Chem. Eur. J.* **2021**, *27*, 6713–6718.
[31] a) M. Abdellaoui, T. Deis, M.-A. Wiethoff, C. Bahri, G. Lemiere, C. Ollivier, L. Fensterbank, *Adv. Synth. Cat.* **2023**, *365,* 884–891; b) M.-A. Wiethoff, M. Abdellaoui, T. Deis, V. Corcé, G. Lemiere, C. Ollivier, L. Fensterbank *Synlett* **2023** DOI: 10.1055/a-2059-3498.
[32] A. Millanvois, C. Ollivier, L. Fensterbank, *Eur. J. Inorg. Chem.* **2022**, *2022*, e202101109.
[33] V. Corcé, C. Ollivier, L. Fensterbank, *Chem. Soc. Rev.* **2022**, *51*, 1470–1510.
[34] R. R. Holmes, *Chem. Rev.* **1990**, *90*, 17–31.
[35] W. B. Farnham, J. F. Whitney, *J. Am. Chem. Soc.* **1984**, *106*, 3992–3994.
[36] a) G. K. S. Prakash, F. Wang, Z. Zhang, R. Haiges, M. Rahm, K. O. Christe, T. Mathew, G. A. Olah, *Angew. Chem. Int. Ed.* **2014**, *53*, 11575–11578; *Angew. Chem.* **2014**, *126*, 11759–11762; b) G. K. S. Prakash, F. Wang, Z. Zhang, R. Haiges, M. Rahm, K. O. Christe, T. Mathew, G. A. Olah, *Angew. Chem.* **2014**, *126*, 11759–11762; *Angew. Chem. Int. Ed.* **2014**, *53*, 11575–11578.
[37] See Supporting Information: Preparation of [Li][$C_6F_{12}H$] from $C_6F_{12}H_2$ and addition on Martin spirosilane.
[38] P. Erdmann, J. Leitner, J. Schwarz, L. Greb, *ChemPhysChem* **2020**, *21*, 987–994.
[39] P. Erdmann, L. Greb, *ChemPhysChem* **2021**, *22*, 935–943.
[40] F. Neese, *WIREs Comput. Mol. Sci.* **2022**, *12*, e1606.

[41] *Deposition Number 2223436–2223438, others strucutre has been identified during our investigation (2223436 (a 9.8876(4) b 17.2753(6) c 28.9811(12) P-1) and 2223438 (a 17.6739(8) b 17.4789(9) c 19.7450(10) P21).*
[42] R. R. Holmes, J. A. Deiters, *J. Am. Chem. Soc.* **1977**, *99*, 3318–3326.
[43] *Data from recently submitted research article on [NEt_4][SiL_2Me].*
[44] a) A. Tlili, S. Lakhdar, *Angew. Chem. Int. Ed.* **2021**, *60*, 19526–19549; *Angew. Chem.* **2021**, *133*, 19678–19701; b) A. Tlili, S. Lakhdar, *Angew. Chem.* **2021**, *133*, 19678–19701; *Angew. Chem. Int. Ed.* **2021**, *60*, 19526–19549.
[45] X. Yang, G. C. Tsui, *Org. Lett.* **2020**, *22*, 4562–4567.
[46] Z. Luo, G. C. Tsui, *Org. Chem. Front.* **2022**, *9*, 4969–4974.
[47] G. Knizia, *J. Chem. Theory Comput.* **2013**, *9*, 4834–4843.
[48] L. Greb, *Chem. Eur. J.* **2018**, *24*, 17881–17896.
[49] M. K. Beyer, *J. Chem. Phys.* **2000**, *112*, 7307–7312.

Manuscript received: March 10, 2023
Revised manuscript received: April 7, 2023
Accepted manuscript online: April 7, 2023